



Tomas Bata University in Zlín
Centre of Polymer Systems

Doctoral Thesis

**Nanofibrous Polymer Systems for Elimination of
Estrogenic Hormones from Wastewater**

**Nanovláknenné polymerní systémy pro eliminaci estrogenních
hormonů z odpadních vod**

Author: Muhammad Yasir, M.Sc.
Degree programme: P3924 Material Sciences and Engineering
Degree course: 3911V040 Biomaterials and Biocomposites
Supervisor: prof. Ing. Vladimír Sedlářik, Ph.D.
Consultant: Ing. Dušan Kimmer, CSc.

Zlín, 2022

© Muhammad Yasir

Dedication

This Ph.D. thesis is dedicated to my adorable and beloved parents (late): ***Mrs. Tabassum Zahida***, M.A., my mother, and ***Mr. Ashiq Hussain***, M.A. LL.B., my father.

ABSTRACT

Residual estrogenic hormones represent emerging pollutants in the environment. One of the most important aspects of their effective removal is the design and fabrication of an adsorption system with appropriate properties. This thesis reports on the complex research activities aimed at the development, optimized preparation, and characterization of various electrospun nanofibrous polymer systems for simultaneous removal of estrogenic hormones such as estrone, estradiol, ethinylestradiol, and estriol from wastewater. A wide scale of polymers covering polyurethanes, polyamide, cellulose acetate, polysulfone, polyether sulfone, polylactic acid, polyacrylonitrile, and polyvinylidene fluoride was studied as a matrix for nanofibrous sorption materials. A facile method was developed for the simultaneous determination of tested hormones by using a high-performance liquid chromatography technique coupled with a UV-Vis detector. Sorption kinetics modeling and description of the material vs. hormones interaction mechanisms were an integral part of this study.

Key words: *estrogenic hormones, nanofibers, electrospinning, adsorption kinetics, wastewater treatment, polyurethane, polyamide, polysulfone, polylactide, polyvinylidene fluoride, cellulose acetate, polyacryl amide*

ABSTRAKT

Residua estrogenních hormonů představují aktuální problém pro životní prostředí. Návrh, vývoj a produkce absorpčních systémů schopných jejich efektivního zachytu z environmentu jsou důležitými aspekty při řešení této problematiky. Tato práce se věnuje komplexnímu výzkumu cíleného na vývoj, charakterizaci a optimalizaci přípravy nanovlákných systémů, připravených pomocí metody elektrovlákňování polymerních roztoků, pro odstraňování estrogenních hormonů estronu, estradiolu, ethinyestradiolu a estriolu z odpadních vod. Široká škála polymerů zahrnujících polyuretan, polyamid, acetát celulózy, polysulfon, polyetersulfon, polylaktid, polyakrylonitril a polyvinilidenfluorid byla studována jako matrice pro přípravy nanovlákných sorpčních materiálů. V rámci práce byla vyvinuta metoda pro současné stanovení všech použitých hormonů pomocí metody vysoce účinné kapalinové chromatografie se spektrometrickou detekcí v ultrafialové a viditelné oblasti. Modelování sorpčních kinetik a popis interakce mezi estrogenními hormony a připravenými materiály jsou nedílnou součástí práce.

Klíčová slova: *estrogenní hormony, nanovlákná, elektrovlákňování, sorpční kinetika, čištění odpadních vod, polyuretan, polyamid, polysulfon, polylaktid, polyvinilidenfluorid, acetát celulózy, polyakrylamid*

ACKNOWLEDGEMENTS

All praise to almighty Allah, the most merciful and compassionate, the creator of the universe, Who enabled me to complete this research work successfully. I feel privileged to have the honor to acknowledge my research supervisor **Prof. Vladimir Sedlarik**, to whom I owe my indescribable special indebtedness, who was very affectionate and cooperative during this research work. I am thankful to my doctoral study consultant, **Ing. Dusan Kimmer**, for the inspiration throughout my study. Without his kind and sincere efforts, it might not have been possible for me to end this task in time.

Furthermore, I would like to extend my gratitude to **Tomas Bata University in Zlín** for providing me with the necessary infrastructure and financial support in the form of a **Ph.D. extraordinary scholarship (2019-2022)** and **IGA project fund (IGA-2019-2022)** for my research, attending different international scientific conferences and my living in the Czech Republic.

The successful accomplishment of this doctoral thesis has become possible with the sustained support of the dearest ones. I offer my special and sincere thanks to my friends in the dormitory and colleagues in the **Centre of Polymer Systems** who guided me through the rough patches in conducting research. Furthermore, I wish to offer my humble gratitude to my deceased parents for their support in the early phase of my life that paved the way for me to reach this destination. I have realized that my whole life, I have been blessed because of them. Finally, I dedicate my success to my beloved wife, son, sister, sister-in-law, and father-in-law; they are a complete inspiration to me throughout my Engineering Career. Their affection, love, prayers, and true guidance have led me to consistent success.

Moreover, I would also thank **Dr. Agnes Schulze**, head of Surfaces and porous membrane filters at Leibniz institute of Surface Engineering (IOM), Leipzig, Germany, for providing me training opportunity and **Dr. Daniel Breite** for helping me participate in learning electron-beam irradiation technique for the development of adsorptive membrane surfaces for the selective removal of hormones from water.

LIST OF PUBLISHED PAPERS

The doctoral work of Mr. Muhammad Yasir, entitled “*Nanofibrous polymer systems for elimination of estrogenic hormones from wastewater,*” involves the following articles:

Article I

M. Yasir (70%), T. Sopik, L. Lovecka, D. Kimmer, V. Sedlarik, The adsorption, kinetics, and interaction mechanisms of various types of estrogen on electrospun polymeric nanofiber membranes, *Nanotechnology* 33 (2021) 75702, <https://doi.org/10.1088/1361-6528/ac357b>.

Article II

M. Yasir (80%), T. Sopik, R. Patwa, D. Kimmer, V. Sedlarik, Adsorption of estrogenic hormones in aqueous solution using electrospun nanofibers from waste cigarette butts: Kinetics, mechanism, and reusability, *Express Polymer Letters* 16 (2022) 624–648, <https://doi.org/10.3144/expresspolymlett.2022.46>.

Article III

M. Yasir (50%), F. A. Ngwabebhoh, T. Sopik, H. Ali, V. Sedlarik, Electrospun polyurethane nanofibers coated with polyaniline/polyvinyl alcohol as ultrafiltration membranes for the removal of ethinylestradiol hormone micropollutant from aqueous phase, *Journal of Environmental Chemical Engineering* 10 (2022) 107811, <https://doi.org/10.1016/j.jece.2022.107811>.

Article IV

M. Yasir (50%), F. A. Ngwabebhoh, T. Sopik, L. Lovecka, D. Kimmer, V. Sedlarik, The adsorptive behaviour of electrospun hydrophobic polymers for optimized uptake of estrogenic sex hormones from aqueous media: Kinetics, thermodynamics and reusability study, *Journal of Chemical Technology and Biotechnology* (2022), <https://doi.org/10.1002/jctb.7191>.

TABLE OF CONTENT

Dedication.....	3
ABSTRACT	4
ABSTRAKT	5
ACKNOWLEDGEMENTS	6
LIST OF PUBLISHED PAPERS	7
TABLE OF CONTENT	8
1. INTRODUCTION.....	13
2. Theoretical background.....	15
2.1 The global challenge of water filtration.....	15
2.2 Methods of removing contaminants from water	16
i) Conventionally applied methods	16
ii) Advance adsorption methods for wastewater treatment.....	20
2.3 Emerging micropollutants in water	23
2.3.1 Solution preparation and sampling	26
2.3.2 Devised method of High-Performance Liquid Chromatography (HPLC)	28
2.3.3 Detection and quantification	29
2.4 Method of membrane preparation (Electrospinning).....	30
2.4.1 Influence of parameters for electrospinning	32
2.4.2 Influence of parameters while electrospinning	33
3. MATERIALS AND APPLICATIONS.....	35
3.1 Materials used for adsorption in water treatment	35
3.2 Materials and Chemicals required	36
3.3 Preparation of experimental materials via electrospinning	37
3.3.1 Solution preparation for electrospinning.....	37
3.3.2 Fabrication of nanofibers	38
3.4 Method of characterization of material	41
4. MOTIVATION FOR THE DOCTORAL STUDY	57

4.1	Conclusions and bridging the gap.....	57
4.2	Aims of doctoral thesis	58
4.3	Experimental design.....	60
4.3.1	Evaluation of the adsorption properties of polymeric nanofiber structure by discontinuous sorption testing	60
4.3.2	Adsorption kinetics study	62
4.3.3	Thermodynamic study	64
4.3.4	Isotherm modeling	64
4.3.5	Reusability test.....	65
4.3.6	Statistical and error analysis	65
5.	The adsorption, kinetics, and interaction mechanisms of various types of estrogen on electrospun polymeric nanofiber membranes	66
5.1	Characterization of the electrospun nanofibers	67
5.2	Static adsorption study of hormones on the polymeric nanofiber materials	71
5.3	Equilibrium adsorption capacity comparison	72
5.4	Adsorption kinetics	74
5.5	Adsorption mechanism of EH on polyurethane nanofibers.....	77
5.6	Determination of recovery and reusability of comparative electrospun nanofibers.....	80
5.7	Limitations, future works, and practical application	84
5.8	Conclusions.....	85
6.	Adsorption of estrogenic hormones in aqueous solution using electrospun nanofibers from waste cigarette butts: Kinetics, mechanism, and reusability....	86
6.1	Characterization of WCENFs	87
6.2	Batch adsorption study of EH on WCENFs	91
6.3	Adsorption kinetics of EH on WCENFs.....	94
6.4	Adsorption mechanism of EH on WCENFs.....	98
6.5	Determination of recovery and reusability of WCENFs	102
6.6	Instantaneous adsorption test of PET/WCENFs syringe film	104

6.7 EH adsorption on PET/WCENFs fabricated membrane film and commercial application	105
6.8 Restrictions, Further research, and application of WCENFs	107
6.9 Comparative study of WCENFs with other adsorbents for the removal of EH.....	107
6.10 Conclusions	109
7. Electrospun polyurethane nanofibers coated with polyaniline/polyvinyl alcohol as ultrafiltration membranes for the removal of ethinylestradiol hormone micropollutant from the aqueous phase.....	110
7.1 Post-modification of spun PU nanofiber membrane	111
7.2 Adsorption analysis via modeling	111
7.3 Modification of spun nanofibers.....	112
7.4 Material characterization	113
7.4.1 FTIR analysis.....	113
7.4.2 Optical microscopy	114
7.4.3 SEM analysis	115
7.5 Adsorption study of PU-modified nanofibers.....	116
7.6 Batch adsorption optimization study	117
7.6.1 ANOVA for quadratic model	118
7.7 Optimization validation	120
7.8 Effect of two interaction parameters on the removal of EE2 hormone	121
7.9 Effect of single parameters on the optimal removal of EE2 hormone .	125
7.9.1 Effect of solution pH	125
7.9.2 Effect of initial EE2 hormone concentration.....	125
7.9.3 Effect of dosage	125
7.9.4 Effect of temperature	126
7.10 Adsorption mechanism of EE2 hormone on PU-PANI-ES fibers.....	127
7.11 Kinetic modeling for the uptake of EE2 hormone by PU-PANI-ES....	128
7.12 Thermodynamic study for the adsorption of EE2 hormone	130
7.13 Reusability study of PU-PANI-ES nanofibers	131

7.14 Comparative study of PU-PANI-ES with other adsorbents for EE2 hormone removal	132
7.15 Conclusions.....	133
8. The adsorptive behavior of electrospun hydrophobic polymers for optimized uptake of estrogenic sex hormones from aqueous media: Kinetics, thermodynamics and reusability study.....	135
8.1 Characterization of materials	136
8.2 Batch adsorption studies.....	139
8.2.1 Preliminary adsorption for different prepared hydrophobic polymeric nanofibers.....	139
8.2.2 Effect of contact time	140
8.3 Adsorption kinetics for PSU nanofibers.....	140
8.4 Adsorption based on the variation of single parameters	144
8.4.1 Effect of solution pH.....	144
8.4.2 Effect of E1 hormone concentration	145
8.4.3 Effect of PSU adsorbent dosage.....	145
8.4.4 Effect of temperature	146
8.5 Adsorption mechanism of E1 on PSU.....	147
8.6 Thermodynamic study for adsorption of E1 hormone on PSU nanofibers	148
8.7 Isotherm modeling.....	149
8.8 A comparative study with other adsorbents for E1	151
8.9 Adsorption-desorption study of PSU nanofibers	152
8.10 Conclusions.....	153
9 CONCLUDING REMARKS	154
9.1 Conclusions of work done	154
9.2 Contribution to science and practice.....	158
9.3 Future plans.....	159
REFERENCES.....	161
LIST OF FIGURES	178
LIST OF TABLES	183

LIST OF ABBREVIATIONS AND SYMBOLS.....	184
APPENDIX 1	188
CURRICULUM VITAE	202
TOTAL PUBLICATIONS	206
PUBLICATIONS	208

1. INTRODUCTION

Water is the most important and limited resource available on earth, which has been contaminated by toxic metals, pathogens, pharmaceutical chemicals, dust, dyes, pesticides, fertilizers, and organic and inorganic materials. Various methods have been implemented for the remediation of water quality and cleaning, but most of them are expensive, less effective, and time-consuming. In this domain, several solutions related to nanotechnology have been successfully deployed in recent times. In this regard, membranes based on nanofibers produced from different polymeric materials for water treatment applications are promising owing to their benefits, such as affordability, sustainability, efficient performance, durability, high surface area, high aspect ratio, and nanoporous structure. Furthermore, the nanofiber membrane functions precisely in different aquatic conditions without the accumulation of chemicals [1].

Estrogenic hormones (EH) at significant levels are a serious cause of fish femininity and breast and ovarian cancer because of hormonal imbalance. Furthermore, environmental effluents that are being constantly discharged, especially synthetic hormones, are difficult to contain and pose a severe risk to the environment and various forms of life. So far, several techniques have been employed to eliminate such hazardous hormones, such as ozonation, membrane bioreactors, advanced oxidation, membrane filtration, coagulation, and flocculation. These commonly used techniques also result in secondary pollution, which demands secondary water treatment. In this regard, removing synthetic hormones by adsorption via electrospun nanofibers offers a sustainable and relatively environmentally friendly solution for eliminating synthetic hormones with high efficiency and effectiveness of reusability for several adsorption-desorption cycles after regeneration. This brings a practical approach to large-scale production.

The thesis presented here is devoted to fabricating electrospun polymeric nanofibrous membranes that are porous and most suitable for capturing EH, owing to their specific surface area and functional groups on the surfaces involved. The surface treatment of nanofibers further enhances the simultaneous adsorption of EH due to the involvement of several types of interaction mechanisms, such as physical adsorption, hydrophobic interactions, hydrogen bonding, and π - π stacking interaction. This surface modification of the most promising nanofiber is used to evaluate enhanced adsorption in an optimization study with the optimized experimental parameters via the response surface

methodology using a central composite design model and validation of operating parameters by the Design-Expert software. The study also contains devising a facile HPLC method for simultaneous detection and quantification of EH. The core part is devoted to optimized preparation, characterization of the electrospun membranes, testing of adsorption activity under different conditions, optimization of experimental parameters for determination of suitable kinetic models, Isotherms, thermodynamics, and ensuring the effectiveness by reusability of membranes over several adsorption-desorption cycles.

2. Theoretical background

2.1 The global challenge of water filtration

In the last few decades, rapid industrialization and human population growth have raised serious environmental concerns due to the high demand for various synthetic chemicals, which are being released into the environment without proper treatment. Today, the freshwater available on earth is less than 1% for the use of human beings. This freshwater has comprised the form of snow-capped peaks, glaciers, and ice mountains. The earth's water includes freshwater (2.6%) and saltwater (97.4%), which is primarily oceans (Figure 2.1). Of the freshwater, 70% is utilized for the purpose of irrigation, 10% for domestic use, and 20% for industrial work [2]. About 1.3 billion population worldwide cannot acquire safe water for drinking [3]. Approximately 1.8 million people consume unsafe and unclean water and die yearly because of diseases such as diarrhea. The world's population is massively growing, with an expected number to reach 3 billion in the next 30 years. There are almost 2.7 billion people exposed to devastating use of poor water quality due to an economic crisis in the developing world [4]. According to reports, around 5500–6200 children die worldwide per day using contaminated water. Globally, 0.8 million humans have unavailability of safe drinking water because of several reasons such as climatic effects of the growing population, increasing demand for energy, food crisis, ground and surface water pollution, improper use of resources, sanitation problems, soil erosion, excessive use of pesticides and fertilizers, contamination by heavy toxic metals, industrial effluent waste, oils spillage, pharmaceutical chemicals, and steroid hormones which are a significant contributor to contaminated water. These continuously spreading bioactive contaminants have severe consequences on the health of humans and marine life, uptaking water from sources leading to fatal diseases, among them being different kinds of cancer. Thus, micro-pollutants in water are needed to be immediately abolished and eradicated by strict control policies at wastewater treatment plants before consumption. The fabrication of high-performance and sustainable fibrous membranes is a necessity for all environmental applications areas, such as the removal of effluents waste from industries, textiles, dyes, heavy metals in water, nitrates, per- and polyfluoroalkyl substances, bacteria, pharmaceutical chemicals, EH, viruses, desalination and filtration of water for drinking purposes [5].

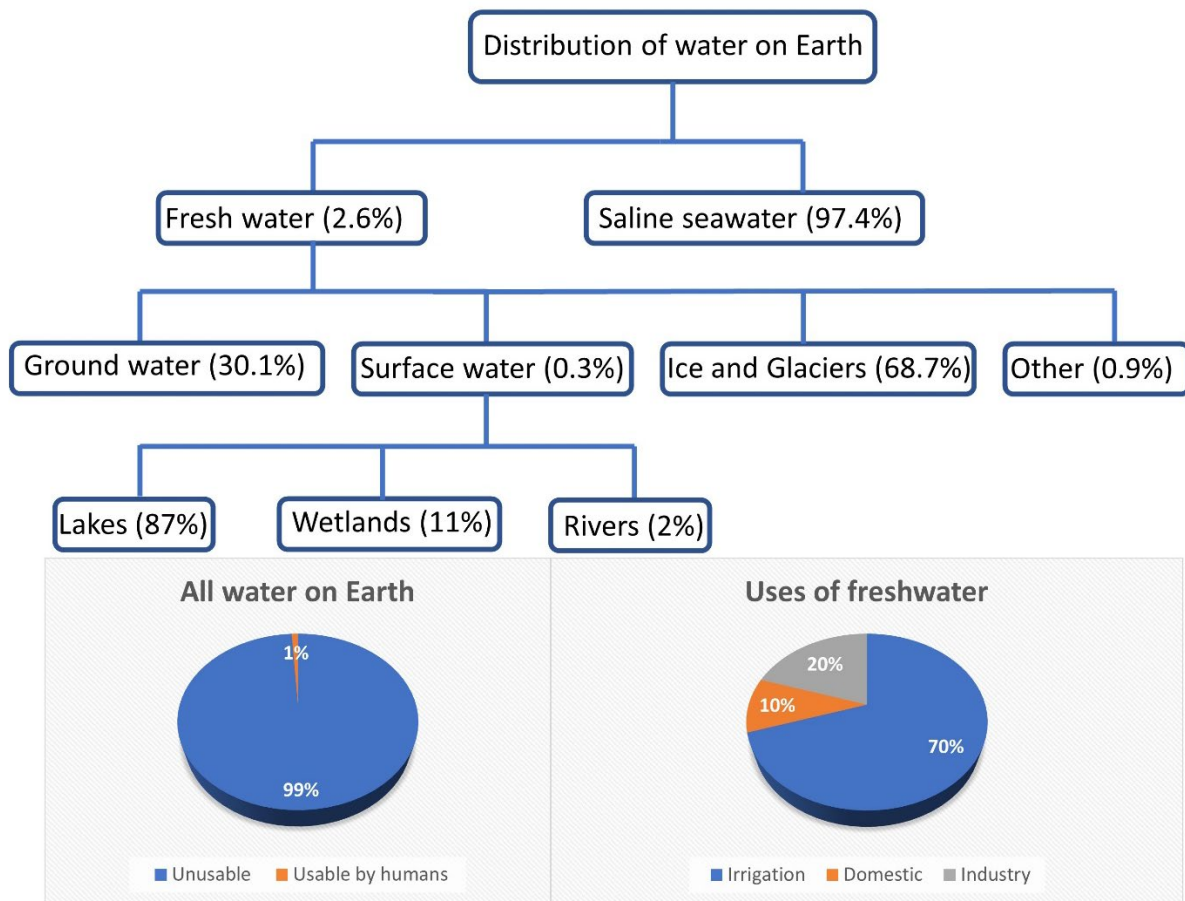


Figure 2.1: Distribution of Earth's water and its uses (Self-representation by the author).

2.2 Methods of removing contaminants from water

The equilibrium between sewage and freshwater resources is achieved by wastewater treatment. Therefore, the efficiency of wastewater treatment has a significant impact on water neutralization and reduces the depletion of precious water resources. Therefore, the most crucial needs of the modern period are technological advancements for wastewater treatment. The traditional and cutting-edge methods of water purification are described in detail here.

i) Conventionally applied methods

The removal of a wide range of hazardous compounds, bacteria, and chemicals contained in wastewater is limited by traditional methods of water filtration [6]. Conventional methods are displayed in Figure 2.2.

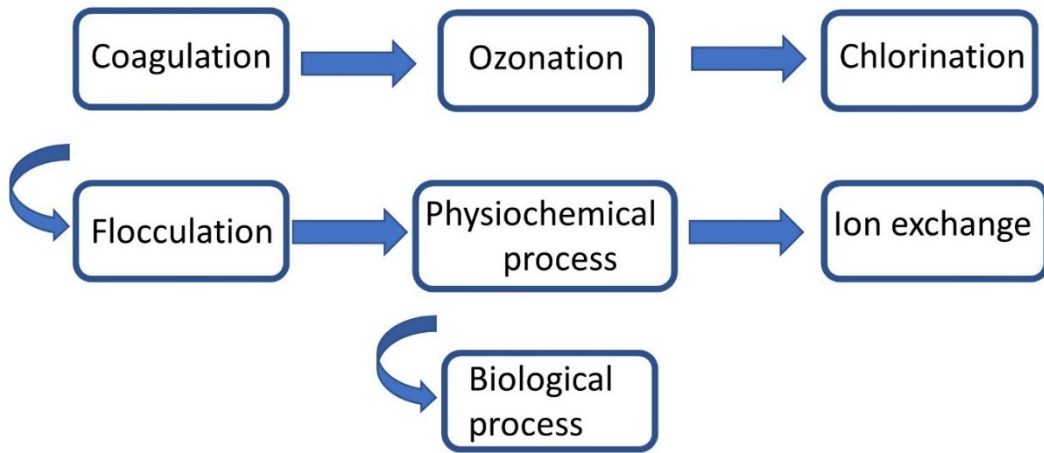


Figure 2.2: Conventional techniques of water filtration (Self-representation by the author).

Coagulation process

Before filtration and sedimentation, the technique of coagulation is used to clean wastewater. In this method, charged coagulants are employed to remove the wastewater's suspended solids and neutralize them. The flocs, which are invisible to the human eye, are formed when neutralized particles clump together. Additionally, the wastewater can be stirred to create micro flocs, as illustrated in Figure 2.3; however, this method is quite endothermic. Numerous academics have been studying the coagulation method for the treatment of wastewater [7,8]. While coagulation is widely used, new pilot plants and fully functional industrial units have also used the ozonation process to purify water.

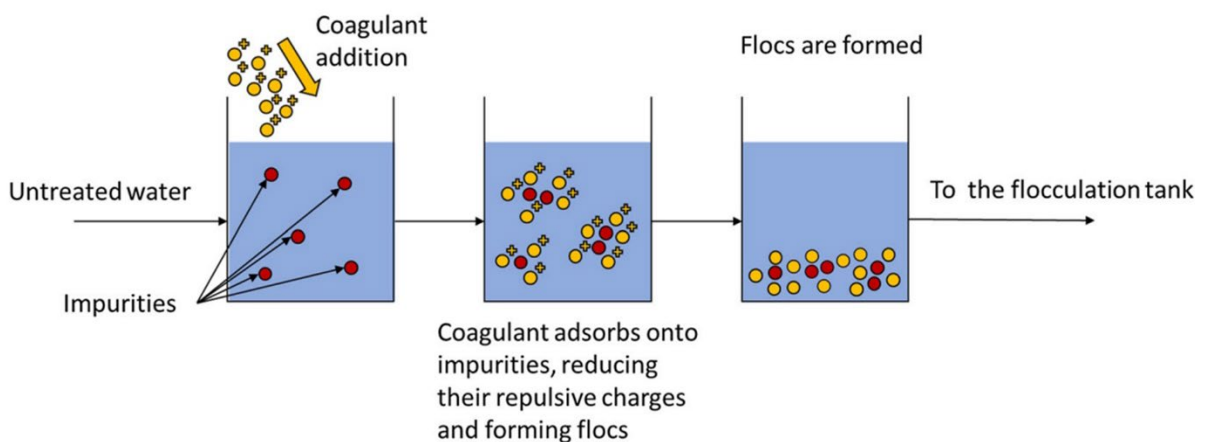


Figure 2.3: The Coagulation Process [9].

Ozonation process

wastewater effluents are taken out using this method, and drinking water is cleaned. By reducing the amount of organic and inorganic compounds in water, ozonation purifies it. Many studies have also reported using the ozonation technique to purify water and eliminate impurities such as effluents, dyes, and particles. Figure 2.4 displays a schematic representation of the procedure. This approach for purifying water is less effective due to its high cost and limited lifespan [10,11]. These ozonation difficulties are handled in the chlorination process, which is one of the most basic methods for purifying water.

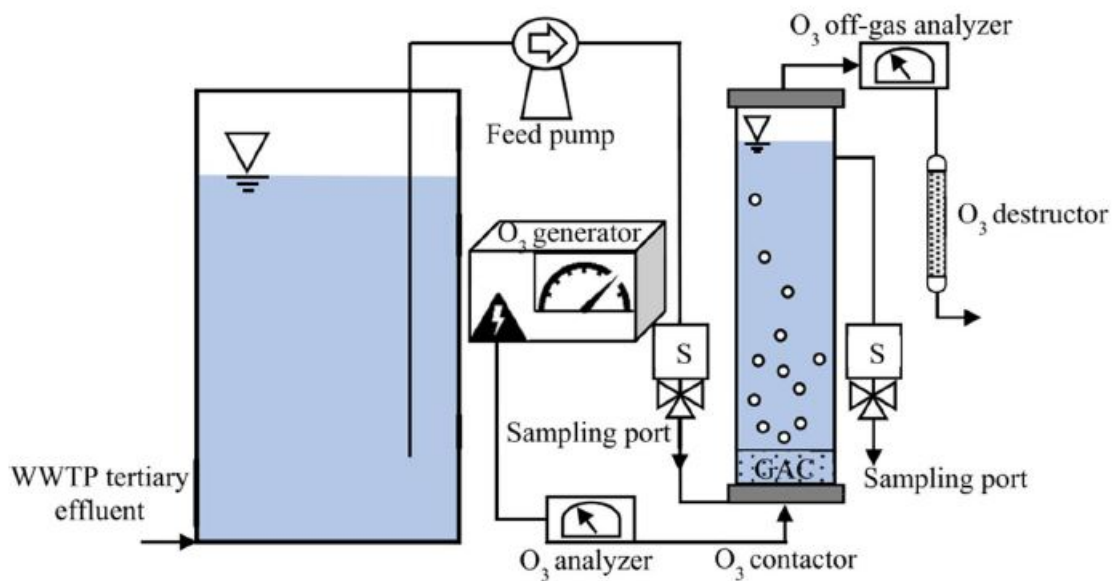


Figure 2.4: The Ozonation Process [1].

Chlorination process

This method is frequently employed to eliminate bacteria, pathogens, and other germs in wastewater because its mechanism offers a residual defense against bacteria and other organisms. Pathogens cause unwanted odor and taste in water. Various scientists have utilized this procedure to purify wastewater [12,13]. Chlorination may alter the taste and aroma of water, which is much less likely to occur in coagulation and flocculation.

Flocculation process

This procedure involves gentle mixing to agglomerate and settles the particles, as seen in Figure 2.5. The settled particles are subsequently removed from the wastewater using a filter. As the molecules are slowly mixed together, a bond is formed that makes the agglomerated particles visible. In order to improve floc density and settling speed, the coagulant can also be used to create a bridge

between the flocs. Once the floc reaches its maximum size, filtering is used to remove it from the media. Several researchers have reported that flocculation can remove pollutants [14].

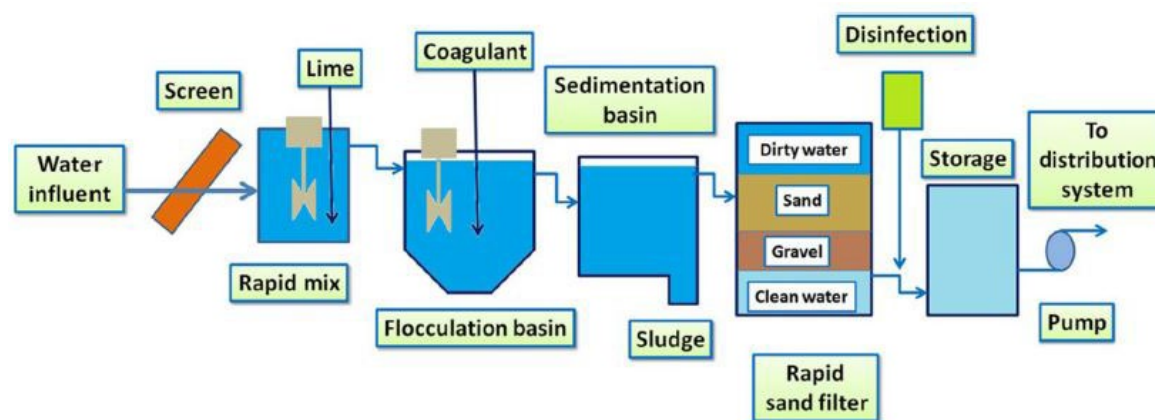


Figure 2.5: The Flocculation Process [1].

Physiochemical process of treatment

This method comprises the softening, coagulation, and flocculation of lime, and it is effective at removing a wide range of endocrine-disrupting compounds (ECDs). Numerous scholars have described a physiochemical method for wastewater cleaning [15,16].

Ion exchange and photolysis technique

Various treatment plants currently utilize ion exchange and photolysis to purify water; however, these methods have drawbacks that limit their utilization. The major downside of this approach is that it cannot be utilized to eliminate water pollutants at the microscale [17,18]. One of the biological processes used in the traditional category of water purification can be used to remove microscale particles.

The biological process of treatment

Due to the biological trickling filter and sludge, which the filtering and purification operations could not remove, several contaminants are still soluble in wastewater. Therefore, the biological process, also known as the cellular method, is employed by bacteria and microorganisms to break down organic waste and remove water contamination. Figure 2.6 depicts a procedure to remove microorganisms and other impurities from wastewater [19,20]. Both domestically and industrially, these traditional techniques are still in use. However, a few

cutting-edge water filtration methods have also been developed that are more effective and offer several benefits.

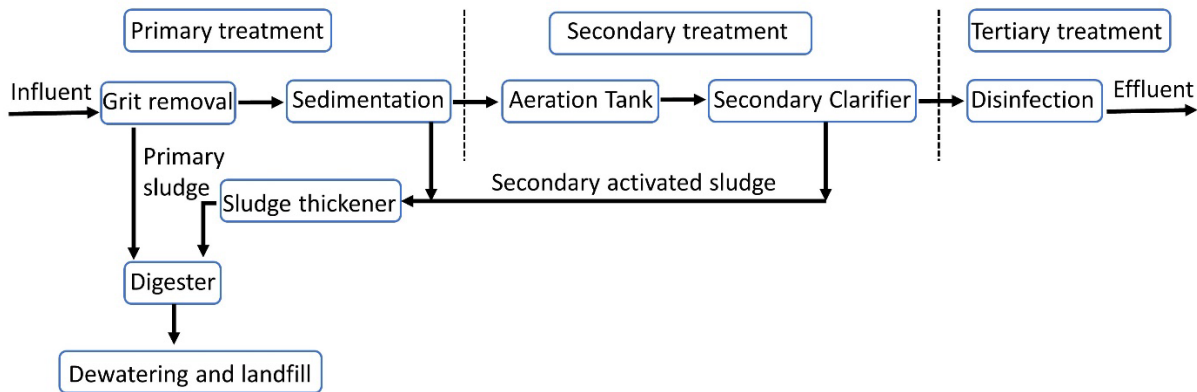


Figure 2.6: Biological treatment of wastewater (Self-representation by the author) [21].

ii) Advance adsorption methods for wastewater treatment

Membrane filtration of water and wastewater is frequently employed to uphold water quality standards. The pressure mechanism in the membrane purification process serves as a barrier between beneficial water and contaminants [22]. These membranes have a variety of advantages, including the fact that they are sturdy, effective, take less time, take up less space, and use fewer chemicals. Additionally, barrier membranes are sufficiently flexible. The type of material from which it is made and the kind of nanomaterials incorporated into it significantly impact how well membrane technology works [23]. According to the porosity of the membranes, there are four types of advanced methods or membrane filtering processes, as depicted in Figure 2.7.

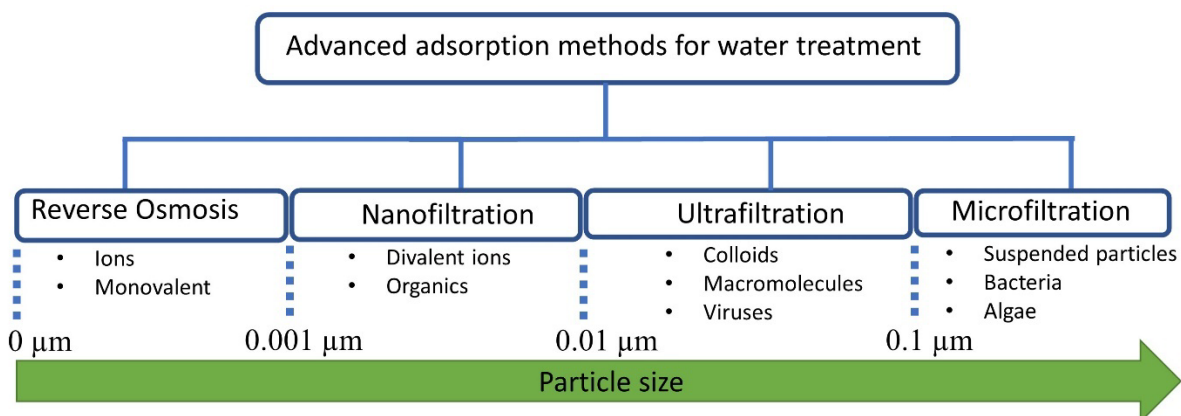


Figure 2.7: Advanced adsorption methods for water treatment (Self-representation by the author) [24].

Ultrafiltration technique

Microorganisms and large molecules can be retained by filters employed in the ultrafiltration process, which operate in the pressure range of 1 to 10 bars and have pores between 5 and 2 nm [25]. The method is displayed in Figure 2.8.

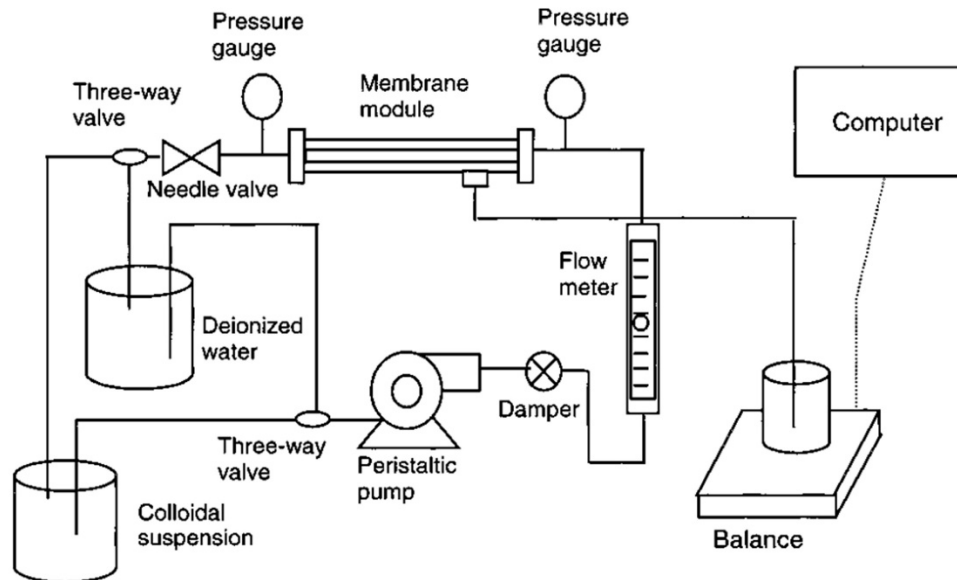


Figure 2.8: Schematic diagram of the cross-flow ultrafiltration technique [26].

Microfiltration technique

Contrary to regular filtering techniques, microfiltration often eliminates colloids and tiny particles with coarse pore sizes of 1–2 μm and works by the driving force. Figure 2.9 illustrates the schematic diagram.

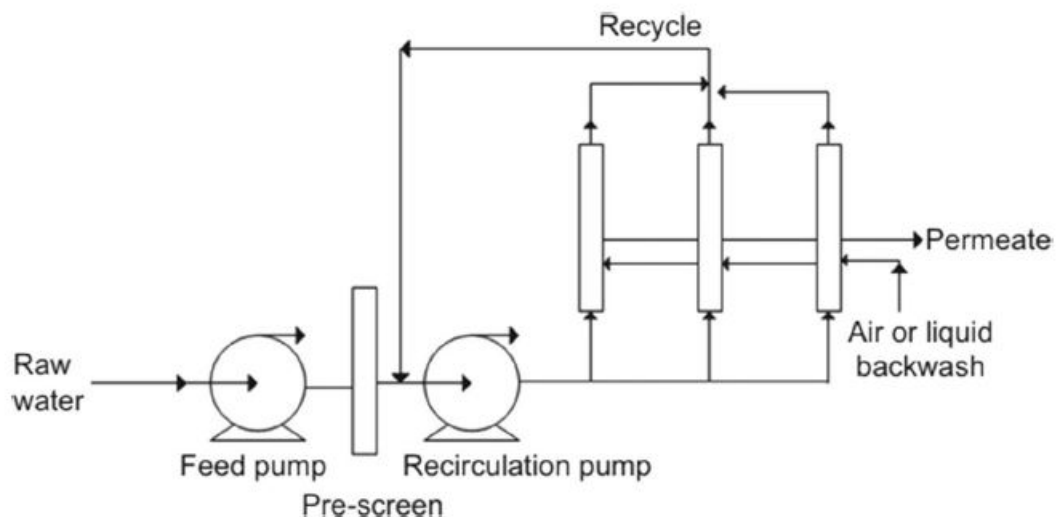


Figure 2.9: Schematic diagram of the microfiltration technique [27].

Reverse osmosis technique

Reverse osmosis is a method that uses a semi-permeable membrane at the highest pressure of 20 to 100 bars. The membrane stops salts and must withstand high pressures, as shown in Figure 2.10.

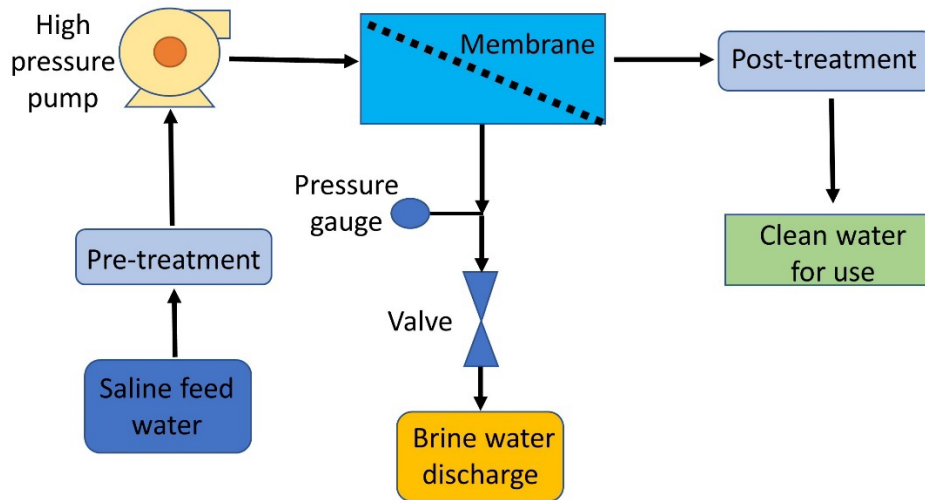


Figure 2.10: Schematic diagram of the reverse osmosis technique (Self-representation by the author) [28].

Nanofiltration technique

The most cutting-edge pressure-obsessed membrane method for molten-stage separation is called nanofiltration (NF), which operates at pressures of 7 to 30 bars and has pores of 1–5 nm that can hold ions and organic contaminants with low molecular weight. Because NF uses less energy but produces more fluidity, it has replaced chiefly reverse osmosis (RO). This method is believed to be more effective where size exclusion is crucial. By combining ions' dimensions, electrical properties, and contact tools like RO, NF allowed ions to be separated. Additionally, the NF's nanoporous shape makes it very effective in excluding tiny amounts of uncharged colloids. At the same time, the exterior electrostatic characteristics document monovalent ions to get conveyed while recalling the multivalent ions. In recent years, NF has developed into a workable technique, which has encouraged its usage in various industries for operations like the treatment of bleaching wastes from textile manufacturing, the separation of pharmaceuticals from fermentation batches, and the removal of viruses. It works pretty well in treating organic and inorganic pollutants in water [29]. Recently, new techniques for purifying water have been introduced. Compared to traditional water purification techniques, these technologies are more effective. The use of nanofiltration, ultrafiltration and microfiltration membranes for water and

wastewater purification has increased because the nanofibrous membranes have a high surface area to volume ratio, higher efficiency, very fine and small pore size, good product quality, easy handling, high selectivity, ease of manufacturing, no use of harsh chemicals, environmentally friendly, and low-cost technology [30]. Figure 2.11 shows a schematic diagram of nanofiltration.

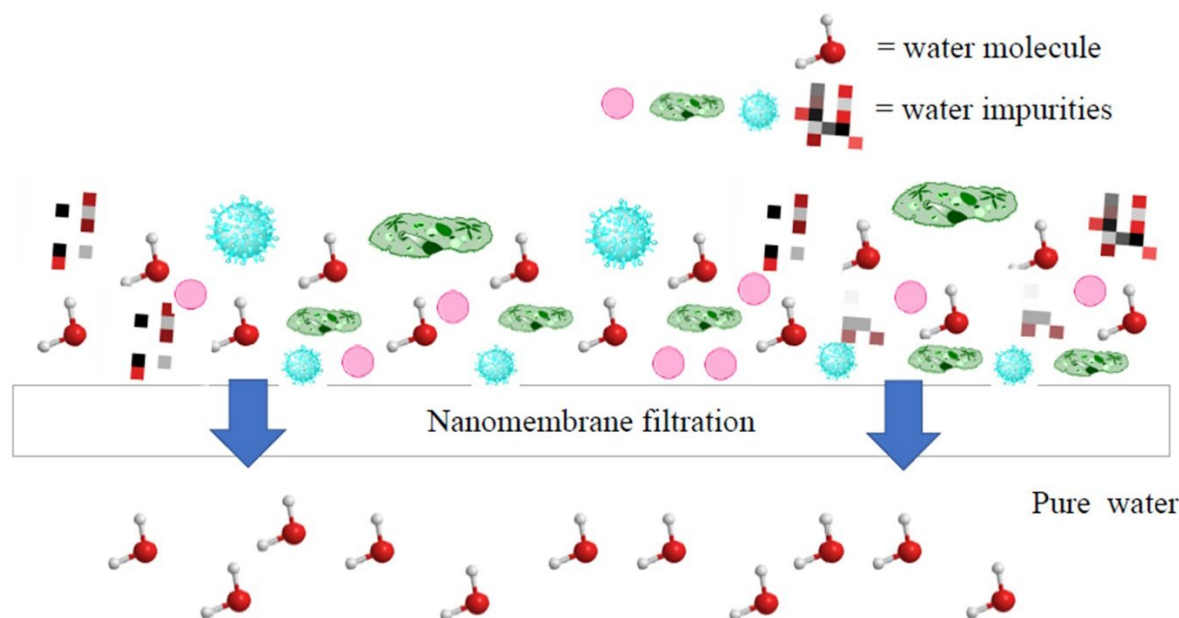


Figure 2.11: Nanofiltration technique as applied in water treatment [31].

2.3 Emerging micropollutants in water

Synthetic EH, also called endocrine-disrupting chemicals (EDCs), have an adverse effect on both human beings and animals [32,33]. Residual micropollutants of this type are observed in low concentrations - at the level of micro-and nanograms - in cleaning reservoirs at wastewater treatment plants [32]. This problem has aroused serious concerns among the scientific community since synthetic hormones are known to interfere with the functional groups of natural hormones by blocking endogenous and mimic ability, which makes it much more dangerous [34–38]. The presence of a minuscule level of hormones represents a severe threat to human and aquatic life through exposure to food sources or drinking water [38,39]. Recently, the European Union directive 2020/2184 concerning drinking water quality recommended a threshold limit of 1 ng/L as a benchmark for assessing the occurrence and treatment of EDCs [40]. The primary sources of hormones and fatal effects are displayed in Figure 2.12.

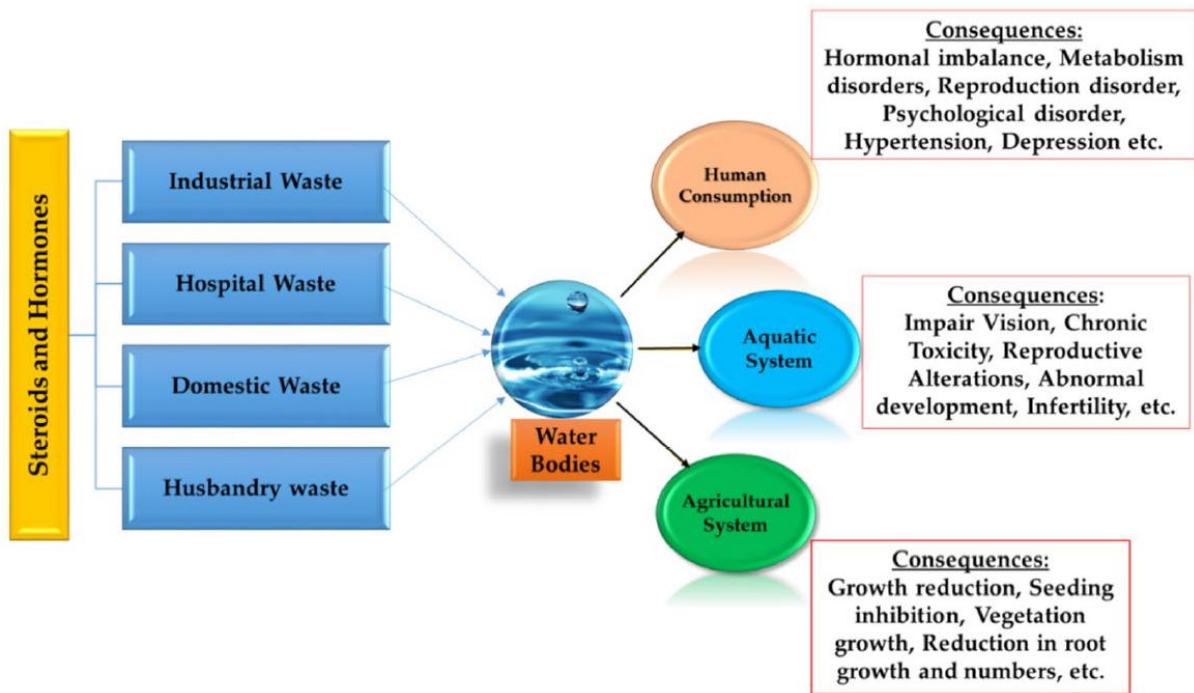


Figure 2.12: Schematic diagram of the primary sources of hormones in the environment and their fatal consequences [41].

The types of natural and steroid hormones found in wastewater can be classified in Figure 2.13 as follows:

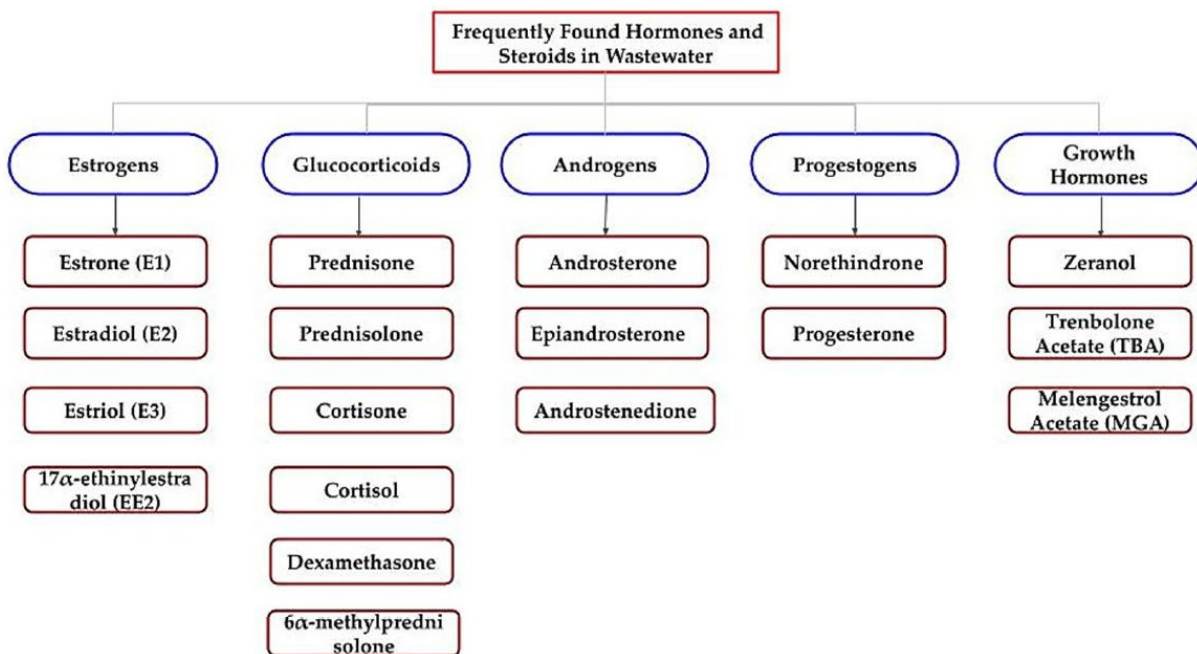


Figure 2.13: Classification of hormones potentially found in the natural environment [41].

EH include estrone (E1), estradiol (E2), ethinylestradiol (EE2), and estriol (E3), which disrupt the reproduction of aquatic species and the function of natural

hormones in the human body [39]. Studies have proven that a rise in femininity occurs in fish, weight loss affects the testicles of quails, and alligators experience issues with fertility [42]. Meanwhile, reports show that humans demonstrate a decline in the sperm counts of males, and the risk of breast and ovarian cancer is heightened in females [43]. Quantities of these EH have been observed downstream of the treatment plants [44–46], with lower limits having been reported of 3.4-41 ng/L at constructed wetlands in the Czech Republic [47]. Of the aforementioned estrogens, EE2 is a modern, formulated, synthetic EH used in oral contraceptive pills in the treatment of prostate cancer and menstrual problems in females [48]. It is considered the most fatal among all the EH as it only degrades partially at wastewater treatment plants and is challenging to be removed [49]. Consequently, the natural environment deconjugates the metabolites of EE2 and makes them active again under a suitable environment [50]. EE2 is the most potent EDC and is considered to have high estrogenicity [51–53]; In general, these EH (natural and synthetic) are majorly from anthropogenic sources, antibiotics, contraceptive pills, chemotherapy drugs and are present in excreting of humans and animals (feces and urine). These EH are released into the environment (e.g., reservoirs, rivers, and lakes) via insufficiently treated effluents. Hence, proper disposal of these EH is immediately required. Figure 2.14 shows the appearance and surface morphology of each hormone; it was captured at 8 kV applied potential and at a magnification of 10000x except for E1, which was 1000x due to the large size of particles. The structure and properties of EH are stated below in Figure 2.15 and Table 2.1.

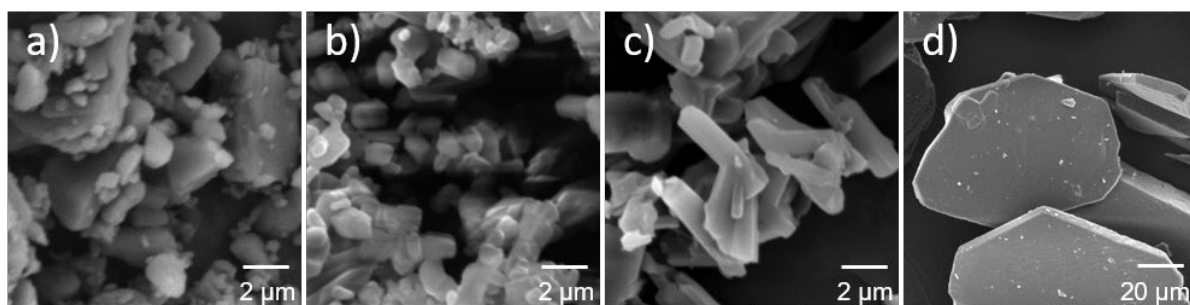


Figure 2.14: SEM of a) E3, b) E2, c) EE2 and d) E1 hormones, respectively (Self-representation by the author).

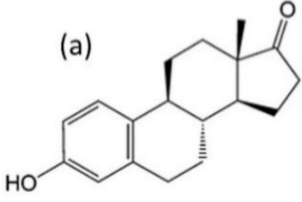
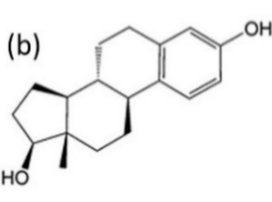
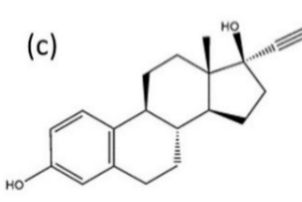
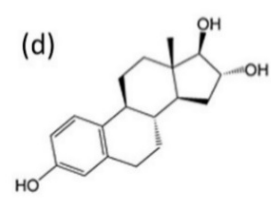
				
$\log K_{ow}$	3.43	3.94	4.15	2.45
pK_a	10.34	10.46	10.40	10.38

Figure 2.15: Steroid estrogenic hormones a) E1, b) E2, c) EE2, d) E3 (self-representation by the author).

Table 2.1: Specific properties of hormones

Estrogenic Hormone	Molecular formula	Molecular weight (g/mol)	Melting point (°C)	Solubility in water (mg/l)
Estrone	C ₁₈ H ₂₂ O ₂	270.37	258.0-260.0	12.42
B-Estradiol	C ₁₈ H ₂₄ O ₂	272.38	178.5	12.96
17α-Ethinyl-Estradiol	C ₂₀ H ₂₄ O ₂	296.40	182.0-183.0	4.83
Estriol	C ₁₈ H ₂₄ O ₃	288.38	282.0	13.25

2.3.1 Solution preparation and sampling

Hormone solution was prepared in three different mediums viz. ethanol, ethanol: water (20:80), and water. For the ethanol, 5 mg/L stock solution was prepared after stirring the solution for 1 h, and it was seen that hormones dissolved immediately. For the ethanol: water system, the concentration of 20 mg/L in solvent 10:90, 10 mg/L 10:90, 20 mg/L 20:80, and 10 mg/l 20:80 was prepared but didn't dissolve completely and stayed as a suspension. However, at a higher volume ratio of ethanol: water 20: 80, solubility was better, as can be seen in Figure 2.16 below.

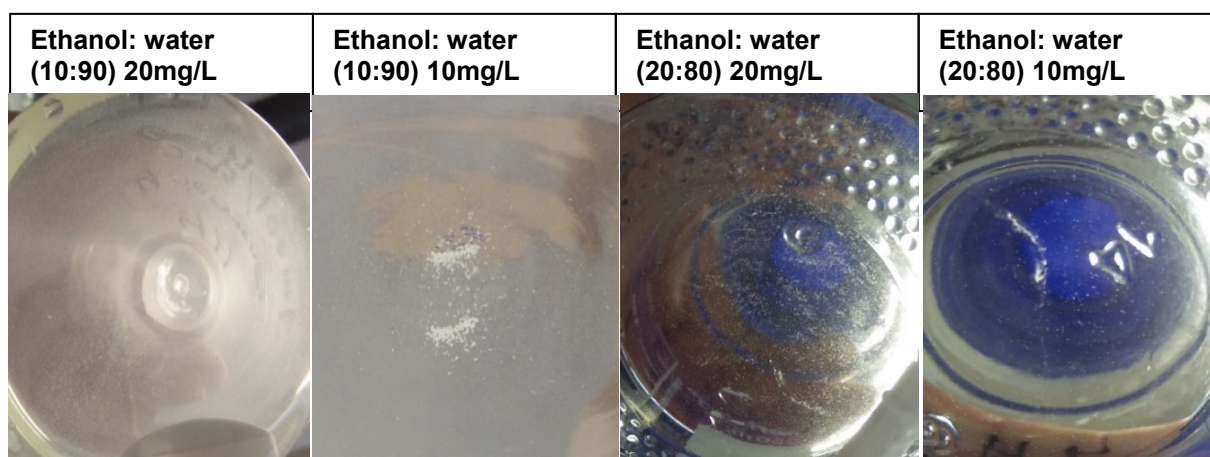


Figure 2.16: Solubility of all four hormones together in a solution at different concentrations (Self-representation by the author).

Hence, using ethanol: water 20:80, 5 mg of each hormone was dissolved in a total of 1000 mL by initially dissolving in 200 mL ethanol, followed by 800 mL of water properly stirred at 800 rpm for 24 hours to make sure complete homogenous mixing and solubility. It was also observed that if hormones are first dissolved in water followed by ethanol, then hormones are only partially dissolved. The descending order of solubility using HPLC is EE2>E3>E2>E1. In the case of water, solubility was a problem because individual solubility of each hormone is available in literature but considering all 4 hormones together in a single solution was challenging, especially for distilled and deionized water. Solubility was lower than the values available in the data, and it was seen that preparing a solution of 1mg/L concentration of each hormone, even after stirring for 1 whole day, there were still some particles at the bottom of the container which could be referred to as E1 because of its least solubility [39]. It was also checked by separately dissolving each hormone in 1 L of water. When the solution was sonicated for 30 mins, there was an increase in peak for E1, proving that its solubility improved. Therefore, finally, a concentration of 0.2 mg/L of each hormone was prepared by adding 1 mg of the given hormone into 5 L of HPLC grade water; magnetic stirring was maintained at 800 rpm for 24 h to prepare 0.8 mg/L of solution and stored in the dark. Samples of concentrations 0.2, 0.15, 0.1, 0.05, 0.03, and 0.02 mg/L were collected by a micropipette and dosed into 1.5 mL screw neck vials after passing through a glass microfiber (GMF) filter of pore size 0.45 μm and 25 mm diameter. HPLC was performed on triplicated samples, resulting in mean concentrations plotted on a calibration curve.

2.3.2 Devised method of High-Performance Liquid Chromatography (HPLC)

Several methods have been devised in the literature using various instruments to quantify EH. However, they are limited to a single or two hormones at a time. Herein, using this procedure, we have devised a facile HPLC method for concurrent detection and quantifying of four EH in a single run. The hormone samples (E1, E2, EE2, E3) were analyzed, and their calibration standards were discerned on an HPLC DionexUltiMate 3000 Series unit (Thermo Fisher Scientific, Germany). Separation took place on a reversed-phase column (Kinetex 2.6 μm C18 100 A, 150x4.6mm; Phenomenex, USA) equipped with an ULTRA precolumn guard, UHPLC C18 (Phenomenex, USA) at 30 °C. A mixture of HPLC grade acetonitrile and water constituted the mobile phase (45:55, vol/vol) applied at the flow rate of 0.8 mL/min over a total isocratic run time of 12 min. The autosampler chamber was set to 5 °C, and a volume of 20 μL was injected each time into the column. Eluates were detected at the wavelengths 200 and 205 nm, and the concentration of hormones was calculated from the findings of the 200 nm tests. A calibration vial with a concentration of 0.02 mg/L was employed to determine the detection limit for each hormone in water; the limit of detection and quantification were found to be 0.560 and 1.867, 1.189 and 3.963, 0.920 and 3.067, and 1.883 and 6.280 $\mu\text{g/L}$ for E3, E2, EE2, and E1, respectively. Values for concentration were quantified by external calibration in software Chromeleon version 7.2 (Thermo Fisher Scientific, USA), as demonstrated in Figure 2.17.

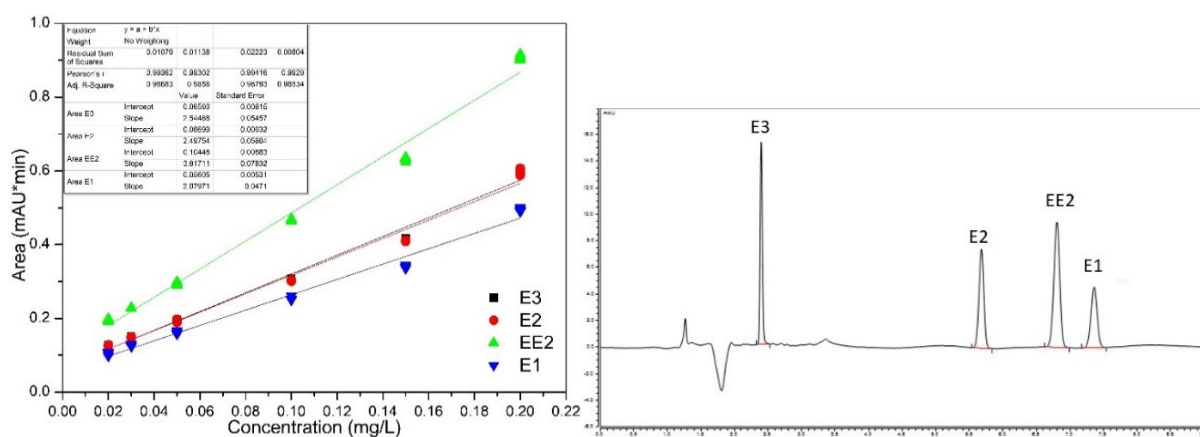


Figure 2.17: Calibration curve and chromatogram of stock solution concentration of 0.8 mg/L containing 0.2 mg/L concentration of each hormone (E1, E2, EE2, E3) in the mixture (Self-representation from experimental data).

2.3.3 Detection and quantification

To identify the peak of hormones, firstly, each hormone solution was tested to detect and identify the retention time (r.t), and then a combined solution of hormones was tested. Also, the limit of detection (LOD) and limit of quantification (LOQ) were calculated from 0.01 mg/L standard as given in the formulas below:

$$LOD = \left(\left(\frac{c}{S/N} \right) \times 3 \right) \quad (2.1)$$

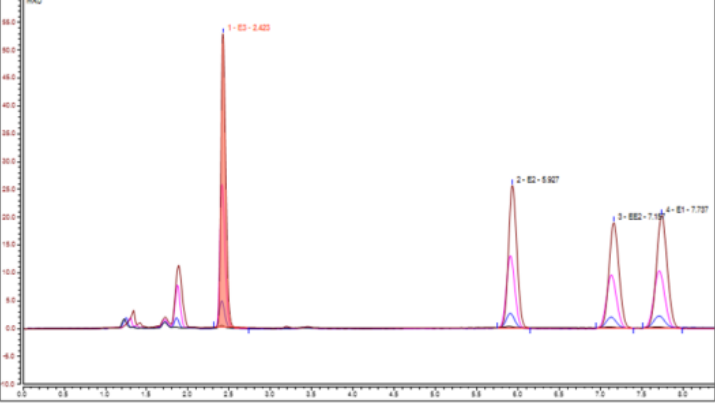
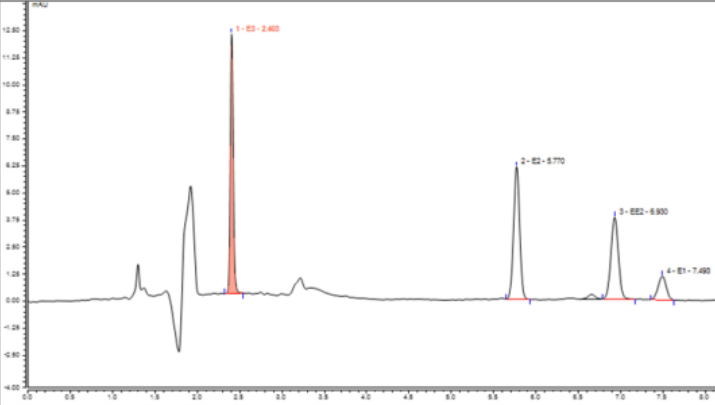
$$LOQ = \left(\left(\frac{c}{S/N} \right) \times 10 \right) \quad (2.2)$$

Where c is the concentration (mg/L) of each hormone and S/N is the signal-to-noise ratio.

Table 2.2 represents intensity peaks, calibration equations along with LOD (mg/L) and LOQ (mg/L) of each hormone at their particular retention time in the ascending order of time of E3, E2, EE2, and E1, respectively, in a given medium.

Table 2.2: Intensity peak, calibration equation, and limits of each hormone when mixed in a specific solution medium (a) ethanol, (b) ethanol: water 20: 80, and (c) water

Ethanol		Equation	Limits
E3		$y = 5.11x + 0.02$ $(R^2 = 1)$	LOD: 0.001 LOQ: 0.004
E2		$y = 5.52x + 0.04$ $(R^2 = 1)$	LOD: 0.002 LOQ: 0.006
EE2		$y = 4.2557x - 0.0004$ $(R^2 = 1)$	LOD: 0.003 LOQ: 0.009
E1		$y = 5.64x + 0.04$ $(R^2 = 1)$	LOD: 0.002 LOQ: 0.007

Ethanol: water 20: 80		Equation	LOQ/LOD
E3		$y = 3.44x + 0.07$ $(R^2 = 1)$	LOD: 0.002 LOQ: 0.006
E2		$y = 2.92x + 0.06$ $(R^2 = 0.9999)$	LOD: 0.003 LOQ: 0.011
EE 2		$y = 2.58x + 0.05$ $(R^2 = 0.9999)$	LOD: 0.005 LOQ: 0.015
E1		$y = 2.99x + 0.06$ $(R^2 = 1)$	LOD: 0.004 LOQ: 0.014
Water		Equation	LOQ/LOD
E3		$y = 2.00x + 0.04$ $(R^2 = 0.9885)$	LOD: 0.0005 LOQ: 0.002
E2		$y = 2.06x + 0.05$ $(R^2 = 0.9918)$	LOD: 0.001 LOQ: 0.004
EE 2		$y = 1.60x + 0.04$ $(R^2 = 0.9939)$	LOD: 0.002 LOQ: 0.005
E1		$y = 0.61x + 0.02$ $(R^2 = 0.9901)$	LOD: 0.005 LOQ: 0.017

2.4 Method of membrane preparation (Electrospinning)

Although a variety of approaches have been used in the literature to remove water pollutants, some of them are appropriate and effective, but they all have drawbacks [54,55]. Conventional treatment plants cannot eliminate EDCs efficiently owing to their properties of low molecular weight and slow biodegradability [56]. This has led to the widespread occurrence of the same

quantity in reservoirs, rivers, and lakes since they are released from treatment plants alongside treated effluents [57,58]. In this regard, various strategies have been applied to capture, eliminate or completely degrade the EDCs and other common toxic chemical effluents, such as ozonation, membrane bioreactors, advanced oxidation, membrane filtration, coagulation, flocculation, and photocatalysis [59–61]. Each technique has certain limitations, such as low efficiency, and any resulting by-products demand further purification and sophisticated methods for processing them. Nano-filtration and reverse osmosis have proven to be interesting, but the extent of energy consumption makes them unfavorable for treatment at a large scale [62,63].

Sorbents based on nanofibers have garnered much attention due to a number of favorable characteristics reported for them, such as large aspect ratio, high surface area, and small pore size [64]. For this purpose, electrospinning is a versatile technique for generating continuous nanofibers, which gives rise to a material's diameter ranging from tens to hundreds of nanometers for adsorption and water filtration processes [65,66]. The large aspect ratio of nanofibers gives significant rise to the filtration efficiency since the pore size is reduced; moreover, the large surface area allows greater contact between the solution and filtration-sorption adsorbent [67]. The apparatus requires an applied voltage between the cathode and anode to allow the electrostatic forces to overcome the tension on the surface of the polymer, thereby ejecting the polymeric solution and solidifying non-woven nanofibers on a collecting electrode covered in a textile substrate [65,68–71]. The quality of nanofibers can be improved by utilizing binary polymers with additives such as acetone and polyethylene oxide (PEO) to obtain beadless nanostructures [67]. The schematic diagram of electrospinning is displayed in Figure 2.18.

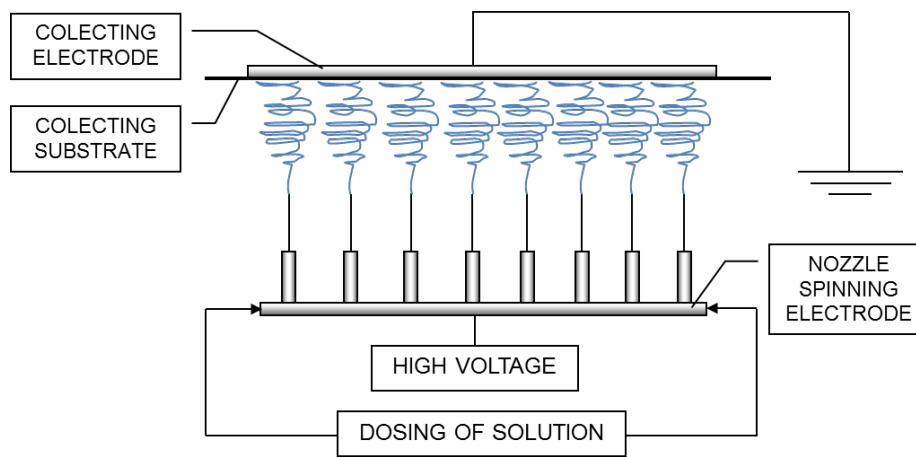


Figure 2.18: Illustration of a needle electrospinning system for the fabrication of nanofiber sheets (Self-representation by the author).

The other types of electrospinning are needleless electrospinning, two-layer fluid electrospinning, rotating roller electrospinning, bubble electrospinning, and conical wire electrospinning.

2.4.1 Influence of parameters for electrospinning

Numerous factors involved in the solution preparation process can be divided into various categories and have a major impact on the morphology of nanofibers are discussed here in detail [72].

Effect of molecular weight and polymer concentration

The molecular weight of the polymer and concentration of the polymer solution directly impact the viscosity of the polymer solution. The entangled molecule chains at the desired molecular weight and concentration prevent the solution jet from breaking during stretching as it advances toward the collector. Similar to the situation of high concentration, a greater number of molecular chains in a polymer solution will result in more entanglements and viscosity. As chain length rises, molecular chains get more entangled, and eventually, viscosity increases with increasing molecular weight. The drawback of high concentration is caused by the nanofibers' small surface area of deposition. To create continuous nanofibers without flaws, sufficient molecular weight and concentration are needed. Increasing the concentration of the solution, which prevents the solvent from moving freely and forming the beads, can remove the beads in nanofibers. Smooth nanofibers that are appropriate for filtering nanoscale particles will form as the molecular weight is further increased while the concentration is held constant. The creation of microribbons, which are appropriate for filtering microsize particles, is caused by raising the molecular weight to a greater level [73].

Additionally, maintaining a lower solution concentration before electrospinning enables the production of nanofibers with the smallest fiber diameter at the given constant molecular weight.

Influence of intrinsic viscosity

Viscosity is a crucial factor in the formation of continuous, bead-free nanofibers. When the viscosity of the polymer solution is extremely low or extremely high, electrospinning is not feasible. It will be challenging to push the fluid through the syringe at greater viscosities. Second, the solvent may evaporate at the needle's tip before the solution can be ejected. Numerous researchers have looked at the beads along the length of nanofibers at low viscosities. They have also looked at how a progressive increase in viscosity causes the shape of the beads to change from spherical to elliptical until smooth fibers are produced. After the creation of smooth fibers, a further rise in viscosity may result in the formation of coarser nanofibers. The main jet may not create secondary jets due to the increased viscosity, which causes the nanofibers' diameter to expand. Similar to this, helix-shaped microribbons that are appropriate for micro-size particles are seen at very high concentrations. Additionally, the low concentration results in nanofibers with narrow pore sizes [74].

Effect of electrical conductivity

To start the viscoelastic jet, the polymer solution must overcome surface tension, which necessitates the delivery of a crucial amount of electrostatic force. Due to the solution's surface tension, the solution jet may fracture during stretching. At low viscosities, the solvent's surface tension begins to take control and forms beads along the length of the nanofibers. Therefore, it is possible to increase the electrical conductivity of the solution and lower its overall surface tension by adding solvents such as ethanol, borax, and citric acid (BC). The wide surfactant varieties can also be utilized to create continuous and smooth nanofibers. The surface tension of the solution has a direct impact on the filtration abilities of nanofiber. Bead fibers can be transformed into a smooth fiber mesh that is ideal for nanoscale particles at low surface tension [75].

2.4.2 Influence of parameters while electrospinning

Variation of voltage

Voltage is a key factor in the creation of smooth, bead-free nanofibers. Most of the time, stronger electrostatic forces at high voltage (greater stretching) cause the finer fibers to form. To create finer or coarser fibers at a certain voltage, flight

duration is also important. By reducing flight time and raising voltage, the solution jet has less time to stretch, resulting in the formation of coarser fibers. Below the minimum voltage necessary to create a Taylor cone at the needle tip, the solution cannot erupt from the needle. Therefore, producing fine and smooth fibers is only possible at a certain voltage level. The smaller pores in the finer fibers make them appropriate for nanoscale particles and other agents [76].

Variation of flow rate

The amount of solution that is accessible for electrospinning at the needle tip depends on the feed rate. A crucial feed rate value should match the applied voltage for a stable Taylor cone. More solution is available at the needle tip at high feed rates, which causes the formation of coarser or beaded nanofibers. The solvent may be fused together and create web-like structures when fed at a greater rate since it doesn't have enough time to dissipate. Lower flow rates are preferred for the production of finer fibers. In comparison to coarser fiber filters, finer fiber nano filters offer more filtration capacity.

Effect of distance between needle and collector

The distance between the needle and the collector has a direct impact on the electric field's strength and flight time. The strength of the electric field increases at very close ranges, causing the solution jet to accelerate and, ultimately, shorten flight time. The flight duration shortens, preventing solvent from evaporating and leading to the formation of an interconnected mesh. Beaded fibers occur because a low distance has the same effect as a high voltage. However, at a higher distance, the stretching of the solution jet is increased due to an increase in flight time; a longer distance produces finer fibers. As a result, finer fibers are favored for removing tiny particulates from water [77].

Type of needle

The process is directly impacted by the needle's interior diameter. Because less solution is exposed to the environment when utilizing smaller inner diameter needles, the likelihood of needle clogging is significantly decreased. The nanofibers' diameter is also decreased due to the smaller inner diameter. Various materials can be electrospun using different types of needle spinnerets depending on their physiochemical needs for the intended usage. The type of needle can be altered based on the level of filtration necessary. Tiny diameter needles are preferred for removing the finer fiber and small particulates. Similar to this, a bigger diameter needle is preferred for prefilter application and the removal of large particles from water [78].

3. MATERIALS AND APPLICATIONS

The major classification for applications of electrospun nanofiber membranes is presented in Figure 3.1.

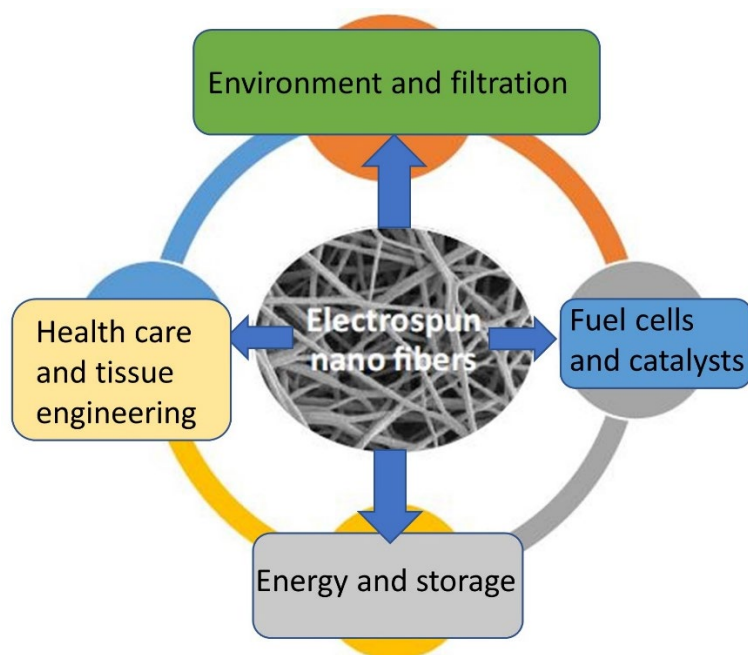


Figure 3.1: Potential applications associated with electrospun nanofiber (self-representation by the author) [79].

3.1 Materials used for adsorption in water treatment

Electrospun nanomembranes are used to remove a variety of wastes from water, including textile waste (dyes, pigments, and colorants), dust, sand, heavy metals, pathogens, microbes, and bacteria, as well as particulates, effluents, and water desalination [5]. The type of water contaminants usually affects the choice of electrospun nanomembranes. In the context of the sorption technique, the choice of material selection is quite crucial. Adsorbent particles for estrogens have been reported, such as granules of activated charcoal [80,81], carbon nanomaterials [82], fullerene [83], carbon nanotubes [84], chitosan, activated carbon, chitin, carbon-based adsorbents prepared from industrial waste [85,86], and activated carbon fibers modified with iron hydroxide [87]. All of these are efficient, yet they require a process of additional separation from wastewater that raises the costs. Some researchers have recently found adsorbents such as nanofibers that could eradicate the need for a subsequent separation procedure [88]. To this end, not many studies have been reported. Therefore, it is necessary to test such high-performance materials with functionalized groups that can optimize the disposal process during the course of research programs.

Past literature describes that electrospun polymers proved an excellent ability to remove heavy metal ions such as copper and organic pollutant dyes from wastewater [89,90]. However, fewer works have been done with electrospun polymers for EH removal applications. According to the literature, research on commercially available nylon, polypropylene (PP), polytetrafluoroethylene, cellulose acetate (CA), regenerated cellulose, and glass microfiber filters have been reported for the removal of E1. Studies also report on polyamide (PA) nanoparticles being employed to extract just EE2, polyethersulfone (PES) nanofibers for the removal of E2, and polyvinylidene fluoride (PVDF) doped with polyvinyl pyrrolidone (PVP) and titanium dioxide (TiO₂) membranes prepared by phase inversion process for the removal of E1 and E2. However, these studies have been solely limited to the filtration of single natural or synthetic hormones [32,48,91,92]. This highlights the necessity of developing the least fiber diameter optimized nanofibers to extract such EH simultaneously and then gauge their kinetics and effectiveness by reusability for comparison [93].

3.2 Materials and Chemicals required

The hormones under test (with purity in percent) comprised E1 $\geq 99\%$, E2 $\geq 98\%$, E3 $\geq 97\%$, and EE2 $\geq 98\%$ purchased from Sigma-Aldrich Chemie GmbH, Germany. Cellulose acetate CA-398-30 (CA) at the molar weight $M_w = 5 \times 10^4$ g/mol came from the Eastman Chemical Company, USA. Polyurethane Elastollan EB_95A (PU Elastollan) at $M_w = 1.1 \times 10^5$ g/mol was bought from BASF Polyurethanes GmbH, Germany. Polyamide 6 (PA) - Silamid EN at $M_w = 1.45 \times 10^5$ g/mol was sourced from Roonamid a.s., Slovakia. Polyacrylonitrile PAN 181315 (PAN) of molecular weight $M_w = 1.5 \times 10^5$ g/mol, 4,4'-methylene-diphenyl diisocyanate (MDI), (poly 3-methyl-1,5-pentanediol-alt-adipic, isophthalic acid) (PAIM), 1,4 butanediol (BD) aniline ($\geq 99\%$ purity), hydrochloric acid, (HCl, 37% purity), ammonium peroxydisulfate, poly(vinyl alcohol) ($M_w \sim 125,000$), ammonium hydroxide (28-30% NH₃ basis), Butylated hydroxytoluene (BHT), and swinnex film holders with Luer lock (25 mm diameter) were purchased from Sigma-Aldrich, Germany. Polyethersulfone Ultrason E2020P SR (PES) at the molecular weight $M_w = 5.5 \times 10^4$ g/mol came from BASF SE, Germany. Acetone, N,N-dimethylformamide (DMF $> 99.5\%$), and sodium hydroxide (CAS: 1310-73-2) were bought from Lach-Ner, s.r.o., Czech Republic. Acetic acid (AA (99%)), formic acid (FA (98%)), sodium tetraborate decahydrate (borax), citric acid, dimethylamylamine (DMA), and 4-methyl-2-pentanone (MIBK) were purchased from PENTA s.r.o., Czech Republic. Polyethylene oxide (PEO) was obtained from scientific polymer

products, Inc, Ontario, The USA. Tetrahydrofuran (THF) was obtained from Carl Roth Rotisolv[®] HPLC (Karlsruhe, Germany). The Kynar Flex[®] 2801, a copolymer composed of poly (vinylidene fluoride)-co-hexafluoro propylene (PVDF) of molecular weight 455 kDa, was purchased from Arkema (France). Ultrason Polysulfone (PSU) S6010 was purchased from BASF, Germany. Polylactic acid (PLA), Ingeo[™] 4060D, biopolymer, was purchased from NatureWorks LLC, The USA. N-Methyl-2-pyrrolidone (NMP) was purchased from Sigma-Aldrich, The USA. The CBs, regardless of brand, were collected over a week from the cigarette waste bins of the Centre of Polymer Systems (CPS), Tomas Bata University in Zlin, Czech Republic. The sample collecting vials (1.5 mL screw neck) were purchased from VWR, Czech Republic.

Furthermore, HPLC solutions of acetonitrile (from Honeywell, Czech Republic) and ethanol (HPLC grade > 99%; from VWR, Czech Republic) were utilized. The micropipette was purchased from HTL Lab Solution, Poland, and GMF filters from Whatman, Czech Republic. Deionized water (pH 7.3, 18.2 M Ω /cm) was created on a laboratory Milli-Q ultrapure (Type 1) water purification system, Biopak[®] Polisher, Merck, The USA, and used throughout the study.

3.3 Preparation of experimental materials via electrospinning

Removing natural and synthetic hormones via electrospun nanofibers offers a sustainable and relatively environmentally friendly solution for eliminating EH.

Each electrospun nanofiber used in the thesis was made from a different polymer; therefore, different solvents were used. We aimed to prepare both hydrophilic and hydrophobic polymeric nanofibers from materials that include polyurethanes (PU Elastollan and PU 918), PA, CA, waste cigarette electrospun nanofibers (WCENFs), polysulfone (PSU), PES, polylactic acid (PLA), polyacrylonitrile (PAN) and PVDF.

3.3.1 Solution preparation for electrospinning

A solution of the conductive components (BC), which was prepared at the ratio of 1:3, respectively and followed by 35 wt% of BC, was dissolved in N, N-dimethylformamide (DMF) solution and stirred in a mixer for 5 h at 400 rpm to make it ready for adjusting the electrical conductivity of each treated solution prior to electrospinning. The synthesis of every electrospun material progressed under the optimized conditions and parameters required for that particular polymer as follows:

PA at the concentration of 18 wt% of the solution was dissolved in acetic acid (AA): formic acid (FA) at the ratio 2:1 for 4 h by stirring at 400 rpm in a mixer (Heidolph, RZR 2041) to homogenize the mixture uniformly. PU Elastollan 18 wt% was dissolved in DMF by treating the solution with BC to enhance electrical conductivity and optimize the electrospinning process. The solution of CA was prepared from 9% of powder in AA (57 wt%), ethanol (19 wt%), water (14.5 wt%), and PEO (0.3 wt%), followed by BC (0.2 wt%), which were stirred together to make a total of 400 g under constant stirring at 400 rpm for 6 h. PES solution (23 wt%) was prepared by dissolving the powder in 73 wt% dimethylamine (DMA): 4-methyl-2-pentanone (MIBK) at the ratio 3:1, supplemented by BC at 4 wt%. PAN powder was dissolved in DMF (9 wt%) under stirring for 5 h at 400 rpm. PSU of 20 wt% was uniformly dissolved in N-Methyl-2-pyrrolidone (NMP). PLA of 16 wt% was dissolved in a solution of DMF/Acetone in a ratio of 4:1. PVDF 20 wt% was dissolved in DMF. PU 918 was prepared via a polyaddition reaction at a Centre of Polymer Systems (CPS) laboratory. PU solution in (DMF), based on 4,4'-methylene-diphenyl diisocyanate (MDI), poly 3-methyl-1,5-pentanediol-alt-adipic, isophthalic acid (PAIM) polymer diol, $M_w = 2 \times 10^3$ g/mol), and 1,4 butanediol (BD) was synthesized at the molar ratio 9:1:8 (PU 918) at 90 °C for 5 h (per partes way of the synthesis, starting with the preparation of a pre-polymer from MDI and PAIM, followed by adding BD and the remaining quantity of MDI. After being supplemented with BC to idealize conductivity, the solution was electrospun at a concentration of 13 wt% PU with $M_w = 9.8 \times 10^4$ g/mol [93]. Waste cigarette butts (CBs) were washed twice with distilled water to remove unwanted debris, dust and dried in a hot-air oven for 6 h at 80 °C. Further, they were washed with ethanol and kept at 40 °C for 4 h. A total of 8 wt% of CBs were dissolved in a binary solution of AA and FA in a ratio (2:1) to make a total solution of 400 g. Then, 3 wt% of PEO of the amount of the CBs was added for stability of the mixture to improve the structural properties of fibers. Finally, the mixture was stirred for 5 h at 400 rpm in a mechanical stirrer (Heidolph, RZR 2041).

3.3.2 Fabrication of nanofibers

The electrospinning process was performed in an electrostatic field on laboratory spin line equipment (CPS, Tomas Bata University, Czech Republic). The apparatus was equipped with a patented rotating electrode with three cotton cord spinning elements (PCT/CZ2010/000042) and a set of nanofiber-forming nozzles (jets) to produce fibers on PP spun-bond non-woven textile of width 40 cm. The voltage applied was 75 kV during the electrospinning process, except for PA, PSU, and PLA, when it equaled 130, 55, and 65 kV, respectively. A set of 32 jet

needles (2 rows of 16 each) was employed for the PU Elastollan, PES, PAN, PSU, PLA, PVDF, and PU 918; solution dosing was set to 0.34, 0.34, 0.13, 0.17, 0.27, 0.41, and 0.24 mL/min., respectively, based on optimum parameters and conditions. The distance between the electrodes equaled 18 cm, apart from PU Elastollan, PSU, PLA, and PVDF, which equaled 19 cm. In the case of PA, CA, and WCENFs, a solution was sprayed from the bath by cords set at 4 rpm, with the distance between the electrodes equaling 22 cm, except for WCENFs, where it is equal 18 cm. The rotational speed of antistatic PP non-woven fabric was set at 10 cm/min., except for PA and PU 918, where the pace was set at 12 and 16 cm/min., respectively. The temperature was gauged as 28 ± 2 °C, and relative air humidity was $< 35\%$. The solutions' electrical conductivity and intrinsic viscosity during preparation were maintained at optimal levels, as shown in Table 3.1.

Table 3.1 shows the optimized properties of the polymeric solutions for subsequent electrospinning and the average mass per unit area of the resultant electrospun nanofibers. PA solution possessed the highest electrical conductivity, while the least was observed for CA. The concentration and intrinsic viscosity of the solutions varied between 8-24% and 0.50-2.00 Pa.s, respectively. The value for average mass per unit area of the electrospun sheets was lowest for PSU and highest for PA. The given properties of solutions varied and set at optimum conditions to aim for defect-free and beadless electrospun nanofibers.

Table 3.1: Solution properties of each polymer prior to electrospinning

Sample	Concentration (%)	Density (g/cm ³)	Intrinsic Viscosity (Pa.s)	Electrical conductivity (μS/cm)	Average mass per unit area (g/m ²)
PES	24	1.350	0.75	102.0	1.02
PU 918	13	1.100	1.50	150.0	0.70
PU Elastollan	18	1.220	1.80	91.8	1.30
CA	9	1.315	1.64	83.4	1.63
PA	18	1.084	0.75	172.0	3.00
PAN	9	1.184	0.53	105.3	0.88
WCENFs	8	1.320	0.95	88.1	0.87
PSU	20	1.25	2.00	116.3	0.59
PLA	16	1.25	0.50	120.1	1.30
PVDF	20	1.78	1.50	118.0	1.85

3.4 Method of characterization of material

General properties of nanofibers and nanoparticles, regardless of their intended application, can be classified as follows:

1. Chemical composition, molecular weight, and structure are characterized by:
 - Fourier transform infrared spectroscopy (FTIR)
 - Gel permeation chromatography (GPC)
 - X-Ray diffraction (XRD)
2. Morphology, surface composition, elemental analysis, surface area, and pore size are characterized by:
 - Optical microscopy
 - Scanning electron microscopy (SEM)
 - BET (Brunauer, Emmett, Teller) analysis
 - Capillary-flow porosimetry
3. Surface wettability is characterized by:
 - Contact angle
4. Thermal stability is characterized by:
 - Thermogravimetric analysis (TGA)
 - Differential scanning calorimetry (DSC)
5. Mechanical properties are characterized by:
 - Tensile test

The following section briefly explains the principle of each characterization technique.

FTIR

Every molecule can undergo electronic, vibration, and rotational transitions. The energy required for electronic transition is higher than that for vibration transition, which is in turn higher than the energy for rotational transition. When a molecule is irradiated by IR radiation, it absorbs energy. Since relatively smaller energy is associated with IR radiation, it can only induce transitions between the vibration and rotational energy levels of a molecule resulting in the IR spectrum, also known as the rotational vibration spectrum of the molecule. As the absorption of

the radiation occurs only if the radiation frequency coincides with the vibration frequency of a bond present in a molecule, by monitoring the absorbed (or transmitted) IR radiation, information about the structure of molecules can be obtained. IR spectroscopy is the most widely used vibration spectroscopy. In the IR region, the position of absorption bands in the spectra is given as wavenumbers (ν) [cm^{-1}]. The IR range consists of three spectral regions, the near IR (NIR – from 4000 to 14000 cm^{-1}), mid-IR (MIR – from 400 to 4000 cm^{-1}), and far IR (FIR 25 – 400 cm^{-1}), of which the MIR, depicting the molecular vibrations, is mostly employed. The standard IR spectroscopy has been significantly improved by utilizing a Fourier transform algorithm, increasing the signal level and enhancing the photometric accuracy. In FTIR spectroscopy, the absorbance frequencies are characteristics of the chemical groups present in a molecule. Hence, the IR spectrum can be considered a fingerprint for identifying unknown compositions or determining the close intermolecular interaction of specific functional groups. The principle of IR in the spectrophotometer is shown in Figure 3.2. Three main factors that affect the IR absorption are the relative mass of the atom (heavier the atom, slower is the vibration frequency of the bond between them), the force constant of bonds (stronger the bond, higher is vibration frequency), and geometry of the atoms [94,95]. The Attenuated total reflection (ATR) mode is used for surface chemical analysis of solid materials nanofibers. In this mode, IR radiation passes through a crystal, for example, germanium (Ge), with a high refractive index causing total internal reflection within that crystal. Consequently, an evanescent wave is extended that moves beyond the crystal's surface and hits the sample's surface in the process. The changes are measured when the sample absorbs energy in contact with the crystal during measurement, and the wave is attenuated in spectral regions. To observe the maximum number of interactions, the IR radiation is reflected many times inside the crystal.

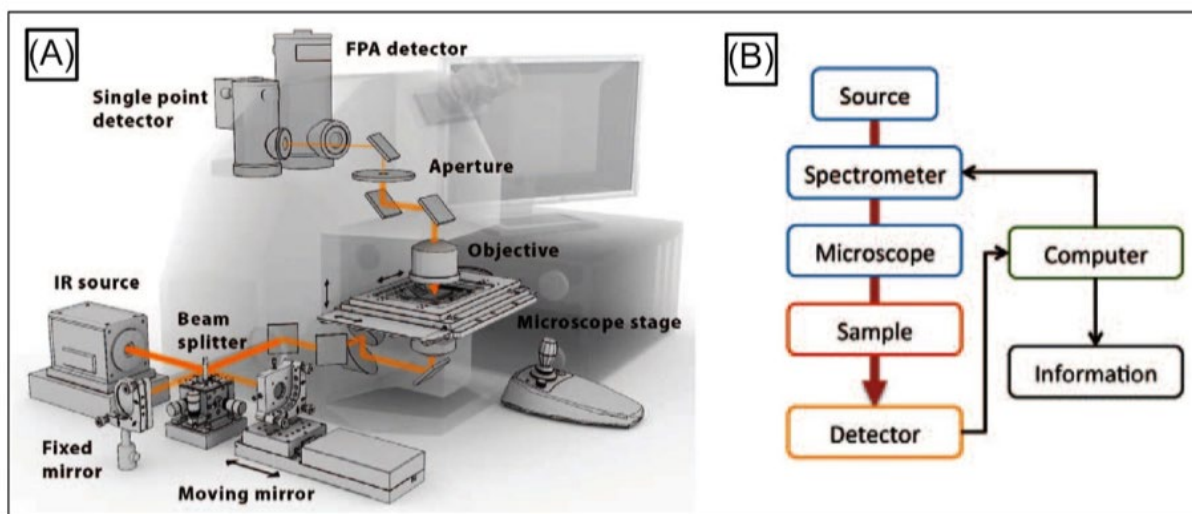


Figure 3.2: A) Illustration of a modern FTIR-imaging spectrometer; B) the conceptual optical path of an FTIR-imaging spectrometer [96].

Fourier transformed infrared spectroscopy (FTIR) was performed on a Nicolet 320 spectrometer (ThermoScientific, USA) equipped with a Ge crystal to determine the functional groups of the polymeric nanofibers tested for adsorption of the EH. Attenuated total reflectance (ATR) spectra were recorded across $400\text{--}4000\text{ cm}^{-1}$ under ambient temperature conditions, with a scan rate of 16, and a resolution of 4 cm^{-1} .

HPLC

This technique can identify and quantify components in a mixture. It is one of the most powerful tools in analytical chemistry. In general, this technique is used to separate a mixture of analytes in solution into its individual components. HPLC has the ability to detect, identify, separate, and quantify compounds that are present in any sample that can be dissolved in a liquid in trace concentrations as low as parts per trillion. In instrumental design, injectors are used to introduce the testing solution mixture into the flowing system. A sample mixture or analyte in a solvent (known as the mobile phase) is pumped at high pressure through a column with chromatographic packing material (stationary phase) to the detector, which monitors and records the separation peaks. Data acquisition accessories control the test automatically, record the results, and calculate the concentration with respect to the calibration curves. Figure 3.3 demonstrates how the sample is injected into the mobile phase and the path the sample takes to reach the detector and is further collected as waste [97].

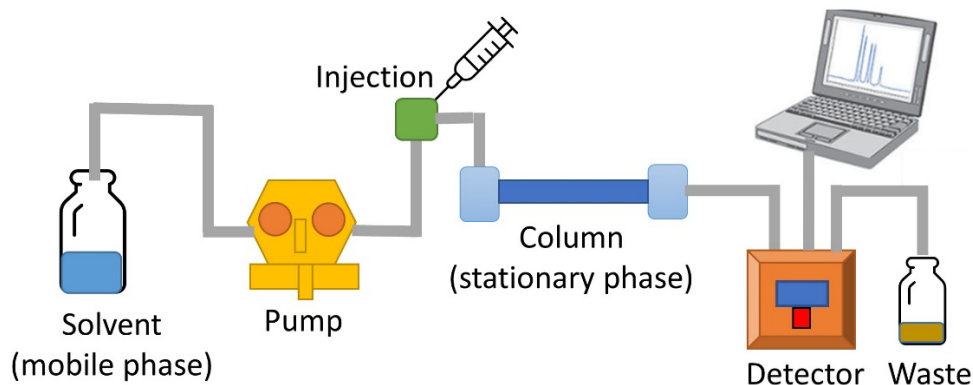


Figure 3.3: Schematic diagram of the high-performance liquid chromatography (Self-representation by the author).

GPC

This one is one of the most potent and useful analytical methods for comprehending and forecasting polymer performance. It is the most practical method for characterizing a polymer's entire molecular weight distribution. GPC breaks down a complex polymeric substance into its constituent polymer, oligomer, monomer, and additives in addition to supplying the molecular weight distribution. By measuring the molecules' effective sizes in solution, GPC separates them. The resin must first be dissolved in the proper solvent in order to prepare a sample for GPC analysis. The dissolved resin is injected into a stream of solvent that is constantly running (mobile phase). Millions of highly porous, hard particles (stationary phase), crammed close together in a column, are traversed by the mobile phase as it moves through them. These particles have regulated pore diameters and come in a variety of sizes. The breadth of each peak reveals the distribution of molecule sizes for a particular resin and its constituent parts. The molecular weight distribution (MWD) curve is another name for the distribution curve. When the peaks are combined, they show a sample's MWD. The peaks get wider when the MWD gets wider and vice versa. The curve shifts farther along the molecular weight axis and vice versa as the average molecular weight increases. Different-sized molecules elute from the column at varied rates. The column retains low molecular weight material longer than high molecular weight material. The term "retention time" refers to the amount of time it takes for a particular fraction to elute.

In the design of instruments, injectors are used to add polymer solutions to flowing systems. Through the columns and system, pumps deliver the sample and solvent. The separation is monitored and recorded by detectors. Accessories for

data acquisition run the test automatically, capture the data, and average the molecular weights. Figure 3.4 shows the procedure for injecting the sample into the mobile phase and the route the sample follows to the detector.

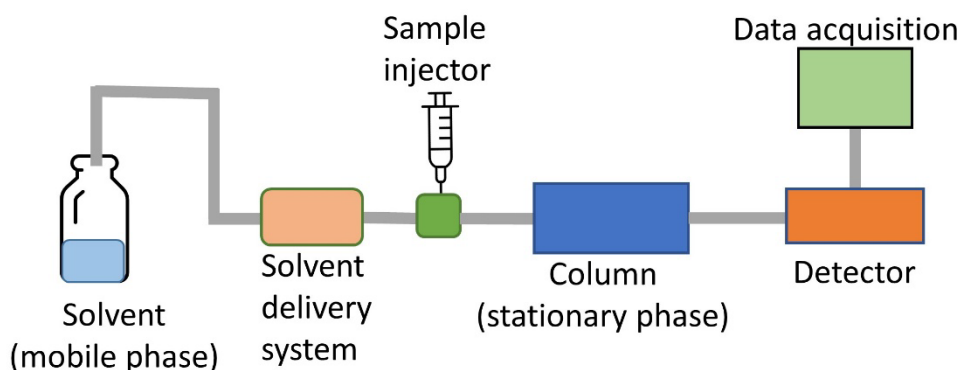


Figure 3.4: Schematic diagram of the gel permeation chromatography technique (Self-representation by the author).

Gel permeation chromatography (GPC) used a Waters HPLC system equipped with a Waters model e2695 and a Waters model 2414 differential refractometer to determine the average molar mass (M_w), number average molar mass (M_n), and polydispersity index ($PDI = M_w/M_n$) of the tested nanofibers samples from peaks corresponding to the polymer fraction using the absolute calibration method (Waters Corporation, Milford, USA). The nanofibers were dissolved in THF (2–3 mg/mL), stabilized with BHT (240 mg/L), and filtered through a 0.45 μm syringe filter. The following procedure was used to separate the samples on a series of gel-mixed bed columns (Polymer Laboratories Ltd, Shropshire, UK): 1 \times PLgel-Mixed-A bed column (300 \times 7.5 mm, 20 μm), 1 \times PLgel-Mixed-B bed column (300 \times 7.5 mm, 10 μm), and 1 \times PLgel-Mixed-D bed column (300 7.5 mm, 5 μm); at 40 $^\circ\text{C}$, the mobile phase contained THF stabilized with BHT (240 mg/L). The mobile phase flow rate was set to 1.0 mL min^{-1} , and the injection volume was 100 μL . All data processing was carried out using Empower 3 software.

XRD

X-ray crystallography is a technique for determining the size of atoms, the lengths, types of chemical bonds, phase identification of a crystalline material, and the atomic and crystalline molecular structure of polymers or metals [98]. The crystalline structure (atoms in crystals) causes a beam of incident X-ray radiation to diffract into many specific directions. The diffraction is the bending of the waves on any obstacle so that these waves deviate from their original. The differential map images a three-dimensional picture of the density of electrons

within the crystal during measuring the angles and intensities of diffracted beams [99]. It can provide information on unit cell dimensions. The analyzed material is finely ground, homogenized, and the average bulk composition is determined. The main principle of XRD analysis is based on constructive interference of monochromatic X-rays through the sample. The basic relationship is given by Bragg's Law:

$$n\lambda = 2d\sin\theta \quad (3.1)$$

Where d is the spacing distance between the layers of atoms in a crystal (\AA), λ is the wavelength of the incident X-ray beam (\AA), n is an integer value of the order of diffraction, θ is the angle of the incident X-ray beam with respect to the layers of atoms ($^\circ$). This law associates the wavelength of electromagnetic radiation λ to the diffraction angle θ and the lattice spacing d in a crystalline sample. A monochromatic X-ray beam is incident on the crystalline material, and the intensity of the scattered beam is measured as a function of the diffraction angle. X-rays scattered from successive planes interact constructively when they eventually reach the X-ray detector [100]. The material is identified by converting the diffracted peaks to d -spacings and further comparison with the stored standard reference patterns. This principle can be seen in Figure 3.5.

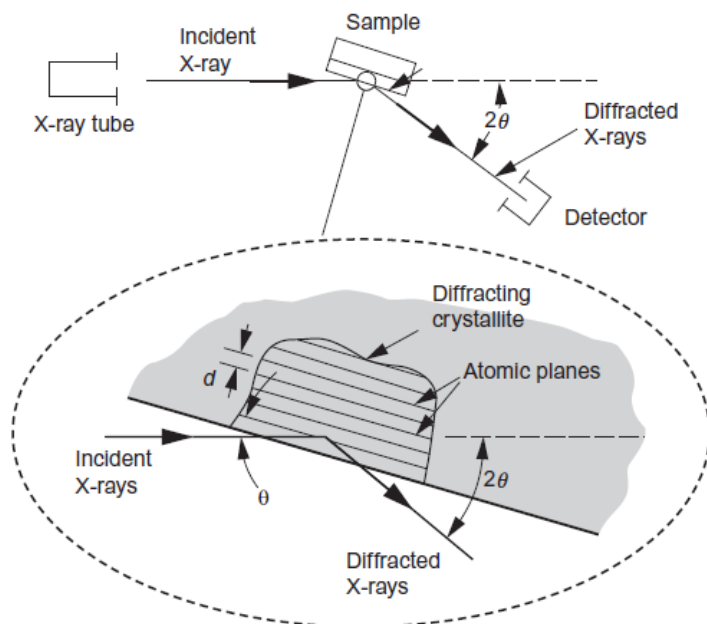


Figure 3.5: Overview of the X-ray diffraction technique [101].

X-ray diffractogram (XRD) of WCENFs was recorded using MiniflexTM 600 X-ray diffractometer (Rigaku, Japan), having $\text{CoK}\beta$ ($\lambda=1.79 \text{ \AA}$) as a source. The angle 2θ was in the range from $5\text{-}90^\circ$ with operating current, step size, step time,

and operational voltage set to 15 mA, 0.02°, 10°/s, and 40 kV, respectively. The diffractograms obtained using Co source were converted to Cu using PowerDLL software converter 2.93 to compare data in the prior art.

Optical microscopy

This method produces optical images that have been enlarged using visible light and a set of lenses. Normal, photosensitive cameras can record an optical microscope's image to create a micrograph. The object is put on a stage and can be seen directly through one or two microscope eyepieces (Figure 3.6). High-power microscopes typically display the same image through both eyepieces, but stereo microscopes employ slightly distinct images to produce a 3-dimensional illusion. There are several different ways to light the sample. Solid objects can be lighted with light coming through the objective lens (bright field) or surrounding it (dark field), while transparent objects can be lit from below. To identify the crystal orientation of metallic objects, utilize polarized light. Typically, a turret is used to install a variety of objective lenses with various magnifications, enabling them to be rotated into position and providing the option to zoom in. Due to the limited resolving power of visible light, optical microscopes typically have a maximum magnification power of about 1000x [102].

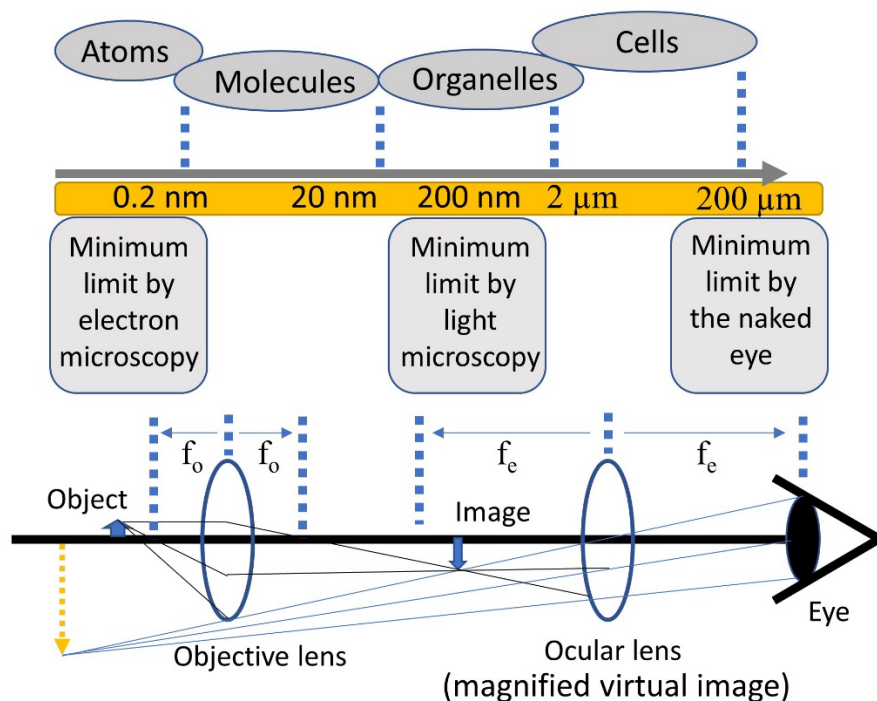


Figure 3.6: Principle of optical microscopy technique and minimum resolvable limits (Self-representation by the author).

Imaging under an optical microscope was collected with a digital microscope of high degree magnification Leica DVM2500 (Leica Microsystems, Czech Republic) in order to observe the coated nanofibrous membranes. Visualization was performed under phase contrast mode, which allows visibility of the coated membranes. Imaging was observed at 100x magnification.

SEM

SEM is used to study surface morphology and identify small areas, for example, polymers that cannot be observed by optical microscopy. A higher magnification is obtained of about 1–2 million times, a large depth of field (up to 100 times), allowing more area of a sample to be focused, and a higher resolution down to sub-nanometric scale can be achieved with a magnification >100,000x. This technique images a different type of sample surface by scanning an energetic electron beam and using electromagnets to control the degree of magnification. The principle of this method is that the primary electrons emitted from an electron gun with energy (100 eV–30 keV) interact in a vacuum with atoms on the sample surface. Therefore, various signals are emitted due to elastic and inelastic scattering. The electrons dislodged from the sample as a result of elastic collision are known as backscattered electrons. They indicate information to distinguish between atoms having a minimum difference in an atomic number of 3. The electrons emitted as a result of an inelastic collision with energy less or equivalent to 50 eV are known as secondary electrons. The signals from these electrons are amplified and useful for analyzing topography. The next is Auger electrons which are released when an inner shell electron is knocked out by a backscattered electron or electron from the primary beam, and an electron from the outer shell loses energy in the form of X-rays to fill the vacancy. Auger electrons come from an escape depth of 0.5 to 2 nm and are used for surface chemistry of materials, while X-rays for EDX analysis. The sample for SEM must be electrically conductive for analysis; otherwise, gold sputtering is used to coat the sample to make it conductive prior to SEM analysis. The apparatus for analysis is shown in Figure 3.7.

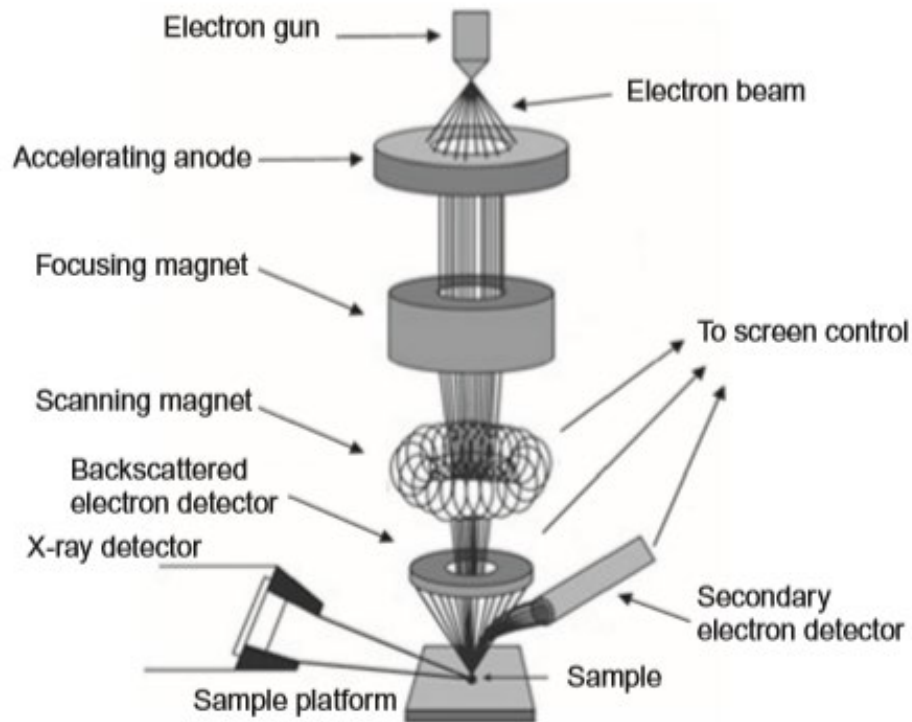


Figure 3.7: Representation of a scanning electron microscope [102].

Imaging on a Nova 450 scanning electron microscope (SEM) (FEI, Thermo Fisher Scientific, USA) was carried out to observe the morphology of the fiber surface, the desired diameter of the fiber and to check for defects such as beads in the structures at the acceleration voltage of 5-10 kV with a through-the-lens detector (TLD), additionally equipped with Octane plus energy dispersive X-ray (EDX) spectroscopy (EDAX, Ametek Inc., PA, USA). A conductive gold coating (~120 s) was applied prior to examining the EH by a sputter coater. The mean fiber diameter of each polymer was determined using software ImageJ version 1.52a.

BET

The physical adsorption of gas molecules on a solid surface is explained by BET theory, which also forms the basis for a crucial analysis method for calculating the precise surface area of materials. The theory applies to multilayer adsorption systems that typically employ a probing gas (referred to as the adsorbate) that does not chemically react with the adsorptive (the material that the gas binds to, and the gas phase is referred to as the adsorptive). Gaseous adsorbates such as nitrogen are frequently used for exploring surfaces. Because of this, the majority of routine BET analyses are carried out at the boiling point (77 K) of N₂. Water, carbon dioxide, and argon are further probing adsorbates. The amount of specific surface area that may be computed using the BET theory may vary on the

adsorbate molecule used and its adsorption cross section because the specific surface area is a scale-dependent feature and cannot be defined at a single true value. This theory is an extended concept of the Langmuir theory, which is limited to the mono adsorption layer of molecules. For multilayer adsorption, the assumptions are briefly described as follows:

1. Infinite layers of gas molecules physically adsorb on a solid.
2. Gas molecules only interact with adjacent layers.
3. The Langmuir hypothesis can be applied to each layer.
4. The first layer's constant adsorption enthalpy is higher than the second layer's (and higher).
5. For the second (and higher) layers, the enthalpy of adsorption is the same as the enthalpy of liquefaction.

With the help of the adsorption isotherm equation, a BET plot is drawn that calculates the total and specific surface area using the slope and y-intercept of the plotted line.

Surface analysis of the nanofibers was carried out according to the Brunauer-Emmett-Teller (BET) method. A high-precision analyzer of surface area and pore size (BELSORP-mini II, BEL Japan Inc., Japan) was used to determine the specific surface area. Outgassing of the substrate occurred at 100 °C for 12 h in a vacuum prior to measurement.

Capillary-flow porosimetry

This method allows the wetting liquid to fill all the accessible pores spontaneously. The fluid from the sample is then displaced with the help of a non-reactive gas under increasing pressure, which depends on the size and distribution of pores. The surface free energy of wetting fluids with respect to the sample must be lower than that of the sample with respect to the gas. This enables the gas, which is capable of displacing the wetting fluid. At high pressures, the gas

extrudes the liquid from the pores and flows through empty pores. On the basis of measured pressure, the pore diameter is obtained by the Young-Laplace formula:

$$P^{1/4} = \frac{4\gamma\cos\theta}{D} \quad (3.2)$$

where D is the pore size diameter, P is the pressure measured, γ is the surface tension of the wetting liquid, and θ is the contact angle between the wetting liquid and the sample.

In the equation, the surface extension γ is a measurable physical characteristic that depends on the wetting liquid used. The contact angle θ depends on the interaction between the material and the wetting liquid [103]. The schematic of the equipment is shown in Figure 3.8.

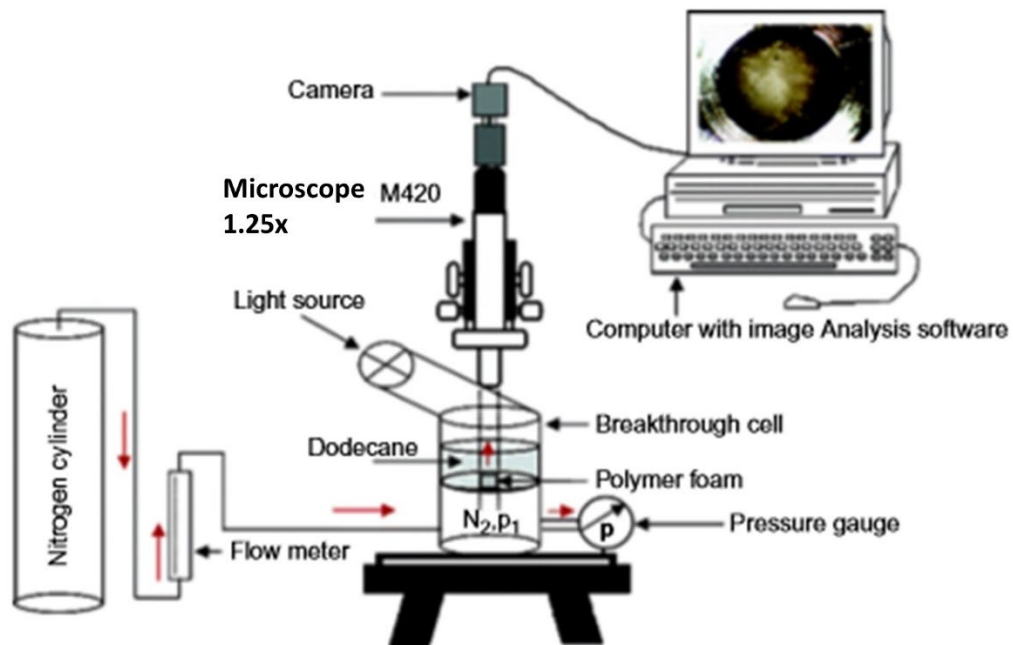


Figure 3.8: Overview of the capillary flow porosimetry equipment [104].

Air permeability and pore size distribution of submicron structures were assessed by flow porosimeter according to ASTM F316-03 (2011). Galpor (Porometer NV, Belgium) was used as a wetting liquid.

Contact angle

Contact angle measurement is commonly used to characterize surface hydrophilicity or hydrophobicity of materials. Contact angle measurement is a relatively simple method for solid samples. The sessile drop method is deployed to capture the image of the drop and measure its contact angle with the sample's surface based on Young's equation ($\gamma_s = \gamma_L \cos \theta + \gamma_{sL}$), as shown in Figure 3.9.

In general, using water as the probe liquid, if the angle is $< 90^\circ$, then the material is considered hydrophilic, which increases as the angle decreases. While if the contact angle is $> 90^\circ$, then the material is considered to be hydrophobic.

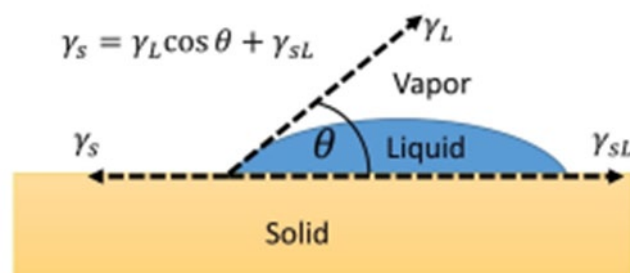


Figure 3.9: Principle of contact angle measurement (Self-representation by the author).

The contact angle measurement was conducted by compressing the nanofibers to make them compact for accurate measurement. To this end, the nanofibers were put onto a single PP sheet that, in turn, was placed upside-down on a sheet of polyethylene terephthalate (PET). Subjected to a thermal press for 10 seconds at a temperature of 110°C , then the layer of PP was detached. The sheet of PET with the nanofibers was covered with a glossy sheet for the thermal press, the same conditions being applied to acquire a smooth, compacted surface. This step ensured that liquid could remain on the surface for measuring the contact angles; without doing this, the surfaces of the nanofibers on the sheet of PP would have been incapable of holding the drops of liquid, which would instantly settle down, penetrating the porous structures. Finally, the contact angle of electrospun nanofibers was measured using the sessile drop technique on a goniometer (Surface Energy Evaluation System (SEE System), Advex Instruments, Brno, Czech Republic) under the conditions of ambient temperature. A $5\ \mu\text{L}$ pipette dropped liquid onto the surface of the samples ($10 \times 10\ \text{mm}^2$), then the shapes of the resulting droplets were observed with the aid of a CCD camera, and the contact angles were measured immediately. Glycerol and Milli Q water were used as the probe liquid to determine the hydrophilicity [105]. The samples were analyzed, and mean values for them are reported herein.

TGA

With respect to methods of thermal analysis, TGA is used to characterize the thermal stability of a material. This technique provides kinetics data for thermal degradation and weight loss of material and also information about the effect caused by additives and chemical composition due to the copolymer. TGA is

performed by heating a sample to a certain temperature under different tunable sample chamber environmental conditions (e.g., an oxidative atmosphere or under dry nitrogen) and then monitoring the variation of its weight loss as a function of temperature. Weight alteration represents polymer degradation or removal of residual solvent. A change in enthalpy may result in a difference in the weight of the test substance, which is the principle of the TGA method [106]. Information about the rate of degradation can be obtained from the results. Hence, the schematic in Figure 3.10 shows the design of TGA equipment.

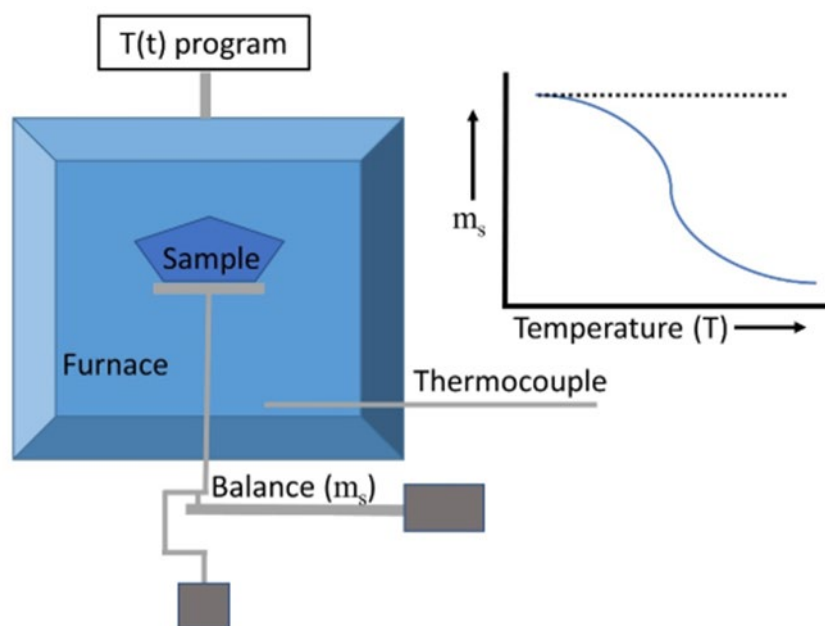


Figure 3.10: Illustration of thermogravimetric analysis instrumentation (Self-representation by the author) [106].

The thermal stability of the fibers was determined using a TGA Q500 thermogravimetric analyzer (TA Instruments, USA). Sample mass ($12 - 20 \pm 0.5$ mg), depending on its density, was heated in an alumina crucible from 25 to 700 °C at a ramp of $15 \text{ }^\circ\text{C}\cdot\text{min}^{-1}$ under an N_2 flow of $100 \text{ mL}\cdot\text{min}^{-1}$.

DSC

DSC technique can provide information about thermal behavior and how the heat capacity (C_p) of a material is changed by the temperature at constant pressure. Samples of known mass are heated or cooled, and the changes in their heat capacity are followed with the help of changes in the heat flow. This process detects phase transitions, such as melting, glass transition, phase changes, and curing. This technique represents the calorimetric method in which the difference in energy supplied to the sample to be tested and reference material is measured

as a function of temperature. For the measurements, the sample of known weight (5 – 20 mg) is placed in a small pan made of aluminum or other metallic or ceramic material. Both reference and tested samples are exposed (in a special atmosphere) to the same controllable temperature program. The temperature difference between the sample and the reference sample is measured by locating them in a common furnace (cell) connected by a bridge (Figure 3.11). The heat flow delivered is proportional to the temperature difference [107,108].

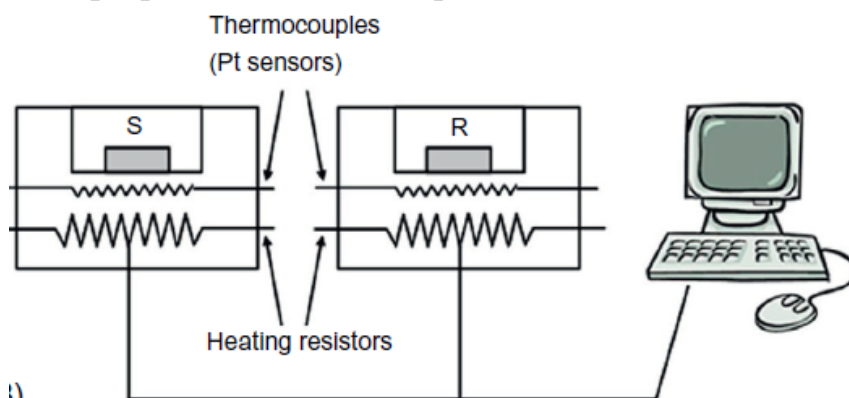


Figure 3.11: Overview of a heat flow DSC chamber with pans for the sample (S) and reference (R) connected by a common bridge [101].

DSC can build the thermogram as a graphic representation, in which the x-axis shows the temperature ($^{\circ}\text{C}$) depending on the heat flow absorbed by the tested material. Figure 3.12 shows the typical DSC analysis where the plot represents the dependence of the heat flow and the temperature that produces characteristic exothermic peaks of crystallization and endothermic peaks of glass transition and melting temperature.

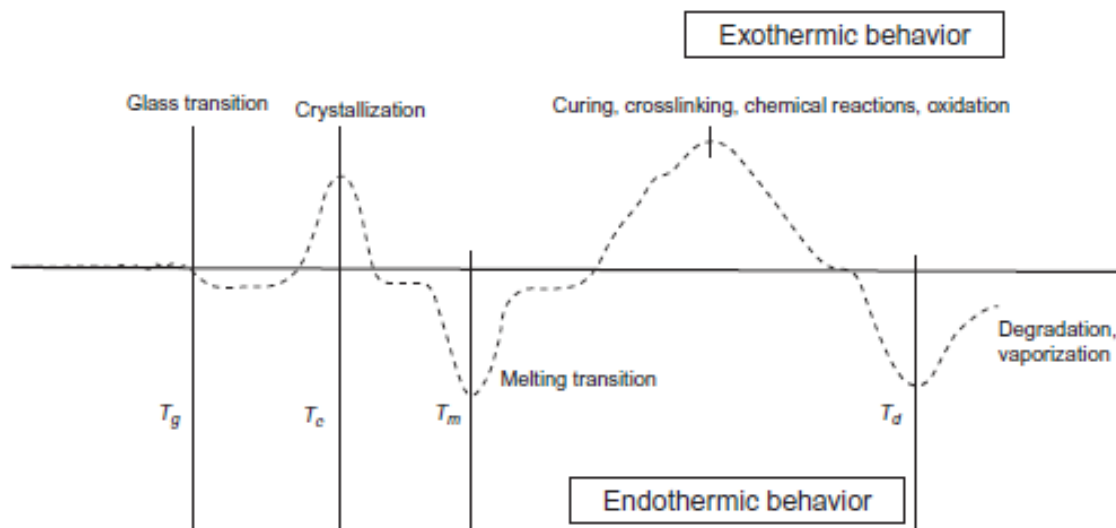


Figure 3.12: DSC thermogram of a polymeric material with various phase transitions - T_g (glass transition temperature), T_c (crystallization temperature), T_m (melting temperature-point), and T_d (temperature of degradation) [101].

To determine the thermal behavior and properties of nanofibers, they were subjected to differential scanning calorimeter (DSC) star[®]System (Mettler Toledo, Switzerland). The sample mass (5.0 ± 0.5 mg) was sealed in an aluminum pan under a nitrogen flow of $50 \text{ mL} \cdot \text{min}^{-1}$ and heated from 25 to 320 °C at a ramp of $10 \text{ }^\circ\text{C} \cdot \text{min}^{-1}$.

Tensile test

A tensile test is used to measure the strength tensile strength, yield strength, elongation, and contraction of the material sample. The test material is loaded with a slowly increasing force in the uniaxial direction until breakage occurs. It also evaluates the modulus of elasticity, the proportionality limit, and the contractual elastic limit [109]. A universal test machine is used to characterize the mechanical properties, e.g., by applying a loading ramp to a geometrically defined sample and recording the resulting deformation. The apparatus includes a frame, a movable crosshead for applying the desired load or constant elongation by a program, and a load transducer. The machine has a universal size and convenient gripping systems for different loading modes, as shown in Figure 3.13.

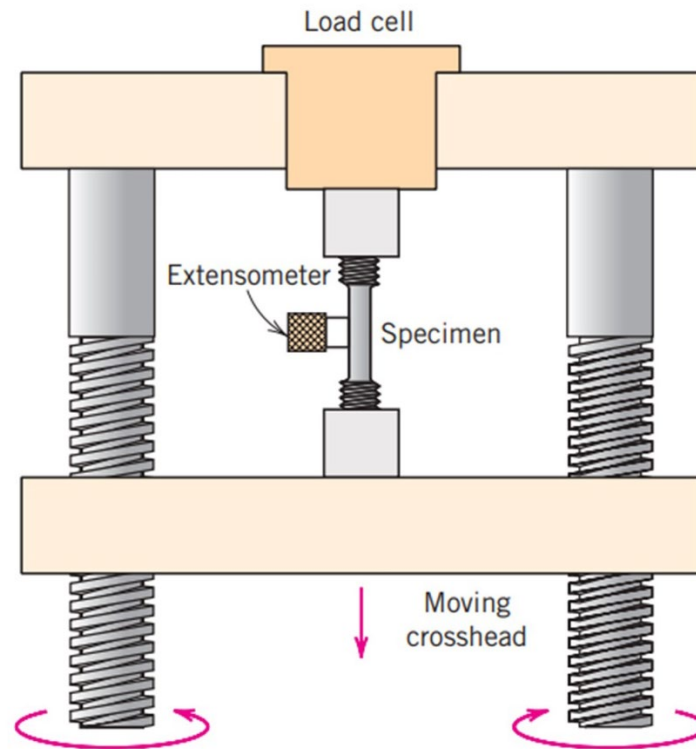


Figure 3.13: Schematic diagram of a universal testing machine for tensile tests [110].

To see the strength of fibers, the tensile test of neat PP and PP substrate with nanofibers was performed and compared because pure nanofibers were very fragile, it was difficult to peel them from the PP sheet to prepare a dumbbell shape and perform a tensile test. Therefore, the tensile tests of samples were carried out on an M350-5CT tensile testing machine (Testometric, UK) supplied with a load cell of 10 kgf. For all measurements, a crosshead pull speed of 10 mm/min and a gauge length of 20 mm was used. A unique die was used to cut specimens in the shape of dumbbells (Type 3, ISO 37:2005). Young's elastic modulus (MPa), ultimate tensile strength (N/mm), percentage elongation (%), and other mechanical properties were obtained. Measurements were conducted in triplicates, and mean values with standard deviation were reported.

4. MOTIVATION FOR THE DOCTORAL STUDY

4.1 Conclusions and bridging the gap

Today, there is a vast awareness of the growing water challenges due to the growing population, use of synthetic chemicals, newly developed pharmaceutical products, industrial waste, pesticides, and especially the use of contraceptive pills that leads to hormonal imbalance, which ultimately ends up in fatal diseases such as breast, ovarian and prostate cancer. Therefore, considering smart, functionalized, and high-performance polymeric materials are highly desired to overcome this nuisance.

In this regard, special attention has been given to EH due to their minuscule concentrations in water streams, and the difficulty is complex methods of detection. Limited methods have been devised in the literature that can simultaneously quantify EH at lower limits of micro and nanograms. These four EH: estrone (E1), estradiol (E2), estriol (E3), and ethinylestradiol (EE2), have high potencies measured in wastewater and the existing conventional wastewater treatment plants are inefficient in removal, recovery, and proper disposal of these EH or have high operating costs.

In literature, nanoparticles for adsorption have been used in this application which further requires additional purification and separation steps that raise the cost of work. However, nanofibers prepared from electrospinning have recently gained great attention due to their high aspect ratio, lightweight, and reusability. Still, they have least been used for this application in water treatment. Therefore, few works have been done with electrospun nanofibers for eradicating these EH from wastewater. Some works have been done with PA, nylon, PVDF, and PES membranes but are limited to just removing a single EH. Hence, it creates a gap that needs more comprehensive work to be done in this area to address this issue properly.

To bridge this gap, this application requires the preparation of more optimized polymeric nanofibers with a facile technique and their surface modification to enhance activity, which can be cost-effective and better in simultaneously adsorbing EH. Further, discuss the mechanisms, measure kinetics, isotherms, and thermodynamics with appropriate models, and finally, prove the effectiveness of materials with several adsorption-desorption cycles for the recovery of EH, as

well as test the reusability of materials to be practically applicable over large-scale use.

4.2 Aims of doctoral thesis

The aims of this doctoral research work are defined in the state-of-the-art study and, based on the conclusions made, are classified into four main categories of work which are demonstrated in the schematic diagram in Figure 4.1 below.

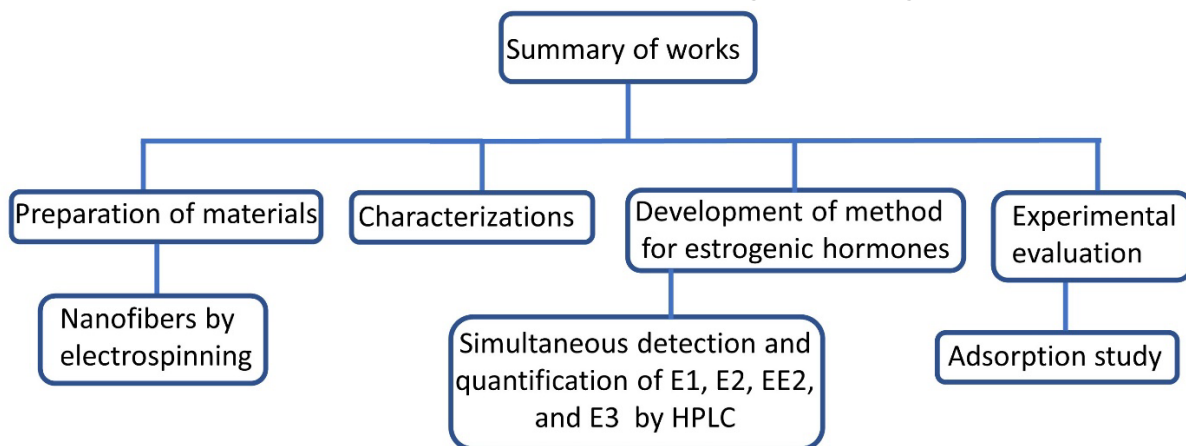


Figure 4.1: Schematic outline of works (Self-representation by the author).

This thesis work includes the preparation of nanofibers based on selective polymers via electrospinning, their characterization, determination of adsorption activity by nanofibers, the study of interactions between polymeric nanofibers and EH, desorption study for the recovery of hormones and reusability of materials. The specifications of these classifications are described in more detail as follows:

- Developing a method for simultaneous detection and quantification of EH (E1, E2, EE2, and E3) via HPLC technique using UV-Vis detector.
- Selection of appropriate polymers for high removal of EH and their optimized synthesis prior to electrospinning. These materials include both hydrophilic and hydrophobic polymers (polyurethanes commercial and lab synthesized (PU Elastollan and PU 918), PA, CA, PSU, PES, PLA, PAN, and PVDF).
- Preparation of solution for each polymer with the desired properties such as solution concentration, intrinsic viscosity, and electrical conductivity of each polymer based on its molecular weight and density.
- The fabrication of nanofibers with the least diameter (ideally < 350 nm) using defined adjusted parameters on electrospinning such as applied

voltage, the distance between electrodes, the rotational speed of collecting PP roll, solution dosage, chamber temperature, and pressure to eliminate and avoid bead defects.

- Determination of adsorption removal efficiency of each EH on the prepared nanofibers via static adsorption test.
- Investigation of adsorption mechanisms (hydrophobic interactions, hydrogen bonding, charge interaction, size exclusion, and π - π stacking interaction) for the promising adsorbent polymers based on their structure and the functional groups of the hormones.
- Determination of contact time study to apply suitable kinetic models (pseudo-first-order, pseudo-second-order, Weber and Morris intraparticle diffusion, Elovich, Boyd, and fractional power models), variation in adsorbate concentration for isothermal models (Freundlich and Langmuir) and thermodynamic study.
- Optimization study with variation in experimental condition parameters such as concentration of adsorbate, adsorbent dosage, pH of the solution, the temperature of interaction, and time of contact.
- Testing reusability of high-performance materials for at least six adsorption-desorption cycles.
- A separate study of recycled CBs to prepare CA electrospun nanofibers (WCENFs) to compare their performance with the commercial CA nanofibers and further fabrication of membrane film for possible comparison of hormone uptake with the commercially available syringe filters (CA, regenerated cellulose (RC), polytetrafluoroethylene (PTFE), and PP).
- Surface modification of the best performance polymeric nanofiber by coating it with polyaniline/polyvinyl alcohol to enhance the adsorption activity of hormones owing to stronger hydrogen bonding interactions.

- Determination of optimum experimental conditions by analysis via response surface methodology using a central composite design model and validation of operating parameters by the Design-Expert software.
- Comparative study of prepared materials' performance of capturing EH with the materials reported in the literature.
- Publish all the data from the mentioned works in Q1/Q2 impact factor journals and international scientific conferences within the frame of university policy and the rector's directive.

4.3 Experimental design

4.3.1 Evaluation of the adsorption properties of polymeric nanofiber structure by discontinuous sorption testing

Static adsorption tests were carried out to determine the adsorption rate. Separate flasks were set aside for testing each polymeric mat in triplicates, utilizing 100 mL from the stock of EH solution at a total concentration of 0.8 mg/L; each flask was then supplemented with 20 mg of a given nanofiber. The flasks were continuously stirred on an orbital incubator shaker (Stuart[®] S1500, Barloworld Scientific Ltd., UK) for adsorption at 250 rpm. Samples of the remaining concentration of the hormones in each flask were collected in vials via a 0.45 μm GMF syringe filter, and readings were taken after intervals of 5 min, 15 min, 30 min, 60 min, and each following hour until a constant value was obtained. At each interval, 4 mL samples were taken with a 20 mL syringe, ensuring that neither the nanofiber was removed nor destroyed in the process, and 4 mL of ultrapure water was added to maintain the total volume. The first 2 mL of the filtrate was discarded, this having passed from the syringe through the GMF filter to eliminate any adsorption during sampling, thereby ensuring accuracy and precision in the results. A flask containing a solution without any nanofiber was labeled as a "control" and included in the experiment to discern the initial reference concentration. It must be noted that adsorption on the glass surface was negligible throughout long-term testing, which was determined by comparing the recorded initial concentration and concentration after 9 h of stirring the control solution. To this end, the hormone solutions were checked prior to the start of the experiment. Each sample reading was conducted in triplicate, and the corresponding values for mean concentration and standard deviation based on Gaussian distribution

were recorded. Finally, the percentage of adsorption for each hormone on the nanofibrous mat was calculated with reference to the aforementioned “control” flask. The stock solution was kept neutral by means of ultrapure deionized water at a pH of 7.3, considering real environmental water samples to be in the range of 6-9. The percentage removed of each hormone at a given time (t) was determined by the expression in Eq. (4.1), as follows [111,112]:

$$Removal (\%) = \frac{C_i - C_t}{C_i} \times 100 \quad (4.1)$$

where C_i is the initial concentration (mg/L), and C_t is the concentration of the solution at time t (mg/L).

Equilibrium adsorption capacity (q_e) and adsorption capacity (q_t) at any instant of time t can also be calculated by the following expressions in Eq. (4.2) and (4.3) [113,114]:

$$q_e = v \times \frac{C_i - C_e}{m} \quad (4.2)$$

$$q_t = v \times \frac{C_i - C_t}{m} \quad (4.3)$$

where m is the mass of adsorbent in grams and v is the volume of solution in liters. It must be noted that q_e is equal to q_t at the last sampling time in the adsorption process.

Applying the average diameter of the nanofibers calculated from SEM, in consideration of the fiber constituting a single continuous cylinder, the length per unit mass (l/m) and surface area (A) of the fiber can be calculated by the following Eq. (4.4), (4.5), and (4.6) [32]:

$$V = \frac{m}{\rho} = \frac{\pi d^2 l}{4} \quad (4.4)$$

By rearranging this expression, the following is obtained:

$$l/m = \frac{4}{\rho \pi d^2} \quad (4.5)$$

where V is the volume (m^3), m is the mass (mg), d is the diameter of the nanofiber (m), and ρ is the density of each given polymer (g/cm^3).

Since $l \gg d$, it is possible to neglect the individual cross-sectional area (A) of the end portions of the fibers, such that the total surface area per unit of mass is expressed as:

$$\frac{A}{m} = \frac{d\pi l}{m} = \frac{4}{\rho d} \quad (4.6)$$

4.3.2 Adsorption kinetics study

The results obtained from the experiment were employed to investigate factors affecting the adsorption process and the rate-limiting step in the process, such as the transfer of mass and type of chemical interaction. Furthermore, the kinetics for selecting optimum conditions for full-scale removal of the hormones were studied. It is often difficult to determine kinetic parameters and explain the mechanisms involved in complex heterogeneous systems since surface effects can be superimposed on top of chemical effects. Therefore, to further understand such adsorption behavior and mechanisms, parameters from five models - pseudo-first-order, pseudo-second-order, and Weber-Morris intraparticle/membrane diffusion, Elovich and fractional power model equations - were employed to test the experimental data and examine the adsorption kinetics of the four EH taken up by each polymer. These models are applicable for describing liquid/solid systems. Pseudo-first-order constitutes a widespread, commonly applied model for analyzing the adsorption of a solute in an aqueous solution. In this context, the rate of sorption of hormones on the surface of the nanofibers was proportional to the amount of hormones adsorbed from the solution phase, expressed by Eq. (4.7) as [115]:

$$q_t = q_e(1 - \exp(-k_1 t)) \quad (4.7)$$

where q_t is the amount of hormone adsorbed per unit mass at time t (mg/g), q_e is the amount of hormone per unit mass at equilibrium (mg/g), and k_1 is the first-order rate constant (L/min).

The pseudo-second-order equation relates to solid-phase adsorption capacity and can predict the behavior of kinetics over a great range for adsorption [116]. In this model, surface adsorption is the rate-determining step, which involves chemisorption due to physicochemical interactions between the solid and liquid phases [117]. The linear form of Eq. (4.8) is expressed as [118]:

$$\frac{t}{q_t} = \frac{1}{k_2 q_e^2} + \frac{t}{q_e} \quad (4.8)$$

where k_2 is the reaction rate constant (g/(mg min)).

The adsorption process usually occurs in consecutive steps, comprising the movement of the adsorbate from the solution bulk to the surface of the adsorbent

and then diffusion through the boundary layer to the outer surface of the adsorbent. This is followed by adsorption on an available active site on the surface of the adsorbent and, finally, intraparticle diffusion through pores. The Weber-Morris intraparticle/membrane diffusion model is diffusion-controlled; the adsorption rate directly depends on the speed at which an adsorbate can diffuse towards the adsorbent. This model is described by Eq. (4.9) as follows [119]:

$$q_t = kt^{\left(\frac{1}{2}\right)} + I \quad (4.9)$$

where k is the reaction rate constant ($\text{mg/g h}^{1/2}$), and I is the y-intercept constant (mg/g), providing data on the thickness of the boundary layer.

For the validity of this model, it is essential to note that the linear, converging line for each EH must pass through the point of origin for intraparticle diffusion to constitute the rate-determining step.

In reactions where chemisorption is a dominant mechanism such that on the surface of the adsorbent, adsorbate is deposited without desorption of products, the rate of adsorption decreases with time as the reaction proceeds, and it is due to the surface coverage. In such reactions, the elovich model is suitable for explaining the chemisorption process by expressing the following linear Eq. (4.10) [120]:

$$q_t = \beta \ln(\alpha\beta) + \beta \ln t \quad (4.10)$$

Where α and β are the coefficients such that α represents the initial adsorption rate (g/mg.min) and β represents the desorption coefficient ($\text{mg}/(\text{g.min})$). These coefficients can be calculated from the slope and y-intercept of the plot.

The fractional power model is the more advanced form of the Freundlich equation, and the linear form is expressed in Eq. (4.11) [121].

$$\ln q_t = \ln a + b \ln t \quad (4.11)$$

Where a and b are the coefficients in the expression and given that $b < 1$, the product of a and b is given as the specific adsorption rate at 1 min after the start of the experiment.

Boyd's model accounts for the free diffusion of a solid spherical adsorbent in a solution phase, and the following Eq. (4.12) is used to express this model.

$$B_t = -0.4977 - \ln(1 - F) \quad (4.12)$$

where, B_t is the Boyd parameter related to the adsorption process, and F is the fraction of solute adsorbed at any time, t (min), estimated from $F = q_t/q_{max}$.

4.3.3 Thermodynamic study

The impact that surrounds temperature influences the adsorption capacity of spun nanofibers was studied in a temperature-controlled system at different temperatures. The thermodynamic parameters were calculated based on the adsorption distribution coefficient (K_D) for the different studied temperatures. The thermodynamics of the adsorption process were estimated using the following equations [122,123].

$$K_D = \frac{C_s}{C_e} \quad (4.13)$$

$$\ln K_D = -\frac{\Delta H}{RT} + \frac{\Delta S}{R} \quad (4.14)$$

$$\Delta G = \Delta H - T\Delta S \quad (4.15)$$

Where, K_D is the distribution coefficient (a ratio of solid phase to solute concentrations), C_s (mg/L) is the concentration of the hormone on the adsorbent, ΔH is the enthalpy change, ΔS is the entropy change, ΔG is the Gibbs free energy change, R (8.314 J/mol K) is the universal gas constant, and T (K) is the absolute temperature. By plotting a Van't Hoff plot of $\ln K_D$ versus $1/T$, ΔS and ΔH were determined from the slope and intercept, respectively.

4.3.4 Isotherm modeling

The adsorption isotherm study was performed at the initial pH of 7, the temperature of 25 °C, and different initial concentrations of the hormone mixture (0.1, 0.2, 0.3, 0.4, and 0.5 mg/L). Spun nanofibers were used as the adsorbent, and samples were collected after 9 h of adsorption. The fitting of the adsorption equilibrium data was evaluated using the Langmuir and Freundlich isotherms. The non-linear regression equations used for the models are shown in Eq. (4.16) and (4.17), respectively [124–126]:

$$q_e = \frac{Q_{max}K_L C_e}{(1 + K_L C_e)} \quad (4.16)$$

$$q_e = K_F C_e^{1/n} \quad (4.17)$$

Where q_e is the amount of adsorbed hormone on adsorbent at equilibrium (mg/g), C_e is the residual equilibrium hormone concentration (mg/L), Q_{max} is the

maximum adsorption capacity (mg/g), K_L is the Langmuir isotherm constant, K_F is the Freundlich constant and n is the Freundlich heterogeneity factor.

4.3.5 Reusability test

For the desorption test in order to determine the reversibility of the polymers for sorption, triplicates of each polymer sample were extracted from the conical flasks containing the hormone solutions and soaked in 50 mL of water, and shaken for 15 min at a constant 250 rpm, which would not significantly reduce the hormone concentration on the nanofibers as a consequence of chemical bonding [32]. Therefore, each sample, after being washed three times with distilled and deionized water, was immersed in 40 mL of pure anhydrous ethanol since all EH exhibit very high solubility in ethanol due to their high partitioning coefficient ($\text{Log-} K_{o/w} = 3.13, 4.01, 2.45, \text{ and } 3.90$ for E1, E2, E3, and EE2, respectively). A strong partitioning effect was expected to occur in combination with a competing hydroxyl group present in the ethanol, which could destabilize the estrogen-nanofiber hydrogen bonds and attract the adsorbed hydrophobic hormones in the ethanol solution [39,127]. The resultant solution was gently stirred for 30 min at 175 rpm, air-dried afterward, and placed in a desiccator until the next adsorption cycle. The procedure was repeated for several cycles until low adsorption efficiencies were observed. For better treatment in the latter chapters, the procedure was slightly modified. The nanofibers after adsorption, were extracted from the conical flasks containing the hormone solutions and washed thoroughly with distilled water, followed by gentle stirring at a constant 100 rpm for 10 min in a 100 mL mixture of 1:1 water and ethanol to remove the hormones entirely and eluted in the mixture. A sample reading was taken to determine the concentration of hormones recovered. Finally, the nanofibers were placed in 100 mL of water until the next adsorption cycle.

4.3.6 Statistical and error analysis

The data are displayed as Mean \pm Standard error. OriginLab v.9.0 and Design expert software v.13.0 were used for statistical analysis. The difference between values was determined by one-way analysis of variance (ANOVA). A value of $p < 0.05$ was determined as statistically significant. Error analysis parameters such as the determination coefficient (R^2) were used to ascertain the difference between the experimental and theoretical data. In addition, the sum of squared errors (SSE) and Chi-squared (χ^2) were employed to minimize errors since inherent bias occurs during the linearization of equations, such as in kinetic modeling.

5. The adsorption, kinetics, and interaction mechanisms of various types of estrogen on electrospun polymeric nanofiber membranes

This chapter primarily investigates the optimized preparation of electrospun nanostructures from polymers CA, polyurethanes (PU 918 and PU Elastollan), PA, PES, and PAN that possess beadless desired attributes of morphology, small diameter of the fiber, high ratio of surface area to volume, lightweight, and numerous sites for adsorption. Research focuses on these nanostructured polymers with high sorption activity for EH (E1, E2, EE2, and E3). A membrane of this type could be employed for the microfiltration of wastewater compared to commercially available microfiltration membranes that exhibit greater flux [71]. The objective is simultaneous adsorption of four EH in a one-step process from wastewater at neutral pH because the pH of rivers is in the range of 6-9. The feasibility of the results is analyzed by applying experimental data, thereby determining adsorption capacity and kinetics via suitable pseudo-first-order, pseudo-second-order, and intraparticle diffusion models to help understand the suitability of characteristics essential for large-scale implementation. Finally, the adsorption mechanisms of the nanofibers are gauged to understand the interaction ability of functional groups present for bonding between polymers and EH. The tests are conducted with the extent of polymers' reusability over several adsorption cycles to discern reliability and effectiveness for the large-scale generation of these polymers. The following Figure 5.1 depicts the preparation and experimental design of the nanofibers.

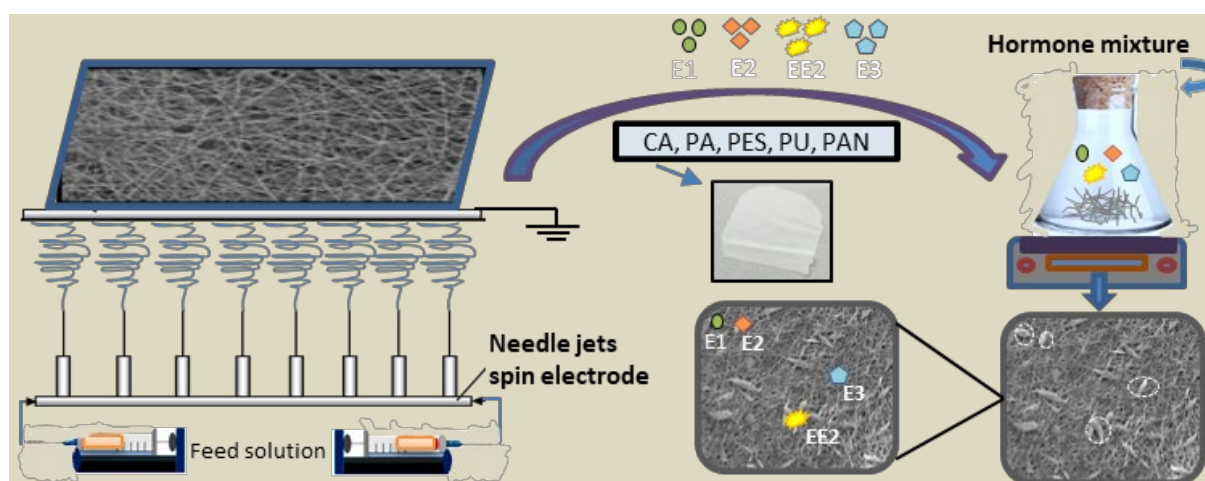


Figure 5.1: Schematic of nanofibers prepared via electrospinning and static adsorption test for hormone removal.

5.1 Characterization of the electrospun nanofibers

The SEM of the nanofibers, along with the distribution of fiber diameter from the various polymers prepared via electrospinning, are shown in Figure 5.2.

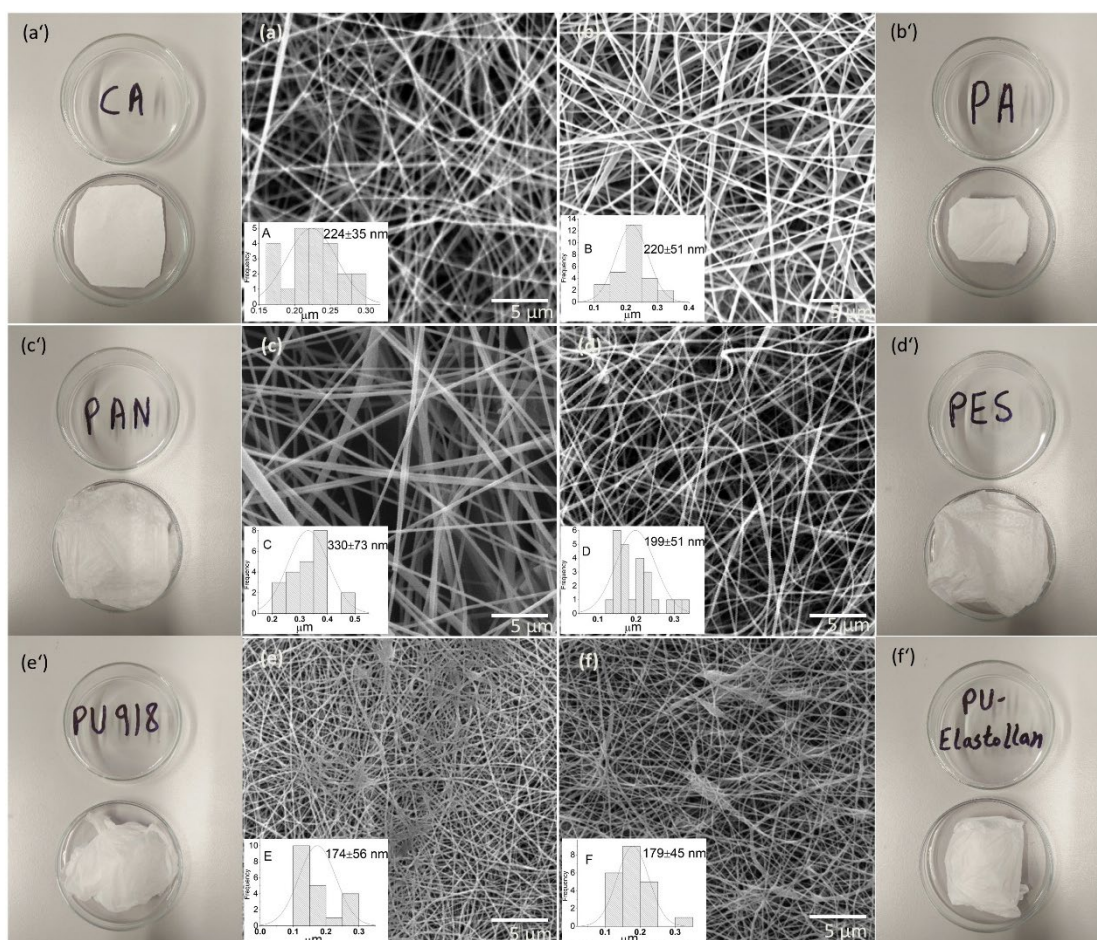


Figure 5.2: Electron micrographs, (inset) distribution of frequency size, and sample images of the electrospun nanofibers (20 mg) of (a, a') CA, (b, b') PA, (c, c') PAN, (d, d') PES, (e, e') PU 918, and (f, f') PU Elastollan, respectively.

The graph above reveals that the uniform nanofibers were produced with minimum beading and a narrow fiber diameter range, i.e., 174-330 nm; PU 918 demonstrated the least value and PAN the greatest. These low averages in the size of diameters were attributed to the optimized electrospinning process (low intrinsic viscosity, low polymer concentration in the solution, and high electrical conductivity prior to said process); the large surface area was the consequence of this. The size and morphology of the EH were also analyzed on an electron microscope, and the micrographs are shown in Appendix 1 (Fig. S2).

Table 5.1 details the recorded diameters from the SEM images, calculated fiber length, and surface area through the application of the above formulas in

experimental design (section 4.3), in addition to the surface area measured by BET.

Table 5.1: Characteristics of the electrospun nanofibers as gauged by BET, contact angle, and calculated values from the SEM images

Nanofiber	Average fiber diameter (nm)	Fiber length per unit of mass (m/mg)	Calculated surface area (m ² /g)	BET surface area (m ² /g)	Contact angle (°)
CA	224 ± 35	19297	13.6	8.66	22.2 ± 0.9
PA	220 ± 51	24268	16.8	5.50	8.8 ± 2.3
PAN	330 ± 73	9875	10.2	5.16	0
PES	199 ± 51	23816	14.9	17.66	72.5 ± 1.8
PU 918	174 ± 56	38231	20.9	5.34	27.4 ± 0.1
PU Elastollan	179 ± 45	32572	18.3	16.34	45.4 ± 1.1

The geometrically determining surface areas, based on SEM, strongly agree with the average fiber diameter because smaller diameter nanofibers possess a larger surface area, which indicates more sites for adsorption. For instance, PU 918 had the smallest average fiber diameter (174 ± 56 nm), so it possessed the largest calculated surface area (20.9 m²/g), and PAN had the largest average fiber diameter (330 ± 73 nm), so it possessed the least calculated surface area (10.2 m²/g); the results correspond to the literature with the values in the range of 9-51 m²/g for surface area and a few hundreds of nanometers for average fiber diameter [32,128]. The estimated surface area of cylindrical geometry was founded on a calculation that assumed the fibers had a smooth surface and no solvent evaporated during electrospinning. Whereas, in BET measurement, the surface area is slightly underestimated because each polymer had a different mass per unit area produced, which could be a plausible reason, especially in PU 918 with 0.7 g/m² (see Table 3.1), which has led to a lower value of BET.

The hydrophilic properties of the electrospun nanofibers were tested using contact angle measurements. It is considered that the hydrophilic surfaces generally have a contact angle of < 90°, and the lesser the contact angle, the more hydrophilic the material is. We observed that the liquid instantly penetrated the nanofibers on PP

completely. Therefore, nanofibers were compressed on a PET sheet, and it exhibited low contact angle values because we observed water percolation into fiber networks. According to the results obtained (Table 5.1), the contact angle values were in the range of $0 - 72.5^\circ$. These values indicated that all the nanofibers were hydrophilic and suitable for the removal of the investigated EH. The contact angle of a particular polymer's nanofibers mainly depends on the concentration of the polymer in the solution during the electrospinning process. The possible reasons for the difference in contact angles of various polymer nanofibers could be their structure, pore size, and fiber diameter [129].

IR studies were conducted to distinguish the functional groups in the electrospun nanofibers of each polymer which are later discussed in the adsorption mechanism section to understand the type of bonding and interactions between EH and nanofibers, as shown in Figure 5.3.

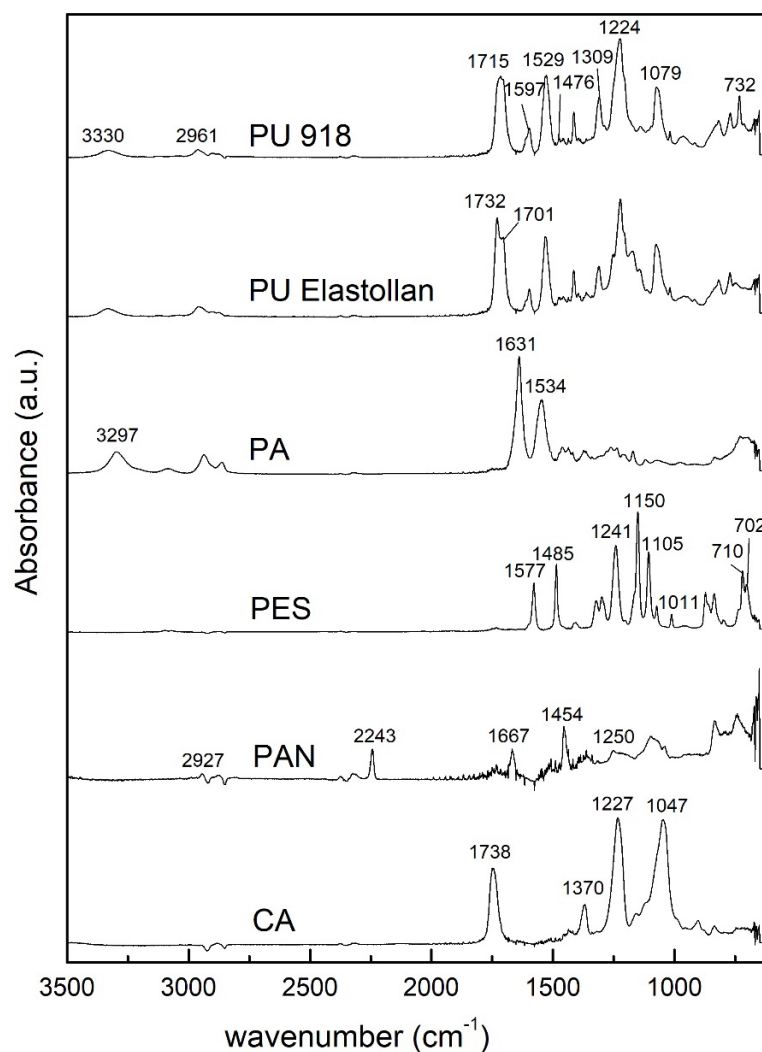


Figure 5.3: FTIR spectra for the electrospun nanofibers from attenuated total reflectance (ATR) sampling.

As can be seen from Figure 5.3, the characteristic peaks for PAN at 1250, 1454, 1667, 2243, and 2927 cm^{-1} correspond to C-N stretching, C-H bending in CH_2 , C=C stretching, $\text{C}\equiv\text{N}$ stretching, and C-H stretching vibrations in the polymer structure, respectively [130]. The small PAN and polyurethanes peaks represent aliphatic CH_2 , reflecting a C-H asymmetrical flexing vibration. The electrospun polyurethanes show an absorption peak at 3330 cm^{-1} caused by the stretching vibrations of N-H and the aliphatic amino group in the carbamate. Strong peaks usually occur between 1700-1736 cm^{-1} , relating to mono or disubstituted compounds, herein denoting the peak at 1732 cm^{-1} attributed to the C=O stretching vibration of the amido ester, while a separate region at 1701 cm^{-1} is observed for PU Elastollan in contrast with a single peak at 1715 cm^{-1} for PU 918. The peak at 1529 cm^{-1} is for N-H bending and C-N stretching vibrations of the amide group. The peak at 1224 cm^{-1} arises through the C-N stretching vibration for the other amide group. As a result of the stretching vibration of the C=C bond in the skeleton of the benzene ring, peaks appear at 1476 and 1597 cm^{-1} . A broad range of peaks occurs at 1079 and 1106 cm^{-1} due to characteristic bands of alkyl ether causing the asymmetric flexing vibration of C-O-C bonds, most prominent for PU Elastollan [131,132].

The vibration of aromatic hydrocarbons is observed in PES at the bands 1577, 1485, and 1105 cm^{-1} . The bands at 1241 and 1150 cm^{-1} could be due to aryloxy and aromatic sulfone groups, respectively. A band arising through a SO_3H symmetrical stretching vibration appears at 1011 cm^{-1} . These peaks indicate that the material is strongly sulfonated [133]. The peaks at 710 and 702 cm^{-1} are attributed to the stretching vibrations of C-O and C-S bonds, respectively [134].

The peak at 1534 cm^{-1} - characteristic of PA - is attributed to amide II, C=O bending, and the amide I band at 1631 cm^{-1} indicates the stretching vibration of C=O in the amide group (-CO-HN-). Lastly, the amide A band at 3297 cm^{-1} corresponds to -NH stretching [127]. In the case of CA, it can be seen that the vibration peak at 1047 cm^{-1} shows a C-O bond, the peak at 1227 cm^{-1} represents a (C-O-C) anti-symmetric stretching ester group, the peak at 1370 cm^{-1} denotes C- CH_3 , and the peak at 1738 is for C=O bond stretching of the carbonyl group [135,136]. Hence, the FTIR spectra measured for the nanofibers are in reasonable compliance with spectra for the original polymeric raw materials from the bank of IR spectra.

5.2 Static adsorption study of hormones on the polymeric nanofiber materials

The experiment was conducted on 100 mL of a solution containing a mixture of the 4 EH (E1, E2, EE2, E3) at a total concentration of 0.8 mg/L, wherein each hormone equated to 0.2 mg/L in concentration, in addition to 20 mg of adsorbent. Figure 5.4 details the static adsorption of each hormone separately on the various electrospun nanofibers at 250 rpm over a period of 9 h.

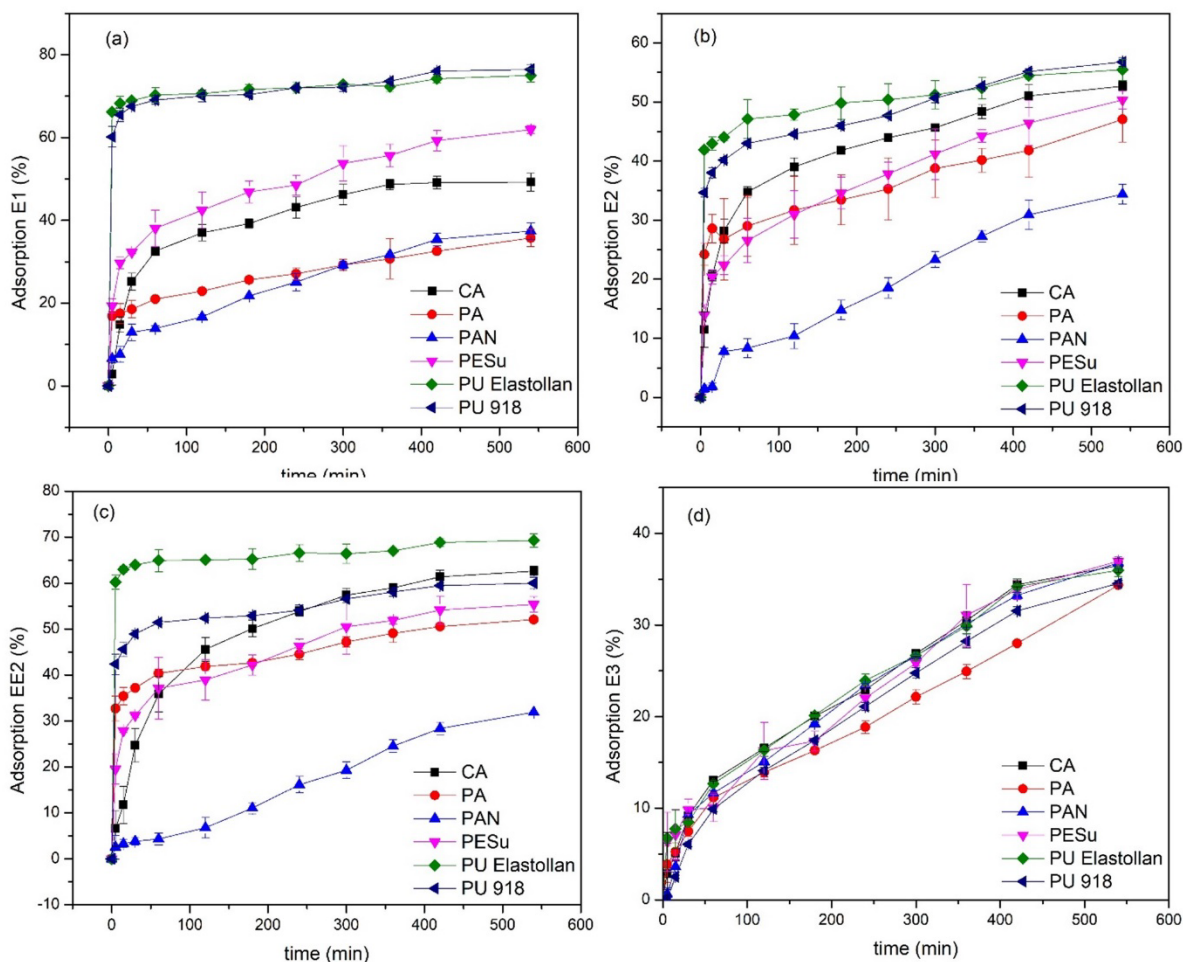


Figure 5.4: Static adsorption of each estrogenic hormone on six different nanofibers from a combined solution of (a) E1, (b) E2, (c) EE2, and (d) E3.

The results in Figure 5.4 demonstrate that polyurethanes were most efficient at removing EE2, E2, and E1, PAN demonstrated the lowest capacity for EE2 and E2 adsorption, while PA was the least effective with E1 and E3. The plausible reason for the least adsorption on PAN could be due to its large fiber diameter (330 ± 73 nm), as depicted by its least calculated total surface area of 10.2 m²/g compared to the other polymers, thereby attributing to its less available sites for adsorption and hydrogen bond interactions with the EH. Comparing the sorption

efficiency of both polyurethanes revealed that PU Elastollan either possessed a superior adsorption effect (for the hormones EE2 and E2) or was identical (E3, E1), potentially due to the lesser content of hard segments in PU Elastollan than PU 918. The active sorption center of PU Elastollan is more easily accessible than the sterically hindered center in the hard segments of PU 918.

All materials showed a similar trend of sorption for the E3 hormone. The conclusion can be drawn that EE2, E2, and E1 were readily adsorbed by these nanostructured materials, with E3 being adsorbed the least. The low percentage of removal of E3 could be attributed to its minimal $\log K_{ow}$ value of 2.45, compared with E1, E2, and EE2 at 3.43, 3.94, and 4.15, respectively. The adsorption of these estrogens was directly related to their hydrophobic nature, as specified by the higher value for K_{ow} [120]. Furthermore, E3 followed a different kinetic trend than the other hormones in that its adsorption was gradual, whereas most of the adsorption of the other hormones occurred within the first 70 minutes for the majority of the materials. CA and PES had similar adsorption behavior for all the hormones, and CA exhibited higher adsorption efficiency for EE2 and E2, though PES was particularly effective with E1. Therefore, it is noteworthy to mention that every material proved sufficient in its response to the simultaneous adsorption of each hormone.

5.3 Equilibrium adsorption capacity comparison

Determination was made as to total adsorption in combination for all four hormones by each polymer, along with cumulative adsorption capacity as a function of time to work out the overall efficiency of each polymer. The various trends are presented in Figure 5.5.

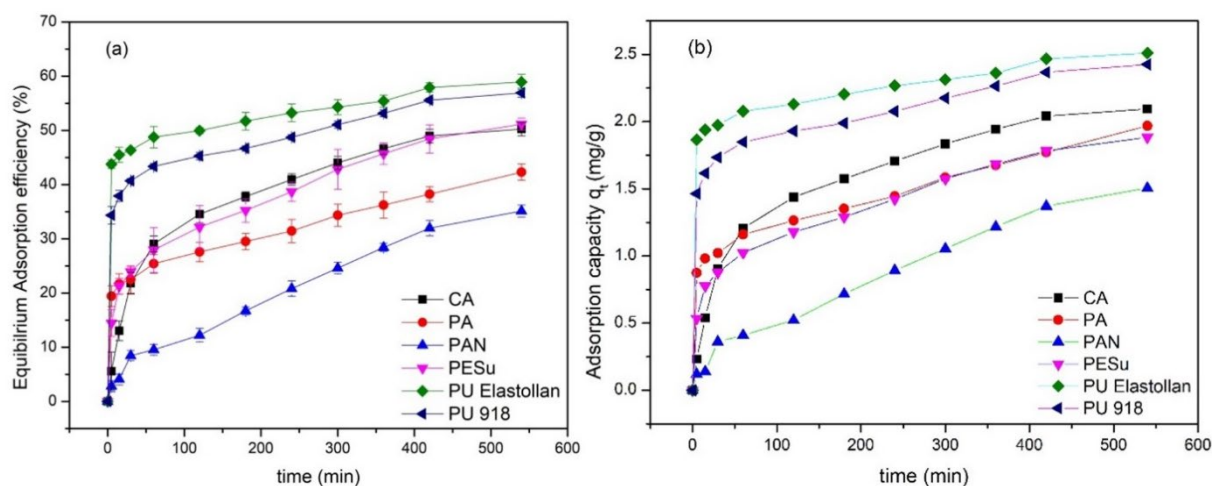


Figure 5.5: Trends for the combined hormones of E1, E2, EE2, and E3 on the nanofibers as to (a) removal efficiency as a function of time and (b) total adsorption capacity as a function of time.

Figure 5.5a shows the total cumulative adsorption of the hormones on the nanofibrous materials to the time of 540 min for equilibrium. The results show that the removal efficiency at equilibrium for the different materials ranged between 30 to 60%. The graph reveals that the polyurethanes had the greatest tendency and fastest rates for adsorption, reaching close to equilibrium with 50% efficiency within the first 100 min, as represented by the initial curve of the graph, reaching a maximum removal efficiency of ca. 60%. Although PAN initially had the lowest rate, it eventually demonstrated the highest rate at the halfway point between 120 min and 420 min, as visible in the steepness of the curve. CA and PES were similar in adsorption behavior, reaching 50% at equilibrium. Thus, PU Elastollan was the best polymer for the adsorption of the estrogens, with PAN being the least effective.

The total adsorption capacity of each material as a function of time is detailed in Figure 5.5b. The results indicate that the cumulative adsorption capacity of the four EH increased for each material until equilibrium was established between the adsorbates and adsorbent. The time to reach equilibrium depended on the concentration of the adsorbate and the amount of adsorbent [137]. Both factors were kept constant to compare the capacities of the different materials. However, it was still necessary to increase the amount of adsorbent to enhance the removal efficiency of the polymers over a shorter time frame. The highest cumulative adsorption capacity calculated was 2.51 mg/g for PU Elastollan, whereas the lowest was 1.51 mg/g for PAN. The adsorption capacities for E1, E2, EE2, and E3 were found to be 0.801, 0.592, 0.736, and 0.382 mg/g for PU Elastollan and 0.396, 0.370, 0.343, and 0.397 mg/g for PAN, respectively. EE2 stood out in terms

of adsorption and was found to have the highest adsorption capacity for all the polymers compared to the other estrogens.

Thus, the results of polymers in the current study are well in compliance with the literature values, and comparing the adsorption capacities herein with previous research showed the suitability of these polymers as a potential adsorbent for removing the EH in comparison with solid particles and membranes. Adsorption capacities reported in the literature were found to be 0.423 mg/g, 0.472 mg/g, and 0.472 mg/g when MWCNTs was used, and 2533.34 ng/g, 2020.78 ng/g, and 2234.09 ng/g when activated sludge was employed for E1, E2, and EE2, respectively. The value for removing E1 was 62 ng/g via a hydrophobic hollow fiber membrane [112]. Hence, PU Elastollan in the current study has a higher adsorption capacity for each hormone compared to the research in the literature. Another aspect that distinguishes these polymeric membranes over solid particles is that solid particles require a further sophisticated purification method to be separated from the treated water, which increases the cost. In addition, solid particles sometimes are toxic, which makes them less preferable for the intended purpose. Whereas these nanofibers can be easily washed, reused, and the EH can be quickly recovered. Furthermore, environment-friendly nanoparticles as adsorbents can be used as additives in these nanofibers during electrospinning which can further enhance their adsorption capacity by increasing the surface area and available sites that can be viable for the entrapment of EH.

5.4 Adsorption kinetics

Removal of the EH by the polymer nanofibers through adsorption increased over time, obtaining a maximum value for every hormone on each polymer type and reaching equilibrium. The adsorption rate was initially rapid until 30 minutes had passed, whereupon it gradually ebbed away in parallel with the duration of contact to an assumed plateau at 540 min.

Figure 5.6 contains plots describing the adsorption kinetics of the four EH on PU Elastollan since this polymer exhibited the highest removal efficiency and adsorption capacity and has proven to be the best nanofiber; the kinetic parameters obtained are given in Table 5.2. The kinetic plots and parameters for the other polymers were also calculated and are provided in Appendix 1 (Fig. S3-7 and Table S1-5).

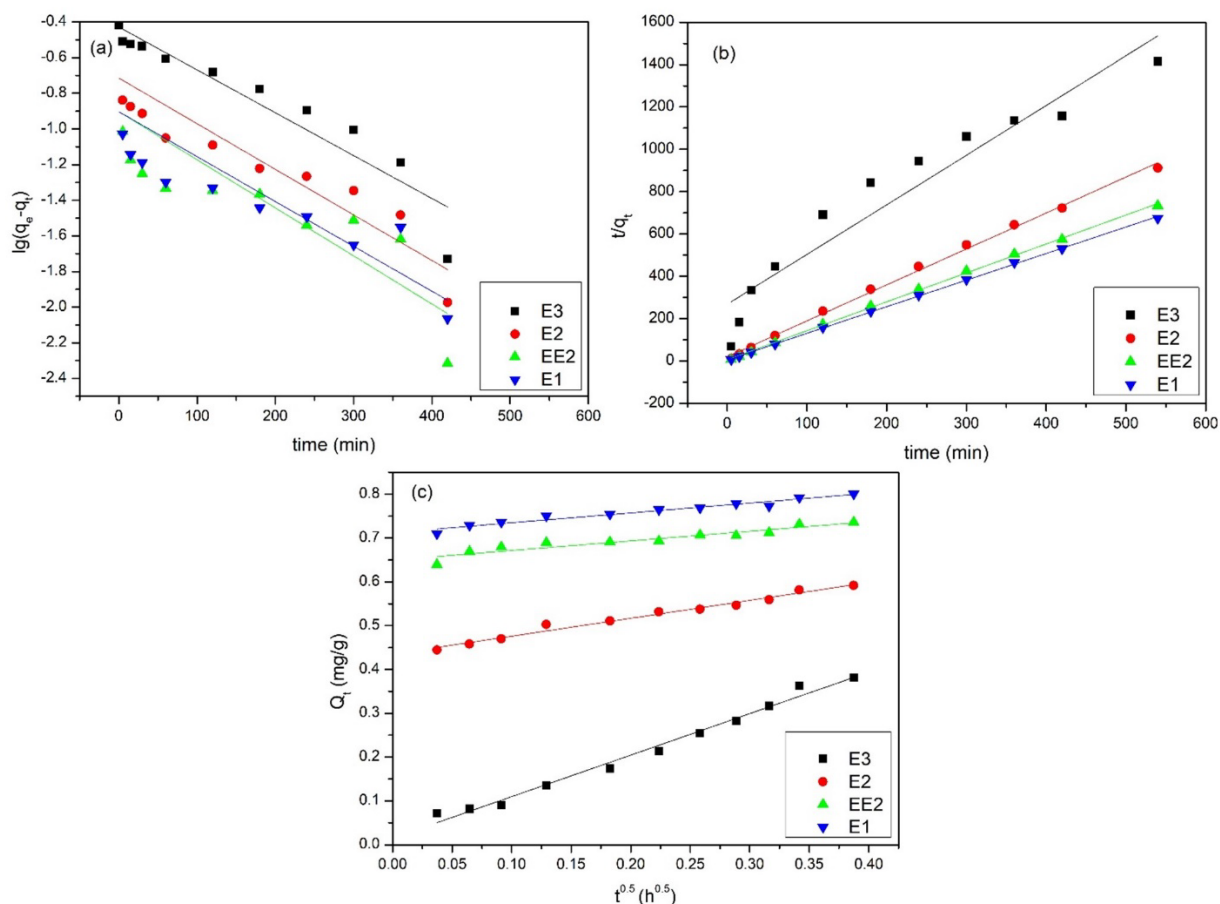


Figure 5.6: Plots of the adsorption kinetics for the four estrogenic hormones (E1, E2, EE2, E3) on PU Elastollan nanofibers: (a) pseudo-first-order, (b) pseudo-second-order, (c) the Weber-Morris intraparticle diffusion model.

The results were examined to obtain fits for the adsorption kinetics of the adsorbate mixture of E1, E2, EE2, and E3 EH on the adsorbent nanofibers by plotting on graphs the pseudo-first-order, pseudo-second-order, and Weber and Morris intraparticle diffusion models. Figure 5.6a shows $\lg(q_e - q_t)$ plotted against t for the E3 hormone, which is in good compliance with the pseudo-first-order equation. The data points are shown together with generated lines for best fits. The agreement between the data set is reflected in the high regression coefficient (0.901) for E3 compared to the other three hormones (E2, EE2, and E1), with the regression coefficients 0.793, 0.630, and 0.619, respectively. The equilibrium adsorption capacity calculated for E3 (0.373) is reasonable compared to the experimental value (0.382). The rate constant k_1 is far more similar, though, and within the range for all hormones. For E2, EE2, and E1, however, this model appears to be less accurate for describing the initial stage ($t \leq 30$ min.), and the theoretical expected yield of 0.193, 0.125, and 0.125 seems unsatisfactory and

much lower than the actual values of 0.592, 0.736 and 0.801 for E2, EE2, and E1, respectively.

The lines plotted in Figure 5.6b of t/q_t vs. t have to be linear to estimate q_e and k_2 from the curve and y-intercept, respectively. The results indicate that the interaction of E2, EE2, and E1 with the material followed second-order kinetics, as shown by the line for best fit adhering fully with the data set points. The regression coefficients are greater than 0.99, and the calculated adsorption capacities of 0.589, 0.733, and 0.796 are incredibly close to the experimental values of 0.592, 0.736, and 0.801, respectively. This suggests that the active sites were not homogeneous on the surface since the rate of adsorption is determined by two factors – the concentration of the hormones and the number of active sites available on the material [137]. These findings confirm the suitability of this model for describing the adsorption of E2, EE2, and E1 on the PU Elastollan nanofibers. Similar results were observed for the other polymers in this study compared with results described in the literature for MWCNTs [112]. E3 exhibits an overall mismatch, though, as two linear portions are visible – one for the first 60 min and another for the period after 100 min. The plot in Figure 5.6b was applied to determine the rate constant (k_2) and the calculated equilibrium adsorption capacity (q_e) expressed in Eq. (4.2) to obtain the regression coefficient (R^2) shown below in Table 5.2.

In the case of q_t vs. $t^{0.5}$, the graph for E3 is linear in progression with a comparatively high and acceptable regression coefficient (0.987) that almost passes through the point of origin. This means that intraparticle diffusion constitutes the rate-limiting step, which is unlikely to happen in the adsorption of the other three hormones (see Figure 5.6c). The plots for the other estrogens do not pass through the point of origin, potentially due to a surface effect that may have controlled the sorption process during the initial time periods, representing a diffusion-controlled or boundary-layer diffusion effect. Thus, for E2, EE2, and E1, intraparticle diffusion could comprise part of the mechanism, though not a step for determining the total rate of diffusion. The values calculated by Eq. (4.7), (4.8), and (4.9) are given in Table 5.2.

Table 5.2: Values for each hormone from the kinetic models in relation to PU Elastollan electrospun nanofibers

Hormone	Experimental	Pseudo-first-order model			Pseudo-second-order model			Intraparticle diffusion model		
		q_e (mg/g)	k_1 (min^{-1})	q_e, cal (mg/g)	R^2	k_2 (g/mg min)	q_e, cal (mg/g)	R^2	k (mg/g $\text{h}^{1/2}$)	I (mg/g)
E3	0.382	0.002	0.373	0.901	0.020	0.426	0.924	0.947	0.015	0.987
E2	0.592	0.003	0.193	0.793	0.145	0.589	0.998	0.406	0.436	0.983
EE2	0.736	0.003	0.125	0.630	0.276	0.733	0.999	0.219	0.650	0.895
E1	0.801	0.003	0.125	0.619	0.286	0.796	0.999	0.228	0.711	0.946

5.5 Adsorption mechanism of EH on polyurethane nanofibers

The possible mechanisms that existed between the estrogens and nanofibers comprise the following: (1) size-exclusion; (2) physical adsorption of estrogens on the external surfaces and inside layers of the nanofibers due to their porous structures; (3) charge interactions between the estrogens and electrospun nanofibers; (4) the bonding of estrogen molecules onto the nanofibers via reaction with the functional groups present on the surfaces of the nanofibers. Size exclusion would not be expected in this system as the reported molecular size of the estrogens was quite small (approximately 0.8 nm for E1 and 0.796 nm for E2), compared to the pore sizes of the electrospun nanofibers and GMF filter used; otherwise, their removal efficiency would have been 100%. As the fiber diameters of the polyurethanes were lesser in size (PU 918 = 174 ± 56 , PU Elastollan = 179 ± 45), their surface area is larger as a consequence (20.9 and 18.3, respectively), providing sufficient availability of active sites for adsorption of the estrogens, as detailed in Table 5.1. Electrostatic charge can also affect adsorption, as Porter and Porter report in the literature on adsorption behavior on microfilters in the presence of cations [138]. The deprotonation of E1, E2, EE2, and E3 is governed by the dissociation of the hydroxyl group attached to the benzene ring. The acid dissociation constants for E1, E2, EE2 and E3 equal 10.34, 10.46, 10.4, and 10.38,

respectively [139,140]. All of them have slightly weaker acidity than phenol ($pK_a = 10$). As a result of the high value of pK_a , most of the molecules of the estrogens were undissociated, and thus, they remained neutral in the solution mixture [42]. Therefore, it is unlikely that charge interaction was the main factor that brought about the significant adsorption of the EH on the nanofibers [39,141].

The high and rapid adsorption of the estrogens on the polyurethanes is noteworthy. The molecules were far smaller in size than the porosity of the nanostructures, indicating that pore size had a negligible dependence on adsorption. Apart from physical adsorption, which gradually reaches equilibrium, the only rational explanation for the strong interaction of these estrogens with the nanofibers is bonding. Hydrogen bonds are stronger than Van der Waals forces involved in physical adsorption. In this context, Figure 5.7 presents the chemical interactions of each estrogen with the polyurethane molecule.

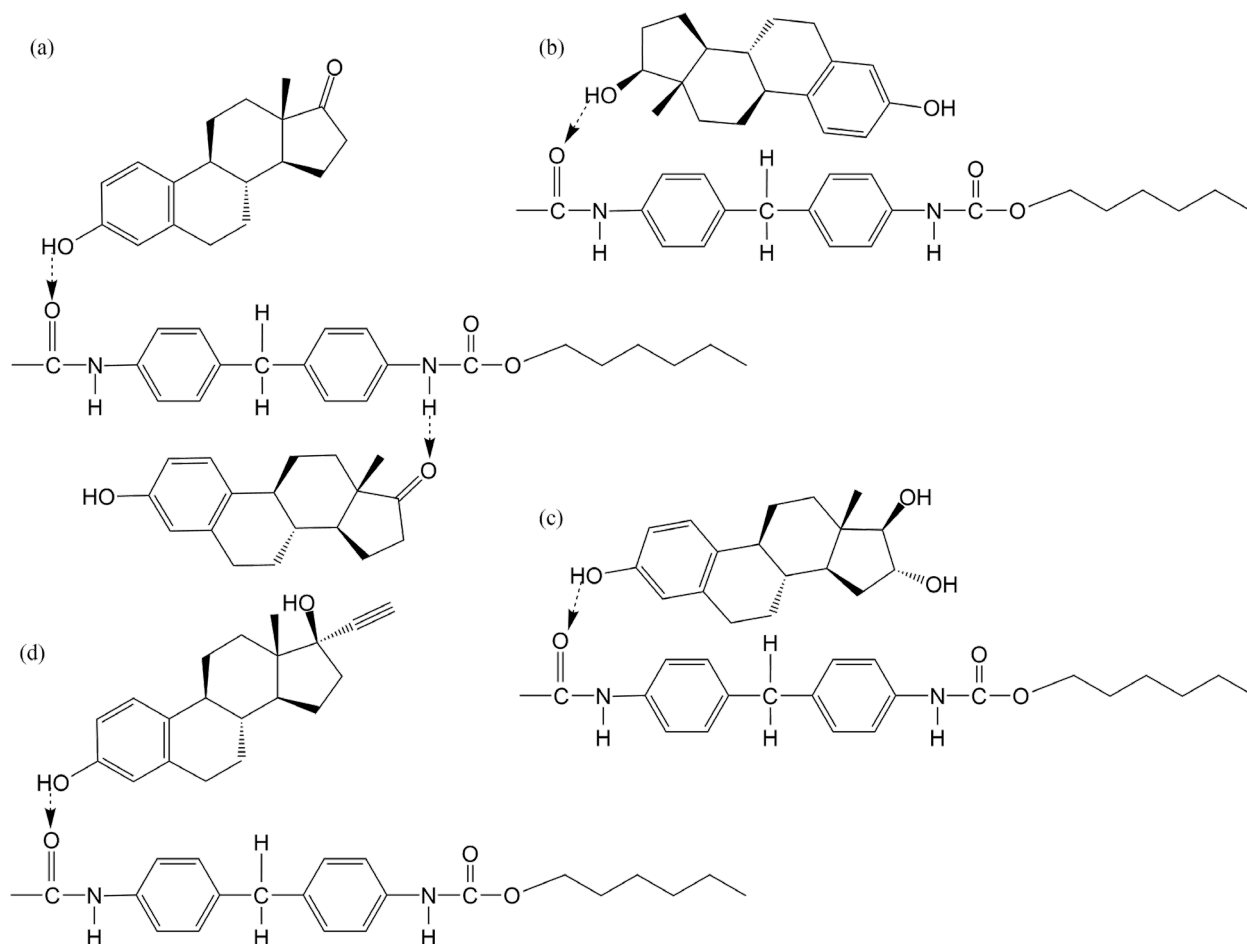


Figure 5.7: Hydrogen bonding between the polyurethane molecule and estrogenic hormones (a) E1, (b) E2, (c) E3, and (d) EE2.

Each estrogen molecule (E1, E2, EE2, E3) in this study contains a hydroxyl group (-OH) acting as a proton donor for hydrogen bonding. Due to the presence of both a nucleophilic carbonyl group (-C=O) and hydroxyl group in E1, this proton can act as both a donor or acceptor in hydrogen bonding and has the highest removal efficiency as a consequence. Han *et al.* describe similar hydrogen bonding by E1 with nylon 6,6 membrane in their research [39,127]. Nylon 6,6 and polyurethanes possess identical functional groups involved in hydrogen bonding. Therefore, the functional groups (N-H and C=O) in PU Elastollan, PU 918, and PA participated in the hydrogen bonding of E1, although only C=O was present for the other three estrogens, as determined by FTIR analysis. These hydrogen bonding interactions would dictate the adsorption of the estrogens on the polyurethane nanofibers, explaining the rapidity of the adsorption process in the initial stage of the experiment. The accurate technique of FTIR analysis was employed to characterize hydrogen bonds on the PU 918 polyurethane, as detailed below.

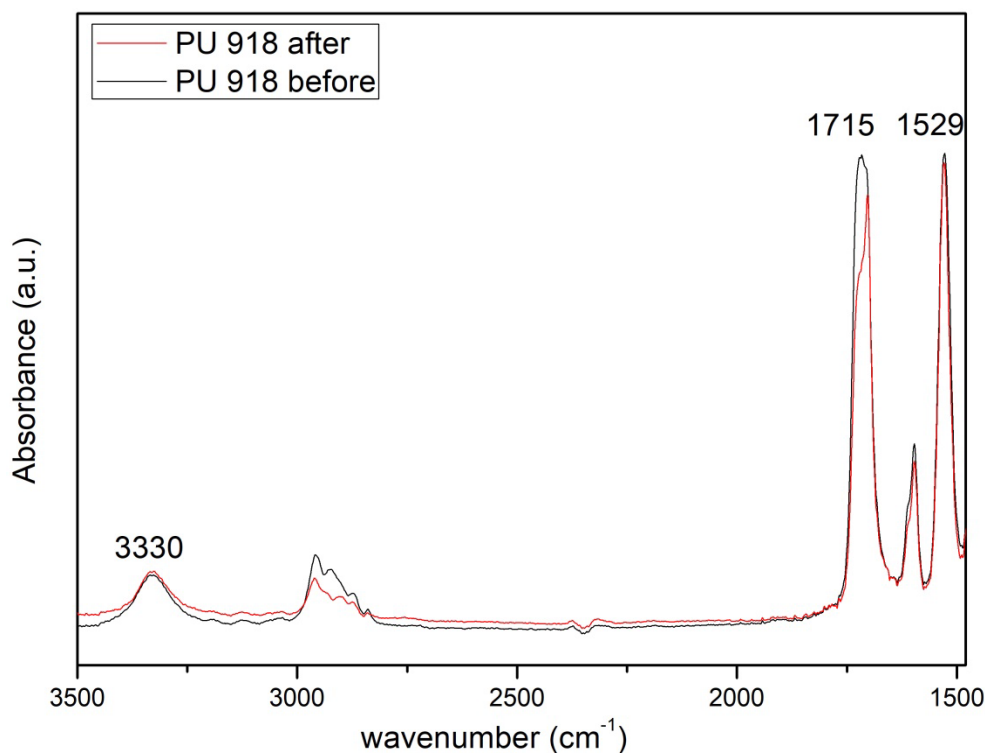


Figure 5.8: FTIR spectra for the PU 918 nanofibers before and after static adsorption (0.8 mg/L mixture of E1, E2, EE2, and E3 of 100 mL volume).

The FTIR spectra for a PU 918 sample saturated with estrogen are presented in Figure 5.8. A notable aspect is a difference in the relative intensity of the peak at 1715 cm⁻¹ that corresponds to C=O stretching. A crucial feature of PU 918 is its cross-linking molecular structure that arises through inter and intra-hydrogen bonds. The band contributes to restricting the stretching of the hydrogen bonds on

the carbonyl group in PU 918 and is evident from the shift of the peak to a reduced frequency of 1700 cm^{-1} . There is also a significant drop in intensity at 1715 cm^{-1} , yet this is not the case for two amide bands (at 3330 cm^{-1} and 1529 cm^{-1}), suggesting a change occurs through the adsorption of the EH. A possible explanation could be the presence of hydroxyl groups on the terminals of the estrogens that compete with -NH groups in acquiring the carbonyl groups present on the polyurethane; this potentially causes weak intermolecular hydrogen bonding, with eventual substitution by the estrogen molecules and the subsequent formation of new bonds.

No notable change occurs for the amide band (3330 cm^{-1}) after adsorption. A possible explanation is that the -NH groups are not set free to interact with hydrogen donors, such as the water and C=O groups of the cyclopentane rings present in E1 molecules, so it cannot forge new hydrogen bonds; otherwise, a new peak would be visible at ca. 3400 cm^{-1} [127]. Han *et al.* report that N-methyl acetamide (NMA), which possesses a simple structure with an amide group, does not interact with the -C=O group when released. The results given herein clearly agree with the study in the literature; thus, the estrogens (E1, E2, EE2, E3) under investigation might form hydrogen bonds with the polyurethanes and PA [141,142].

5.6 Determination of recovery and reusability of comparative electrospun nanofibers

Figure 5.9 presents the adsorption study over the four cycles.

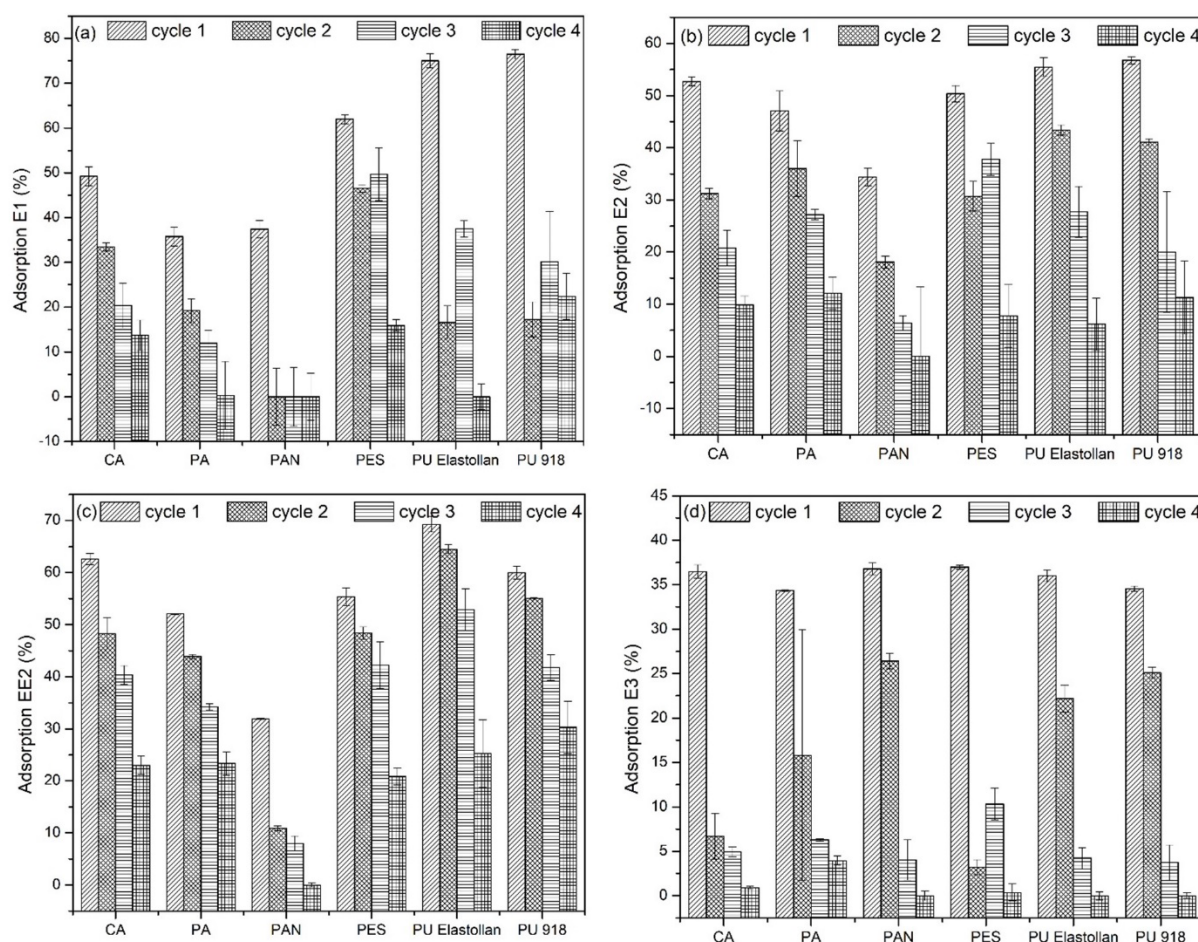


Figure 5.9: Four adsorption cycles for each electrospun material (20 mg) and each estrogenic hormone (a) E1, (b) E2, (c) EE2, and (d) E3, at an initial concentration of 0.2 mg/L in a combined solution of 0.8 mg/L.

The above graphs represent the removal of the hormones in percentage, present at 0.2 mg/L in concentration with 20 mg of each nanofiber adsorbent over four adsorption cycles. As can be seen, the trend is one of decrease for each material after consecutive cycles for all the hormones, except for PES during the second and third cycles as it underwent the least change in surface morphology; the change in average fiber diameter from the original size of 199 nm to 278 nm following ethanol treatment was not as large as for other polymeric nanofibers. The highest removal efficiency is evident for E1 and EE2, with the least for E3. The values for removal efficiency are similar for all the materials during the first cycle of E3. PA shows the least adsorption for E1 and E3, while PAN exhibits the least for EE2 and E2. Notably, PAN cannot be reused for E1 because of the significant effect that transpires during the desorption process, leading to a loss in mass, which brings about a decrease in the amount of active adsorption sites and a reduction in the surface area through an increase in fiber diameter.

PU 918 appears applicable for removing E1 and E2 during the first cycle, whereas PES and PU Elastollan are more suited to E3 and EE2, respectively. A drastic drop in the effectiveness of the materials for E1 and E3 arises during the second cycle, possibly related to the treatment with ethanol they received in the desorption process. However, this is unlikely to occur in the case of EE2 and E2, as the materials seem far more reliable over repeated cycles. It can be concluded that the adsorbent materials under investigation are reusable to a limited extent after being washed with ethanol, i.e., up to four adsorption cycles, with the exception of E3, with a limit of three cycles.

The comparison presented was conducted to discern the reusability of the nanostructured sorption materials. Industrial applications may require the testing of other solvents, and the findings reported herein indicate that the suitable solvent must possess very high solubility of hormones but minimum solubility of these polymers from which the nanofibers were made. Figure 5.10 shows the overall efficiency of each polymer over four adsorption cycles.

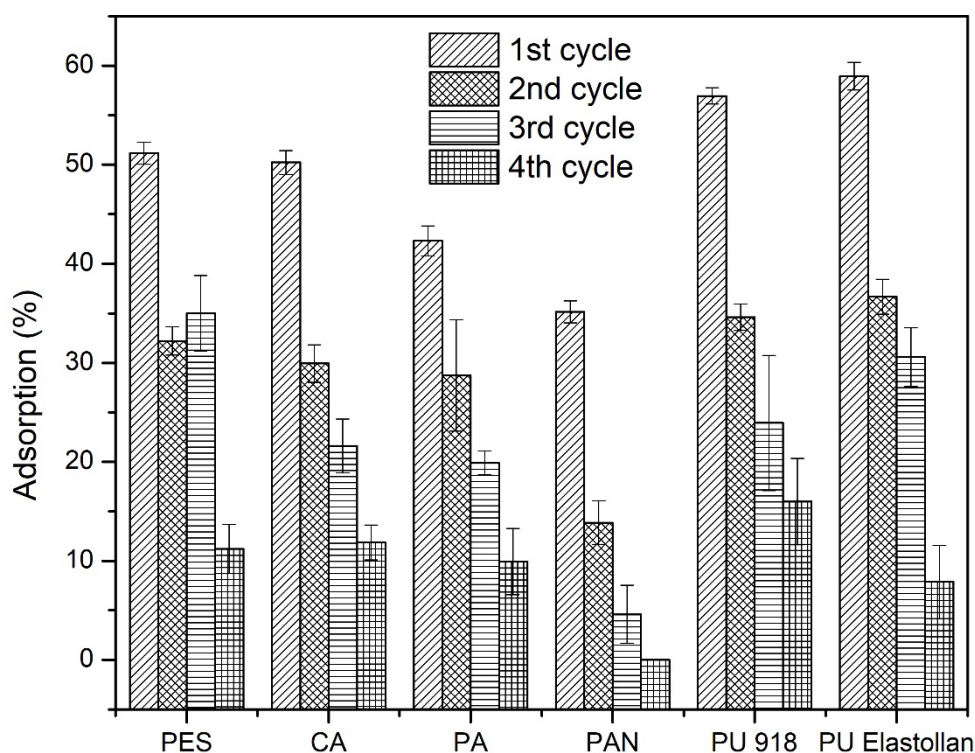


Figure 5.10: Cumulative efficiency of adsorption for the four estrogenic hormones on the various nanofibers over four cycles.

Figure 5.10 illustrates the adsorption efficiency of each polymer for cumulative EH removal over four adsorption cycles. It should also be noted that these percentages are for the mixture of E1, E2, EE2, and E3 for each polymer per cycle.

PU Elastollan demonstrates the highest extent of hormone removal in the first cycle, in contrast with PAN with the least, while PU 918 has the highest efficiency in the 4th cycle. PA exhibits the least drop in effectiveness from the first to the second cycle and better reliability. PES is the most consistent and manages the greatest adsorption in the 3rd cycle. It should be noted that due to repeated treatment with ethanol during desorption, it was evident that the nanofibers became stiff and shrank due to loss in mass until the last cycle. Compact and tightly folded, they provided less surface area for hormone entrapment during the final cycle, as shown in Figure 5.11.

The repeated desorption cycles of estrogen hormones from the nanofibers, wherein ethanol was applied, exerted a significant change in fiber morphology attributed to contact between the nanofibers and ethanol. The nanofibers of these materials are not prone to dissolving in ethanol, and their porous structure facilitates the complete penetration of ethanol molecules. This is why, after several cycles and a period of contact, the structure of the nanofibers collapsed and swelled, and the effectiveness of the adsorption process diminished, as is evident in the SEM images of the nanofiber structures after four cycles in Figure 5.11.

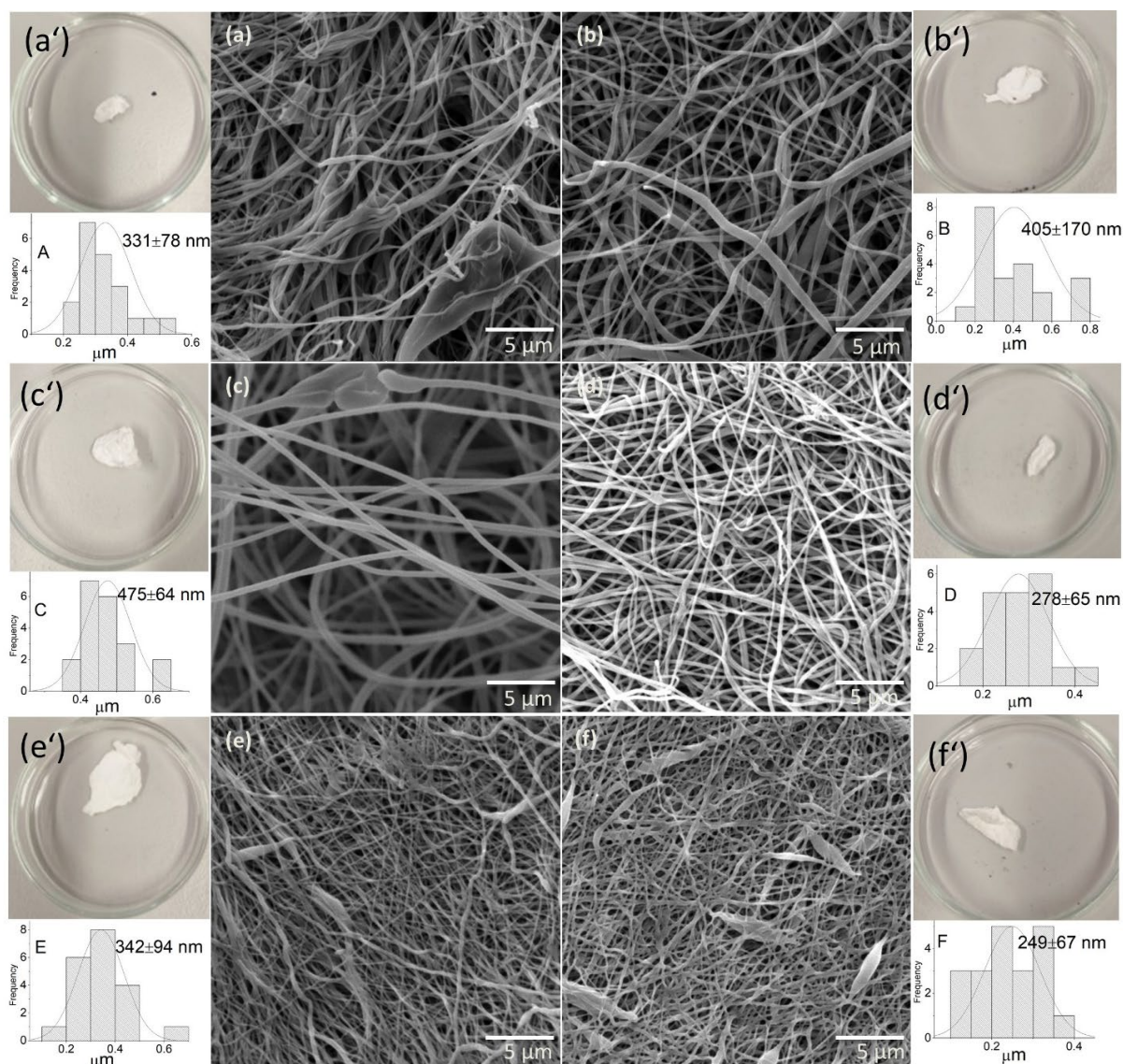


Figure 5.11: SEM Images, sample images of the nanofibers, and distribution of their fiber diameter after four adsorption-desorption cycles: (a, a', A) CA, (b, b', B) PA, (c, c', C) PAN, (d, d', D) PES, (e, e', E) PU918, and (f, f', F) PU Elastollan.

Figure 5.11 presents the surface morphology for each nanofiber after four adsorption-desorption cycles. It is visible that the diameter of the nanofibers increased for each type of polymer, ranging from 249-475 nm (PU Elastollan experienced the least, and PAN the highest), in comparison with the range in diameter prior to adsorption, which was 174-330 nm, respectively.

5.7 Limitations, future works, and practical application

This is a preliminary model study for testing various electrospun polymers for simultaneous adsorption of a set of four EH using ultrapure water. However, certain limitations exist that require extra investigation and improvement to devise

a continuous adsorption technique that functions at high pressures. Additionally, several aspects of the process that include membrane fouling, solution characteristics, varying concentrations of adsorbent, and adsorbate need to be addressed to make this process amenable for large-scale use. Future works shall encompass testing the electrospun materials with actual water samples from a reservoir. Doing this would enable the authors to observe the competing behavior and influence of inorganic ions and organic pollutants on entrapping estrogens during continuous adsorption by dead-end flow and cross-flow measurements. A similar concept for research could involve varying the pH, temperature, ionic strength, and concentration of adsorbent and adsorbate in order to discern the optimum applicability of kinetics and determine thermodynamic parameters. These matters will be subjected to in future research.

5.8 Conclusions

This study investigated the simultaneous removal of various EH by polymeric electrospun nanostructures. A one-step group detection method was devised for concurrent quantification of the EH. It was found that all the nanofibrous membranes were capable of successfully removing all types of estrogens. Overall adsorption efficiency diminished in the following order: PU Elastollan >PU- 918 >PES >CA >PA >PAN. The chemical composition and functional groups in the structure of the nanofibers played a major role in possessing hydrogen bonds between different types of estrogens and nanofibers, elaborated in the adsorption mechanism. The percentage efficiency of removal was the greatest for E1 (76.5), declining through EE2 (69.3) and E2 (56.8) to E3 (37.0). PU Elastollan demonstrated the highest capacity for total adsorption over the other NF membranes and also compared to literature values, equaling 2.51 mg/g due to its carbonyl functionality and surface area. Based on results from kinetic models for all the polymers, pseudo-first-order is applicable for E3, with pseudo-second-order being suitable for E1, E2, and EE2; the exception is PAN, where the estrogens follow the pseudo-first-order kinetic model. Consequently, both models are considered appropriate due to their high regression coefficients compared to other kinetic models. Desorption tests to discern the recovery of the hormones and the reusability of the sorption nanostructures were conducted and found to be valid for four cycles. The research carried out shows that polymeric nanofibrous membranes are worthy of consideration as potential adsorbents for the simultaneous removal of estrogens from wastewater streams.

6. Adsorption of estrogenic hormones in aqueous solution using electrospun nanofibers from waste cigarette butts: Kinetics, mechanism, and reusability

Herein, this chapter aims to prepare waste cigarette electrospun nanofibers (WCENFs) for the batch adsorption of four EH (E1, E2, E3, and EE2). The nanofibers are based on small fiber diameter formation to achieve high surface area and aspect ratio, thereby creating more sites available for adsorption. The objective is to focus on single and simultaneous adsorption of various EH in a one-step process. Further, to investigate the feasibility of the results using the experimental data, adsorption capacity and apply different kinetic models such as pseudo-first-order, pseudo-second-order, intraparticle diffusion, elovich, and fractional power models for evaluation. These models help to understand the characteristics of adsorption kinetics that are essential for the selection of optimum conditions for the large-scale removal application of EH. The study also includes establishing the fibers' adsorption mechanism to understand interactions between WCENFs and EH. Then, the reusability in several adsorption-desorption cycles to assess the reliable effectiveness of this material. Finally, a comparative study on the instant adsorption efficiency of PET/WCENFs (Polyethylene terephthalate) syringe film against commercially available CA syringe film to analyze their performance. The schematic display in Figure 6.1 shows the method of nanofibers preparation via electrospinning technique and batch adsorption study in the form of nanofibers and syringe film.

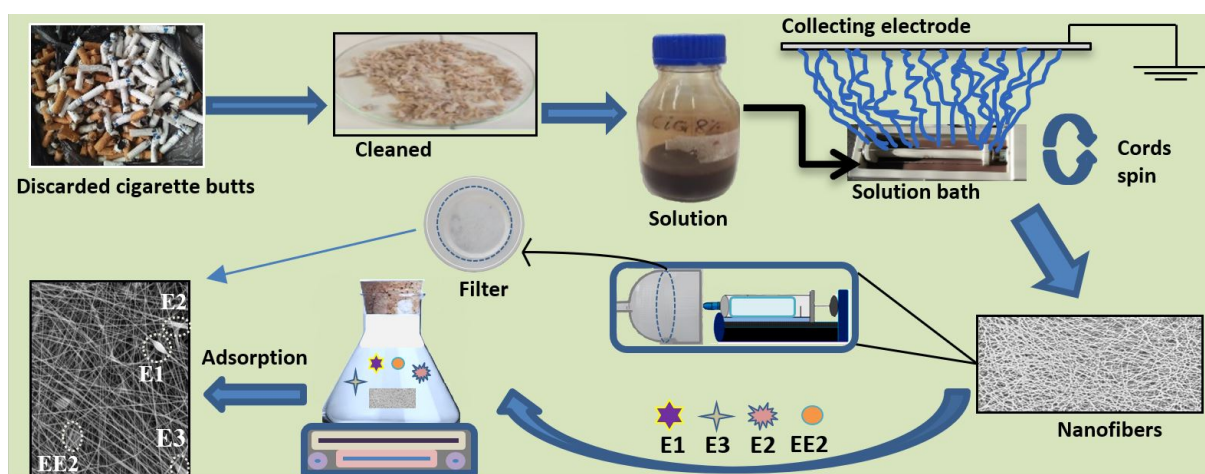


Figure 6.1: schematic representation of fabrication of WCENFs used for simultaneous removal of EH by batch adsorption test and instantaneous syringe film test.

6.1 Characterization of WCENFs

SEM imaging was carried out for morphological analysis of the electrospun fibers.

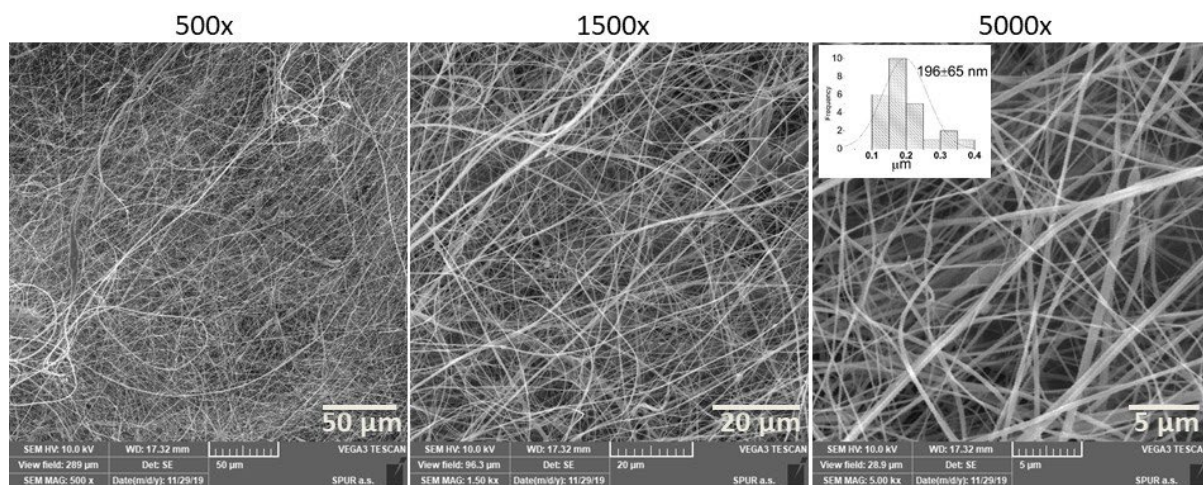


Figure 6.2: SEM micrograph and (inset) size distribution for WCENFs at different magnifications of 500x, 1500x, and 5000x.

Figure 6.2 illustrates that uniform submicron fibers were produced with minimum possible beads and a relatively narrow fiber diameter distribution of 196 ± 65 nm compared with the CA having 224 ± 35 nm and a calculated surface area of $13.6 \text{ m}^2/\text{g}$ [143]. This indicates that WCENFs possess a higher surface area of $15.5 \text{ m}^2/\text{g}$ (Table 6.1) and more available adsorption sites. The such low average diameter is attributed to properties mentioned in Table 3.1: lower intrinsic viscosity, low polymer concentration in the solution, and high electrical conductivity prior to electrospinning, which has led to the development of a high surface area of WCENFs. Also, the molecular properties calculated from GPC were $M_n = 90,000$, $M_w = 210,000$, and $PDI = 2.3$. To further understand the physicochemical properties of the structure, XRD results revealed a broad single peak near $2\theta = 15^\circ$, which denotes that WCENFs are semi-amorphous by nature [113]. The functional groups are further discussed in FTIR. The mean diameter of pores in the submicron structure was $1.4 \mu\text{m}$, and the maximum pore diameter was $2.2 \mu\text{m}$. The permeability of the submicron structure for the dry air was $247 \text{ L}\cdot\text{min}^{-1}\cdot\text{bar}^{-1}\cdot\text{cm}^2$. Also, the results from the TGA thermograph showed no material degradation was observed up to 110°C , and the degradation temperature was found to be 355.7°C [144]. The initial dip in DSC thermogram could be due to evaporation of water and the graph revealed that the glass transition temperature (T_g) of WCENFs was well above standard room operating

temperatures (~180 °C) and given that the material’s degradation range started around 250 °C and was spread over a wide range. The thermogram indicates that the material was thermally stable; therefore, these fibers would not be subjected to any softening and deformation at room temperature during the whole adsorption study [135,145].

ImageJ analysis software obtained the average diameter of fibers observed through SEM. The calculated diameters from the SEM images, calculated fiber length, surface area using the formulas in experimental design, the surface area measured by BET, and porosity by porosimetry are shown in Table 6.1.

Table 6.1: Characteristics values of WCENFs calculated using SEM micrographs, BET, and porosimetry

BET before adsorption		BET after adsorption		Porosimetry		Fiber analysis from SEM	
Surface area (m ² /g)	18.05	Surface area (m ² /g)	3.61	Mean pore size (μm)	1.4	Average fiber diameter (nm)	196 ± 65
Mean pore diameter (nm)	13.49	Mean pore diameter (nm)	17.19	Maximum pore size (μm)	2.2	Fiber length per unit mass calculated (m/mg)	25105
Total pore volume (cm ³ /g)	0.061	Total pore volume (cm ³ /g)	0.016	Air permeability (l/cm ² .min.bar)	247	Calculated surface area (m ² /g)	15.5

The geometrically determined surface area based on SEM compared to that by BET analysis is well in compliance. The BET surface area is well comparable to the literature values in the range of 9-51 m²/g and the average fiber diameter of 167-2737 nm [32]. The calculated surface area from the average fiber diameter (196 ± 65 nm), considered as a cylindrical shape, calculated from SEM is 15.5 m²/g. The actual surface area measured from BET is 18.05 m²/g which is slightly higher. The plausible reason for the lower calculated surface area value based on geometry compared with the BET value could be due to a much lower density

than the bulk polymer density because of pore formation and other effects during electrospinning. The presence of pores on the fibers' surface is confirmed by BET mean pore diameter (13.49 nm). Furthermore, the estimated surface area is based on the assumption that the fibers have a smooth surface without pores. In reality, solvent evaporation during electrospinning has resulted in a smaller diameter of fibers seen from the SEM micrograph (Figure 6.2), which has resulted in increased surface area. We can also see that the surface area of fiber decreased after four adsorption cycles from 18.05 to 3.61 m²/g due to interaction with ethanol during desorption cycles that caused swelling (discussed in detail in the reusability section). However, the mean pore diameter increased from 13.49 to 17.19 nm due to the wear-off of material during several desorption cycles. Still, a reduced total pore volume was observed from 0.061 to 0.016 cm³/g, which justifies the adsorption and entrapment of hormones in the fibers during interaction in the batch adsorption study.

The contact angle was measured to determine the hydrophilicity of the fibers. WCENFs mainly contain CA, which has polar hydroxyl groups. Thus, CA is hydrophilic by nature [129]. We observed both the liquids penetrated the WCENFs on PP completely. Therefore, WCENFs were compressed on a PET sheet, and they exhibited contact angle values of 14.6 ± 3.3 with water and 87.3 ± 0.8 with glycerol. It is generally agreed that a hydrophilic surface shows a low water contact angle ($\theta < 90^\circ$). It is reported that the surface roughness, average fiber diameter, and concentration of the polymer in the solution before electrospinning also have a direct influence on the wetting properties [105,129]. The reported electrospun CA in the literature had a water contact angle of $22.2 \pm 0.9^\circ$, which is higher compared to the water contact angle of WCENFs ($14.6 \pm 3.3^\circ$) in the current study; This indicates that WCENFs are slightly more hydrophilic compared to electrospun CA in literature [143]. The investigated WCENFs in the present research possess a low contact angle which indicates high hydrophilicity. The hydrophilic nature of WCENFs provides feasibility to the fibers to interact with EH in water and supports the adsorption process because the stronger interaction between EH and WCENFs is due to the hydrogen bonding interaction and Van der Waals forces which essentially requires the hydrophilic nature of the fiber [146].

To see the mechanical properties of WCENFs, the stress vs. strain graph below explains Young's modulus, ultimate tensile strength, maximum elongation before fracture, and stress at breakage.

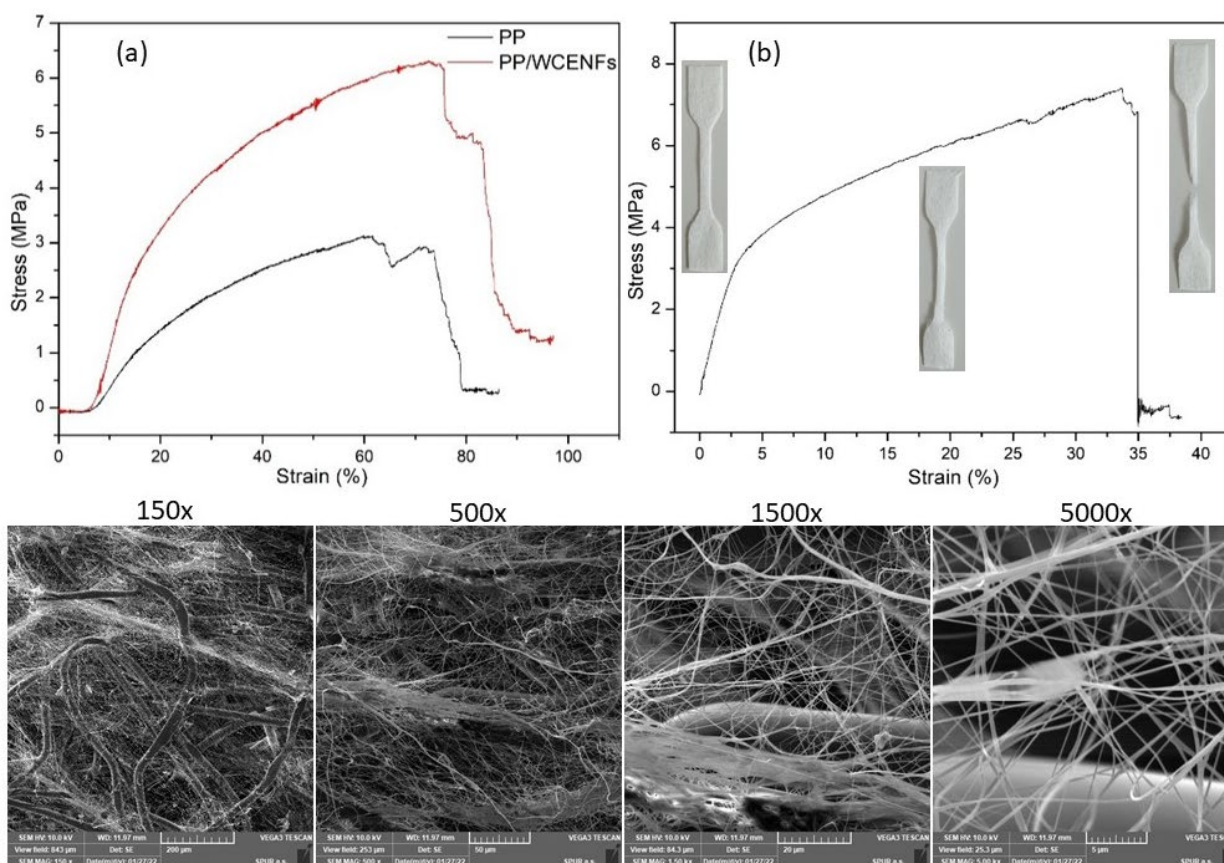


Figure 6.3: Stress vs. strain curves for (a) PP and PP/WCENFs, and (b) PET/WCENFs along with micrographs after breakage at a different magnification of 150x, 500x, 1500x, and 5000x.

Figure 6.3 demonstrates the stress vs. strain curve of PP and PP with WCENFs up to the breaking point. It can be seen that Young's modulus has increased from 8.9 to 28.8 MPa, which is evident from the steep slope in the graph, and the ultimate tensile strength has improved to almost 122% (3.1 to 6.9 N/mm²). Similarly, a slight increase in stress at breakage from 0.4 to 1.4 MPa and the total elongation from 19.3 to 19.9 mm was observed, showing that the difference between the two values in each case determined the value of that physical quantity of WCENFs. Similar values of the mechanical properties of electrospun fibers were reported in the literature [147].

However, throughout the batch adsorption study, WCENFs were used alone after peeling off from the PP sheet, which was only used for the collection of fiber. Herein, PP was used as a support material for measuring mechanical properties as alone WCENFs were too fragile and could not maintain shape after peeling off owing to their weak inter-fiber adhesion [147], low average area mass (0.865 g/m²), and thickness (0.003 mm) compared to CA spun fibers with 1.630 g/m² and

0.005 mm, respectively. The mean values for each sample are reported below in Table 6.2.

Table 6.2: Summary of mechanical properties of the WCENFs with substrates

Materials	Thickness (mm)	Young's Modulus, E (Mpa)	Ultimate Tensile Strength, σ (N/mm ²)	Elongation at break, ϵ (mm)	Stress at Break (MPa)
PP	0.14±0.01	8.9±4.3	3.1±1.0	19.3±5.1	0.4±0.2
PP/WCENFs	0.17±0.01	28.8±2.4	6.9±1.2	19.9±0.7	1.4±0.2
PET/WCENFs	0.14±0.01	109.0±23.1	7.5±0.9	8.6±1.3	0.10±0.4

Similarly, the mechanical properties were observed for the fabricated PET/WCENFs syringe film, and an improvement in strength and Young's modulus were reported to be 7.5 N/mm² and 109 MPa, respectively. PET/WCENFs film was used for the syringe adsorption test to compare the removal percentage with the commercial CA syringe film. Herein, WCENFs were embedded on a PET sheet of a thickness of 0.43 mm by the thermal press. The significant increase in each mechanical property is illustrated in Table 6.2, and micrograph images at different magnifications are represented in Figure 6.3 to see the behavior at the time of fracture. It can be seen that the strength for elongation is primarily provided by the PET sheet, which breaks following the ductile failure, whereas WCENFs were relatively brittle. They gradually broke after a slight elongation when the fiber chain straightened up (evident at 500x and 1500x magnification) owing to their non-woven and non-crosslinked structure [148]. It can be seen that only a few fiber treads remained intact over a long elongation. The results also reveal that the PET/WCENFs film can be used for continuous filtration removal of hormones in future research.

6.2 Batch adsorption study of EH on WCENFs

The study of four EH (E1, E2, EE2, E3) was conducted with a total concentration of 0.8 mg/L and 20 mg of WCENFs. Figure 6.4a below shows the batch adsorption study of each hormone on WCENFs for a period of time till no further significant adsorption was observed and the material reached almost saturation.

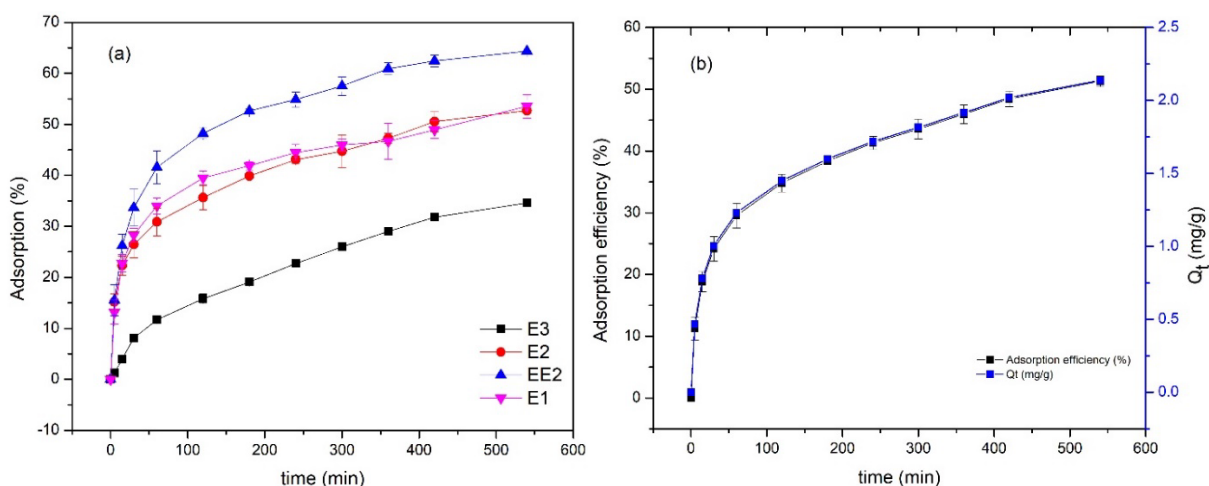


Figure 6.4: (a) Batch adsorption study of each EH on WCENFs from a combined solution, (b) Cumulative adsorption removal efficiency as a function of time of EH (E1, E2, EE2, E3) together on WCENFs on the primary y-axis, and the total adsorption capacity (Q_t) of WCENFs as a function of time on the secondary y-axis.

Figure 6.4a depicts WCENFs adsorption behavior with each hormone, and as can be seen, the ascending order of adsorption of EH is as $E3 < E2 < E1 < EE2$, with removal efficiencies of 34.6%, 52.7%, 53.6%, and 64.3%, respectively. WCENFs showed the best sorption of EE2 and the worst sorption of E3 hormone. It could also be concluded that WCENFs can readily adsorb EE2, E2, and E1, while gradually adsorb E3. The low percentage removal of E3 could be attributed to its low $\log K_{ow}$ value, 2.45, compared to E1, E2, and EE2; 3.43, 3.94, and 4.15, respectively. $\log K_{ow}$ is a parameter used to determine the value of hydrophobicity for EH by measuring the partitioning between water and octanol. The values ranged between -3 (very hydrophilic) and $+10$ (extremely hydrophobic). Generally, the values above 2.5 indicate that the material would accumulate in the solid phase and not be dissolved in an aqueous medium. Therefore, its interaction with the membrane would be hydrophobic. High $\log K_{ow}$ values tend to adsorb more readily to organic matter because of their low affinity for water [146]. The adsorption of these estrogens is directly dependent on their hydrophobic nature, which is specified by the higher value of K_{ow} [120]. Furthermore, E3 follows a different kinetic trend than the other EH because the adsorption is gradual throughout the experiment. While for other EH, most of the adsorption occurs within 30 min from the starting time. WCENFs have similar adsorption behavior for all EH compared to the CA fibers, which also follow adsorption efficiency in decreasing order of $EE2 > E1 > E2 > E3$. However, the removal efficiencies of EH with WCENFs are more significant than CA

electrospun fibers [143]. Hence, it can be concluded that electrospun WCENFs can be sufficiently responsible for the adsorption of each EH simultaneously.

Figure 6.4b above shows the percentage of total cumulative adsorption of EH on WCENFs and the total adsorption capacity of WCENFs in a given time. The results show that the total equilibrium removal efficiency lies at 51.3%. It is evident from the graph that WCENFs had a high adsorption tendency and fast adsorption rates reaching nearly half of their efficiency within the first 30 min, as represented by the steep initial slope of the graph corresponding to the removal efficiency mark of about 25%. However, the trend of the gradient changed from steep to steady after almost 60 min of the continuous adsorption experiment and remained the same till the end.

The total adsorption capacity (Q_t) as a function of time is also demonstrated in Figure 6.4b with a secondary y-axis. The results indicate that the cumulative four EH adsorption capacities increased similarly for WCENFs until equilibrium was established between the adsorbates and adsorbent. The time to reach equilibrium depends on the concentration of adsorbate and the amount of adsorbent. Both factors were kept constant to compare the capacities with the literature. However, it was still necessary to increase the amount of adsorbent to enhance the removal efficiency in a lesser time. The equilibrium adsorption capacity of WCENFs was found to be 2.14 mg/g, and adsorption capacities of E1, E2, EE2, and E3 were found to be 0.551, 0.532, 0.687, and 0.369 mg/g, respectively. Compared to the literature, Yasir *et al.* in previous research (chapter 5) reported the equilibrium adsorption capacity of CA to be 2.095 mg/g and individual adsorption capacities of E1, E2, EE2, and E3 to be 0.506, 0.532, 0.668, and 0.389 mg/g, respectively [143]. Therefore, the results of WCENFs are well in the range and strongly comply with the literature values of CA, which indicates that WCENFs are better in adsorption than electrospun CA fibers. Additionally, the as-prepared WCENFs are a cost-effective and efficient substitute.

Additionally, in the previous work, the highest equilibrium adsorption capacity was observed for PU Elastollan at 2.51 mg/g and the lowest for PAN at 1.51 mg/g. Furthermore, the reported adsorption capacities for E1, E2, EE2, and E3 were 0.801, 0.592, 0.736, and 0.382 mg/g for PU Elastollan and 0.396, 0.370, 0.343, and 0.397 mg/g for PAN, respectively [143].

Moreover, EE2 was found to have a strong affinity for adsorption as a result; the highest adsorption capacity compared to the other three EH for all the other

polymers mentioned in the literature. The adsorption capacities for MWCNTs in the literature were found to be 0.423 mg/g, 0.472 mg/g, and 0.472 mg/g, and for the activated sludge were 2533.34 ng/g, 2020.78 ng/g, and 2234.09 ng/g for E1, E2, and EE2, respectively, which are lower values compared to the current research. Furthermore, the value for removing E1 was 62 ng/g when a hydrophobic hollow fiber membrane was used [120]. Thus, comparing the present study's adsorption capacity with the previous research works proves the suitability of WCENFs as a potential adsorbent for removing these EH, comparing the other solid particles and membrane adsorbents. Hence, it is evident that WCENFs have a pretty high adsorption capacity and is a useful polymeric material for reusing it for these EH adsorptions.

6.3 Adsorption kinetics of EH on WCENFs

The removal of EH on WCENFs by adsorption increased with time, obtaining a maximum value for reaching equilibrium. The adsorption rate was fast initially until 30 min and gradually decreased as the contact time increased to an assumed plateau at 540 min.

The adsorption kinetic plots for the adsorption of four EH on WCENFs are shown in Figure 6.5, and the obtained kinetic parameters from the models mentioned above are presented in Table 6.3.

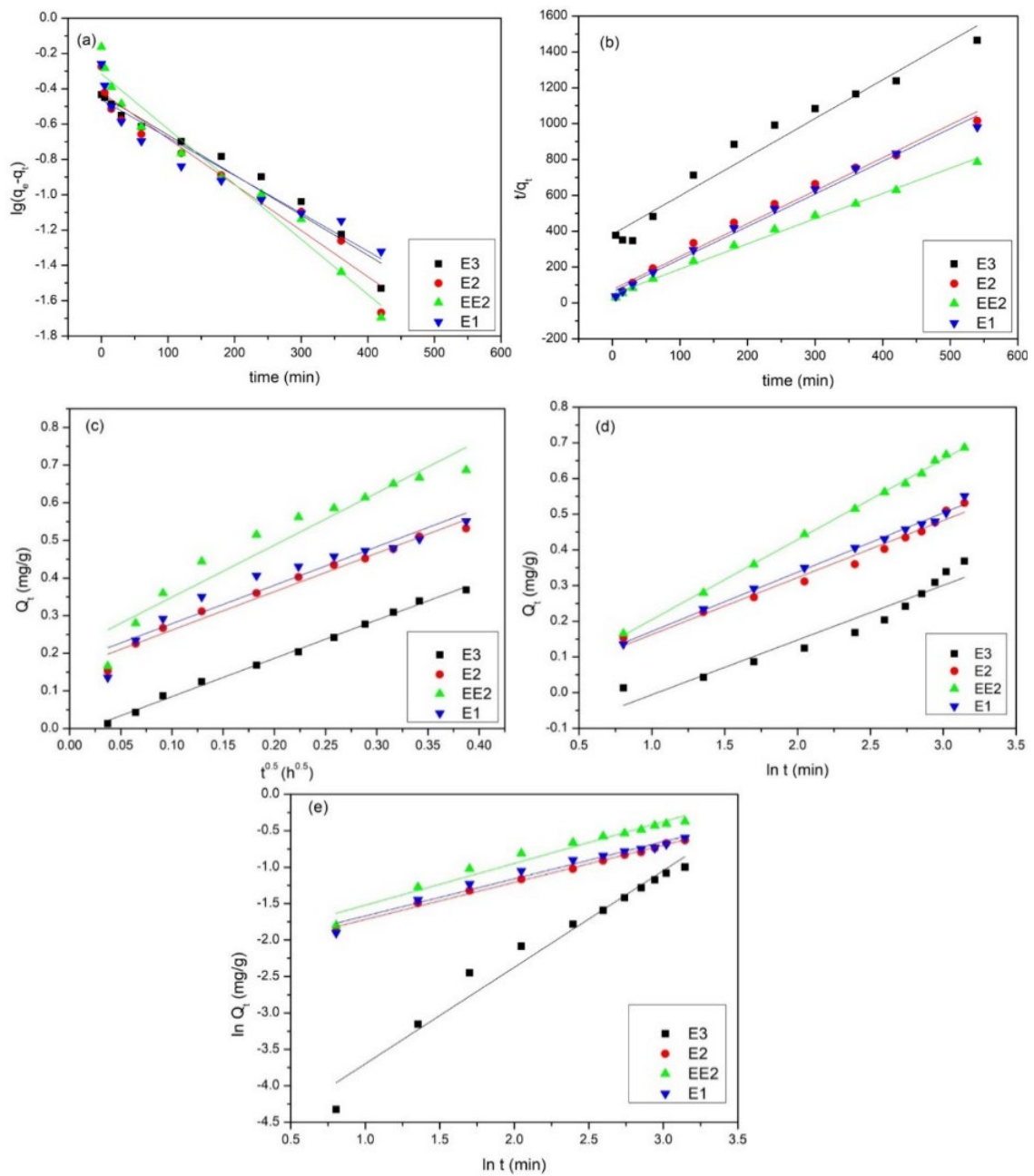


Figure 6.5: Adsorption kinetics plots of four EH (E1, E2, EE2, E3) on WCENFs, (a) Pseudo-first-order, (b) Pseudo-second-order, (c) Weber-Morris interparticle diffusion model, (d) Elovich model, and (e) Fractional power model.

The results were examined to obtain adsorption kinetics fits of the adsorbate mixture of E1, E2, EE2, and E3 EH on the adsorbent fibers using several model plots. In Figure 6.5a, the plotting $\ln(q_e - q_t)$ vs. t for E3 hormone shows good compliance with the pseudo-first-order equation. The data points are shown

together with the generated lines of best fit. The agreement between the data set is reflected by the high regression coefficient (0.962) for E3, and the equilibrium adsorption capacity calculated for E3 (0.368) is extremely close to the experimental value (0.369), which indicates that the predicted adsorption capacity by this model is almost the same as the actual value. The rate constant k_1 is similar and in the range for all EH. However, this model appears less accurate for E2, EE2, and E1 for describing the initial stage ($t \leq 30$ min). The theoretical expected yield of 0.350, 0.444, and 0.306 seems unsatisfactory and far less than the actual 0.532, 0.687, and 0.551 for E2, EE2, and E1.

The lines plotted in Figure 6.5b of t/q_t vs. t must be linear to estimate q_e and k_2 from the slope and y-intercept, respectively. The results indicated that the interaction of E2, EE2, and E1 with the material followed a line of best fit, completely matching the data set points. The regression coefficients are 0.99, and the calculated adsorption capacities of E2, EE2, and E1 are 0.544, 0.711, and 0.549 compared to the experimental values of 0.532, 0.687, and 0.551, respectively. The slight difference indicates that the active sites were not homogenous on the surface because the adsorption rate is determined by the hormone concentration and the number of active sites available on the material [137]. These findings confirm the suitability of this model for describing E1, E2, and EE2 adsorption on WCENFs. Similar results were observed when comparing the results described in the literature for MWCNTs by Al-Khateeb *et al.* [120]. Whereas E3 shows an overall non-linear trend; instead, two linear portions can be seen. One for the first 60 min and the second for the time interval after 100 min. The plot in Figure 6.5b was used to determine the rate constant (k_2) and the calculated equilibrium adsorption capacity (q_e) expressed in Eq. (4.2) to obtain the regression coefficient (R^2) shown below in Table 6.3.

Regarding Figure 6.5c of q_t vs. $t^{0.5}$, the graph for E3 is a linear plot with a comparatively high regression coefficient, but the plot does not pass through the origin. This specifies that intraparticle diffusion is not entirely the rate-limiting step, which is likely to happen in the adsorption of the other three EH as well, as shown in Figure 6.5c. The plausible reason for EH could be that they do not converge properly and the overall best fits do not pass through the origin; this could be due to a surface effect that may have dominantly controlled the sorption process after an hour of time interval and be considered a diffusion-controlled or boundary layer diffusion effect. Furthermore, two linear trends can be seen clearly. In the first 60 min, a sharper and steeper slope trend of a line is observed, which could pass through the origin and indicate that intraparticle diffusion is the

rate-limiting step in this region. While in the second region, the diffusion slows down, shown by a gentle slope because the lesser remaining concentration of EH is left in the solution. Thus, for E2, EE2, and E1, intra-particle diffusion can be part of the mechanism, but it can not be a total rate-determining step [120].

The plot in Figure 6.5d of q_t vs. $\ln t$ shows that EE2 has the highest regression coefficient (0.999), which explains that chemisorption is the most prominent mechanism for the adsorption of EE2 on WCENFs. This is also proven when EE2 had the most rapid adsorption (see Figure 6.4a) and the highest equilibrium capacity of 0.687 mg/g compared to the other EH.

In the case of Figure 6.5e of $\ln q_t$ vs. $\ln t$, a mismatch is seen for E3, while a linear relationship is seen for E1, E2, and EE2 but not for overall adsorption time. The regression coefficients are not satisfactory in most of the cases. This indicates that the fractional power model is not appropriate for EH. The calculated parameters using Eq. (4.7), (4.8), (4.9), (4.10), and (4.11) are shown in Table 6.3.

Table 6.3: The kinetic models' parameters with each EH using WCENFs

Models	Hormones			
	Estrone (E1)	β -Estradiol (E2)	17 α -Ethinylestradiol (EE2)	Estriol (E3)
Experimental q_e (mg/g)	0.551	0.532	0.687	0.369
Pseudo First Order model				
k_1 (min ⁻¹)	0.002	0.003	0.003	0.002
q_e, cal (mg/g)	0.306	0.350	0.444	0.368
R^2	0.951	0.958	0.977	0.962
Pseudo Second Order model				
k_2 (g/mg.min)	0.055	0.045	0.041	0.012

q_e , cal (mg/g)	0.549	0.544	0.711	0.464
R^2	0.991	0.988	0.995	0.966
Intraparticle diffusion model				
k (mg/g.h ^{1/2})	1.006	1.022	1.386	1.017
I (mg/g)	0.181	0.159	0.210	-0.017
R^2	0.931	0.975	0.926	0.996
Elovich Model				
α (g/mg.min)	14.964	12.962	7.414	1.636
β (mg/g.min)	0.081	0.080	0.112	0.077
R^2	0.994	0.979	0.999	0.930
Fractional power model				
A	0.113	0.108	0.123	0.007
B	0.255	0.255	0.286	0.663
Ab	0.368	0.362	0.409	0.669
R^2	0.973	0.994	0.967	0.969

6.4 Adsorption mechanism of EH on WCENFs

The four possible adsorption mechanisms between EH and the WCENFs could be (1) size-exclusion; (2) physical adsorption of estrogens on the external surface and inside layers of fibers due to their porous structures; (3) charge interactions

between EH and WCENFs; (4) Hydrogen bonding of EH molecules onto fibers by reaction with the functional groups present on the surface of fibers. Size exclusion is unexpected in this system because the reported molecular size of estrogens by Han *et al.* is quite small (approximately 0.8 nm for E1 and 0.796 nm for E2) than the pore sizes of the WCENFs (1.4 μm) and GMF film (0.45 μm) used. Otherwise, the removal efficiency would have been 100%. A smaller fiber diameter in WCENFs (196 ± 65 nm) leads to a larger surface area (15.5 m^2/g) that provides sufficient active sites for adsorption of EH on the fibers, as shown in Table 6.1. The electrostatic charge might also influence adsorption, as Porter and Porter already reported adsorption behavior on microfilms in the presence of cations [138]. The deprotonation of E1, E2, EE2, and E3 is governed by the hydroxyl group's dissociation attached to the benzene ring. The acid dissociation constants for E1, E2, EE2 and E3 are 10.34, 10.46, 10.4 and 10.38, respectively [140,146]. They all have slightly weaker acidity than phenol ($pK_a = 10$). As a result of the high value of pK_a , most of the molecules for all these estrogens are undissociated; thus, they stay neutral in the solution mixture. As a result, it is unlikely that the influence of charge interaction can be the main factor for the significant adsorption of these EH on the fibers [39].

The high and rapid adsorption of the EH on the WCENFs is particularly interesting. The size of molecules is far tiny compared to the porosity of this structure. Therefore, the pore size has negligible dependence on adsorption. Apart from the physical adsorption, which gradually reaches equilibrium, the only rational explanation is the strong interaction of these EH with the fibers due to the hydrogen bonding. Hydrogen bonds are more robust than the Van der Waals forces involved in physical adsorption. Figure 6.6 below shows the chemical interactions of each EH with the WCENFs molecule.

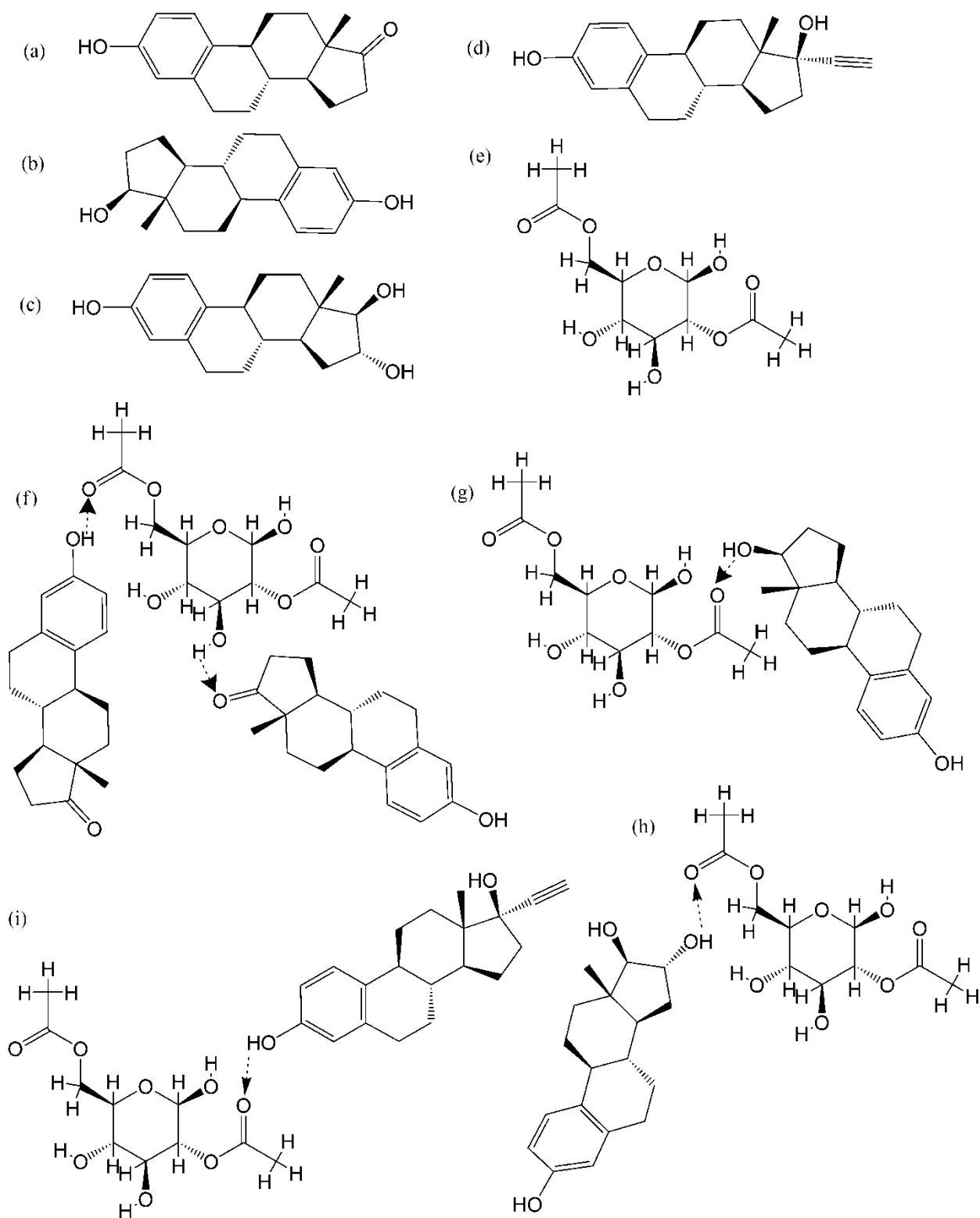


Figure 6.6: Displayed structures of (a) E1, (b) E2, (c) E3, (d) EE2, (e) WCENFs molecule and hydrogen bonding between WCENFs molecule with EH (f) E1, (g) E2, (h) E3, and (i) EE2.

The EH molecules (E1, E2, EE2, E3) in this study contain a hydroxyl group (-OH) acting as a proton donor for hydrogen bonding. Due to the presence of both

nucleophilic carbonyl group (-C=O) and hydroxyl group in E1, this proton can act as both donor or acceptor in the hydrogen bonding because CA also contains both C=O and O-H groups. Han *et al.* have described and explained similar hydrogen bonding of E1 with nylon 6,6 membrane in their investigation [39,127]. Nylon 6,6 and cellulose acetate have a common C=O functional group involved in hydrogen bonding with the estrogens during the adsorption process. Therefore, the functional groups (C=O), (C-O-C), and (C-O-H) present in WCENFs are involved in hydrogen bonding due to lone pair electrons present on oxygen atoms with (C=O) and (O-H) groups present in E1, whereas only (O-H) group of the other three EH (E2, EE2, and E3) is involved in chemisorption as shown in Figure 6.6 and presented in FTIR analysis in Figure 6.7. These hydrogen bonding interactions would dictate the EH adsorption on WCENFs, explaining the fast adsorption process for EH in the initial stage of the experiment. FTIR analysis is a sensitive technique used in the study to characterize the hydrogen bonds on WCENFs, as shown below.

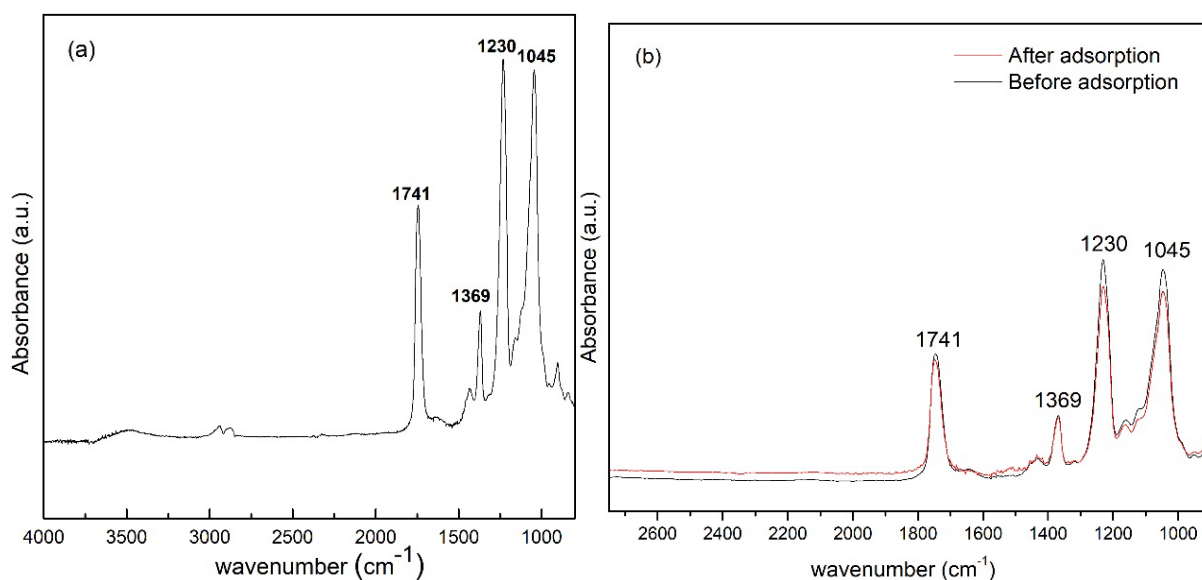


Figure 6.7: Attenuated total reflectance (ATR) mode FTIR spectra of (a) WCENFs and (b) before and after batch adsorption.

The ATR-FTIR characterization of WCENFs was performed to observe the functional groups present. The superimposed FTIR spectra of WCENFs before and after the adsorption study are presented in Figure 6.7. The broadband near $3400\text{-}3600\text{ cm}^{-1}$ indicates OH group presence in fibers. It is noteworthy to see a slight peak shift and the difference in the peak's relative intensities at 1741 cm^{-1} , 1230 cm^{-1} , and 1045 cm^{-1} corresponding to C=O stretching, C-O-C anti-symmetric stretching, and C-O bonds, respectively [136]. Their intensities

significantly decreased after the adsorption study due to the developed intermolecular hydrogen bonding interactions. In contrast, no change is noticed in the peak intensity at 1369 cm^{-1} belonging to the C-CH₃ bond because it can not undergo hydrogen bonding. This assures the existence of the chemisorption at 1741 cm^{-1} , 1230 cm^{-1} , and 1045 cm^{-1} of all these EH on the fibers' surface. In addition, the variation in the peak intensity depends on the number of active available functional groups present in the system and their competing behavior for the available sites [127]. Hence, the results supporting the previous literature suggest that EH (E1, E2, EE2, E3) could form hydrogen bonding with oxygen-containing groups on WCENFs. In our previous research, a similar study reported hydrogen bond interaction of carbonyl group (C=O) in polyurethane with these EH [143].

6.5 Determination of recovery and reusability of WCENFs

The adsorption and desorption process was repeated for four consecutive cycles, and considering the efficiency of WCENFs below 10% during the 4th cycle, it was not further reused. The adsorption study of each cycle is reported in Figure 6.8.

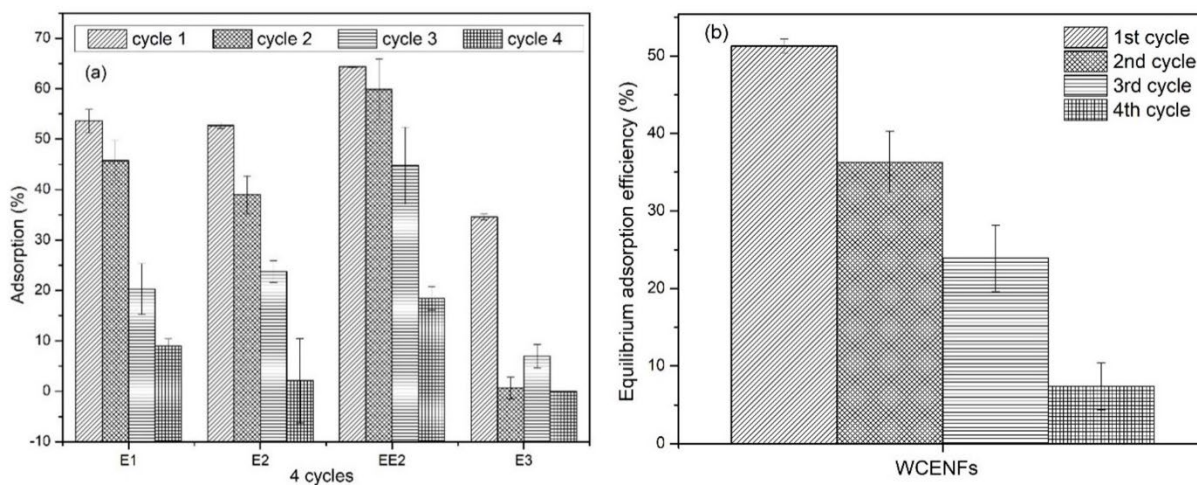


Figure 6.8: (a) Adsorption cycles of each EH (E1, E2, EE2, E3) with an initial concentration of 0.2 mg/L in a combined solution of 0.8 mg/L on WCENFs (20 mg), (b) Cumulative efficiency of all EH adsorption on WCENFs during four cycles

Figure 6.8a represents the percentage removal of each EH concurrently on WCENFs during four consecutive adsorption cycles. As can be seen, the trend is decreasing after every successive cycle for all EH except for E3, where the adsorption percentage remains below 10% after the first cycle due to fewer available active sites for adsorption and intense competition among the functional

groups of EH. The highest removal efficiencies are observed for EE2 (~64.3%), while least for E3 (~34.6%), and the trend is similar in each adsorption cycle. The gradual decrease in adsorption after each cycle is because of mass loss during the desorption process, leading to a reduction of the active adsorptive sites and, thus, a drop in the surface area due to the increase in the fiber diameter (see Figure 6.9).

Figure 6.8b above illustrates the equilibrium adsorption efficiency of WCENFs for cumulative EH removal during four adsorption cycles. As can be seen, the highest reduction of EH in the first cycle is 51.3%, and the trend follows a gradual decrease which ends at 7.4% in the fourth adsorption cycle. Furthermore, it should also be noted that due to the continuous treatment with ethanol during desorption, it was evident that the fibers became stiff and shrank due to mass loss after the last cycle. Therefore, fibers were compact and tightly folded, providing less surface area for EH entrapment during the previous cycle. Thus, providing lesser removal efficiency. The presented comparison was made as a modeling study for the reusability of submicron structure from WCENFs for sorption. In industrial applications, some other solvents have to be tested. According to this model study, the more requested properties of a suitable solvent must be a very high solubility of EH with no solubility of the polymer.

With the repeated desorption cycles of EH from fibers using ethanol, there was a significant change in the fiber morphology attributed to the contact of fibers with ethanol. However, fibers were unlikely to dissolve in ethanol, and their porous structure allowed complete penetration of ethanol molecules. Therefore, after several cycles and contact time, it has led to the collapse and swelling of the structure of the fibers and the effectiveness of the adsorption process [32]. It is evident in the SEM image of the fiber structure after the complete adsorption study, as shown. Figure 6.9 shows the fiber's surface morphology after four adsorption-desorption cycles. As can be seen, the fiber's diameter increased from 196-351 nm, with the high swelling experienced on several fibers, as shown above (white arrows).

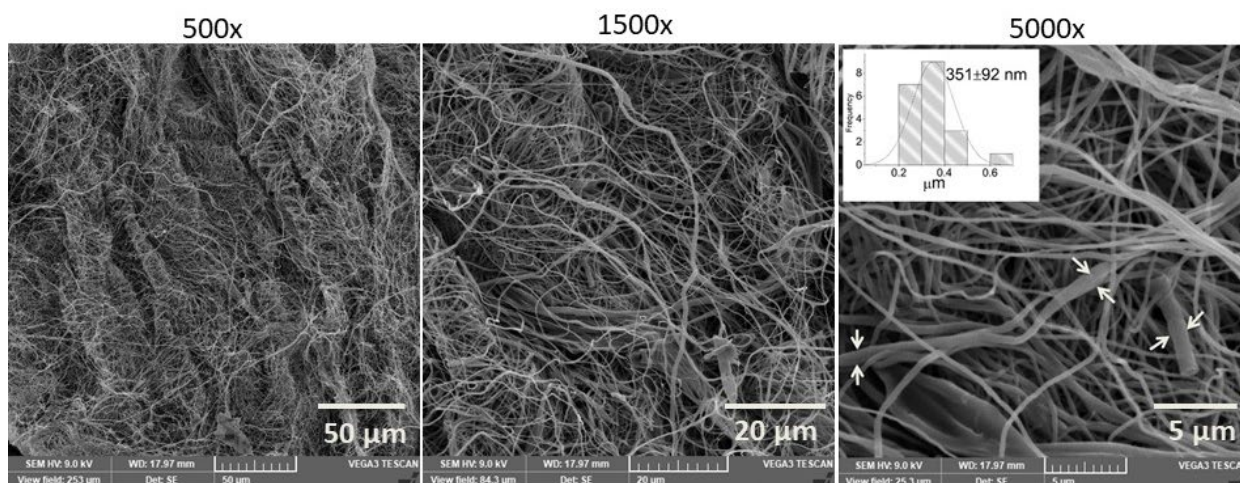


Figure 6.9: SEM image of WCENFs and their fiber diameter distribution after four adsorption-desorption cycles at different magnifications of 500x, 1500x, and 5000x.

6.6 Instantaneous adsorption test of PET/WCENFs syringe film

To perform the syringe film test, the WCENFs due to their fragility were preferably compressed on the PET sheet and used instead of WCENFs alone or with a PP sheet because PP can itself adsorb hormones as previously reported at 96.3% of E1 using a 0.2 μm membrane film [39]. In addition, PET is stiffer to hold fiber straight as a film, providing better strength and enduring high pressures during the filtration process [149]. Therefore, the adsorption of EH was first tested on a neat PET mat to see any influence of adsorption. A batch adsorption test was conducted in the same manner as for WCENFs previously, and no adsorption of any EH was observed on PET. The HPLC chromatograms of solution before and after adsorption perfectly overlap, and no decrease was observed in EH concentration (Figure 6.10). Then, WCENFs compressed on a PET sheet were cut into a 25 mm circular disc in triplicates and placed in the swinnex film holders.

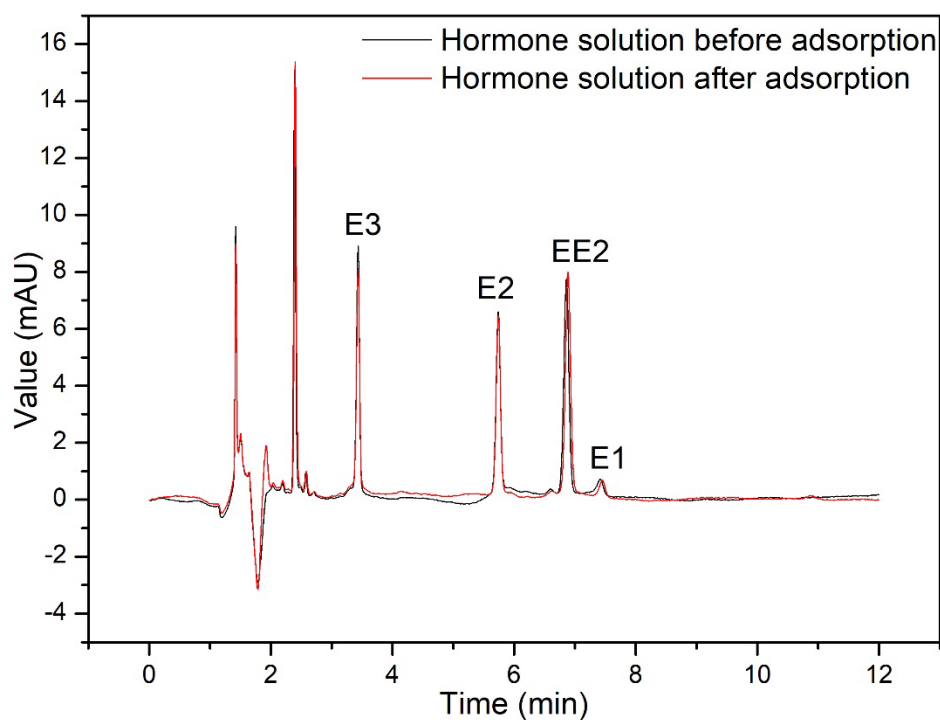


Figure 6.10: Chromatogram of before and after adsorption on PET with stock solution (0.8 mg/L) containing 0.2 mg/L concentration of each EH (E3, E2, EE2, E1) in a mixture.

6.7 EH adsorption on PET/WCENFs fabricated membrane film and commercial application

The adsorption equilibrium of EH solution was observed in these films, and a characteristic value of volume to reach equilibrium (V_{eq}) was noted. This concept of determining V_{eq} is used to conveniently and approximately mitigate the effect of these hormones simultaneously on WCENFs. V_{eq} is defined as the minimum volume of feed solution that passes through the film and can withstand to achieve adsorption equilibrium for this set of EH. Suppose the value of V_{eq} is significantly considerable; in that case, this method can instantly remove EH from wastewater. Figure 6.11 below shows the comparative results of E1, E2, EE2, and E3 adsorption on the PET/WCENFs film, where the residual concentration of the mixed EH solution permeates normalized (expressed in percentage values) against the initial concentration of each hormone in the feed versus the accumulated feed solution. It must be noted that these results were compared with the commercial CA syringe film reported by Han *et al.* for E1 adsorption [39].

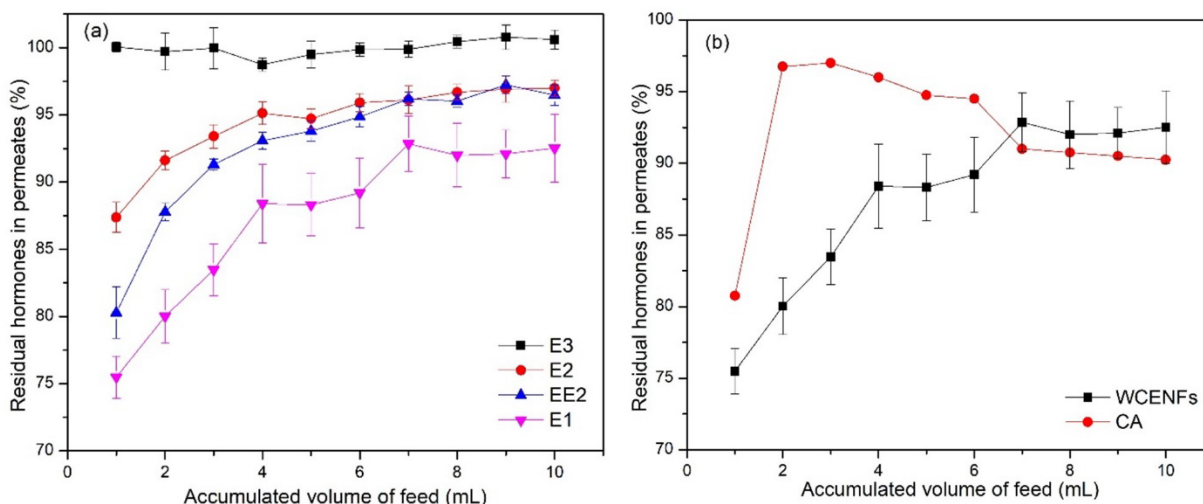


Figure 6.11: (a) Concurrent adsorption of EH (E1, E2, EE2, and E3) on 1.4 μm PET/WCENFs syringe film using 0.8 mg/L EH aqueous solution as feed containing 0.2 mg/L of each hormone and (b) 1.4 μm PET/WCENFs film adsorption comparison with 0.45 μm commercial CA syringe film for E1.

Figure 6.11a shows simultaneous adsorption of all EH on the WCENFs film. It can be seen that the highest adsorption is experienced for E1 and the lowest for E3 until equilibrium was achieved at 7 mL of feed. It can be seen that maximum adsorption for E1, E2, EE2, and E3 were found to be 24.5%, 12.6%, 19.7%, and 0.5%, respectively. A gradual decrease in adsorption was seen for the PET/WCENFs film in a syringe adsorption test, which suggests the process of physical adsorption of EH on the PET/WCENFs film.

Figure 6.11b compares the results of WCENFs film with the commercial CA syringe film over 10 mL accumulated volume of feed. As can be seen, the total E1 adsorption of 18.6% was seen for commercial CA film with the initial solution concentration of 0.4 mg/L while 24.5% for WCENFs with the initial concentration of 0.2 mg/L. Also, 14.2% total adsorption on PET/WCENFs was noticed from the mixture of all four EH with the solution concentration of 0.8 mg/L, which is twice that of commercial CA. Furthermore, after the 1st mL of permeate passed through the commercial CA film, a decrease in adsorption was observed drastically during the next few permeates for commercial CA and then a slight increase in adsorption until it gets stagnant after 6 mL; this could be due to experimental error or loss of some already adsorbed E1 molecules on the surface of commercial CA film. While, a gradual decrease in adsorption was seen for PET/WCENFs syringe film, which suggests that physical adsorption could be the primary cause of EH adsorption but without any EH losses from the surface. The membrane's adsorption sites were occupied by EH molecules when more and more feed was

passed, and eventually, an equilibrium was established when the adsorption sites were saturated. The derived V_{eq} value was 7 mL for both PET/WCENFs and commercial CA films. After these volumes, no significant change was observed. This suggests that the film reached saturation with EH at 7 mL. Similar results were reported in the literature for E1 adsorption reaching equilibrium at 8 mL for PP, 7 mL for polytetrafluoroethylene (PTFE), and 6 mL for regenerated cellulose (RC) films [39].

The PET/WCENFs film in the current study has a high retention volume for these EH with twice the initial concentration of EH solution compared to the commercial GMF, RC, PTFE, CA, and PP films reported by Han *et al.* Therefore, PET/WCENFs film can be used within this capacity for instant and concurrent removal of these EH solutes from wastewater. It can be a cheap and viable method by using waste CBs to make a WCENFs film for replacing the commercially available films for water treatment. The PET/WCENFs film can be an excellent substitute for the already available commercial films because this can be disposed of after several cycles, easily be detached, and replaced from a swinnex film holder. Additionally, the WCENFs used as a film can be prepared by facile electrospinning technique, which is not costly.

6.8 Restrictions, Further research, and application of WCENFs

This model study was limited to working with one concentration due to the restriction of solubility of four EH together, their detection, and quantification limits set on HPLC. Moreover, continuous long-term membrane testing on the cross and dead-end flow measurement under high pressures and flow rates, including membrane fouling, needs to be investigated. Furthermore, the influence of pH variation, interference of organic matter, ionic strength, temperature, the competing behavior of inorganic ions, varied concentrations of adsorbate and adsorbent dosage are some matters to be addressed in future research to help optimize the kinetics, determine isotherms and thermodynamic parameters. These works shall focus on actual reservoir samples to conclude the feasibility of this process for large-scale production.

6.9 Comparative study of WCENFs with other adsorbents for the removal of EH

The following Table 6.4 illustrates the type of fibers and particles used for the removal of hormones and pollutants from water. As can be seen, the WCENFs have a cumulative adsorption capacity of 2.14 mg/g, which is greater than most

of the electrospun fibers (individual values are specified in Table 6.4) reported in the literature. Apart from that, the given particles (PA612, Darco AC, and Norit AC) have higher adsorption capacities than WCENFs due to their higher surface area based on the nature of those materials. Also, the individual adsorption capacities of WCENFs are firmly in compliance with those of electrospun CA fibers.

Table 6.4: Comparison of adsorbents used for the specified water pollutants

Adsorbents	Pollutant	Adsorption capacity (mg/g)	Reference
MWCNTs	E1, E2, EE2	0.423, 0.472, 0.472	[120]
PA612, Darco AC, Norit AC	EE2	25.4 27.6 10.4	[48]
Un-anthracite, 4 K anthracite	EE2, BPA	0.2147, 0.1221 0.6209, 0.1540	[119]
PU Elastollan, PU 918, CA, PAN, PES, PA	E1, E2, EE2, E3	0.801, 0.592, 0.736, 0.382 0.816, 0.606, 0.637, 0.366 0.506, 0.532, 0.668, 0.389 0.396, 0.370, 0.343, 0.397 0.442, 0.487, 0.591, 0.363 0.331, 0.543, 0.611, 0.485	[143]
WCENFs	E1, E2, EE2, E3	0.551, 0.532, 0.687, 0.369	Present study

6.10 Conclusions

This study focused on the concurrent removal of four EH (E1, E2, EE2, E3) to replicate real-time waste streams using WCENFs, recycling, and a green approach. A one-step detection and concomitant quantification method based on HPLC was devised for these EH. It is noteworthy to mention that the WCENFs membrane could successfully remove all of these EH. The chemical composition of polymer, functional groups present, and structure of WCENFs played an essential role in the rapid adsorption process, which is elaborated in the adsorption mechanism. The strong affinity of WCENFs was found to be towards all EH due to abundant hydrogen bonding interactions. The highest percentage removal efficiencies from the batch adsorption were 64.3%, 53.6%, 52.7%, and 34.6% for EE2, E1, E2, and E3, respectively. The total adsorption capacity obtained was 2.14 mg/g, and reported individual adsorption capacities of E1, E2, EE2, and E3 were found to be 0.551, 0.532, 0.687, and 0.369 mg/g, respectively. Based on the kinetic modeling results, the pseudo-first-order suits E3 and the pseudo-second-order model is suitable for E1, E2, and EE2. Therefore, both models are considered most appropriate due to their high regression coefficients than the other kinetic models. Desorption studies for the recovery of EH and reuse of submicron WCENFs was conducted and validated for four cycles using HPLC grade ethanol as the most suitable solvent. To summarize, the fabricated PET/WCENFs syringe film successfully responded to the retention time for these EH compared to the commercial CA syringe film. It also implies that recycled WCENFs can be considered a promising adsorbent for the rapid remediation of wastewater streams and possibly replacing the commercially available CA syringe film.

7. Electrospun polyurethane nanofibers coated with polyaniline/polyvinyl alcohol as ultrafiltration membranes for the removal of ethinylestradiol hormone micropollutant from the aqueous phase

Post modification of spun nanofibers to enhance functionality properties with high nitrogen-containing compounds has been limited. This process has proven to greatly enhance adsorption performance for different persistent environmental pollutants [150,151]. Polyaniline (PANI) is a widely used conducting and electroactive polymer due to its cost-effective synthesis via either simple chemical or electrochemical oxidation [152,153]. This conductive polymer possessed benzenoid and quinonoid rings in its structural units linked by amine- and/or imine-type nitrogen atoms via π - π interactions and hydrogen bonding [154,155]. This makes PANI and its related composite materials promising adsorbents of organic pollutants. However, PANI in combination with supporting polymers such as polyvinyl alcohol can enhance the materials both with appreciable electrical conductivity and mechanical integrity [156]. In water pollution treatment, the incorporation of such polymer in the adsorbent material increases the presence of nitrogen atoms, which in turn enhances the ability to interact with pollutants via the formation of complexes with various organic and inorganic substances to reduce their prevalence in the aqueous phase.

In this chapter, the polyurethane (PU) membrane prepared via electrospinning is post-modified by coating with PANI in a polyvinyl alcohol solution for the enhanced removal of EE2 micropollutant hormone. To understand the characteristics of the coated PU membranes, FTIR, SEM, and optical microscopy were performed. The adsorptive interaction and performance for the removal of EE2 were further investigated via optimization study using response surface methodology to evaluate the experimental data by analysis of variance (ANOVA) to determine optimum adsorption capacity via adsorptive two parameters interactions. Furthermore, the determined optimal adsorption condition was validated by studying effects on single parameters of solution pH, temperature, initial concentration of the hormone, and adsorbent dosage. The kinetics and thermodynamics of the adsorption process were also calculated. Finally, a reusability analysis of the prepared adsorbent over six adsorption-desorption cycles was performed in order to determine the consistent effectiveness of coated PU membrane.

7.1 Post-modification of spun PU nanofiber membrane

Polyaniline (PANI) stabilized with poly(vinyl alcohol) (PVA) system was prepared by the oxidation of aniline in hydrochloride with ammonium peroxydisulfate as previously described [143,157] with slight modifications. In brief, aniline (0.1 M) dissolved in 1M HCL solution was mixed with 4 wt% aqueous solution of PVA to form a 50 mL solution. Weighed 0.5 g spun PU nanofiber was dipped in the above-prepared solution for 2 h to allow for the adsorption of the aniline monomer on the surface of the fibers. An equal volume (50 mL) of 0.125 M of ammonium peroxydisulfate solution was added to the mixture, shortly stirred, and allowed at room temperature for 24 h for the polymerization of aniline to occur and coating on the spun fibers. The originally white solution turned dark green/black as PANI was produced. The coated spun fibers were then removed and repeatedly re-suspended in 0.2 M HCL to remove residual or unreacted monomers, followed by washing them severally with distilled water to neutral pH. The coated sample known as PU-PANI emeraldine salt (PU-PANI-ES) was subsequently freeze-dried for further use. PU-PANI-ES was further converted to PU-PANI emeraldine base (PU-PANI-EB) by suspension of the coated membranes in excess of 1 M ammonium hydroxide for 24 h [158]. Thus, blue PANI base coated PU nanofibrous membranes were collected by filtering the residual solution, washed with acetone and water repeatedly, then dried as above.

7.2 Adsorption analysis via modeling

Central Composite Design (CCD) model was employed using the Design-Expert software v13.0 to estimate and optimize the most influencing factors and their interaction effects on EE2 hormone removal by the coated spun PU nanofiber membranes. CCD is composed of factorial points corresponding to axial and central points [126,159]. The levels of the main investigated factors are given in Table 7.1. The relationship between these independent factors based on the obtained responses is fitted to a second-order polynomial equation that allows for the modelling of responses of the hormone, which is expressed by Eq. (7.1).

$$Y = \beta_0 + \sum_{i=1}^k \beta_i X_i + \sum_{i=1}^k \beta_{ii} X_i^2 + \sum_{i=1}^k \sum_{j=i+1}^k \beta_{ij} X_i X_j + \varepsilon \quad (7.1)$$

Where Y is the response (removal efficiency), X_i and X_{ij} are the encoded parameters, and β_0 , β_i , β_{ii} , and β_{ij} are the linear, quadratic, and interaction coefficients, respectively. Based on the results generated, the desirability function

is then employed to obtain the optimization of investigated parameters (best levels for each factor).

Table 7.1: Investigated experimental factors and their levels in the central composite design

Factors	Low(-1)	Center (0)	High (+1)
<i>A – Temperature (°C)</i>	25.00	40.00	55.00
<i>B – Solution pH</i>	5.00	7.00	9.00
<i>C – Initial conc. of hormone (mg/L)</i>	0.20	0.30	0.40
<i>D – Adsorbent dosage (mg)</i>	10.00	20.00	30.00

7.3 Modification of spun nanofibers

PANI is typically achieved by the oxidation of aniline with ammonium peroxydisulfate in an acidic aqueous medium at room temperature, followed by deprotonation with ammonium hydroxide for PANI base (Scheme 7.1a). The treatment of the PU nanofibrous membrane with PANI serves as an alternative to improve the functional properties of materials. In order to obtain soft conducting and filtration membranes, another component, such as a water-soluble supporting polymer, in this case, PVA was incorporated into the system to enhance homogenous PANI being formed with low agglomeration and increase surface interaction with the PU fibers [143,160]. PVA, as a supporting polymer, forms a skeletal network between the PANI particles and PU fibers that further strengthens the integrity of the membrane [143]. Considering that PANI is produced in the vicinity of the PVA phase, where the reactants are gradually concentrated during polymerization and bind to the PU fiber surface to form PU-PANI-ES, which is then deprotonated to PU-PANI-EB in the basic medium (Scheme 7.1b and c). This leads to the formation of modified PU nanofibrous membranes rich in nitrogen atoms, which are composed of conducting and supporting polymer phases possessing a composite nature. This makes them suited as good adsorbents to be explored for the removal of micropollutants (such as EH) from the aqueous phase.

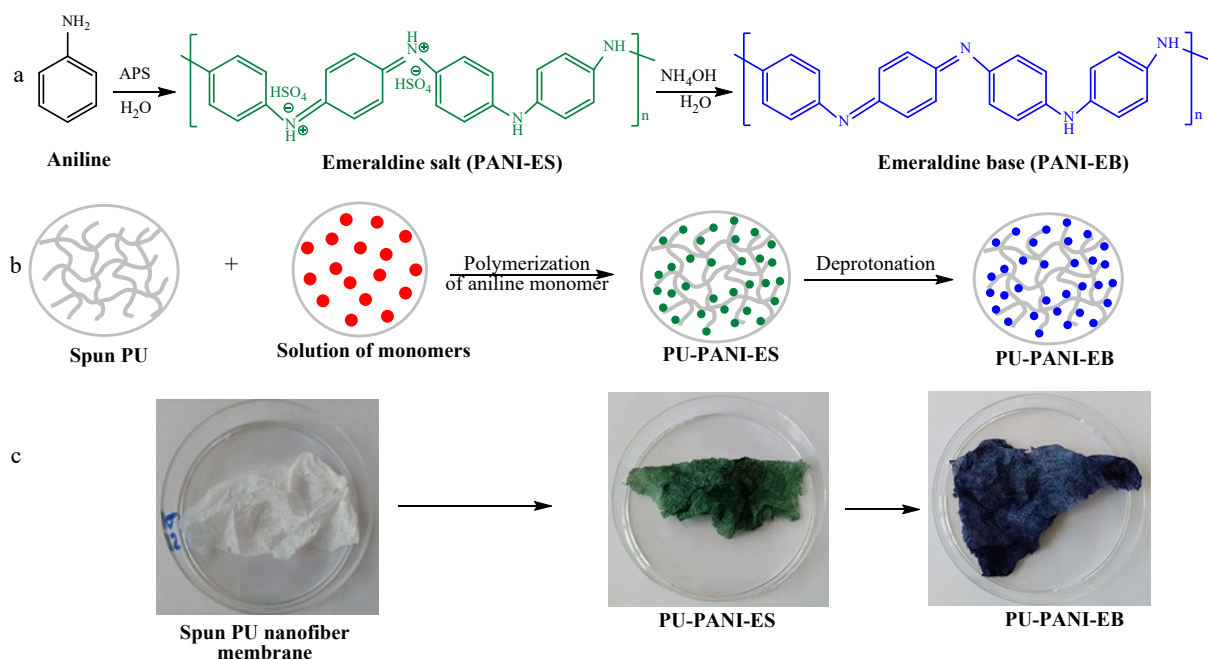


Figure 7.1: (a) Aniline is oxidized to PANI (emeraldine) salt (PANI-ES) with ammonium peroxydisulfate and deprotonated to PANI (emeraldine) base (PANI-EB) using ammonium hydroxide. (b) Spun PU membrane (gray spirals) mixed with a solution of monomers (red circles) subsequently monomer polymerizes to a polymer (green objects) and adheres to PU fiber surface. After that green PANI is deprotonated to an emeraldine base (blue objects). (c) Images of neat spun PU membrane, PU-PANI-ES and PU-PANI-EB coated membranes.

7.4 Material characterization

7.4.1 FTIR analysis

The FTIR spectra of neat PU, PU-PANI-ES, and PU-PANI-EB are presented in Figure 7.2. The FTIR spectra of PU show a broad peak between 3700-3200 cm^{-1} , corresponding to the N-H bond stretching vibrations from the aliphatic amino group of carbamate. The peaks at 2952 and 2889 cm^{-1} reflect C-H asymmetrical flexing vibration of aliphatic CH_2 groups, respectively [161]. The strong absorption peak around 1710 cm^{-1} is ascribed to amido ester C=O stretching vibration [162,163]. The peaks at 1590 and 1522 cm^{-1} are attributed to the N-H bending of the amide group. The characteristic peaks arising at 1410 and 1307 cm^{-1} illustrate the stretching vibration in the skeleton of the benzene ring due to the C=C bond [164]. The stretching vibration peak at 1240 cm^{-1} relates to the C-N bond from the amide group. The asymmetric flexing vibration of C-O-C bonds is caused by alkyl ether and is represented by a sharp peak at 1080 cm^{-1} [143,165]. The peak at 708 and 730 cm^{-1} are attributed to aryl C-H bending. PVA did not

show any obvious absorption band in the study, which may be attributed to overlapping its peak with PU.

The FT-IR spectra of PU-PANI-ES and PU-PANI-EB showed a characteristic broad band between 3700-3200 cm^{-1} , attributed to the overlapping stretching vibrations of N-H from PU, PANI, and OH from PVA. The peaks at about 1590 and 1522 cm^{-1} which showed increased intensity for coated PU materials with PANI, are ascribed to the absorption of quinone and benzene rings of PANI [166]. The peaks at 1307 and 1136 cm^{-1} also depicted increased intensity for PANI-coated PU materials and related to the alkyl C-N stretching vibration from PU and PANI. The peak at 815 cm^{-1} further showed increased intensity for the PANI-coated samples and is attributed to the π localized polaron band of coated PANI on PU fibers [167].

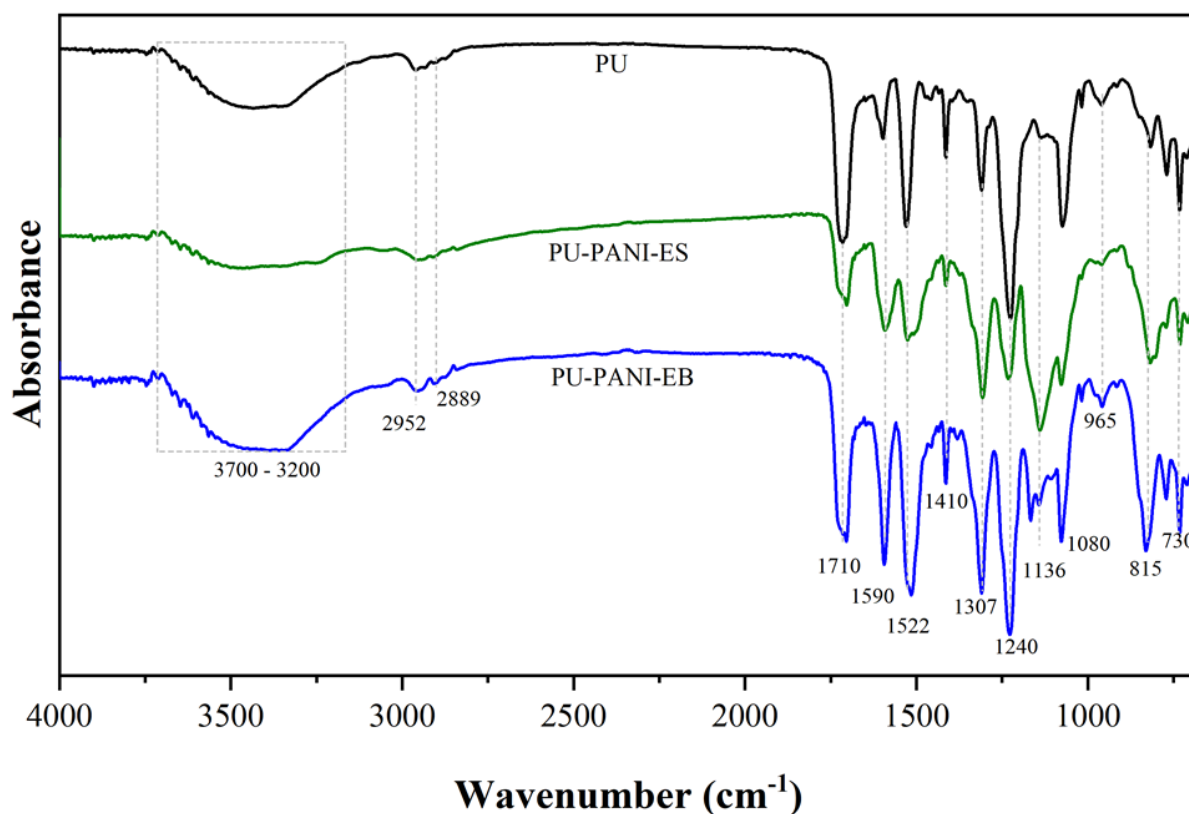


Figure 7.2: FTIR spectra of neat PU as control, PU-PANI-ES, and PU-PANI-EB treated fibers from attenuated total reflectance (ATR) sampling.

7.4.2 Optical microscopy

It is visible by the optical microscopy (Figure 7.3) that the coated samples (either green or blue) provide good phase contrast while showing the fibrillary structure of the membranes. After freeze-drying, they convert to lightweight membranes.

Considering the change in color of the PU membranes from white to green and blue confirms the coating of PANI on the fiber surface of PU during preparation. This makes the formed, modified PU membranes suited to be exploited as novel adsorbents.

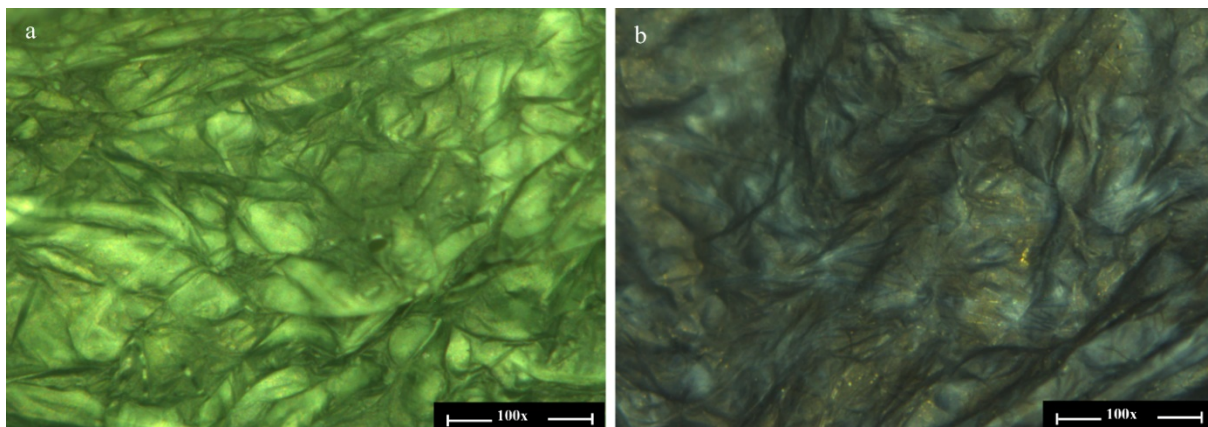


Figure 7.3: Optical micrograph of coated (a) PU-PANI-ES and (b) PU-PANI-EB membranes at 100x magnification.

7.4.3 SEM analysis

The micrographs in Figure 7.4 show that the electrospun nanofiber of PU exhibit a minimum diameter of approximately 174 ± 56 nm (Table 5.1), as previously reported by Yasir *et al.* [143]. These fibers, after treatment with PANI, become more dense and thicker due to the adsorption of polymerized PANI particles on the surface of fibers. This makes the structure more compact, as seen in the case of PU-PANI-ES and PU-PANI-EB. However, PU-PANI-ES is more denser compared to PU-PANI-EB because the latter was further deprotonated, which may have resulted in the loss of some particles during treatment, making it less dense. Overall, both of the modified materials appear to have a better morphology compared to the PU control, and it is also proved further by the improvement in the performance of the materials shown in the following section.

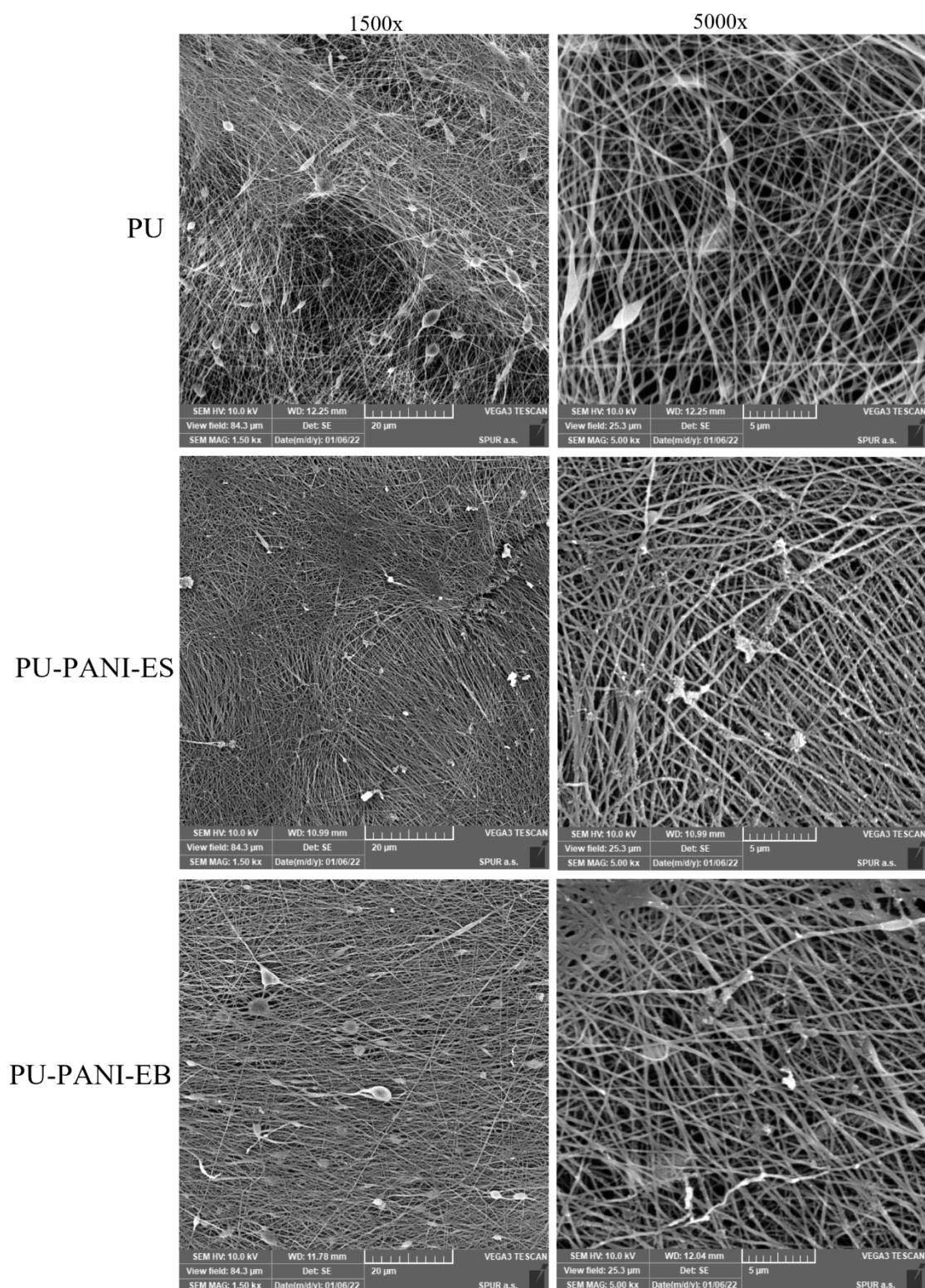


Figure 7.4: SEM images of PU as control, PU-PANI-ES, and PU-PANI-EB treated fibers at different magnifications of 1500x and 5000x.

7.5 Adsorption study of PU-modified nanofibers

In order to test the efficiency of prepared materials as suitable adsorbents, a preliminary adsorption study was performed for neat PU and coated PU samples

(PU-PANI-ES and PU-PANI-EB). Figure 7.5 presents the results obtained from the experiment done with 20 mg of each adsorbent in 100 mL EE2 hormone solution with a concentration of 0.20 mg/L for 3.5 h at 150 rpm, room temperature, and pH 7. The results show that the coated PU materials with PANI significantly improved the adsorption of EE2. The neat PU had a removal efficiency and adsorption capacity of 55.38% (0.612 mg/g), which increased to 81.46% (0.900 mg/g), and 90.33% (0.998 mg/g) for PU-PANI-EB and PU-PANI-ES, respectively. Based on the achieved results, the best sample (PU-PANI-ES) was further studied via an optimization study to determine the optimum removal conditions for the EE2 hormone.

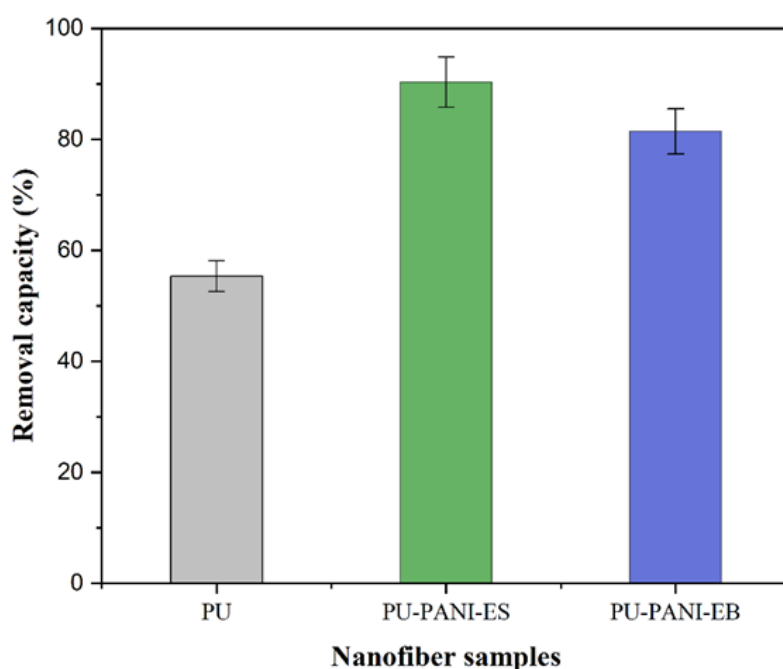


Figure 7.5: Adsorption removal of EE2 using PU as control, PU-PANI-ES, and PU-PANI-EB treated nanofibrous membranes.

7.6 Batch adsorption optimization study

The optimum adsorption parametric conditions for the present study were determined by analysis of the obtained experimental data (Table 7.2) via the CCD model using response surface methodology. The recorded experimental response values (removal capacity) were fitted to a second-order polynomial equation generated by the Design-Expert 9 software (Stat-Ease Inc., The USA). Herein, 20 experimental runs were evaluated according to the response surface design method. Four operating factors were investigated in the optimization study, including temperature, solution pH, initial concentration of the hormone, and adsorbent dosage, coded as A, B, C, and D, respectively. Experimental runs were

generated and ran in random sequence to determine the actual removal efficiency response values from the collected experimental data, while the predicted response values were determined using the quadratic polynomial model as given in Eq. (7.2):

$$\text{Removal \%} = +84.09 - 3.59A + 8.35B - 1.59C + 7.65D + 0.1841AB - 2.16AC + 1.72AD - 2.85BC - 8.24BD - 0.1004CD - 7.25A^2 + 3.79B^2 - 2.95C^2 - 2.01D^2 \quad (7.2)$$

Table 7.2: The different experiment runs with their actual and predicted responses

Runs	Factors				Removal capacity (%)	
	A	B	C	D	Actual response	Predicted response
1	40	7	0.2	20	84.58	82.72
2	40	7	0.3	20	82.12	84.09
3	40	7	0.3	40	89.17	89.72
4	40	7	0.3	30	85.85	84.09
5	55	9	0.2	10	85.52	85.98
6	40	5	0.3	20	78.98	79.53
7	25	9	0.4	30	83.46	82.72
8	40	9	0.3	20	95.67	96.23
9	55	7	0.3	20	72.70	73.25
11	55	9	0.4	10	85.85	84.09
13	55	5	0.4	30	73.72	72.98
14	40	7	0.3	10	85.85	84.09
15	55	5	0.2	30	80.90	80.16
16	25	5	0.2	10	73.88	74.43
17	25	7	0.3	20	81.68	82.15
18	40	7	0.4	20	52.93	53.39
19	25	5	0.4	10	79.87	80.42
20	25	9	0.2	30	76.59	79.55

7.6.1 ANOVA for quadratic model

The analysis of variance (ANOVA) was employed to support the acceptability of the design model. Table 7.3 shows the obtained ANOVA data from the Design-Expert software. According to the results presented, the F-value of the model was 20.66, implying that the model is significant, and there is only a 0.17% chance that an F-value this large could occur due to noise. The significance of the studied model was also confirmed by the very low P-value of the model (P model =

0.0017). This value also relates to describing the close agreement between actual and predicted responses observed in Table 7.2 [168,169]. The P-value for the linear and quadratic terms of the model was also studied. In this case, the model terms B, D, AD, BC, BD, A², and B² are significant, showing that solution pH (B), adsorbent dosage (D), and quadratic terms are highly significant, while the other linear and quadratic terms of the model showed low significance.

Table 7.3: ANOVA data for removal of estrogenic hormone based on CCD quadratic model

Source	Sum of Squares	df	F-value	p-value	
Model	1752.04	14	20.66	0.0017	significant
<i>A-Temperature</i>	25.72	1	4.24	0.094	
<i>B-pH</i>	139.43	1	23.01	0.004	
<i>C-Conc of hormone</i>	25.13	1	4.15	0.097	
<i>D-Dosage of adsorbent</i>	116.93	1	19.30	0.007	
<i>AB</i>	0.05	1	0.09	0.093	
<i>AC</i>	37.39	1	6.17	0.056	
<i>AD</i>	4.76	1	7.85	0.042	
<i>BC</i>	65.17	1	10.76	0.022	
<i>BD</i>	108.62	1	17.93	0.008	
<i>CD</i>	0.08	1	0.01	0.913	
<i>A²</i>	133.88	1	22.10	0.005	
<i>B²</i>	36.58	1	6.04	0.006	
<i>C²</i>	22.18	1	3.66	0.114	
<i>D²</i>	10.29	1	1.70	0.249	
Residual	30.29	5			
<i>Lack of Fit</i>	19.85	2	2.85	0.202	not significant
<i>Pure Error</i>	10.44	3			
Cor Total	1982.33	19			

The Lack of Fit value of 2.85 implies not significant, which is good because we want the model to fit. There is a 20.23% chance that a Lack of Fit F-value this large could occur due to noise. The determination coefficient (R^2) had a value of 0.983, implying that 98% of the variations in this model were predicted and calculated using the established quadratic model. In addition, the calculated adjusted R^2 value (0.935) was close to the predicted R^2 value (0.845), with a difference of less than 0.20. Considering the three R^2 values were high, this

indicates that the polynomial model is validated and well fitted to the experimental design responses [126]. The adequacy of the model was further confirmed and validated by the correlation plot between the predicted and actual responses, as shown in Figure 7.6a. Moreover, the observed residuals verse the fitted predicted responses were also plotted in Figure 7.6b and displayed a normal random distribution of residuals [170].

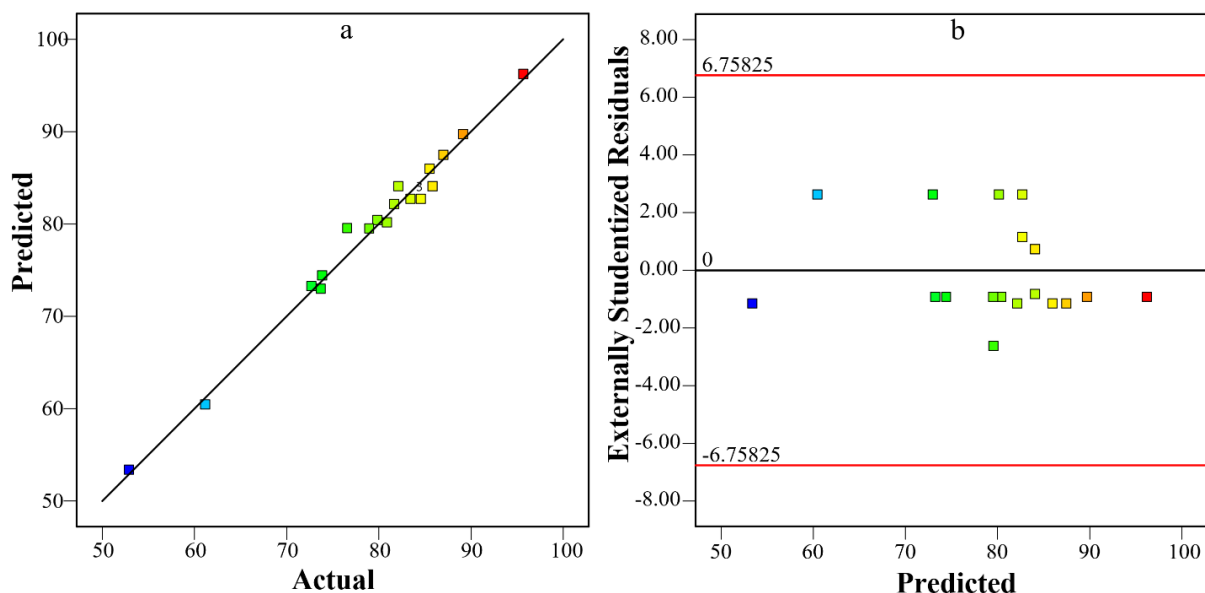


Figure 7.6: (a) Plot of predicted and actual response values and (b) residual plot for EE2 hormone removal.

7.7 Optimization validation

The optimized operating factors suggested by the Design-Expert software were determined as follows; solution pH 7.0 (considering that wastewater or river water is in the range of pH 6-8), initial EE2 hormone concentration 0.30 mg/L, adsorbent dosage 20 mg, and temperature 40 °C. To optimize the operating parameters, the lower and upper limits of the operating parameters were chosen based on the studied ranges. The target was selected based on the most desirable conditions. The deduced predicted values for removal percentage and adsorption capacity are provided in Table 7.4. To confirm the generated predicted values, a validation test was performed using the determined optimum conditions. Results showed a close correlation between the predicted and experimental responses, validating the significance of the model.

Table 7.4: Point prediction and validation of optimized parameters at 95% confidence interval

Response	Predicted Mean	Observed	Std Dev	SE Mean	Desirability
Removal percentage (%)	84.08	82.20	2.46	0.85	1.00
Adsorption capacity (mg/g)	1.88	2.11	0.29	0.10	1.00

7.8 Effect of two interaction parameters on the removal of EE2 hormone

The 3-dimensional response surface plots help in the comprehensive evaluation of the operation of the system under the framed experimental design and elaborate on understanding the effects caused on the response by variation of the experimental factors. The observation obtained are discussed as follows:

Figure 7.7a demonstrates the effect of temperature and solution pH on the removal percentage of EE2. As can be seen, an increase and then a decrease in removal percentage was observed with an increase in temperature ranging from 25 - 55 °C. Whereas a linear rise in removal percentage was seen with an increase in pH because EE2 remains undissociated in this pH range till pH reaches its value of pK_a (10.50) [112,118]. The highest removal percentage recorded was 95.60% at 40 °C temperature and pH 9. On the other hand, the lowest removal percentage occurred at pH 5 and a temperature of 55 °C. This is because the adsorption here is of exothermic nature and spontaneous, which favors lower temperatures [111].

In Figure 7.7b, the effect on EE2 removal percentage is observed by varying temperatures and concentrations of the hormone solution. The EE2 removal percentage increased and then decreased with an increase in temperature, which indicates that the adsorption of EE2 on PU-PANI-ES is exothermic, favoring high removal efficiency at a lower temperature [171]. At a high concentration of hormone 0.4 mg/L and a temperature of 55 °C, the removal percentage appears to be the least. The highest removal percentage of 82.10% is found to be at optimum parameters of 40 °C and 0.3 mg/L concentration of the hormone.

Figure 7.7c depicts the effect of temperature and dosage of adsorbent on the removal percentage of EE2. The temperature ranged from 25 - 55 °C, and the dosage of the adsorbent from 10-30 mg. An increase in removal efficiency followed by a decrease with increasing temperature, as described above, relates to the exothermic nature of the adsorption process. However, the removal percentage increased linearly with an increase in the dosage of the adsorbent. This could be due to the increase in the number of sites leading to an increase in the contact surface area as the amount of adsorbent increased [172]. The highest removal percentage achieved was nearly 90%, with a 30 mg dosage of the adsorbent at 40 °C.

In Figure 7.7d, the effect of changing solution pH and concentration of the hormone is seen on the removal percentage. The solution pH ranges from 5-9 and concentration from 0.20 - 0.40 mg/L. The removal percentage is slightly high at pH 5 and at a higher concentration of 0.4 mg/L. However, there is a sharp rise in removal percentage from nearly 70.00% at pH 5 to 96.00% at pH 9. The highest removal percentage is found to be at 0.20 mg/L concentration and pH 9. However, the removal percentage is seen to decrease by an increase in concentration from 0.20 - 0.40 mg/L at constant pH 9. A plausible reason could be that all the active sites are already occupied, reaching saturation, and a rise in concentration led to a drop in removal percentage [172].

Figure 7.7e illustrates the effect of dosage of adsorbent and solution pH on the removal percentage of EE2. It is evident from the graph that at pH 5 and 10 mg of dosage, the least removal percentage was achieved. Furthermore, the removal percentage linearly increased by either solely an increase in pH of the solution or an increase in the dosage of adsorbent. Whereas at pH 9, increasing the dosage of adsorbent had a negligible effect on removal percentage, but at pH 5, the difference was distinguishing; a rise in removal percentage from 50.00% at a dosage of 10 mg to around 92.00% at a dosage of 30 mg was seen which indicates a rapid rise in adsorption. The highest removal percentage of about 96.00% interpreted from this graph was at pH 9 and 20 mg of dosage.

Figure 7.7f represents the influence of the concentration of hormone and the dosage of adsorbent on EE2 removal percentage. As can be seen, at a dosage of 10 mg, the removal percentage is the least and is almost unaffected by an increase in the concentration of the solution. However, the removal percentage is high at a lower concentration if the dosage is kept constant. Whereas there is a gradual rise in the removal percentage by increased dosage of adsorbent for all the given

concentrations of the solution. At a dosage of 30 mg, a slight increase and then decrease is observed in the removal percentage of EE2 by the increase in the concentration of the solution. This indicates that the rise was due to an increase in the amount of EE2 hormones adsorbed on the sites of the adsorbent until the 0.30 mg/L concentration of the solution. At this point, all the available sites on the adsorbent were completely filled by EE2 hormones, and a further increase in concentration led to a decrease in removal percentage because no additional EE2 hormone molecule could be adsorbed on the adsorbent's surface [118].

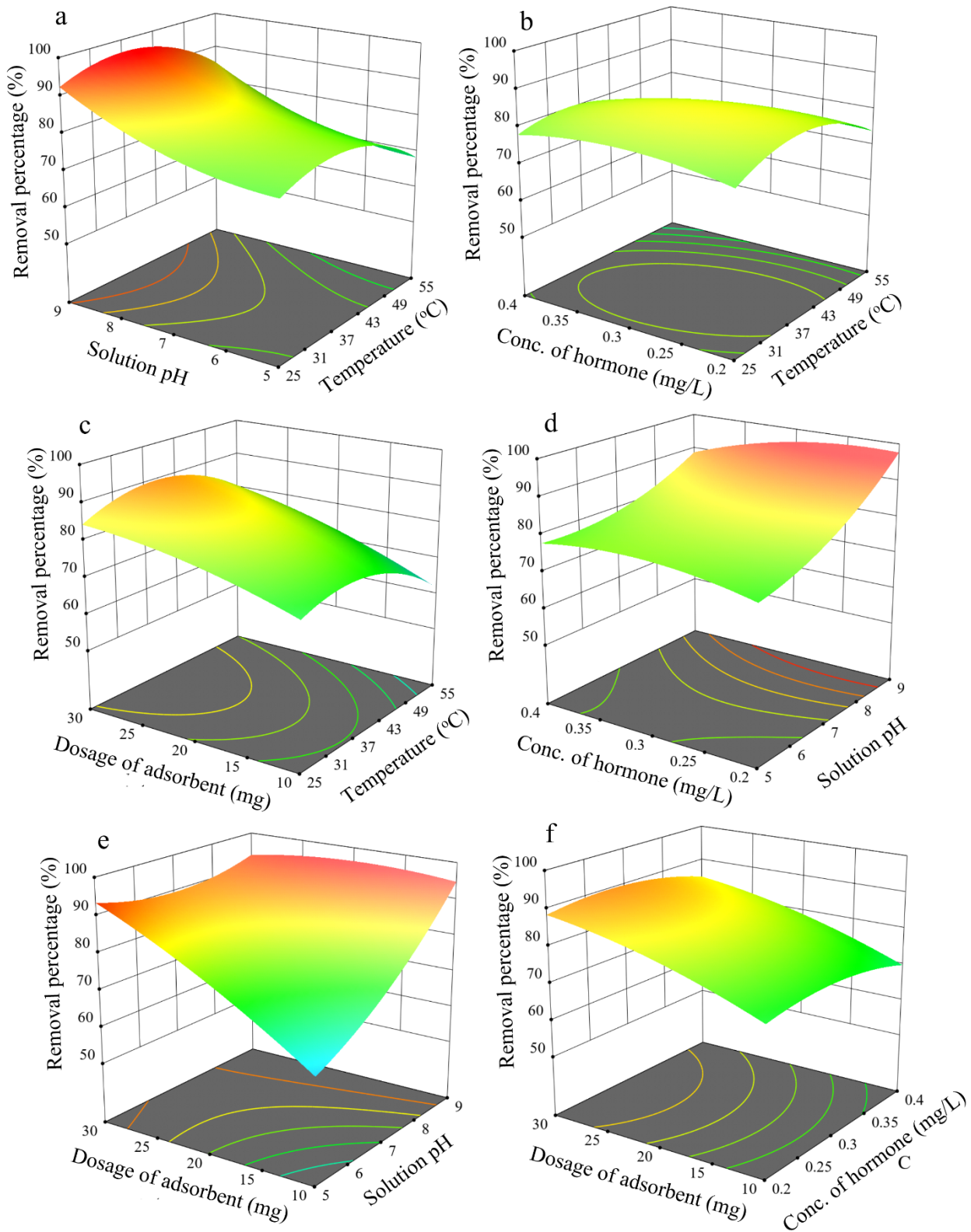


Figure 7.7: 3D two-parameter interaction response surface plot on the removal of EE2 hormone using PU-PANI-ES membrane.

7.9 Effect of single parameters on the optimal removal of EE2 hormone

In order to further validate the determined optimum conditions for the removal of EE2 hormone, the removal efficiency and adsorption capacity of PU-PANI-ES adsorbent was evaluated by varying a single factor (solution pH, initial EE2 concentration, dosage, and temperature) while keeping the other factors constant at determining optimum values.

7.9.1 Effect of solution pH

In Figure 7.8a, an increasing trend is observed with an increase in the pH of the solution. There is a gentle rise in efficiency from 79.90% at pH 5 to about 82.10% at pH 7; however, there is a sharp increase in efficiency, reaching 95.70% at pH 9. A similar trend was followed for the values of adsorption capacities which were about 1.67, 1.70, and 2.00 mg/g for pH 5, 7, and 9, respectively. Usually, pK_a represents the acid dissociation constant at which EE2 can lose its hydrogen atom and become negatively charged. The pK_a of EE2 is in the range of 10.25 - 10.50; therefore, in this case, the pH of the solutions remained below 9.5. Thus, no cation-anionic attraction was expected to occur between EE2 and adsorbent, and EE2 remained neutral [42]. However, at higher pH above pK_a , adsorption efficiency is expected to decrease due to charge repulsion [146].

7.9.2 Effect of initial EE2 hormone concentration

Figure 7.8b represents the influence of the initial concentration of EE2 in the solution on the efficiency of PU-PANI-ES fibers. It can clearly be seen that the efficiency of fibers linearly decreased, whereas the adsorption capacity increased with an increase in the concentration of EE2 in the solution. At 0.20 mg/L concentration, the highest removal efficiency of 84.62% and lowest adsorption capacity of 1.09 mg/g was reported, while at 0.40 mg/L concentration, the lowest removal efficiency of 76.64% and highest adsorption capacity of 2.21 mg/g was reported. This is because high removal efficiency is expected with a large number of active sites available for adsorption. However, at a higher initial concentration of the solution, less number of sites are left gradually due to saturation leading to a reduction in removal efficiency [172].

7.9.3 Effect of dosage

In Figure 7.8c, the effect of adsorbent dosage was determined on its removal efficiency and adsorption capacity. The removal efficiency linearly increased

from 73.90% at a dosage of 10 mg to 89.20% at a 40 mg of fiber dosage. The response for adsorption capacity was the opposite. It was 3.04 mg/g observed at 10 mg of dosage, which decreased to 0.91 mg/g for 40 mg of dosage. This is expected to happen due to the large surface area available at high dosage, creating more number of sites for adsorption. Thus, high removal percentage is observed [118,172].

7.9.4 Effect of temperature

In Figure 7.8d, the effect of temperature variation was observed on the performance of the coated PU membrane. It can be seen that both removal efficiency and adsorption capacity of coated PU increased between 25 - 35 °C, and then they decreased with further increase in temperature to 55 °C. The optimum temperature observed was 35 °C, with a removal efficiency of 82.10%, and an adsorption capacity of 1.70 mg/g was recorded. The values at a higher temperature of 55 °C were 72.70% and 1.58 mg/g, respectively, which were lower than the values obtained at room temperature of 79.90% and 1.63 mg/g, respectively. This is because the nature of adsorption is exothermic in this case which favors higher adsorption as lower temperature [171]. A more detailed description is given in the later section about thermodynamics.

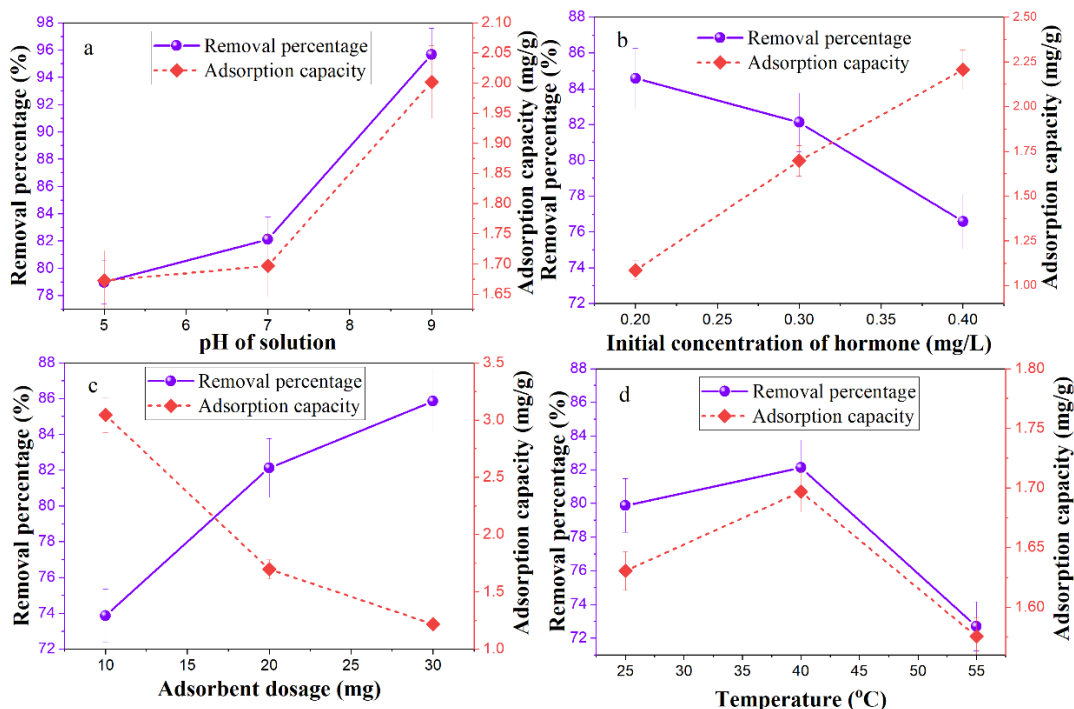


Figure 7.8: Effects of different adsorption parameters on removal percentage and adsorption capacity: a) pH of the solution, b) initial concentration of EE2, c) adsorbent dosage, and d) temperature on the removal of EE2 hormone using PU-PANI-ES fibers.

7.10 Adsorption mechanism of EE2 hormone on PU-PANI-ES fibers

The aim of this section is to elucidate the types of mechanisms that occur simultaneously and contribute to the adsorption of EE2 on PU-PANI-ES, as presented in Figure 7.9. The extent of such mechanisms depends on the types of functional groups present on the fiber, the nature of the hormone (hydrophobicity), and the amount of surface available on fibers for interaction. Based on the studied material, the types of adsorption interaction mechanisms include physical adsorption, hydrophobic interaction, π - π stacking interaction, cation- π interaction, and hydrogen bonding. EE2 has an OH terminal group, which can act as a strong donor and acceptor, while the benzene ring chain can act as a weak π acceptor [146]. In addition, the presence of high amounts of nitrogen atoms from PU and PANI increases the interaction of the adsorbent with the hormone via a hydrogen bond, electrostatic interaction, and weak van der Waals forces. Furthermore, the physical adsorption of EE2 on the surface of PU-PANI-ES with an approximate average diameter (174 ± 56 nm) and inner pores (16.99 nm) present on the fiber's surface possess a large surface area that contains active sites for accumulation of EE2 hormones [143].

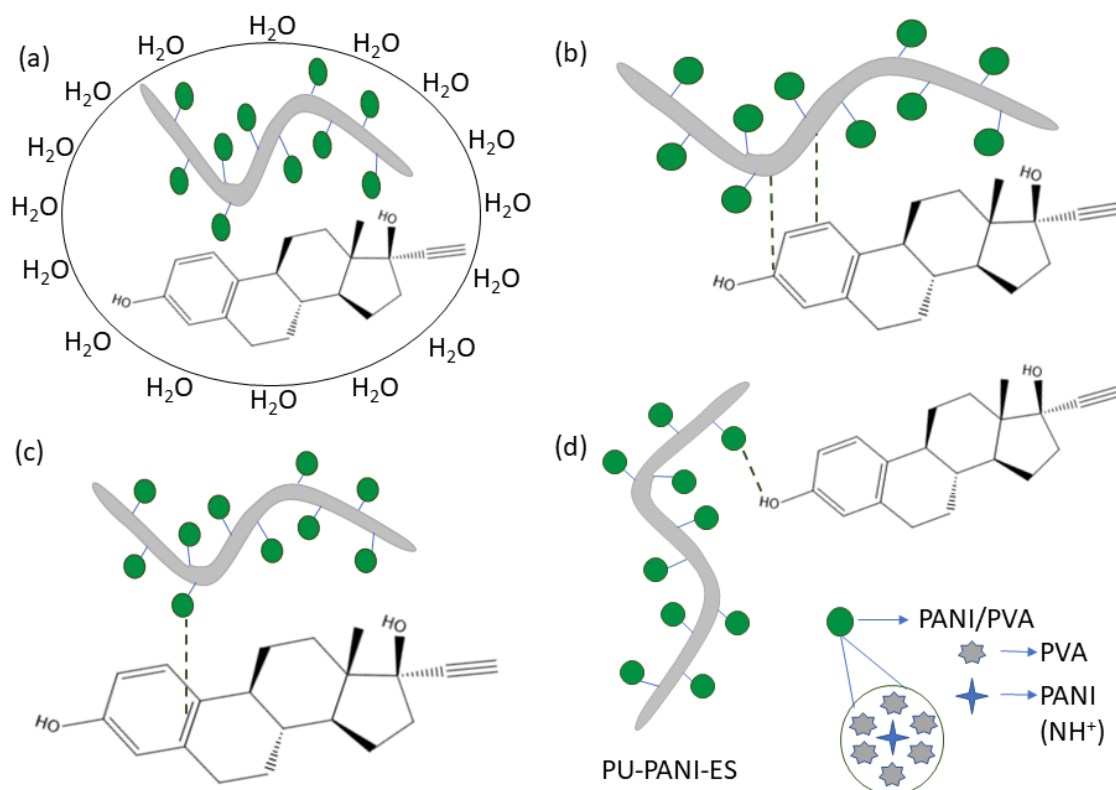


Figure 7.9: Possible interaction mechanisms between EE2 and PU-PANI-ES fibers; (a) hydrophobic interactions, (b) π - π stacking interaction, (c) Cation- π interaction, and (d) hydrogen bonding.

K_{ow} is the parameter value to determine the hydrophobicity of EE2 by partitioning between octanol and water. Hormones with a value greater than 2.50 are generally expected to accumulate in the solid phase instead of dissolving in an aqueous solution. The K_{ow} of EE2 is 3.67, which is above 2.50; thus, it is likely to undergo hydrophobic interaction with PU. Weak π - π stacking interaction also occurs between the electron-rich and deficient benzene aromatic rings (phenol group) available in PU, PANI, and EE2 hormone by overlapping of double bonds [146]. Comparing the results in Figure 7.5, the decrease in adsorption percentage from 90.30% for PU-PANI-ES to 81.50% for PU-PANI-EB is a consequence of the loss of positively charged amine groups in PU-PANI-ES when deprotonated to PU-PANI-EB, which in turn decreases the forms cation- π interaction with the aromatic benzene rings of EE2 [146]. PU is the most robust adsorbing polymer tested among other polymers in the previous study, owing to its polar nature [143]. PU consists of N-H and C=O functional groups that can form hydrogen bonding with the O-H terminal groups present in EE2 [173]. Herein, PU-PANI-ES fibers were chemically functionalized with an excess of amine groups present on the surface, as a result, enhanced the adsorption of EE2 on its surface as compared to the non-coated PU (as control). Furthermore, size-exclusion is another factor essential for membrane filtration, but it is unexpected here in the adsorption mechanism, which is primarily dependent on the molecule size of EE2, the pore size of fibers, and functional properties. The molecular size of hormones reported in the literature (0.79 nm) is far less than the mean porosity of the control PU fibers structure (0.47 μ m); hence this factor is excluded from consideration [32,143].

7.11 Kinetic modeling for the uptake of EE2 hormone by PU-PANI-ES

Comparing Figure 7.10a and b, the difference between the dotted data set experimental points is far away scattered from the line of best fit (Figure 7.10a), which indicates that the model was not completely suitable to describe the adsorption interaction between EE2 hormone and PU-PANI-ES adsorbent. Whereas Figure 7.10b showed the best fitting with the experimental data indicating the pseudo-second-order model best describes the adsorption process. This is also evident by high regression coefficients and close agreement between the experimental adsorption capacities and the calculated values, represented in Table 7.5. Figures 7.10c and d describe the kind of adsorption process occurring during the uptake of EE2 hormone by PU-PANI-ES. From Figure 7.10c, two linear regions are visible (initial half and latter half), which relates to the initial

and gradual adsorption phase and then the equilibrium phase. In addition, the boundary-layer effect was depicted not to pass through the origin region, which indicates that the process was more intraparticle diffusion-controlled in the latter half of the experiment as a consequence of the surface control effect [111,112].

Among all the calculated models from the experimental data, it can be seen that EE2 adsorption on PU-PANI-ES fibers follows the pseudo-second-order model. The experimental data set points adhere completely to the line of best fit, also observed by the high regression coefficient (R^2) of 0.998 and the calculated adsorption capacity of 2.16 mg/g is extremely close to the experimental value of 2.11 mg/g. The plausible reason that indicates these findings could be the inhomogeneous surface of available active sites on the modified adsorbent PU membrane since the adsorption rate is dependent on the concentration of hormone in the solution and the number of available sites that can actively accommodate the hormone [137]. All the supporting values of the used models are presented in Table 7.5.

Table 7.5: Kinetic models and their determining parameters related to the removal of EE2 hormone using PU-PANI-ES fibers

Pseudo-first-order		Pseudo-second order	
$q_e, exp (mg/g)$	2.11	$q_e, exp (mg/g)$	2.11
$q_e, cal (mg/g)$	1.13	$q_e, cal (mg/g)$	2.16
$K_1 (min^{-1})$	0.02	$K_2 (g/mg min)$	0.04
R^2	0.892	R^2	0.998
χ^2	0.03	χ^2	0.12
SSE	0.16	SSE	0.57
Intraparticle diffusion		Boyd	
$K_3 (mg/g min^{0.5})$	0.11	R^2	0.939
$C (mg/g)$	0.62	χ^2	0.07
R^2	0.872	SSE	0.29
χ^2	0.14		
SSE	0.84		

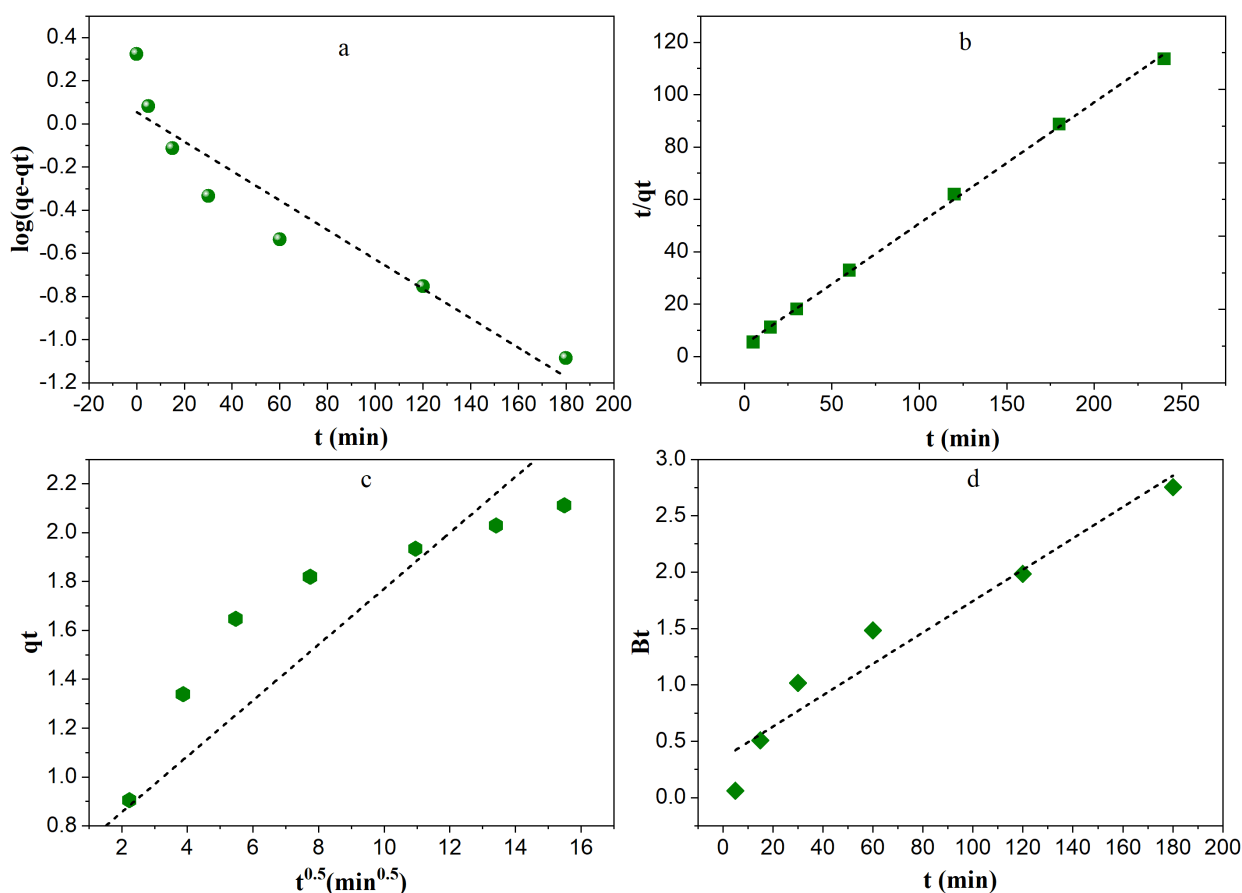


Figure 7.10: Plots of the adsorption kinetics for the EE2 hormone on PU-PANI-ES fibers: (a) pseudo-first-order, (b) pseudo-second-order, (c) intraparticle diffusion model, and (d) Boyd model.

7.12 Thermodynamic study for the adsorption of EE2 hormone

In order to understand the thermodynamic behavior of the adsorption process for the removal of EE2 by PU-PANI-ES adsorbent, the Gibbs free energy change (ΔG), enthalpy change (ΔH), and entropy change (ΔS) were determined using Eq. (4.13), (4.14), and (4.15) [122,123]. Values of ΔG at different temperatures were then calculated and are given in Table 7.6.

Table 7.6: Thermodynamic parametric values for the adsorption of EE2 hormone

Parameters	Temperature		
	298 K	313 K	328 K
ΔG (kJ/mol)	-37.52	-33.03	-28.53
ΔH (kJ/mol)		-12.67	
ΔS (J/mol K)		-29.94	

In accordance with calculated results, ΔG was determined to be negative, which is expected, indicating that the adsorption process was favorable and the reaction was spontaneous. ΔH value was negative, which confirmed the adsorption of EE2 onto the PU-PANI-ES membrane to be exothermic in nature. This explains the decrease in adsorption capacity at higher temperatures. In addition, the low ΔH value depicts that the adsorption process favors more physical adsorption rather than chemical adsorption. The values deduced and phenomena observed in the present study are in close agreement with similar previous studies on the adsorption of EH [112,174]. The negative ΔS value indicates the adsorption process was more enthalpy driven.

7.13 Reusability study of PU-PANI-ES nanofibers

After adsorption, the adsorbent material was treated by desorption of the adsorbed EE2 hormone. For the desorption test, the PU adsorbents were extracted from the conical flasks containing the hormone solutions and washed with distilled water, followed by gentle stirring at a constant 100 rpm for 10 min in a 100 mL mixture of 1:1 water and ethanol to remove the hormones entirely and eluted in the aqueous phase. Then, the PU adsorbent was re-placed in 100 mL water until the next adsorption cycle. The procedure was repeated for six consecutive adsorption-desorption cycles. Readings were collected in triplicates, and the average value was recorded.

It could be noticed from the results in Figure 7.11 that the adsorption efficiency of PU-PANI-ES for EE2 hormone remains over 80% throughout the six adsorption cycles, while desorption gradually decreases and stay stagnant at around 60% in the last two cycles. A slight rise in adsorption with the increase in the number of cycles up to four cycles was observed, which could be due to improved swelling of the adsorbent when in contact with the ethanol (alkaline medium), resulting in high adsorption. However, the efficiency gets constant and near to that of the first cycle during the fifth and sixth cycles, which can be attributed to the decrease in the swelling reversibility of PU-PANI-ES. A similar increasing and then decreasing trend was reported in the literature for acid orange II and methylene blue removal [175].

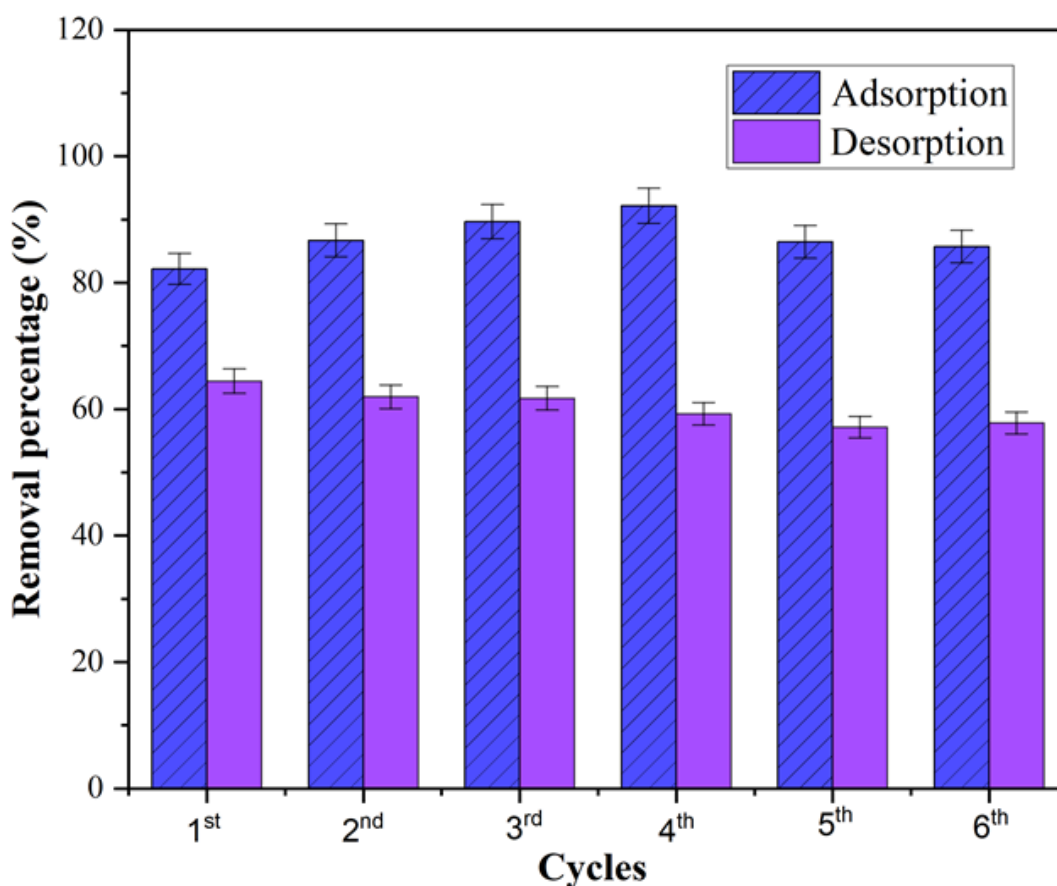


Figure 7.11: Six adsorption-desorption cycles of EE2 by PU-PANI-ES fibers.

7.14 Comparative study of PU-PANI-ES with other adsorbents for EE2 hormone removal

The following Table 7.7 demonstrates the adsorbent fibers and particles reported in the literature with their total adsorption capacities for capturing EE2 hormone compared to this study. As can be seen, the adsorption capacity of PU-PANI-ES reported in this study is 2.11 mg/g. This value is relatively high compared to similar reported previous studies. It is noteworthy to mention the significance of produced electrospun modified nanofibrous membrane in this study. However, considering Norit AC, Darco AC, and PA612 particles, the adsorption capacity value of these materials is still quite higher than the current study, which can be attributed to the nature of those materials and the relatively large surface area they possess (5.12 - 17.64 m²/g) in general as compared to fibrous materials.

Table 7.7: Comparison of adsorbents for EE2 hormone removal

Adsorbents	pH and temperature (°C)	Adsorption capacity (mg/g)	Reference
MWCNTs	6.30 and 25	0.47	[112]
PA612, Darco AC, Norit AC	7.00 and 25	25.42 27.61 10.40	[176]
Un-anthracite, 4 K anthracite	7.00 and 25	0.21 0.62	[177]
PU Elastollan, PU 918, PA	7.00 and 25	0.74 0.64 0.61	Our previous work [143]
PU-PANI-ES	7.00 and 40	2.11	Present study

7.15 Conclusions

In this study, we successfully investigated the removal of a steroid hormone from water by lab synthesized spun polyurethane nanofiber membrane modified with PANI in PVA solution as the supporting polymer. The different spun and treated PU nanofiber membranes were chemically and morphologically characterized via FTIR, SEM, and optical microscopy. PU-PANI-ES as a modified material was demonstrated to be the most efficient with 90.30% removal efficiency of the studied hormone as compared to its base form PU-PANI-EB (81.50%) and neat PU (55.40%) as control. PU-PANI-ES was further evaluated via an optimization study using the CCD model to determine its optimum removal conditions for EE2 hormone. According to the results obtained, the model proved to be significant for the optimization of the removal of the EE2 hormone with a high regression coefficient (R^2) of 0.983. The optimum parameters were found to be pH 7 (considering that wastewater or river water is in the range of pH 6-8), the temperature of 40 °C, 0.3 mg/L concentration of EE2, and 20 mg of PU-PANI-ES dosage. In addition, the adsorption was studied kinetically using different kinetic models, and the results depicted that the removal of EE2 hormone best fitted the pseudo-second-order model with maximum adsorption capacity determined as 2.11 mg/g. This obtained value proved to be significantly high compared to the other similar adsorbents in the literature. Furthermore, the adsorption efficiency was demonstrated to be temperature sensitive and decreased considerably at a higher temperature. This was supported by a thermodynamic

study that showed the adsorption process is spontaneous and exothermic in nature. Finally, the recovery of EE2 hormone and reusability of PU-PANI-ES adsorbent depicted a good removal percentage which remained over 80% for tested six consecutive adsorption-desorption cycles. Overall, the reported results proved that the modification of the spun PU nanofiber with PANI significantly improved hormone removal from water and can be considered a promising adsorbent membrane for the remediation of different steroid hormones from water.

8. The adsorptive behavior of electrospun hydrophobic polymers for optimized uptake of estrogenic sex hormones from aqueous media: Kinetics, thermodynamics and reusability study

The study in this chapter aims to fabricate and test hydrophobic electrospun nanostructures of the thinnest fiber diameter and ample surface area to volume ratio for more adsorption sites. To remove EH from wastewater, it is focused on using nanostructured membranes constructed from polymers with strong sorption activity. The goal is to simultaneously adsorb multiple EH from wastewater at neutral pH in a one-step procedure and quantify by HPLC. To understand the characteristics, and interactions mechanisms involved, further investigate the feasibility of the results using the experimental data to determine adsorption capacity with contact time and measure kinetics with appropriate models of pseudo-first-order, pseudo-second-order, intraparticle diffusion, Elovich, and fractional power models. Furthermore, one-way variance in ANOVA was deployed for optimized adsorption process by varying conditions such as pH, temperature, the concentration of adsorbate, and adsorbent dosage to determine suitable Isothermal model and thermodynamics. Finally, the research evaluates the reusability of prepared spun fibers over six adsorption-desorption cycles to determine their consistent effectiveness and recovery of EH.

8.1 Characterization of materials

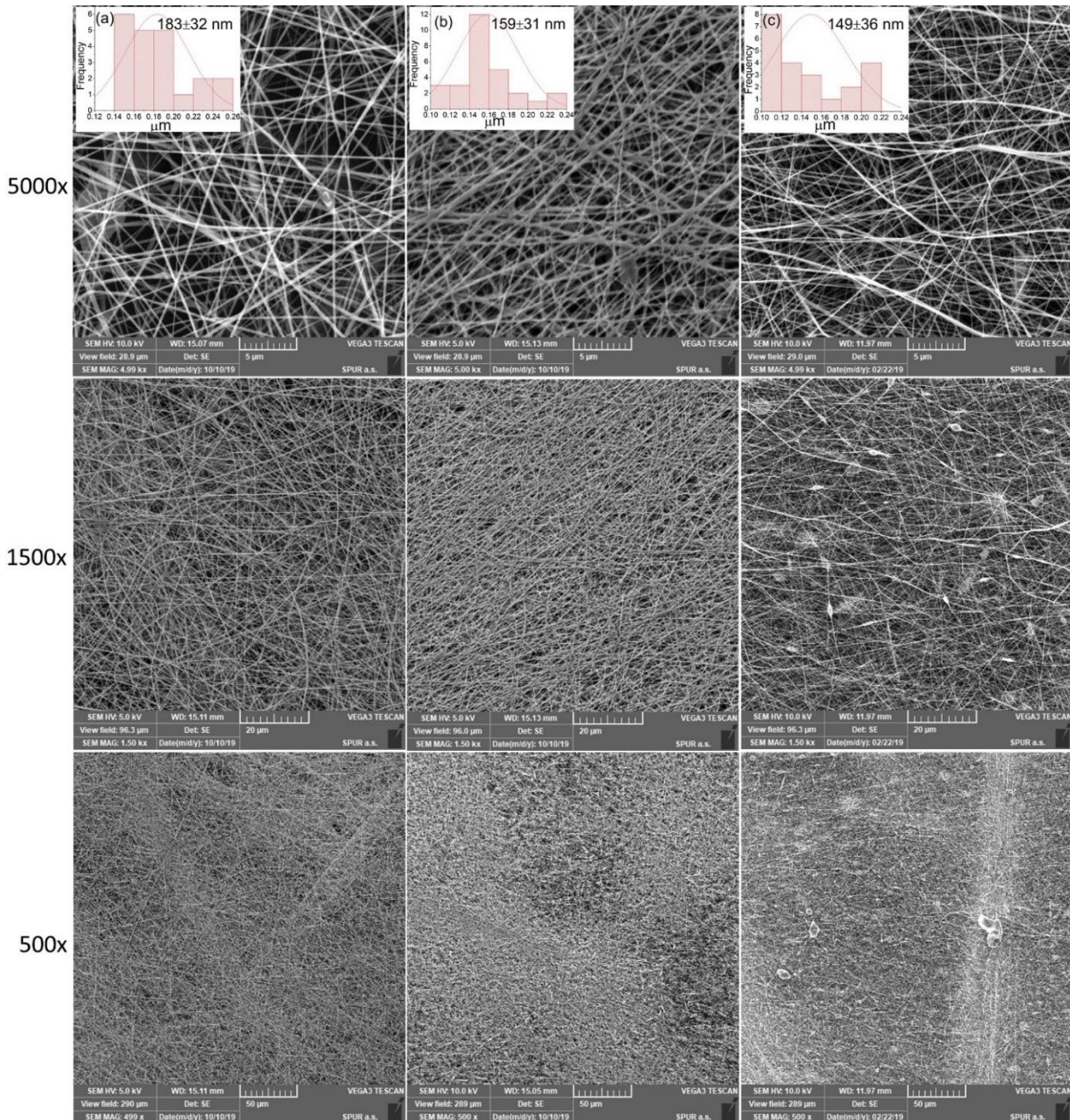


Figure 8.1: Electron micrographs with (inset) distribution of frequency size of the electrospun nanofibers (a) PSU, (b) PLA, and (c) PVDF at different magnifications of 500x, 1500x, and 5000x.

Figure 8.1 reveals that the electrospun nanofibers were produced without beads or defects, as desired. The calculated average fiber diameters from SEM were in the range of 149–183 nm, which are firmly in compliance with the range of electrospun nanofiber (174–330 nm) reported in Table 5.1 and literature [143]. These low achieved diameters are attributed to the optimized parameters used to prepare electrospinning solutions, including low polymer concentration in the

solution, intrinsic viscosity, and electrical conductivity (Table 3.1). Further properties are mentioned in Table 8.1.

Table 8.1: SEM, BET, and porosimetry data of electrospun polymeric fiber materials

Nanofiber	Average fiber diameter SEM (nm)	Porometry Mean pore size (μm)	Air permeability ($\text{l}/\text{cm}^2\cdot\text{min}\cdot\text{bar}$)	BET surface area (m^2/g)
PSU	183 ± 32	0.91	244	6.267
PLA	159 ± 31	1.10	197	0.302
PVDF	149 ± 36	0.39	077	1.612

It can be seen in Table 8.1 that the mean pore size ranged from 0.39 - 1.10 μm and air permeability from 77-244 $\text{l}/\text{cm}^2\cdot\text{min}\cdot\text{bar}$, which are inversely dependent on the average mass of nanofiber per unit area (Table 3.1), the relative structural porosity is also visible in SEM micrographs at the same magnification. The measured BET surface area ranged from 0.3 - 6.3 m^2/g , which is directly dependent on the intrinsic viscosities of the solutions (PSU ~ 2.0 , PLA ~ 0.5 , and PVDF ~ 1.5 Pa.s) prior to electrospinning. The effect of the surface area is also evident in the preliminary test for the adsorption of hormones, where PSU was observed to adsorb and remove the highest percentage of hormones.

To investigate the physiochemical features of electrospun nanofibers. The TGA graphs in Figures 8.2 (a, b, and c) displayed that no nanofibers degradation was observed up to 100 $^{\circ}\text{C}$ for any polymer. A slight initial dip in Figures 8.2a, b, and c is due to the evaporation of water, while the weight loss started at around 200 $^{\circ}\text{C}$ for PSU, about 300 $^{\circ}\text{C}$ for PLA, and nearly 400 $^{\circ}\text{C}$ for PVDF, which is far above the tested experimental range for adsorption in this study. Additionally, the degradation with a rapid weight loss was observed at 517.73, 345.69, and 480.22 $^{\circ}\text{C}$ for PSU, PLA, and PVDF, respectively. The XRD (Figure 8.2d) also revealed that a broad peak region was observed for each polymer around $2\theta = 17-20^{\circ}$, which indicates the semi-amorphous nature of the polymer electrospun nanofibers. For PVDF, two broad spikes are seen at around 18° and 22° that belong to the α and β phases, respectively [178].

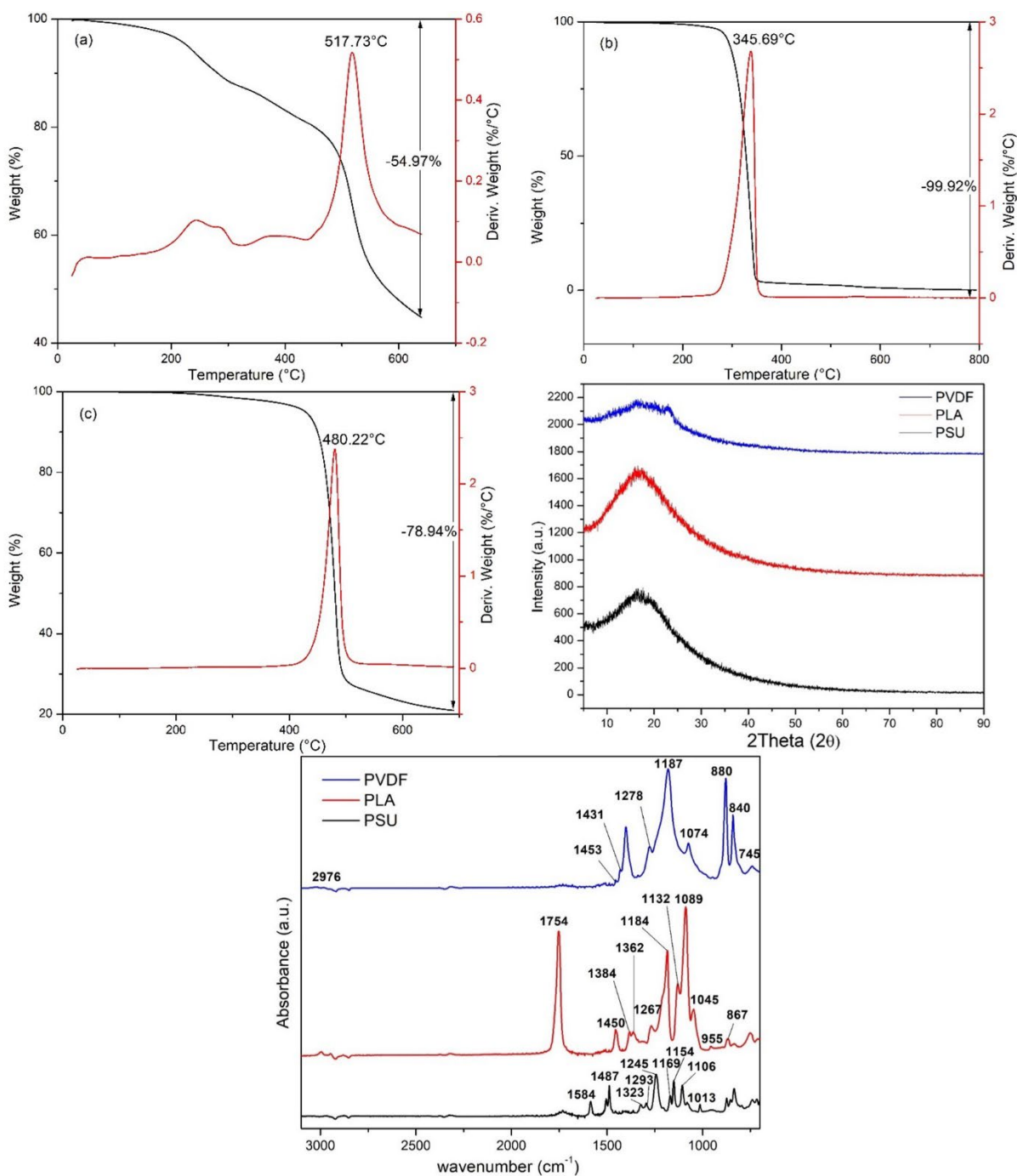


Figure 8.2: Thermogravimetric analysis of (a) PSU, (b) PLA, (c) PVDF, (d) X-ray diffractograms, and (e) FTIR spectra of the different electrospun nanofibers.

The IR spectra in Figure 8.2e shows a characteristic peak at about 2974 cm⁻¹ assigned to CH₂ symmetric stretching present in all three polymeric nanofibers. Then, the spike at 1453 cm⁻¹ for PVDF is the scissoring or in-plane bending of CH₂ in the α -phase. Furthermore, the rocking of CH₂ or CF₂ asymmetric stretching is observed at 840 cm⁻¹, and in-plane bending at 745 cm⁻¹ is seen in the β -phase [179]. PVDF appears in different crystal phases; the spike at 840 cm⁻¹ is

considerably large, representing the β -phase, as well as the peaks at 1431 and 1278 cm^{-1} define the crystalline phase. The peak at 1074 cm^{-1} is mainly due to the β -phase, but traces of other phases could also be found around this location in the literature [178]. The absorption peak at 1187 cm^{-1} is due to the combination of β and γ phases, and the large peak at 880 cm^{-1} is a result of the combination of all existing phases. Whereas peaks at 840 and 1278 cm^{-1} are the usual β -phase peaks [180].

In PLA, the characteristic peaks observed at 1754, 1267, and 754 cm^{-1} assigned to $\text{C}=\text{O}$ are due to the strength vibration, bending vibration, and torsion vibration, respectively. The peak located at 955 cm^{-1} corresponds to $\text{C}-\text{C}$ group. In addition, the spikes at 1132, 1045, and 867 cm^{-1} belong to $\text{C}-\text{O}$ groups for strength vibration. The deformation of $\text{C}-\text{H}$ appears at 1450 cm^{-1} , and the symmetric and asymmetric strength vibration of the -CH bond is indicated at 1362 and 1384 cm^{-1} . The formed peaks at 867 and 754 cm^{-1} are evidence of the amorphous and crystalline regions present in PLA, respectively [181].

The spectra peak intensity for PSU revealed at 1323, and 1293 cm^{-1} corresponds to the asymmetric absorption of the $\text{S}=\text{O}$ group, while the peak at 1169 cm^{-1} belongs to the symmetric absorption of the $\text{S}=\text{O}$ group. In addition, the characteristic absorption peaks at 1584 and 1487 cm^{-1} are attributed to the benzene rings [182]. The main characterized peaks are present at 1584, 1245, 1323, 1154, 1106, and 1013 cm^{-1} , corresponding to the stretching caused by aromatic $\text{C}=\text{C}$, $\text{C}-\text{O}-\text{C}$ (ether group), and $\text{O}=\text{S}=\text{O}$ bonds, respectively [183].

8.2 Batch adsorption studies

8.2.1 Preliminary adsorption for different prepared hydrophobic polymeric nanofibers

To evaluate and distinguish the efficiency of the prepared spun PSU, PLA, and PVDF nanofibers, short-term batch tests using the materials were performed to ascertain their adsorption efficiency against four different hormones of E1, E2, EE2, and E3. According to deduced results (Figure 8.3a), spun PSU showed more than 50% removal efficiency for almost all studied hormones. Removal efficiency for the different spun nanofibers was in the magnitude of $\text{PSU} > \text{PLA} > \text{PVDF}$. Based on this initial evaluation, spun PSU material was used for subsequent study due to its high adsorption capacity for different EH.

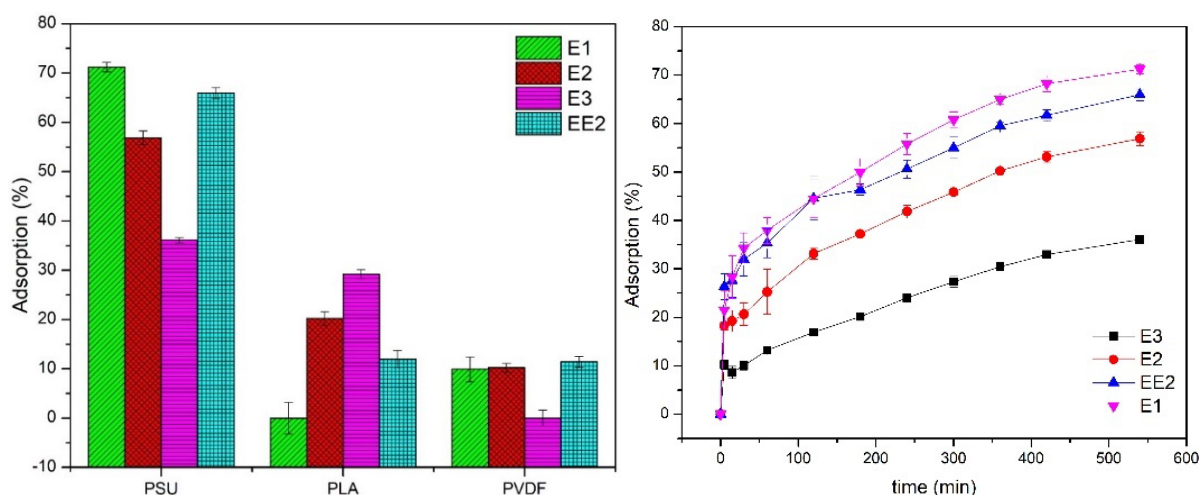


Figure 8.3: (a) Comparative adsorption efficiency of hormones (E1, E2, E3, and EE2) on PSU, PLA, and PVDF electrospun nanofibers (left panel), and (b) Adsorption efficiency trends of E1, E2, E3, and EE2 hormones on PSU nanofibers as a function of time (right panel). (pH: 7, concentration of each hormone: 0.2 mg/L, and testing duration: 9 h)

8.2.2 Effect of contact time

The contact time plays a major role in the adsorption of the hormones onto the different spun nanofibers. The effect of contact time on the adsorption of the various hormones (E1, E2, EE2, and E3) by spun PSU as the adsorbent with the highest adsorption capacity was further investigated and is shown in Figure 8.3b. It can be observed that the initial uptake of the hormones occurred within the first 2 h, and after that, a gradual increase with time up to 9 h depicted as apparent equilibrium. This initial rapid uptake of the hormones could be due to the availability of the adsorption sites on the adsorbent materials. It was evident that the adsorbed amount of the hormones adsorbed onto the adsorbent increased by increasing the contact time. After 4 h, the removal of the hormones from the aqueous phase was more than 50%. The removal capacity of PSU for the different hormones was in the magnitude of $E1 > EE2 > E2 > E3$. This indicated that the E1 hormone had the highest binding affinity to PSU. This may be due to the stoichiometric structural arrangement of the E1 hormone molecule that favored more hydrogen bonds and π - π interaction with the adsorbent [143].

8.3 Adsorption kinetics for PSU nanofibers

The adsorption of EH on PSU increased with time until equilibrium was achieved. The initial rate was fast for 60 min, and then it gradually decreased with an increased contact time, assuming saturation at 540 min. The adsorption kinetic plots for the adsorption of E1 on PSU nanofibers are shown in Figure 8.4, and the

obtained kinetic parameters from the models mentioned above are presented in Table 8.2. Several kinetic models were used to investigate the experimental data that can best fit to understand the ability of concomitant adsorption of EH on the surface of PSU fibers. In Figure 8.4a, the plotting $\ln (q_e - q_t)$ vs. t shows a strong agreement of E3 hormone with a linear best fit line covering the data set points, and the predicted adsorption capacity of 0.307 mg/g is close to the experimental equilibrium adsorption capacity of 0.354 mg/g with a high regression coefficient of 0.954. Whereas the theoretical adsorption capacities for E1, E2, and EE2 are 0.367, 0.423, and 0.451, which are unsatisfactory and reasonably less expected compared to the experimental values of 0.508, 0.550, and 0.703 mg/g, respectively. However, the rate constant K_1 is precise and similar for each EH, but the data set points do not match the generated lines of best fit for E1, E2, and EE2 for the pseudo-first-order equation.

For Figure 8.4b, the plots of t/q_t vs. t must be linear lines to accurately and precisely estimate the q_e and k_2 values from the slopes and y-intercepts of each data set, respectively. The results obtained clearly indicate that E1, E2, and EE2 EH follow Pseudo-second order model kinetics. The data set points mostly match the lines of best fit with a high regression coefficient of 0.962, 0.970, and 0.975 for E1, E2, and EE2, respectively. Also, the calculated adsorption capacities of 0.528, 0.576, and 0.715 are strongly in compliance with the experimentally achieved values of 0.508, 0.550, and 0.703, respectively. The slightly lower values obtained during the experiment are referred to as the inhomogeneous active sites on the surface of PSU because the rate of adsorption is primarily dependent on the concentration of hormone solution and the number of available active sites present on the surface of the adsorbent material. Similar results have been observed and reported by Al-Khateeb *et al.* in the literature using MWCNTs as an adsorbent for these hormones. The adsorption capacities reported were 0.423, 0.472, and 0.472 for E1, E2, and EE2, respectively [120]. Furthermore, E3 shows a clear mismatch using the pseudo-second-order model. The data points do not fit the linear best fit line, and in fact, two separate portions are observed; one for the first 120 min and the second from 180 min till the end of the experiment. The plots in Figure 8.4b were used to determine the rate constants (k_2) and the calculated equilibrium adsorption capacities (q_e) expressed in Eq. (4.2) to obtain the regression coefficient (R^2) shown in Table 8.2.

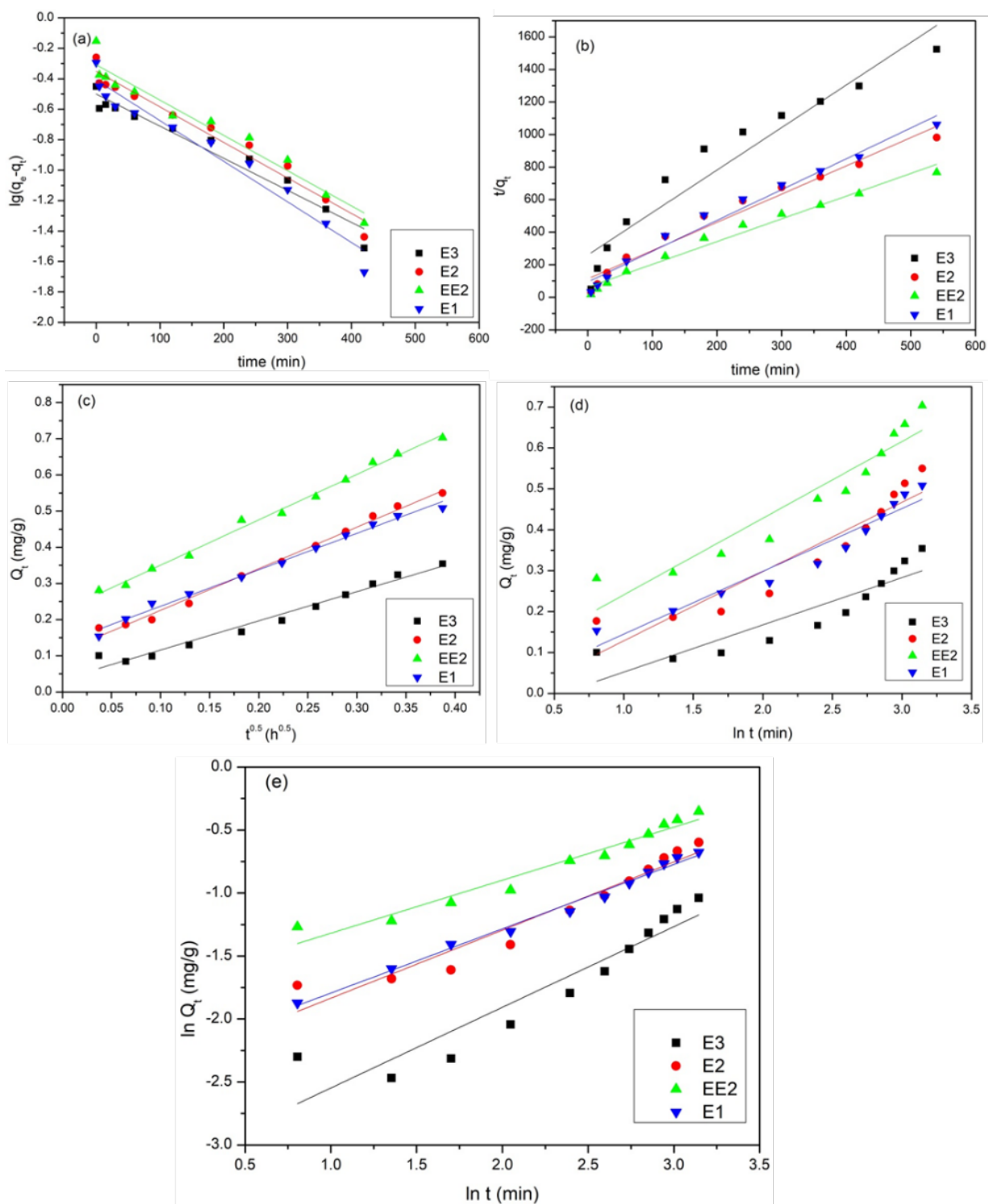


Figure 8.4: Adsorption kinetics plots of the four estrogenic hormones (E1, E2, EE2, E3) on PSU nanofibers, (a) Pseudo-first-order, (b) Pseudo-second-order, (c) Weber-Morris intraparticle diffusion, (d) Elovich, and (e) Fractional power model.

The plot of q_t vs. $t^{0.5}$ is shown in Figure 8.4c, representing the intraparticle diffusion model. The linear plots of all EH have a high regression coefficient of 0.992, 0.993, 0.995, and 0.975 for E1, E2, EE2, and E3, respectively, but the plots

do not intercept through the origin. This indicates that intraparticle diffusion is involved in the adsorption process, but it is only a part of the mechanism and is not wholly the rate-determining step. The plausible reason could be that EH do not converge properly. This could be due to the surface boundary layer effects that might have dominated the interaction of the adsorption process in the latter half. Therefore, the diffusion rate decreases as the adsorption progresses, and a gentle slope is observed because of the low concentration of EH remaining in the solution.

The plot in Figure 8.4d of q_t vs. $\ln t$ depicts high adsorption rates per minute, which indicates and elucidates that chemisorption is the most dominant adsorption mechanism in the interaction of EH with PSU nanofibers. EE2 had the highest adsorption capacity of 0.703 mg/g and an initial adsorption rate of 18.870 g/mg.min. The descending order of removal rates is in the magnitude of EE2>E1>E2>E3, with E1 having the highest regression coefficient of 0.942 and the highest overall adsorption removal percentage (Figure 8.3) owing to its binding affinity to PSU. The plausible reason could be the stoichiometric structural arrangement of the E1 molecule that favored more hydrogen bonds and π - π interactions with the PSU fibers based on its structure.

In Figure 8.4e, the plots of $\ln q_t$ vs. $\ln t$ are represented. As can be seen, an entire mismatch is evident for most of the EH, except for E1, where a linear relationship is seen with a regression coefficient of 0.990, but the adsorption capacity is unsatisfactory. This indicates that the fractional power model is not appropriate for these EH. The calculated parameters using Equations (4.7), (4.8), (4.9), (4.10), and (4.11) are shown in Table 8.2.

Table 8.2: The kinetic models' parameters with each hormone using PSU electrospun nanofibers

Models parameters	Hormones			
	E1	E2	EE2	E3
q_e , expt (mg/g)	0.508	0.550	0.703	0.354
<i>Pseudo-First Order model</i>				
k_1 (min ⁻¹)	0.003	0.002	0.002	0.002
q_e , cal (mg/g)	0.367	0.423	0.451	0.307
R^2	0.962	0.970	0.975	0.954
<i>Pseudo-Second Order model</i>				
k_2 (g/mg.min)	0.038	0.027	0.031	0.026
q_e , cal (mg/g)	0.528	0.576	0.715	0.383
R^2	0.980	0.968	0.981	0.929
<i>Intraparticle diffusion model</i>				
k (mg/g h ^{0.5})	1.009	1.152	1.256	0.807
I (mg/g)	0.136	0.110	0.225	0.035
R^2	0.992	0.993	0.995	0.975
<i>Elovich Model</i>				
α (g/mg.min)	11.641	7.302	18.870	5.796
β (mg/g.min)	0.077	0.085	0.094	0.058
R^2	0.942	0.881	0.909	0.819
<i>Fractional power model</i>				
a	0.100	0.093	0.176	0.041
b	0.255	0.270	0.210	0.320
$a+b$	0.025	0.025	0.037	0.013
R^2	0.990	0.939	0.957	0.885

8.4 Adsorption based on the variation of single parameters

Following the preliminary adsorption, contact time, and kinetic studies, the E1 hormone was selected as the most suitable hormone for further investigation of adsorption due to its high interaction with the adsorbents, leading to the highest removal efficiency. As one of three major endogenous estrogens found in humans, this hormone serves as a suitable candidate. Different adsorption parameters of solution pH, hormone concentration, adsorbent dosage, and temperature effect were investigated by varying one factor and keeping the others constant.

8.4.1 Effect of solution pH

Solution pH is a vital index-controlling parameter for the adsorption performance of an adsorbent. The solution pH was varied from 3 to 9 at a constant dosage of

20 mg, 0.2 mg/L hormone concentration, pH 7, and temperature 25 °C under shaking at 150 rpm. Figure 8.5a reveals that the hormone uptake by PSU is slightly affected by the initial solution pH ranging from 3.0 to 7.0, while the adsorption efficiency significantly increased from pH 7 to 9. The lowest removal efficiency was observed at pH 3 at 44.32% compared to 79.92% determined at pH 9.0. This observation can be traceable to the ionization state of the estrone (E1) hormone molecule. Generally, EH is considered weak Lewis acid, and its ionization state is strongly dependent on solution pH. The reported value in literature for pK_a of E1 is approximately 10.34 [146]. pK_a represents the acid dissociation constant of E1, which above this value, the hormone deprotonates and becomes negatively charged, thereby losing its hydrogen atom affinity. As such, the adsorption study was investigated below pH 9 to favor interaction between the hormone molecules and the adsorbent materials [184]. Though maximum adsorption was achieved at pH 9, for environmental and better safety handling of the system, pH 7, which shows more than 50% removal efficiency, was selected as the most suitable solution pH.

8.4.2 Effect of E1 hormone concentration

The effect of the initial concentration of the hormone on spun PSU adsorption properties was investigated as presented in Figure 8.5b. According to the plot, the amount of hormone adsorbed on spun PSU was evaluated by varying initial concentrations from 0.1 to 0.5 mg/L at a dosage of 20 mg, pH 7, and temperature of 25 °C under shaking at 150 rpm. It was observed that the amount of hormone adsorption increased with an increase in initial concentration. However, the removal efficiency decreases with an increase in initial hormone concentration. As seen depicted in Figure 8.5b, the removal efficiency decreased from 52.95% to 48.62%. This phenomenon was attributed to the gradual saturation of the adsorbent adsorption sites with an increase in initial hormone concentration [185].

8.4.3 Effect of PSU adsorbent dosage

The dosage of adsorbent plays a crucial role in the whole adsorption process. Investigations were performed by varying the amount of spun PSU (10, 20, 30, and 40 mg) while keeping the other factors constant at 0.2 mg/L, pH 7, and temperature 25 °C under shaking at 150 rpm. Figure 8.5c shows that increasing the amount of adsorbent led to increased adsorption capacity. This is ascribed to more available adsorption sites as the amount of the adsorbent increases, allowing for an increase in the number of hormone pollutants attached to the adsorbent [186]. It is evident that increasing the amount of the adsorbent directly increases

the adsorption surface giving rise to an increased removal percentage of the hormone from an aqueous phase. The removal efficiency rises from 37.42% to 79.82% by increasing the adsorbent amount from 10 mg to 40 mg. In addition, it was observed that the removal percentage was greater than 50% using adsorbent amounts ≥ 20 mg.

8.4.4 Effect of temperature

The effect on removal efficiency of the hormone by spun PSU was investigated by varying the medium's temperature (25, 35, and 45 °C) at constant 20 mg, 0.2 mg/L, and pH 7 under shaking at 150 rpm. Based on obtained results (Figure 8.5d), low temperatures (25 and 35 °C) favored higher adsorption capacity as compared to a decrease in adsorption at elevated temperatures (45 °C). This observation was mainly attributed to the exothermic nature of the adsorption process [187]. In addition, low adsorption at elevated temperatures may relate to the denaturing of the molecular hormone structure, affecting binding affinity to the adsorbent adsorption sites. The adsorption efficiency of the hormone was most significant at 35 °C, with a removal capacity of 65.33% compared to 40.26% for higher temperatures. This suggested that adsorption at mild room temperature best suited the removal of the hormone, and continued heating would decrease the adsorption efficiency. Thus, for economic and environmental considerations, the best conditions for removing the EH were suitable for temperatures between 25 – 35 °C.

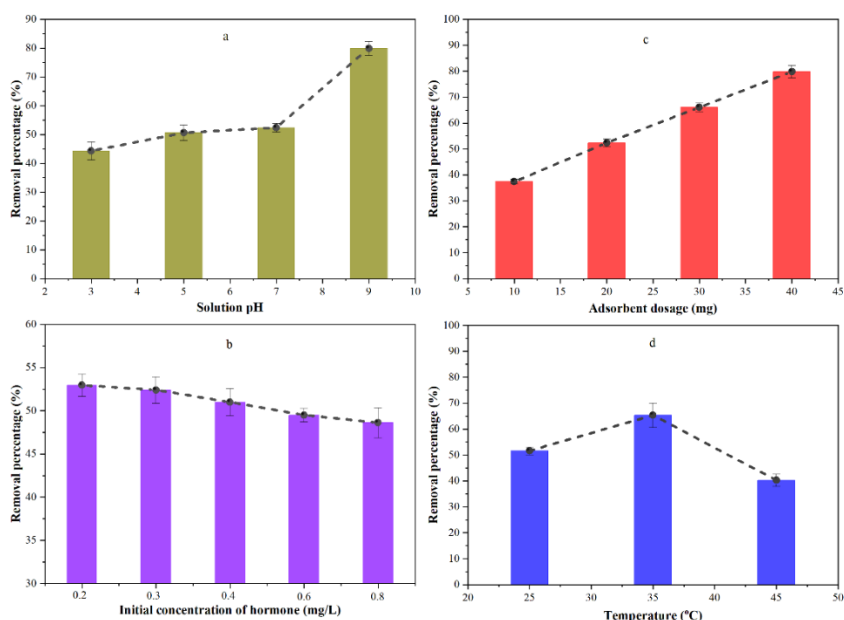


Figure 8.5: Effects of different adsorption parameters: a) solution pH, b) initial adsorbate concentration, c) adsorbent dosage, and d) temperature on the removal of E1 hormone using spun PSU nanofibers.

8.5 Adsorption mechanism of E1 on PSU

The types of mechanism depend on several factors such as the hydrophobic nature of the hormone, surface area of the polymeric nanofiber available for active sites interaction, functional groups present on hormone and nanofiber, and pH of the solution. There can be more adsorption mechanisms present together that contribute to and can lead to the adsorption of E1 on PSU nanofibers, as shown in Figure 8.6. Size exclusion can contribute to a negligible amount of adsorption on the surface of PSU nanofibers (BET mean pore diameter on fiber surface was 10.288 nm and SEM mean fiber diameter equaled 183 ± 32 nm). This is expected because the reported diameter size of the E1 molecule in literature is approximately 0.8 nm using the Stokes-Einstein equation [188]. Thus, a minuscule amount of E1 molecules can be entrapped in the pores on the fibers' surface. However, most of the E1 molecules can readily pass through the porous non-woven structure of nanofibers owing to its mean porosity of 0.91 μm and similarly for PLA (1.10 μm) and PVDF (0.39 μm). Additionally, the dissociation of hydroxyl groups of E1 attached to its aromatic rings is dependent on the acid dissociation constant (pK_a); this value of E1 is 10.34, which is higher than that of phenol ($pK_a = 10$). This indicates that E1 would not deprotonate and stay predominantly neutral at $\text{pH} < 10.5$; therefore, the influence of electrostatic charge is absent in this system. The other possibility of E1 adsorption on the PSU internal and external surfaces could be due to the hydrophobic interactions; the $\log K_{ow}$ (octanol-water partitioning coefficient) is 3.43, which is a greater value than 2.5; therefore, it suggests that E1 could readily be adsorbed on hydrophobic surfaces of PSU, PLA and PVDF nanofibers. Next, the electron-rich and deficient benzene aromatic rings possessed by both adsorbate (E1) and the adsorbent (PSU) will lead to π - π interactions by overlapping double-bonded C=C atoms present in the two molecules. Furthermore, the phenolic hydroxyl and carbonyl functional groups present on E1 can facilitate the formation of hydrogen bonding by acting as either a proton donor or acceptor. However, in this case, the -OH terminal group present in E1 molecules will serve as a proton donor and bind with the groups containing highly electronegative oxygen atoms in the structure of PSU nanofibers [188]. Similarly, the C=O bond present at 1754 cm^{-1} in PLA (Figure 8.2e) is responsible for its hydrogen bonding with hormones; however, this interaction is absent in the case of PVDF. This is the strongest of all the interactions and provides a boost in the rapid adsorption of the E1 hormone. Similar hydrogen bonding interactions of nylon 6,6 membrane and electrospun polyurethane fibers with E1 are reported in the literature [39,143]. Hence, a

similar interaction behavior is expected to occur in the remaining hormones (E2, EE2, E3) of the same estrogenic family [146].

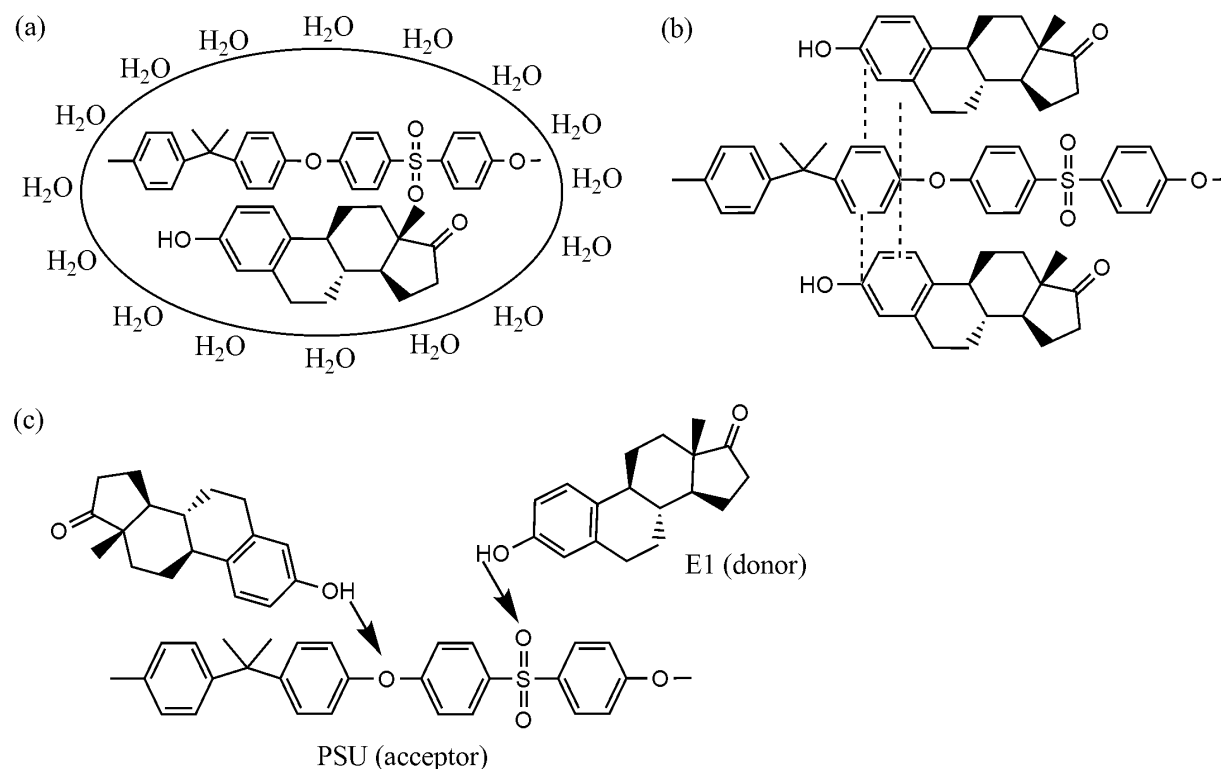


Figure 8.6: Schematic representation of the possible different interaction mechanisms between PSU nanofibers and E1 hormone; (a) hydrophobic interactions, (b) π - π stacking interaction, and (c) hydrogen bonding. Strong bonding interactions are represented with bold arrows, while weak interactions are represented with dotted lines.

Therefore, comparing the types of adsorption interaction mechanisms between EH and PSU nanofibers with PLA and PVDF, the overall descending trend of hormones adsorption on nanofibers is PSU > PLA > PVDF, which is also evident from Figure 8.3a.

8.6 Thermodynamic study for adsorption of E1 hormone on PSU nanofibers

The thermodynamic parameters were estimated by plotting a Van't Hoff plot of $\ln K_D$ versus $1/T$, while values of ΔS and ΔH were determined from the slope and intercept, respectively. Values of ΔG at different temperatures were then calculated using Eq. (4.13), (4.14), and (4.15) are given in Table 8.3. In general, the adsorption capacities of the PSU sample decreased at higher temperatures (Figure 8.5d). The highest increase in adsorption capacity occurred by increasing the temperature from 25 to 35 °C. This increase in temperature may have

facilitated diffusion of the hormone molecules through the spun PSU material's matrix, thereby favoring adsorption. The calculated thermodynamic parameters summarized in Table 8.3 depicted ΔH and ΔG values to be negative. This indicated that the adsorption process of the EH onto PSU was exothermic and spontaneous, demonstrating favourability at lower temperatures. The values of ΔG , ranging from -0.536 to -0.59 kJ/mol, imply that evaluated EH was adsorbed onto PSU through the mechanism of physical adsorption. The ΔH value (≤ 20 kJ/mol) determined for the hormone adsorption on PSU also suggested that adsorption occurred through the mechanism of physical adsorption [184]. The negative ΔS entropy value suggested a decrease in randomness at the solute/solid interface.

Table 8.3: Thermodynamic parametric values for the adsorption of E1 hormone

Parameters	Temperature		
	298 K	308 K	318 K
ΔG° (kJ/mol)	-0.596	-0.566	-0.536
ΔH° (kJ/mol)		-1.478	
ΔS° (J/mol K)		-2.958	

8.7 Isotherm modeling

By plotting q_e vs. C_e , the equilibrium adsorption data were fitted with isotherm models as presented in Figure 8.7, while the calculated isothermal parameters are given in Table 8.4.

The Langmuir model is based on the assumption of monolayer coverage on a homogenous surface with identical adsorption sites, given there is no interaction between the adsorbate molecules, while the Freundlich model describes multilayer adsorption with the interaction between adsorbate molecules and heterogeneous adsorbent surface for various adsorption sites [189,190]. Adsorption capacities of spun PSU increased with initial hormone concentration, although the characteristic plateau was not achieved in the investigated concentration range. According to R^2 values (> 0.990), both models fit well with

the experimental. This was supported by the low values obtained for the other error analysis parameters (Sum of squared errors and Chi-squared). However, the experimental data best fit with the Freundlich isotherm model. This indicates that the adsorption of the hormones on the surface of PSU was mainly heterogeneous. Freundlich parameter K_F is an indication of the PSU capacity, while n is a measure of surface heterogeneity. For the investigated hormone, the n value was below one, indicating the heterogeneous surface of the adsorbent. Maximum adsorption capacities calculated from the Langmuir isotherm was 10.65 mg/g for hormone, which was in close agreement with that calculated from the combined Langmuir-Freundlich isotherms was 12.88 mg/g, indicating the suitability of these isotherms in describing the adsorption process of the hormone on the adsorbent. Similar results for the same hormone have been reported by Patel *et al.* [186] and Prokic *et al.* [124], with maximum adsorption capacities determined as 10.12 mg/g and 12.66 mg/g, respectively.

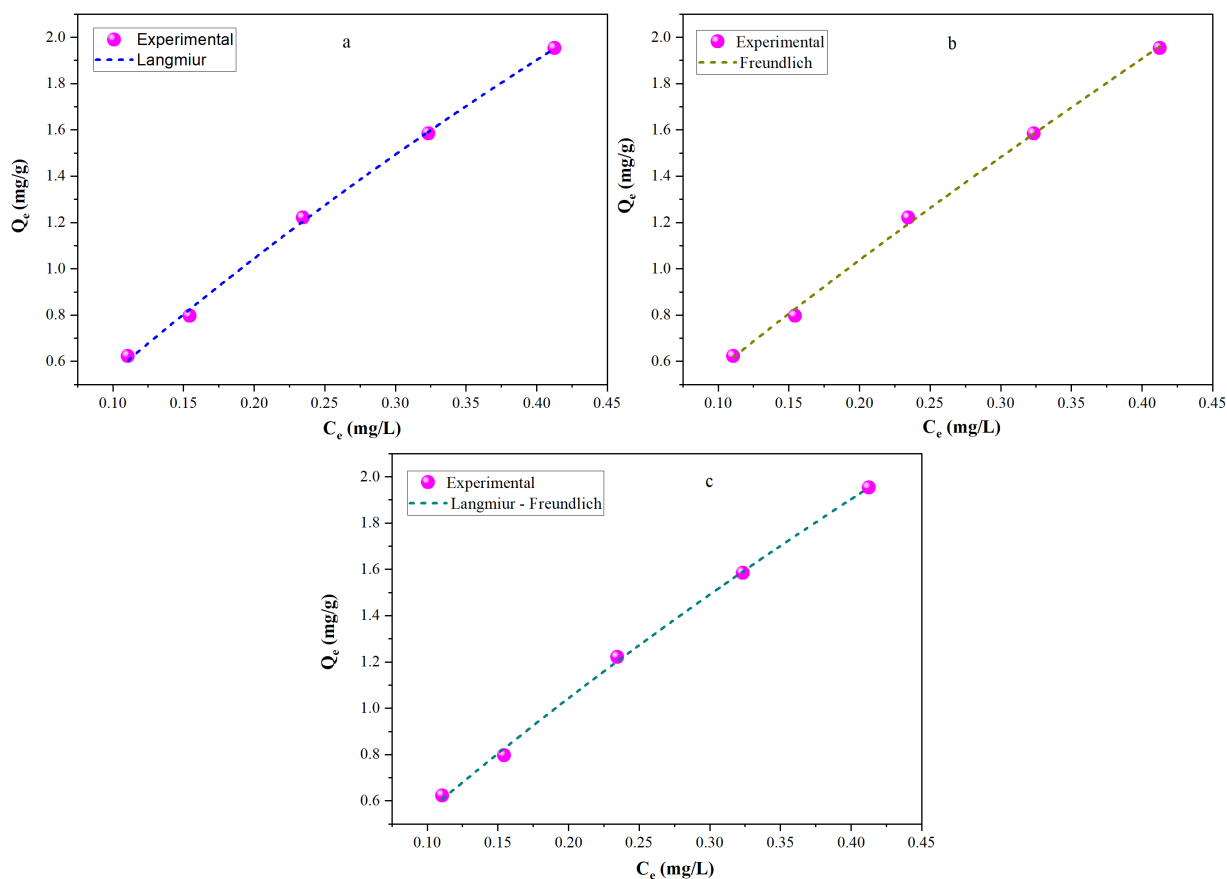


Figure 8.7: Adsorption isotherms for E1 hormone using PSU electrospun nanofibers; a) Langmuir, b) Freundlich and c) Langmuir-Freundlich model.

Table 8.4: Calculated adsorption isotherm parameters for the adsorption of the E1 hormone

<i>Langmuir model</i>					
Q_{\max} (mg/g)	K_L (L/mg)	R_L	R^2	SSE	χ^2
10.651	0.543	0.696 – 0.887	0.998	0.00144	0.00048
<i>Freundlich model</i>					
K_F (mg/g)(L/mg)	n		R^2	SSE	χ^2
4.267	0.878		0.999	0.00172	0.00057
<i>Langmuir – Freundlich model</i>					
Q_{\max} (mg/g)	K_{LF}	n	R^2	SSE	χ^2
12.888	0.424	0.975	0.996	0.00142	0.00071

SSE = Sum of squared errors, $\chi^2 = Chi-square$

8.8 A comparative study with other adsorbents for E1

The following Table 8.5 compares the reported electrospun nanofibers and other adsorbent particles reported in the literature for effective removal of E1 hormone. PSU possesses a high adsorption capacity owing to its surface area of 6.3 m²/g, which is relatively low for the other compared materials reported in the literature. The results revealed that PSU nanofibers at pH 7 and room temperature (25 °C) possessed a cumulative adsorption capacity of 2.115 mg/g with an individual adsorption capacity of E1 to be 0.508 mg/g. This value is higher than the adsorption capacity of the compared electrospun nanofibers, MWCNTs, activated sludge, and hollow fiber membrane shown in Table 8.5. However, the value is slightly low compared to carbonized hydrothermal carbon owing to its high surface area compared to electrospun nanofibers based on the nature of that material. When comparing PSU with the other electrospun nanofiber reported in the literature, the value for PSU nanofibers is high owing to its high surface area and small average fiber diameter of 183 ± 32 nm (PES: 199 ± 51 nm, PAN: 330 ± 73, PA: 220 ± 51 nm), the structure that allows hydrophobic and π - π interactions, and functional groups present on the surface that facilitate hydrogen bonding with E1 hormone, as discussed in adsorption mechanism.

Table 8.5: Comparison of adsorption capacity of E1 hormone using PSU to various adsorbents

Material	Hormone	pH and Temperature (°C)	Adsorption capacity (mg/g)	Reference
PES nanofibers	E1	7 and 25	0.442	[143]
PAN nanofibers	E1	7 and 25	0.396	[143]
PA nanofibers	E1	7 and 25	0.331	[143]
MWCNTs	E1	7 and 25	0.423	[120]
Activated sludge	E1	7 and 25	0.002533	[120]
Hydrophobic hollow fiber membrane	E1	7 and 25	0.000062	[120]
Carbonized hydrothermal carbon	E1	7 and 25	0.95	[125]
PSU nanofibers	E1	7 and 25	0.508	Present study

8.9 Adsorption-desorption study of PSU nanofibers

The consecutive adsorption cycles were performed at optimum conditions of pH 7, temperature 35, 0.2 mg/L concentration of adsorbate (E1), and 40 mg dosage of adsorbent (PSU). It can be seen in Figure 8.8 that the highest adsorption was achieved at around 82.2%, which was gradually reduced, reaching the efficiency of about 60% in six adsorption cycles which is evidence of the high performance of PSU nanofibers. Similarly, desorption cycles followed the same trend; however, the efficiency remained slightly higher in most of the cycles using desorption of E1 from PSU nanofibers which clearly indicates the effectiveness of the process for recovery of E1 hormones from the nanofibers. Additionally, The SEM image shows the surface morphology of nanofibers after six cycles. A slight increase in the diameter of nanofiber is observed, rising from 183 to 246 nm. A plausible reason for swelling is attributed to the interaction of nanofiber with ethanol while in contact during the desorption cycles [143].

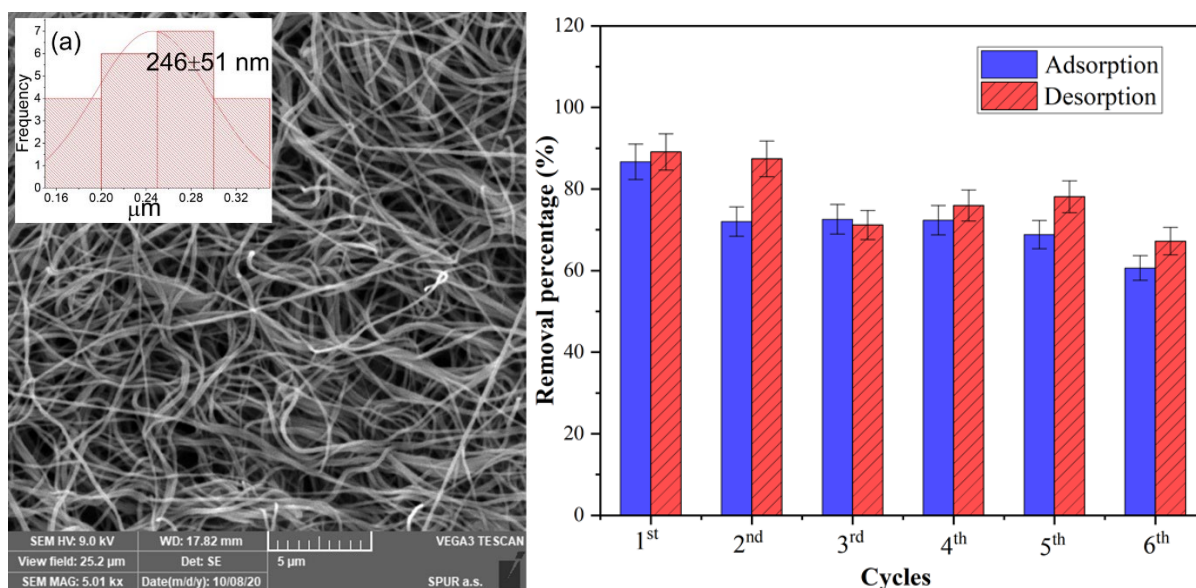


Figure 8.8: SEM micrograph after study with (inset) distribution of the fiber diameter (in the left panel) and cycles of adsorption-desorption for E1 by PSU nanofibers (in the right panel).

8.10 Conclusions

Polymeric nanofibers that include PSU, PLA, and PVDF were successfully produced via the facile electrospinning method and could adsorb all types of EH. These fibers possessed a mean fiber diameter of 149 - 183 nm and a specific surface area of 1.6 - 6.3 m²/g. The preliminary study showed that PSU was the best among these polymers, with the highest percentage of removal (71.2%) of E1. The adsorption of hormones on PSU is significantly high compared to other polymers owing to the hydrogen bonding interactions. Therefore, five models (pseudo-first-order, pseudo-second-order, intraparticle diffusion, Elovich, and fractional power model) were deployed on experimental data to obtain the adsorption kinetics and to understand the characteristics of PSU fibers with contact time. The obtained results showed that E3 followed pseudo-first-order kinetics while E1, E2, and EE2 best fitted pseudo-second-order kinetics. It was found that PSU fibers had maximum removal efficiency of 71.2, 65.9, 56.9, and 36.1 % for E1, EE2, E2, and E3, respectively. Adsorption obeyed Langmuir-Freundlich isothermal adsorption models; thermodynamics and mechanisms were evaluated, revealing that the adsorption process of E1 was exothermic and spontaneous in nature. The adsorption-desorption cycles were conducted over six cycles to determine the reusability and effectiveness of PSU, which remained above 60%. Overall, the results indicate that PSU can be a potential and efficient adsorbent for the effective simultaneous removal of EH from water streams.

9 CONCLUDING REMARKS

9.1 Conclusions of work done

This doctoral work focused on developing and characterizing *electrospun nanofibrous polymeric materials that were tested for the elimination of estrogenic hormones from wastewater by adsorption*. All the mentioned aims were successfully achieved, and the **brief summary** of this doctoral work which was prepared and published in the form of articles, is explained below:

Article I entitled “*The adsorption, kinetics, and interaction mechanisms of various types of estrogen on electrospun polymeric nanofiber membranes.*” This work comprised of preparation and characterization of six different electrospun polymeric nanofibers: CA, PA, PES, polyurethanes (918 and Elastollan), and PAN to simultaneously adsorbing four EH (E1, E2, EE2, and E3) in a single step process and to compare their performance (adsorption efficiency and adsorption capacity). The nanofibers possessed an average fiber diameter in the range of 174–330 nm, and their specific surface area ranged between 10.2 and 20.9 m² g⁻¹. The adsorption-desorption process was investigated in four cycles. The pseudo-first-order, pseudo-second-order, and intraparticle diffusion models were deployed on experimental data to determine the kinetics. Findings showed that E1, E2, and EE2 best fitted pseudo-second-order kinetics, while E3 followed pseudo-first-order kinetics. It was found that PU Elastollan nanofibers were the best and had maximum adsorption capacities of 0.801, 0.590, 0.736, and 0.382 mg g⁻¹ for E1, E2, EE2, and E3, respectively. In addition, the results revealed that PU Elastollan nanofibers had the highest percentage efficiency of estrogens removal at ~58.9% due to its strong hydrogen bonding with EH, which was explained in the mechanism. In comparison, the least removal efficiency was observed for PAN at ~35.1%. These mentioned results were **reported and published in** “*Nanotechnology*” 33, (2021), 75702, <https://doi.org/10.1088/1361-6528/ac357b> (Web of Science Indexed [Materials Science], Q2, J_{imp}: 3.953)

Article II entitled “*Adsorption of estrogenic hormones in aqueous solution using electrospun nanofibers from waste cigarette butts: Kinetics, mechanism, and reusability.*” This study emphasized recycling waste CBs to produce defect-free electrospun nanofibers (WCENFs) to adsorb EH simultaneously. The WCENFs were characterized by SEM, XRD, FTIR, BET, porosimetry, contact angle by sessile drop technique, TGA, DSC, GPC, and tensile test. Five models (pseudo-first-order, pseudo-second-order, intraparticle diffusion, elovich, and fractional power model) were deployed to determine the kinetics. The strong

affinity of WCENFs was found to be towards all EH due to abundant hydrogen bonding interactions between functional groups (C=O, C–O–C, and C–O–H) of WCENFs and O–H of all EH (additionally, with C=O group of E1). The highest percentage removal efficiencies from the batch adsorption were 64.3, 53.6, 52.7, and 34.6% for EE2, E1, E2, and E3, respectively. Results showed that the total adsorption capacity achieved was 2.14 mg/g, whereas the individual values for E1, E2, EE2, and E3 were 0.551, 0.532, 0.687, and 0.369 mg/g, respectively. To summarize, the WCENFs was further thermally pressed to fabricate PET/WCENFs syringe film. It successfully and better responded to the retention time for these EH compared to the commercial CA syringe film. Therefore, it implies that recycled WCENFs can be considered a promising adsorbent for rapidly remediation wastewater streams to eliminate hormones and possibly replace the commercially available CA syringe film. These results were **reported and published in** “*Express Polymer Letters*” 16, (2022), 624–648, <https://doi.org/10.3144/expresspolymlett.2022.46> (Web of Science Indexed [Polymer Science], Q2, J_{imp}: 3.952)

Article III entitled “*Electrospun polyurethane nanofibers coated with polyaniline/polyvinyl alcohol as ultrafiltration membranes for the removal of ethinylestradiol hormone micropollutant from aqueous phase.*” This study reported the fabrication of electrospun polyurethane (PU 918) nanofibers modified by coating with polyaniline/polyvinyl alcohol (PANI/PVA) to form filtration membranes for the enhanced removal of ethinylestradiol (EE2) hormone. Structural and morphological characterization was performed by FTIR, SEM, and optical microscopy, while the detection and quantification of EE2 were analyzed using HPLC. PU-PANI-ES as a modified material demonstrated to be the most efficient with 90.30% removal efficiency of the studied hormone compared to its base form PU-PANI-EB (81.50%) and neat PU 918 (55.40%) as control. Findings demonstrated that EE2 best fitted pseudo-second-order kinetics. Furthermore, the adsorption process was optimized via response surface methodology using a central composite design model by varying parameters such as pH, temperature, the concentration of adsorbate, and adsorbent dosage to determine. The model proved to be significant for optimizing the removal of the EE2 hormone with a high regression coefficient (R^2) of 0.983. The optimum parameters were found to be pH 7 (considering that wastewater or river water is in the range of pH 6–8), the temperature of 40 °C, 0.3 mg/L concentration of EE2, and 20 mg of PU-PANI-ES dosage. It was found that the modified PU membranes had a maximum adsorption capacity of 2.11 mg/g and high removal percentage

efficiency of ~82.20% for EE2. Adsorption mechanism and thermodynamics were also evaluated, and the results depicted the adsorption process of EE2 occurred via intraparticle diffusion and was exothermic in nature. Finally, a reusability study was done over six adsorption-desorption cycles to test the consistent effectiveness of the modified PU membrane, which remained above 80% removal capacity. Overall, the reported results proved that the modification of the spun PU nanofiber with PANI significantly improved hormone removal from water and can be considered a promising adsorbent membrane for the remediation of different steroid hormones from water. The results mentioned above were **reported and published in** “*Journal of Environmental Chemical Engineering*” 10, (2022), 107811, <https://doi.org/10.1016/j.jece.2022.107811> (Web of Science Indexed [Chemical Engineering], Q1, J_{imp} : 7.968)

Article IV entitled “*The adsorptive behaviour of electrospun hydrophobic polymers for optimized uptake of estrogenic sex hormones from aqueous media: Kinetics, thermodynamics and reusability study.*” This study focused on hydrophobic polymeric nanofibers of PSU, PVDF, and PLA, that were prepared via an electrospinning process and characterized using SEM, FTIR, TGA, BET, XRD, and porosimetry. Nanofibers possessed a mean fiber diameter of 149 - 183 nm and a specific surface area of 1.6 - 6.3 m²/g. The adsorption efficiency of simultaneous removal of E1, E2, E3, and EE2 in a mixed concentration was investigated using HPLC. The preliminary study showed that PSU was the best among these polymers, with the highest percentage of removal (71.2%) of E1. The adsorption of hormones on PSU was significantly high compared to other polymers owing to the hydrogen bonding interactions. Therefore, five models (pseudo-first-order, pseudo-second-order, intraparticle diffusion, Elovich, and fractional power model) were deployed on experimental data to obtain the adsorption kinetics and to understand the characteristics of PSU fibers with contact time. The results indicated that spun PSU fibers exhibited the highest removal of all four estrogens, with a maximum removal efficiency of 71.2, 65.9, 56.9, and 36.1 % and adsorption capacity of 0.508, 0.703, 0.550, and 0.354 mg/g for E1, EE2, E2, and E3, respectively. Additionally, the adsorption was optimized by varying parameters such as concentration of adsorbate, pH, adsorbent dosage, and temperature to analyze one-way variance using ANOVA statistically. The pseudo-second-order is best fitted for E1, EE2, and E2, while the pseudo-first-order is for E3. The Langmuir-Freundlich isothermal model was most suitable for evaluation, and the thermodynamics depicted the adsorption of E1 on PSU was exothermic and spontaneous. The results indicated that spun PSU can be an

efficient adsorbent in the simultaneous elimination of estrogens from wastewater and exhibits high regeneration performance of over 60% after six adsorption-desorption cycles. These mentioned results were **reported and published in** “*Journal of Chemical Technology and Biotechnology*” (2022), <https://doi.org/10.1002/jctb.7191> (Web of Science Indexed [Chemical Engineering], Q2, J_{imp}: 3.709)

Apart from the adsorption study of hormones on nanofibers, some photocatalyst materials (nanoparticles, nanowires, and nanorods) were prepared to test the photodegradation of these hormones as secondary work. The results of work with nanoparticles titled “***Green synthesis of titanium and zinc oxide nanoparticles for simultaneous photocatalytic removal of estrogens in wastewater***” was **reported and published in** “*AIP Proceedings of the 13th International Conference on Nanomaterials, Brno, Czech Republic*” 189-196, (2021), <https://doi.org/10.37904/nanocon.2021.4333>. In this study, titanium and zinc oxide nanoparticles (ZnO-NPs) were green synthesized using lemon juice and peel extract, zinc acetate, ethylene glycol, and titanium IV isopropoxide as precursors. The prepared TiO₂ and ZnO-NPs were characterized and subjected to the photocatalytic degradation of EH (E1, E2, EE2, and E3) under UV light irradiation at 365 nm, which resulted in promising photocatalytic activity. All four EH were significantly degraded owing to the photocatalytic activity combined with a slight contribution of hormonal adsorption (4-11 %) onto the surface of the photocatalysts. Overall hormonal degradation rates were in the range of 84-93 %, and approximately 99 % removal was achieved in 60 minutes under UV light irradiation by ZnO and TiO₂, respectively.

The second work entitled “***ZnO nanowires and nanorods based ZnO/WO₃/Pt heterojunction for efficient photocatalytic degradation of Estriol (E3) hormone***” was based on the removal of E3 hormone (which had least been adsorbed by nanofibers) by heterojunction photocatalytic nanowire and nanorod thin films. It was done because nanofibers possessed the least adsorption efficiency with this hormone. In this work, ZnO nanowires and nanorods based on ZnO/WO₃/Pt heterojunction were successfully grown on glass substrates via a facile hydrothermal method followed by spraying. The photocatalytic performance was evaluated by the degradation of the E3 hormone under UV light irradiation (~365 nm) in a closed continuous flow reactor. The as-prepared samples achieved an excellent photodegradation rate in the range of 23-37 % and 63- 86 % for the nanorods and nanowires morphology, respectively. This article provided new insight into the construction of suitable geometrically optimized

heterojunctions for the remediation of persistent bio toxicants such as E3, which are the most difficult to be removed from wastewaters by adsorption. The above-mentioned results were **reported and published in** “*Materials Letters*” (2022), 132291, <https://doi.org/10.1016/j.matlet.2022.132291> (Web of Science Indexed [Applied Physics], Q2, J_{imp} : 3.574)

9.2 Contribution to science and practice

In the present scenario, a minuscule level of EH present are a severe threat to human and aquatic life through their exposure via food sources or drinking water. As a result, fish femininity, breast, ovarian, and prostate cancer caused by hormonal disorders is a serious threat and problem to society. The current European Union directive 2020/2184 concerning drinking water quality recommended a threshold limit of 1 ng/L as a benchmark for assessing the occurrence and treatment of EDCs. Thus, this doctoral work focuses on the preparation and characterization of smart materials that can be utilized for the simultaneous elimination of estrogenic hormones from wastewater by means of an adsorption technique for practical application.

The commonly used techniques are incapable of capturing EH at water treatment plants and result in secondary pollution due to insufficiently treated effluents, which demand secondary water treatment. Moreover, adsorbent nanoparticles which are promising for estrogens, have been reported in the literature, but they require an additional separation process from wastewater that raises the costs. In this regard, removing EH by adsorption via electrospun nanofibers offers a sustainable and relatively environmentally friendly solution for eliminating synthetic hormones with high efficiency and effectiveness of reusability for several adsorption-desorption cycles after regeneration. This brings a practical approach to large-scale production. Polymeric materials for water treatment applications are promising owing to their benefits, such as affordability, sustainability, efficient performance, durability, high surface area, high aspect ratio, and nanoporous structure. Furthermore, the nanofiber membrane functions precisely in different aquatic conditions without the accumulation of chemicals. In literature, commercially available nylon, PP, polytetrafluoroethylene, CA, regenerated cellulose, and glass microfiber filters have been reported for the removal of E1. Meanwhile, PA nanoparticles were employed to extract just EE2, PES nanofibers for the removal of E2, and PVDF doped with PVP and TiO₂ membranes prepared by the phase inversion process for the removal of E1 and E2. However, these studies were solely limited to the filtration of a single natural

or synthetic hormone. Therefore, different combinations of polymeric materials have been utilized to develop electrospun nanofibers, which can be utilized in simultaneous adsorption removal of four EH. Additionally, CBs were recycled to fabricate WCENFs that were used for comparison with the commercially available filters in the market. The studies were optimized using modeling to obtain the best conditions, understand interaction mechanisms, and apply kinetics, Isotherms, and thermodynamics. Also, the most promising lab synthesized polyurethane (PU 918) was surface coated with PANI/PVA to enhance adsorption removal capacity owing to ionic interaction and improved hydrogen bonding. Furthermore, ZnO and TiO₂ nanoparticles were green synthesized, considering environmental protection to test their photodegradation performance. Later these particles can be used in nanofibers for combining the photodegradation and adsorption processes. Finally, ZnO-based nanorods and nanowires thin films were prepared, characterized, and tested in a continuous cross-flow closed system for E3 hormone, which was least adsorbed by nanofiber membranes.

This doctoral study elaborated on the use of several hydrophilic and hydrophobic polymeric electrospun nanofibers, especially recycled WCENFs for adsorption and smartly functionalized polymers for optimized removal of hormones considering wastewater treatment applications. As a secondary work, nanoparticles, rods, and wires heterojunctions were tested for photodegradation of these hormones. This provides an opportunity for the next generation of scientific researchers to develop further modified and extremely specific polymeric nanofiber membranes incorporated with such photocatalysts intended for the eradication of micropollutants at wastewater treatment plants.

9.3 Future plans

The primary goal of this doctoral work was the *development and characterization of electrospun nanofibrous polymeric materials that were tested for the elimination of estrogenic hormones from wastewater by means of an adsorption technique*. This aim was successfully achieved by preparing smart electrospun polymeric nanofibers for the adsorption removal of EH. However, the experimental work was restricted to batch adsorption study. Furthermore, as a secondary work, photocatalyst materials such as nanoparticles, nanorods, and nanowires were synthesized and were successful with a high performance of photocatalytic degradation of these EH but only in the presence of UV light. Additionally, the studies were limited to the use of these materials individually and separately for adsorption and photodegradation techniques. Thus, this

generates the following aims of studies that could be achieved before the final application of these studies can be implemented over large-scale use.

- Optimized fabrication jointly of high-performing electrospun nanofiber membranes (PU and WCENFs) incorporated with highly efficient photocatalysts that can operate at both UV and visible light conditions to have rapid simultaneous adsorption removal and photocatalytic degradation of micropollutants such as EH from wastewater.
- Determination of the possible enhanced adsorption activity by surface functionalization in the presence of an incorporated photocatalyst and observing the stability of nanofibers in different mediums.
- Determination of contact time study to apply suitable kinetic models in continuous crossflow and dead-end flow closed systems to obtain high flux and true removal percentages in natural water samples for complete wastewater remediation.
- Testing the reusability of material for at least ten cycles to be economically viable where the performance must remain high above 90% and the recovery of EH is significantly possible.
- Optimization study with variation in experimental condition parameters such as the influence of competing ions and interacting media, the concentration of adsorbate, adsorbent dosage, pH of the solution, the temperature of interaction, and time of contact to precisely evaluate the types of the mechanism involved, apply thermodynamics, Isothermal models, identify the most suitable cost-effective operating conditions, and determine the economic feasibility.
- Observe the adsorption and photodegradation capacities of the prepared materials to analyze their performance in capturing EH and compare them with the best materials reported in the literature.

REFERENCES

- [1] Uddin, Z.; Ahmad, F.; Ullan, T.; Nawab, Y.; Ahmad, S.; Azam, F.; Rasheed, A.; Zafar, M. S.: Recent trends in water purification using electrospun nanofibrous membranes. *International Journal of Environmental Science and Technology*, (2021).
<http://doi:10.1007/s13762-021-03603-9>.
- [2] Dongre, R. S.; Sadasivuni, K. K.; Deshmukh, K.; Mehta, A.; Basu, S.; Meshram, J. S.; Al-Maadeed, M. A. A.; Karim, A.: Natural polymer based composite membranes for water purification: a review. *Polymer-Plastics Technology and Materials*, **58**, 1295–1310 (2019).
<http://doi:10.1080/25740881.2018.1563116>.
- [3] Mishra, R. K.; Sabu, A.; Tiwari, S. K.: Materials chemistry and the futurist eco-friendly applications of nanocellulose: Status and prospect. *Journal of Saudi Chemical Society*, **22**, 949–978 (2018).
<http://doi:10.1016/j.jscs.2018.02.005>.
- [4] Alim, M. A.; Rahman, A.; Tao, Z.; Samali, B.; Khan, M. M.; Shirin, S.: Suitability of roof harvested rainwater for potential potable water production: A scoping review. *Journal of Cleaner Production*, **248** (2020).
<http://doi:10.1016/j.jclepro.2019.119226>.
- [5] Wadhawan, S.; Jain, A.; Nayyar, J.; Mehta, S. K.: Role of nanomaterials as adsorbents in heavy metal ion removal from waste water: A review. *Journal of Water Process Engineering*, **33**, 101038 (2020).
<http://doi:10.1016/j.jwpe.2019.101038>.
- [6] Jain, P.; Pradeep, T.: Potential of silver nanoparticle-coated polyurethane foam as an antibacterial water filter. *Biotechnology and Bioengineering*, **90**, 59–63 (2005). <http://doi:10.1002/bit.20368>.
- [7] Matilainen, A.; Gjessing, E. T.; Lahtinen, T.; Hed, L.; Bhatnagar, A.; Sillanpää, M.: An overview of the methods used in the characterisation of natural organic matter (NOM) in relation to drinking water treatment. *Chemosphere*, **83**, 1431–1442 (2011).
<http://doi:10.1016/j.chemosphere.2011.01.018>.
- [8] Jiang, J. Q.: The role of coagulation in water treatment. *Current Opinion in Chemical Engineering*, **8**, 36–44 (2015).
<http://doi:10.1016/j.coche.2015.01.008>.
- [9] Turner, T.; Wheeler, R.; Stone, A.; Oliver, I.: Potential Alternative Reuse Pathways for Water Treatment Residuals. *Water, Air, and Soil Pollution*, **230** (2019).
- [10] Glaze, W. H.; Kang, J. W.; Chapin, D. H.: The chemistry of water treatment processes involving ozone, hydrogen peroxide and ultraviolet radiation. *Ozone: Science & Engineering*, **9**, 335–352 (1987).
<http://doi:10.1080/01919518708552148>.
- [11] Rice, R. G.: The use of ozone to control trihalomethanes in drinking water

- treatment. *Ozone: Science & Engineering*, **2**, 75–99 (1980).
<http://doi:10.1080/01919518008550870>.
- [12] Kim, J.; Chung, Y.; Shin, D.; Kim, M.; Lee, Y.; Lim, Y.; Lee, D.: Chlorination by-products in surface water treatment process. *Desalination*, **151**, 1–9 (2003). [http://doi:10.1016/S0011-9164\(02\)00967-0](http://doi:10.1016/S0011-9164(02)00967-0).
- [13] Shi, P.; Jia, S.; Zhang, X. X.; Zhang, T.; Cheng, S.; Li, A.: Metagenomic insights into chlorination effects on microbial antibiotic resistance in drinking water. *Water Research*, **47**, 111–120 (2013).
<http://doi:10.1016/j.watres.2012.09.046>.
- [14] Golob, V.; Vinder, A.; Simonič, M.: Efficiency of the coagulation/flocculation method for the treatment of dyebath effluents. *Dyes and Pigments*, **67**, 93–97 (2005).
<http://doi:10.1016/j.dyepig.2004.11.003>.
- [15] Sher, F.; Malik, A.; Liu, H.: Industrial polymer effluent treatment by chemical coagulation and flocculation. *Journal of Environmental Chemical Engineering*, **1**, 684–689 (2013). <http://doi:10.1016/j.jece.2013.07.003>.
- [16] Yang, Y.; Zhu, G.; Zhang, H.; Chen, J.; Zhong, X.; Lin, Z.; Su, Y.; Bai, P.: Triboelectric Nanogenerator for Harvesting Wind Energy and as Self-. *ACS Nano*, **7**, 9461–9468 (2013).
- [17] Rengaraj, S.; Yeon, K. H.; Moon, S. H.: Removal of chromium from water and wastewater by ion exchange resins. *Journal of Hazardous Materials*, **87**, 273–287 (2001). [http://doi:10.1016/S0304-3894\(01\)00291-6](http://doi:10.1016/S0304-3894(01)00291-6).
- [18] Dąbrowski, A.; Hubicki, Z.; Podkościelny, P.; Robens, E.: Selective removal of the heavy metal ions from waters and industrial wastewaters by ion-exchange method. *Chemosphere*, **56**, 91–106 (2004).
<http://doi:10.1016/j.chemosphere.2004.03.006>.
- [19] Joss, A.; Keller, E.; Alder, A. C.; Göbel, A.; McArdell, C. S.; Ternes, T.; Siegrist, H.: Removal of pharmaceuticals and fragrances in biological wastewater treatment. *Water Research*, **39**, 3139–3152 (2005).
<http://doi:10.1016/j.watres.2005.05.031>.
- [20] Oller, I.; Malato, S.; Sánchez-Pérez, J. A.: Combination of Advanced Oxidation Processes and biological treatments for wastewater decontamination-A review. *Science of the Total Environment*, **409**, 4141–4166 (2011). <http://doi:10.1016/j.scitotenv.2010.08.061>.
- [21] Ting, Y. F.; Praveena, S. M.: Sources, mechanisms, and fate of steroid estrogens in wastewater treatment plants: a mini review. *Environmental Monitoring and Assessment*, **189** (2017). <http://doi:10.1007/s10661-017-5890-x>.
- [22] Qu, X.; Alvarez, P. J. J.; Li, Q.: Applications of nanotechnology in water and wastewater treatment. *Water Research*, **47**, 3931–3946 (2013).
<http://doi:10.1016/j.watres.2012.09.058>.
- [23] Lee, J.; Yoon, J.; Kim, J. H.; Lee, T.; Byun, H.: Electrospun PAN–GO composite nanofibers as water purification membranes. *Journal of Applied*

- Polymer Science, **135**, 1–9 (2018). <http://doi:10.1002/app.45858>.
- [24] Yalcinkaya, F.: A review on advanced nanofiber technology for membrane distillation. *Journal of Engineered Fibers and Fabrics*, **14** (2019). <http://doi:10.1177/1558925018824901>.
- [25] Ma, H.; Burger, C.; Hsiao, B. S.; Chu, B.: Ultra-fine cellulose nanofibers: New nano-scale materials for water purification. *Journal of Materials Chemistry*, **21**, 7507–7510 (2011). <http://doi:10.1039/c0jm04308g>.
- [26] Zhang, M.; Song, L.: Mechanisms and parameters affecting flux decline in cross-flow microfiltration and ultrafiltration of colloids. *Environmental Science and Technology*, **34**, 3767–3773 (2000). <http://doi:10.1021/es990475u>.
- [27] Koyuncu, I.; Sengur, R.; Turken, T.; Guclu, S.; Pasaoglu, M. E.: *Advances in water treatment by microfiltration, ultrafiltration, and nanofiltration*; Vol. 2019; ISBN 9781782421269.
- [28] Islam, M. S.; Sultana, A.; Saadat, A. H. M.; Islam, M. S.; Shammi, M.; Uddin, M. K.: Desalination Technologies for Developing Countries: A Review. *Journal of Scientific Research*, **10**, 77–97 (2018). <http://doi:10.3329/jsr.v10i1.33179>.
- [29] Bjorge, D.; Daels, N.; De Vrieze, S.; Dejans, P.; Van Camp, T.; Audenaert, W.; Hogie, J.; Westbroek, P.; De Clerck, K.; Van Hulle, S. W. H.: Performance assessment of electrospun nanofibers for filter applications. *Desalination*, **249**, 942–948 (2009). <http://doi:10.1016/j.desal.2009.06.064>.
- [30] Barhate, R. S.; Ramakrishna, S.: Nanofibrous filtering media: Filtration problems and solutions from tiny materials. *Journal of Membrane Science*, **296**, 1–8 (2007). <http://doi:10.1016/j.memsci.2007.03.038>.
- [31] Mahdi A. Shirazi, M.; Bazgir, S.; Meshkani, F.: Electrospun Nanofibrous Membranes for Water Treatment. *Advances in Membrane Technologies*, (2020). <http://doi:10.5772/intechopen.87948>.
- [32] Schäfer, A. I.; Stelzl, K.; Faghieh, M.; Sen Gupta, S.; Krishnadas, K. R.; Heißler, S.; Pradeep, T.: Poly(ether sulfone) Nanofibers Impregnated with β -Cyclodextrin for Increased Micropollutant Removal from Water. *ACS Sustainable Chemistry and Engineering*, **6**, 2942–2953 (2018). <http://doi:10.1021/acssuschemeng.7b02214>.
- [33] McLachlan, J. A.; Simpson, E.; Martin, M.: Endocrine disrupters and female reproductive health. *Best Pract. Res. Clin. Endocrinol. Metab.* (2006), **20**, 63–75.
- [34] Montes-Grajales, D.; Olivero-Verbel, J.: EDCs databank: 3D-structure database of endocrine disrupting chemicals. *Toxicology*, **327**, 87–94 (2015). <http://doi:10.1016/j.tox.2014.11.006>.
- [35] Gyllenhammar, I.; Glynn, A.; Jönsson, B. A. G.; Lindh, C. H.; Darnerud, P. O.; Svensson, K.; Lignell, S.: Diverging temporal trends of human exposure to bisphenols and plastizisers, such as phthalates, caused by

- substitution of legacy EDCs? *Environmental Research*, **153**, 48–54 (2017). <http://doi:10.1016/j.envres.2016.11.012>.
- [36] Sood, S.; Shekhar, S.; Santosh, W.: Dimorphic placental stress: A repercussion of interaction between endocrine disrupting chemicals (EDCs) and fetal sex. *Medical Hypotheses*, **99**, 73–75 (2017). <http://doi:10.1016/j.mehy.2017.01.002>.
- [37] Luo, L.; Yang, Y.; Xiao, M.; Bian, L.; Yuan, B.; Liu, Y.; Jiang, F.; Pan, X.: A novel biotemplated synthesis of TiO₂/wood charcoal composites for synergistic removal of bisphenol A by adsorption and photocatalytic degradation. *Chemical Engineering Journal*, **262**, 1275–1283 (2015). <http://doi:10.1016/j.cej.2014.10.087>.
- [38] Chen, Y.; Zhang, Y.; Luo, L.; Shi, Y.; Wang, S.; Li, L.; Long, Y.; Jiang, F.: A novel templated synthesis of C/N-doped β -Bi₂O₃ nanosheets for synergistic rapid removal of 17 α -ethynylestradiol by adsorption and photocatalytic degradation. *Ceramics International*, **44**, 2178–2185 (2018). <http://doi:10.1016/j.ceramint.2017.10.173>.
- [39] Han, J.; Qiu, W.; Gao, W.: Adsorption of estrone in microfiltration membrane filters. *Chemical Engineering Journal*, **165**, 819–826 (2010). <http://doi:10.1016/j.cej.2010.10.024>.
- [40] European Commission: Directive (EU) 2020/2184 of the European Parliament and of the Council of 16 December 2020 on the quality of water intended for human consumption. *Official Journal of the European Union*, **2019**, 1–61 (2020).
- [41] Yazdan, M. S.; Kumar, R.; Leung, S. W.: The Environmental and Health Impacts of Steroids and Hormones in Wastewater Effluent , as Well as Existing Removal Technologies : A Review. , 206–224 (2022).
- [42] Nghiem, L. D.; Schäfer, A. I.: Adsorption and transport of trace contaminant estrone in NF/RO membranes. *Environmental Engineering Science*, **19**, 441–451 (2002). <http://doi:10.1089/109287502320963427>.
- [43] Solomon, G. M.; Schettler, T.: Environment and health: 6. Endocrine disruption and potential human health implications. *Cmaj* (2000), **163**, 1471–1476.
- [44] Cartinella, J. L.; Cath, T. Y.; Flynn, M. T.; Miller, G. C.; Hunter, K. W.; Childress, A. E.: Removal of natural steroid hormones from wastewater using membrane contactor processes. *Environmental Science and Technology*, **40**, 7381–7386 (2006). <http://doi:10.1021/es060550i>.
- [45] Johnson, A. C.; Aerni, H. R.; Gerritsen, A.; Gibert, M.; Giger, W.; Hylland, K.; Jürgens, M.; Nakari, T.; Pickering, A.; Suter, M. J. F.; Svenson, A.; Wettstein, F. E.: Comparing steroid estrogen, and nonylphenol content across a range of European sewage plants with different treatment and management practices. *Water Research*, **39**, 47–58 (2005). <http://doi:10.1016/j.watres.2004.07.025>.
- [46] Sarmah, A. K.; Northcott, G. L.; Leusch, F. D. L.; Tremblay, L. A.: A

- survey of endocrine disrupting chemicals (EDCs) in municipal sewage and animal waste effluents in the Waikato region of New Zealand. *Science of the Total Environment*, **355**, 135–144 (2006).
<http://doi:10.1016/j.scitotenv.2005.02.027>.
- [47] Vymazal, J.; Březinová, T.; Koželuh, M.: Occurrence and removal of estrogens, progesterone and testosterone in three constructed wetlands treating municipal sewage in the Czech Republic. *Science of the Total Environment*, **536**, 625–631 (2015).
<http://doi:10.1016/j.scitotenv.2015.07.077>.
- [48] Han, J.; Qiu, W.; Cao, Z.; Hu, J.; Gao, W.: Adsorption of ethinylestradiol (EE2) on polyamide 612: Molecular modeling and effects of water chemistry. *Water Research*, **47**, 2273–2284 (2013).
<http://doi:10.1016/j.watres.2013.01.046>.
- [49] Braga, O.; Smythe, G. A.; Schäfer, A. I.; Feitz, A. J.: Fate of steroid estrogens in Australian inland and coastal wastewater treatment plants. *Environmental Science and Technology*, **39**, 3351–3358 (2005).
<http://doi:10.1021/es0501767>.
- [50] Limpiyakorn, T.; Homklin, S.; Ong, S. K.: Fate of estrogens and estrogenic potentials in sewerage systems. *Critical Reviews in Environmental Science and Technology*, **41**, 1231–1270 (2011).
<http://doi:10.1080/10643380903488680>.
- [51] Aris, A. Z.; Shamsuddin, A. S.; Praveena, S. M.: Occurrence of 17 α -ethinylestradiol (EE2) in the environment and effect on exposed biota: A review. *Environ. Int.* (2014), **69**, 104–119.
- [52] Adeel, M.; Song, X.; Wang, Y.; Francis, D.; Yang, Y.: Environmental impact of estrogens on human, animal and plant life: A critical review. *Environ. Int.* (2017), **99**, 107–119.
- [53] Siegenthaler, P. F.; Bain, P.; Riva, F.; Fent, K.: Effects of antiandrogenic progestins, chlormadinone and cyproterone acetate, and the estrogen 17 α -ethinylestradiol (EE2), and their mixtures: Transactivation with human and rainbowfish hormone receptors and transcriptional effects in zebrafish (*Danio rerio*). *Aquatic Toxicology*, **182**, 142–162 (2017).
<http://doi:10.1016/j.aquatox.2016.11.001>.
- [54] Srinivasan, J.; Ramakrishnan, G.; Mukhopadhyay, S.; Manoharan, S.: A study of knitted fabrics from polyester microdenier fibres. *Journal of the Textile Institute*, **98**, 31–35 (2007). <http://doi:10.1533/joti.2005.0180>.
- [55] Aende, A.; Gardy, J.; Hassanpour, A.: Seawater desalination: A review of forward osmosis technique, its challenges, and future prospects. *Processes*, **8** (2020). <http://doi:10.3390/PR8080901>.
- [56] Semião, A. J. C.; Schäfer, A. I.: Xenobiotics Removal by Membrane Technology: An Overview. In: (2010); pp. 307–338.
- [57] Luo, Y.; Guo, W.; Ngo, H. H.; Nghiem, L. D.; Hai, F. I.; Zhang, J.; Liang, S.; Wang, X. C.: A review on the occurrence of micropollutants in the

- aquatic environment and their fate and removal during wastewater treatment. *Sci. Total Environ.* (2014), 473–474, 619–641.
- [58] Tijani, J. O.; Fatoba, O. O.; Petrik, L. F.: A review of pharmaceuticals and endocrine-disrupting compounds: Sources, effects, removal, and detections. *Water, Air, and Soil Pollution*, **224** (2013).
<http://doi:10.1007/s11270-013-1770-3>.
- [59] Onesios, K. M.; Yu, J. T.; Bouwer, E. J.: Biodegradation and removal of pharmaceuticals and personal care products in treatment systems: A review. *Biodegradation* (2009), *20*, 441–466.
- [60] Pham, T. T.; Nguyen, V. A.; Van der Bruggen, B.: Pilot-Scale Evaluation of GAC Adsorption Using Low-Cost, High-Performance Materials for Removal of Pesticides and Organic Matter in Drinking Water Production. *Journal of Environmental Engineering*, **139**, 958–965 (2013).
[http://doi:10.1061/\(asce\)ee.1943-7870.0000704](http://doi:10.1061/(asce)ee.1943-7870.0000704).
- [61] ALI, H.; MASAR, M.; URBANEK, M.; GULER, A. C.; URBANEK, P.; MACHOVSKY, M.; KURITKA, I.: Effect of annealing on luminescence and photocatalytic activity of ZnS nanocrystals under UV light irradiation. *NANOCON 2020 Conference Proceedings*, **2020**, 261–266 (2020).
<http://doi:10.37904/nanocon.2020.3707>.
- [62] Pendergast, M. M.; Hoek, E. M. V.: A review of water treatment membrane nanotechnologies. *Energy Environ. Sci.* (2011), *4*, 1946–1971.
- [63] Shannon, M. A.; Bohn, P. W.; Elimelech, M.; Georgiadis, J. G.; Mariñas, B. J.; Mayes, A. M.: Science and technology for water purification in the coming decades. *Nature* (2008), *452*, 301–310.
- [64] Augusto, F.; Hantao, L. W.; Mogollón, N. G. S.; Braga, S. C. G. N.: New materials and trends in sorbents for solid-phase extraction. *TrAC - Trends in Analytical Chemistry*, **43**, 14–23 (2013).
<http://doi:10.1016/j.trac.2012.08.012>.
- [65] Bhardwaj, N.; Kundu, S. C.: Electrospinning: A fascinating fiber fabrication technique. *Biotechnol. Adv.* (2010), *28*, 325–347.
- [66] Yang, Z.; Peng, H.; Wang, W.; Liu, T.: Crystallization behavior of poly(ϵ -caprolactone)/layered double hydroxide nanocomposites. *Journal of Applied Polymer Science*, **116**, 2658–2667 (2010).
<http://doi:10.1002/app>.
- [67] Yudanova, T. N.; Filatov, I. Y.; Afanasov, I. M.: Production of ultrafine cellulose acetate fibers. *Theoretical Foundations of Chemical Engineering*, **50**, 508–512 (2016). <http://doi:10.1134/S004057951604031X>.
- [68] Dzenis, Y.: Spinning continuous fibers for nanotechnology. *Science (80-)*. (2004), *304*, 1917–1919.
- [69] Shabafrooz, V.; Mozafari, M.; Vashae, D.; Tayebi, L.: Electrospun nanofibers: From filtration membranes to highly specialized tissue engineering scaffolds. *J. Nanosci. Nanotechnol.* (2014), *14*, 522–534.
- [70] Hemamalini, T.; Karunakaran, S. A.; Siva Elango, M. K.; Senthil Ram, T.;

- Giri Dev, V. R.: Regeneration of cellulose acetate nanofibrous mat from discarded cigarette butts. *Indian Journal of Fibre and Textile Research*, **44**, 248–252 (2019).
- [71] Kimmer, D.; Vincent, I.; Lovecka, L.; Kazda, T.; Giurg, A.; Skorvan, O.: Some aspects of applying nanostructured materials in air filtration, water filtration and electrical engineering. In *AIP Conference Proceedings*; (2017); Vol. 1843.
- [72] F. Cengiz, TA. Dao, O. Jirsak: Influence of solution properties on the roller electrospinning of poly(vinyl alcohol). *Society*, , 1–10 (2010). <http://doi:10.1002/pen>.
- [73] Haider, A.; Haider, S.; Kang, I.: REVIEW A comprehensive review summarizing the effect of electrospinning parameters and potential applications of nanofibers in biomedical and biotechnology. *Arabian Journal of Chemistry*, **11**, 1165–1188 (2018). <http://doi:10.1016/j.arabjc.2015.11.015>.
- [74] Sagitha, P.; Reshmi, C. R.; Manaf, O.; Sundaran, S. P.; Juraij, K.; Sujith, A.: *Development of nanocomposite membranes by electrospun nanofibrous materials*; Elsevier Inc.; ISBN 9780128167106.
- [75] Wasim, M.; Sabir, A.; Shafiq, M.; Jamil, T.: *Chapter 11 - Electrospinning: A Fiber Fabrication Technique for Water Purification*; Elsevier Inc.; ISBN 9780128139264.
- [76] Ray, S. S.; Chen, S.; Li, C.; Nguyen, C.: RSC Advances A comprehensive review : electrospinning technique for fabrication and surface modification. *RSC Advances*, **6**, 85495–85514 (2016). <http://doi:10.1039/C6RA14952A>.
- [77] Schiffman, J. D.; Schauer, C. L.: A Review : Electrospinning of Biopolymer Nanofibers and their Applications A Review : Electrospinning of Biopolymer Nanofibers and their Applications. **3724** (2008). <http://doi:10.1080/15583720802022182>.
- [78] Eng, J. T. S.; Lin, T.: *Journal of Textile Science & Engineering Needleless Electrospinning : A Practical Way to Mass Production of Nanofibers*. **2**, 2–4 (2012). <http://doi:10.4172/2165-8064.1000e109>.
- [79] Wang, X.; Hsiao, B. S.: Electrospun nanofiber membranes. *Current Opinion in Chemical Engineering*, **12**, 62–81 (2016). <http://doi:10.1016/j.coche.2016.03.001>.
- [80] Kumar, A. K.; Mohan, S. V.: Endocrine disruptive synthetic estrogen (17 α -ethynylestradiol) removal from aqueous phase through batch and column sorption studies: Mechanistic and kinetic analysis. *Desalination*, **276**, 66–74 (2011). <http://doi:10.1016/j.desal.2011.03.022>.
- [81] Kumar, A. K.; Mohan, S. V.; Sarma, P. N.: Sorptive removal of endocrine-disruptive compound (estriol, E3) from aqueous phase by batch and column studies: Kinetic and mechanistic evaluation. *Journal of Hazardous Materials*, **164**, 820–828 (2009).

- <http://doi:10.1016/j.jhazmat.2008.08.075>.
- [82] Pan, B.; Lin, D.; Mashayekhi, H.; Xing, B.: Adsorption and hysteresis of bisphenol A and 17 α -ethinyl estradiol on carbon nanomaterials. *Environmental Science and Technology*, **42**, 5480–5485 (2008). <http://doi:10.1021/es8001184>.
- [83] Jin, X.; Hu, J. Y.; Tint, M. L.; Ong, S. L.; Biryulin, Y.; Polotskaya, G.: Estrogenic compounds removal by fullerene-containing membranes. *Desalination*, **214**, 83–90 (2007). <http://doi:10.1016/j.desal.2006.10.019>.
- [84] Kiran Kumar, A.; Venkata Mohan, S.: Removal of natural and synthetic endocrine disrupting estrogens by multi-walled carbon nanotubes (MWCNT) as adsorbent: Kinetic and mechanistic evaluation. *Separation and Purification Technology*, **87**, 22–30 (2012). <http://doi:10.1016/j.seppur.2011.11.015>.
- [85] Krupadam, R. J.; Sridevi, P.; Sakunthala, S.: Removal of endocrine disrupting chemicals from contaminated industrial groundwater using chitin as a biosorbent. *Journal of Chemical Technology and Biotechnology*, **86**, 367–374 (2011). <http://doi:10.1002/jctb.2525>.
- [86] Zhang, Y.; Zhou, J. L.: Removal of estrone and 17 β -estradiol from water by adsorption. In *Water Research*; (2005); Vol. 39, pp. 3991–4003.
- [87] Hristovski, K. D.; Nguyen, H.; Westerhoff, P. K.: Removal of arsenate and 17 α -ethinyl estradiol (EE2) by iron (hydr)oxide modified activated carbon fibers. *Journal of Environmental Science and Health - Part A Toxic/Hazardous Substances and Environmental Engineering*, **44**, 354–361 (2009). <http://doi:10.1080/10934520802659695>.
- [88] Wang, J.; Pan, K.; Giannelis, E. P.; Cao, B.: Polyacrylonitrile/polyaniline core/shell nanofiber mat for removal of hexavalent chromium from aqueous solution: Mechanism and applications. *RSC Advances*, **3**, 8978–8987 (2013). <http://doi:10.1039/c3ra40616d>.
- [89] Chigome, S.; Torto, N.: A review of opportunities for electrospun nanofibers in analytical chemistry. *Anal. Chim. Acta* (2011), **706**, 25–36.
- [90] Chigome, S.; Darko, G.; Torto, N.: Electrospun nanofibers as sorbent material for solid phase extraction. *Analyst* (2011), **136**, 2879–2889.
- [91] Niavarani, Z.; Breite, D.; Prager, A.; Abel, B.; Schulze, A.: Estradiol removal by adsorptive coating of a microfiltration membrane. *Membranes*, **11**, 1–13 (2021). <http://doi:10.3390/membranes11020099>.
- [92] Wang, M.; Qu, F.; Jia, R.; Sun, S.; Li, G.; Liang, H.: Preliminary study on the removal of steroidal estrogens using TiO₂-doped PVDF ultrafiltration membranes. *Water (Switzerland)*, **8**, 1–12 (2016). <http://doi:10.3390/w8040134>.
- [93] Kimmer, D.; Vincent, I.; Fenyk, J.; Petras, D.; Zatloukal, M.; Sambaer, W.; Zdimal, V.: Morphology of nano and micro fiber structures in ultrafine particles filtration. In *AIP Conference Proceedings*; (2011); Vol. 1375, pp. 295–311.

- [94] Chittur, K. K. K.: FTIR/ATR for protein adsorption to biomaterial surfaces. *Biomaterials*. (1998), *19*, 357–369.
- [95] Ismail, A. A.; van de Voort, F. R.; Sedman, J.: Chapter 4 Fourier transform infrared spectroscopy: Principles and applications. In *Instrumental Methods in Food Analysis*; Paré, J. R. J., Bélanger, J. M. R. B. T.-T. and I. in A. C., Eds.; Elsevier, (1997); Vol. 18, pp. 93–139 ISBN 0167-9244.
- [96] Bhargava, R.: Infrared spectroscopic imaging: The next generation. *Applied Spectroscopy*, **66**, 1091–1120 (2012). <http://doi:10.1366/12-06801>.
- [97] Gerber, F.; Krummen, M.; Potgeter, H.; Roth, A.; Siffrin, C.; Spoendlin, C.: Practical aspects of fast reversed-phase high-performance liquid chromatography using 3 μm particle packed columns and monolithic columns in pharmaceutical development and production working under current good manufacturing practice. *Journal of Chromatography A*, **1036**, 127–133 (2004). <http://doi:10.1016/j.chroma.2004.02.056>.
- [98] Serra, A.; Bacon, D. J.; Pond, R. C.: The crystallography and core structure of twinning dislocations in H.C.P. metals. *Acta Metallurgica*, **36**, 3183–3203 (1988). [http://doi:10.1016/0001-6160\(88\)90054-5](http://doi:10.1016/0001-6160(88)90054-5).
- [99] Otwinowski, Z.; Minor, W. B. T.-M. in E.: [20] Processing of X-ray diffraction data collected in oscillation mode. In *Macromolecular Crystallography Part A*; Academic Press, (1997); Vol. 276, pp. 307–326 ISBN 0076-6879.
- [100] Sampath Kumar, T. S.: Chapter 2 - Physical and Chemical Characterization of Biomaterials. In; Bandyopadhyay, A., Bose, S. B. T.-C. of B., Eds.; Academic Press: Oxford, (2013); pp. 11–47 ISBN 978-0-12-415800-9.
- [101] Tanzi, M. C.: *Characterization of thermal properties and crystallinity of polymer biomaterials*; Elsevier Ltd.; ISBN 9780081007372.
- [102] Brunella, M. F.; Serafini, A.; Tanzi, M. C.: *Characterization of 2D polymeric biomaterial structures or surfaces*; Elsevier Ltd.; ISBN 9780081007372.
- [103] Nisbet, D. R.; Rodda, A. E.; Finkelstein, D. I.; Horne, M. K.; Forsythe, J. S.; Shen, W.: Surface and bulk characterisation of electrospun membranes: Problems and improvements. *Colloids and Surfaces B: Biointerfaces*, **71**, 1–12 (2009). <http://doi:https://doi.org/10.1016/j.colsurfb.2009.01.022>.
- [104] Safinia, L.; Mantalaris, A.; Bismarck, A.: Nondestructive technique for the characterization of the pore size distribution of soft porous constructs for tissue engineering. *Langmuir*, **22**, 3235–3242 (2006). <http://doi:10.1021/la051762g>.
- [105] Szewczyk, P. K.; Ura, D. P.; Metwally, S.; Knapczyk-Korczyk, J.; Gajek, M.; Marzec, M. M.; Bernasik, A.; Stachewicz, U.: Roughness and fiber fraction dominated wetting of electrospun fiber-based porous meshes. *Polymers*, **11** (2018). <http://doi:10.3390/polym11010034>.

- [106] Brown, M. E.: *Handbook of thermal analysis and calorimetry*; Vol. 1; ISBN 9772081415.
- [107] Weldon, D. G.: *Differential scanning calorimetry*; Vol. 31; ISBN 9783642055935.
- [108] Voronin, G.; Harte, F.: Differential scanning calorimetry. *Encyclopedia of Dairy Sciences: Third edition*, **2**, 348–355 (2021).
<http://doi:10.3139/9781569906446.007>.
- [109] Patwa, R.; Saha, N.; Sáha, P.: Magnetic hydrogel based shoe insoles for prevention of diabetic foot. *Journal of Magnetism and Magnetic Materials*, **514**, 167153 (2020). <http://doi:10.1016/j.jmmm.2020.167153>.
- [110] Callister, W. D.; Rethwisch, D. G.: *Fundamentals of Materials Science and Engineering*; ISBN 9780470125373.
- [111] Qi, F. F.; Cao, Y.; Wang, M.; Rong, F.; Xu, Q.: Nylon 6 electrospun nanofibers mat as effective sorbent for the removal of estrogens: Kinetic and thermodynamic studies. *Nanoscale Research Letters*, **9**, 1–10 (2014).
<http://doi:10.1186/1556-276X-9-353>.
- [112] Al-Khateeb, L. A.; Obaid, A. Y.; Asiri, N. A.; Abdel Salam, M.: Adsorption behavior of estrogenic compounds on carbon nanotubes from aqueous solutions: Kinetic and thermodynamic studies. *Journal of Industrial and Engineering Chemistry*, **20**, 916–924 (2014).
<http://doi:10.1016/j.jiec.2013.06.023>.
- [113] Taha, A. A.; Wu, Y. na; Wang, H.; Li, F.: Preparation and application of functionalized cellulose acetate/silica composite nanofibrous membrane via electrospinning for Cr(VI) ion removal from aqueous solution. *Journal of Environmental Management*, **112**, 10–16 (2012).
<http://doi:10.1016/j.jenvman.2012.05.031>.
- [114] Tian, Y.; Wu, M.; Liu, R.; Li, Y.; Wang, D.; Tan, J.; Wu, R.; Huang, Y.: Electrospun membrane of cellulose acetate for heavy metal ion adsorption in water treatment. *Carbohydrate Polymers*, **83**, 743–748 (2011).
<http://doi:10.1016/j.carbpol.2010.08.054>.
- [115] Luo, Z.; Li, H.; Yang, Y.; Lin, H.; Yang, Z.: Adsorption of 17 α -ethinylestradiol from aqueous solution onto a reduced graphene oxide-magnetic composite. *Journal of the Taiwan Institute of Chemical Engineers*, **80**, 797–804 (2017). <http://doi:10.1016/j.jtice.2017.09.028>.
- [116] Günay, A.; Arslankaya, E.; Tosun, I.: Lead removal from aqueous solution by natural and pretreated clinoptilolite: Adsorption equilibrium and kinetics. *Journal of Hazardous Materials*, **146**, 362–371 (2007).
<http://doi:10.1016/j.jhazmat.2006.12.034>.
- [117] Ersali, S.; Hadadi, V.; Moradi, O.; Fakhri, A.: Pseudo-second-order kinetic equations for modeling adsorption systems for removal of ammonium ions using multi-walled carbon nanotube. *Fullerenes, Nanotubes and Carbon Nanostructures*, , 150527104639002 (2013).
<http://doi:10.1080/1536383x.2013.787610>.

- [118] Esmaceli, F.; Gorbanian, S. A.; Moazezi, N.: Removal of Estradiol Valerate and Progesterone using Powdered and Granular Activated Carbon from Aqueous Solutions. *International Journal of Environmental Research*, **11**, 695–705 (2017). <http://doi:10.1007/s41742-017-0060-0>.
- [119] He, J.; Zhou, Q.; Guo, J.; Fang, F.: Characterization of potassium hydroxide modified anthracite particles and enhanced removal of 17 α -ethinylestradiol and bisphenol A. *Environmental Science and Pollution Research*, **25**, 22224–22235 (2018). <http://doi:10.1007/s11356-018-2287-5>.
- [120] Al-Khateeb, L. A.; Obaid, A. Y.; Asiri, N. A.; Abdel Salam, M.: Adsorption behavior of estrogenic compounds on carbon nanotubes from aqueous solutions: Kinetic and thermodynamic studies. *Journal of Industrial and Engineering Chemistry*, **20**, 916–924 (2014). <http://doi:10.1016/j.jiec.2013.06.023>.
- [121] Ho, Y. S.; McKay, G.: Application of kinetic models to the sorption of copper (II) on to peat. *Adsorption Science and Technology*, **20**, 797–815 (2002). <http://doi:10.1260/026361702321104282>.
- [122] Ngwabebhoh, F. A.; Mammadli, N.; Yildiz, U.: Bioinspired modified nanocellulose adsorbent for enhanced boron recovery from aqueous media: Optimization, kinetics, thermodynamics and reusability study. *Journal of Environmental Chemical Engineering*, **7**, 103281 (2019). <http://doi:10.1016/j.jece.2019.103281>.
- [123] Carballa, M.; Fink, G.; Omil, F.; Lema, J. M.; Ternes, T.: Determination of the solid-water distribution coefficient (K_d) for pharmaceuticals, estrogens and musk fragrances in digested sludge. *Water Research*, **42**, 287–295 (2008). <http://doi:10.1016/j.watres.2007.07.012>.
- [124] Prokić, D.; Vukčević, M.; Kalijadis, A.; Maletić, M.; Babić, B.; Đurkić, T.: Removal of Estrone, 17 β -Estradiol, and 17 α -Ethinylestradiol from Water by Adsorption onto Chemically Modified Activated Carbon Cloths. *Fibers and Polymers*, **21**, 2263–2274 (2020). <http://doi:10.1007/s12221-020-9758-2>.
- [125] Proki, D.; Vuk, M.; Mitrovi, A.; Maleti, M.; Kalijadis, A.; Jankovi, I.; Tatjana, Đ.: from water onto modified multi-walled carbon nanotubes , carbon cryogel , and carbonized hydrothermal carbon. (2021).
- [126] Ngwabebhoh, F. A.; Erdem, A.; Yildiz, U.: Synergistic removal of Cu(II) and nitrazine yellow dye using an eco-friendly chitosan-montmorillonite hydrogel: Optimization by response surface methodology. *Journal of Applied Polymer Science*, **133**, 1–14 (2016). <http://doi:10.1002/app.43664>.
- [127] Han, J.; Qiu, W.; Hu, J.; Gao, W.: Chemisorption of estrone in nylon microfiltration membranes: Adsorption mechanism and potential use for estrone removal from water. *Water Research*, **46**, 873–881 (2012). <http://doi:10.1016/j.watres.2011.11.066>.

- [128] Celebioglu, A.; Demirci, S.; Uyar, T.: Cyclodextrin-grafted electrospun cellulose acetate nanofibers via “click” reaction for removal of phenanthrene. *Applied Surface Science*, **305**, 581–588 (2014). <http://doi:10.1016/j.apsusc.2014.03.138>.
- [129] Mikaeili, F.; Gouma, P. I.: Super Water-Repellent Cellulose Acetate Mats. *Scientific Reports*, **8**, 1–8 (2018). <http://doi:10.1038/s41598-018-30693-2>.
- [130] Karbownik, I.; Rac-Rumijowska, O.; Fiedot-Toboła, M.; Rybicki, T.; Tetrycz, H.: The preparation and characterization of polyacrylonitrile-polyaniline (PAN/PANI) fibers. *Materials*, **12** (2019). <http://doi:10.3390/ma12040664>.
- [131] Han, X. J.; Cheng, B. J.; Li, Y. J.; Huang, Z. M.; Huang, C.; Du, Z. F.; Wang, J.: The effects of electrospinning parameters on coaxial polyacrylonitrile/polyurethane nanofibers: Morphology and water vapour transmission rate. *Fibers and Polymers*, **16**, 2237–2243 (2015). <http://doi:10.1007/s12221-015-5458-8>.
- [132] Sundaran, S. P.; Reshmi, C. R.; Sujith, A.: Tailored design of polyurethane based fouling-tolerant nanofibrous membrane for water treatment. *New Journal of Chemistry*, **42**, 1958–1972 (2018). <http://doi:10.1039/c7nj03997b>.
- [133] Kwak, N. S.; Jung, W. H.; Park, H. M.; Hwang, T. S.: Electrospun polyethersulfone fibrous mats: Sulfonation, its characterization and solution-phase ammonium sorption behavior. *Chemical Engineering Journal*, **215–216**, 375–382 (2013). <http://doi:10.1016/j.cej.2012.10.065>.
- [134] Xu, Y.; Bao, J.; Zhang, X.; Li, W.; Xie, Y.; Sun, S.; Zhao, W.; Zhao, C.: Functionalized polyethersulfone nanofibrous membranes with ultra-high adsorption capacity for organic dyes by one-step electrospinning. *Journal of Colloid and Interface Science*, **533**, 526–538 (2019). <http://doi:10.1016/j.jcis.2018.08.072>.
- [135] Benavente, M. J.; Caballero, M. J. A.; Silvero, G.; López-Coca, I.; Escobar, V. G.: Cellulose Acetate Recovery from Cigarette Butts. *Proceedings*, **2**, 1447 (2019). <http://doi:10.3390/proceedings2201447>.
- [136] Nasir, M.; Subhan, A.; Prihandoko, B.; Lestariningsih, T.: Nanostructure and Property of Electrospun SiO₂-Cellulose Acetate Nanofiber Composite by Electrospinning. *Energy Procedia*, **107**, 227–231 (2017). <http://doi:10.1016/j.egypro.2016.12.133>.
- [137] Vazquez-Velez, E.; Lopez-Zarate, L.; Martinez-Valencia, H.: Electrospinning of polyacrylonitrile nanofibers embedded with zerovalent iron and cerium oxide nanoparticles, as Cr(VI) adsorbents for water treatment. *Journal of Applied Polymer Science*, **137**, 1–10 (2020). <http://doi:10.1002/app.48663>.
- [138] Porter, J. J.; Porter, R. S.: Filtration studies of selected anionic dyes using asymmetric titanium dioxide membranes on porous stainless-steel tubes.

- Journal of Membrane Science, **101**, 67–81 (1995).
[http://doi:10.1016/0376-7388\(94\)00278-7](http://doi:10.1016/0376-7388(94)00278-7).
- [139] Auriol, M.; Filali-Meknassi, Y.; Adams, C. D.; Tyagi, R. D.: Natural and synthetic hormone removal using the horseradish peroxidase enzyme: Temperature and pH effects. *Water Research*, **40**, 2847–2856 (2006).
<http://doi:10.1016/j.watres.2006.05.032>.
- [140] Behera, S. K.; Kim, H. W.; Oh, J. E.; Park, H. S.: Occurrence and removal of antibiotics, hormones and several other pharmaceuticals in wastewater treatment plants of the largest industrial city of Korea. *Science of the Total Environment*, **409**, 4351–4360 (2011).
<http://doi:10.1016/j.scitotenv.2011.07.015>.
- [141] Bayode, A. A.; dos Santos, D. M.; Omorogie, M. O.; Olukanni, O. D.; Moodley, R.; Bodede, O.; Agunbiade, F. O.; Taubert, A.; de Camargo, A. S. S.; Eckert, H.; Vieira, E. M.; Unuabonah, E. I.: Carbon-mediated visible-light clay-Fe₂O₃–graphene oxide catalytic nanocomposites for the removal of steroid estrogens from water. *Journal of Water Process Engineering*, **40**, 101865 (2021). <http://doi:10.1016/j.jwpe.2020.101865>.
- [142] Pinto, A. M.; Moreira, S.; Gonçalves, I. C.; Gama, F. M.; Mendes, A. M.; Magalhães, F. D.: Biocompatibility of poly(lactic acid) with incorporated graphene-based materials. *Colloids and Surfaces B: Biointerfaces*, **104**, 229–238 (2013). <http://doi:10.1016/j.colsurfb.2012.12.006>.
- [143] Yasir, M.; Šopík, T.; Lovecká, L.; Kimmer, D.; Sedlařík, V.: The adsorption, kinetics, and interaction mechanisms of various types of estrogen on electrospun polymeric nanofiber membranes. *Nanotechnology*, **33**, 75702 (2021). <http://doi:10.1088/1361-6528/ac357b>.
- [144] Arroyo, F. D.; Castro-Guerrero, C. F.; León-Silva, U.: Thin films of cellulose acetate nanofibers from cigarette butt waste. *Progress in Rubber, Plastics and Recycling Technology*, **36**, 3–17 (2020).
<http://doi:10.1177/1477760619895024>.
- [145] Alhokbany, N. S.; Naushad, M.; Kumar, V.; Al hatim, S.; Alshehri, S. M.; Ahamad, T.: Self-nitrogen doped carbons aerogel derived from waste cigarette butts (cellulose acetate) for the adsorption of BPA: Kinetics and adsorption mechanisms. *Journal of King Saud University - Science*, **32**, 3351–3358 (2020). <http://doi:10.1016/j.jksus.2020.09.021>.
- [146] Schäfer, A. I.; Akanyeti, I.; Semião, A. J. C.: Micropollutant sorption to membrane polymers: A review of mechanisms for estrogens. *Advances in Colloid and Interface Science*, **164**, 100–117 (2011).
<http://doi:10.1016/j.cis.2010.09.006>.
- [147] Cao, W.; Ma, W.; Lu, T.; Jiang, Z.; Xiong, R.; Huang, C.: Multifunctional nanofibrous membranes with sunlight-driven self-cleaning performance for complex oily wastewater remediation. *Journal of Colloid and Interface Science*, **608**, 164–174 (2022). <http://doi:10.1016/j.jcis.2021.09.194>.
- [148] Kanu, N. J.; Gupta, E.; Vates, U. K.; Singh, G. K.: Electrospinning process

- parameters optimization for biofunctional curcumin/gelatin nanofibers. *Materials Research Express*, **7**, 0–27 (2020). <http://doi:10.1088/2053-1591/ab7f60>.
- [149] Ma, H.; Burger, C.; Hsiao, B. S.; Chu, B.: Nanofibrous microfiltration membrane based on cellulose nanowhiskers. *Biomacromolecules*, **13**, 180–186 (2012). <http://doi:10.1021/bm201421g>.
- [150] Araga, R.; Sharma, C. S.: Amine Functionalized Electrospun Cellulose Nanofibers for Fluoride Adsorption from Drinking Water. *Journal of Polymers and the Environment*, (2019). <http://doi:10.1007/s10924-019-01394-2>.
- [151] Qian, L.; Li, X.; Qi, F.; Li, J.; Lu, L.; Xu, Q.: An amino-functionalized grooved nanofiber mat for solid-phase extraction of phenolic pollutants. *Microchimica Acta*, (2017). <http://doi:10.1007/s00604-017-2313-1>.
- [152] Stejskal, J.; Bober, P.; Trchová, M.; Kovalcik, A.; Hodan, J.; Hromádková, J.; Prokeš, J.: Polyaniline Cryogels Supported with Poly(vinyl alcohol): Soft and Conducting. *Macromolecules*, (2017). <http://doi:10.1021/acs.macromol.6b02526>.
- [153] Zhang, Z.; Wei, Z.; Wan, M.: Nanostructures of polyaniline doped with inorganic acids. *Macromolecules*, (2002). <http://doi:10.1021/ma020199v>.
- [154] Stejskal, J.: Interaction of conducting polymers, polyaniline and polypyrrole, with organic dyes: polymer morphology control, dye adsorption and photocatalytic decomposition. *Chem. Pap.* (2020).
- [155] Ayad, M.; El-Hefnawy, G.; Zaghlol, S.: Facile synthesis of polyaniline nanoparticles; its adsorption behavior. *Chemical Engineering Journal*, (2013). <http://doi:10.1016/j.cej.2012.11.099>.
- [156] Stejskal, J.: Conducting polymers are not just conducting: a perspective for emerging technology. *Polymer International*, (2020). <http://doi:10.1002/pi.5947>.
- [157] Zaghlol, S.; Amer, W. A.; Shaaban, M. H.; Ayad, M. M.; Bober, P.; Stejskal, J.: Conducting macroporous polyaniline/poly(vinyl alcohol) aerogels for the removal of chromium(VI) from aqueous media. *Chemical Papers*, **74**, 3183–3193 (2020). <http://doi:10.1007/s11696-020-01151-z>.
- [158] Humpolicek, P.; Kasparkova, V.; Saha, P.; Stejskal, J.: Biocompatibility of polyaniline. *Synthetic Metals*, (2012). <http://doi:10.1016/j.synthmet.2012.02.024>.
- [159] Huang, T.; Zhang, S. wen; Xie, J.; Zhou, L.; Liu, L. fei: Effective adsorption of quadrivalent cerium by synthesized laurylsulfonate green rust in a central composite design. *Journal of Environmental Sciences (China)*, (2021). <http://doi:10.1016/j.jes.2021.01.028>.
- [160] Wang, J.; Chi, H.; Zhou, A.; Zheng, R.; Bai, H.; Zhang, T.: Facile synthesis of multi-functional elastic polyaniline/polyvinyl alcohol composite gels by a solution assembly method. *RSC Advances*, (2020). <http://doi:10.1039/d0ra02238a>.

- [161] Erdem, A.; Ngwabebhoh, F. A.; Çetintaş, S.; Bingöl, D.; Yildiz, U.: Fabrication and characterization of novel macroporous Jeffamine/diamino hexane cryogels for enhanced Cu(II) metal uptake: Optimization, isotherms, kinetics and thermodynamic studies. *Chemical Engineering Research and Design*, (2017). <http://doi:10.1016/j.cherd.2016.10.010>.
- [162] Saleh, T. A.: Isotherm, kinetic, and thermodynamic studies on Hg(II) adsorption from aqueous solution by silica- multiwall carbon nanotubes. *Environmental Science and Pollution Research*, **22**, 16721–16731 (2015). <http://doi:10.1007/s11356-015-4866-z>.
- [163] Saleh, T. A.: The influence of treatment temperature on the acidity of MWCNT oxidized by HNO₃ or a mixture of HNO₃ /H₂SO₄. *Applied Surface Science*, **257**, 7746–7751 (2011). <http://doi:10.1016/j.apsusc.2011.04.020>.
- [164] Saleh, T. A.: Simultaneous adsorptive desulfurization of diesel fuel over bimetallic nanoparticles loaded on activated carbon. *Journal of Cleaner Production*, **172**, 2123–2132 (2018). <http://doi:10.1016/j.jclepro.2017.11.208>.
- [165] Bahadur, A.; Shoaib, M.; Saeed, A.; Iqbal, S.: FT-IR spectroscopic and thermal study of waterborne polyurethane-acrylate leather coatings using tartaric acid as an ionomer. *E-Polymers*, (2016). <http://doi:10.1515/epoly-2016-0154>.
- [166] Shahi, M.; Moghimi, A.; Naderizadeh, B.; Maddah, B.: Electrospun PVA-PANI and PVA-PANI-AgNO₃ composite nanofibers. *Scientia Iranica*, (2011). <http://doi:10.1016/j.scient.2011.08.013>.
- [167] Huang, H.; Yao, J.; Li, L.; Zhu, F.; Liu, Z.; Zeng, X.; Yu, X.; Huang, Z.: Reinforced polyaniline/polyvinyl alcohol conducting hydrogel from a freezing–thawing method as self-supported electrode for supercapacitors. *Journal of Materials Science*, (2016). <http://doi:10.1007/s10853-016-0137-8>.
- [168] Khasawneh, O. F. S.; Palaniandy, P.; Palaniandy, P.; Ahmadipour, M.; Mohammadi, H.; Bin Hamdan, M. R.: Removal of acetaminophen using Fe₂O₃-TiO₂nanocomposites by photocatalysis under simulated solar irradiation: Optimization study. *Journal of Environmental Chemical Engineering*, (2021). <http://doi:10.1016/j.jece.2020.104921>.
- [169] Galedari, M.; Mehdipour Ghazi, M.; Rashid Mirmasoomi, S.: Photocatalytic process for the tetracycline removal under visible light: Presenting a degradation model and optimization using response surface methodology (RSM). *Chemical Engineering Research and Design*, (2019). <http://doi:10.1016/j.cherd.2019.03.031>.
- [170] Lambropoulou, D.; Evgenidou, E.; Saliverou, V.; Kosma, C.; Konstantinou, I.: Degradation of venlafaxine using TiO₂/UV process: Kinetic studies, RSM optimization, identification of transformation products and toxicity evaluation. *Journal of Hazardous Materials*, (2017).

- <http://doi:10.1016/j.jhazmat.2016.04.074>.
- [171] Kovalova, L.; Knappe, D. R. U.; Lehnberg, K.; Kazner, C.; Hollender, J.: Removal of highly polar micropollutants from wastewater by powdered activated carbon. *Environmental Science and Pollution Research*, (2013). <http://doi:10.1007/s11356-012-1432-9>.
- [172] Abdel-Gawad, S. A.; Abdel-Aziz, H. M.: Removal of ethinylestradiol by adsorption process from aqueous solutions using entrapped activated carbon in alginate biopolymer: isotherm and statistical studies. *Applied Water Science*, **9**, 1–8 (2019). <http://doi:10.1007/s13201-019-0951-7>.
- [173] Yasir, M.; Sopik, T.; Patwa, R.; Kimmer, D.; Sedlarik, V.: Adsorption of estrogenic hormones in aqueous solution using electrospun nanofibers from waste cigarette butts : Kinetics, mechanism, and reusability. *Express polymer letters*, **16**, 624–648 (2022).
- [174] Ren, Y. X.; Nakano, K.; Nomura, M.; Chiba, N.; Nishimura, O.: A thermodynamic analysis on adsorption of estrogens in activated sludge process. *Water Research*, (2007). <http://doi:10.1016/j.watres.2007.01.058>.
- [175] Wang, W.; Hu, J.; Zhang, R.; Yan, C.; Cui, L.; Zhu, J.: A pH-responsive carboxymethyl cellulose/chitosan hydrogel for adsorption and desorption of anionic and cationic dyes. *Cellulose*, **28**, 897–909 (2021). <http://doi:10.1007/s10570-020-03561-4>.
- [176] Han, J.; Qiu, W.; Cao, Z.; Hu, J.; Gao, W.: Adsorption of ethinylestradiol (EE2) on polyamide 612: Molecular modeling and effects of water chemistry. *Water Research*, **47**, 2273–2284 (2013). <http://doi:10.1016/j.watres.2013.01.046>.
- [177] He, J.; Zhou, Q.; Guo, J.; Fang, F.: Characterization of potassium hydroxide modified anthracite particles and enhanced removal of 17 α -ethinylestradiol and bisphenol A. *Environmental Science and Pollution Research*, **25**, 22224–22235 (2018). <http://doi:10.1007/s11356-018-2287-5>.
- [178] Kaspar, P.; Sobola, D.; Částková, K.; Knápek, A.; Burda, D.; Orudzhev, F.; Dallaev, R.; Tofel, P.; Trčka, T.; Grmela, L.; Hadaš, Z.: Characterization of polyvinylidene fluoride (Pvdf) electrospun fibers doped by carbon flakes. *Polymers*, **12**, 1–15 (2020). <http://doi:10.3390/polym12122766>.
- [179] Lanceros-Méndez, S.; Mano, J. F.; Costa, A. M.; Schmidt, V. H.: FTIR and DSC studies of mechanically deformed β -PVDF films. *Journal of Macromolecular Science - Physics*, **40 B**, 517–527 (2001). <http://doi:10.1081/MB-100106174>.
- [180] Sengupta, D.; Kottapalli, A. G. P.; Chen, S. H.; Miao, J. M.; Kwok, C. Y.; Triantafyllou, M. S.; Warkiani, M. E.; Asadnia, M.: Characterization of single polyvinylidene fluoride (PVDF) nanofiber for flow sensing applications. *AIP Advances*, **7** (2017). <http://doi:10.1063/1.4994968>.

- [181] Sepahi, S.; Kalae, M.; Mazinani, S.; Abdouss, M.; Hosseini, S. M.: Introducing electrospun polylactic acid incorporating etched halloysite nanotubes as a new nanofibrous web for controlled release of Amoxicillin. *Journal of Nanostructure in Chemistry*, **11**, 245–258 (2021). <http://doi:10.1007/s40097-020-00362-w>.
- [182] Rosid, S. M.; Ajji, A.; Hasbullah, H.; Rosid, S. J. M.; Ismail, A. F.; Goh, P. S.: Physicochemical characteristics of polysulfone nanofiber membranes with iron oxide nanoparticles via electrospinning. *Journal of Applied Polymer Science*, **139**, 1–10 (2022). <http://doi:10.1002/app.51661>.
- [183] Mazoochi, T.; Hamadian, M.; Ahmadi, M.; Jabbari, V.: Investigation on the morphological characteristics of nanofibrous membrane as electrospun in the different processing parameters. *International Journal of Industrial Chemistry*, **3**, 1–8 (2012). <http://doi:10.1186/2228-5547-3-2>.
- [184] Duan, Q.; Li, X.; Wu, Z.; Alsaedi, A.; Hayat, T.; Chen, C.; Li, J.: Adsorption of 17 β -estradiol from aqueous solutions by a novel hierarchically nitrogen-doped porous carbon. *Journal of Colloid and Interface Science*, **533**, 700–708 (2019). <http://doi:10.1016/j.jcis.2018.09.007>.
- [185] Zhang, J.; Nguyen, M. N.; Li, Y.; Yang, C.; Schäfer, A. I.: Steroid hormone micropollutant removal from water with activated carbon fiber-ultrafiltration composite membranes. *Journal of Hazardous Materials*, **391**, 122020 (2020). <http://doi:10.1016/j.jhazmat.2020.122020>.
- [186] Patel, S.; Han, J.; Gao, W.: Sorption of 17 β -estradiol from aqueous solutions on to bone char derived from waste cattle bones: Kinetics and isotherms. *Journal of Environmental Chemical Engineering*, **3**, 1562–1569 (2015). <http://doi:10.1016/j.jece.2015.04.027>.
- [187] Gong, K.; Lin, Y.; Wu, P.; Jin, X.; Owens, G.; Chen, Z.: Removal mechanism of 17 β -estradiol by carbonized green synthesis of Fe/Ni nanoparticles. *Chemosphere*, **291**, 132777 (2022). <http://doi:10.1016/j.chemosphere.2021.132777>.
- [188] Jin, X.; Hu, J.: Role of water chemistry on estrone removal by nanofiltration with the presence of hydrophobic acids. *Frontiers of Environmental Science and Engineering*, **9**, 164–170 (2015). <http://doi:10.1007/s11783-014-0747-9>.
- [189] Tagliavini, M.; Engel, F.; Weidler, P. G.; Scherer, T.; Schäfer, A. I.: Adsorption of steroid micropollutants on polymer-based spherical activated carbon (PBSAC). *Journal of Hazardous Materials*, **337**, 126–137 (2017). <http://doi:10.1016/j.jhazmat.2017.03.036>.
- [190] Ngwabebhoh, F. A.; Gazi, M.; Oladipo, A. A.: Adsorptive removal of multi-azo dye from aqueous phase using a semi-IPN superabsorbent chitosan-starch hydrogel. *Chemical Engineering Research and Design*, **112**, 274–288 (2016). <http://doi:10.1016/j.cherd.2016.06.023>.

LIST OF FIGURES

Figure 2.1: Distribution of Earth's water and its uses (Self-representation by the author).	16
Figure 2.2: Conventional techniques of water filtration (Self-representation by the author).	17
Figure 2.3: The Coagulation Process [9].	17
Figure 2.4: The Ozonation Process [1].	18
Figure 2.5: The Flocculation Process [1].	19
Figure 2.6: Biological treatment of wastewater (Self-representation by the author) [21].	20
Figure 2.7: Advanced adsorption methods for water treatment (Self-representation by the author) [24].	20
Figure 2.8: Schematic diagram of the cross-flow ultrafiltration technique [26].	21
Figure 2.9: Schematic diagram of the microfiltration technique [27].	21
Figure 2.10: Schematic diagram of the reverse osmosis technique (Self-representation by the author) [28].	22
Figure 2.11: Nanofiltration technique as applied in water treatment [31].	23
Figure 2.12: Schematic diagram of the primary sources of hormones in the environment and their fatal consequences [41].	24
Figure 2.13: Classification of hormones potentially found in the natural environment [41].	24
Figure 2.14: SEM of a) E3, b) E2, c) EE2 and d) E1 hormones, respectively (Self-representation by the author).	25
Figure 2.15: Steroid estrogenic hormones a) E1, b) E2, c) EE2, d) E3 (self-representation by the author).	26
Figure 2.16: Solubility of all four hormones together in a solution at different concentrations (Self-representation by the author).	27
Figure 2.17: Calibration curve and chromatogram of stock solution concentration of 0.8 mg/L containing 0.2 mg/L concentration of each hormone (E1, E2, EE2, E3) in the mixture (Self-representation from experimental data).	28
Figure 2.18: Illustration of a needle electrospinning system for the fabrication of nanofiber sheets (Self-representation by the author).	32
Figure 3.1: Potential applications associated with electrospun nanofiber (self-representation by the author) [79].	35

Figure 3.2: A) Illustration of a modern FTIR-imaging spectrometer; B) the conceptual optical path of an FTIR-imaging spectrometer [96].....	43
Figure 3.3: Schematic diagram of the high-performance liquid chromatography (Self-representation by the author).	44
Figure 3.4: Schematic diagram of the gel permeation chromatography technique (Self-representation by the author).	45
Figure 3.5: Overview of the X-ray diffraction technique [101].	46
Figure 3.6: Principle of optical microscopy technique and minimum resolvable limits (Self-representation by the author).	47
Figure 3.7: Representation of a scanning electron microscope [102].	49
Figure 3.8: Overview of the capillary flow porosimetry equipment [104].	51
Figure 3.9: Principle of contact angle measurement (Self-representation by the author).	52
Figure 3.10: Illustration of thermogravimetric analysis instrumentation (Self-representation) [106].	53
Figure 3.11: Overview of a heat flow DSC chamber with pans for the sample (S) and reference (R) connected by a common bridge [101].....	54
Figure 3.12: DSC thermogram of a polymeric material with various phase transitions - T_g (glass transition temperature), T_c (crystallization temperature), T_m (melting temperature-point), and T_d (temperature of degradation) [101].	55
Figure 3.13: Schematic diagram of a universal testing machine for tensile tests [110].	56
Figure 4.1: Schematic outline of works (Self-representation by the author).....	58
Figure 5.1: Schematic of nanofibers prepared via electrospinning and static adsorption test for hormone removal.	66
Figure 5.2: Electron micrographs, (inset) distribution of frequency size, and sample images of the electrospun nanofibers (20 mg) of (a, a') CA, (b, b') PA, (c, c') PAN, (d, d') PES, (e, e') PU 918, and (f, f') PU Elastollan, respectively.	67
Figure 5.3: FTIR spectra for the electrospun nanofibers from attenuated total reflectance (ATR) sampling.....	69
Figure 5.4: Static adsorption of each estrogenic hormone on six different nanofibers from a combined solution of (a) E1, (b) E2, (c) EE2, and (d) E3.....	71

Figure 5.5: Trends for the combined hormones of E1, E2, EE2, and E3 on the nanofibers as to (a) removal efficiency as a function of time and (b) total adsorption capacity as a function of time.	73
Figure 5.6: Plots of the adsorption kinetics for the four estrogenic hormones (E1, E2, EE2, E3) on PU Elastollan nanofibers: (a) pseudo-first-order, (b) pseudo-second-order, (c) the Weber-Morris interparticle diffusion model.	75
Figure 5.7: Hydrogen bonding between the polyurethane molecule and estrogenic hormones (a) E1, (b) E2, (c) E3, and (d) EE2.	78
Figure 5.8: FTIR spectra for the PU 918 nanofibers before and after static adsorption (0.8 mg/L mixture of E1, E2, EE2, and E3 of 100 mL volume).	79
Figure 5.9: Four adsorption cycles for each electrospun material (20 mg) and each estrogenic hormone (a) E1, (b) E2, (c) EE2, and (d) E3, at an initial concentration of 0.2 mg/L in a combined solution of 0.8 mg/L.	81
Figure 5.10: Cumulative efficiency of adsorption for the four estrogenic hormones on the various nanofibers over four cycles.	82
Figure 5.11: SEM Images, sample images of the nanofibers, and distribution of their fiber diameter after four adsorption-desorption cycles: (a, a', A) CA, (b, b', B) PA, (c, c', C) PAN, (d, d', D) PES, (e, e', E) PU918, and (f, f', F) PU Elastollan.	84
Figure 6.1: schematic representation of fabrication of WCENFs used for simultaneous removal of EH by batch adsorption test and instantaneous syringe film test.	86
Figure 6.2: SEM micrograph and (inset) size distribution for WCENFs at different magnifications of 500x, 1500x, and 5000x.	87
Figure 6.3: Stress vs. strain curves for (a) PP and PP/WCENFs, and (b) PET/WCENFs along with micrographs after breakage at a different magnification of 150x, 500x, 1500x, and 5000x.	90
Figure 6.4: (a) Batch adsorption study of each EH on WCENFs from a combined solution, (b) Cumulative adsorption removal efficiency as a function of time of EH (E1, E2, EE2, E3) together on WCENFs on the primary y-axis, and the total adsorption capacity (Q_t) of WCENFs as a function of time on the secondary y-axis.	92
Figure 6.5: Adsorption kinetics plots of four EH (E1, E2, EE2, E3) on WCENFs, (a) Pseudo-first-order, (b) Pseudo-second-order, (c) Weber-Morris interparticle diffusion model, (d) Elovich model, and (e) Fractional power model.	95

Figure 6.6: Displayed structures of (a) E1, (b) E2, (c) E3, (d) EE2, (e) WCENFs molecule and hydrogen bonding between WCENFs molecule with EH (f) E1, (g) E2, (h) E3, and (i) EE2.	100
Figure 6.7: Attenuated total reflectance (ATR) mode FTIR spectra of (a) WCENFs and (b) before and after batch adsorption.....	101
Figure 6.8: (a) Adsorption cycles of each EH (E1, E2, EE2, E3) with an initial concentration of 0.2 mg/L in a combined solution of 0.8 mg/L on WCENFs (20 mg), (b) Cumulative efficiency of all EH adsorption on WCENFs during four cycles.....	102
Figure 6.9: SEM image of WCENFs and their fiber diameter distribution after four adsorption-desorption cycles at different magnifications of 500x, 1500x, and 5000x.	104
Figure 6.10: Chromatogram of before and after adsorption on PET with stock solution (0.8 mg/L) containing 0.2 mg/L concentration of each EH (E3, E2, EE2, E1) in a mixture.....	105
Figure 6.11: (a) Concurrent adsorption of EH (E1, E2, EE2, and E3) on 1.4 μm PET/WCENFs syringe film using 0.8 mg/L EH aqueous solution as feed containing 0.2 mg/L of each hormone and (b) 1.4 μm PET/WCENFs film adsorption comparison with 0.45 μm commercial CA syringe film for E1.	106
Figure 7.1: (a) Aniline is oxidized to PANI (emeraldine) salt (PANI-ES) with ammonium peroxydisulfate and deprotonated to PANI (emeraldine) base (PANI-EB) using ammonium hydroxide. (b) Spun PU membrane (gray spirals) mixed with a solution of monomers (red circles) subsequently monomer polymerizes to a polymer (green objects) and adheres to PU fiber surface. After that green PANI is deprotonated to an emeraldine base (blue objects). (c) Images of neat spun PU membrane, PU-PANI-ES and PU-PANI-EB coated membranes.	113
Figure 7.2: FTIR spectra of neat PU as control, PU-PANI-ES, and PU-PANI-EB treated fibers from attenuated total reflectance (ATR) sampling.	114
Figure 7.3: Optical micrograph of coated (a) PU-PANI-ES and (b) PU-PANI-EB membranes at 100x magnification.	115
Figure 7.4: SEM images of PU as control, PU-PANI-ES, and PU-PANI-EB treated fibers at different magnifications of 1500x and 5000x.....	116
Figure 7.5: Adsorption removal of EE2 using PU as control, PU-PANI-ES, and PU-PANI-EB treated nanofibrous membranes.....	117

Figure 7.6: (a) Plot of predicted and actual response values and (b) residual plot for EE2 hormone removal.	120
Figure 7.7: 3D two-parameter interaction response surface plot on the removal of EE2 hormone using PU-PANI-ES membrane.	124
Figure 7.8: Effects of different adsorption parameters on removal percentage and adsorption capacity: a) pH of the solution, b) initial concentration of EE2, c) adsorbent dosage, and d) temperature on the removal of EE2 hormone using PU-PANI-ES fibers.....	126
Figure 7.9: Possible interaction mechanisms between EE2 and PU-PANI-ES fibers; (a) hydrophobic interactions, (b) π - π stacking interaction, (c) Cation- π interaction, and (d) hydrogen bonding.	127
Figure 7.10: Plots of the adsorption kinetics for the EE2 hormone on PU-PANI-ES fibers: (a) pseudo-first-order, (b) pseudo-second-order, (c) intraparticle diffusion model, and (d) Boyd model.	130
Figure 7.11: Six adsorption-desorption cycles of EE2 by PU-PANI-ES fibers.	132
Figure 8.1: Electron micrographs with (inset) distribution of frequency size of the electrospun nanofibers (a) PSU, (b) PLA, and (c) PVDF at different magnifications of 500x, 1500x, and 5000x.	136
Figure 8.2: Thermogravimetric analysis of (a) PSU, (b) PLA, (c) PVDF, (d) X-ray diffractograms, and (e) FTIR spectra of the different electrospun nanofibers.	138
Figure 8.3: (a) Comparative adsorption efficiency of hormones (E1, E2, E3, and EE2) on PSU, PLA, and PVDF electrospun nanofibers (left panel), and (b) Adsorption efficiency trends of E1, E2, E3, and EE2 hormones on PSU nanofibers as a function of time (right panel). (pH: 7, concentration of each hormone: 0.2 mg/L, and testing duration: 9 h).....	140
Figure 8.4: Adsorption kinetics plots of the four estrogenic hormones (E1, E2, EE2, E3) on PSU nanofibers, (a) Pseudo-first-order, (b) Pseudo-second-order, (c) Weber-Morris intraparticle diffusion, (d) Elovich, and (e) Fractional power model.	142
Figure 8.5: Effects of different adsorption parameters: a) solution pH, b) initial adsorbate concentration, c) adsorbent dosage, and d) temperature on the removal of E1 hormone using spun PSU nanofibers.....	146
Figure 8.6: Schematic representation of the possible different interaction mechanisms between PSU nanofibers and E1 hormone; (a) hydrophobic	

interactions, (b) π - π stacking interaction, and (c) hydrogen bonding. Strong bonding interactions are represented with bold arrows, while weak interactions are represented with dotted lines.....	148
Figure 8.7: Adsorption isotherms for E1 hormone using PSU electrospun nanofibers; a) Langmuir, b) Freundlich and c) Langmuir-Freundlich model. .	150
Figure 8.8: SEM micrograph after study with (inset) distribution of the fiber diameter (in the left panel) and cycles of adsorption-desorption for E1 by PSU nanofibers (in the right panel).....	153

LIST OF TABLES

Table 2.1: Specific properties of hormones	26
Table 2.2: Intensity peak, calibration equation, and limits of each hormone when mixed in a specific solution medium (a) ethanol, (b) ethanol: water 20: 80, and (c) water	29
Table 3.1: Solution properties of each polymer prior to electrospinning	40
Table 5.1: Characteristics of the electrospun nanofibers as gauged by BET, contact angle, and calculated values from the SEM images.....	68
Table 5.2: Values for each hormone from the kinetic models in relation to PU Elastollan electrospun nanofibers	77
Table 6.1: Characteristics values of WCENFs calculated using SEM micrographs, BET, and porosimetry	88
Table 6.2: Summary of mechanical properties of the WCENFs with substrates	91
Table 6.3: The kinetic models' parameters with each EH using WCENFs	97
Table 6.4: Comparison of adsorbents used for the specified water pollutants .	108
Table 7.1: Investigated experimental factors and their levels in the central composite design.....	112
Table 7.2: The different experiment runs with their actual and predicted responses	118
Table 7.3: ANOVA data for removal of estrogenic hormone based on CCD quadratic model.....	119

Table 7.4: Point prediction and validation of optimized parameters at 95% confidence interval	121
Table 7.5: Kinetic models and their determining parameters related to the removal of EE2 hormone using PU-PANI-ES fibers.....	129
Table 7.6: Thermodynamic parametric values for the adsorption of EE2 hormone	130
Table 7.7: Comparison of adsorbents for EE2 hormone removal.....	133
Table 8.1: SEM, BET, and porosimetry data of electrospun polymeric fiber materials.....	137
Table 8.2: The kinetic models' parameters with each hormone using PSU electrospun nanofibers.....	144
Table 8.3: Thermodynamic parametric values for the adsorption of E1 hormone	149
Table 8.4: Calculated adsorption isotherm parameters for the adsorption of the E1 hormone.....	151
Table 8.5: Comparison of adsorption capacity of E1 hormone using PSU to various adsorbents	152

LIST OF ABBREVIATIONS AND SYMBOLS

Alphabetically ordered

AA	Acetic acid
ATR	Attenuated total reflection
BC	Borax and citric acid
BD	1,4 butanediol
BET	Brunauer, Emmett, Teller
BHT	Butylated hydroxytoluene
Borax	Sodium tetra-borate decahydrate
CA	Cellulose acetate
CBs	Cigarette butts

CCD	Central composite design
DMA	Dimethylamylamine
DMF	N, N-dimethylformamide
DSC	Differential scanning calorimetry
ECDs	Endocrine disrupting compound
EH	Estrogenic hormones
E1	Estrone
E2	Estradiol
EE2	Ethinylestradiol
E3	Estriol
FA	Formic acid
FTIR	Fourier transform infrared spectroscopy
GMF	Glass microfiber
GPC	Gel permeation chromatography
HPLC	High performance liquid chromatography
LOD	Limit of detection
LOQ	Limit of quantification
MDI	4,4'-methylene-diphenyl diisocyanate
MIBK	4-methyl-2-pentanone
M_n	number average molar mass
M_w	Average molar mass
MWCNTs	Multiwalled carbon nanotubes
MWD	Molecular weight distribution
NF	Nanofiltration

NMA	N-methyl acetamide
NMP	N-Methyl-2-pyrrolidone
NPs	Nanoparticles
PA	Polyamide
PAIM	Poly 3-methyl-1,5-pentanediol-alt-adipic, isophthalic acid
PAN	Polyacrylonitrile
PANI	Polyaniline
PDI	Polydispersity index
PEO	Polyethylene oxide
PES	Polyethersulfone
PET	Polyethylene terephthalate
PLA	Poly lactide
PSU	Polysulfone
PU Elasollan	Polyurethane Elastollan
PU 918	Polyurethane 918
PU-PANI- ES	Polyurethane modified with polyaniline emeraldine salt
PU-PANI- EB	Polyurethane modified with polyaniline emeraldine base
PVA	Polyvinyl alcohol
PVDF	Polyvinylidene fluoride
PVP	Polyvinyl pyrrolidone
PP	Polypropylene
PTFE	Polytetrafluoroethylene

RC	Regenerated cellulose
RO	Reverse osmosis
SEM	Scanning electron microscopy
TGA	Thermogravimetric analysis
THF	Tetrahydrofuran
TiO ₂	Titanium dioxide
TLD	Through-the-lens detector
WCENFs	Waste cigarette electrospun nanofibers
XRD	X-Ray diffraction
ZnO	Zinc oxide

APPENDIX 1

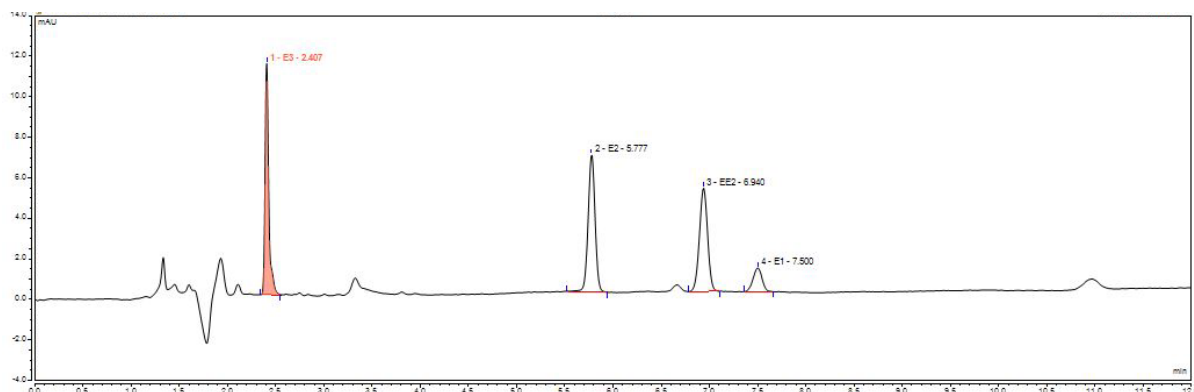


Fig. S1: Chromatogram of stock solution concentration of 0.8 mg/L containing 0.2 mg/L concentration of each hormone (E1, E2, EE2, E3) in the mixture.

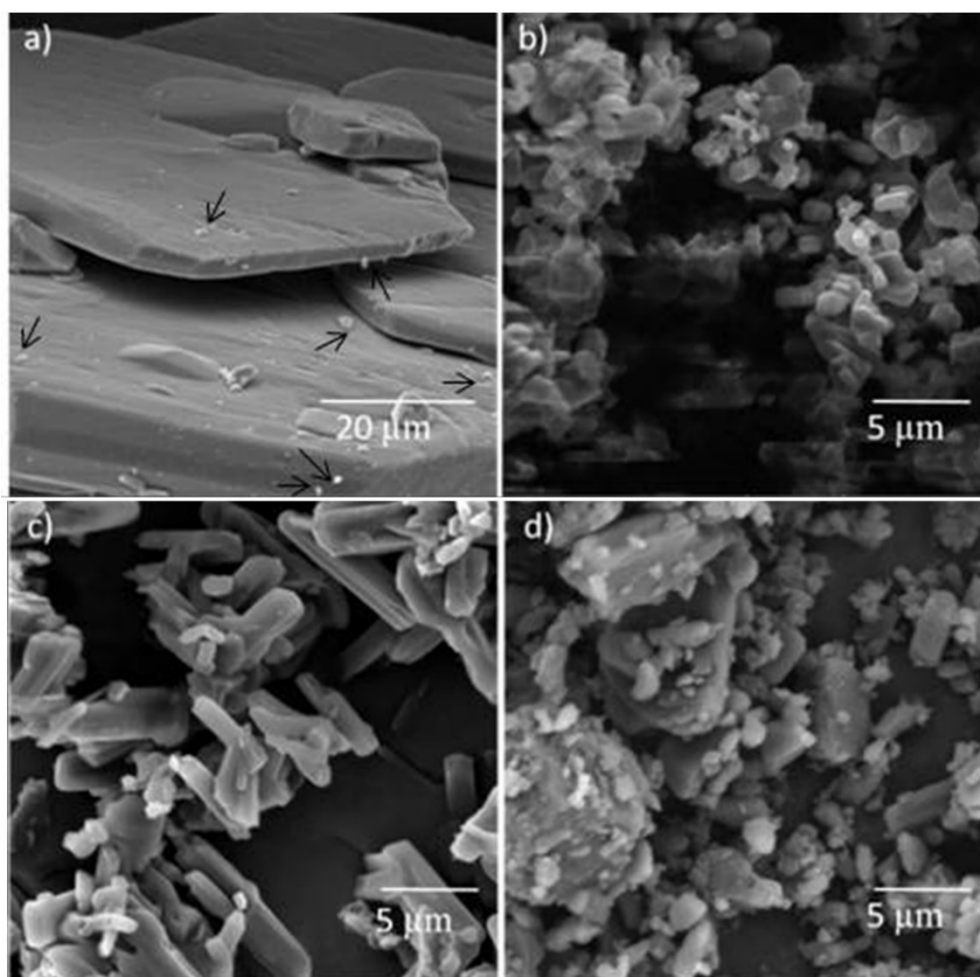
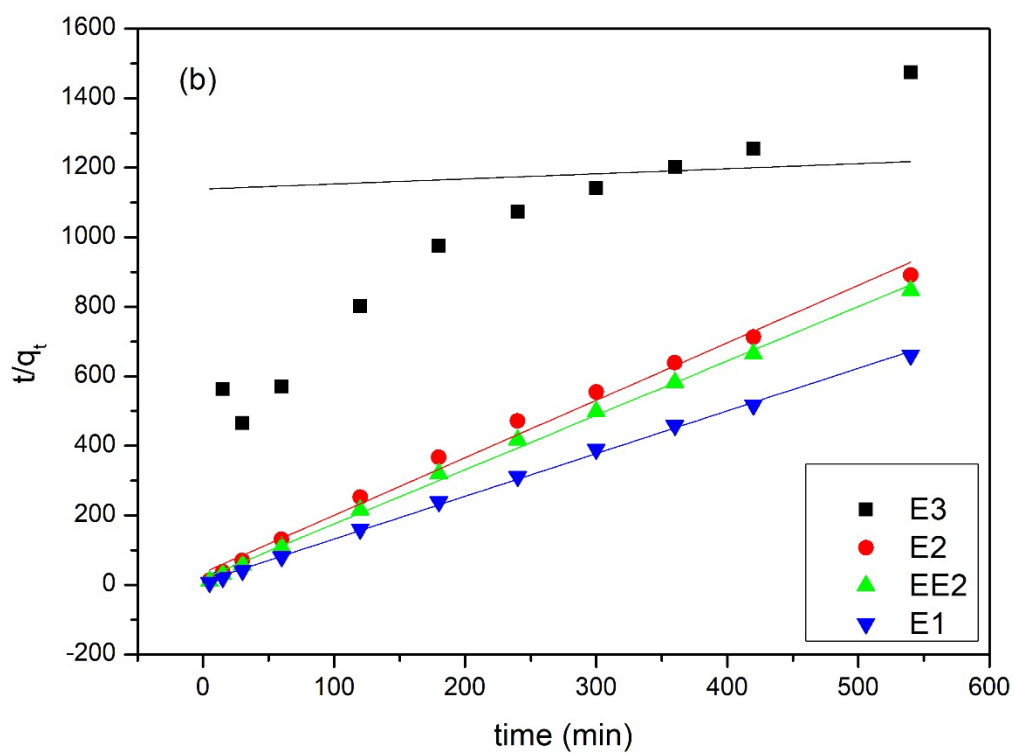
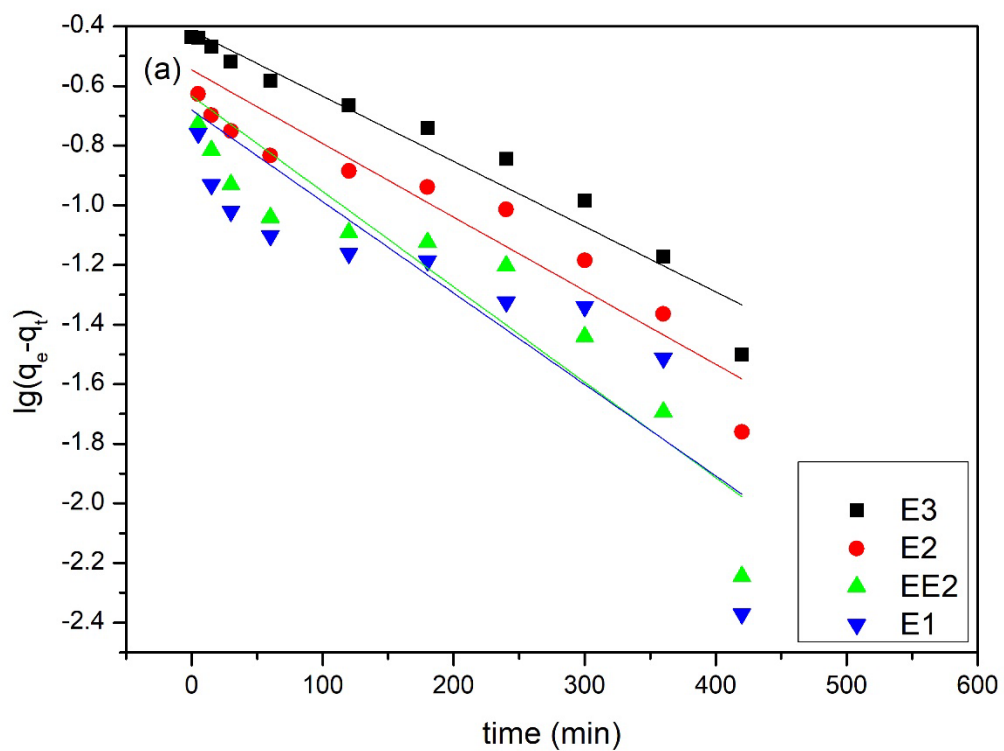


Fig. S2: Electron micrographs of estrogen crystals (a) E1 (black arrows), (b) E2, (c) EE2 and (d) E3 hormones, respectively.



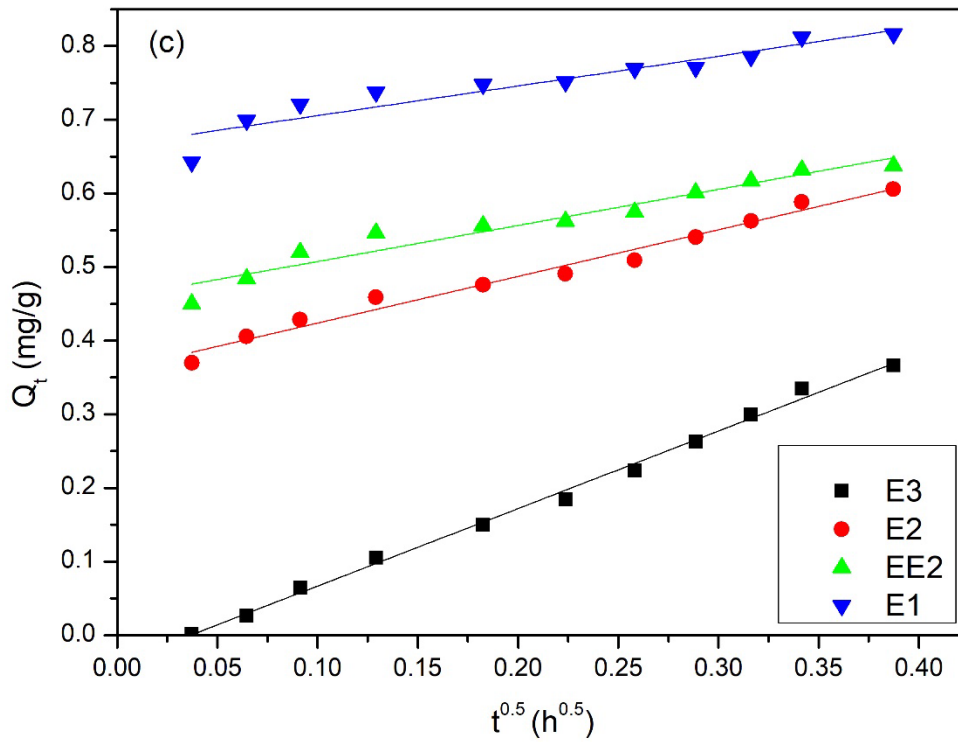
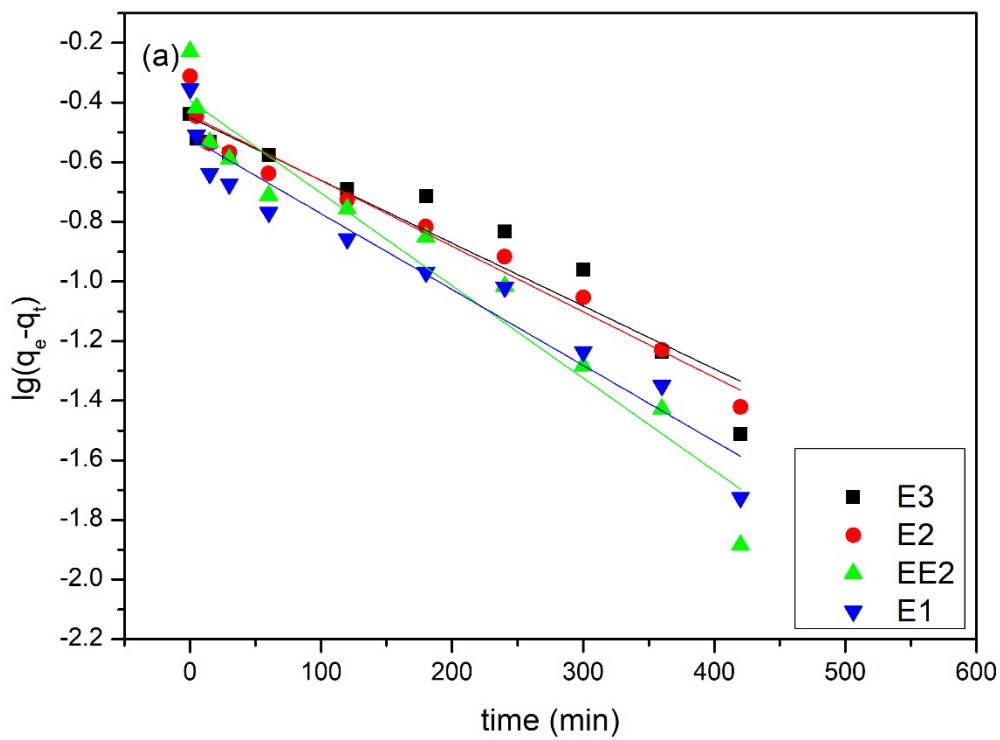


Fig. S3: Adsorption kinetics plots of four estrogenic hormones (E1, E2, EE2, E3) on PU 918 nanofibers, (a) Pseudo-first-order, (b) Pseudo-second-order, (c) Weber-Morris interparticle diffusion model.



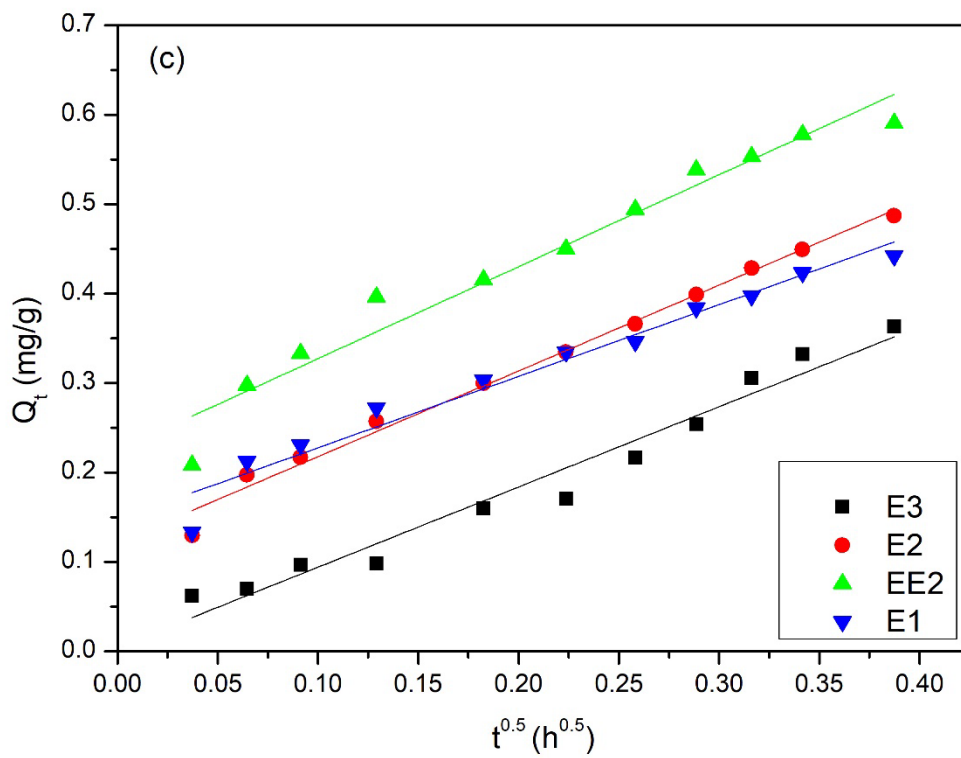
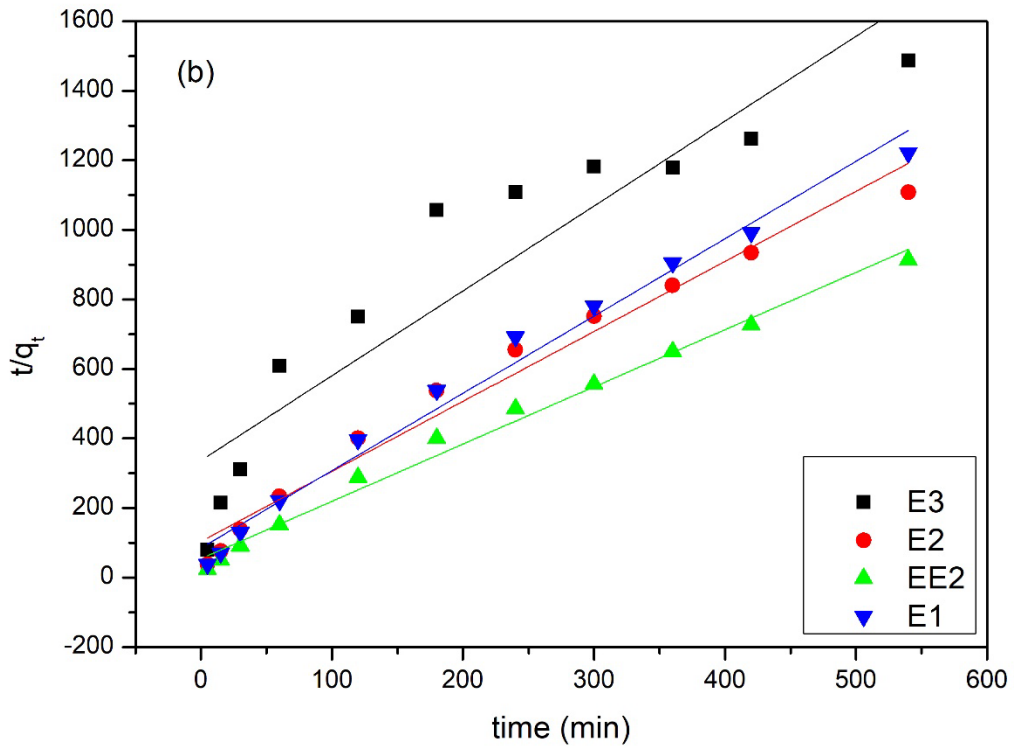
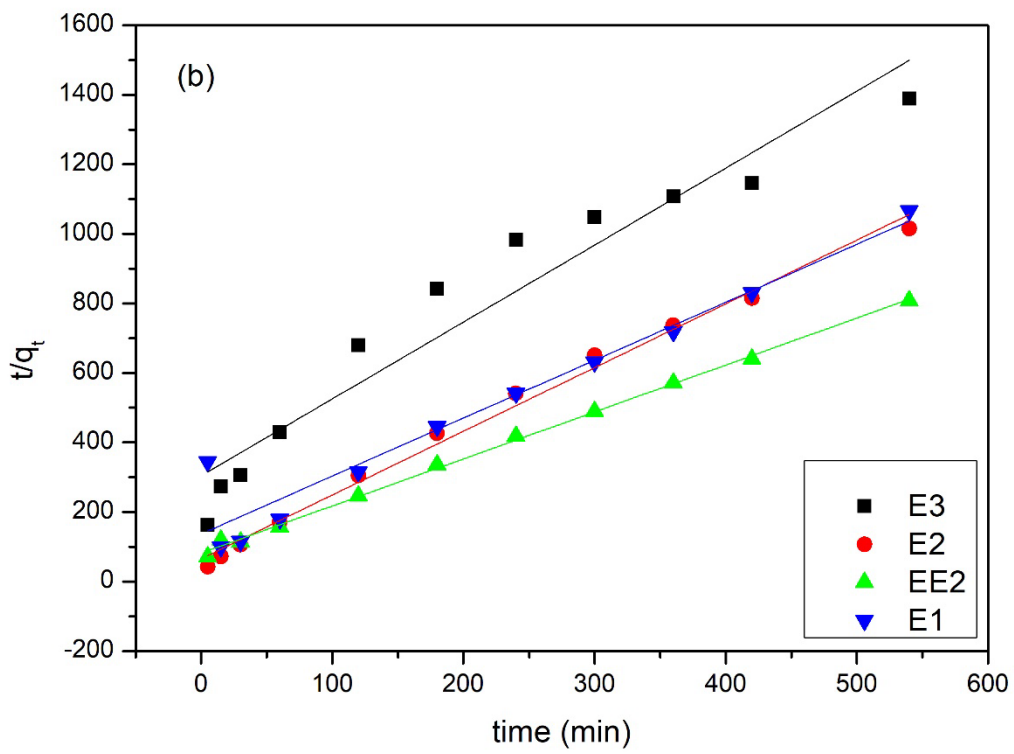
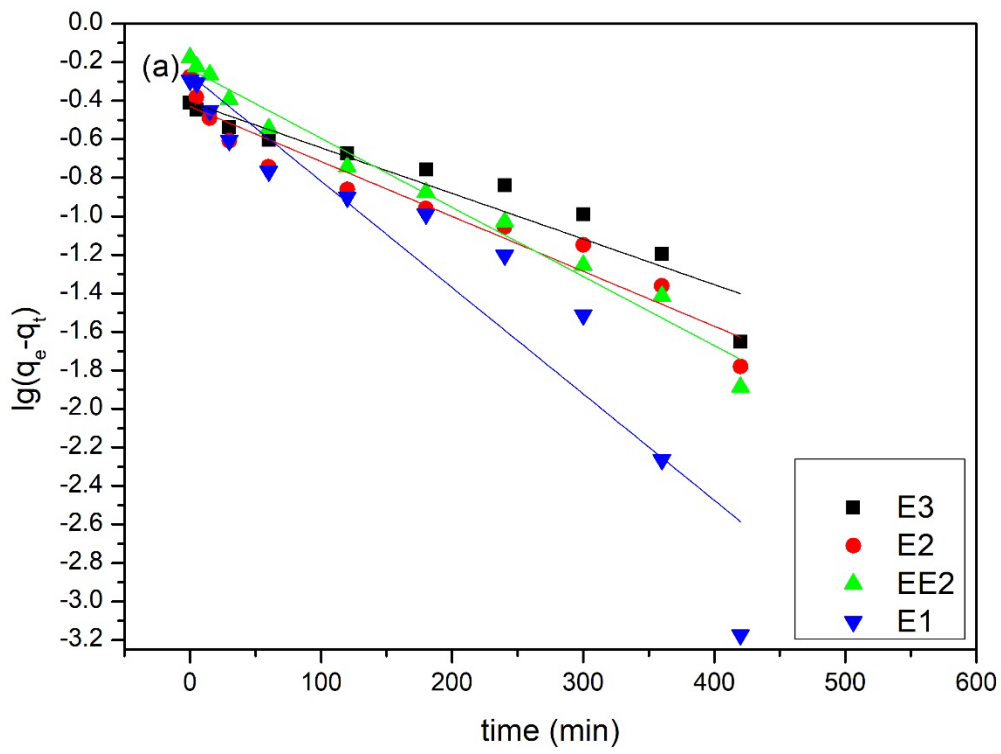


Fig. S4: Adsorption kinetics plots of four estrogenic hormones (E1, E2, EE2, E3) on PES nanofibers, (a) Pseudo-first-order, (b) Pseudo-second-order, (c) Weber-Morris interparticle diffusion model.



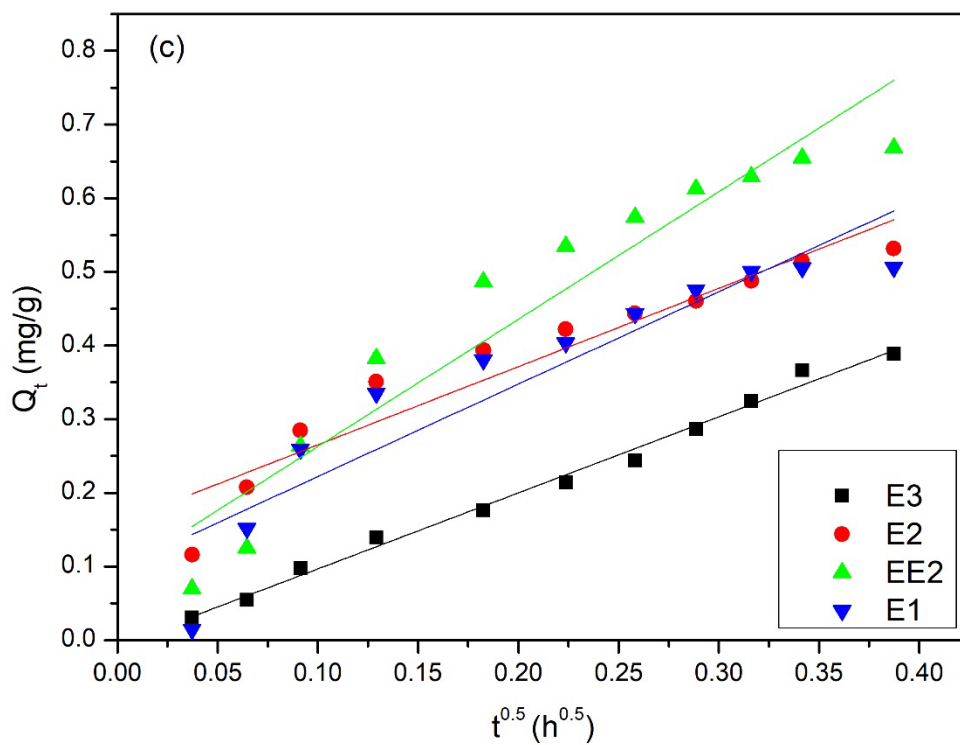
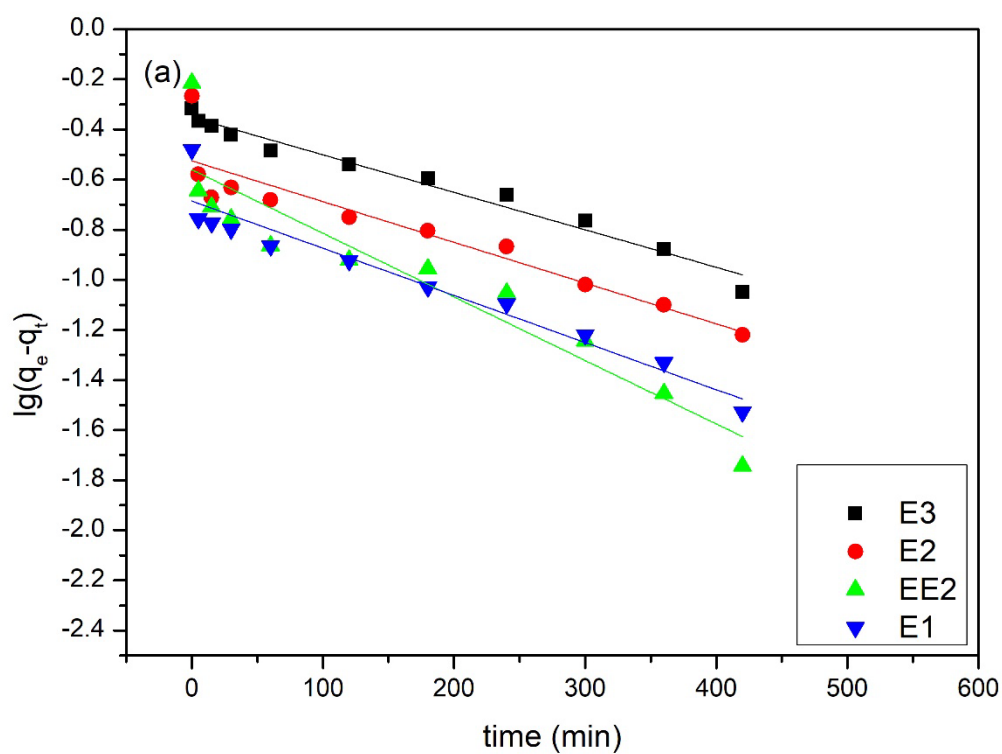


Fig. S5: Adsorption kinetics plots of four estrogenic hormones (E1, E2, EE2, E3) on CA nanofibers, (a) Pseudo-first-order, (b) Pseudo-second-order, (c) Weber-Morris interparticle diffusion model.



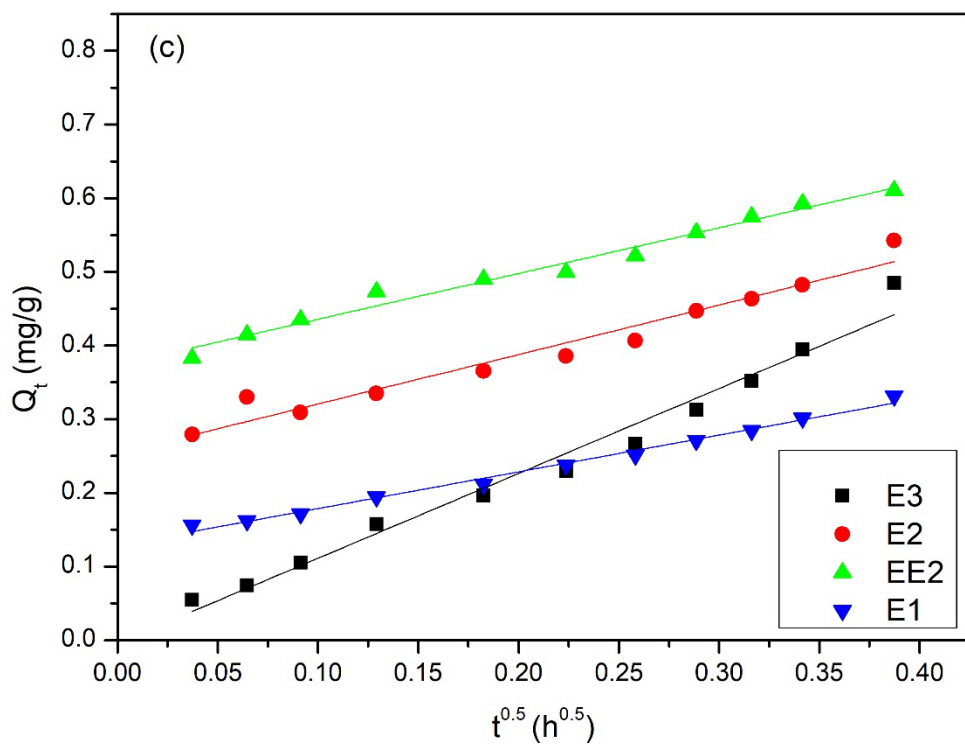
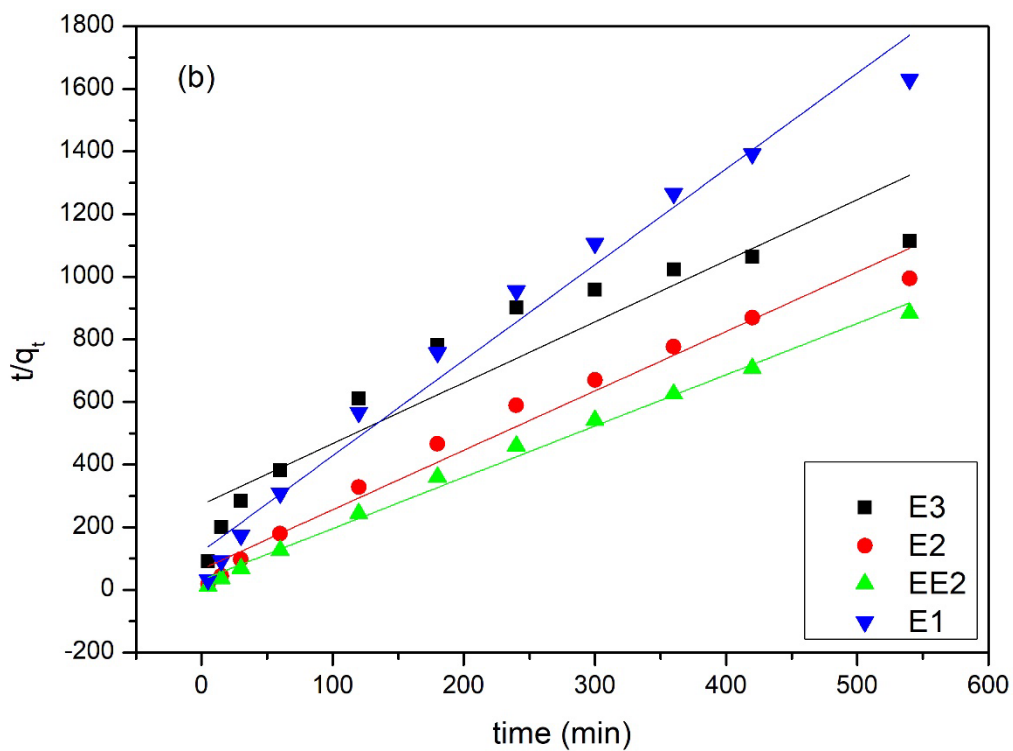
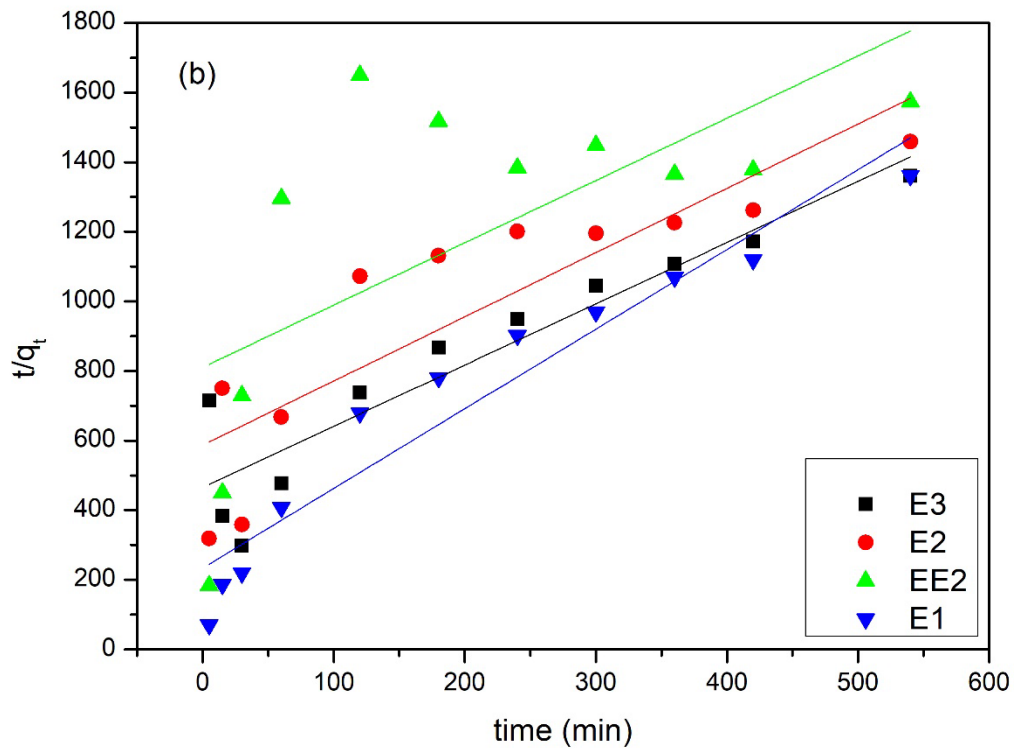
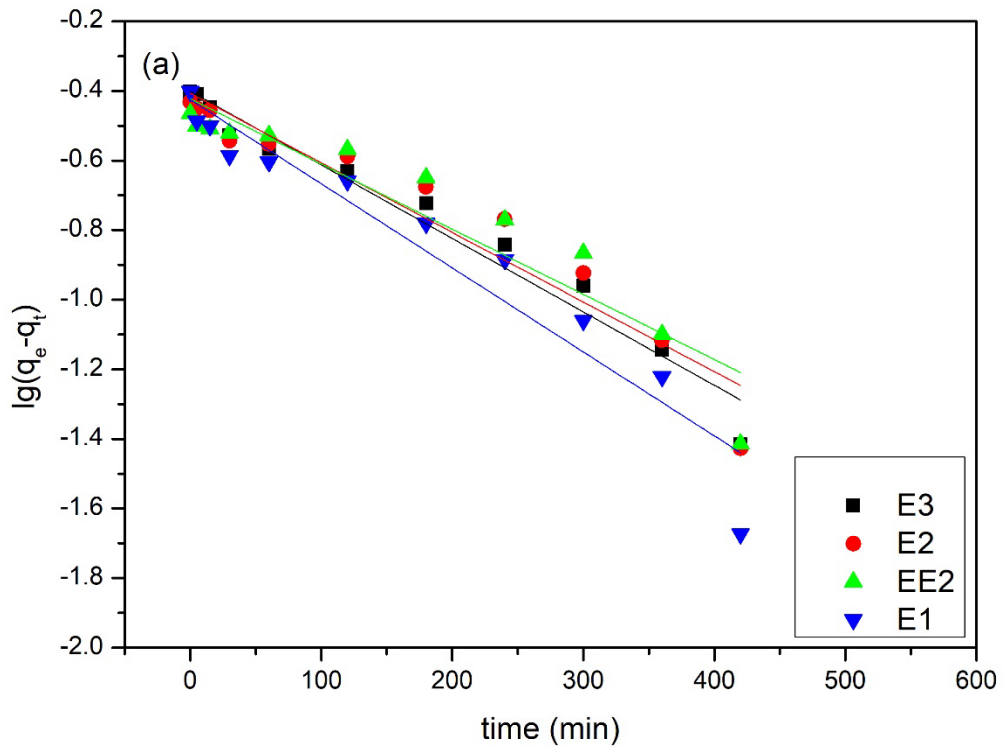


Fig. S6: Adsorption kinetics plots of four estrogenic hormones (E1, E2, EE2, E3) on PA nanofibers, (a) Pseudo-first-order, (b) Pseudo-second-order, (c) Weber-Morris interparticle diffusion model.



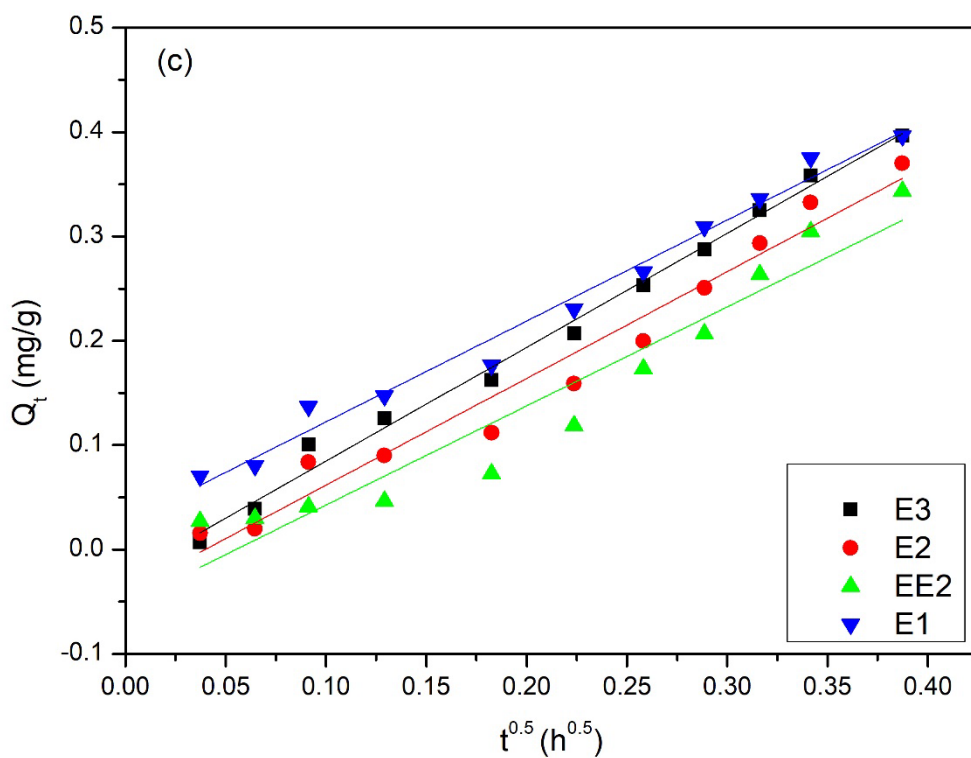


Fig. S7: Adsorption kinetics plots of four estrogenic hormones (E1, E2, EE2, E3) on PAN nanofibers, (a) Pseudo-first-order, (b) Pseudo-second-order, (c) Weber-Morris interparticle diffusion model.

Table S1: The kinetic models' parameters of each hormone with PU 918 electrospun nanofiber

Models	Hormones			
Parameters	Estrone (E1)	β -Estradiol (E2)	17 α -Ethinylestradiol (EE2)	Estriol (E3)
Experimental q_e (mg/g)	0.816	0.606	0.637	0.366
Pseudo First Order model				
k_1 (min ⁻¹)	0.003	0.003	0.003	0.002
q_e, cal (mg/g)	0.208	0.284	0.233	0.384
R^2	0.723	0.861	0.839	0.954
Pseudo Second Order model				
k_2 (g/mg.min)	0.164	0.078	0.130	0.007
q_e, cal (mg/g)	0.814	0.604	0.639	0.538
R^2	0.999	0.992	0.998	0.949
Intraparticle diffusion model				
k (mg/g.h ^{1/2})	0.403	0.633	0.490	1.052
I (mg/g)	0.665	0.361	0.459	-0.038
R^2	0.897	0.981	0.944	0.996

Table S2: The kinetic models' parameters of each hormone with PES electrospun nanofiber

Models	Hormones			
Parameters	Estrone (E1)	β -Estradiol (E2)	17 α -Ethinylestradiol (EE2)	Estriol (E3)
Experimental q_e (mg/g)	0.442	0.487	0.591	0.363
Pseudo First Order model				
k_1 (min ⁻¹)	0.003	0.002	0.003	0.002
q_e , cal (mg/g)	0.302	0.360	0.404	0.355
R ²	0.943	0.968	0.944	0.924
Pseudo Second Order model				
k_2 (g/mg.min)	0.058	0.039	0.050	0.018
q_e , cal (mg/g)	0.449	0.496	0.607	0.410
R ²	0.986	0.977	0.990	0.865
Intraparticle diffusion model				
k (mg/g.h ^{1/2})	0.795	0.953	1.028	0.897
I (mg/g)	0.149	0.124	0.225	0.004
R ²	0.970	0.993	0.960	0.967

Table S3: The kinetic models' parameters of each hormone with CA electrospun nanofiber

Models	Hormones			
Parameters	Estrone (E1)	β -Estradiol (E2)	17 α -Ethinylestradiol (EE2)	Estriol (E3)
Experimental q_e (mg/g)	0.506	0.532	0.668	0.389
Pseudo First Order model				
k_1 (min ⁻¹)	0.006	0.003	0.004	0.002
q_e, cal (mg/g)	0.540	0.371	0.581	0.391
R^2	0.897	0.941	0.979	0.918
Pseudo Second Order model				
k_2 (g/mg.min)	0.020	0.051	0.022	0.016
q_e, cal (mg/g)	0.560	0.545	0.740	0.452
R^2	0.992	0.993	0.998	0.935
Intraparticle diffusion model				
k (mg/g.h ^{1/2})	1.255	1.063	1.730	1.032
I (mg/g)	0.097	0.159	0.090	-0.007
R^2	0.869	0.914	0.915	0.992

Table S4: The kinetic models' parameters of each hormone with PA electrospun nanofiber

Models	Hormones			
Parameters	Estrone (E1)	β -Estradiol (E2)	17 α -Ethinylestradiol (EE2)	Estriol (E3)
Experimental q_e (mg/g)	0.331	0.543	0.611	0.485
Pseudo First Order model				
k_1 (min ⁻¹)	0.002	0.002	0.003	0.002
q_e , cal (mg/g)	0.206	0.298	0.275	0.445
R ²	0.929	0.866	0.875	0.975
Pseudo Second Order model				
k_2 (g/mg.min)	0.076	0.055	0.084	0.014
q_e , cal (mg/g)	0.327	0.527	0.610	0.513
R ²	0.978	0.978	0.994	0.880
Intraparticle diffusion model				
k (mg/g.h ^{1/2})	0.498	0.673	0.621	1.151
I (mg/g)	0.129	0.253	0.374	-0.004
R ²	0.992	0.957	0.982	0.979

Table S5: The kinetic models' parameters of each hormone with PAN electrospun nanofiber

Models	Hormones			
Parameters	Estrone (E1)	β -Estradiol (E2)	17 α -Ethinylestradiol (EE2)	Estriol (E3)
Experimental q_e (mg/g)	0.396	0.370	0.343	0.397
Pseudo First Order model				
k_1 (min ⁻¹)	0.002	0.002	0.002	0.002
q_e , cal (mg/g)	0.376	0.392	0.389	0.397
R ²	0.928	0.927	0.893	0.966
Pseudo Second Order model				
k_2 (g/mg.min)	0.022	0.006	0.002	0.007
q_e , cal (mg/g)	0.437	0.542	0.664	0.568
R ²	0.932	0.762	0.357	0.873
Intraparticle diffusion model				
k (mg/g.h ^{1/2})	0.967	1.023	0.978	1.092
I (mg/g)	0.026	-0.041	-0.061	-0.025
R ²	0.985	0.969	0.925	0.992

CURRICULUM VITAE

Personal information Muhammad Yasir
Address: Vaclavska 930/18a, Brno (Czech Republic)
Contact: yasir@utb.cz
Sex: Male | Date of birth: 18/3/91 | Nationality: Pakistani

Education 2019 – present

Doctoral degree

Centre of polymer systems, Tomas Bata University in Zlin (Czech Republic)

Material Science and Engineering

Biomaterials and Biocomposites

2015 – 2017

Master's degree

Faculty of Earth Science and Engineering, University of Miskolc (Hungary)

Petroleum Engineering

2011 – 2015

Bachelor's degree

School of Chemical and Materials Engineering, National University of Sciences and Technology (Pakistan)

Materials Engineering

2008 – 2010

A-Levels

Beaconhouse educational complex, Islamabad (Pakistan)
(University of Cambridge Examination, England)

2006 – 2008

O-Levels

Beaconhouse school system, Islamabad (Pakistan)
(University of Cambridge Examination, England)

Work experience 2017 – 2018

Lecturer (TVF)

School of Chemical and Materials Engineering and
School of Art Design and Architecture, National
University of Sciences and Technology (Pakistan)

2017 – 2018

Coach for O & A-Levels
Internik Academy

2008 – 2015

Private home tutor
O & A-Levels

Internships 2022 (8 weeks)

Research traineeship (Ph.D. degree)
Leibniz Institute of Surface Engineering (IOM), Germany

2017 (4 weeks)

Corrosion control and maintenance (Master's degree)
MOL GROUP, Hungary

2014 (6 weeks)

Quality control (Bachelor's degree)
Velosi Integrity & Safety Pakistan (PVT) LTD, Pakistan

Work on 2022 – present
projects of Project IGA/CPS/2022/003,
Internal Grant Member of project team
Agency (IGA)

2021

Project IGA/CPS/2021/002, Preparation and
characterization of nanocomposite systems
Member of project team

2020

Project IGA/CPS/2020/002, Bioactive polymer systems
for environmental applications

Member of project team

2019

Project IGA/CPS/2019/006, Polymeric composites for
bio-applications

Member of project team

Network and membership **2017 – present**

Registered Materials Engineer

Pakistan Engineering Council, Islamabad, Pakistan

2013 – 2014

NUST Bazm-e-Pakistan

National University of Sciences and Technology (NUST),
Islamabad, Pakistan

Conferences and Seminars *Nanocon2021 (20th – 22nd October 2021)*

International scientific conference Brno, Czech Republic

Academic English writing for Research and Publication
(Webinar) (26th – 29th April 2021)

Department of English, University of Liverpool, England,
United Kingdom

Tips and Tricks for Handling Reference Materials (8th
December 2020)

RESTEK (Webinar), France

HPLC Troubleshooting – Part 2 (1st December 2020)

RESTEK (Webinar), France

HPLC Troubleshooting – Part 1 (24th November 2020)

RESTEK (Webinar), France

Nanocon2020 (21st – 23rd October 2020)

International scientific conference Brno, Czech Republic

Model United Nations (LUMUN) (27th – 31st December
2009)

Lahore University of Management Sciences (LUMS),
Lahore, Pakistan

*The Champion's Leadership Summit (14th September
2008)* Islamabad, Pakistan

Honours and awards *UESTP Overseas PhD Scholarship (2018)*
Higher Education Commission (HEC),
Pakistan

Monash PhD Research Scholarship (2018)
Faculty of Engineering International Postgraduate
Research Scholarship (FEIPRS),
Australia

Bronze Medal (2017)
M.Sc Petroleum Engineering, University of Miskolc,
Hungary

Laptop winner (2016)
5th position in Materials engineering batch
Prime minister's Laptop scheme, Government of Pakistan

Name twice on the dean's list (2014)
High GPA achievement in 2 consecutive semesters
(Collected certificate and scholarship)
National University of Sciences and Technology (NUST)

Shield for 5A grades in O-Levels (2008)
66% tuition fee waiver scholarship in AS-level and 50%
in A2-level
Beaconhouse school system

Languages

Mother tongue Urdu

Other languages English

TOTAL PUBLICATIONS

Papers published in international journals with impact factor:

1. M. Yasir, T. Sopik, L. Lovecka, D. Kimmer, V. Sedlarik, The adsorption, kinetics, and interaction mechanisms of various types of estrogen on electrospun polymeric nanofiber membranes, *Nanotechnology* 33 (2021) 75702, <https://doi.org/10.1088/1361-6528/ac357b>.
2. M. Yasir, T. Sopik, R. Patwa, D. Kimmer, V. Sedlarik, Adsorption of estrogenic hormones in aqueous solution using electrospun nanofibers from waste cigarette butts: Kinetics, mechanism, and reusability, *Express Polymer Letters* 16 (2022) 624–648, <https://doi.org/10.3144/expresspolymlett.2022.46>.
3. M. Yasir, M. Masar, T. Sopik, H. Ali, M. Urbanek, J. Antos, M. Machovsky, I. Kuritka, ZnO nanowires and nanorods based ZnO/WO₃/Pt heterojunction for efficient photocatalytic degradation of Estriol (E3) hormone, *Materials Letters* (2022) 132291, <https://doi.org/10.1016/j.matlet.2022.132291>.
4. M. Yasir, F. A. Ngwabebhoh, T. Sopik, H. Ali, V. Sedlarik, Electrospun polyurethane nanofibers coated with polyaniline/polyvinyl alcohol as ultrafiltration membranes for the removal of ethinylestradiol hormone micropollutant from aqueous phase, *Journal of Environmental Chemical Engineering* 10 (2022) 107811, <https://doi.org/10.1016/j.jece.2022.107811>.
5. M. Yasir, F. A. Ngwabebhoh, T. Sopik, L. Lovecka, D. Kimmer, V. Sedlarik, The adsorptive behaviour of electrospun hydrophobic polymers for optimized uptake of estrogenic sex hormones from aqueous media: Kinetics, thermodynamics and reusability study. in the *Journal of Chemical Technology and Biotechnology*. (2022) <https://doi.org/10.1002/jctb.7191>.

Papers published in international conferences:

1. M. Yasir, T. Sopik, D. Kimmer, V. Sedlarik, Facile HPLC technique for simultaneous detection of estrogenic hormones in wastewater. in ‘Proceedings of the 12th International Conference on Nanomaterials, Brno, Czech Republic’ 272–276 (2020). <https://doi.org/10.37904/nanocon.2020.3710>.

2. M. Yasir, T. Sopik, H. Ali, D. Kimmer, V. Sedlarik, Green synthesis of titanium and zinc oxide nanoparticles for simultaneous photocatalytic removal of estrogens in wastewater. in 'Proceedings of the 13th International Conference on Nanomaterials, Brno, Czech Republic' 189-196 (2021). <https://doi.org/10.37904/nanocon.2021.4333>.
3. H. Ali, M. Masar, M. Yasir, T. Sopik, P. Urbanek, M. Machovsky, I. Kuritka, Silica supported WO₃/Cu₂O heterostructured nanoparticles for photocatalytic degradation of hormones. in 'Proceedings of the 13th International Conference on Nanomaterials, Brno, Czech Republic' 104-109 (2021). <https://doi.org/10.37904/nanocon.2021.4343>.
4. Z. Krchnackova, D. Kimmer, L. Lovecka, M. Kovarova, H. Pistekova, D. Vesela, I. Vincent, M. Yasir, V. Sedlarik, Antimicrobial properties of polymeric nanofibrous membranes containing ferrous sulphate. in 'Proceedings of the 13th International Conference on Nanomaterials, Brno, Czech Republic' 317-322 (2021). <https://doi.org/10.37904/nanocon.2021.4347>.
5. H. Ali, M. Masar, M. Yasir, F. A. Ngwabebhoh, O. Zandraa, T. Sopik, M. Machovsky, I. Kuritka, Silica supported visible light active graphitic carbon nitride (g-C₃N₄) photocatalyst for estrogenic hormones removal and antibacterial activity, submitted in 'Proceedings of the 2nd International Conference on Energy Fuels Environment, Krakow, Poland' (2022).

Papers accepted as coauthor in international journals with impact factor:

1. B. Ahmad, N. M. Ahmad, M. Yasir, Z. A. Khan, S. Rafiq, High-Performance Anticorrosive Polyester Coatings on Mild Steel in Mixed Acid Mixtures Environments. in *Advances in Polymer Technology*. (2019) <https://doi.org/10.1155/2019/3954784>
2. A. Salim, M. A. Abbas, M. I. Khan, M. Z. Khan, F. Javaid, S. Mushtaq, M. Batool, M. Yasir, A. L. Khan, A. U. Khan, K. M. Deen, N. M. Ahmad, Graphene Oxide incorporated Polyether Sulfone Nanocomposite Antifouling Ultrafiltration Membranes with Enhanced Hydrophilicity. in *Materials Research Express*. (2022) <https://doi.org/10.1088/2053-1591/ac81a3>.
3. P. Drohsler, M. Yasir, D. R. C. Fabian, J. Cisar, Z. Yadollahi, V. Sedlarik, Comparative degradation study of a biodegradable composite based on polylactide with halloysite nanotubes and a polyacrylic acid copolymer. in *the Journal of Materials Today Communications*. (2022) <https://doi.org/10.1016/j.mtcomm.2022.104400>.

PUBLICATIONS

PAPER

The adsorption, kinetics, and interaction mechanisms of various types of estrogen on electrospun polymeric nanofiber membranes

To cite this article: Muhammad Yasir *et al* 2022 *Nanotechnology* **33** 075702

View the [article online](#) for updates and enhancements.

You may also like

- [Using of some hormones in the creation of estrus and ovulation to improvement reproductive in local cows](#)
Makki khalaf hussein AL dulaimi
- [Effect of Flaxseed on some hormonal profile and genomic DNA concentration in Karadi lambs](#)
A N Yousif
- [The effect of methanol extract of soybean \(*Glycine max* L. Merr.\) on rat testicular steroid hormones](#)
R Aryani, H Manurung, S Moeljopawiro et al.



The Electrochemical Society
Advancing solid state & electrochemical science & technology

241st ECS Meeting

May 29 – June 2, 2022 Vancouver • BC • Canada

Extended abstract submission deadline: Dec 17, 2021

Connect. Engage. Champion. Empower. Accelerate.
Move science forward



Submit your abstract



The adsorption, kinetics, and interaction mechanisms of various types of estrogen on electrospun polymeric nanofiber membranes

Muhammad Yasir^{*} , Tomáš Šopík, Lenka Lovecká, Dušan Kimmer and Vladimír Sedlařík^{*}

Centre of Polymer Systems, University Institute, Tomas Bata University in Zlín, Třída Tomáše Bati 5678, 760 01 Zlín, Czech Republic

E-mail: yasir@utb.cz and sedlarik@utb.cz

Received 11 August 2021, revised 14 October 2021

Accepted for publication 1 November 2021

Published 24 November 2021



CrossMark

Abstract

This study focuses on the adsorption kinetics of four highly potent sex hormones (estrone (E1), 17 β -estradiol (E2), 17 α -ethinylestradiol (EE2), and estriol (E3)), present in water reservoirs, which are considered a major cause of fish feminization, low sperm count in males, breast and ovarian cancer in females induced by hormonal imbalance. Herein, electrospun polymeric nanostructures were produced from cellulose acetate, polyamide, polyethersulfone, polyurethanes (918 and elastollan), and polyacrylonitrile (PAN) to simultaneously adsorb these estrogenic hormones in a single step process and to compare their performance. These nanofibers possessed an average fiber diameter in the range 174–330 nm and their specific surface area ranged between 10.2 and 20.9 m² g⁻¹. The adsorption–desorption process was investigated in four cycles to determine the effective reusability of the adsorption systems. A one-step high-performance liquid chromatography technique was developed to detect and quantify concurrently each hormone present in the solution. Experimental data were obtained to determine the adsorption kinetics by applying pseudo-first-order, pseudo-second-order and intraparticle diffusion models. Findings showed that E1, E2 and EE2 best fitted pseudo-second-order kinetics, while E3 followed pseudo-first-order kinetics. It was found that polyurethane Elastollan nanofibers had maximum adsorption capacities of 0.801, 0.590, 0.736 and 0.382 mg g⁻¹ for E1, E2, EE2 and E3, respectively. In addition, the results revealed that polyurethane Elastollan nanofibers had the highest percentage efficiency of estrogens removal at ~58.9% due to its strong hydrogen bonding with estrogenic hormones, while the least removal efficiency for PAN at ~35.1%. Consecutive adsorption–desorption cycles demonstrated that polyurethane maintained the best efficiency, even after being repeatedly used four times compared to the other polymers. Overall, the findings indicate that all the studied nanostructures have the potential to be effective adsorbents for concurrently eradicating such estrogens from the environment.

Supplementary material for this article is available [online](#)

Keywords: wastewater treatment, estrogenic hormones, static adsorption, kinetics, electrospun nanofibers

(Some figures may appear in colour only in the online journal)

^{*} Authors to whom any correspondence should be addressed.

1. Introduction

Synthetic estrogenic hormones, also called endocrine-disrupting chemicals (EDCs), have an adverse effect on both human beings and animals [1, 2]. Residual micropollutants of this type are observed in low concentrations—at the level of micro- and nanograms—in cleaning reservoirs at wastewater treatment plants [1]. This problem has aroused serious concerns among the scientific community since synthetic hormones are known to interfere with the functional groups of natural hormones by blocking endogenous and mimic ability, which makes it much more dangerous [3–7]. The presence of estrogenic hormones represents a severe threat to human and aquatic life through exposure via food sources or drinking water [7, 8].

Estrogenic hormones include estrone (E1), estradiol (E2), ethinylestradiol (EE2) and estriol (E3), which disrupt the reproduction of aquatic species and the function of natural hormones in the human body [8]. Studies have proven that a rise in femininity occurs in fish, weight loss affects the testicles of quails and alligators experience issues with fertility [9]. Meanwhile, reports show that humans demonstrate a decline in the sperm counts of males and the risk of breast and ovarian cancer is heightened in females [10]. Quantities of these estrogenic hormones have been observed downstream of the treatment plants [11–13], with lower limits having been reported of 3.4–41 ng l⁻¹ at constructed wetlands in the Czech Republic [14]. Of the aforementioned estrogens, EE2 is a modern, formulated, synthetic estrogenic hormone used in oral contraceptive pills in the treatment of prostate cancer and menstrual problems in females [15]. It is considered the most fatal among all the estrogenic hormones as it only degrades partially at wastewater treatment plants and is challenging to be removed [16]. Consequently, the natural environment deconjugates the metabolites of EE2 and makes them active again under a suitable environment [17]. EE2 is the most potent EDC and is considered to have high estrogenicity [18–20]; hence, proper disposal of these estrogenic hormones is immediately required.

Conventional treatment plants cannot eliminate EDCs efficiently owing to their properties of low molecular weight and slow biodegradability [21]. This has led to the widespread occurrence of the same quantity in reservoirs, rivers and lakes since they are released from treatment plants alongside treated effluents [22, 23]. In this regard, various strategies have been applied to capture, eliminate or completely degrade the EDCs and other common toxic chemical effluents, such as ozonation, membrane bioreactors, advanced oxidation, membrane filtration, coagulation, flocculation and photocatalysis [24–26]. Each technique has certain limitations, such as low efficiency and any resulting by-products demand further purification and sophisticated methods for processing them. Nano-filtration and reverse osmosis have proven to be interesting, but the extent of energy consumption makes them unfavorable for the treatment at a large scale [27, 28].

In the context of the sorption technique, the choice of material selection is quite crucial. Adsorbent particles for estrogens have been reported, such as granules of activated charcoal [29, 30], carbon nanomaterials [31], fullerene [32], carbon nanotubes [33], chitosan, activated carbon, chitin,

carbon-based adsorbents prepared from industrial waste [34, 35] and activated carbon fibers modified with iron hydroxide [36]. All of these are efficient, yet they require a process of additional separation from wastewater that raises the costs. Some researchers have recently found adsorbents such as nanofibers that could eradicate the need for a subsequent separation procedure [37]. To this end, not many studies have been reported. Therefore, it is necessary to test such high-performance materials with functionalized groups that can optimize the disposal process during the course of research programs.

Sorbents based on nanofibers have garnered much attention due to a number of favorable characteristics reported for them, such as large aspect ratio, high surface area and small pore size [38]. For this purpose, a versatile technique for generating continuous nanofibers is electrospinning, which gives rise to a material's diameter ranging from tens to hundreds of nanometers for adsorption and water filtration processes [39, 40]. The large aspect ratio of nanofibers gives significant rise to the filtration efficiency since the pore size is reduced; moreover, the large surface area allows greater contact between the solution and filtration-sorption adsorbent [41]. The apparatus requires an applied voltage between the cathode and anode to allow the electrostatic forces to overcome the tension on the surface of the polymer, thereby ejecting the polymeric solution and solidifying non-woven nanofibers on a collecting electrode covered in a textile substrate [39, 42–45]. The quality of nanofibers can be improved by utilizing binary polymers with additives such as acetone and polyethylene oxide to obtain beadless nanostructures [41].

Past literature describes that electrospun polymers proved an excellent ability in removing heavy metal ions such as copper and organic pollutant dyes from wastewater [46, 47]. However, fewer works have been done with electrospun polymers for estrogenic hormone removal applications. According to literature, research on commercially available nylon, polypropylene (PP), polytetrafluoroethylene, cellulose acetate, regenerated cellulose and glass microfiber filters have been reported for the removal of E1. Studies also report on polyamide (PA) nanoparticles being employed to extract just EE2. While polyethersulfone (PES) nanofibers for the removal of E2 and polyvinylidene fluoride (PVDF) doped with polyvinyl pyrrolidone (PVP) and titanium dioxide (TiO₂) membranes prepared by phase inversion process for the removal of E1 and E2 have been reported. However, these studies have been solely limited to the filtration of single natural or synthetic hormones [1, 15, 48, 49]. This highlights the necessity of developing the least fiber diameter optimized nanofibers to extract such estrogenic hormones simultaneously and then gauge their kinetics for comparison [50].

This paper primarily investigates the optimized preparation of electrospun nanostructures from polymers (cellulose-acetate (CA), polyurethanes (PU 918 and PU Elastollan), polyamide 6 (PA), polyethersulfone (PES) and polyacrylonitrile (PAN)) that possess beadless desired attributes of morphology, small diameter of the fiber, high ratio of surface area to volume, lightweight and numerous sites for adsorption. Research focuses on these nanostructured polymers with high sorption activity for estrogenic hormones (E1, E2, EE2 and E3). A membrane of this type could be

employed for the microfiltration of wastewater compared to commercially available microfiltration membranes that exhibit greater flux [45]. The objective is simultaneous adsorption of four estrogenic hormones in a one-step process from wastewater at neutral pH because the pH of rivers is in the range of 6–9. The feasibility of the results is analyzed by applying experimental data, thereby determining adsorption capacity and kinetics via suitable models of pseudo-first-order, pseudo-second-order and intraparticle diffusion to help understand the suitability of characteristics essential for large scale implementation. Finally, the adsorption mechanisms of the nanofibers are gauged to understand the interaction ability of functional groups present for bonding between polymers and estrogenic hormones. The tests are conducted with the extent of polymers' reusability over several adsorption cycles to discern reliability and effectiveness for large scale generation of these polymers.

2. Materials and methods

2.1. Materials and reagents

The hormones under test (with purity in percent) comprised E1 \geq 99%, E2 \geq 98%, E3 \geq 97% and EE2 \geq 98% purchased from Sigma-Aldrich Chemie GmbH, Germany. Cellulose acetate CA-398-30 (CA) at the molar weight $M_w = 5 \times 10^4$ g mol⁻¹ came from the Eastman Chemical Company, USA. Poly-urethane Elastollan EB_95A (PU Elastollan) at $M_w = 1.1 \times 10^5$ g mol⁻¹ was bought from BASF Polyurethanes GmbH, Germany. Polyamide 6 (PA)—Silamid EN at $M_w = 1.45 \times 10^5$ g mol⁻¹ was sourced from Roonamid a.s., Slovakia. Polyacrylonitrile PAN 181315 (PAN) of molecular weight $M_w = 1.5 \times 10^5$ g mol⁻¹ was purchased from Sigma Aldrich, Germany. Polyethersulfone Ultrason E2020P SR (PES) at the molecular weight $M_w = 5.5 \times 10^4$ g mol⁻¹ came from BASF SE, Germany. 4,4'-methylene-diphenyl diisocyanate (MDI), (poly 3-methyl-1,5-pentanediol-alt-adipic, isophthalic acid) (PAIM) and 1,4-butanediol (BD) were sourced from Sigma Aldrich, Germany. N,N-dimethylformamide (DMF >99.5%) was bought from Lach-Ner, s.r.o., Czech Republic. Acetic acid (AA (99%)), formic acid (FA (98%)), sodium tetra-borate decahydrate (borax), citric acid, polyethylene oxide (PEO), dimethylamylamine (DMA) and 4-methyl-2-pentanone (MIBK) were purchased from PENTA s.r.o., Czech Republic.

Furthermore, HPLC solutions of acetonitrile (from Honeywell, Czech Republic) and ethanol (HPLC grade >99%; from VWR, Czech Republic) were utilized. Deionized water (pH 7.3, 18.2 M Ω cm⁻¹) was created on a laboratory Milli-Q ultrapure (Type 1) water purification system, Biopak[®] Polisher, Merck, USA and used throughout the study.

2.2. Preparation of the nanofibers

Each electrospun nanofiber was made from a different polymer; therefore, different solvents were used. A solution of the conductive components, borax and citric acid (BC), which

was prepared at the ratio of 1:3, respectively and followed by 35 wt% of BC, was dissolved in DMF solution and stirred in a mixer for 5 h at 400 rpm to make it ready for adjusting the electrical conductivity of each treated solution prior to electrospinning. The synthesis of every electrospun material progressed under the optimized conditions and parameters required for that particular polymer as follows:

PA at the concentration of 18 wt% of the solution was dissolved in AA: FA at the ratio 2:1 for 4 h by stirring at 400 rpm in a mixer (Heidolph, RZR 2041) to homogenize the mixture uniformly. PU Elastollan 18 wt% was dissolved in DMF by treating the solution with BC to enhance electrical conductivity and optimize the electrospinning process. The solution of CA was prepared from 9% of powder in AA (57 wt%), ethanol (19 wt%), water (14.5 wt%) and PEO (0.3 wt%), followed by BC (0.2 wt%), which were stirred together to make a total of 400 g under constant stirring at 400 rpm for 6 h. PES solution (23 wt%) was prepared by dissolving the powder in 73 wt% DMA: MIBK at the ratio 3:1, supplemented by BC at 4 wt%. PAN powder was dissolved in DMF (9 wt%) under stirring for 5 h at 400 rpm. PU 918 was prepared via a polyaddition reaction at a centre of polymer systems (CPS) laboratory. PU solution in (DMF), based on MDI, PAIM polymer diol, $M_w = 2 \times 10^3$ g mol⁻¹) and BD was synthesized at the molar ratio 9:1:8 (PU 918) at 90 °C for 5 h per partes way of the synthesis, starting with the preparation of a pre-polymer from MDI and PAIM, followed by adding BD and the remaining quantity of MDI. After being supplemented with BC to idealize conductivity, the solution was electrospun at a concentration of 13 wt% PU with $M_w = 9.8 \times 10^4$ g mol⁻¹ [50].

The electrospinning process was performed in an electrostatic field on laboratory spin line equipment (CPS, Tomas Bata University, Czech Republic). The apparatus was equipped with a patented rotating electrode with three cotton cord spinning elements (PCT/CZ2010/000042) and a set of nanofiber-forming nozzles (jets) to produce fibers on polypropylene (PP) spun-bond non-woven textile of width 40 cm. The voltage applied was 75 kV during the electrospinning process, except for polyamide, when it equaled 130 kV. A set of 32 jet needles (2 rows of 16 each) was employed for the PU Elastollan, PES, PAN and PU 918; solution dosing was set to 0.34, 0.34, 0.13 and 0.24 ml min⁻¹, respectively, based on optimum parameters and conditions. The distance between the electrodes equaled 18 cm, apart from PU Elastollan, which equaled 19 cm. In the case of PA and CA, a solution was sprayed from the bath by cords set at 4 rpm, with the distance between the electrodes equaling 22 cm. The rotational speed of antistatic PP non-woven fabric was set at 10 cm min⁻¹, except for PA and PU 918, where the pace was set at 12 and 16 cm min⁻¹, respectively. The temperature was gauged as 28 \pm 2 °C and relative air humidity was <35%. The solutions' electrical conductivity and intrinsic viscosity during preparation were maintained at optimal levels, as shown in table 1.

Table 1 shows the optimized properties of the polymeric solutions for subsequent electrospinning and the average mass per unit area of the resultant electrospun nanofibers. PA solution possessed the highest electrical conductivity, while

Table 1. Properties of the polymeric solutions.

Sample	Concentration (%)	Density (g cm ⁻³)	Intrinsic viscosity (Pa.s)	Electrical conductivity (μS cm ⁻¹)	Average mass per unit area (g m ⁻²)
PES	24	1.350	0.75	102.0	1.02
PU 918	13	1.100	1.50	150.0	0.70
PU Elastollan	18	1.220	1.80	91.8	1.30
CA	9	1.315	1.64	83.4	1.63
PA	18	1.084	0.75	172.0	3.00
PAN	9	1.184	0.53	105.3	0.88

the least was observed for CA. The concentration and intrinsic viscosity of the solutions varied between 9%–24% and 0.53–1.80 Pa.s, respectively. The value for average mass per unit area of the electrospun sheets was lowest for PU 918 and highest for PA. The given properties of solutions varied and set at optimum conditions to aim defect-free and beadless electrospun nanofibers.

2.3. Characterization

Imaging on a Nova 450 scanning electron microscope (SEM) (FEI, Thermo Fisher Scientific, USA) was carried out to observe the morphology of the fiber surface, the desired diameter of the fiber and to check for defects such as beads in the structures at the acceleration voltage of 5–10 kV with a through-the-lens detector. A conductive gold coating (~120 s) was applied prior to examining the estrogenic hormones by a sputter coater. The mean fiber diameter of each polymer was determined using software ImageJ version 1.52a.

Fourier transformed infrared spectroscopy (FTIR) was performed on a Nicolet 320 spectrometer (ThermoScientific, USA) equipped with a Ge crystal to determine the functional groups of the polymeric nanofibers tested for adsorption of the estrogenic hormones. Attenuated total reflectance spectra were recorded across 400–4000 cm⁻¹ under ambient temperature conditions, a scan rate of 16 and a resolution of 4 cm⁻¹.

Surface analysis of the nanofibers was carried out according to the Brunauer–Emmett–Teller (BET) method. A high-precision analyzer of surface area and pore size (BEL-SORP-mini II, BEL Japan Inc, Japan) was used to determine the specific surface area. Outgassing of the substrate occurred at 100 °C for 12 h in a vacuum prior to measurement.

The contact angle measurement was conducted by compressing the nanofibers to make them compact for accurate measurement. To this end, the nanofibers were put onto a single PP sheet that, in turn, was placed upside-down on a sheet of polyethylene terephthalate (PET). Subjected to a thermal press for 10 s at a temperature of 110 °C, then the layer of PP was detached. The sheet of PET with the nanofibers was covered with a glossy sheet for the thermal press, the same conditions being applied to acquire a smooth, compacted surface. This step ensured that liquid could remain on the surface for measuring the contact angles; without doing this, the surfaces of the nanofibers on the sheet of PP would

have been incapable of holding the drops of liquid, which would instantly settle down, penetrating the porous structures. Finally, the contact angle of electrospun nanofibers was measured using the sessile drop technique on a goniometer (surface energy evaluation system (SEE System), Advex Instruments, Brno, Czech Republic) under the conditions of ambient temperature. A 5 μl pipette dropped liquid onto the surface of the samples (10 × 10 mm²), then the shapes of the resulting droplets were observed with the aid of a CCD camera and the contact angles measured immediately. Milli Q water was used as the probe liquid to determine the hydrophilicity [51]. The samples were analyzed and mean values for them are reported herein.

2.4. Solution preparation and sampling

A concentration of 0.2 mg l⁻¹ of each hormone was prepared by adding 1 mg of the given hormone into 5 l of water; magnetic stirring was maintained at 800 rpm for 24 h to prepare 0.8 mg l⁻¹ of solution and stored in the dark. Samples of 0.2, 0.15, 0.1, 0.05, 0.03 and 0.02 mg l⁻¹ were collected by a micropipette (HTL Lab Solution, Poland) and dosed into 1.5 ml screw neck vials (VWR, Czech Republic) after passing through a glass microfiber (GMF) filter (Whatman, Czech Republic; of pore size 0.45 μm and 25 mm diameter). HPLC was performed on triplicated samples, resulting in mean concentrations plotted on a calibration curve.

2.5. High-performance liquid chromatography (HPLC)

The hormone samples (E1, E2, EE2, E3) were analyzed and their calibration standards were discerned on an HPLC DionexUltiMate 3000 Series unit (Thermo Fisher Scientific, Germany). Separation took place on a reversed-phase column (Kinetex 2.6 μm C18 100 A, 150 × 4.6 mm; Phenomenex, USA) equipped with an ULTRA precolumn guard, UHPLC C18 (Phenomenex, USA) at 30 °C. A mixture of HPLC grade acetonitrile and water constituted the mobile phase (45:55, vol/vol) applied at the flow rate of 0.8 ml min⁻¹ over a total isocratic run time of 12 min. The autosampler chamber was set to 5 °C and a volume of 20 μl was injected each time into the column. Eluates were detected at the wavelengths 200 and 205 nm and the concentration of hormones was calculated from the findings of the 200 nm tests (supplementary data, figure S1 (available online at stacks.iop.org/NANO/33/075702/mmedia)). A calibration vial with a concentration of

0.02 mg l⁻¹ was employed to determine the detection limit for each hormone; the limits equaled 1 μg l⁻¹ for E3, E2 and EE2 and 6 μg l⁻¹ for E1. Values for concentration were quantified by external calibration in software Chromeleon version 7.2 (Thermo Fisher Scientific, USA) [52].

2.6. Evaluation of the adsorption properties of polymeric nanofiber structure by discontinuous sorption testing

Static adsorption tests were carried out to determine the adsorption rate. Separate flasks were set aside for testing each polymeric mat in triplicates, utilizing 100 ml from the stock of estrogenic hormone solution at a total concentration of 0.8 mg l⁻¹; each flask was then supplemented with 20 mg of a given nanofiber. The flasks were continuously stirred on an orbital incubator shaker (Stuart® S1500, Barloworld Scientific Ltd, UK) for adsorption at 250 rpm. Samples of the remaining concentration of the hormones in each flask were collected in vials via a 0.45 μm GMF syringe filter and readings were taken after intervals of 5 min, 15 min, 30 min, 60 min and each following hour until a constant value was obtained. At each interval, 4 ml samples were taken with a 20 ml syringe, ensuring that neither the nanofiber was removed nor destroyed in the process and 4 ml of ultrapure water was added to maintain total volume. The first 2 ml of the filtrate was discarded, this having passed from the syringe through the GMF filter to eliminate any adsorption during sampling, thereby ensuring accuracy and precision in the results. A flask containing a solution without any nanofiber was labeled as 'control' and included in the experiment to discern the initial reference concentration. It must be noted that adsorption on the glass surface was negligible throughout long-term testing, which was determined by comparing the recorded initial concentration and concentration after 9 h of stirring the control solution. To this end, the hormone solutions were checked prior to the start of the experiment. Each sample reading was conducted in triplicate and the corresponding values for mean concentration and standard deviation based on Gaussian distribution were recorded. Finally, the percentage of adsorption for each hormone on the nanofibrous mat was calculated with reference to the aforementioned 'control' flask. The stock solution was kept neutral by means of ultrapure deionized water at a pH of 7.3, considering real environmental water samples to be in the range of 6–9. The percentage removed of each hormone at a given time (*t*) was determined by the expression in equation (1), as follows [53, 54]:

$$\text{Removal (\%)} = \frac{C_i - C_t}{C_i} \times 100, \quad (1)$$

where C_i is the initial concentration (mg l⁻¹) and C_t is the concentration of the solution at time t (mg l⁻¹).

Equilibrium adsorption capacity (q_e) and adsorption capacity (q_t) at any instant of time t can also be calculated by the following expressions in equations (2) and (3) [55, 56]:

$$q_e = v \times \frac{C_i - C_e}{m}, \quad (2)$$

$$q_t = v \times \frac{C_i - C_t}{m}, \quad (3)$$

where m is the mass of adsorbent in grams and v is the volume of solution in liters. It must be noted that q_e is equal to q_t at the last sampling time in the adsorption process.

2.7. Reusability test

For the desorption test, the nanofibers were extracted from the conical flasks containing the hormone solutions and washed thoroughly with distilled water, followed by stirring at a constant 250 rpm for 15 min in deionized water. They were subsequently placed in an oven at 30 °C for 6 h to remove excess moisture and dried in the air; the nanofibers remained unaffected by this. They were then soaked in 40 ml of pure ethanol and continuously stirred for 30 min at 175 rpm to remove the hormones entirely and eluted in ethanol [1]. Finally, the nanofibers were dried at room temperature and placed in a desiccator until the next adsorption cycle. The procedure was repeated for several cycles until low adsorption efficiencies were observed.

3. Results and discussion

3.1. Characterization of the electrospun nanofibers

The SEM of the nanofibers, along with the distribution of fiber diameter from the various polymers prepared via electrospinning, are shown in figure 1.

The graph above reveals that the uniform nanofibers were produced with minimum beading and a narrow fiber diameter range, i.e 174–330 nm; PU 918 demonstrated the least value and PAN the greatest. These low averages in the size of diameters were attributed to the optimized electrospinning process (low intrinsic viscosity, low polymer concentration in the solution and high electrical conductivity prior to said process); the large surface area was the consequence of this. The size and morphology of the estrogenic hormones were also analyzed on an electron microscope and the micrographs are shown as supplementary data (figure S2).

Applying the average diameter of the nanofibers calculated from SEM, in consideration of the fiber constituting a single continuous cylinder, the length per unit mass (l/m) and surface area (A) of the fiber can be calculated by the following equations (4)–(6) [1]:

$$V = \frac{m}{\rho} = \frac{\pi d^2 l}{4}, \quad (4)$$

By rearranging this expression, the following is obtained:

$$l/m = \frac{4}{\rho \pi d^2}, \quad (5)$$

where V is the volume (m³), m is the mass (mg), d is the diameter of the nanofiber (m) and ρ is the density of each given polymer (g cm⁻³).

Since $l \gg d$, it is possible to neglect the individual cross-sectional area (A) of the end portions of the fibers, such that

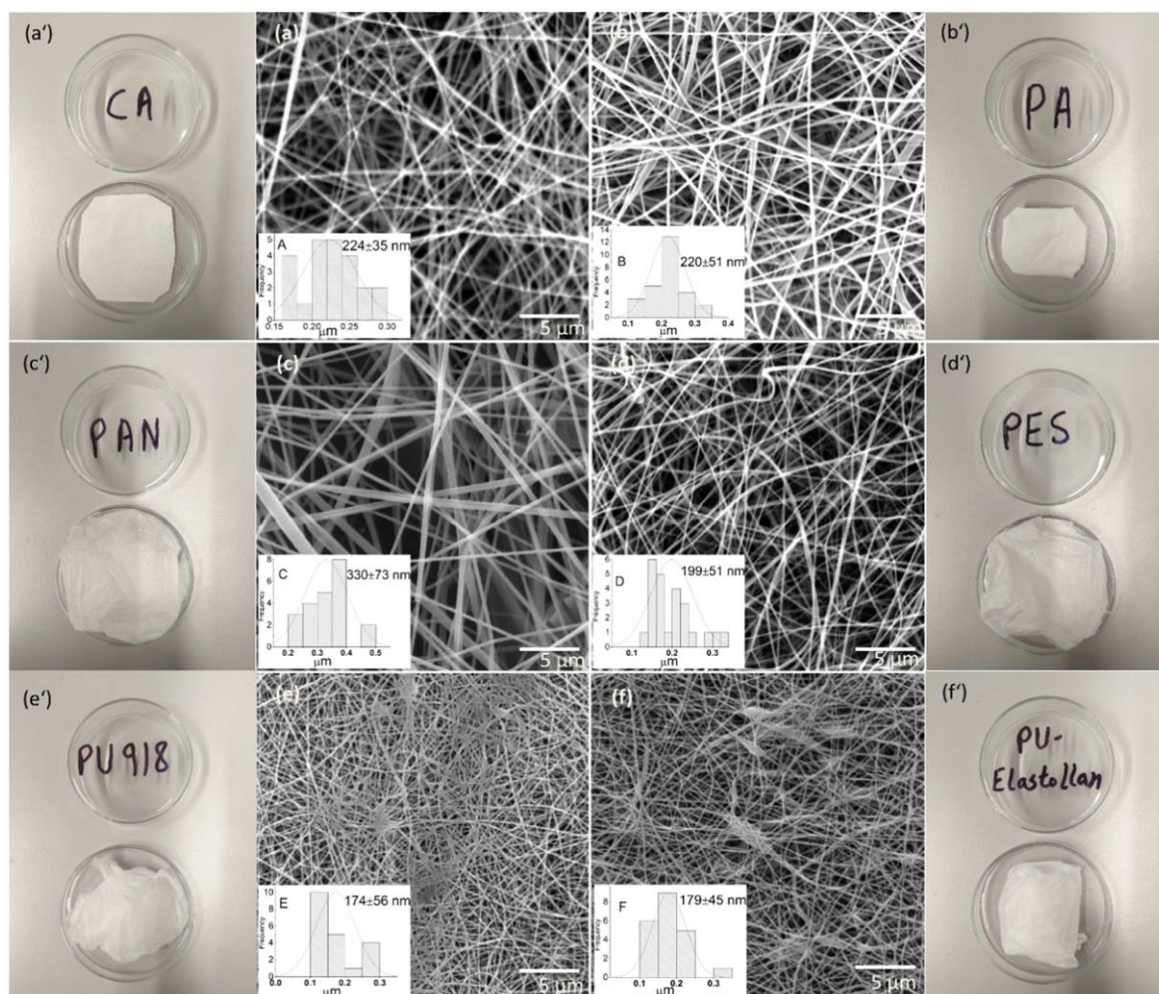


Figure 1. Electron micrographs, (inset) distribution of frequency size and sample images of the electrospun nanofibers (20 mg) of ((a), (a')) CA, ((b), (b')) PA, ((c), (c')) PAN, ((d), (d')) PES, ((e), (e')) PU 918 and ((f), (f')) PU Elastollan, respectively.

Table 2. Characteristics of the electrospun nanofibers as gauged by BET, contact angle and calculated values from the SEM images.

Nanofiber	Average fiber diameter (nm)	Fiber length per unit of mass (m mg^{-1})	Calculated surface area ($\text{m}^2 \text{g}^{-1}$)	BET surface area ($\text{m}^2 \text{g}^{-1}$)	Contact angle($^\circ$)
CA	224 ± 35	19 297	13.6	8.66	22.2 ± 0.9
PA	220 ± 51	24 268	16.8	5.50	8.8 ± 2.3
PAN	330 ± 73	9875	10.2	5.16	0
PES	199 ± 51	23 816	14.9	17.66	72.5 ± 1.8
PU 918	174 ± 56	38 231	20.9	5.34	27.4 ± 0.1
PU Elastollan	179 ± 45	32 572	18.3	16.34	45.4 ± 1.1

total surface area per unit of mass is expressed as:

$$\frac{A}{m} = \frac{d\pi l}{m} = \frac{4}{\rho d}. \quad (6)$$

Table 2 details the recorded diameters from the SEM images, calculated fiber length and surface area through the application of the above formulas, in addition to the surface area measured by BET.

The geometrically determined surface areas, based on SEM, strongly agree with the average fiber diameter because smaller diameter nanofibers possess a larger surface area,

which indicates more sites for adsorption. For instance, PU 918 had the smallest average fiber diameter (174 ± 56 nm), so it possessed the largest calculated surface area ($20.9 \text{ m}^2 \text{g}^{-1}$) and PAN had the largest average fiber diameter (330 ± 73 nm), so it possessed the least calculated surface area ($10.2 \text{ m}^2 \text{g}^{-1}$); the results correspond to the literature with the values in the range of $9\text{--}51 \text{ m}^2 \text{g}^{-1}$ for surface area and a few hundreds of nanometers for average fiber diameter [1, 57]. The estimated surface area of cylindrical geometry was founded on a calculation that assumed the fibers had a smooth surface and no solvent evaporated during electrospinning. Whereas, in

BET measurement, the surface area is slightly underestimated because each polymer had a different mass per unit area produced, which could be a plausible reason, especially in PU 918 with 0.7 g m^{-2} (see table 1), which has led to a lower value of BET.

The hydrophilic properties of the electrospun nanofibers were tested using contact angle measurements. It is considered that the hydrophilic surfaces generally have a contact angle of $<90^\circ$ and the lesser the contact angle, the more hydrophilic the material is. We observed that the liquid instantly penetrated the nanofibers on pp completely. Therefore, nanofibers were compressed on a PET sheet and it exhibited low contact angle values because we observed water percolation into fiber networks. According to the results obtained (table 2), the contact angle values were in the range of 0° – 72.5° . These values indicated that all the nanofibers were hydrophilic and suitable for the removal of the investigated estrogenic hormones. The contact angle of a particular polymer's nanofibers mainly depends on the concentration of the polymer in solution during the electrospinning process. The possible reasons for the difference in contact angles of various polymer nanofibers could be their structure, pore size and fiber diameter [58].

IR studies were conducted to distinguish the functional groups in the electrospun nanofibers of each polymer which are later discussed in the adsorption mechanism section to understand the type of bonding and interactions between estrogenic hormones and nanofibers, as shown in figure 2.

As can be seen from figure 2, the characteristic peaks for PAN at 1250 , 1454 , 1667 , 2243 and 2927 cm^{-1} correspond to C–N stretching, C–H bending in CH_2 , C=C stretching, $\text{C}\equiv\text{N}$ stretching and C–H stretching vibrations in the polymer structure, respectively [59]. The small PAN and polyurethanes peaks represent aliphatic CH_2 , reflecting a C–H asymmetrical flexing vibration. The electrospun polyurethanes show an absorption peak at 3330 cm^{-1} caused by the stretching vibrations of N–H and the aliphatic amino group in the carbamate. Strong peaks usually occur between 1700 and 1736 cm^{-1} , relating to mono or disubstituted compounds, herein denoting the peak at 1732 cm^{-1} attributed to the C=O stretching vibration of the amido ester, while a separate region at 1701 cm^{-1} is observed for PU Elastollan in contrast with a single peak at 1715 cm^{-1} for PU 918. The peak at 1529 cm^{-1} is for N–H bending and C–N stretching vibrations of the amide group. The peak at 1224 cm^{-1} arises through the C–N stretching vibration for the other amide group. As a result of the stretching vibration of the C=C bond in the skeleton of the benzene ring, peaks appear at 1476 and 1597 cm^{-1} . A broad range of peaks occurs at 1079 and 1106 cm^{-1} due to characteristic bands of alkyl ether causing the asymmetric flexing vibration of C–O–C bonds, most prominent for PU Elastollan [60, 61].

The vibration of aromatic hydrocarbons is observed in PES at the bands 1577 , 1485 and 1105 cm^{-1} . The bands at 1241 and 1150 cm^{-1} could be due to aryloxy and aromatic sulfone groups, respectively. A band arising through a SO_3H symmetrical stretching vibration appears at 1011 cm^{-1} . These peaks indicate that the material is strongly sulfonated [62].

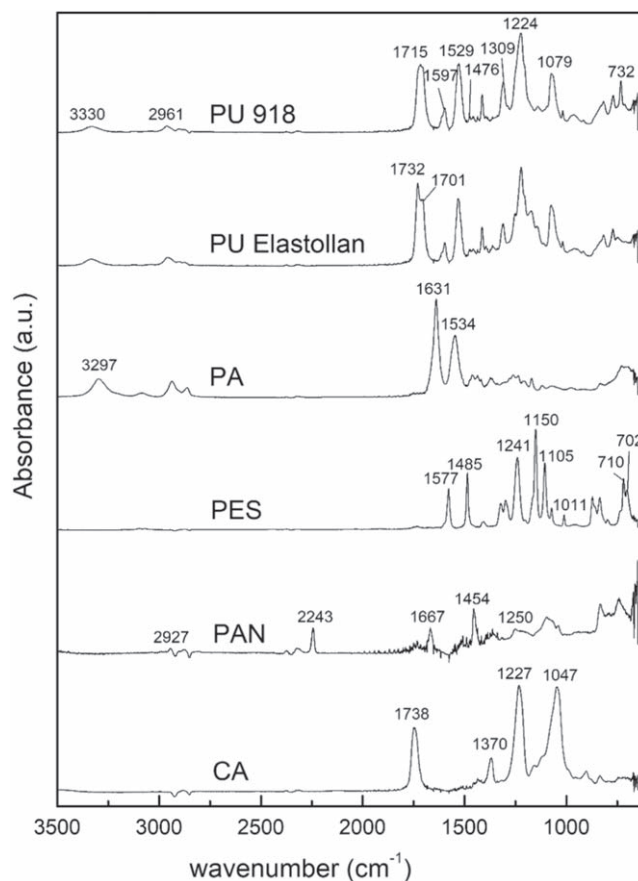


Figure 2. FTIR spectra for the electrospun nanofibers from attenuated total reflectance (ATR) sampling.

The peaks at 710 and 702 cm^{-1} are attributed to the stretching vibrations of C–O and C–S bonds, respectively [63].

The peak at 1534 cm^{-1} —characteristic of PA—is attributed to amide II, C=O bending and the amide I band at 1631 cm^{-1} indicates the stretching vibration of C=O in the amide group (–CO–HN–). Lastly, the amide A band at 3297 cm^{-1} corresponds to –NH stretching [64]. In the case of CA, it can be seen that the vibration peak at 1047 cm^{-1} shows a C–O bond, the peak at 1227 cm^{-1} represents a (C–O–C) anti-symmetric stretching ester group, the peak at 1370 cm^{-1} denotes C–CH₃ and the peak at 1738 cm^{-1} is for C=O bond stretching of the carbonyl group [65, 66]. Hence, the FTIR spectra measured for the nanofibers are in reasonable compliance with spectra for the original polymeric raw materials from the bank of IR spectra.

3.2. Static adsorption study of hormones on the polymeric materials

The experiment was conducted on 100 ml of a solution containing a mixture of the 4 estrogenic hormones (E1, E2, EE2, E3) at a total concentration of 0.8 mg l^{-1} , wherein each hormone equated to 0.2 mg l^{-1} in concentration, in addition to 20 mg of adsorbent. Figure 3 details the static adsorption of each hormone separately on the various electrospun nanofibers at 250 rpm over a period of 9 h .

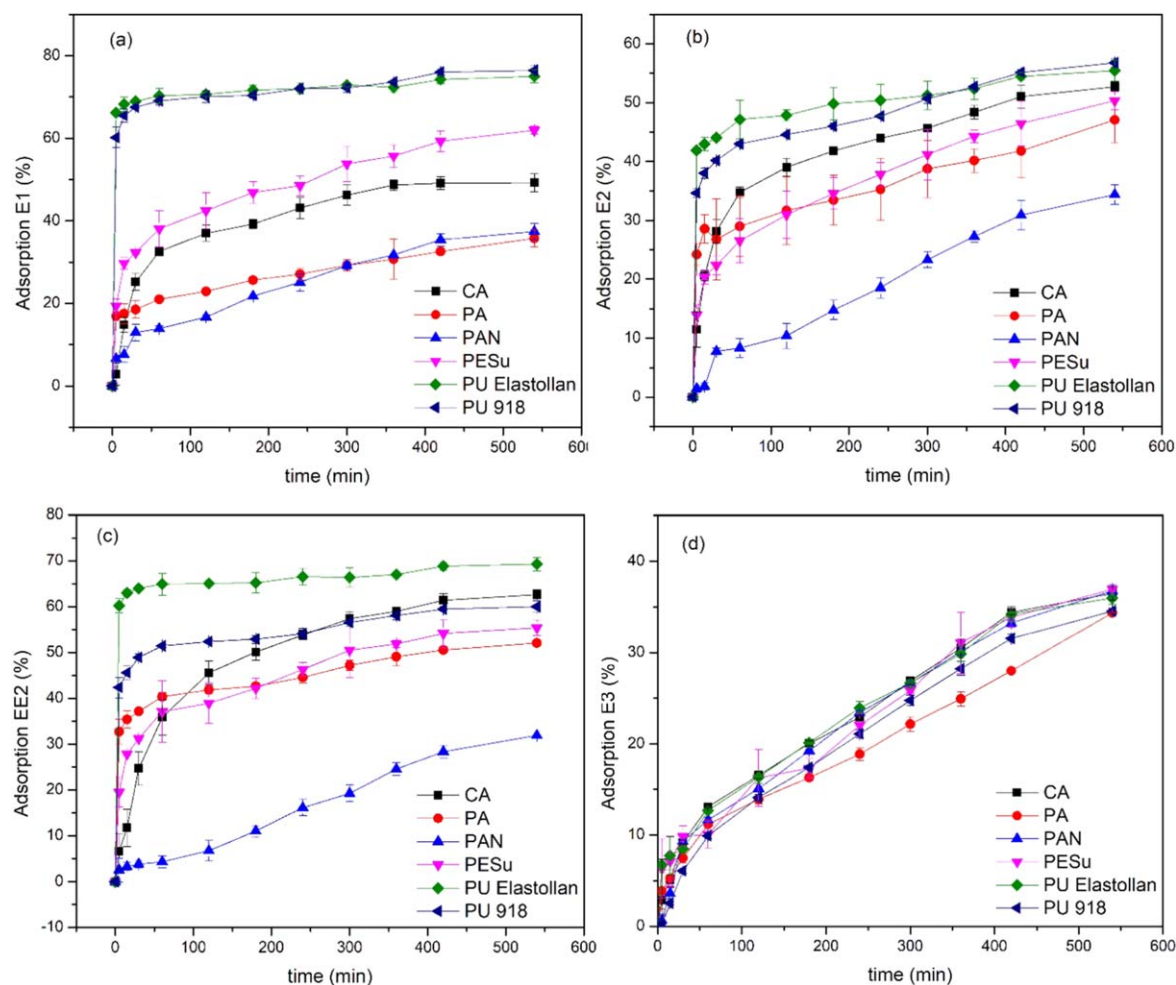


Figure 3. Static adsorption of each estrogenic hormone on six different nanofibers from a combined solution of (a) E1, (b) E2, (c) EE2 and (d) E3.

The results in figure 3 demonstrate that polyurethanes were most efficient at removing EE2, E2 and E1, PAN demonstrated the lowest capacity for EE2 and E2 adsorption, while PA was the least effective with E1 and E3. The plausible reason for the least adsorption on PAN could be due to its large fiber diameter (330 ± 73 nm), as depicted by its least calculated total surface area of $10.2 \text{ m}^2 \text{ g}^{-1}$ compared to the other polymers, thereby attributing to its less available sites for adsorption and hydrogen bond interactions with the estrogenic hormones. Comparing the sorption efficiency of both polyurethanes revealed that PU Elastollan either possessed a superior adsorption effect (for the hormones EE2 and E2) or was identical (E3, E1), potentially due to the lesser content of hard segments in PU Elastollan than PU 918. The active sorption center of PU Elastollan is more easily accessible than the sterically hindered center in the hard segments of PU 918.

All materials showed a similar trend of sorption for the E3 hormone. The conclusion can be drawn that EE2, E2 and E1 were readily adsorbed by these nanostructured materials, with E3 being adsorbed the least. The low percentage of removal of E3 could be attributed to its minimal $\log K_{ow}$ value of 2.45, compared with E1, E2 and EE2 at 3.43, 3.94

and 4.15, respectively. The adsorption of these estrogens was directly related to their hydrophobic nature, as specified by the higher value for K_{ow} [54]. Furthermore, E3 followed a different kinetic trend than the other hormones in that its adsorption was gradual, whereas most of the adsorption of the other hormones occurred within the first 70 min for the majority of the materials. CA and PES had similar adsorption behavior for all the hormones and CA exhibited higher adsorption efficiency for EE2 and E2, though PES was particularly effective with E1. Therefore, it is noteworthy to mention that every material proved sufficient in its response to simultaneous adsorption of each hormone.

3.3. Equilibrium adsorption capacity comparison

Determination was made as to total adsorption in combination for all four hormones by each polymer, along with cumulative adsorption capacity as a function of time to work out the overall efficiency of each polymer. The various trends are presented in figure 4.

Figure 4(a) above shows the total cumulative adsorption of the hormones on the nanofibrous materials to the time of 540 min for equilibrium. The results show that the removal efficiency at

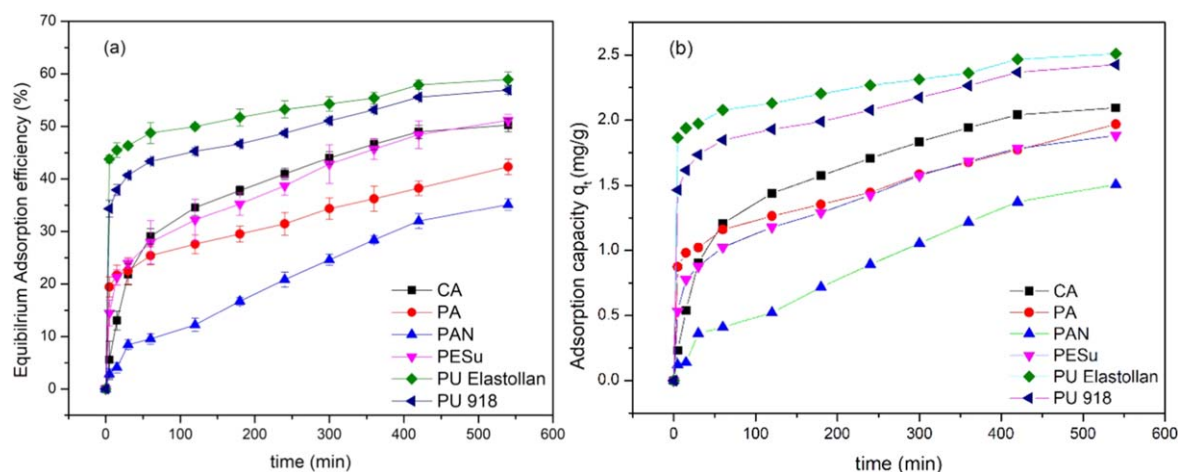


Figure 4. Trends for the combined hormones of E1, E2, EE2 and E3 on the nanofibers as to (a) removal efficiency as a function of time and (b) total adsorption capacity as a function of time.

equilibrium for the different materials ranged between 30% and 60%. The graph reveals that the polyurethanes had the greatest tendency and fastest rates for adsorption, reaching close to equilibrium with 50% efficiency within the first 100 min, as represented by the initial curve of the graph, reaching a maximum removal efficiency of ca. 60%. Although PAN initially had the lowest rate, it eventually demonstrated the highest rate at the halfway point between 120 and 420 min, as visible in the steepness of the curve. CA and PES were similar in adsorption behavior, reaching 50% at equilibrium. Thus, PU Elastollan was the best polymer for adsorption of the estrogens, with PAN being the least effective.

The total adsorption capacity of each material as a function of time is detailed in figure 4(b). The results indicate that the cumulative adsorption capacity of the four estrogenic hormones increased for each material until equilibrium was established between the adsorbates and adsorbent. The time to reach equilibrium depended on the concentration of the adsorbate and the amount of adsorbent [67]. Both factors were kept constant to compare the capacities of the different materials. However, it was still necessary to increase the amount of adsorbent to enhance the removal efficiency of the polymers over a shorter time frame. The highest cumulative adsorption capacity calculated was 2.51 mg g^{-1} for PU Elastollan, whereas the lowest was 1.51 mg g^{-1} for PAN. The adsorption capacities for E1, E2, EE2 and E3 were found to be 0.801, 0.592, 0.736 and 0.382 mg g^{-1} for PU Elastollan and 0.396, 0.370, 0.343 and 0.397 mg g^{-1} for PAN, respectively. EE2 stood out in terms of adsorption and was found to have the highest adsorption capacity for all the polymers compared to the other estrogens.

Thus, the results of polymers in the current study are well in compliance with the literature values and comparing the adsorption capacities herein with previous research showed the suitability of these polymers as a potential adsorbent for removing the estrogenic hormones, in comparison with solid particles and membranes. Adsorption capacities reported in the literature were found to be 0.423 mg g^{-1} , 0.472 mg g^{-1} and 0.472 mg g^{-1} when MWCNTs was used and $2533.34 \text{ ng g}^{-1}$,

$2020.78 \text{ ng g}^{-1}$ and $2234.09 \text{ ng g}^{-1}$ when activated sludge was employed for E1, E2 and EE2, respectively. The value for removing E1 was 62 ng g^{-1} via a hydrophobic hollow fiber membrane [54]. Hence, PU Elastollan in the current study has a higher adsorption capacity for each hormone compared to the research in the literature. Another aspect that distinguishes these polymeric membranes over solid particles is that solid particles require a further sophisticated purification method to be separated from the treated water, which increases the cost. In addition, solid particles sometimes are toxic, which makes them less preferable for the intended purpose. Whereas these nanofibers can be easily washed, reused and the estrogenic hormones can be quickly recovered. Furthermore, environment-friendly nanoparticles as adsorbents can be used as additives in these nanofibers during electrospinning which can further enhance their adsorption capacity by increasing the surface area and available sites that can be viable for the entrapment of estrogenic hormones.

3.4. Adsorption kinetics

Removal of the estrogenic hormones by the polymer nanofibers through adsorption increased over time, obtaining a maximum value for every hormone on each polymer type and reaching equilibrium. The adsorption rate was initially rapid until 30 min had passed, whereupon it gradually ebbed away in parallel with the duration of contact, to an assumed plateau at 540 min.

The results obtained from the experiment were employed to investigate factors affecting the adsorption process and the rate-limiting step in the process, such as the transfer of mass and type of chemical interaction. Furthermore, the kinetics for selecting optimum conditions for full-scale removal of the hormones were studied. It is often difficult to determine kinetic parameters and explain the mechanisms involved in complex heterogeneous systems since surface effects can be superimposed on top of chemical effects. Therefore, to further understand such adsorption behavior and mechanisms, parameters from three models—pseudo-first-order, pseudo-second-order and Weber–Morris intraparticle/membrane diffusion model equations—were employed to test the experimental data and examine the adsorption kinetics of the

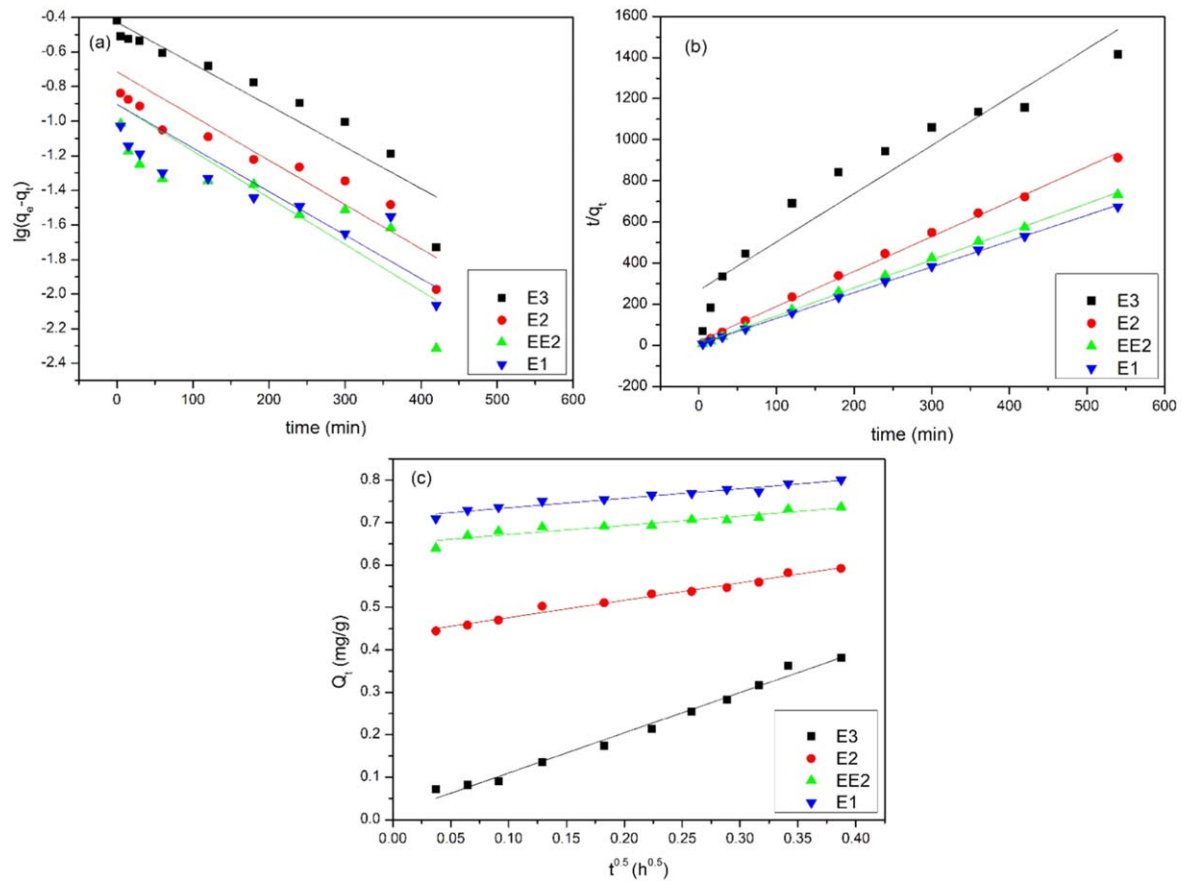


Figure 5. Plots of the adsorption kinetics for the four estrogenic hormones (E1, E2, EE2, E3) on PU Elastollan nanofibers: (a) pseudo-first-order, (b) pseudo-second-order, (c) the Weber–Morris interparticle diffusion model.

four estrogenic hormones taken up by each polymer. These models are applicable for describing liquid/solid systems. Pseudo-first-order constitutes a widespread, commonly applied model for analyzing the adsorption of a solute in an aqueous solution. In this context, the rate of sorption of hormones on the surface of the nanofibers was proportional to the amount of hormones adsorbed from the solution phase, expressed by equation (7) as [68]:

$$q_t = q_e(1 - \exp(-k_1 t)), \quad (7)$$

where q_t is the amount of hormone adsorbed per unit mass at time t (mg g^{-1}), q_e is the amount of hormone per unit mass at equilibrium (mg g^{-1}) and k_1 is the first-order rate constant (l min^{-1}).

The pseudo-second-order equation relates to solid-phase adsorption capacity and can predict the behavior of kinetics over a great range for adsorption [69]. In this model, surface adsorption is the rate-determining step, which involves chemisorption due to physicochemical interactions between the solid and liquid phases [70]. The linear form of equation (8) is expressed as [71]:

$$\frac{t}{q_t} = \frac{1}{k_2 q_e^2} + \frac{t}{q_e}, \quad (8)$$

where k_2 is the reaction rate constant (g (mg min)^{-1}).

The adsorption process usually occurs in consecutive steps, comprising movement of the adsorbate from the solution bulk to the surface of the adsorbent and then diffusion through the boundary layer to the outer surface of the adsorbent. This is followed by adsorption on an available active site on the surface of the adsorbent and, finally, intraparticle diffusion through pores. The Weber–Morris intraparticle/membrane diffusion model is diffusion-controlled; the adsorption rate directly depends on the speed at which an adsorbate can diffuse towards the adsorbate. This model is described by equation (9), as follows [72]:

$$q_t = kt\left(\frac{1}{2}\right) + I, \quad (9)$$

where k is the reaction rate constant ($\text{mg g}^{-1} \text{h}^{1/2}$) and I is the y-intercept constant (mg g^{-1}) providing data on the thickness of the boundary layer.

For the validity of this model, it is essential to note that the linear, converging line for each estrogenic hormone must pass through the point of origin for intraparticle diffusion to constitute the rate-determining step.

Figure 5 contains plots describing the adsorption kinetics of the four estrogenic hormones on PU Elastollan since this polymer exhibited the highest removal efficiency, adsorption capacity and has proven to be the best nanofiber; the kinetic parameters obtained are given in table 3. The kinetic plots and

Table 3. Values for each hormone from the kinetic models in relation to PU Elastollan electrospun nanofibers.

Hormone	Experimental q_e (mg g ⁻¹)	Pseudo-first-order model			Pseudo-second-order model			Intraparticle diffusion model		
		k_1 (min ⁻¹)	q_e , cal (mg g ⁻¹)	R^2	k_2 (g mg ⁻¹ min ⁻¹)	q_e , cal (mg g ⁻¹)	R^2	k (mg g ⁻¹ h ^{1/2})	I (mg g ⁻¹)	R^2
E3	0.382	0.002	0.373	0.901	0.020	0.426	0.924	0.947	0.015	0.987
E2	0.592	0.003	0.193	0.793	0.145	0.589	0.998	0.406	0.436	0.983
EE2	0.736	0.003	0.125	0.630	0.276	0.733	0.999	0.219	0.650	0.895
E1	0.801	0.003	0.125	0.619	0.286	0.796	0.999	0.228	0.711	0.946

parameters for the other polymers were also calculated and are provided in the supplementary data (figures S3–7 and tables S1–5).

The results were examined to obtain fits for the adsorption kinetics of the adsorbate mixture of E1, E2, EE2 and E3 estrogenic hormones on the adsorbent nanofibers by plotting on graphs the pseudo-first-order, pseudo-second-order and Weber and Morris intraparticle diffusion models. Figure 5(a) shows $\lg(q_e - q_t)$ plotted against t for the E3 hormone, which is in good compliance with the pseudo-first-order equation. The data points are shown together with generated lines for best fits. The agreement between the data set is reflected in the high regression coefficient (0.901) for E3 compared to the other three hormones (E2, EE2 and E1) with the regression coefficients 0.793, 0.630 and 0.619, respectively. The equilibrium adsorption capacity calculated for E3 (0.373) is reasonable compared to the experimental value (0.382). The rate constant k_1 is far more similar, though and within the range for all hormones. For E2, EE2 and E1, however, this model appears to be less accurate for describing the initial stage ($t \leq 30$ min) and the theoretical expected yield of 0.193, 0.125 and 0.125 seems unsatisfactory and much lower than the actual values of 0.592, 0.736 and 0.801 for E2, EE2 and E1, respectively.

The lines plotted in figure 5(b) of t/q_t versus t have to be linear to estimate q_e and k_2 from the curve and y-intercept, respectively. The results indicate that the interaction of E2, EE2 and E1 with the material followed second-order kinetics, as shown by the line for best fit adhering fully with the data set points. The regression coefficients are greater than 0.99 and the calculated adsorption capacities of 0.589, 0.733 and 0.796 are incredibly close to the experimental values 0.592, 0.736 and 0.801, respectively. This suggests that the active sites were not homogeneous on the surface since the rate of adsorption is determined by two factors—the concentration of the hormones and the number of active sites available on the material [67]. These findings confirm the suitability of this model for describing the adsorption of E2, EE2 and E1 on the PU Elastollan nanofibers. Similar results were observed for the other polymers in this study compared with results described in the literature for MWCNTs [54]. E3 exhibits an overall mismatch, though, as two linear portions are visible—one for the first 60 min and another for the period after 100 min. The plot in figure 5(b) was applied to determine the rate constant (k_2) and the calculated equilibrium adsorption

capacity (q_e) expressed in equation (8) to obtain the regression coefficient (R^2) shown below in table 3.

In the case of q_t versus $t^{0.5}$, the graph for E3 is linear in progression with a comparatively high and acceptable regression coefficient (0.987) that almost passes through the point of origin. This means that intraparticle diffusion constitutes the rate-limiting step, which is unlikely to happen in the adsorption of the other three hormones (see figure 5(c)). The plots for the other estrogens do not pass through the point of origin, potentially due to a surface effect that may have controlled the sorption process during the initial time periods, representing a diffusion-controlled or boundary layer diffusion effect. Thus, for E2, EE2 and E1, intraparticle diffusion could comprise part of the mechanism, though not a step for determining the total rate of diffusion. The values calculated by equations (7)–(9) are given in table 3.

3.5. Adsorption mechanism

The possible mechanisms that existed between the estrogens and nanofibers comprise the following: (1) size-exclusion; (2) physical adsorption of estrogens on the external surfaces and inside layers of the nanofibers due to their porous structures; (3) charge interactions between the estrogens and electrospun nanofibers; (4) the bonding of estrogen molecules onto the nanofibers via reaction with the functional groups present on the surfaces of the nanofibers. Size exclusion would not be expected in this system as the reported molecular size of the estrogens was quite small (approximately 0.8 nm for E1 and 0.796 nm for E2), compared to the pore sizes of the electrospun nanofibers and GMF filter used; otherwise, their removal efficiency would have been 100%. As the fiber diameters of the polyurethanes were lesser in size (PU 918 = 174 ± 56 , PU Elastollan = 179 ± 45), their surface area is larger as a consequence (20.9 and 18.3, respectively), providing sufficient availability of active sites for adsorption of the estrogens, as detailed in table 2. Electrostatic charge can also affect adsorption, as Porter and Porter report in the literature on adsorption behavior on microfilters in the presence of cations [73]. The deprotonation of E1, E2, EE2 and E3 is governed by the dissociation of the hydroxyl group attached to the benzene ring. The acid dissociation constants for E1, E2, EE2 and E3 equal 10.34, 10.46, 10.4 and 10.38, respectively [74, 75]. All of them have slightly weaker acidity than phenol ($pK_a = 10$). As a result of the high value of pK_a , most of the molecules of the estrogens were undissociated and

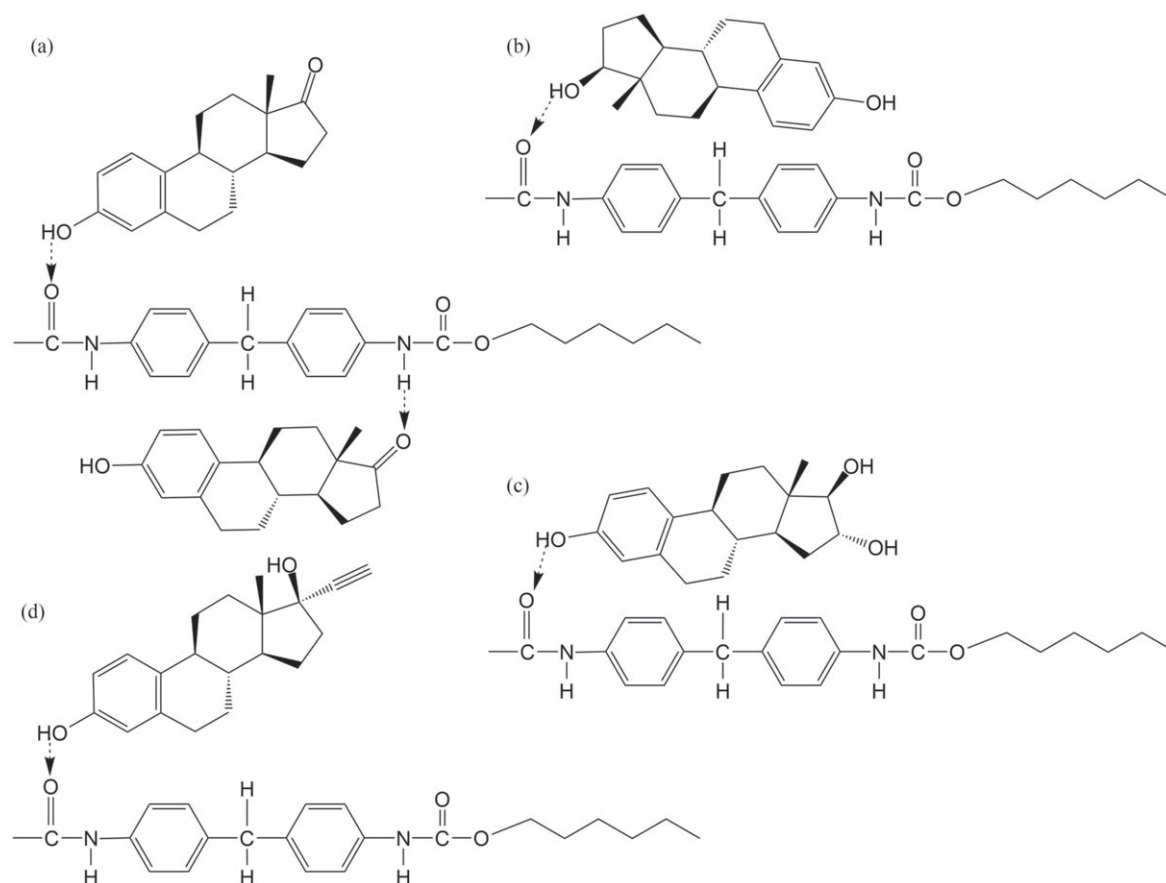


Figure 6. Hydrogen bonding between the polyurethane molecule and estrogenic hormones (a) E1, (b) E2, (c) E3 and (d) EE2.

thus, they remained neutral in the solution mixture [9]. Therefore, it is unlikely that charge interaction was the main factor that brought about the significant adsorption of the estrogenic hormones on the nanofibers [8, 76].

The high and rapid adsorption of the estrogens on the polyurethanes is noteworthy. The molecules were far smaller in size than the porosity of the nanostructures, indicating that pore size had a negligible dependence on adsorption. Apart from physical adsorption, which gradually reaches equilibrium, the only rational explanation for the strong interaction of these estrogens with the nanofibers is bonding. Hydrogen bonds are stronger than Van der Waals forces involved in physical adsorption. In this context, figure 6 presents the chemical interactions of each estrogen with the polyurethane molecule.

Each estrogen molecule (E1, E2, EE2, E3) in this study contains a hydroxyl group ($-OH$) acting as a proton donor for hydrogen bonding. Due to the presence of both a nucleophilic carbonyl group ($-C=O$) and hydroxyl group in E1, this proton can act as both a donor or acceptor in hydrogen bonding and has the highest removal efficiency as a consequence. Han *et al* describe similar hydrogen bonding by E1 with nylon 6,6 membrane in their research [8, 64]. Nylon 6,6 and polyurethanes possess identical functional groups involved in hydrogen bonding. Therefore, the functional groups ($N-H$ and $C=O$) in PU Elastollan, PU 918 and PA participated in the hydrogen bonding of E1, although only $C=O$ was present for the other three estrogens, as determined by FTIR analysis.

These hydrogen bonding interactions would dictate the adsorption of the estrogens on the polyurethane nanofibers, explaining the rapidity of the adsorption process in the initial stage of the experiment. The accurate technique of FTIR analysis was employed to characterize hydrogen bonds on the PU 918 polyurethane, as detailed below.

The FTIR spectra for a PU 918 sample saturated with estrogen are presented in figure 7. A notable aspect is the difference in the relative intensity of the peak at 1715 cm^{-1} that corresponds to $C=O$ stretching. A crucial feature of PU 918 is its cross-linking molecular structure that arises through inter and intra-hydrogen bonds. The band contributes to restricting the stretching of the hydrogen bonds on the carbonyl group in PU 918 and is evident from the shift of the peak to a reduced frequency of 1700 cm^{-1} . There is also a significant drop in intensity at 1715 cm^{-1} , yet this is not the case for two amide bands (at 3330 cm^{-1} and 1529 cm^{-1}), suggesting a change occurs through adsorption of the estrogenic hormones. A possible explanation could be the presence of hydroxyl groups on the terminals of the estrogens that compete with $-NH$ groups in acquiring the carbonyl groups present on the polyurethane; this potentially causes weak intermolecular hydrogen bonding, with eventual substitution by the estrogen molecules and the subsequent formation of new bonds.

No notable change occurs for the amide band (3330 cm^{-1}) after adsorption. A possible explanation is that the $-NH$ groups

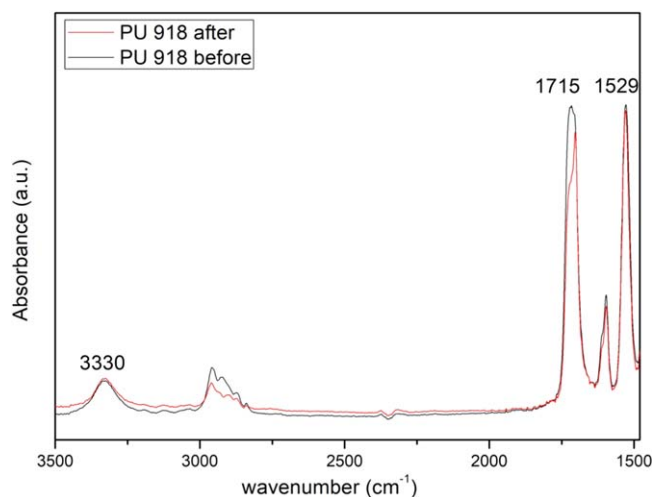


Figure 7. FTIR spectra for the PU 918 nanofibers before and after static adsorption (0.8 mg l^{-1} mixture of E1, E2, EE2 and E3 of 100 ml volume).

are not set free to interact with hydrogen donors, such as the water and C=O groups of the cyclopentane rings present in E1 molecules, so it cannot forge new hydrogen bonds; otherwise, a new peak would be visible at ca. 3400 cm^{-1} [64]. Han *et al* report that N-methyl acetamide (NMA), which possesses a simple structure with an amide group, does not interact with the $\text{C}=\text{O}$ group when released. The results are given herein clearly agree with the study in the literature; thus, the estrogens (E1, E2, EE2, E3) under investigation might form hydrogen bonds with the polyurethanes and PA [76, 77].

3.6. Determination of recovery and reusability

In order to determine the reversibility of the polymers for sorption, triplicates of each polymer sample were soaked in 50 ml of water and shaken for 15 min, which would not significantly reduce the hormone concentration on the nanofibers as a consequence of chemical bonding [1]. Therefore, each sample, after being washed three times with distilled and deionized water, was immersed in 40 ml of pure anhydrous ethanol since all estrogenic hormones exhibit very high solubility in ethanol due to their high partitioning coefficient ($\text{Log-} K_{o/w} = 3.13, 4.01, 2.45$ and 3.90 for E1, E2, E3 and EE2, respectively). A strong partitioning effect was expected to occur in combination with a competing hydroxyl group present in the ethanol, which could destabilize the estrogen-nanofiber hydrogen bonds and attract the adsorbed hydrophobic hormones in the ethanol solution [8, 64]. The resultant solution was gently stirred for 30 min at 175 rpm and air-dried afterward, a process repeated up to four consecutive cycles. Figure 8 presents the adsorption study over the four cycles.

The above graphs represent the removal of the hormones in percentage, present at 0.2 mg l^{-1} in concentration with 20 mg of each nanofiber adsorbent over four adsorption cycles. As can be seen, the trend is one of decrease for each material after consecutive cycles for all the hormones, except for PES during the second and third cycles as it underwent the least change in surface morphology; the change in average fiber

diameter from the original size of 199–278 nm following ethanol treatment was not as large as for other polymeric nanofibers. The highest removal efficiency is evident for E1 and EE2, with the least for E3. The values for removal efficiency are similar for all the materials during the first cycle of E3. PA shows the least adsorption for E1 and E3, while PAN exhibits the least for EE2 and E2. Notably, PAN cannot be reused for E1 because of the significant effect that transpires during the desorption process, leading to a loss in mass, which brings about a decrease in the amount of active adsorption sites and reduction in the surface area through an increase in fiber diameter.

PU 918 appears applicable for removing E1 and E2 during the first cycle, whereas PES and PU Elastollan are more suited to E3 and EE2, respectively. A drastic drop in the effectiveness of the materials for E1 and E3 arises during the second cycle, possibly related to the treatment with ethanol they received in the desorption process. However, this is unlikely to occur in the case of EE2 and E2, as the materials seem far more reliable over repeated cycles. It can be concluded that the adsorbent materials under investigation are reusable to a limited extent after being washing with ethanol, i.e up to four adsorption cycles, with the exception of E3 with a limit of three cycles.

The comparison presented was conducted to discern the reusability of the nanostructured sorption materials. Industrial applications may require the testing of other solvents and the findings reported herein indicate that the suitable solvent must possess very high solubility of hormones but minimum solubility of these polymers from which the nanofibers were made. Figure 9 shows the overall efficiency of each polymer over four adsorption cycles.

Figure 9 illustrates the adsorption efficiency of each polymer for cumulative estrogenic hormone removal over four adsorption cycles. It should also be noted that these percentages are for the mixture of E1, E2, EE2 and E3 for each polymer per cycle. PU Elastollan demonstrates the highest extent of hormone removal in the first cycle, in contrast with PAN with the least, while PU 918 has the highest efficiency in the 4th cycle. PA exhibits the least drop in effectiveness from the first to the second cycle and better reliability. PES is the most consistent and manages the greatest adsorption in the 3rd cycle. It should be noted that due to repeated treatment with ethanol during desorption, it was evident that the nanofibers became stiff and shrank due to loss in mass until the last cycle. Compact and tightly folded, they provided less surface area for hormone entrapment during the final cycle, as shown in figure 10.

The repeated desorption cycles of estrogen hormones from the nanofibers, wherein ethanol was applied, exerted a significant change in fiber morphology attributed to contact between the nanofibers and ethanol. The nanofibers of these materials are not prone to dissolving in ethanol and their porous structure facilitates the complete penetration of ethanol molecules. This is why, after several cycles and a period of contact, the structure of the nanofibers collapsed and swelled and the effectiveness of the adsorption process

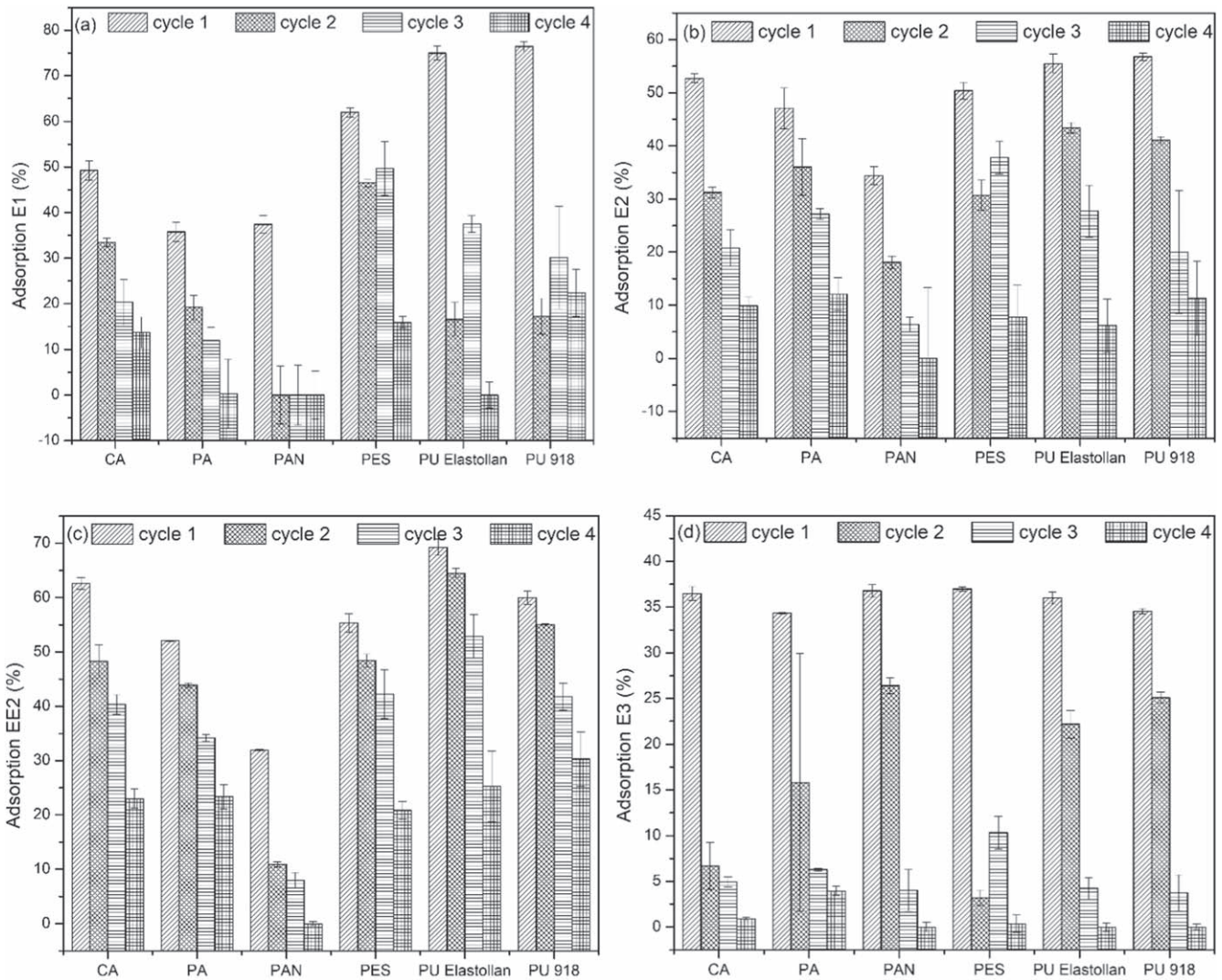


Figure 8. Four adsorption cycles for each electrospun material (20 mg) and each estrogenic hormone (a) E1, (b) E2, (c) EE2 and (d) E3, at an initial concentration of 0.2 mg l⁻¹ in a combined solution of 0.8 mg l⁻¹.

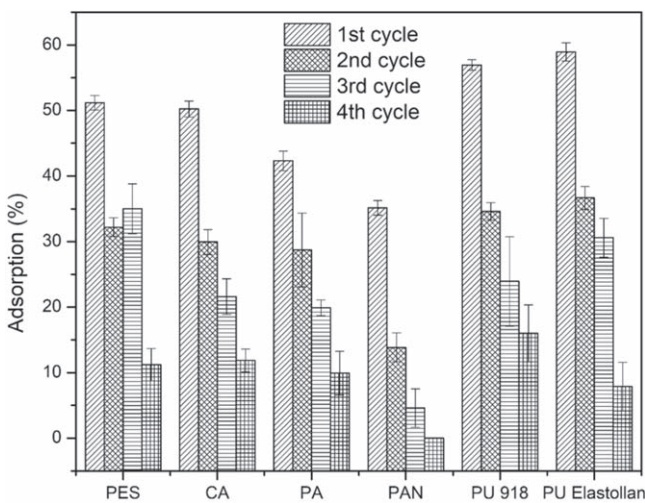


Figure 9. Cumulative efficiency of adsorption for the four estrogenic hormones on the various nanofibers over four cycles.

diminished, as is evident in the SEM images of the nanofiber structures after four cycles in figure 10.

Figure 10 presents the surface morphology for each nanofiber after four adsorption–desorption cycles. It is visible that the diameter of the nanofibers increased for each type of polymer, ranging from 249 to 475 nm (PU Elastollan experienced the least and PAN the highest), in comparison with the range in diameter prior to adsorption, which was 174–330 nm, respectively.

3.7. Limitations, future works and practical application

This is a preliminary model study for testing various electrospun polymers for simultaneous adsorption of a set of four estrogenic hormones using ultrapure water. However, certain limitations exist that require extra investigation and improvement to devise a continuous adsorption technique that functions at high pressures. Additionally, several aspects of

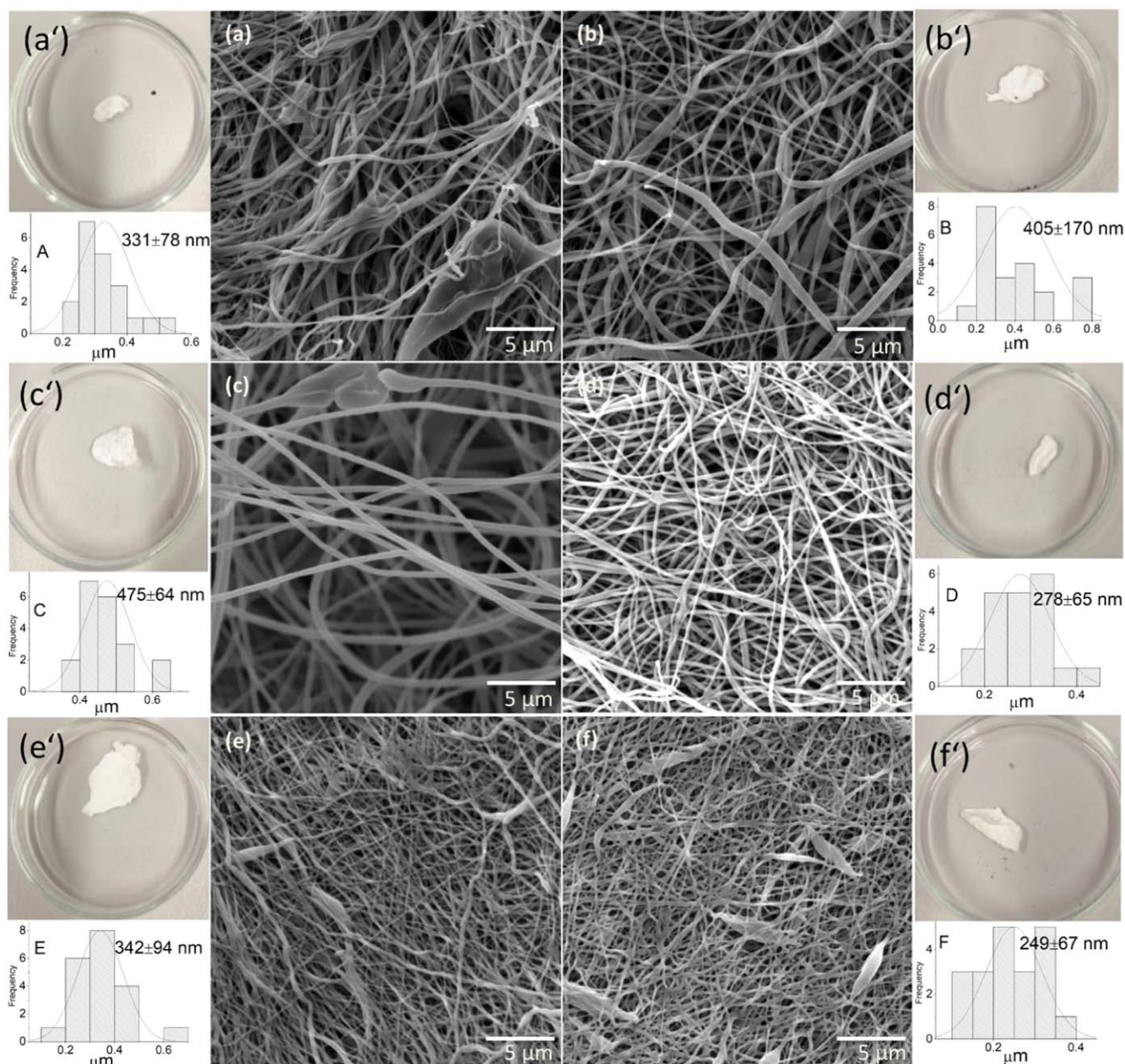


Figure 10. SEM Images, sample images of the nanofibers and distribution of their fiber diameter after four adsorption-desorption cycles: ((a), (a'), (A)) CA, ((b), (b'), (B)) PA, ((c), (c'), (C)) PAN, ((d), (d'), (D)) PES, ((e), (e'), (E)) PU 918 and ((f), (f'), (F)) PU Elastollan.

the process that include membrane fouling, solution characteristics, varying concentrations of adsorbent and adsorbate need to be addressed to make this process amenable for large scale use. Future works shall encompass testing the electrospun materials with actual water samples from a reservoir. Doing this would enable the authors to observe the competing behavior and influence of inorganic ions and organic pollutants on entrapping estrogens during continuous adsorption by dead-end flow and cross-flow measurements. A similar concept for research could involve varying the pH, temperature, ionic strength and concentration of adsorbent and adsorbate in order to discern the optimum applicability of kinetics and determine thermodynamic parameters. These matters will be subjected to in future research.

4. Conclusions

This study investigated the simultaneous removal of various estrogenic hormones by polymeric electrospun nanostructures. A one-step group detection method was devised for concurrent quantification of the estrogenic hormones. It was found that all the nanofibrous membranes were capable of successfully removing all types of estrogens. Overall adsorption efficiency diminished in the following order: PU Elastollan > PU-918 > PES > CA > PA > PAN. The chemical composition and functional groups in the structure of the nanofibers played a major role in possessing hydrogen bonds between different types of estrogens and nanofibers, elaborated in the adsorption mechanism. The percentage efficiency

of removal was the greatest for E1 (76.5), declining through EE2 (69.3) and E2 (56.8) to E3 (37.0). PU Elastollan demonstrated the highest capacity for total adsorption over the other NF membranes and also compared to literature values, equaling 2.51 mg g^{-1} due to its carbonyl functionality and surface area. Based on results from kinetic models for all the polymers, pseudo-first-order is applicable for E3, with pseudo-second-order being suitable for E1, E2 and EE2; the exception is PAN, where the estrogens follow the pseudo-first-order kinetic model. Consequently, both models are considered appropriate due to their high regression coefficients compared to other kinetic models. Desorption tests to discern recovery of the hormones and the reusability of the sorption nanostructures were conducted and found to be valid for four cycles. The research carried out shows that polymeric nanofibrous membranes are worthy of consideration as potential adsorbents for the simultaneous removal of estrogens from wastewater streams.

Acknowledgments

The authors gratefully acknowledge the financial support of the Ministry of Education, Youth and Sports of the Czech Republic (grant no. RP/CPS/2020/002), the Internal Grant Agency of TBU in Zlin (grant no. IGA/CPS/2020/002) and the Technological Agency of the Czech Republic (grant no. FW01010588).

Data availability statement

All data that support the findings of this study are included within the article (and any supplementary files).

CrediT authorship contribution statement

Muhammad Yasir: Conceptualization, Methodology, Investigation, Formal analysis, Data curation, Writing-original draft, Writing- review & editing.

Tomáš Šopík: Methodology, Formal analysis, Data curation.

Lenka Lovecka: Methodology.

Dušan Kimmer: Conceptualization, Supervision, Review & editing.

Vladimír Sedlařík: Conceptualization, Supervision, Project administration, Funding acquisition, Review & editing.

Conflicts of interest

The authors declare that they have no known competing financial interests or personal connections that would influence the work reported in this paper.

ORCID iDs

Muhammad Yasir  <https://orcid.org/0000-0001-8999-2779>

References

- [1] Schäfer A I, Stelzl K, Faghih M, Sen Gupta S, Krishnadas K R, Heißler S and Pradeep T 2018 Poly(ether sulfone) nanofibers impregnated with β -cyclodextrin for increased micropollutant removal from water *ACS Sustain. Chem. Eng.* **6** 2942–53
- [2] McLachlan J A, Simpson E and Martin M 2006 Endocrine disruptors and female reproductive health *Best Pract. Res. Clin. Endocrinol. Metab.* **20** 63–75
- [3] Montes-Grajales D and Olivero-Verbel J 2015 EDCs databank: 3D-structure database of endocrine disrupting chemicals *Toxicology.* **327** 87–94
- [4] Gyllenhammar I, Glynn A, Jönsson B A G, Lindh C H, Darnerud P O, Svensson K and Lignell S 2017 Diverging temporal trends of human exposure to bisphenols and plastizisers, such as phthalates, caused by substitution of legacy EDCs? *Environ. Res.* **153** 48–54
- [5] Sood S, Shekhar S and Santosh W 2017 Dimorphic placental stress: a repercussion of interaction between endocrine disrupting chemicals (EDCs) and fetal sex *Med. Hypotheses* **99** 73–5
- [6] Luo L, Yang Y, Xiao M, Bian L, Yuan B, Liu Y, Jiang F and Pan X 2015 A novel biotemplated synthesis of TiO_2 /wood charcoal composites for synergistic removal of bisphenol A by adsorption and photocatalytic degradation *Chem. Eng. J.* **262** 1275–83
- [7] Chen Y, Zhang Y, Luo L, Shi Y, Wang S, Li L, Long Y and Jiang F 2018 A novel templated synthesis of C/N-doped β - Bi_2O_3 nanosheets for synergistic rapid removal of 17 α -ethynylestradiol by adsorption and photocatalytic degradation *Ceram. Int.* **44** 2178–85
- [8] Han J, Qiu W and Gao W 2010 Adsorption of estrone in microfiltration membrane filters *Chem. Eng. J.* **165** 819–26
- [9] Nghiem L D and Schäfer A I 2002 Adsorption and transport of trace contaminant estrone in NF/RO membranes *Environ. Eng. Sci.* **19** 441–51
- [10] Solomon G M and Schettler T 2000 Environment and health: 6. Endocrine disruption and potential human health implications *Cmaj* **163** 1471–6
- [11] Cartinella J L, Cath T Y, Flynn M T, Miller G C, Hunter K W and Childress A E 2006 Removal of natural steroid hormones from wastewater using membrane contactor processes *Environ. Sci. Technol.* **40** 7381–6
- [12] Johnson A C et al 2005 Comparing steroid estrogen and nonylphenol content across a range of European sewage plants with different treatment and management practices *Water Res.* **39** 47–58
- [13] Sarmah A K, Northcott G L, Leusch F D L and Tremblay L A 2006 A survey of endocrine disrupting chemicals (EDCs) in municipal sewage and animal waste effluents in the Waikato region of New Zealand *Sci. Total Environ.* **355** 135–44
- [14] Vymazal J, Březinová T and Koželuh M 2015 Occurrence and removal of estrogens, progesterone and testosterone in three constructed wetlands treating municipal sewage in the Czech Republic *Sci. Total Environ.* **536** 625–31
- [15] Han J, Qiu W, Cao Z, Hu J and Gao W 2013 Adsorption of ethynylestradiol (EE2) on polyamide 612: molecular modeling and effects of water chemistry *Water Res.* **47** 2273–84

- [16] Braga O, Smythe G A, Schäfer A I and Feitz A J 2005 Fate of steroid estrogens in Australian inland and coastal wastewater treatment plants *Environ. Sci. Technol.* **39** 3351–8
- [17] Limpiyakorn T, Homklin S and Ong S K 2011 Fate of estrogens and estrogenic potentials in sewerage systems *Crit. Rev. Environ. Sci. Technol.* **41** 1231–70
- [18] Aris A Z, Shamsuddin A S and Praveena S M 2014 Occurrence of 17 α -ethynylestradiol (EE2) in the environment and effect on exposed biota: a review *Environ. Int.* **69** 104–19
- [19] Adeel M, Song X, Wang Y, Francis D and Yang Y 2017 Environmental impact of estrogens on human, animal and plant life: a critical review *Environ. Int.* **99** 107–19
- [20] Siegenthaler P F, Bain P, Riva F and Fent K 2017 Effects of antiandrogenic progestins, chlormadinone and cyproterone acetate and the estrogen 17 α -ethynylestradiol (EE2) and their mixtures: transactivation with human and rainbowfish hormone receptors and transcriptional effects in zebrafish (*Danio rerio*) *Aquatic Toxicol.* **182** 142–62
- [21] Semião A J C and Schäfer A I 2010 Xenobiotics removal by membrane technology: an overview *Xenobiotics in the Urban Water Cycle (Environmental Pollution)* ed D Fatta-Kassinos, K Bester and K Kümmerer vol 16 (Dordrecht: Springer) 307–38
- [22] Luo Y, Guo W, Ngo H H, Nghiem L D, Hai F I, Zhang J, Liang S and Wang X C 2014 A review on the occurrence of micropollutants in the aquatic environment and their fate and removal during wastewater treatment *Sci. Total Environ.* **473–474** 619–41
- [23] Tijani J O, Fatoba O O and Petrik L F 2013 A review of pharmaceuticals and endocrine-disrupting compounds: sources, effects, removal and detections *Water Air Soil Pollut.* **224** 1770
- [24] Onesios K M, Yu J T and Bouwer E J 2009 Biodegradation and removal of pharmaceuticals and personal care products in treatment systems: a review *Biodegradation.* **20** 441–66
- [25] Pham T T, Nguyen V A and Van der Bruggen B 2013 Pilot-scale evaluation of gac adsorption using low-cost, high-performance materials for removal of pesticides and organic matter in drinking water production *J. Environ. Eng.* **139** 958–65
- [26] Ali H, Masar M, Urbanek M, Guler A C, Urbanek P, Machovsky M and Kuritka I 2020 Effect of annealing on luminescence and photocatalytic activity of ZnS nanocrystals under UV light irradiation *NANOCON 2020 Conf. Proc.* pp 261–6
- [27] Pendergast M M and Hoek E M V 2011 A review of water treatment membrane nanotechnologies *Energy Environ. Sci.* **4** 1946–71
- [28] Shannon M A, Bohn P W, Elimelech M, Georgiadis J G, Mariñas B J and Mayes A M 2008 Science and technology for water purification in the coming decades *Nature* **452** 301–10
- [29] Kumar A K and Mohan S V 2011 Endocrine disruptive synthetic estrogen (17 α -ethynylestradiol) removal from aqueous phase through batch and column sorption studies: Mechanistic and kinetic analysis *Desalination* **276** 66–74
- [30] Kumar A K, Mohan S V and Sarma P N 2009 Sorptive removal of endocrine-disruptive compound (estriol, E3) from aqueous phase by batch and column studies: kinetic and mechanistic evaluation *J. Hazard. Mater.* **164** 820–8
- [31] Pan B, Lin D, Mashayekhi H and Xing B 2008 Adsorption and hysteresis of bisphenol A and 17 α -ethinyl estradiol on carbon nanomaterials *Environ. Sci. Technol.* **42** 5480–5
- [32] Jin X, Hu J Y, Tint M L, Ong S L, Biryulin Y and Polotskaya G 2007 Estrogenic compounds removal by fullerene-containing membranes *Desalination* **214** 83–90
- [33] Kiran Kumar A and Venkata Mohan S 2012 Removal of natural and synthetic endocrine disrupting estrogens by multi-walled carbon nanotubes (MWCNT) as adsorbent: kinetic and mechanistic evaluation *Sep. Purif. Technol.* **87** 22–30
- [34] Krupadam R J, Sridevi P and Sakunthala S 2011 Removal of endocrine disrupting chemicals from contaminated industrial groundwater using chitin as a biosorbent *J. Chem. Technol. Biotechnol.* **86** 367–74
- [35] Zhang Y and Zhou J L 2005 Removal of estrone and 17 β -estradiol from water by adsorption *Water Res.* **39** 3991–4003
- [36] Hristovski K D, Nguyen H and Westerhoff P K 2009 Removal of arsenate and 17 α -ethinyl estradiol (EE2) by iron (hydr) oxide modified activated carbon fibers *J. Environ. Sci. Heal. A* **44** 354–61
- [37] Wang J, Pan K, Giannelis E P and Cao B 2013 Polyacrylonitrile/polyaniline core/shell nanofiber mat for removal of hexavalent chromium from aqueous solution: mechanism and applications *RSC Adv.* **3** 8978–87
- [38] Augusto F, Hantao L W, Mogollón N G S and Braga S C G N 2013 New materials and trends in sorbents for solid-phase extraction *TrAC Trends Anal. Chem.* **43** 14–23
- [39] Bhardwaj N and Kundu S C 2010 Electrospinning: a fascinating fiber fabrication technique *Biotechnol. Adv.* **28** 325–47
- [40] Yang Z, Peng H, Wang W and Liu T 2010 Crystallization behavior of poly(ϵ -caprolactone)/layered double hydroxide nanocomposites *J. Appl. Polym. Sci.* **116** 2658–67
- [41] Yudanova T N, Filatov I Y and Afanasov I M 2016 Production of ultrafine cellulose acetate fibers *Theor. Found. Chem. Eng.* **50** 508–12
- [42] Dzenis Y 2004 Spinning continuous fibers for nanotechnology *Science* **304** 1917–9
- [43] Shabafrooz V, Mozafari M, Vashaei D and Tayebi L 2014 Electrospun nanofibers: from filtration membranes to highly specialized tissue engineering scaffolds *J. Nanosci. Nanotechnol.* **14** 522–34
- [44] Hemamalini T, Karunakaran S A, Siva Elango M K, Senthil Ram T and Giri Dev V R 2019 Regeneration of cellulose acetate nanofibrous mat from discarded cigarette butts *Indian J. Fibre Text. Res.* **44** 248–52
- [45] Kimmer D, Vincent I, Lovecka L, Kazda T, Giurg A and Skorvan O 2017 Some aspects of applying nanostructured materials in air filtration, water filtration and electrical engineering *AIP Conf. Proc.* **1843** 060001
- [46] Chigome S and Torto N 2011 A review of opportunities for electrospun nanofibers in analytical chemistry *Anal. Chim. Acta* **706** 25–36
- [47] Chigome S, Darko G and Torto N 2011 Electrospun nanofibers as sorbent material for solid phase extraction *Analyst* **136** 2879–89
- [48] Niavarani Z, Breite D, Prager A, Abel B and Schulze A 2021 Estradiol removal by adsorptive coating of a microfiltration membrane *Membranes* **11** 1–13
- [49] Wang M, Qu F, Jia R, Sun S, Li G and Liang H 2016 Preliminary study on the removal of steroidal estrogens using TiO₂-doped PVDF ultrafiltration membranes *Water* **8** 1–12
- [50] Kimmer D, Vincent I, Fenyk J, Petras D, Zatloukal M, Sambaer W and Zdimal V 2011 Morphology of nano and micro fiber structures in ultrafine particles filtration *AIP Conf. Proc.* **1375** 295–311
- [51] Szewczyk P K, Ura D P, Metwally S, Knapczyk-Korczak J, Gajek M, Marzec M M, Bernasik A and Stachewicz U 2018 Roughness and fiber fraction dominated wetting of electrospun fiber-based porous meshes *Polymers* **11** 34
- [52] Yasir M, Šopík T, Kimmer D and Sedlářik V 2021 Facile hplc technique for simultaneous detection of estrogenic hormones in wastewater *Nanocon Conf. Proc.—Int. Conf. Nanomater (2021 October 2021)*, pp 272–6
- [53] Qi F F, Cao Y, Wang M, Rong F and Xu Q 2014 Nylon 6 electrospun nanofibers mat as effective sorbent for the

- removal of estrogens: kinetic and thermodynamic studies *Nanoscale Res. Lett.* **9** 1–10
- [54] Al-Khateeb L A, Obaid A Y, Asiri N A and Abdel Salam M 2014 Adsorption behavior of estrogenic compounds on carbon nanotubes from aqueous solutions: kinetic and thermodynamic studies *J. Ind. Eng. Chem.* **20** 916–24
- [55] Taha A A, Na Wu Y, Wang H and Li F 2012 Preparation and application of functionalized cellulose acetate/silica composite nanofibrous membrane via electrospinning for Cr(VI) ion removal from aqueous solution *J. Environ. Manage.* **112** 10–6
- [56] Tian Y, Wu M, Liu R, Li Y, Wang D, Tan J, Wu R and Huang Y 2011 Electrospun membrane of cellulose acetate for heavy metal ion adsorption in water treatment *Carbohydrate Polym.* **83** 743–8
- [57] Celebioglu A, Demirci S and Uyar T 2014 Cyclodextrin-grafted electrospun cellulose acetate nanofibers via 'click' reaction for removal of phenanthrene *Appl. Surf. Sci.* **305** 581–8
- [58] Mikaeili F and Gouma P I 2018 Super water-repellent cellulose acetate mats *Sci. Rep.* **8** 1–8
- [59] Karbownik I, Rac-Rumijowska O, Fiedot-Toboła M, Rybicki T and Teterycz H 2019 The preparation and characterization of polyacrylonitrile-polyaniline (PAN/PANI) fibers *Materials* **12** 664
- [60] Han X J, Cheng B J, Li Y J, Huang Z M, Huang C, Du Z F and Wang J 2015 The effects of electrospinning parameters on coaxial polyacrylonitrile/polyurethane nanofibers: morphology and water vapour transmission rate *Fibers Polym.* **16** 2237–43
- [61] Sundaran S P, Reshmi C R and Sujith A 2018 Tailored design of polyurethane based fouling-tolerant nanofibrous membrane for water treatment *New J. Chem.* **42** 1958–72
- [62] Kwak N S, Jung W H, Park H M and Hwang T S 2013 Electrospun polyethersulfone fibrous mats: sulfonation, its characterization and solution-phase ammonium sorption behavior *Chem. Eng. J.* **215–216** 375–82
- [63] Xu Y, Bao J, Zhang X, Li W, Xie Y, Sun S, Zhao W and Zhao C 2019 Functionalized polyethersulfone nanofibrous membranes with ultra-high adsorption capacity for organic dyes by one-step electrospinning *J. Colloid Interface Sci.* **533** 526–38
- [64] Han J, Qiu W, Hu J and Gao W 2012 Chemisorption of estrone in nylon microfiltration membranes: adsorption mechanism and potential use for estrone removal from water *Water Res.* **46** 873–81
- [65] Benavente M J, Caballero M J A, Silvero G, López-Coca I and Escobar V G 2019 Cellulose acetate recovery from cigarette butts *Proceedings.* **2** 1447
- [66] Nasir M, Subhan A, Prihandoko B and Lestariningsih T 2017 Nanostructure and property of electrospun SiO_2 -cellulose acetate nanofiber composite by electrospinning *Energy Proc.* **107** 227–31
- [67] Vazquez-Velez E, Lopez-Zarate L and Martinez-Valencia H 2020 Electrospinning of polyacrylonitrile nanofibers embedded with zerovalent iron and cerium oxide nanoparticles, as Cr(VI) adsorbents for water treatment *J. Appl. Polym. Sci.* **137** 1–10
- [68] Luo Z, Li H, Yang Y, Lin H and Yang Z 2017 Adsorption of 17α -ethinylestradiol from aqueous solution onto a reduced graphene oxide-magnetic composite *J. Taiwan Inst. Chem. Eng.* **80** 797–804
- [69] Günay A, Arslankaya E and Tosun I 2007 Lead removal from aqueous solution by natural and pretreated clinoptilolite: adsorption equilibrium and kinetics *J. Hazard. Mater.* **146** 362–71
- [70] Ersali S, Hadadi V, Moradi O and Fakhri A 2013 Pseudo-second-order kinetic equations for modeling adsorption systems for removal of ammonium ions using multi-walled carbon nanotube *Fullerenes, Nanotube Carbon Nanostructures* **14** 1217112133007
- [71] Esmaeeli F, Gorbanian S A and Moazezi N 2017 Removal of estradiol valerate and progesterone using powdered and granular activated carbon from aqueous solutions *Int. J. Environ. Res.* **11** 695–705
- [72] He J, Zhou Q, Guo J and Fang F 2018 Characterization of potassium hydroxide modified anthracite particles and enhanced removal of 17α -ethinylestradiol and bisphenol A *Environ. Sci. Pollut. Res.* **25** 22224–35
- [73] Porter J J and Porter R S 1995 Filtration studies of selected anionic dyes using asymmetric titanium dioxide membranes on porous stainless-steel tubes *J. Membr. Sci.* **101** 67–81
- [74] Auriol M, Filali-Meknassi Y, Adams C D and Tyagi R D 2006 Natural and synthetic hormone removal using the horseradish peroxidase enzyme: temperature and pH effects *Water Res.* **40** 2847–56
- [75] Behera S K, Kim H W, Oh J E and Park H S 2011 Occurrence and removal of antibiotics, hormones and several other pharmaceuticals in wastewater treatment plants of the largest industrial city of Korea *Sci. Total Environ.* **409** 4351–60
- [76] Bayode A A et al 2021 Carbon-mediated visible-light clay- Fe_2O_3 -graphene oxide catalytic nanocomposites for the removal of steroid estrogens from water *J. Water Proc. Eng.* **40** 101865
- [77] Pinto A M, Moreira S, Gonçalves I C, Gama F M, Mendes A M and Magalhães F D 2013 Biocompatibility of poly(lactic acid) with incorporated graphene-based materials *Colloids Surf. B* **104** 229–38

Research article

Adsorption of estrogenic hormones in aqueous solution using electrospun nanofibers from waste cigarette butts: Kinetics, mechanism, and reusability

Muhammad Yasir*^{ID}, Tomáš Šopík^{ID}, Rahul Patwa^{ID}, Dušan Kimmer^{ID}, Vladimír Sedlařík^{ID}

Centre of Polymer Systems, University Institute, Tomas Bata University in Zlín, Třída Tomáše Bati 5678, 76001 Zlín, Czech Republic

Received 9 December 2021; accepted in revised form 14 February 2022

Abstract. This study emphasizes rapid and simultaneous adsorptive removal of estrogenic hormones (EH): estrone (E1), estradiol (E2), ethinylestradiol (EE2), and estriol (E3) from wastewater using recycled waste cigarette electrospun fibers (WCENFs). The submicron fibers exhibited a strong affinity towards all EH due to abundant hydrogen bonding interactions. The adsorption kinetics pseudo-first-order, pseudo-second-order, intra-particle diffusion, Elovich, and fractional power models were explored and fitted towards optimum conditions for the large-scale removal process of the EH. Results showed that E1, E2, and EE2 followed pseudo-second-order kinetics while E3 followed the pseudo-first-order kinetic model. In combination, the total adsorption capacity achieved was 2.14 mg/g, whereas the individual values for E1, E2, EE2, and E3 were 0.551, 0.532, 0.687, and 0.369 mg/g, respectively. The percentage efficiency of WCENFs was highest with EE2 ~64.3% and least with E3 ~34.6%. The WCENFs could repeatedly be used for four adsorption-desorption cycles as an effective adsorbent for the simultaneous removal of four EH via batch adsorption studies. According to the results obtained, the repurposing of waste cigarette butts to WCENFs presented itself as a suitable alternative for removing EH and possibly other organic pollutants from water.

Keywords: industrial application, water treatment, estrogens removal, adsorption kinetics

1. Introduction

Reportedly, over 5.5 trillion cigarettes are produced a year globally, with 4.5 trillion waste cigarette butts (CBs) causing approximately 2 million tons of littered butts a year without proper disposal [1, 2]. Cigarette smoking not only causes significant health damage to the smoker but also to the passive smoker, ultimately leading to continuous air pollution. The open disposal of CB in public areas such as bus stops, stations, parks, and gardens pollutes soil and water [3]. It degrades the chemical, physical and biological conditions of nature [1, 4]. The available cigarette in the market consists of 95% cellulose acetate (CA) [5]; the remaining are paper, polyvinyl alcohol, and tobacco.

CB is approximately 30% in length and contains monofilament tow of CA combined with some additives and chemicals. The accumulation of traces of tobacco in these CBs and their disposal as wastes is a severe issue and a major threat to the ecosystem since they are non-degradable. These CB wastes are flushed away by rain drained into rivers, seas, and further into the oceans, which is devastating for marine life [6] as the contaminants of CBs are likely to enter the food chain. It is considered one of the most critical waste due to its high dispersion worldwide, causing severe health effects on the lives of humans [7]. Thus, it is necessary to identify a new method of recycling and repurposing CBs to counter this inevitable waste [8].

*Corresponding author, e-mail: yasir@utb.cz

© BME-PT

Estrogenic hormones (EH) include estrone (E1), estradiol (E2), ethinylestradiol (EE2), and estriol (E3), also called endocrine-disrupting chemicals (EDCs), have adverse effects on humans and wildlife [9]. Residual of these micropollutants are present in micro and nanograms concentrations in local cleaning reservoirs of wastewater treatment [9]. In general, these EH (natural and synthetic) are majorly from anthropogenic sources, antibiotics, contraceptive pills, chemotherapy drugs and are present in excreting of humans and animals (feces and urine). These EH are released into the environment (*e.g.*, reservoirs, rivers, and lakes) via insufficiently treated effluents [10, 11]. For example, EH in the range of 3.4–41 ng/l has been reported in constructed wetlands of the Czech Republic [12]. At such high concentrations, they may harm the reproduction tendency of aquatic species and interrupt natural body hormones' function [13]. Studies have shown an increase in fish femininity, testicles weight loss in quails, and fertility disorder in alligators, which are a few of the many side effects [14]. Furthermore, a decline in male sperm count high breast and ovarian cancer risks in humans have been reported [15]. Amongst all EH, EE2 is the most dangerous due to its partial degradation, while its treatment and inadequate removal lead to colossal estrogenicity [16]. This issue has aroused deep concerns in the scientific world because these synthetic EH can interfere with functional groups of hormones synthesized naturally inside the body by mimicking them [17–21]. Thus, the presence of these EH is a severe threat to both human and aquatic life based on the source of food or drinking water [13, 21]. Hence, the EH require proper concurrent disposal and elimination from wastewater.

The conventional wastewater treatment plants cannot properly remove these hormones with low molecular weight and low biodegradability because they are difficult to be detected and quantified at extremely low concentrations [22]. Reportedly, various treatments have been applied, such as ozonation, membrane bioreactors, advanced oxidation, membrane filtration, photocatalytic degradation, and coagulation-flocculation, to counter this issue [23–25]. Each technique has some limitations, such as complexity, low efficiency, and by-products generated during the procedure require further sophisticated purification steps. Nano-filtration and reverse osmosis have also emerged as interesting methods, but the intense energy requirements make them unfeasible for selection

[26, 27]. Adsorption is one such promising technique that has been found to address the issue of EH removal.

In addition to the sorption technique, the sorbent material is the most important and dominant factor. Several adsorbents have been reported for EH removal in previous studies, such as granules of activated charcoal [28, 29], fullerene [30, 31], carbon nanotubes [32], chitosan, activated carbon, chitin, multi-walled carbon nanotubes, carbon-based adsorbents prepared from industrial waste [33, 34], and activated carbon fibers modified with iron hydroxide [35]. All these materials in particles form are efficient in adsorbing EH when dispersed in solution due to the large surface area. Hence, they require modification and a further operable filtration technique after adsorption from wastewater, which increases the overall cost. Recently, submicron fibers as sorbents have an emerging interest because of their characteristic features such as lightweight, small fiber diameter, small pore size, high aspect ratio, and large specific surface area of fibers providing a greater contact of the solution with the adsorbent to significantly raise the filtration efficiency [36, 37]. In addition, this class of materials has been proven as suitable adsorbents to eradicate the subsequent additional separation step [38, 39]. Thus, the research essentially needs a new high-performance material specifically with an optimum disposal process efficiency. In the context of recycling materials, electrospinning is a versatile technique for generating a continuous fiber sheet with a diameter from tens to hundreds of nanometres for sophisticated solar cells, air purification, and water filtration techniques [40]. Moreover, electrospun polymers have proven to be an excellent choice for removing heavy metal ions, organic pollutants, and dyes from wastewater and have been used in wound healing, orthopedic and anti-bacterial applications [41–44]. Therefore, taking both aspects of recycling and removing organic molecules by efficient use of repurposed waste CBs will keep the environment clean and be an excellent solution to reduce micropollutants from wastewater. Presently, few studies have been done with CBs in different applications such as asphalt production, biofilm carrier, metal corrosion inhibitors [1], insecticides, fired clay brick filler [6], energy storage devices, and removal of bisphenol-A from wastewater [8]. However, modification of the CBs into spun fibers [45] will improve the adsorption efficiency of these materials due to

readily available functional groups (C=O, C–O–C, and C–O–H) to form hydrogen bonding with organic pollutants such as EH [8, 46]. So far, the adsorption of EH, to the best of our knowledge, has been explored to a lesser extent. Recently, few studies on the removal of different EH hormones by polyamide (PA) fibers, polyethersulfone (PES), and polyvinylidene (PVDF) membrane modified with polyvinyl pyrrolidone and titanium dioxide have been reported [9, 13, 47–49]. These studies were restricted to the filtration of single hormones. In our previous study, we reported the use of polyurethane (PU), cellulose acetate (CA), polyacrylonitrile (PAN), PA, and PES fibers for adsorption removal of different EH [50]. Hence, it is necessary to fill this gap by developing fibers produced from recycling CBs at optimum conditions with achieved desired least fiber diameter, thereby increasing surface area making the material an ideal candidate for the simultaneous removal of different EH. This process will not only reduce litter waste created from CBs, but it is a less costly method owing to the electrospinning technique, which requires less energy for the fabrication of fibers [51]. Herein, this paper aims to prepare waste cigarette electrospun nanofibers (WCENFs) for the batch adsorption of four EH (E1, E2, E3, and EE2). The prepared fibers are based on small fiber diameter formation to achieve high surface area and aspect ratio, thereby creating more sites available for adsorption. The objective is to focus on single and simultaneous adsorption of various EH in a one-step process. Further, to investigate the feasibility of the results using the experimental data, adsorption capacity and apply different kinetic models such as pseudo-first-order, pseudo-second-order, intraparticle diffusion, Elovich, and fractional power models were evaluated. These models help to understand the characteristics of adsorption kinetics that are essential for the selection of optimum conditions for the large-scale removal application of EH. The study also includes establishing the fibers' adsorption mechanism to understand interactions between WCENFs and EH. Then, the reusability in several adsorption-desorption cycles to assess the reliable effectiveness of this material. Finally, a comparative study on the instant adsorption efficiency of prepared PET/WCENFs (polyethylene terephthalate) syringe film against commercially available CA syringe film was analyzed.

2. Materials and methods

2.1. Materials and reagents

The CBs, regardless of brand, were collected over a week from the cigarette waste bins of Centre of Polymer Systems (CPS), Tomas Bata University in Zlin, Czech Republic. Four EH *viz.* estrone (E1) $\geq 99\%$, 17β -estradiol (E2) $\geq 98\%$, estriol (E3) $\geq 97\%$, and 17α -ethinylestradiol (EE2) $\geq 98\%$ were purchased from Sigma-Aldrich Chemie GmbH, Germany. Butylated hydroxytoluene (BHT) and Swinnex film holders with Luer lock (25 mm diameter) were purchased from Sigma-Aldrich, Germany. Tetrahydrofuran (THF) were obtained from Carl Roth Rotisolv[®] HPLC (Karlsruhe, Germany). Acetonitrile (HPLC grade) and ethanol (HPLC grade $>99\%$ pure) were purchased from Honeywell and VWR, Czech Republic, respectively. Furthermore, sodium tetra-borate decahydrate (borax), citric acid, acetic acid (99%), and formic acid (98%) were purchased from PENTA s.r.o., the Czech Republic, and *N,N*-dimethylformamide (DMF $>99.5\%$) from Lach-Ner, s.r.o., Czech Republic. Polyethylene oxide (PEO) from Scientific Polymer Products, Inc., Ontario, the USA. Deionized water (18.3 M Ω /cm, pH 7.3) was sourced from a Milli-Q ultra-pure (type 1) water purification system, Biopak[®] Polisher, Merck, the USA, and was used throughout the study.

2.2. Submicron-fibers fabrication

CBs were washed twice with distilled water to remove unwanted debris dust and dried in a hot-air oven for 6 h at 80 °C. Further, they were washed with ethanol and kept at 40 °C for 4 h. A total of 8 wt% of CBs were dissolved in a binary solution of acetic acid and formic acid in a ratio (2:1) to make a total solution of 400 g. Then, 3 wt% of PEO of the amount of the CBs was added for stability of the mixture to improve the structural properties of fibers. Finally, the mixture was stirred for 5 h at 400 rpm in a mechanical stirrer (Heidolph, RZR 2041). Electrical conductivity was adjusted to about 88.1 μ S/cm by using a solution of borax and citric acid (BC) in a ratio (1:3), prior to electrospinning; this solution was prepared by dissolving 35 wt% of BC in DMF solution and stirring for 5 h at 400 rpm on a magnetic stirrer and viscosity of the solution during the preparation was kept at 0.95 Pa·s.

The electrospinning process was performed by nano spider technology using the NS Lab 200S equipment

(Elmarco, Czech Republic) to produce WCENFs on a polypropylene (PP) spun-bond non-woven sheet with a width of 40 cm. The applied supply was 75 kV, solution coming out of the bath to be sprayed from cord strings was set at 0.34 ml/min. The distance between the electrodes was 18 cm, the rotational speed of collecting fiber sheet fabric was 10 cm/min, and the temperature was 27 ± 1 °C with the relative air humidity <35%. The solution properties were optimized before the electrospinning process, and the properties of the WCENFs are shown in Table 1.

The table shows the optimized properties of the polymer solution prepared from CBs for electrospinning and the average area mass of produced electrospun fibers. The aim of optimizing these parameters was to prepare the least diameter, defect-free, and beadless submicron fibrous mats from waste CBs.

2.3. Characterization

Morphological analysis was carried out using Nova 450 scanning electron microscope (SEM) (FEI, Thermo Fisher Scientific, USA) at 5–10 kV applied potential using a through-the-lens detector (TLD). It was done to observe the fiber surface morphology, the diameter size of fibers, and the defects in the structures such as beads. The software ImageJ version 1.52a was used to determine the average fiber diameter of samples.

X-ray diffractogram (XRD) of WCENFs was recorded using Miniflex™ 600 X-ray diffractometer (Rigaku, Japan), having $\text{CoK}\beta$ ($\lambda = 1.79$ Å) as a source. The angle 2θ was in the range from 5–90° with operating current, step size, step time, and operational voltage set to 15 mA, 0.02°, 10°/s, and 40 kV, respectively. The diffractograms obtained using Co source were converted to Cu using PowerDLL software converter 2.93 to compare data in the prior art.

To determine the functional groups present in WCENFs used for the adsorption of EH, Nicolet 320 Fourier transformed infrared spectroscopy (FTIR) (ThermoScientific, USA) equipped with Ge crystal was used. The attenuated total reflectance (ATR)

spectra were recorded from 400–4000 cm^{-1} at ambient temperature with a scan rate of 16 and a resolution of 4 cm^{-1} .

The surface area analysis of WCENFs was made utilizing the Brunauer-Emmett-Teller (BET) high precision surface area and pore size analyzer BELSORP-mini II (BEL Japan, Inc., Japan) to determine the specific surface area. The substrate's outgassing was done at 100 °C for 12 h under vacuum before starting measurement. Air permeability and pore size distribution of submicron structure were assessed by flow porometer according to ASTM F316-03 (2011). Galpor (Porometer NV, Belgium) was used as a wetting liquid.

To determine the contact angle of the electrospun fibers, they were made more compact for accurate measurement. First, the WCENFs on the PP substrate was placed upside-down on the PET sheet and subjected to thermal press for 10 seconds at a temperature of 120 °C, and then, PP was detached. Next, the WCENFs on PET were covered with a glossy sheet for a thermal press again with the same conditions to acquire a smooth and more compact surface. This step was done so that liquid could stay on the surface for angle measurement; otherwise, the surface would not hold the drop in the case of WCENFs alone or with PP substrate, and it would instantly settle down and penetrate through the structure. Finally, the contact angle of electrospun fibers was measured using the sessile drop technique on a goniometer (Surface Energy Evaluation System (SEE System), Advex Instruments, Brno, Czech Republic) at ambient temperature. A 5 μl pipette was used to drop liquid on the sample surface (10×10 mm^2), the drop shape was observed using a CCD camera, and the angle was measured instantly. Glycerol and Milli Q water were used as the probe liquids to determine hydrophilicity. The samples were analyzed in triplicates, and the mean values with standard deviation were reported.

The thermal stability of the fibers was determined using a TGA Q500 thermogravimetric analyzer (TA Instruments, USA). Sample mass ($\sim 19.0 \pm 0.5$ mg),

Table 1. Representative properties of the solution prior to electrospinning and of produced WCENFs compared with CA fibers [50].

Sample	Concentration [%]	Density [g/cm^3]	Intrinsic viscosity [$\text{Pa}\cdot\text{s}$]	Electrical conductivity [$\mu\text{S}/\text{cm}$]	Average area mass [g/m^2]
WCENFs	8	1.320	0.95	88.1	0.865
CA	9	1.315	1.64	83.4	1.630

depending on its density, was heated in alumina crucible from 25 to 700 °C at a ramp of 15 °C/min under N₂ flow of 100 ml/min. To determine the thermal behavior and properties of WCENFs, they were subjected to differential scanning calorimeter (DSC) star[®]System (Mettler Toledo, Switzerland). The sample mass (5.0±0.5 mg) was sealed in an aluminum pan under a nitrogen flow of 50 ml/min and heated from 25 to 320 °C at a ramp of 10 °C/min. Gel permeation chromatography (GPC) used a Waters HPLC system equipped with a Waters model e2695 and a Waters model 2414 differential refractometer to determine the average molar mass (M_w), number average molar mass (M_n), and polydispersity index ($PDI = M_w/M_n$) of the tested WCENFs samples from peaks corresponding to the polymer fraction using the absolute calibration method (Waters Corporation, Milford, USA). The WCENFs was dissolved in THF (2–3 mg/ml), stabilized with BHT (240 mg/l), and filtered through a 0.45 µm syringe filter. The following procedure was used to separate the samples on a series of gel-mixed bed columns (Polymer Laboratories Ltd, Shropshire, UK): 1 × PLgel-Mixed-A bed column (300×7.5 mm, 20 µm), 1 × PLgel-Mixed-B bed column (300×7.5 mm, 10 µm), and 1 × PLgel-Mixed-D bed column (300×7.5 mm, 5 µm); at 40 °C, the mobile phase contained THF stabilized with BHT (240 mg/l). The mobile phase flow rate was set to 1.0 ml/min, and the injection volume was 100 µl. All data processing was carried out using Empower 3 software. To see the strength of fibers, the tensile test of neat PP and PP substrate with WCENFs was performed and compared because pure WCENFs were very fragile, it was difficult to peel them from the PP sheet to prepare a dumbbell shape and perform a tensile test. Further to test the WCENFs as syringe film in the last section, PET was used as a support substrate for WCENFs. Therefore, the tensile tests of PP, PP/WCENFs, and PET/WCENFs were carried out on an M350-5CT tensile testing machine (Testometric, UK) supplied with a load cell of 10 kgf. For all measurements, a crosshead pull speed of 10 mm/min and a gauge length of 20 mm was used. A unique die was used to cut specimens in the shape of dumbbells (Type 3, ISO 37:2005). Young's elastic modulus [MPa], ultimate tensile strength [N/mm], percentage elongation [%], and other mechanical properties were obtained. Measurements were conducted in triplicates, and mean values with standard deviation were reported.

2.4. High-performance liquid chromatography (HPLC) analytical method

A HPLC DionexUltiMate 3000 Series (Thermo Fisher Scientific, Germany) was used to analyze EH (E1, E2, EE2, E3) calibration standards and samples. The separation was carried out at 30 °C on a Kinetex 2.6 µm C18 100 A (150×4.6 mm; Phenomenex, USA) reversed-phase column with a pre-column security guard ULTRA, UHPLC C18 (Phenomenex, USA). A mobile phase of acetonitrile and water (45:55, vol/vol) was utilized at a flow rate of 0.8 ml/min for a total isocratic run of 12 min. A volume of 20 µl was injected into the column, and the sampler chamber was set at 5 °C. The eluates were recorded, and the EH concentrations were determined using the 200 nm test results. The external calibration method for EH concentration quantification was performed using the Chromeleon version 7.2 software (Thermo Fisher Scientific, USA) [52].

2.5. Solution preparation and sampling

Preliminary experiments were carried out to determine the exact concentration when all four EH were completely dissolved together in a mixture. The solubility of individual hormones was lower than the values available in the literature. When 1 mg/l concentration of each EH was prepared separately, it was observed that E1 partially remained undissolved after 24 h of stirring, with some solute particles staying at the bottom of the container. A similar observation was reported by Han *et al.* [13] that it took 12 days for E1 to reach a plateau concentration of 0.61 mg/l. Therefore, considering a solution with a mixture of four different EH, it was necessary to have a lower solution concentration from this value. The method of EH detection and quantification via HPLC was developed earlier. Hence, a solution containing all four EH was prepared by adding 1 mg of each EH in a total of 5 l of water, kept under magnetic stirring at 800 rpm for 24 h, making an overall concentration of 0.8 mg/l solution with the individual concentrations of 0.2 mg/l. For calibration, samples in a concentration of 0.2, 0.15, 0.1, 0.05, 0.03, 0.02, 0.005 mg/l were collected using a micropipette (HTL Lab Solution, Poland) in 1.5 ml screw neck vials (VWR, Czech Republic) after passing through glass microfiber (GMF) filter (Whatman, Czech Republic) with pore size 0.45 µm and 25 mm in diameter before placing in HPLC. A calibration curve was

obtained using mean concentrations from the triplicate values. The calibration vial with a concentration of 0.005 mg/l was used to identify each hormone's detection limit. The limit was set at 0.5, 1.0, 2.0, and 5.0 µg/l for E3, E2, EE2, and E1, respectively [52].

2.6. Batch adsorption test of WCENFs

The experimental kinetics were carried out to determine the adsorption rate. Tests for WCENFs were performed in triplicates using 100 ml of EH solution taken from stock with a total concentration of 0.8 mg/l, and 20 mg of WCENFs were placed in each flask. The flasks were continuously stirred at 250 rpm using an orbital incubator shaker (GFL 3005, MERCI s.r.o., Germany). To determine the remaining concentration of EH present in the solution, samples were drawn at fixed intervals of time each after 5, 15, 30, 60 min, and after each hour until a plateau was reached. At each specified time interval, 4 ml samples were drawn carefully without any contact with fibers using a 20 ml syringe and collected in vials after passing through a 0.45 µm GMF filter. The first 2 ml filtrate was discarded by passing from a syringe through a GMF filter to eliminate any negligible adsorption within the filter and rinse out any remaining liquid from the previous reading while sampling to ensure accuracy and precision. Proper care was taken to ensure that neither fiber was removed nor destroyed during the sampling and was replaced by 4 ml of ultrapure water to maintain the total flask volume. A control flask containing only solution was also placed as a starting reference concentration in the experiment. It must be noted that negligible adsorption was observed on the glass surface of the flask throughout the experimentation, which was calculated by comparing the initial measured concentration with the concentration of control after 9 h of shaking. Then, the results of triplicated experimental values were obtained to calculate mean concentration values and standard deviations that were recorded and reported. Finally, the percentage of adsorption of each EH on WCENFs was calculated with reference to the control. The solution was maintained neutral at a pH of 7.3 using ultrapure deionized water because river water samples are in the pH range of 6–9. The percentage removal of each EH at a given time (t) was measured using the expression shown in Equation (1) [53]:

$$\text{Removal} [\%] = \frac{C_i - C_t}{C_i} \cdot 100 \quad (1)$$

where C_i is the initial concentration [mg/l] and C_t is the concentration of solution at time t [mg/L].

Also, equilibrium adsorption capacity (q_e) and adsorption capacity (q_t) at time t can be calculated by the following expressions shown in Equation (2) and (3):

$$q_e = v \cdot \frac{C_i - C_e}{m} \quad (2)$$

$$q_t = v \cdot \frac{C_i - C_t}{m} \quad (3)$$

where m is the mass of adsorbent in grams, C_e is the concentration of the solution at equilibrium, and v is the volume of solution in liters.

2.7. Desorption and reusability of material

To determine the reversibility of WCENFs sorption, the fibers in triplicates were taken out from the EH solution and washed thoroughly with distilled and deionized water followed by immersion in 50 ml of water and shaken for 20 min at 250 rpm. This step would just clean the surface of fibers and nominally remove some physically adsorbed hormones, but it would not significantly reduce EH concentration on fibers due to chemical bonding [9]. The fibers were then placed in the oven at 30 °C for 6 h to remove the excess moisture, followed by air drying without any effect on fibers. This step was performed in triplicates by immersing the fibers in 40 ml pure anhydrous ethanol, given that all estrogenic hormones have a very high solubility in ethanol based on their high partitioning coefficient ($\log K_{ow} = 3.13, 4.01, 2.45,$ and 3.90 for E1, E2, E3, and EE2, respectively). Then, a strong partition effect was expected to occur in combination with a competing hydroxyl group present in ethanol that could destabilize the EH-fiber hydrogen bonds and attract the adsorbed hydrophobic hormones in the ethanol solution [13, 54]. Next, the solution system was gently stirred for 30 min at 175 rpm for complete elution of EH from the fibers; after that, air-dried at room temperature and placed in a desiccator until used for the next adsorption cycle. The procedure was repeated for several cycles until very low adsorption was expected.

2.8. Instantaneous adsorption test of PET/WCENFs syringe film

To perform the syringe film test, the WCENFs, due to their fragility, were preferably compressed on the PET sheet and used instead of WCENFs alone or with PP sheet because PP can itself adsorb hormones as previously reported at 96.3% of E1 using a 0.2 μm membrane film [13]. In addition, PET is stiffer to hold fiber straight as a film, providing better strength and enduring high pressures during the filtration process [55]. Therefore, the adsorption of EH was first tested on a neat PET mat to see any influence of adsorption. A batch adsorption test was conducted in the same manner as for WCENFs previously, and no adsorption of any EH was observed on PET. The HPLC chromatograms of solution before and after adsorption perfectly overlap, and no decrease was observed in EH concentration (Figure 1). Then, WCENFs compressed on a PET sheet were cut into a 25 mm circular disc in triplicates and placed in the Swinnex film holders.

3. Results and discussion

3.1. Characterization of adsorbent

SEM imaging was carried out for morphological analysis of the electrospun fibers.

Figure 2 illustrates that uniform submicron fibers were produced with minimum possible beads and a relatively narrow fiber diameter distribution of 196 ± 65 nm compared with the CA having 224 ± 35 nm and calculated surface area of $13.6 \text{ m}^2/\text{g}$ [50]. This indicates that WCENFs possess a higher surface area of $15.5 \text{ m}^2/\text{g}$ (Table 2) and more available adsorption

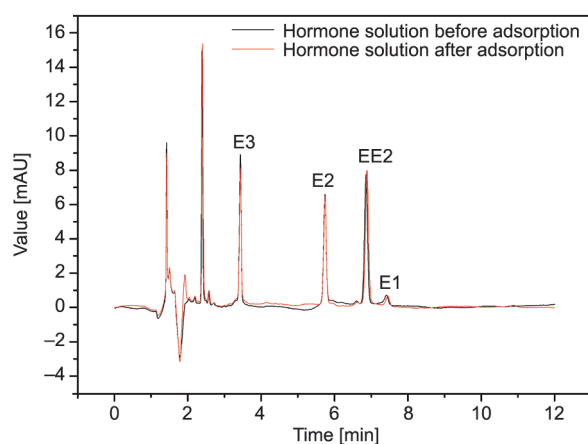


Figure 1. Chromatogram of before and after adsorption on PET with stock solution (0.8 mg/l) containing 0.2 mg/l concentration of each EH (E3, E2, EE2, E1) in a mixture.

sites. Such low average diameter is attributed to properties mentioned in Table 1: lower intrinsic viscosity, low polymer concentration in the solution, and high electrical conductivity prior to electrospinning, which has led to the development of a high surface area of WCENFs. Also, the molecular properties calculated from GPC were $M_n = 90\,000 \text{ g/mol}$, $M_w = 210\,000 \text{ g/mol}$, and $PDI = 2.3$. To further understand the physicochemical properties of the structure, XRD results revealed a broad single peak near $2\theta = 15^\circ$, which denotes that WCENFs are semi-amorphous by nature [56]. The functional groups are further discussed in FTIR. The mean diameter of pores in the submicron structure was $1.4 \mu\text{m}$, and the maximum pore diameter was $2.2 \mu\text{m}$. The permeability of the submicron structure for the dry air was $247 \text{ l}/(\text{min} \cdot \text{bar} \cdot \text{cm}^2)$. Also, the results from the TGA thermograph showed no material degradation was observed up to 110°C , and the degradation temperature was found to be 355.7°C [45]. The initial dip in DSC thermogram could be due to evaporation of water and the graph revealed that the glass transition temperature (T_g) of WCENFs was well above standard room operating temperatures ($\sim 180^\circ\text{C}$) and given that the material's degradation range started around 250°C and was spread over a wide range. The thermogram indicates that the material was thermally stable; therefore, these fibers would not be subjected to any softening and deformation at room temperature during the whole adsorption studies [5, 8]. ImageJ analysis software obtained the average diameter of fibers observed through SEM. Considering the fiber as a single continuous cylinder, the length per unit mass [l/m] and surface area (A) of the fiber can be calculated using the expressions given in Equation (4), and (5) [9]:

$$V = \frac{m}{\rho} = \frac{\pi d^2 l}{4} \quad (4)$$

By rearranging this expression, we get:

$$\frac{l}{m} = \frac{4}{\rho \pi d^2} \quad (5)$$

where V is the volume [m^3], m is the mass [mg], d is the diameter of fiber [m], and ρ is the density of material [$1.32 \text{ g}/\text{cm}^3$].

Since $l \gg d$; therefore, individual cross-sectional area (A) of the end corners of the fibers can be neglected, and the total surface area per unit mass can be expressed as (Equation (6)):

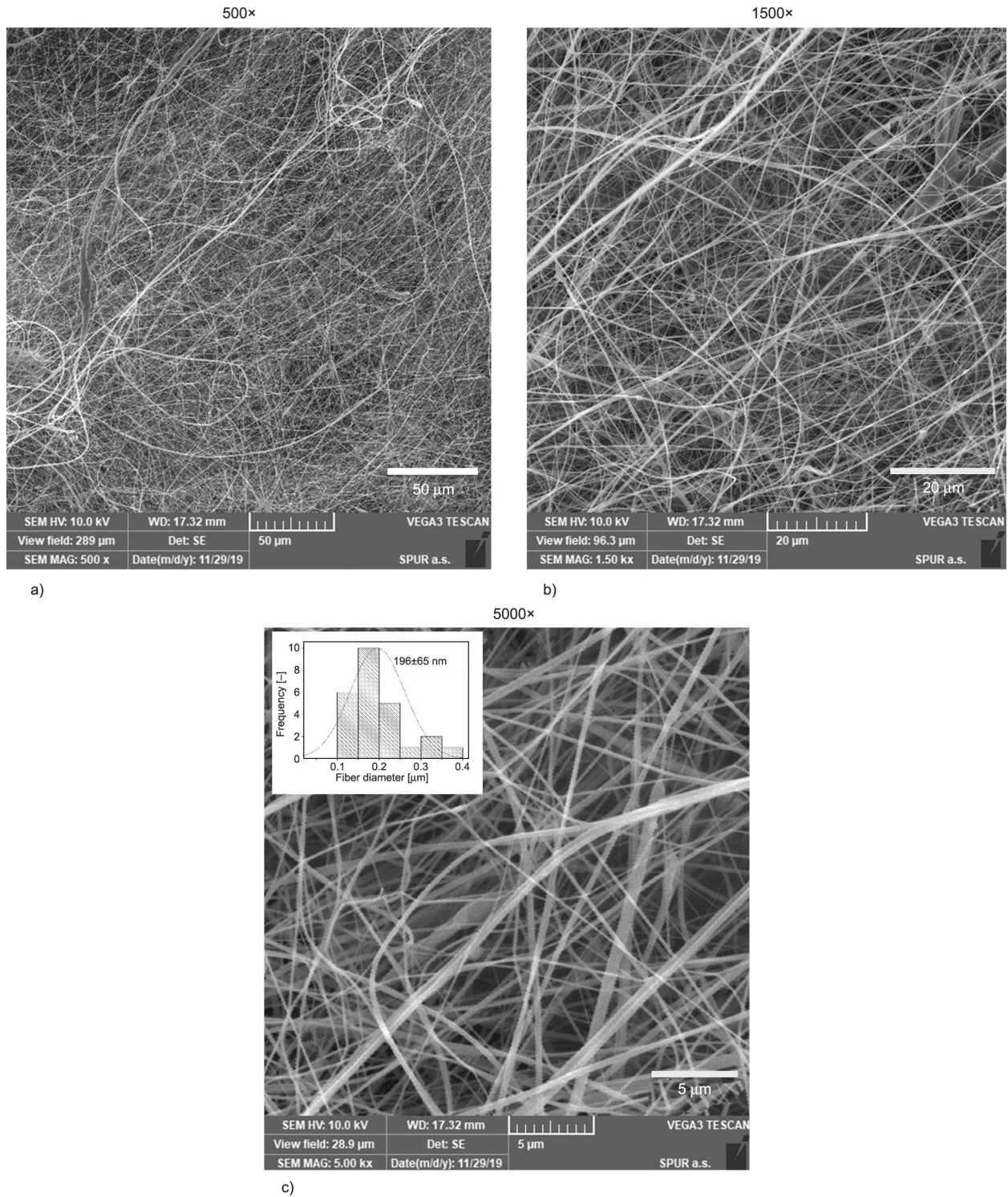


Figure 2. SEM micrograph and (inset) size distribution for WCENFs at different magnification of (a) 500×, (b) 1500× and (c) 5000×.

$$\frac{A}{m} = \frac{d\pi l}{m} = \frac{4}{\rho d} \quad (6)$$

The calculated diameters from the SEM images, calculated fiber length, surface area using the above formulas, the surface area measured by BET, and porosity by porometry are shown in Table 2.

The geometrically determined surface area based on SEM compared to that by BET analysis is well in compliance. The BET surface area is well comparable to the literature values in the range of 9–51 m²/g and the average fiber diameter of 167–2737 nm [9]. The calculated surface area from the average fiber diameter (196 ± 65 nm) considered as cylindrical

Table 2. Characteristics values of WCENFs calculated using SEM micrographs, BET, and porometry.

BET before adsorption		BET after adsorption		Porometry		Fiber analysis from SEM	
Surface area [m ² /g]	18.05	Surface area [m ² /g]	3.61	Mean pore size porometry [μm]	1.4	Average fiber diameter [nm]	196±65
Mean pore diameter [nm]	13.49	Mean pore diameter [nm]	17.19	Maximum pore size porometry [μm]	2.2	Fiber length per unit mass calculated [m/mg]	25 105
Total pore volume [cm ³ /g]	0.061	Total pore volume [cm ³ /g]	0.016	Air permeability porometry [l/(cm ² ·min·bar)]	247	Calculated surface area [m ² /g]	15.5

shape calculated from SEM is 15.5 m²/g. The actual surface area measured from BET is 18.05 m²/g which is slightly higher. The plausible reason for lower calculated surface area value based on geometry compared with BET value could be due to much lower density than the bulk polymer density because of pore formation and other effects during electrospinning. The presence of pores on the fibers' surface is confirmed by BET mean pore diameter (13.49 nm). Furthermore, the estimated surface area is based on the assumption that the fibers have a smooth surface without pores. In reality, solvent evaporation during electrospinning has resulted in a smaller diameter of fibers seen from the SEM micrograph (Figure 2), which has resulted in increased surface area. We can also see that the surface area of fiber decreased after four adsorption cycles from 18.05 to 3.61 m²/g due to interaction with ethanol during desorption cycles that caused swelling (discussed in detail in the reusability section). However, the mean pore diameter increased from 13.49 to 17.19 nm due to the wear-off of material during several desorption cycles. Still, a reduced total pore volume was observed from 0.061 to 0.016 cm³/g, which justifies the adsorption and entrapment of hormones in the fibers during interaction in the batch adsorption study.

The contact angle was measured to determine the hydrophilicity of the fibers. WCENFs mainly contain CA, which has polar hydroxyl groups. Thus, CA is hydrophilic by nature [57]. We observed both the liquids penetrated the WCENFs on PP completely. Therefore, WCENFs were compressed on a PET sheet, and they exhibited contact angle values of 14.6±3.3° with water and 87.3±0.8° with glycerol. It is generally agreed that a hydrophilic surface shows a low water contact angle ($\theta < 90^\circ$). It is reported that the surface roughness, average fiber diameter, and concentration of the polymer in the solution before electrospinning also have a direct influence on the wetting properties [57, 58]. The reported electrospun CA in the literature had a water contact angle of

22.2±0.9°, which is higher compared to the water contact angle of WCENFs (14.6±3.3°) in the current study; This indicates that WCENFs are slightly more hydrophilic compared to electrospun CA in literature [50]. The investigated WCENFs in the present research possess a low contact angle which indicates high hydrophilicity. The hydrophilic nature of WCENFs provides feasibility to the fibers to interact with EH in water and support the adsorption process because the stronger interaction between EH and WCENFs is due to the hydrogen bonding interaction and Van der Waals forces which essentially requires the hydrophilic nature of the fiber [59].

To see the mechanical properties of WCENFs, the stress vs. strain graph below explains Young's modulus, ultimate tensile strength, maximum elongation before fracture, and stress at breakage.

Figure 3 demonstrates the stress vs. strain curve of PP and PP with WCENFs up to the breaking point. It can be seen that Young's modulus has increased from 8.9 to 28.8 MPa, which is evident from the steep slope in the graph, and the ultimate tensile strength has improved to almost 122% (3.1 to 6.9 N/mm²). Similarly, a slight increase in stress at breakage from 0.4 to 1.4 MPa and the total elongation from 19.3 to 19.9 mm was observed, showing that the difference between the two values in each case determined the value of that physical quantity of WCENFs. Similar values of the mechanical properties of electrospun fibers were reported in the literature [51].

However, throughout the batch adsorption study, WCENFs were used alone after peeling off from the PP sheet, which was only used for the collection of fiber. Herein, PP was used as a support material for measuring mechanical properties as alone WCENFs were too fragile and could not maintain shape after peeling off owing to their weak inter-fiber adhesion [51], low average area mass (0.865 g/m²), and thickness (0.003 mm) compared to CA spun fibers with 1.630 g/m² and 0.005 mm, respectively. The mean values for each sample are reported below in Table 3.

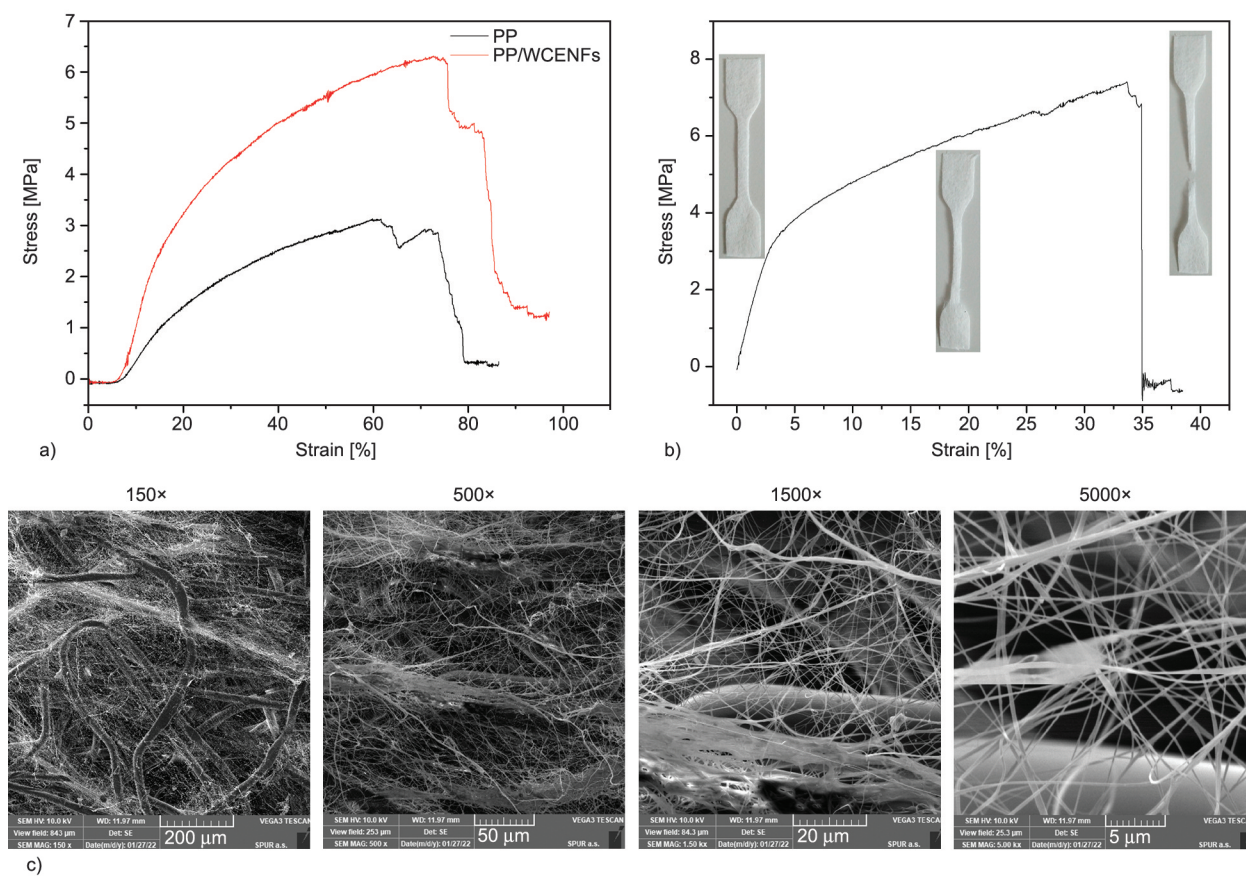


Figure 3. Stress vs. strain curves for (a) PP and PP/WCENFs, and (b) PET/WCENFs along with micrographs after breakage at a different magnification of 150×, 500×, 1500×, and 5000×(c).

Table 3. Summary of mechanical properties of the WCENFs with substrates.

Materials	Thickness [mm]	Young’s modulus, E [MPa]	Ultimate tensile strength, σ [N/mm ²]	Elongation at break, ϵ [mm]	Stress at break [MPa]
PP	0.14±0.01	8.9±4.3	3.1±1.0	19.3±5.1	0.4±0.2
PP/WCENFs	0.17±0.01	28.8±2.4	6.9±1.2	19.9±0.7	1.4±0.2
PET/WCENFs	0.14±0.01	109.0±23.1	7.5±0.9	8.6±1.3	0.1±0.4

Similarly, the mechanical properties were observed for the fabricated PET/WCENFs syringe film, and an improvement in strength and Young’s modulus was reported to be 7.5 N/mm² and 109 MPa, respectively. PET/WCENFs film was used for the syringe adsorption test to compare the removal percentage with the commercial CA syringe film. Herein, WCENFs were embedded on a PET sheet of thickness 0.43 mm by the thermal press. The significant increase in each mechanical property is illustrated in Table 3, and micrograph images at different magnifications are represented in Figure 3 to see the behavior at the time of fracture. It can be seen that the strength for elongation is primarily provided by the PET sheet, which breaks following the ductile failure, whereas WCENFs were relatively brittle. They gradually broke after a slight elongation when the

fiber chain straightened up (evident at 500× and 1500× magnification) owing to their non-woven and non-crosslinked structure [44]. It can be seen that only a few fiber threads remained intact over a long elongation. The results also reveal that the PET/WCENFs film can be used for continuous filtration removal of hormones in future research.

3.2. Batch adsorption study of EH on WCENFs

The study of four EH (E1, E2, EE2, E3) was conducted with a total concentration of 0.8 mg/l and 20 mg of WCENFs. Figure 4a below shows the batch adsorption study of each hormone on WCENFs for a period of time till no further significant adsorption was observed and the material reached almost saturation.

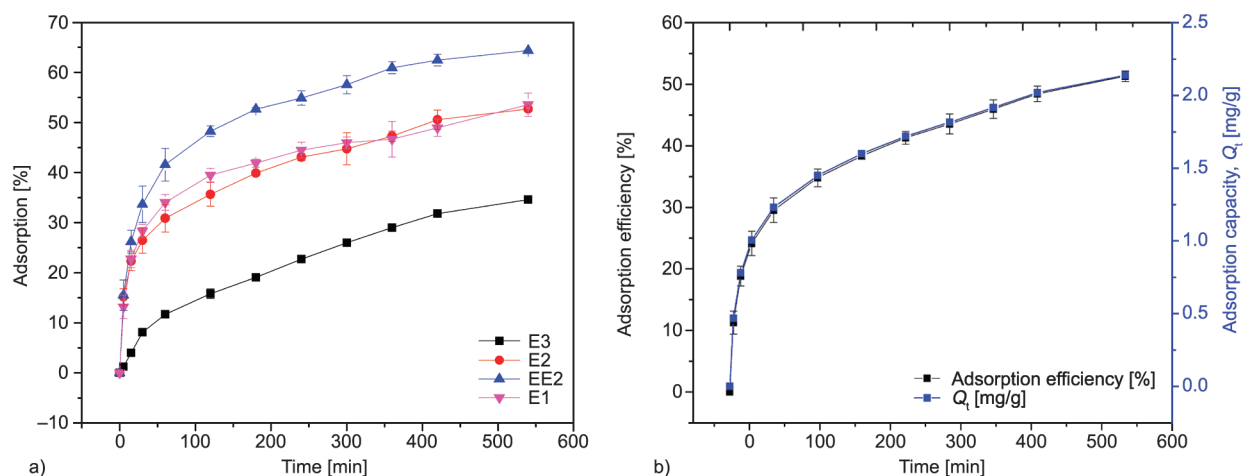


Figure 4. (a) Batch adsorption study of each EH on WCENFs from a combined solution, (b) cumulative adsorption removal efficiency as a function of time of EH (E1, E2, EE2, E3) together on WCENFs on the primary y -axis, and the total adsorption capacity (Q_t) of WCENFs as a function of time on the secondary y -axis.

Figure 4a depicts WCENFs adsorption behavior with each hormone, and as can be seen, the ascending order of adsorption of EH is as $E3 < E2 < E1 < EE2$ with removal efficiencies of 34.6, 52.7, 53.6, and 64.3%, respectively. WCENFs showed the best sorption of EE2 and the worst sorption of E3 hormone. It could also be concluded that WCENFs can readily adsorb EE2, E2, and E1, while gradually adsorb E3. The low percentage removal of E3 could be attributed to its low $\log K_{ow}$ value; 2.45, compared to E1, E2, and EE2; 3.43, 3.94, and 4.15, respectively. $\log K_{ow}$ is a parameter used to determine the value of hydrophobicity for EH by measuring the partitioning between water and octanol. The values are ranged between -3 (very hydrophilic) and $+10$ (extremely hydrophobic). Generally, the values above 2.5 indicate that the material would accumulate in the solid phase and not be dissolved in an aqueous medium. Therefore, its interaction with the membrane would be hydrophobic. High $\log K_{ow}$ values tend to adsorb more readily to organic matter because of their low affinity for water [59]. The adsorption of these estrogens is directly dependent on their hydrophobic nature, which is specified by the higher value of K_{ow} [60]. Furthermore, E3 follows a different kinetic trend than the other EH because the adsorption is gradual throughout the experiment. While for other EH, most of the adsorption occurs within 30 min from the starting time. WCENFs have similar adsorption behavior for all EH compared to the CA fibers, which also follows adsorption efficiency in decreasing order of $EE2 > E1 > E2 > E3$. However, the removal efficiencies of EH with WCENFs are

more significant than CA electrospun fibers [50]. Hence, it can be concluded that electrospun WCENFs can be sufficiently responsible for the adsorption of each EH simultaneously.

Figure 4b above shows the percentage of total cumulative adsorption of EH on WCENFs and the total adsorption capacity of WCENFs in a given time. The results show that the total equilibrium removal efficiency lies at 51.3%. It is evident from the graph that WCENFs had a high adsorption tendency and fast adsorption rates reaching nearly half of their efficiency within the first 30 min, as represented by the steep initial slope of the graph corresponding to the removal efficiency mark of about 25%. However, the trend of gradient changed from steep to steady after almost 60 min of the continuous adsorption experiment and remained the same till the end.

The total adsorption capacity (Q_t) as a function of time is also demonstrated in Figure 4b with a secondary y -axis. The results indicate that the cumulative of four EH adsorption capacities increased similarly for WCENFs until equilibrium was established between the adsorbates and adsorbent. The time to reach equilibrium depends on the concentration of adsorbate and the amount of adsorbent. Both factors were kept constant to compare the capacities with the literature. However, it was still necessary to increase the amount of adsorbent to enhance the removal efficiency with a lesser time. The equilibrium adsorption capacity of WCENFs was found to be 2.14 mg/g, and adsorption capacities of E1, E2, EE2, and E3 were found to be 0.551, 0.532, 0.687, and 0.369 mg/g, respectively. Compared to the literature,

Yasir *et al.* [50] in previous research reported the equilibrium adsorption capacity of CA to be 2.095 mg/g and individual adsorption capacities of E1, E2, EE2, and E3 to be 0.506, 0.532, 0.668, and 0.389 mg/g, respectively. Therefore, the results of WCENFs are well in the range and strongly comply with the literature values of CA, which indicates that WCENFs are better in adsorption than electrospun CA fibers. Additionally, the as-prepared WCENFs are a cost-effective and efficient substitute.

Additionally, in the previous work, the highest equilibrium adsorption capacity was observed for PU Elastollan of 2.51 mg/g and the lowest for PAN of 1.51 mg/g. Furthermore, the reported adsorption capacities for E1, E2, EE2, and E3 were 0.801, 0.592, 0.736, and 0.382 mg/g for PU Elastollan and 0.396, 0.370, 0.343, and 0.397 mg/g for PAN, respectively [50].

Moreover, EE2 was found to have a strong affinity for adsorption as a result; highest adsorption capacity compared to the other three EH for all the other polymers mentioned in the literature. The adsorption capacities for MWCNTs in literature were found to be 0.423, 0.472, and 0.472 mg/g, and for the activated sludge were 2533.34, 2020.78, and 2234.09 ng/g for E1, E2, and EE2, respectively, which are lower values compared to the current research. Furthermore, the value for removing E1 was 62 ng/g when a hydrophobic hollow fiber membrane was used [60]. Thus, comparing the present study's adsorption capacity with the previous research works proves the suitability of WCENFs as a potential adsorbent for removing these EH comparing the other solid particles and membrane adsorbents. Hence, it is evident that WCENFs have a pretty high adsorption capacity and is a useful polymeric material for reusing it for these EH adsorption.

3.3. Adsorption kinetics

The removal of EH on WCENFs by adsorption increased with time, obtaining a maximum value for reaching equilibrium. The adsorption rate was fast initially until 30 min and gradually decreased as the contact time increased to an assuming plateau at 540 min. The results obtained from the experiment were used for studying the factors affecting the adsorption process and the rate-limiting step in this process, such as transfer of mass and type of chemical interaction processes. In addition, kinetics information helps select optimum conditions for full-scale

removal of the EH process. However, it is often difficult to determine the kinetic parameters and explain the mechanisms involved in the complex heterogeneous systems because the surface effects can superimpose on the chemical effects. Therefore, to further understand the adsorption behaviors and mechanism, parameters from five models; Pseudo-first-order, Pseudo-second-order, and Weber-Morris intra-particle/membrane diffusion, Elovich and fractional power model equations were used to test the experimental data to examine the adsorption kinetics of four EH uptaken by WCENFs. These models are used best to describe the liquid/solid systems. The pseudo-first-order by Lagergren is a widely used and most common model for any adsorption study of different solutes in an aqueous solution. It explains that the rate of sorption of EH on the surface of the fibers is proportional to the number of hormones adsorbed from the solution phase, and it can be expressed by Equation (7) as [53]:

$$q_t = q_e (1 - \exp(-k_1 t)) \quad (7)$$

where q_t is the amount of hormone adsorbed per unit mass at time t [mg/g], q_e is the amount of hormone adsorbed per unit mass at equilibrium [mg/g], and k_1 is the first-order rate constant [1/min].

The pseudo-second-order equation is related to the solid phase adsorption capacity and can usually predict kinetics behavior over a long adsorption range. In this model, surface adsorption is the rate-determining step involving chemisorption because of physicochemical interactions between the solid and liquid phases [61]. Therefore, the linear form of Equation (8) can be expressed as:

$$\frac{t}{q_t} = \frac{1}{k_2 q_e^2} + \frac{t}{q_e} \quad (8)$$

where k_2 is the reaction rate constant [g/(mg·min)]. Usually, the adsorption process occurs in consecutive steps; these include movement of the adsorbate from the solution bulk to the surface of the adsorbent and then diffusion through the boundary layer to the outer surface of the adsorbent. It is followed by the adsorption on an available active site on the adsorbent's surface and, at last, intra-particle diffusion through pores. The Weber-Morris intra-particle/membrane diffusion model is diffusion-controlled; the adsorption rate directly depends on the speed at which an adsorbate can diffuse towards the provided

adsorbent. Therefore, this model is described using Equation (9) [62]:

$$q_t = kt^{\frac{1}{2}} + I \quad (9)$$

where k is the reaction rate constant [$\text{mg}/(\text{g}\cdot\text{h}^{1/2})$], and I is the y -intercept constant [mg/g], gives the information about the boundary layer thickness.

For the validity of this model, it is essential to note that the linear converging line for each EH must pass through the origin for intra-particle diffusion to be the rate-determining step.

In reactions where chemisorption is a dominant mechanism such that on the surface of the adsorbent, adsorbate is deposited without desorption of products, the rate of adsorption decreases with time as the reaction proceeds, and it is due to the surface coverage. In such reactions, the Elovich model is suitable for explaining the chemisorption process by expressing the following linear Equation (10) [60]:

$$q_t = \beta \ln(\alpha\beta) + \beta \ln t \quad (10)$$

where α and β are the coefficients such that α represent the initial adsorption rate [$\text{g}/(\text{mg}\cdot\text{min})$] and β represents the desorption coefficient [$\text{g}/(\text{g}\cdot\text{min})$]. These coefficients can be calculated from the slope and y -intercept of the plot given in Figure 5d.

The fractional power model is the more advanced form of the Freundlich equation, and the linear form is expressed in Equation (11) [63]:

$$\ln q_t = \ln a + b \ln t \quad (11)$$

where a and b are the coefficients in the expression and given that $b < 1$, the product of a and b is given as the specific adsorption rate at 1 min after the start of the experiment.

The adsorption kinetic plots for the adsorption of four EH on WCENFs are shown in Figure 5, and the obtained kinetic parameters from the models mentioned above are presented in Table 4.

The results were examined to obtain adsorption kinetics fits of adsorbate mixture of E1, E2, EE2, and E3 EH on the adsorbent fibers using several model plots. In Figure 5a, the plotting $\ln(q_e - q_t)$ vs. t for E3 hormone shows good compliance with the pseudo-first-order equation. The data points are shown together with the generated lines of best fits. The agreement between the data set is reflected by the

high regression coefficient (0.962) for E3, and the equilibrium adsorption capacity calculated for E3 (0.368) is extremely close to the experimental value (0.369), which indicates that predicted adsorption capacity by this model is almost the same as the actual value. The rate constant k_1 is similar and in the range for all EH. However, this model appears less accurate for E2, EE2, and E1 for describing the initial stage ($t \leq 30$ min). The theoretical expected yield of 0.350, 0.444, and 0.306 seems unsatisfactory and far less than the actual 0.532, 0.687, and 0.551 for E2, EE2, and E1.

The lines plotted in Figure 5b of t/q_t vs. t must be linear to estimate q_e and k_2 from the slope and y -intercept, respectively. The results indicated that the interaction of E2, EE2, and E1 with the material followed a line of best fit, completely matching the data set points. The regression coefficients are 0.99, and the calculated adsorption capacities of E2, EE2, and E1 are 0.544, 0.711, and 0.549 compared to the experimental values 0.532, 0.687, and 0.551, respectively. The slight difference indicates that the active sites were not homogenous on the surface because the adsorption rate is determined by the hormone concentration and the number of active sites available on the material [64]. These findings confirm the suitability of this model for describing E1, E2, and EE2 adsorption on WCENFs. Similar results were observed when comparing the results described in the literature for MWCNTs by Al-Khateeb *et al.* [60]. Whereas E3 shows an overall non-linear trend; instead, two linear portions can be seen. One for the first 60 min and the second for the time interval after 100 min. The plot in Figure 5b was used to determine the rate constant (k_2) and the calculated equilibrium adsorption capacity (q_e) expressed in Equation (8) to obtain the regression coefficient (R^2) shown below in Table 4.

Regarding Figure 5c of q_t vs. $t^{1/2}$, the graph for E3 is a linear plot with a comparatively high regression coefficient, but the plot does not pass through the origin. This specifies that the intraparticle diffusion is not entirely the rate-limiting step, which is likely to happen in the adsorption of the other three EH as well, as shown in Figure 5c. The plausible reason for EH could be that they do not converge properly and the overall best fits do not pass through the origin; this could be due to a surface effect that may have dominantly controlled the sorption process after an hour of time interval and be considered a diffusion-controlled

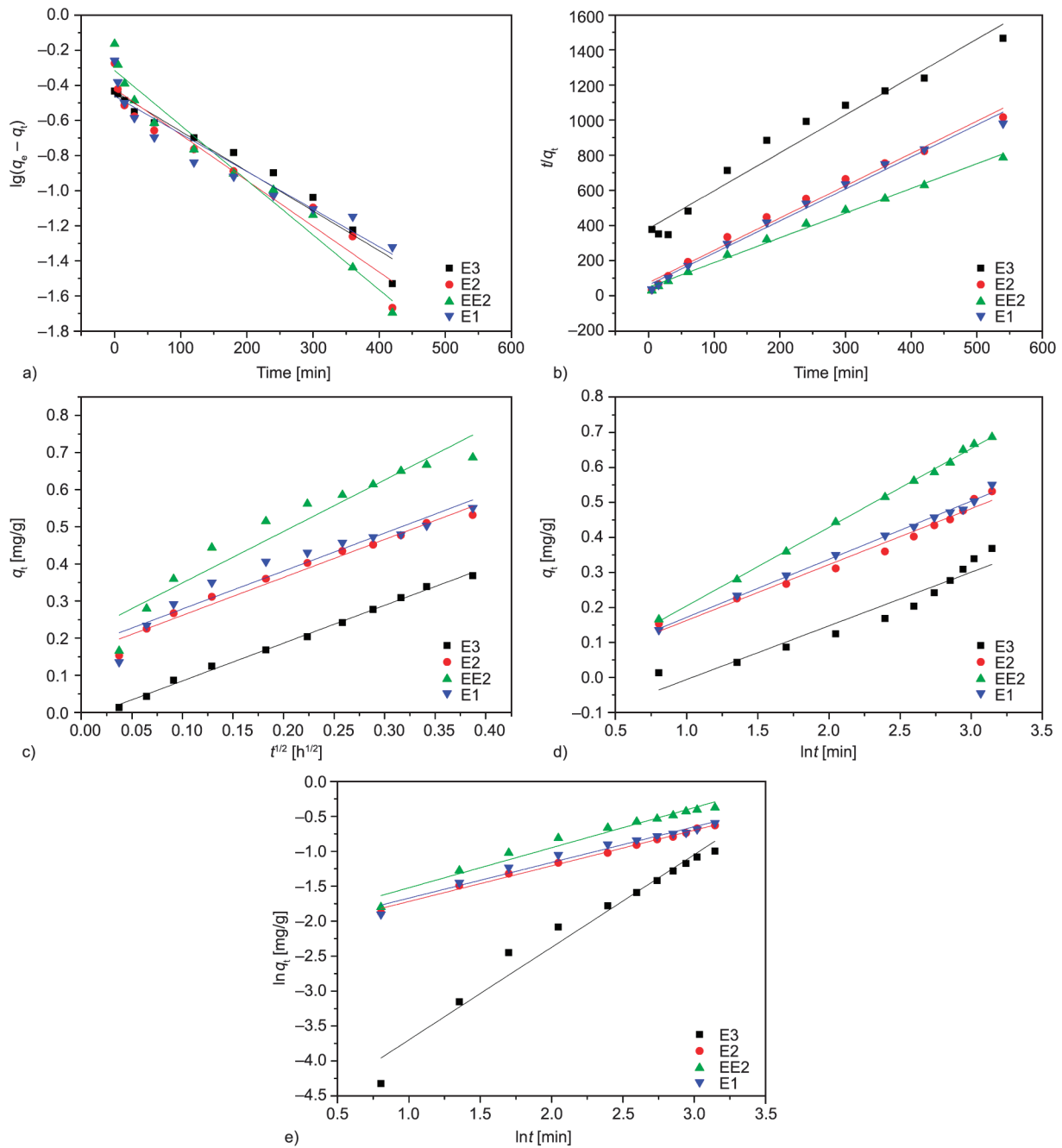


Figure 5. Adsorption kinetics plots of four EH (E1, E2, EE2, E3) on WCENFs, (a) Pseudo-first-order, (b) Pseudo-second-order, (c) Weber-Morris interparticle diffusion model, (d) Elovich model, and (e) fractional power model.

or boundary layer diffusion effect. Furthermore, two linear trends can be seen clearly. In the first 60 min, a sharper and steeper slope trend of a line is observed, which could pass through the origin and indicate that intraparticle diffusion is the rate-limiting step in this region. While in the second region, the diffusion slows down, shown by a gentle slope because the lesser remaining concentration of EH is left in the solution. Thus, for E2, EE2, and E1, intraparticle diffusion can be part of the mechanism, but it can not be a total rate-determining step [60].

The plot in Figure 5d of q_t vs. $\ln t$ shows that EE2 has the highest regression coefficient (0.999), which explains that chemisorption is the most prominent mechanism for the adsorption of EE2 on WCENFs. This is also proven when EE2 had the most rapid adsorption (see Figure 4a) and the highest equilibrium capacity of 0.687 mg/g compared to the other EH. In the case of Figure 5e of $\ln q_t$ vs. $\ln t$, a mismatch is seen for E3, while a linear relationship is seen for E1, E2, and EE2 but not for overall adsorption time. The regression coefficients are not satisfactory in

Table 4. The kinetic models parameters with each EH using WCENFs.

Models		Hormones			
Parameters		Estrone (E1)	β -Estradiol (E2)	17 α -ethinylestradiol (EE2)	Estriol (E3)
Experimental q_e [mg/g]		0.551	0.532	0.687	0.369
Pseudo first order model					
k_1	[min ⁻¹]	0.002	0.003	0.003	0.002
$q_{e, cal}$	[mg/g]	0.306	0.350	0.444	0.368
R^2	[-]	0.951	0.958	0.977	0.962
Pseudo second order model					
k_2	[g/(mg·min)]	0.055	0.045	0.041	0.012
$q_{e, cal}$	[mg/g]	0.549	0.544	0.711	0.464
R^2	[-]	0.991	0.988	0.995	0.966
Intraparticle diffusion model					
k	[mg/(g·h ^{1/2})]	1.006	1.022	1.386	1.017
I	[mg/g]	0.181	0.159	0.210	-0.017
R^2	[-]	0.931	0.975	0.926	0.996
Elovich model					
α	[g/(mg·min)]	14.964	12.962	7.414	1.636
β	[mg/(mg·min)]	0.081	0.080	0.112	0.077
R^2	[-]	0.994	0.979	0.999	0.930
Fractional power model					
a	[-]	0.113	0.108	0.123	0.007
b	[-]	0.255	0.255	0.286	0.663
$a + b$	[-]	0.368	0.362	0.409	0.669
R^2	[-]	0.973	0.994	0.967	0.969

most of the cases. This indicates that the fractional power model is not appropriate for EH. The calculated parameters using Equations (7)–(11) are shown in Table 4.

3.4. Adsorption mechanism

The four possible adsorption mechanisms between EH and the WCENFs could be (1) size-exclusion; (2) physical adsorption of estrogens on the external surface and inside layers of fibers due to their porous structures; (3) charge interactions between EH and WCENFs; (4) Hydrogen bonding of EH molecules onto fibers by reaction with the functional groups present on the surface of fibers. Size exclusion is unexpected in this system because the reported molecular size of estrogens by Han *et al.* [54] is quite small (approximately 0.8 nm for E1 and 0.796 nm for E2) than the pore sizes of the WCENFs (1.4 μ m) and GMF film (0.45 μ m) used. Otherwise, the removal efficiency would have been 100%. A smaller fiber diameter in WCENFs (196 \pm 65 nm) leads to a larger surface area (15.5 m²/g) that provides sufficient active sites for adsorption of EH on the fibers, as shown in Table 2. The electrostatic charge might also influence adsorption, as Porter and Porter already reported

adsorption behavior on microfilms in the presence of cations [65]. The deprotonation of E1, E2, EE2, and E3 is governed by the hydroxyl group's dissociation attached to the benzene ring. The acid dissociation constants for E1, E2, EE2 and E3 are 10.34, 10.46, 10.4 and 10.38, respectively [59, 66]. They all have slightly weaker acidity than phenol ($pK_a = 10$). As a result of the high value of pK_a , most of the molecules for all these estrogens are undissociated; thus, they stay neutral in the solution mixture. As a result, it is unlikely that the influence of charge interaction can be the main factor for the significant adsorption of these EH on the fibers [13].

The high and rapid adsorption of the EH on the WCENFs is particularly interesting. The size of molecules is far tiny compared to the porosity of this structure. Therefore, the pore size has negligible dependence on adsorption. Apart from the physical adsorption, which gradually reaches equilibrium, the only rational explanation is the strong interaction of these EH with the fibers due to the hydrogen bonding. Hydrogen bonds are more robust than the van der Waals forces involved in the physical adsorption. Figure 6 below shows the chemical interactions of each EH with the WCENFs molecule.

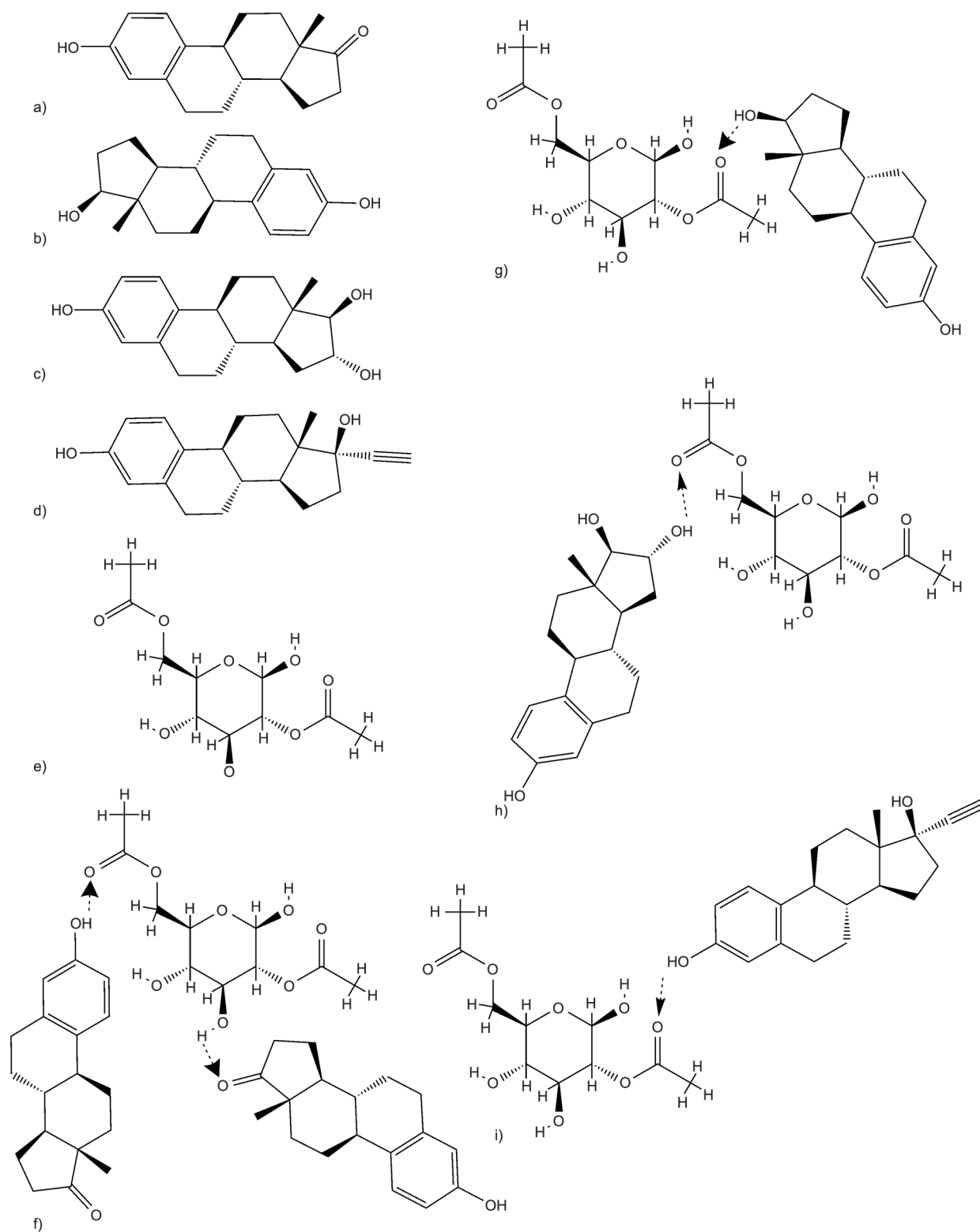


Figure 6. Displayed structures of (a) E1, (b) E2, (c) E3, (d) EE2, (e) WCENFs molecule and hydrogen bonding between WCENFs molecule with EH (f) E1, (g) E2, (h) E3, and (i) EE2.

The EH molecules (E1, E2, EE2, E3) in this study contain a hydroxyl group ($-OH$) acting as a proton donor for hydrogen bonding. Due to the presence of both nucleophilic carbonyl group ($-C=O$) and hydroxyl group in E1, this proton can act as both donor

or acceptor in the hydrogen bonding because CA also contains both $C=O$ and $O-H$ groups. Han and coworkers [13, 54] have described and explained similar hydrogen bonding of E1 with nylon 6,6 membrane in their investigation. Nylon 6,6 and cellulose

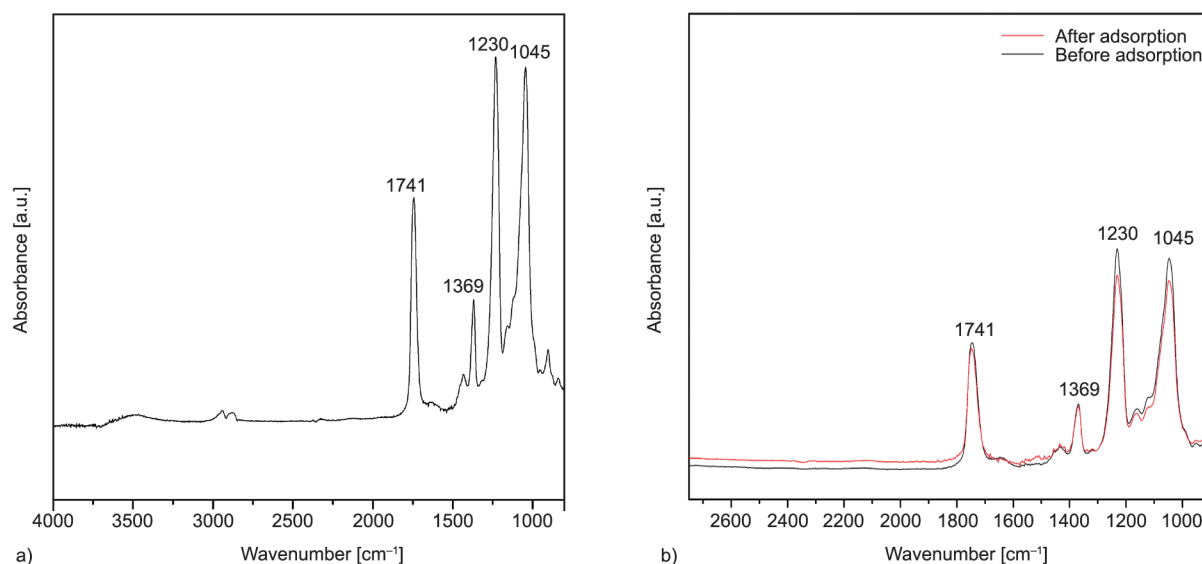


Figure 7. Attenuated total reflectance (ATR) mode FTIR spectra of (a) WCENFs and (b) before and after batch adsorption.

acetate have a common C=O functional group involved in the hydrogen bonding with the estrogens during the adsorption process. Therefore, the functional groups (C=O), (C–O–C), and (C–O–H) present in WCENFs are involved in hydrogen bonding due to lone pair electrons present on oxygen atoms with (C=O) and (O–H) groups present in E1, whereas only (O–H) group of the other three EH (E2, EE2, and E3) is involved in chemisorption as shown in Figure 6 and presented in FTIR analysis in Figure 7. These hydrogen bonding interactions would dictate the EH adsorption on WCENFs, explaining the fast adsorption process for EH in the initial stage of the experiment. FTIR analysis is a sensitive technique used in the study to characterize the hydrogen bonds on WCENFs, as shown below.

The ATR-FTIR characterization of WCENFs was performed to observe the functional groups present. The superimposed FTIR spectra of WCENFs before and after the adsorption study are presented in Figure 7. The broadband near 3400–3600 cm^{-1} indicates OH group presence in fibers. It is noteworthy to see a slight peak shift and the difference in the peak's relative intensities at 1741, 1230, and 1045 cm^{-1} corresponding to C=O stretching, C–O–C anti-symmetric stretching, and C–O bonds, respectively [67]. Their intensities significantly decreased after the adsorption study due to the developed inter-molecular hydrogen bonding interactions. In contrast, no change is noticed in the peak intensity at 1369 cm^{-1} belonging to the C–CH₃ bond because it can not undergo hydrogen bonding. This assures the existence of the

chemisorption at 1741, 1230, and 1045 cm^{-1} of all these EH on the fibers' surface. In addition, the variation in the peak intensity depends on the number of active available functional groups present in the system and their competing behavior for the available sites [54]. Hence, the results supporting the previous literature suggest that EH (E1, E2, EE2, E3) could form hydrogen bonding with oxygen-containing groups on WCENFs. In our previous research, a similar study reported hydrogen bond interaction of carbonyl group (C=O) in polyurethane with these EH [50].

3.5. Determination of recovery and reusability

The adsorption and desorption process was repeated for four consecutive cycles, and considering the efficiency of WCENFs below 10% during the 4th cycle, it was not further reused. The adsorption study of each cycle is reported in Figure 8.

Figure 8a represents the percentage removal of each EH concurrently on WCENFs during four consecutive adsorption cycles. As can be seen, the trend is decreasing after every successive cycle for all EH except for E3, where the adsorption percentage remains below 10% after the first cycle due to fewer available active sites for adsorption and intense competition among the functional groups of EH. The highest removal efficiencies are observed for EE2 (~64.3%), while least for E3 (~34.6%), and the trend is similar in each adsorption cycle. The gradual decrease in adsorption after each cycle is because of mass loss during the desorption process, leading to a reduction of

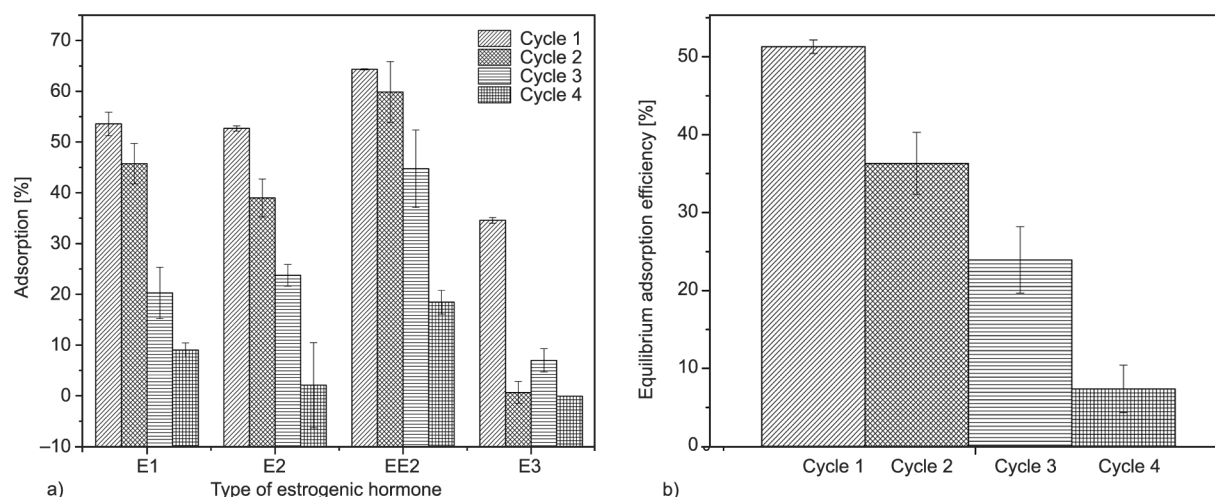


Figure 8. (a) Adsorption cycles of each EH (E1, E2, EE2, E3) with an initial concentration of 0.2 mg/l in a combined solution of 0.8 mg/l on WCENFs (20 mg), (b) cumulative efficiency of all EH adsorption on WCENFs during four cycles.

the active adsorptive sites and, thus, a drop in the surface area due to the increase in the fiber diameter (see Figure 9).

Figure 8b above illustrates the equilibrium adsorption efficiency of WCENFs for cumulative EH removal during four adsorption cycles. As can be seen, the highest reduction of EH in the first cycle is 51.3%, and the trend follows a gradual decrease which ends at 7.4% in the fourth adsorption cycle. Furthermore, it should also be noted that due to the continuous treatment with ethanol during desorption, it was evident that the fibers became stiff and shrank due to mass loss after the last cycle. Therefore, fibers were compact and tightly folded, providing less surface area for EH entrapment during the previous cycle. Thus, providing lesser removal efficiency. The presented comparison was made as a modeling study for the reusability of submicron structure from WCENFs for sorption. In industrial applications, some other solvents have to be tested. According to this model study, the more requested properties of a suitable solvent must be a very high solubility of EH with no solubility of the polymer.

With the repeated desorption cycles of EH from fibers using ethanol, there was a significant change in the fiber morphology attributed to the contact of fibers with ethanol. However, fibers were unlikely to dissolve in ethanol, and their porous structure allowed complete penetration of ethanol molecules. Therefore, after several cycles and contact time, it has led to collapse and swelling of the structure of the fibers and the effectiveness of the adsorption process [9]. It is evident in the SEM image of the fiber structure after the complete adsorption study, as shown.

Figure 9 shows the fiber's surface morphology after four adsorption-desorption cycles. As can be seen, the fiber's diameter increased from 196–351 nm, with the high swelling experienced on several fibers as shown above (white arrows).

3.6. EH adsorption on PET/WCENFs fabricated membrane film and commercial application

The adsorption equilibrium of EH solution was observed in these films, and a characteristic value of volume to reach equilibrium (V_{eq}) was noted. This concept of determining V_{eq} is used to conveniently and approximately mitigate the effect of these hormones simultaneously on WCENFs. V_{eq} is defined as the minimum volume of feed solution that passes through the film and can withstand to achieve adsorption equilibrium for this set of EH. Suppose the value of V_{eq} is significantly considerable; in that case, this method can instantly remove EH from wastewater. Figure 10 below shows the comparative results of E1, E2, EE2, and E3 adsorption on the PET/WCENFs film, where the residual concentration of the mixed EH solution permeates normalized (expressed in percentage values) against the initial concentration of each hormone in the feed versus the accumulated feed solution. It must be noted that these results were compared with the commercial CA syringe film reported by Han *et al.* [13] for E1 adsorption.

Figure 10a shows simultaneous adsorption of all EH on the WCENFs film. It can be seen that the highest adsorption is experienced for E1 and the lowest for E3 until equilibrium was achieved at 7 ml of feed. It can be seen that maximum adsorption for E1, E2,

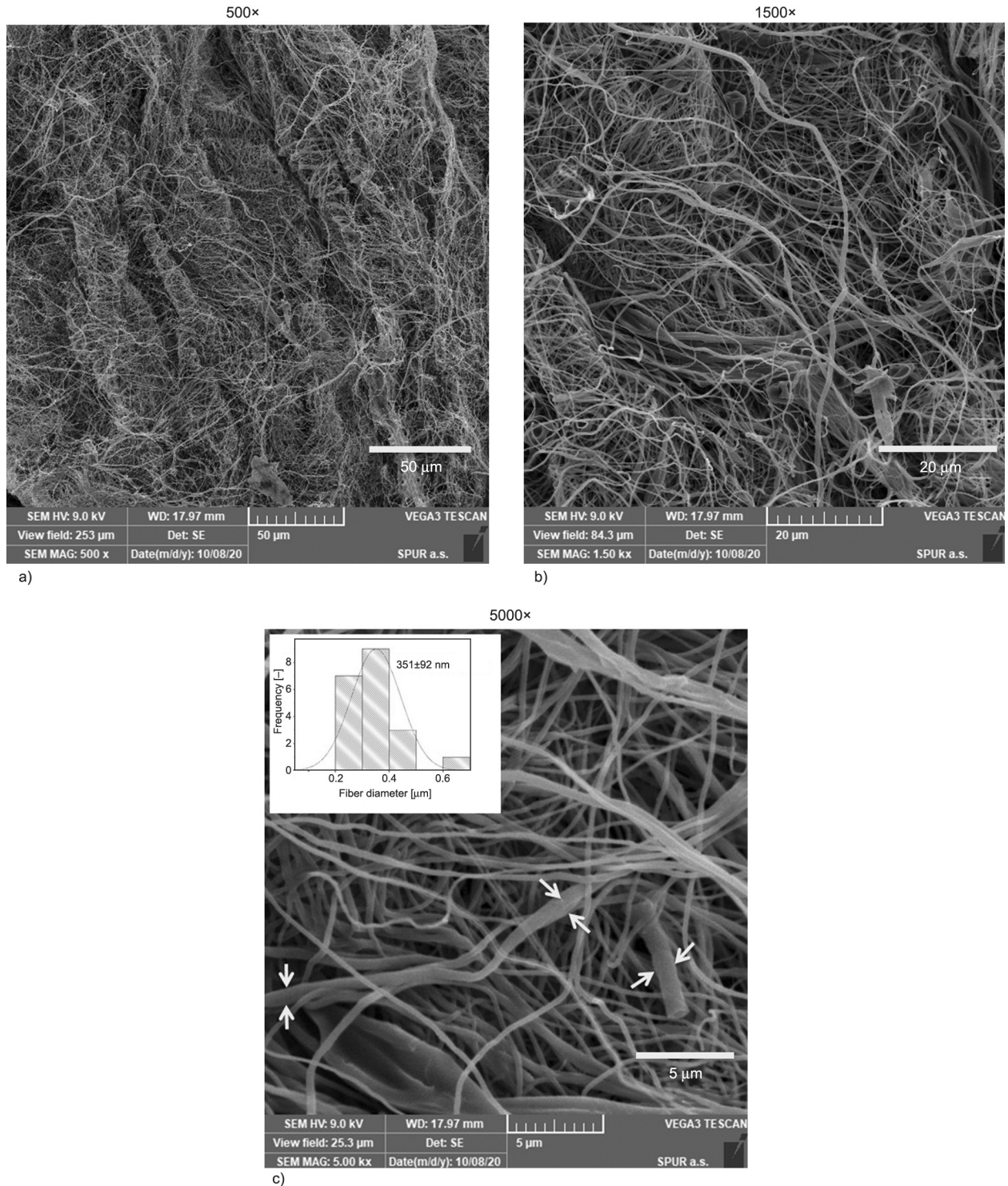


Figure 9. SEM image of WCENFs and their fiber diameter distribution after four adsorption-desorption cycles at a different magnification of (a) 500×, (b) 1500×, and (c) 5000×.

EE2, and E3 were found to be 24.5, 12.6, 19.7, and 0.5%, respectively. A gradual decrease in adsorption was seen for the PET/WCENFs film in a syringe adsorption test, which suggests the process of physical adsorption of EH on the PET/WCENFs film.

Figure 10b compares the results of WCENFs film with the commercial CA syringe film over 10 ml

accumulated volume of feed. As can be seen, the total E1 adsorption of 18.6% was seen for commercial CA film with the initial solution concentration of 0.4 mg/l while 24.5% for WCENFs with the initial concentration of 0.2 mg/l. Also, 14.2% total adsorption on PET/WCENFs was noticed from the mixture of all four EH with the solution concentration

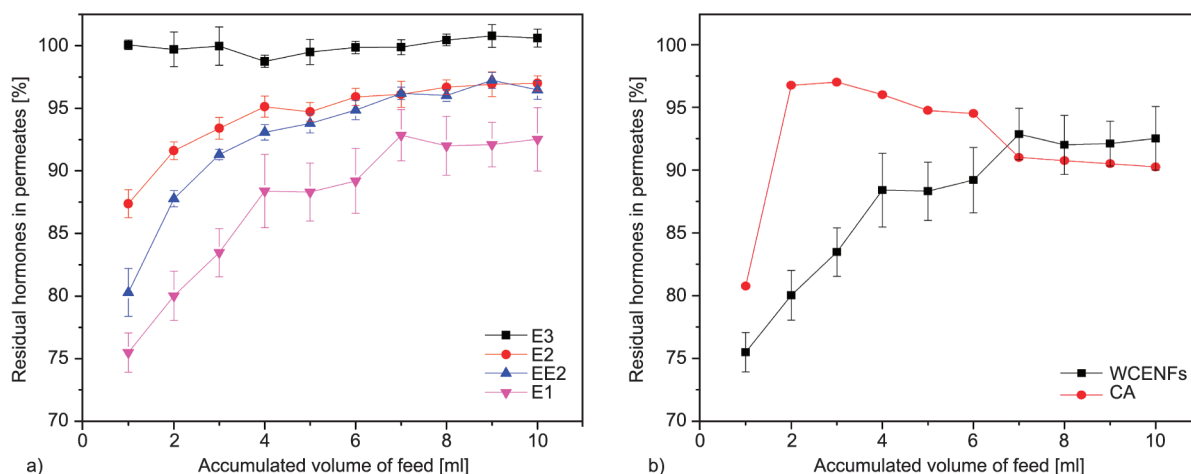


Figure 10. (a) Concurrent adsorption of EH (E1, E2, EE2, and E3) on 1.4 μm PET/WCENFs syringe film using 0.8 mg/l EH aqueous solution as feed containing 0.2 mg/l of each hormone and (b) 1.4 μm PET/WCENFs film adsorption comparison with 0.45 μm commercial CA syringe film for E1 [13].

of 0.8 mg/l, which is twice that of commercial CA. Furthermore, after the 1st mL of permeate passed through the commercial CA film, a decrease in adsorption was observed drastically during the next few permeates for commercial CA and then a slight increase in adsorption until it gets stagnant after 6 ml; this could be due to experimental error or loss of some already adsorbed E1 molecules on the surface of commercial CA film. While, a gradual decrease in adsorption was seen for PET/WCENFs syringe film, which suggests that physical adsorption could be the primary cause of EH adsorption but without any EH losses from the surface. The membrane's adsorption sites were occupied by EH molecules when more and more feed was passed, and eventually, an equilibrium was established when the adsorption sites were saturated. The derived V_{eq} value was 7 ml for both PET/WCENFs and commercial CA films. After these volumes, no significant change was observed. This suggests that the film reached saturation with EH at 7 ml. Similar results were reported in the literature for E1 adsorption reaching equilibrium at 8 ml for PP, 7 ml for polytetrafluoroethylene (PTFE), and 6 ml for regenerated cellulose (RC) films [13]. The PET/WCENFs film in the current study has a high retention volume for these EH with twice the initial concentration of EH solution compared to the commercial GMF, RC, PTFE, CA, and PP films reported by Han *et al.* [13]. Therefore, PET/WCENFs film can be used within this capacity for instant and concurrent removal of these EH solutes from wastewater. It can be a cheap and viable method by using waste CBs to make a WCENFs film for replacing

the commercially available films for water treatment. The PET/WCENFs film can be an excellent substitute for the already available commercial films because this can be disposed of after several cycles, easily be detached, and replaced from a Swinnex film holder. Additionally, the WCENFs used as a film can be prepared by facile electrospinning technique, which is not costly.

3.7. Restrictions, further research, and application

This model study was limited to working with one concentration due to the restriction of solubility of four EH together, their detection, and quantification limits set on HPLC. Moreover, continuous long-term membrane testing on the cross and dead-end flow measurement under high pressures and flow rates, including membrane fouling, needs to be investigated. Furthermore, the influence of pH variation, interference of organic matter, ionic strength, temperature, the competing behavior of inorganic ions, varied concentrations of adsorbate and adsorbent dosage are some matters to be addressed in future research to help optimize the kinetics, determine isotherms and thermodynamic parameters. These works shall focus on actual reservoir samples to conclude the feasibility of this process for large-scale production.

3.8. Comparative study

Table 5 illustrates the type of fibers and particles used for the removal of hormones and pollutants from water. As can be seen, the WCENFs have a cumulative adsorption capacity of 2.14 mg/g, which is

Table 5. Comparison of adsorbents used for the specified water pollutants.

Adsorbents	Pollutant adsorption capacity [mg/g]					Reference
	E1	E2	E3	EE2	BPA	
MWCNTs	0.423	0.472	–	0.472	–	[60]
PA612	–	–	–	25.4	–	[47]
Darco AC	–	–	–	27.6	–	
Norit AC	–	–	–	10.4	–	
Un-anthracite	–	–	–	0.2147	0.1221	[68]
4 K anthracite	–	–	–	0.6209	0.1540	
PU Elastollan	0.801	0.592	0.382	0.736	–	[50]
PU 918	0.816	0.606	0.366	0.637	–	
CA	0.506	0.532	0.389	0.668	–	
PAN	0.396	0.370	0.397	0.343	–	
PES	0.442	0.487	0.363	0.591	–	
PA	0.331	0.543	0.485	0.611	–	
WCENFs	0.551	0.532	0.369	0.687	–	

greater than most of the electrospun fibers (individual values are specified in Table 5) reported in the literature. Apart from that, the given particles (PA612, Darco AC, and Norit AC) have higher adsorption capacities than WCENFs due to their higher surface area based on the nature of those materials. Also, the individual adsorption capacities of WCENFs are firmly in compliance with those of electrospun CA fibers.

4. Conclusions

This study focused on concurrent removal of four EH (E1, E2, EE2, E3) to replicate real-time waste streams using WCENFs, recycling, and green approach. A one-step detection and concomitant quantification method based on HPLC was devised for these EH. It is noteworthy to mention that the WCENFs membrane could successfully remove all of these EH. The chemical composition of polymer, functional groups present, and structure of WCENFs played an essential role in the rapid adsorption process, which is elaborated in the adsorption mechanism. The strong affinity of WCENFs was found to be towards all EH due to abundant hydrogen bonding interactions. The highest percentage removal efficiencies from the batch adsorption were 64.3, 53.6, 52.7, and 34.6% for EE2, E1, E2, and E3, respectively. The total adsorption capacity obtained was 2.14 mg/g, and reported individual adsorption capacities of E1, E2, EE2, and E3 were found to be 0.551, 0.532, 0.687, and 0.369 mg/g, respectively. Based on the kinetic modeling results, the pseudo-first-order suits E3 and the pseudo-second-order model

is suitable for E1, E2, and EE2. Therefore, both models are considered most appropriate due to their high regression coefficients than the other kinetic models. Desorption studies for the recovery of EH and reuse of submicron WCENFs was conducted and validated for four cycles using HPLC grade ethanol as the most suitable solvent. To summarize, the fabricated PET/WCENFs syringe film successfully responded to the retention time for these EH compared to the commercial CA syringe film. It also implies that recycled WCENFs can be considered a promising adsorbent for rapidly remediation of wastewater streams and possibly replacing the commercially available CA syringe film.

Acknowledgements

The authors gratefully acknowledge the financial support by the Ministry of Education, Youth, and Sports of the Czech Republic (grant no. RP/CPS/2020/002), the Internal Grant Agency of TBU in Zlin (grant no. IGA/CPS/2021/002). We would also like to acknowledge the Centre of Polymer Systems (CPS) situated at Tomas Bata University in Zlin, Czech Republic, to use the available research facilities to conduct this research work. Furthermore, the authors very much appreciate the assistance in laboratory equipment by Dr. Lenka Lovecka in CPS.

References

- [1] Torkashvand J., Farzadkia M.: A systematic review on cigarette butt management as a hazardous waste and prevalent litter: Control and recycling. *Environmental Science and Pollution Research*, **26**, 11618–11630 (2019).
<https://doi.org/10.1007/s11356-019-04250-x>

- [2] Shen F., Tian D., Yang G., Deng S., Shen F., He J., Zhu Y., Huang C., Hu J.: Deacetylation processing of waste cigarette butts for high-titer bioethanol production toward a clean recycling process. *ACS Sustainable Chemistry and Engineering*, **8**, 11253–11262 (2020).
<https://doi.org/10.1021/acssuschemeng.0c03979>
- [3] Rebischung F., Chabot L., Biauudet H., Pandard P.: Cigarette butts: A small but hazardous waste, according to European regulation. *Waste Management*, **82**, 9–14 (2018).
<https://doi.org/10.1016/j.wasman.2018.09.038>
- [4] Montalvão M. F., Chagas T. Q., da Silva Alvarez T. G., Mesak C., da Costa Araújo A. P., Gomes A. R., de Andrade Vieira J. E., Malafaia G.: How leachates from wasted cigarette butts influence aquatic life? A case study on freshwater mussel *Anodontites trapesialii*. *Science of the Total Environment*, **689**, 381–389 (2019).
<https://doi.org/10.1016/j.scitotenv.2019.06.385>
- [5] Benavente M. J., Caballero M. J. A., Silvero G., López-Coca I., Escobar V. G.: Cellulose acetate recovery from cigarette butts. *Proceedings*, **2**, 1447 (2019).
<https://doi.org/10.3390/proceedings2201447>
- [6] Hemamalini T., Karunakaran S. A., Siva Elango M. K., Senthil Ram T., Giri Dev V. R.: Regeneration of cellulose acetate nanofibrous mat from discarded cigarette butts. *Indian Journal of Fibre and Textile Research*, **44**, 248–252 (2019).
- [7] Bilge S., Bakirhan N. K., Osman Donar Y., Smağ A., Ozkan S. A.: Turning toxic cigarette butt waste into the sensor material for the sensitive determination of anti-hypertensive drug trandolapril from its dosage form and biological samples. *Sensors and Actuators, B: Chemical*, **296**, 126626 (2019).
<https://doi.org/10.1016/j.snb.2019.126626>
- [8] Alhokbany N. S., Naushad M., Kumar V., Al hatim S., Alshehri S. M., Ahamad T.: Self-nitrogen doped carbons aerogel derived from waste cigarette butts (cellulose acetate) for the adsorption of BPA: Kinetics and adsorption mechanisms. *Journal of King Saud University – Science*, **32**, 3351–3358 (2020).
<https://doi.org/10.1016/j.jksus.2020.09.021>
- [9] Schäfer A. I., Stelzl K., Faghih M., Sen Gupta S., Krishnadas K. R., Heißler S., Pradeep T.: Poly(ether sulfone) nanofibers impregnated with β -cyclodextrin for increased micropollutant removal from water. *ACS Sustainable Chemistry and Engineering*, **6**, 2942–2953 (2018).
<https://doi.org/10.1021/acssuschemeng.7b02214>
- [10] Luo Y., Guo W., Ngo H. H., Nghiem L. D., Hai F. I., Zhang J., Liang S., Wang X. C.: A review on the occurrence of micropollutants in the aquatic environment and their fate and removal during wastewater treatment. *Science of the Total Environment*, **473–474**, 619–641 (2014).
<https://doi.org/10.1016/j.scitotenv.2013.12.065>
- [11] Tijani J. O., Fatoba O. O., Petrik L. F.: A review of pharmaceuticals and endocrine-disrupting compounds: Sources, effects, removal, and detections. *Water, Air, and Soil Pollution*, **224**, 1770 (2013).
<https://doi.org/10.1007/s11270-013-1770-3>
- [12] Vymazal J., Březinová T., Koželuh M.: Occurrence and removal of estrogens, progesterone and testosterone in three constructed wetlands treating municipal sewage in the Czech Republic. *Science of the Total Environment*, **536**, 625–631 (2015).
<https://doi.org/10.1016/j.scitotenv.2015.07.077>
- [13] Han J., Qiu W., Gao W.: Adsorption of estrone in microfiltration membrane filters. *Chemical Engineering Journal*, **165**, 819–826 (2010).
<https://doi.org/10.1016/j.cej.2010.10.024>
- [14] Nghiem L. D., Schäfer A. I.: Adsorption and transport of trace contaminant estrone in NF/RO membranes. *Environmental Engineering Science*, **19**, 441–451 (2002).
<https://doi.org/10.1089/109287502320963427>
- [15] Solomon G. M., Schettler T.: Environment and health: 6. Endocrine disruption and potential human health implications. *CMAJ*, **163**, 1471–1476 (2000).
- [16] Braga O., Smythe G. A., Schäfer A. I., Feitz A. J.: Fate of steroid estrogens in Australian inland and coastal wastewater treatment plants. *Environmental Science and Technology*, **39**, 3351–3358 (2005).
<https://doi.org/10.1021/es0501767>
- [17] Montes-Grajales D., Olivero-Verbel J.: EDCs databank: 3D-structure database of endocrine disrupting chemicals. *Toxicology*, **327**, 87–94 (2015).
<https://doi.org/10.1016/j.tox.2014.11.006>
- [18] Gyllenhammar I., Glynn A., Jönsson B. A. G., Lindh C. H., Darnerud P. O., Svensson K., Lignell S.: Diverging temporal trends of human exposure to bisphenols and plasticizers, such as phthalates, caused by substitution of legacy EDCs? *Environmental Research*, **153**, 48–54 (2017).
<https://doi.org/10.1016/j.envres.2016.11.012>
- [19] Sood S., Shekhar S., Santosh W.: Dimorphic placental stress: A repercussion of interaction between endocrine disrupting chemicals (EDCs) and fetal sex. *Medical Hypotheses*, **99**, 73–75 (2017).
<https://doi.org/10.1016/j.mehy.2017.01.002>
- [20] Luo L., Yang Y., Xiao M., Bian L., Yuan B., Liu Y., Jiang F., Pan X.: A novel biotemplated synthesis of TiO₂/wood charcoal composites for synergistic removal of bisphenol A by adsorption and photocatalytic degradation. *Chemical Engineering Journal*, **262**, 1275–1283 (2015).
<https://doi.org/10.1016/j.cej.2014.10.087>
- [21] Chen Y., Zhang Y., Luo L., Shi Y., Wang S., Li L., Long Y., Jiang F.: A novel templated synthesis of C/N-doped β -Bi₂O₃ nanosheets for synergistic rapid removal of 17 α -ethynylestradiol by adsorption and photocatalytic degradation. *Ceramics International*, **44**, 2178–2185 (2018).
<https://doi.org/10.1016/j.ceramint.2017.10.173>

- [22] Semião A. J. C., Schäfer A. I.: Xenobiotics removal by membrane technology: An overview. in 'Xenobiotics in the urban water cycle' (eds.: Fatta-Kassinos D., Bester K., Kümmerer K.) Springer, Edinburgh, Vol. 16, 307–338 (2010).
https://doi.org/10.1007/978-90-481-3509-7_17
- [23] Onesios K. M., Yu J. T., Bouwer E. J.: Biodegradation and removal of pharmaceuticals and personal care products in treatment systems: A review. *Biodegradation*, **20**, 441–466 (2009).
<https://doi.org/10.1007/s10532-008-9237-8>
- [24] Pham T. T., Nguyen V. A., van der Bruggen B.: Pilot-scale evaluation of GAC adsorption using low-cost, high-performance materials for removal of pesticides and organic matter in drinking water production. *Journal of Environmental Engineering*, **139**, 958–965 (2013).
[https://doi.org/10.1061/\(asce\)jee.1943-7870.0000704](https://doi.org/10.1061/(asce)jee.1943-7870.0000704)
- [25] Ali H., Guler A. C., Masar M., Urbanek P., Urbanek M., Skoda D., Suly P., Machovsky M., Galusek D., Kuritka I.: Solid-state synthesis of direct z-scheme Cu₂O/WO₃ nanocomposites with enhanced visible-light photocatalytic performance. *Catalysts*, **11**, 293 (2021).
<https://doi.org/10.3390/catal11020293>
- [26] Pendergast M. M., Hoek E. M. V.: A review of water treatment membrane nanotechnologies. *Energy and Environmental Science*, **4**, 1946–1971 (2011).
<https://doi.org/10.1039/c0ee00541j>
- [27] Shannon M. A., Bohn P. W., Elimelech M., Georgiadis J. G., Mariñas B. J., Mayes A. M.: Science and technology for water purification in the coming decades. *Nature*, **452**, 301–310 (2008).
<https://doi.org/10.1038/nature06599>
- [28] Kumar A. K., Mohan S. V.: Endocrine disruptive synthetic estrogen (17 α -ethynylestradiol) removal from aqueous phase through batch and column sorption studies: Mechanistic and kinetic analysis. *Desalination*, **276**, 66–74 (2011).
<https://doi.org/10.1016/j.desal.2011.03.022>
- [29] Kumar A. K., Mohan S. V., Sarma P. N.: Sorptive removal of endocrine-disruptive compound (estriol, E3) from aqueous phase by batch and column studies: Kinetic and mechanistic evaluation. *Journal of Hazardous Materials*, **164**, 820–828 (2009).
<https://doi.org/10.1016/j.jhazmat.2008.08.075>
- [30] Pan B., Lin D., Mashayekhi H., Xing B.: Adsorption and hysteresis of bisphenol A and 17 α -ethinyl estradiol on carbon nanomaterials. *Environmental Science and Technology*, **42**, 5480–5485 (2008).
<https://doi.org/10.1021/es8001184>
- [31] Jin X., Hu J. Y., Tint M. L., Ong S. L., Biryulin Y., Polotskaya G.: Estrogenic compounds removal by fullerene-containing membranes. *Desalination*, **214**, 83–90 (2007).
<https://doi.org/10.1016/j.desal.2006.10.019>
- [32] Kiran Kumar A., Venkata Mohan S.: Removal of natural and synthetic endocrine disrupting estrogens by multi-walled carbon nanotubes (MWCNT) as adsorbent: Kinetic and mechanistic evaluation. *Separation and Purification Technology*, **87**, 22–30 (2012).
<https://doi.org/10.1016/j.seppur.2011.11.015>
- [33] Krupadam R. J., Sridevi P., Sakunthala S.: Removal of endocrine disrupting chemicals from contaminated industrial groundwater using chitin as a biosorbent. *Journal of Chemical Technology and Biotechnology*, **86**, 367–374 (2011).
<https://doi.org/10.1002/jctb.2525>
- [34] Zhang Y., Zhou J. L.: Removal of estrone and 17 β -estradiol from water by adsorption. *Water Research*, **39**, 3991–4003 (2005).
<https://doi.org/10.1016/j.watres.2005.07.019>
- [35] Hristovski K. D., Nguyen H., Westerhoff P. K.: Removal of arsenate and 17 α -ethinyl estradiol (EE2) by iron (hydr)oxide modified activated carbon fibers. *Journal of Environmental Science and Health Part A: Toxic/Hazardous Substances and Environmental Engineering*, **44**, 354–361 (2009).
<https://doi.org/10.1080/10934520802659695>
- [36] Lu T., Liang H., Cao W., Deng Y., Qu Q., Ma W., Xiong R., Huang C.: Blow-spun nanofibrous composite self-cleaning membrane for enhanced purification of oily wastewater. *Journal of Colloid and Interface Science*, **608**, 2860–2869 (2022).
<https://doi.org/10.1016/j.jcis.2021.11.017>
- [37] Ma W., Jiang Z., Lu T., Xiong R., Huang C.: Light-weight, elastic and superhydrophobic multifunctional nanofibrous aerogel for self-cleaning, oil/water separation and pressure sensing. *Chemical Engineering Journal*, **430**, 132989 (2022).
<https://doi.org/10.1016/j.cej.2021.132989>
- [38] Wang J., Pan K., Giannelis E. P., Cao B.: Polyacrylonitrile/polyaniline core/shell nanofiber mat for removal of hexavalent chromium from aqueous solution: Mechanism and applications. *RSC Advances*, **3**, 8978–8987 (2013).
<https://doi.org/10.1039/c3ra40616d>
- [39] Zhao J., Lu Z., He X., Zhang X., Li Q., Xia T., Zhang W., Lu C., Deng Y.: One-step fabrication of Fe(OH)₃@cellulose hollow nanofibers with superior capability for water purification. *ACS Applied Materials and Interfaces*, **9**, 25339–25349 (2017).
<https://doi.org/10.1021/acsami.7b07038>
- [40] Kale S. M., Kirange P. M., Kale T. V., Kanu N. J., Gupta E., Chavan S. S., Vates U. K., Singh G. K.: Synthesis of ultrathin ZnO, nylon-6,6 and carbon nanofibers using electrospinning method for novel applications. *Materials Today: Proceedings*, **47**, 3186–3189 (2021).
<https://doi.org/10.1016/j.matpr.2021.06.289>
- [41] Chigome S., Torto N.: A review of opportunities for electrospun nanofibers in analytical chemistry. *Analytica Chimica Acta*, **706**, 25–36 (2011).
<https://doi.org/10.1016/j.aca.2011.08.021>

- [42] Chigome S., Darko G., Torto N.: Electrospun nanofibers as sorbent material for solid phase extraction. *Analyst*, **136**, 2879–2889 (2011).
<https://doi.org/10.1039/c1an15228a>
- [43] Kanu N. J., Gupta E., Sutar V., Singh G. K., Vates U. K.: An insight into biofunctional curcumin/gelatin nanofibers. in *Nanofibers – Synthesis, properties and applications* (ed.: Kumar B.) Intech Open, London, 1–22 (2021).
<https://doi.org/10.5772/intechopen.97113>
- [44] Kanu N. J., Gupta E., Vates U. K., Singh G. K.: Electrospinning process parameters optimization for bio-functional curcumin/gelatin nanofibers. *Materials Research Express*, **7**, 035022 (2020).
<https://doi.org/10.1088/2053-1591/ab7f60>
- [45] Arroyo F. D., Castro-Guerrero C. F., León-Silva U.: Thin films of cellulose acetate nanofibers from cigarette butt waste. *Progress in Rubber, Plastics and Recycling Technology*, **36**, 3–17 (2020).
<https://doi.org/10.1177/1477760619895024>
- [46] Filep T., Szabó L., Kondor A. C., Jakab G., Szalai Z.: Evaluation of the effect of the intrinsic chemical properties of pharmaceutically active compounds (PhACs) on sorption behaviour in soils and goethite. *Ecotoxicology and Environmental Safety*, **215**, 112120 (2021).
<https://doi.org/10.1016/j.ecoenv.2021.112120>
- [47] Han J., Qiu W., Cao Z., Hu J., Gao W.: Adsorption of ethinylestradiol (EE2) on polyamide 612: Molecular modeling and effects of water chemistry. *Water Research*, **47**, 2273–2284 (2013).
<https://doi.org/10.1016/j.watres.2013.01.046>
- [48] Niavarani Z., Breite D., Prager A., Abel B., Schulze A.: Estradiol removal by adsorptive coating of a microfiltration membrane. *Membranes*, **11**, 99 (2021).
<https://doi.org/10.3390/membranes11020099>
- [49] Wang M., Qu F., Jia R., Sun S., Li G., Liang H.: Preliminary study on the removal of steroidal estrogens using TiO₂-doped PVDF ultrafiltration membranes. *Water*, **8**, 134 (2016).
<https://doi.org/10.3390/w8040134>
- [50] Yasir M., Šopík T., Lovecká L., Kimmer D., Sedlařík V.: The adsorption, kinetics, and interaction mechanisms of various types of estrogen on electrospun polymeric nanofiber membranes. *Nanotechnology*, **33**, 75702 (2021).
<https://doi.org/10.1088/1361-6528/ac357b>
- [51] Cao W., Ma W., Lu T., Jiang Z., Xiong R., Huang C.: Multifunctional nanofibrous membranes with sunlight-driven self-cleaning performance for complex oily wastewater remediation. *Journal of Colloid and Interface Science*, **608**, 164–174 (2022).
<https://doi.org/10.1016/j.jcis.2021.09.194>
- [52] Yasir M., Šopík T., Kimmer D., Sedlařík V.: Facile HPLC technique for simultaneous detection of estrogenic hormones in wastewater. in *‘Proceedings of the 12th International Conference on Nanomaterials, Brno, Czech Republic’* 272–276 (2021).
<https://doi.org/10.37904/nanocon.2020.3710>
- [53] Qi F-F., Cao Y., Wang M., Rong F., Xu Q.: Nylon 6 electrospun nanofibers mat as effective sorbent for the removal of estrogens: Kinetic and thermodynamic studies. *Nanoscale Research Letters*, **9**, 353 (2014).
<https://doi.org/10.1186/1556-276X-9-353>
- [54] Han J., Qiu W., Hu J., Gao W.: Chemisorption of estrone in nylon microfiltration membranes: Adsorption mechanism and potential use for estrone removal from water. *Water Research*, **46**, 873–881 (2012).
<https://doi.org/10.1016/j.watres.2011.11.066>
- [55] Ma H., Burger C., Hsiao B. S., Chu B.: Nanofibrous microfiltration membrane based on cellulose nanowhiskers. *Biomacromolecules*, **13**, 180–186 (2012).
<https://doi.org/10.1021/bm201421g>
- [56] Taha A. A., Wu Y-N., Wang H., Li F.: Preparation and application of functionalized cellulose acetate/silica composite nanofibrous membrane *via* electrospinning for Cr(VI) ion removal from aqueous solution. *Journal of Environmental Management*, **112**, 10–16 (2012).
<https://doi.org/10.1016/j.jenvman.2012.05.031>
- [57] Mikaeili F., Gouma P. I.: Super water-repellent cellulose acetate mats. *Scientific Reports*, **8**, 12472 (2018).
<https://doi.org/10.1038/s41598-018-30693-2>
- [58] Szewczyk P. K., Ura D. P., Metwally S., Knapczyk-Korcza J., Gajek M., Marzec M. M., Bernasik A., Stachewicz U.: Roughness and fiber fraction dominated wetting of electrospun fiber-based porous meshes. *Polymers*, **11**, 34 (2018).
<https://doi.org/10.3390/polym11010034>
- [59] Schäfer A. I., Akanyeti I., Semião A. J. C.: Micropollutant sorption to membrane polymers: A review of mechanisms for estrogens. *Advances in Colloid and Interface Science*, **164**, 100–117 (2011).
<https://doi.org/10.1016/j.cis.2010.09.006>
- [60] Al-Khateeb L. A., Obaid A. Y., Asiri N. A., Abdel Salam M.: Adsorption behavior of estrogenic compounds on carbon nanotubes from aqueous solutions: Kinetic and thermodynamic studies. *Journal of Industrial and Engineering Chemistry*, **20**, 916–924 (2014).
<https://doi.org/10.1016/j.jiec.2013.06.023>
- [61] Ersali S., Hadadi V., Moradi O., Fakhri A.: Pseudo-second-order kinetic equations for modeling adsorption systems for removal of ammonium ions using multi-walled carbon nanotube. *Fullerenes, Nanotubes and Carbon Nanostructures*, **3**, 150527104639002 (2013).
<https://doi.org/10.1080/1536383x.2013.787610>
- [62] Tian Y., Wu M., Liu R., Li Y., Wang D., Tan J., Wu R., Huang Y.: Electrospun membrane of cellulose acetate for heavy metal ion adsorption in water treatment. *Carbohydrate Polymers*, **83**, 743–748 (2011).
<https://doi.org/10.1016/j.carbpol.2010.08.054>
- [63] Ho Y. S., McKay G.: Application of kinetic models to the sorption of copper(II) on to peat. *Adsorption Science and Technology*, **20**, 797–815 (2002).
<https://doi.org/10.1260/026361702321104282>

- [64] Vazquez-Velez E., Lopez-Zarate L., Martinez-Valencia H.: Electrospinning of polyacrylonitrile nanofibers embedded with zerovalent iron and cerium oxide nanoparticles, as Cr(VI) adsorbents for water treatment. *Journal of Applied Polymer Science*, **137**, 48663 (2020).
<https://doi.org/10.1002/app.48663>
- [65] Porter J. J., Porter R. S.: Filtration studies of selected anionic dyes using asymmetric titanium dioxide membranes on porous stainless-steel tubes. *Journal of Membrane Science*, **101**, 67–81 (1995).
[https://doi.org/10.1016/0376-7388\(94\)00278-7](https://doi.org/10.1016/0376-7388(94)00278-7)
- [66] Behera S. K., Kim H. W., Oh J-E., Park H-S.: Occurrence and removal of antibiotics, hormones and several other pharmaceuticals in wastewater treatment plants of the largest industrial city of Korea. *Science of the Total Environment*, **409**, 4351–4360 (2011).
<https://doi.org/10.1016/j.scitotenv.2011.07.015>
- [67] Nasir M., Subhan A., Prihandoko B., Lestariningsih T.: Nanostructure and property of electrospun SiO₂-cellulose acetate nanofiber composite by electrospinning. *Energy Procedia*, **107**, 227–231 (2017).
<https://doi.org/10.1016/j.egypro.2016.12.133>
- [68] He J., Zhou Q., Guo J., Fang F.: Characterization of potassium hydroxide modified anthracite particles and enhanced removal of 17 α -ethinylestradiol and bisphenol A. *Environmental Science and Pollution Research*, **25**, 22224–22235 (2018).
<https://doi.org/10.1007/s11356-018-2287-5>



Electrospun polyurethane nanofibers coated with polyaniline/polyvinyl alcohol as ultrafiltration membranes for the removal of ethinylestradiol hormone micropollutant from aqueous phase

Muhammad Yasir^{*}, Fahanwi Asabuwa Ngwabebhoh, Tomáš Šopík, Hassan Ali, Vladimír Sedlářik^{*}

Centre of Polymer Systems, University Institute, Tomas Bata University in Zlín, Trída Tomáše Bati 5678, 76001 Zlín, Czech Republic

ARTICLE INFO

Editor: Pei Xu

Keywords:

Hormone removal
Electrospun nanofibers
in situ coating
Adsorption
Water remediation

ABSTRACT

Estrogenic hormones at significant levels are a serious cause of fish femininity, breast and ovarian cancer as a consequence of hormonal imbalance. This study reports the fabrication of electrospun polyurethane (PU) nanofibers modified by coating with polyaniline/polyvinyl alcohol (PANI/PVA) to form filtration membranes for the enhanced removal of ethinylestradiol (EE2) estrogenic hormone. Structural and morphological characterization was performed by FTIR, SEM and optical microscopy, while the detection and quantification of EE2 were analysed using HPLC. To understand the material characteristics, the feasibility of the results based on contact time and kinetics to determine the adsorption capacity coated PU nanofibers was further investigated. Findings demonstrated that EE2 best fitted pseudo-second-order kinetics. Furthermore, the adsorption process was optimised via response surface methodology using a central composite design model by varying parameters such as pH, temperature, the concentration of adsorbate, and adsorbent dosage to determine. It was found that the modified PU membranes had a maximum adsorption capacity of 2.11 mg/g and high removal percentage efficiency of ~82.20% for EE2. Adsorption mechanism and thermodynamics were also evaluated, and the results depicted the adsorption process of EE2 occurred via intraparticle diffusion and was exothermic in nature. Finally, a reusability study was done over six adsorption-desorption cycles to test the consistent effectiveness of the modified PU membrane, which remained above 80% removal capacity. Overall, the findings indicate that treated PU with stabilized PANI particles possess the potential to form an effective adsorbent for eradicating EE2 and other estrogenic hormones from the environment.

1. Introduction

In the last few decades, rapid industrialization and human population growth have raised serious environmental concerns due to the high demand for various synthetic chemicals, which are being released into the environment without proper treatment. These synthetic chemicals contain micropollutants as by-products that tend to pose grave risks to animals and humans, thereby threatening the planet's ecosystem. Amongst all, discharged micropollutants from the pesticide and pharmaceutical industry are of special interest due to their relatively high bio-toxicity. The commonly discharged micropollutants are steroidal hormones such as estrogen, testosterone, estrone, β -estradiol, ethinylestradiol, and estriol that possess bio-potency even at sub nanogram scale [1–3]. These micropollutants along with other synthetically

produced chemicals such as bisphenols and polyfluoroalkyl are known as endocrine-disrupting chemicals (EDCs) due to their adverse interaction with the endocrine system [4–6]. They circulate in the body and are released into the blood via the endocrine system as a primary response to hunger, starvation, obesity, and other physiological functions. The presence of any EDC leads to impairment in many important bodily functions vital for maintaining a healthy body [7]. So far, the scientific consensus is clear about the growing incidence rate of several diseases such as reproductive problems, leukaemia, brain cancer, and neurological disorders associated with exposure to EDCs [6]. Therefore, to alleviate the risk of EDCs, several major health and regulatory institutions around the world have established a threshold level for the concentration of contaminants present in drinking water. Recently, the European Union directive 2020/2184 concerning the quality of drinking

^{*} Corresponding authors.

E-mail addresses: yasir@utb.cz (M. Yasir), sedlarik@utb.cz (V. Sedlářik).

<https://doi.org/10.1016/j.jece.2022.107811>

Received 31 January 2022; Received in revised form 19 April 2022; Accepted 25 April 2022

Available online 28 April 2022

2213-3437/© 2022 Elsevier Ltd. All rights reserved.

water recommended a threshold limit of 1 ng/L as a benchmark for assessing the occurrence and treatment of EDCs [8].

Ethinylestradiol (EE2) is one of the most commonly occurring synthetic steroid due to its extensive use in contraceptive pills and treatment of sexual dysfunctions in females [9]. Unlike the naturally released estradiol, synthetically produced EE2 is 10–50 times more potent and has a high degree of bioaccumulation in vertebrates. Therefore, proper environmental remediation and removal of EE2 has been of main research goal due to relatively high adverse effects on the bio-ecosystems [10]. Over the past few years, EE2 concentration in fresh water resources has been rising gradually as conventional waste water treatment plants are ineffective for the total or partial removal of EE2. To address this problem, several strategies have been implemented to remediate this hormone EE2 as a micropollutant alongside other related environmentally persistent toxicants. Different treatment techniques such as biological degradation, advanced oxidation process, catalytic reduction, photocatalysis, and adsorption method have been investigated [11–19]. Out of these methods, the elimination of EDCs by adsorption process has proven to be more beneficial due to low concentration target compounds, simplicity, and cost-effectiveness [20]. Moreover, the formation of toxic by-products is avoided, which are generated in the case of other conventional techniques. The removal of EDCs by highly adsorbent materials such as activated carbon, carbonaceous materials, biochar, etc., have been investigated [21–23]. However, these materials pose a risk of secondary pollution due to difficult separation from the solution and are usually discarded after limited usage [24]. To resolve this issue, polymer-based nanofibers have been recently investigated with a high degree of recyclability and water permeability, demonstrating their potential for practical application compared to conventional membranes [25,26].

Electrospinning is the most common process by which ultrafine nanofibers in precisely controlled conditions can be fabricated, having small pore size distribution, high surface area, and increased surface flexibility [27,28]. In addition, this technique allows ease in modification of the prepared materials by incorporation of additional components with functionalized properties to achieve higher performance [29]. So far, various types of polymers have been used for fabricating electrospun nanofibers, such as polyacrylonitrile, cellulose acetate, polyamide, and polyvinylidene fluoride [30–34]. Depending on the targeted type of pollutant, additional functional molecules have been introduced in the fibrous matrix, such as polydiacetylene, Au/Ag nanoparticles, Schiff base, polyethyleneimine, and rhodamine derivatives [35–38]. However, post modification of these spun nanofibers to enhance functionality properties with high nitrogen containing compounds is limited. This process has proven to greatly enhance adsorption performance for different persistent environmental pollutants [39,40]. Polyaniline (PANI) is a widely used conducting and electroactive polymer due to its cost-effective synthesis via either simple chemical or electrochemical oxidation [41,42]. This conductive polymer possessed benzenoid and quinonoid rings in its structural units linked by amine- and/or imine-type nitrogen atoms via π - π interactions and hydrogen bonding [43,44]. This makes PANI and its related composite materials promising adsorbents of organic pollutants. However, PANI in combination with supporting polymers such as polyvinyl alcohol, can enhance the materials both with appreciable electrical conductivity and mechanical integrity [45]. In water pollution treatment, the incorporation of such polymer in the adsorbent material increases the presence of nitrogen atoms, which in turn enhances the ability to interact with pollutants via formation of complexes with various organic and inorganic substances to reduce their prevalence in the aqueous phase.

In this study, polyurethane (PU) membranes are prepared via electrospinning and further post modified by coating with polyaniline in a polyvinyl alcohol solution for the enhanced removal of EE2 micropollutant hormone. To understand the characteristics of the coated PU membranes, FTIR, SEM, and optical microscopy were performed. The adsorptive interaction and performance for the removal of EE2 were

further investigated via optimization study using response surface methodology to evaluate the experimental data by analysis of variance (ANOVA) to determine optimum adsorption capacity via adsorptive two parameters interactions. Furthermore, we validated the determined optimal adsorption condition by studying effects on single parameters of solution pH, temperature, initial concentration of the hormone, and adsorbent dosage. Kinetics and thermodynamics of the adsorption process were also calculated. Finally, a reusability analysis of the prepared adsorbent over six adsorption-desorption cycles was performed in order to determine the consistent effectiveness of coated PU membrane.

2. Materials and methods

2.1. Materials and reagents

17 α -ethinylestradiol (EE2, $\geq 98\%$) as the model estrogenic hormone, 4,4'-methylene-diphenyl diisocyanate (MDI), (poly 3-methyl-1,5-pentanediol-alt-adipic, isophthalic acid) (PAIM), 1,4 butanediol (BD), aniline ($\geq 99\%$ purity), hydrochloric acid, (HCl, 37% purity), ammonium peroxydisulfate, poly(vinyl alcohol) (Mowiol 20–98, molecular weight 125,000) and ammonium hydroxide (28–30% NH₃ basis) were purchased from Sigma-Aldrich, Germany. Sodium tetra-borate decahydrate (borax) and citric acid were purchased from PENTA s.r.o., N,N-dimethylformamide (DMF >99.5%) from Lach-Ner, s.r.o., Acetonitrile (HPLC grade) from Honeywell and ethanol (HPLC grade > 99%) from VWR, Czech Republic. Deionized water (pH 7, 18.2 M Ω /cm) was prepared in a laboratory Milli-Q ultrapure (Type 1) water purification system (Biopak® Polisher, Merck, USA) and used for preparation/purification purposes.

2.2. Fabrication of nanofibers

2.2.1. Step 1: preparation of polymer solution

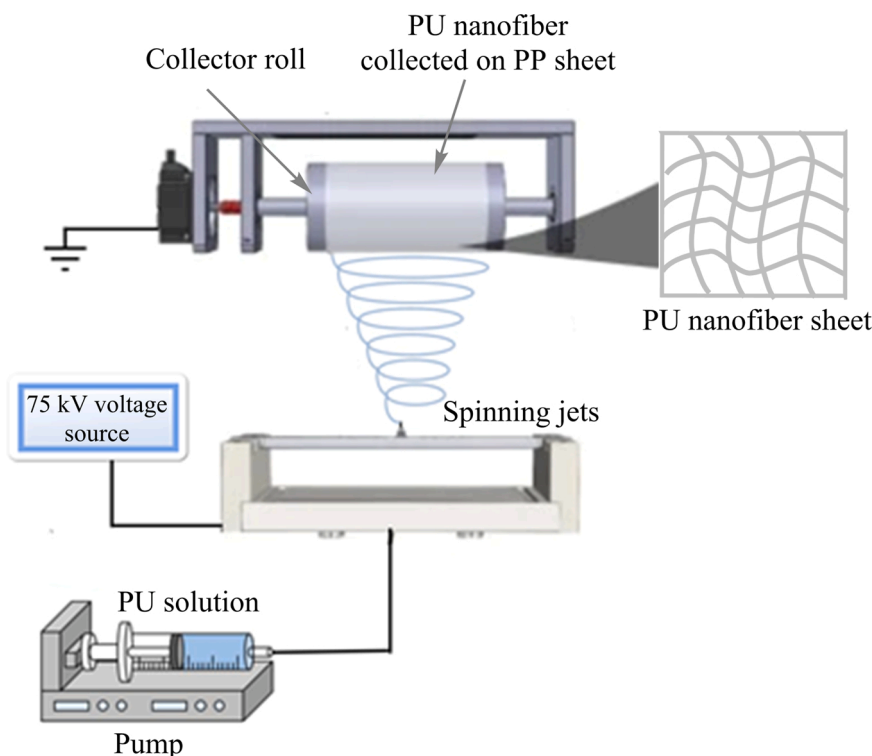
Polyurethane (PU), also known as PU918, was prepared by a polyaddition reaction in the Centre of Polymer Systems (CPS), Zlin, Czech Republic). Initially, MDI, PAIM polymer diol (Mw = 2×10^3 g/mol), and BD in a molar ratio 9:1:8 were synthesized at 90 °C for 5 h (per parts way of the synthesis). The preparation of a pre-polymer started with MDI and PAIM as precursors, followed by the addition of BD and MDI in appropriate amounts. Then, 13 wt% of prepared polyurethane with Mw = 9.8×10^4 g/mol was dissolved in DMF. A separate solution of borax and citric acid (BC) was prepared in a ratio of 1:3, respectively. Then, 35 wt% of BC was dissolved in DMF solution and agitated in a mixer for 5 h at 400 rpm. The electrical conductivity of PU solution was adjusted and optimized to ideal by supplementing with BC solution prior to electrospinning [46].

2.2.2. Step 2: electrospinning process for the production of PU nanofibers

The nanofiber layers were prepared from PU solutions in DMF with a spin line machine in CPS, equipped with a patented rotating electrostatic electrode with nanofibers forming jets (CZ305037; PCT/CZ2010/000042). A schematic illustration of the electrospinning system is illustrated in Scheme 1. The optimum experimental conditions to produce free of defect PU nanofiber membranes were as follows: electric voltage applied to PU solution: 75 kV, PU solution dosing: 0.24 mL/min, relative humidity: 30%, temperature: 22 ± 2 °C, the distance between electrodes: 18 cm, rotational speed of supporting polypropylene (PP) fabric sheet collecting nanofibers: 16 cm/min, and dimension of polypropylene (PP) roll collector: 40 cm of width.

2.3. Post-modification of spun PU nanofiber membrane

Polyaniline (PANI) stabilized with poly(vinyl alcohol) (PVA) system was prepared by the oxidation of aniline in hydrochloride with ammonium peroxydisulfate as previously described [46,47] with slight modifications. In brief, aniline (0.1 M) dissolved in 1 M HCL solution was



Scheme 1. Illustration of the electrospinning system for the production of the PU nanofiber sheets.

mixed with 4 wt% aqueous solution of PVA to form a 50 mL solution. Weighed 0.5 g spun PU nanofiber was dipped in the above prepared solution for 2 h to allow for the adsorption of the aniline monomer on the surface of the fibers. An equal volume (50 mL) of 0.125 M of ammonium peroxydisulfate solution was added to the mixture, shortly stirred, and allowed at room temperature for 24 h for the polymerization of aniline to occur and coating on the spun fibers. The originally white solution turned dark green/black as PANI was produced. The coated spun fibers were then removed and repeatedly re-suspended in 0.2 M HCL to remove residual or unreacted monomers, followed by washing severally with distilled water to neutral pH. The coated sample known as PU-PANI emeraldine salt (PU-PANI-ES) was subsequently freeze-dried for further use. PU-PANI-ES was further converted to PU-PANI emeraldine base (PU-PANI-EB) by suspension of the coated membranes in excess 1 M ammonium hydroxide for 24 h [48]. Thus, blue PANI base coated PU nanofibrous membranes were collected by filtering the residual solution, washed with acetone and water repeatedly, then dried as above.

2.4. Characterization technique

2.4.1. Fourier-transform infrared spectroscopy (FTIR)

FTIR analysis was conducted on a Nicolet 320 spectrometer (ThermoScientific, USA), equipped with Ge crystal to identify the functional groups present on the treated and control PU nanofiber membranes. Attenuated total reflectance (ATR) spectra were recorded across 400–4000 cm^{-1} under standard conditions. The resolution was set to 4 cm^{-1} and the scan rate to 64.

2.4.2. Optical microscopy

Imaging under an optical microscope was collected with a digital microscope of high degree magnification Leica DVM2500 (Leica Microsystems, Czech Republic) in order to observe the coated PU nanofibrous membranes. Visualization was performed under phase contrast mode, which allows visibility of the coated membranes. Imaging was observed at 100x magnification.

2.4.3. Scanning electron microscopy

Micro images were recorded to witness the surface morphology of the fibers on a Nova 450 scanning electron microscope (SEM) (FEI, Thermo Fisher Scientific, USA). Also, the desired fiber diameter and any sort of defects, for instance, beads in the structure, were checked at the acceleration voltage of 5–10 kV via a through-the-lens detector (TLD).

2.4.4. High-performance liquid chromatography (HPLC) analysis

Standard calibration of EE2 hormone and concentration measurement of samples was performed on an HPLC DionexUltiMate 3000 Series (Thermo Fisher Scientific, Germany). A reversed-phase column (Kinetex 2.6 u C18 100 A (150 \times 4.6 mm; Phenomenex, USA)) guarded with a security column (Phenomenex, USA) was used for the separation at 30 $^{\circ}\text{C}$. The mobile phase was a mixture of acetonitrile and water in a ratio (45:55, v/v), and the flow rate was set to 0.8 mL/min under isocratic mode for a total run time of 12 min 20 μL of testing volume was injected onto the column from the sampler chamber at 5 $^{\circ}\text{C}$. The EE2 hormone elute concentrations were detected and quantified at a wavelength of 200 nm.

2.5. Adsorption experimental design

Batch static adsorption was performed to determine the removal capacity of investigated coated spun PU nanofiber membranes. 100 mL hormone solutions in 250 mL conical flasks were used to investigate the adsorption efficiency. The flasks were under continuous shaking on an orbital incubator shaker (Stuart® S1500, Barloworld Scientific Ltd., UK) at 250 rpm by varying different parameters of initial concentration of hormone (mg/L), solution pH, adsorbent dosage (mg), and temperature of adsorbate solution ($^{\circ}\text{C}$). At predetermined time intervals, 4 mL of residual solution was collected, followed by readings performed in triplicate and the average values recorded. The equilibrium adsorption capacity and removal percentages of the hormone were then determined using the mathematical Eqs. (1) and (2), respectively [46,49].

$$\text{Hormone uptake}(q_e) = v \times \frac{(C_i - C_t)}{M} \quad (1)$$

$$\text{Hormone removal } (\%) = \frac{C_i - C_t}{C_i} \times 100 \quad (2)$$

where C_i is the initial concentration (mg/L), and C_t is the concentration of the solution at time t (mg/L). M is the mass of adsorbent (g), V is the volume of solution (L), and q_e is equal to the equilibrium adsorption capacity (mg/g).

Central Composite Design (CCD) model was employed using the Design-Expert software v13.0 to estimate and optimize the most influencing factors and their interaction effects on EE2 hormone removal by the coated spun PU nanofiber membranes. CCD is composed of factorial points corresponding to axial and central points [50,51]. The levels of the main investigated factors are given in Table 1. The relationship between these independent factors based on the obtained responses is fitted to a second-order polynomial equation that allows for the modelling of responses of the hormone, which is expressed by Eq. (3).

$$Y = \beta_0 + \sum_{i=1}^k \beta_i X_i + \sum_{i=1}^k \beta_{ii} X_i^2 + \sum_{i=1}^k \sum_{j=i+1}^k \beta_{ij} X_i X_j + \varepsilon \quad (3)$$

Where Y is the response (removal efficiency), X_i and X_{ij} are the encoded parameters, and β_0 , β_i , β_{ii} , and β_{ij} are the linear, quadratic, and interaction coefficients, respectively. Based on the results generated, the desirability function is then employed to obtain the optimization of investigated parameters (best levels for each factor).

2.6. Adsorption-desorption analysis

After adsorption, the adsorbent material was treated by desorption of the adsorbed EE2 hormone. For the desorption test, the PU adsorbents were extracted from the conical flasks containing the hormone solutions and washed with distilled water, followed by gentle stirring at a constant 100 rpm for 10 min in a 100 mL mixture of 1:1 water and ethanol to remove the hormones entirely and eluted in the aqueous phase. Then, the PU adsorbent was re-placed in 100 mL water until the next adsorption cycle. The procedure was repeated for six consecutive adsorption-desorption cycles. Readings were collected in triplicates, and the average value was recorded.

2.7. Statistical and error analysis

The data are displayed as Mean \pm Standard error. OriginLab v.9.0 and Design expert software v.13.0 were used for statistical analysis. The difference between values was determined by a one-way analysis of variance (ANOVA). A value of $p < 0.05$ was determined as statistically significant. Error analysis parameters such as the determination coefficient (R^2) were used to ascertain the difference between the experimental and theoretical data. In addition, the sum of squared errors (SSE) and Chi-squared (χ^2) were employed to minimize errors since inherent bias occurs during the linearization of equations, such as in kinetic modelling.

Table 1

Investigated experimental factors and their levels in the central composite design.

Factors	Low (-1)	Center (0)	High (+1)
A - Temperature (°C)	25.00	40.00	55.00
B - Solution pH	5.00	7.00	9.00
C - Initial conc. of hormone (mg/L)	0.20	0.30	0.40
D - Adsorbent dosage (mg)	10.00	20.00	30.00

3. Results and discussion

3.1. Modification of spun nanofibers

PANI is typically achieved by the oxidation of aniline with ammonium peroxydisulfate in an acidic aqueous medium at room temperature, followed by deprotonation with ammonium hydroxide for PANI base (Scheme 2a). The treatment of the PU nanofibrous membrane with PANI serves as an alternative to improve the functional properties of materials. In order to obtain soft conducting and filtration membranes, another component, such as a water-soluble supporting polymer, in this case, PVA was incorporated into the system to enhance homogenous PANI being formed with low agglomeration and increase surface interaction with the PU fibers [46,52]. PVA, as a supporting polymer, forms a skeletal network between the PANI particles and PU fibers that further strengthens the integrity of the membrane [46]. Considering that PANI is produced in the vicinity of the PVA phase, where the reactants are gradually concentrated during polymerization and bind to the PU fiber surface to form PU-PANI-ES, which is then deprotonated to PU-PANI-EB in the basic medium (Scheme 2b and c). This leads to the formation of modified PU nanofibrous membranes rich in nitrogen atoms, which is composed of conducting and supporting polymer phases possessing a composite nature. This makes them suited as good adsorbents to be explored for the removal of micropollutants (such as estrogenic hormones) from the aqueous phase.

3.2. Material characterization

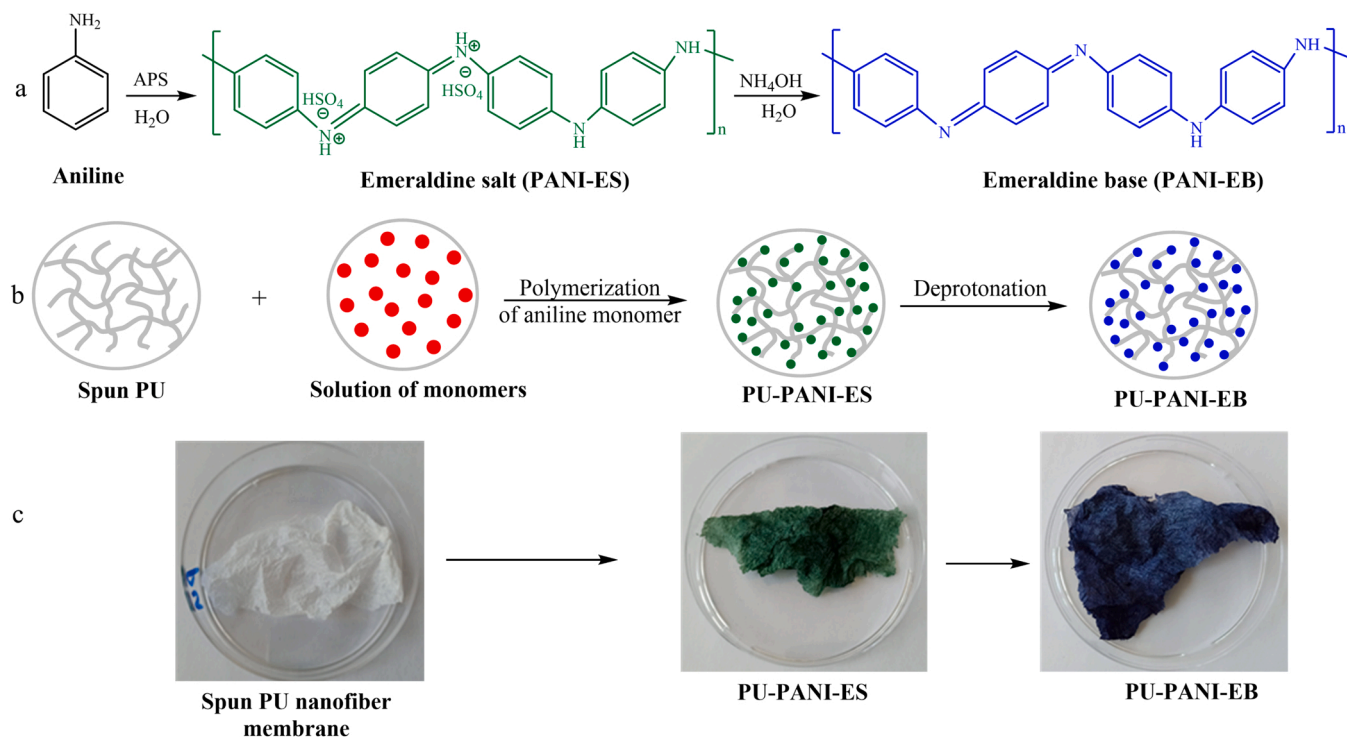
3.2.1. FTIR analysis

The FTIR spectra of neat PU, PU-PANI-ES, and PU-PANI-EB are presented in Fig. 1. The FTIR spectra of PU shows a broad peak between 3700 and 3200 cm^{-1} corresponds to the N-H bond stretching vibrations from the aliphatic amino group of carbamate. The peaks at 2952 and 2889 cm^{-1} reflect C-H asymmetrical flexing vibration of aliphatic CH_2 groups, respectively [53]. The strong absorption peak around 1710 cm^{-1} is ascribed to amido ester C=O stretching vibration [54,55]. The peaks at 1590 and 1522 cm^{-1} are attributed to the N-H bending of the amide group. The characteristic peaks arising at 1410 and 1307 cm^{-1} illustrate the stretching vibration in the skeleton of the benzene ring due to the C=C bond [56]. The stretching vibration peak at 1240 cm^{-1} relates to the C-N bond from the amide group. The asymmetric flexing vibration of C-O-C bonds is caused by alkyl ether and is represented by a sharp peak at 1080 cm^{-1} [46,57]. The peak at 708 and 730 cm^{-1} are attributed to aryl C-H bending. PVA did not show any obvious absorption band in the study, which may be attributed to overlapping its peak with PU.

The FT-IR spectra of PU-PANI-ES and PU-PANI-EB showed a characteristic broad band between 3700 and 3200 cm^{-1} , attributed to the overlapping stretching vibrations of N-H from PU, PANI, and OH from PVA. The peaks at about 1590 and 1522 cm^{-1} which showed increased intensity for coated PU materials with PANI are ascribed to the absorption of quinone and benzene rings of PANI [58]. The peaks at 1307 and 1136 cm^{-1} also depicted increased intensity for PANI coated PU materials and relates to the alkyl C-N stretching vibration from PU and PANI. The peak at 815 cm^{-1} further showed increased intensity for the PANI coated samples and is attributed to the π localized polaron band of coated PANI on PU fibers [59].

3.2.2. Optical microscopy

It is visible by the optical microscopy (Fig. 2) that the coated samples (either green or blue) provide good phase contrast while showing the fibrillary structure of the membranes. After freeze-drying, they convert to lightweight membranes. Considering the change in color of the PU membranes from white to green and blue confirms the coating of PANI on the fiber surface of PU during preparation. This makes the formed modified PU membranes suited to be exploited as novel adsorbents.



Scheme 2. (a) Aniline is oxidized to PANI (emeraldine) salt (PANI-ES) with ammonium peroxydisulfate and deprotonated to PANI (emeraldine) base (PANI-EB) using ammonium hydroxide. (b) Spun PU membrane (gray spirals) mixed with a solution of monomers (red circles) subsequently monomer polymerize to a polymer (green objects) and adhere to PU fiber surface. After that green PANI is deprotonated to an emeraldine base (blue objects). (c) Images of neat spun PU membrane, PU-PANI-ES and PU-PANI-EB coated membranes.

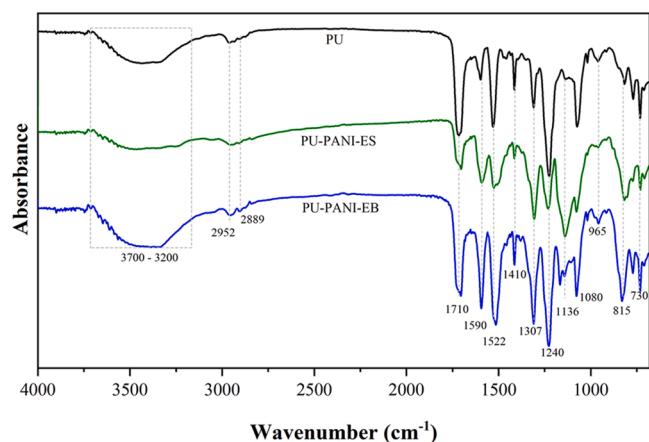


Fig. 1. FTIR spectra of neat PU as control, PU-PANI-ES, and PU-PANI-EB treated fibers from attenuated total reflectance (ATR) sampling.

3.2.3. SEM analysis

The micrographs in Fig. 3 show that the electrospun nanofiber of PU exhibit a minimum diameter of approximately 174 ± 56 nm, as previously reported by Yasir et al. [46]. These fibers, after treatment with PANI become more dense and thicker due to the adsorption of polymerized PANI particles on the surface of fibers. This makes the structure more compact, as seen in the case of PU-PANI-ES and PU-PANI-EB. However, PU-PANI-ES is more denser compared to PU-PANI-EB because the latter was further deprotonated, which may have resulted in the loss of some particles during treatment, making it less dense. Overall, both of the modified materials appear to have a better

morphology compared to the PU control, and it is also proved further by the improvement in the performance of the materials shown in the following section.

3.3. Adsorption study

In order to test the efficiency of prepared materials as suitable adsorbents, a preliminary adsorption study was performed for neat PU and coated PU samples (PU-PANI-ES and PU-PANI-EB). Fig. 4 presents the results obtained from the experiment done with 20 mg of each adsorbent in 100 mL EE2 hormone solution with a concentration of 0.20 mg/L for 3.5 h at 150 rpm, room temperature, and pH 7. The results show that the coated PU materials with PANI significantly improved the adsorption of EE2. The neat PU had a removal efficiency and adsorption capacity of 55.38% (0.612 mg/g), which increased to 81.46% (0.900 mg/g), and 90.33% (0.998 mg/g) for PU-PANI-EB and PU-PANI-ES, respectively. Based on the achieved results, the best sample (PU-PANI-ES) was further studied via an optimization study to determine the optimum removal conditions for the EE2 hormone.

3.4. Batch adsorption optimization study

The optimum adsorption parametric conditions for the present study were determined by analysis of the obtained experimental data (Table 2) via CCD model using response surface methodology. The recorded experimental response values (removal capacity) were fitted to a second-order polynomial equation generated by the Design-Expert 9 software (Stat-Ease Inc., USA). Herein, 20 experimental runs were evaluated according to the response surface design method. Four operating factors were investigated in the optimization study, including temperature, solution pH, initial concentration of the hormone, and

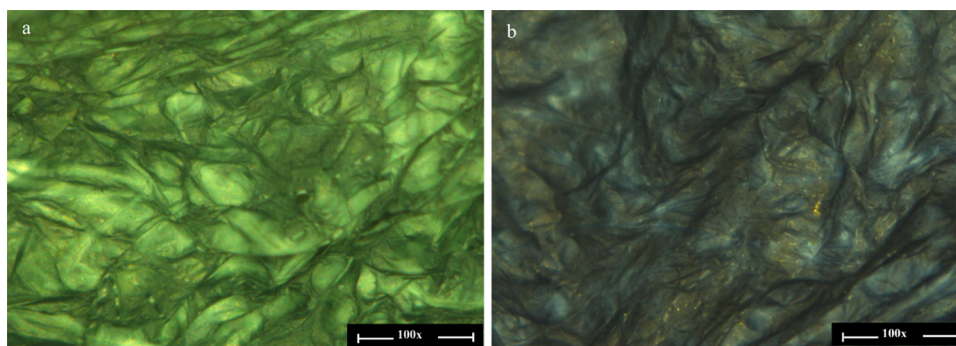


Fig. 2. Optical micrograph of coated (a) PU-PANI-ES and (b) PU-PANI-EB membranes at 100x magnification.

adsorbent dosage, coded as A, B, C, and D, respectively. Experimental runs were generated and ran in random sequence to determine the actual removal efficiency response values from the collected experimental data, while the predicted response values were determined using the quadratic polynomial model as given in Eq. (4):

$$\begin{aligned} \text{Removal\%} = & +84.09 - 3.59A + 8.35B - 1.59C + 7.65D + 0.1841AB \\ & - 2.16AC + 1.72AD - 2.85BC - 8.24BD - 0.1004CD - 7.25A^2 \\ & + 3.79B^2 - 2.95C^2 - 2.01D^2 \end{aligned} \quad (4)$$

3.4.1. ANOVA for quadratic model

The analysis of variance (ANOVA) was employed to support the acceptability of the design model. Table 3 shows the obtained ANOVA data from the Design-Expert software. According to the results presented, the F-value of the model was 20.66, implying that the model is significant, and there is only a 0.17% chance that an F-value this large could occur due to noise. The significance of the studied model was also confirmed by the very low P-value of the model (P model = 0.0017). This value also relates to describe the close agreement between actual and predicted responses observed in Table 2 [60,61]. The P-value for the linear and quadratic terms of the model was also studied. In this case, the model terms B, D, AD, BC, BD, A², and B² are significant, showing that solution pH (B), adsorbent dosage (D), and quadratic terms are highly significant, while the other linear and quadratic terms of the model showed low significance.

The Lack of Fit value of 2.85 implies not significant, which is good because we want the model to fit. There is a 20.23% chance that a Lack of Fit F-value this large could occur due to noise. The determination coefficient (R²) had a value of 0.983, implying that 98% of the variations in this model were predicted and calculated using the established quadratic model. In addition, the calculated adjusted R² value (0.935) was close to the predicted R² value (0.845) with a difference of less than 0.20. Considering the three R² values were high, this indicates that the polynomial model is validated and well fitted to the experimental design responses [51]. The adequacy of the model was further confirmed and validated by the correlation plot between the predicted and actual responses, as shown in Fig. 5a. Moreover, the observed residuals versus the fitted predicted responses were also plotted in Fig. 5b and displayed a normal random distribution of residuals [62].

3.5. Optimization validation

The optimized operating factors suggested by the Design-Expert software were determined as follows; solution pH 7.0 (considering that wastewater or river water is in the range of pH 6–8), initial EE2 hormone concentration 0.30 mg/L, adsorbent dosage 20 mg, and temperature 40 °C. To optimize the operating parameters, the lower and upper limits of the operating parameters were chosen based on the studied ranges. The target was selected based on the most desirable conditions. The deduced predicted values for removal percentage and

adsorption capacity are provided in Table 4. To confirm the generated predicted values, a validation test was performed using the determined optimum conditions. Results showed a close correlation between the predicted and experimental responses, validating the significance of the model.

3.6. Effect of two interaction parameters on the removal of EE2 hormone

The 3D response surface plots help in the comprehensive evaluation of the operation of the system under the framed experimental design and elaborate to understand the effects caused on the response by variation of the experimental factors. The observation obtained are discussed as follows:

Fig. 6a demonstrates the effect of temperature and solution pH on the removal percentage of EE2. As can be seen, an increase and then decrease in removal percentage was observed with an increase in temperature ranging from 25 to 55 °C. Whereas, a linear rise in removal percentage was seen with an increase in pH because EE2 remains undissociated in this pH range till pH reaches its value of pK_a (10.50) [63, 64]. The highest removal percentage recorded was 95.60% at 40 °C temperature and pH 9. On the other hand, the lowest removal percentage occurred at pH 5 and a temperature of 55 °C. This is because the adsorption here is of exothermic nature and spontaneous, which favors lower temperatures [65]. In Fig. 6b, the effect on EE2 removal percentage is observed by varying temperature and concentration of the hormone solution. The EE2 removal percentage increased and then decreased with an increase in temperature, which indicates that the adsorption of EE2 on PU-PANI-ES is exothermic, favoring high removal efficiency at a lower temperature [66]. At a high concentration of hormone 0.4 mg/L and temperature 55 °C, the removal percentage appears to be the least. The highest removal percentage of 82.10% is found to be at optimum parameters of 40 °C and 0.3 mg/L concentration of the hormone. Fig. 6c depicts the effect of temperature and dosage of adsorbent on the removal percentage of EE2. The temperature ranged from 25 to 55 °C, and the dosage of the adsorbent from 10 to 30 mg. An increase in removal efficiency followed by a decrease with increasing temperature, as described above, relates to the exothermic nature of the adsorption process. However, the removal percentage increased linearly with an increase in the dosage of the adsorbent. This could be due to the increase in the number of sites leading to an increase in the contact surface area as the amount of adsorbent increased [67]. The highest removal percentage achieved was nearly 90%, with a 30 mg dosage of the adsorbent at 40 °C.

In Fig. 6d, the effect of changing solution pH and concentration of the hormone is seen on the removal percentage. The solution pH ranges from 5 to 9 and concentration from 0.20 to 0.40 mg/L. The removal percentage is slightly high at pH 5 and at a higher concentration of 0.4 mg/L. However, there is a sharp rise in removal percentage from nearly 70.00% at pH 5–96.00% at pH 9. The highest removal percentage is found to be at 0.20 mg/L concentration and pH 9. However, the

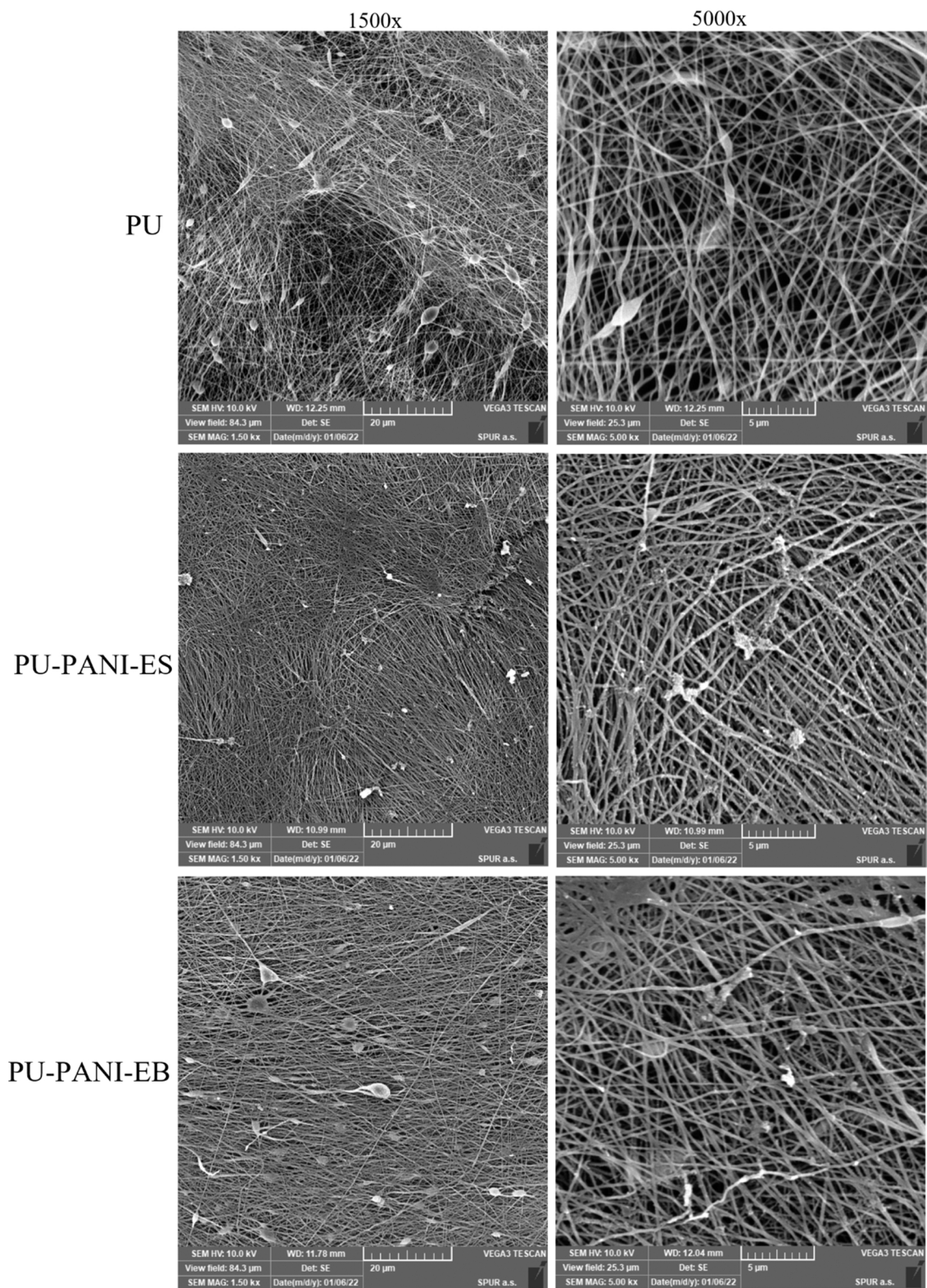


Fig. 3. SEM images of PU as control, PU-PANI-ES, and PU-PANI-EB treated fibers at different magnifications of 1500x and 5000x.

removal percentage is seen to decrease by an increase in concentration from 0.20 to 0.40 mg/L at constant pH 9. A plausible reason could be that all the active sites are already occupied, reaching saturation, and a rise in concentration led to a drop in removal percentage [67]. Fig. 6e illustrates the effect of dosage of adsorbent and solution pH on the removal percentage of EE2. It is evident from the graph that at pH 5 and

10 mg of dosage, the least removal percentage was achieved. Furthermore, the removal percentage linearly increased by either solely an increase in pH of the solution or an increase in the dosage of adsorbent. Whereas, at pH 9, increasing the dosage of adsorbent had a negligible effect on removal percentage, but at pH 5, the difference was distinguishing; a rise in removal percentage from 50.00% at a dosage of

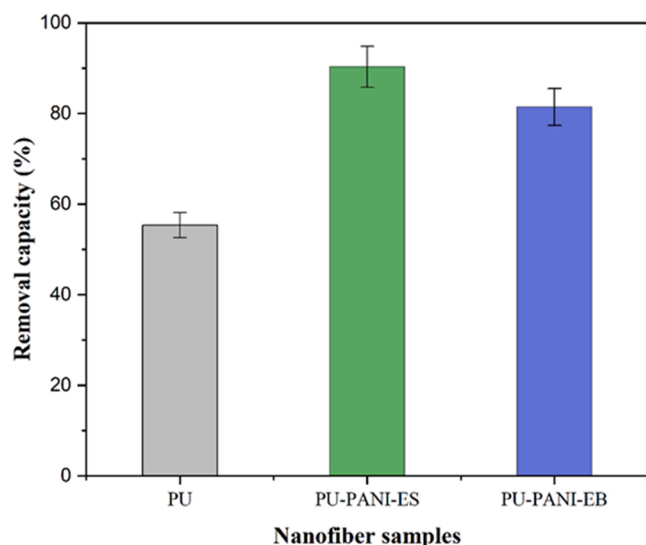


Fig. 4. Adsorption removal of EE2 using PU as control, PU-PANI-ES, and PU-PANI-EB treated nanofibrous membranes.

Table 2

The different experiment runs with their actual and predicted responses.

Runs	Factors				Removal capacity (%)	
	A	B	C	D	Actual response	Predicted response
1	40	7	0.2	20	84.58	82.72
2	40	7	0.3	20	82.12	84.09
3	40	7	0.3	40	89.17	89.72
4	40	7	0.3	30	85.85	84.09
5	55	9	0.2	10	85.52	85.98
6	40	5	0.3	20	78.98	79.53
7	25	9	0.4	30	83.46	82.72
8	40	9	0.3	20	95.67	96.23
9	55	7	0.3	20	72.70	73.25
11	55	9	0.4	10	85.85	84.09
13	55	5	0.4	30	73.72	72.98
14	40	7	0.3	10	85.85	84.09
15	55	5	0.2	30	80.90	80.16
16	25	5	0.2	10	73.88	74.43
17	25	7	0.3	20	81.68	82.15
18	40	7	0.4	20	52.93	53.39
19	25	5	0.4	10	79.87	80.42
20	25	9	0.2	30	76.59	79.55

10 mg to around 92.00% at a dosage of 30 mg was seen which indicates a rapid rise in adsorption. The highest removal percentage of about 96.00% interpreted from this graph was at pH 9 and 20 mg of dosage. Fig. 6f represents the influence of the concentration of hormone and the dosage of adsorbent on EE2 removal percentage. As can be seen, at a dosage of 10 mg, the removal percentage is the least and is almost unaffected by an increase in the concentration of the solution. However, the removal percentage is high at a lower concentration if the dosage is kept constant. Whereas, there is a gradual rise in the removal percentage by increased dosage of adsorbent for all the given concentrations of the solution. At a dosage of 30 mg, a slight increase and then decrease is observed in the removal percentage of EE2 by the increase in the concentration of the solution. This indicates that the rise was due to an increase in the amount of EE2 hormones adsorbed on the sites of the adsorbent until the 0.30 mg/L concentration of the solution. At this point, all the available sites on the adsorbent were completely filled by EE2 hormones, and a further increase in concentration led to a decrease in removal percentage because no additional EE2 hormone molecule could be adsorbed on the adsorbent's surface [63].

Table 3

ANOVA data for removal of estrogenic hormone based on CCD quadratic model.

Source	Sum of Squares	df	F-value	p-value	
Model	1752.04	14	20.66	0.0017	significant
A-Temperature	25.72	1	4.24	0.094	
B-pH	139.43	1	23.01	0.004	
C-Conc of hormone	25.13	1	4.15	0.097	
D-Dosage of adsorbent	116.93	1	19.30	0.007	
AB	0.05	1	0.09	0.093	
AC	37.39	1	6.17	0.056	
AD	4.76	1	7.85	0.042	
BC	65.17	1	10.76	0.022	
BD	108.62	1	17.93	0.008	
CD	0.08	1	0.01	0.913	
A ²	133.88	1	22.10	0.005	
B ²	36.58	1	6.04	0.006	
C ²	22.18	1	3.66	0.114	
D ²	10.29	1	1.70	0.249	
Residual	30.29	5			
Lack of Fit	19.85	2	2.85	0.202	not significant
Pure Error	10.44	3			
Cor Total	1982.33	19			

3.7. Effect of single parameters on the optimal removal of EE2 hormone

In order to further validate the determined optimum conditions for the removal of EE2 hormone, the removal efficiency and adsorption capacity of PU-PANI-ES adsorbent was evaluated by varying a single factor (solution pH, initial EE2 concentration, dosage, and temperature) while keeping the other factors constant at determining optimum values.

3.7.1. Effect of solution pH

In Fig. 7a, an increasing trend is observed with an increase in the pH of the solution. There is a gentle rise in efficiency from 79.90% at pH 5 to about 82.10% at pH 7; however, there is a sharp increase in efficiency, reaching 95.70% at pH 9. A similar trend was followed for the values of adsorption capacities which were about 1.67, 1.70, and 2.00 mg/g for pH 5, 7, and 9, respectively. Usually, pK_a represents the acid dissociation constant at which EE2 can lose its hydrogen atom and become negatively charged. The pK_a of EE2 is in the range of 10.25–10.50; therefore, in this case, the pH of the solutions remained below 9.5. Thus, no cation-anionic attraction was expected to occur between EE2 and adsorbent, and EE2 remained neutral [68]. However, at higher pH above pK_a , adsorption efficiency is expected to decrease due to charge repulsion [69].

3.7.2. Effect of initial EE2 hormone concentration

Fig. 7b represents the influence of the initial concentration of EE2 in the solution on the efficiency of PU-PANI-ES fibers. It can clearly be seen that the efficiency of fibers linearly decreased, whereas the adsorption capacity increased with an increase in the concentration of EE2 in the solution. At 0.20 mg/L concentration, the highest removal efficiency of 84.62% and lowest adsorption capacity of 1.09 mg/g was reported, while at 0.40 mg/L concentration, the lowest removal efficiency of 76.64% and highest adsorption capacity of 2.21 mg/g was reported. This is because high removal efficiency is expected with a large number of active sites available for adsorption. However, at a higher initial concentration of the solution, less number of sites are left gradually due to saturation leading to a reduction in removal efficiency [67].

3.7.3. Effect of dosage

In Fig. 7c, the effect of adsorbent dosage was determined on its removal efficiency and adsorption capacity. The removal efficiency linearly increased from 73.90% at a dosage of 10 mg to 89.20% at a 40 mg of fiber dosage. The response for adsorption capacity was the

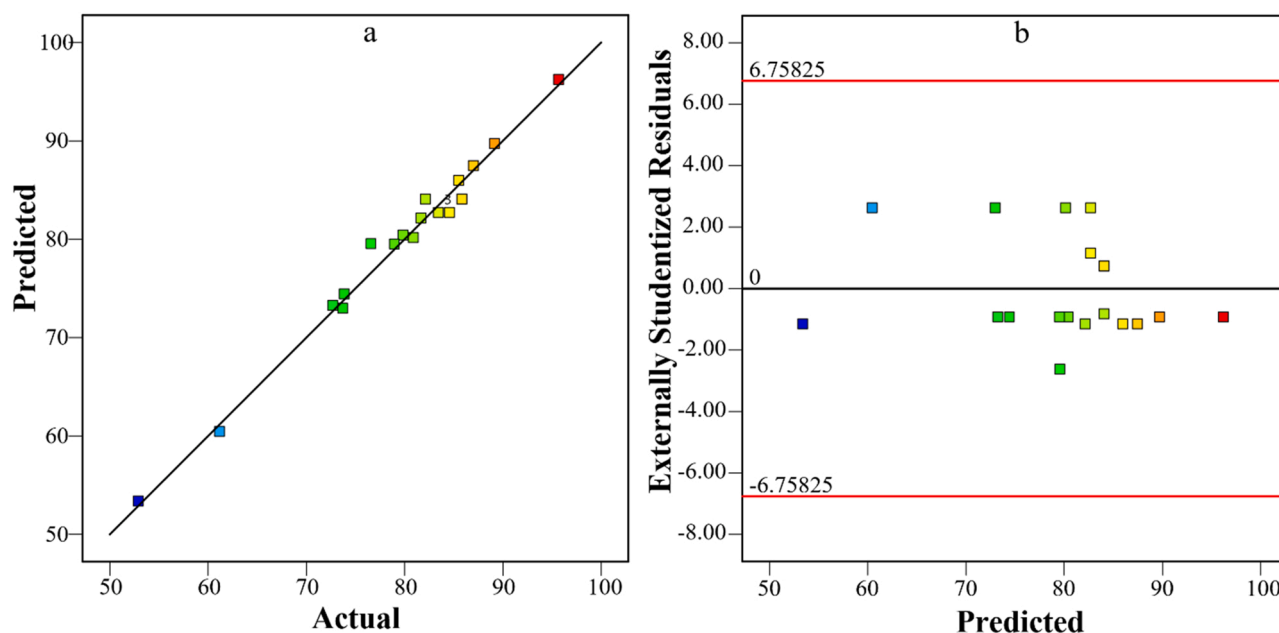


Fig. 5. (a) Plot of predicted and actual responses values and (b) residual plot for EE2 hormone removal.

Table 4

Point prediction and validation of optimized parameters at 95% confidence interval.

Response	Predicted Mean	Observed	Std Dev	SE Mean	Desirability
Removal percentage (%)	84.08	82.20	2.46	0.85	1.00
Adsorption capacity (mg/g)	1.88	2.11	0.29	0.10	1.00

opposite. It was 3.04 mg/g observed at 10 mg of dosage, which decreased to 0.91 mg/g for 40 mg of dosage. This is expected to happen due to the large surface area available at high dosage, creating more number of sites for adsorption. Thus, high removal percentage is observed [63,67].

3.7.4. Effect of temperature

In Fig. 7d, the effect of temperature variation was observed on the performance of the coated PU membrane. It can be seen that both removal efficiency and adsorption capacity of coated PU increased between 25 and 35 °C, and then they decreased with further increase in temperature to 55 °C. The optimum temperature observed was 35 °C, with a removal efficiency of 82.10%, and an adsorption capacity of 1.70 mg/g was recorded. The values at a higher temperature of 55 °C were 72.70% and 1.58 mg/g, respectively, which were lower than the values obtained at room temperature of 79.90% and 1.63 mg/g, respectively. This is because the nature of adsorption is exothermic in this case which favors higher adsorption as lower temperature [66]. A more detailed description is given in the later section about thermodynamics.

3.8. Adsorption mechanism

The aim of this section is to elucidate the types of mechanisms that occur simultaneously and contribute to the adsorption of EE2 on PU-PANI-ES, as presented in Scheme 3. The extent of such mechanisms depends on the types of functional groups present on the fiber, the nature of the hormone (hydrophobicity), and the amount of surface available on fibers for interaction. Based on the studied material, the

types of adsorption interaction mechanisms include physical adsorption, hydrophobic interaction, π - π stacking interaction, cation- π interaction, and hydrogen bonding. EE2 has an OH terminal group, which can act as a strong donor and acceptor, while the benzene ring chain can act as a weak π acceptor [69]. In addition, the presence of high amounts of nitrogen atoms from PU and PANI increases the interaction of the adsorbent with the hormone via a hydrogen bond, electrostatic interaction, and weak van der Waals forces. Furthermore, the physical adsorption of EE2 on the surface of PU-PANI-ES with an approximate average diameter (174 ± 56 nm) and inner pores (16.99 nm) present on the fiber's surface possess a large surface area that contains active sites for accumulation of EE2 hormones [46].

K_{ow} is the parameter value to determine the hydrophobicity of estrogenic hormone by partitioning between octanol and water. Hormones with a value greater than 2.50 are generally expected to accumulate in the solid phase instead of dissolving in an aqueous solution. The K_{ow} of EE2 is 3.67, which is above 2.50; thus, it is likely to undergo hydrophobic interaction with PU. Weak π - π stacking interaction also occurs between the electron-rich and deficient benzene aromatic rings (phenol group) available in PU, PANI, and EE2 hormone by overlapping of double bonds [69]. Comparing the results in Fig. 4, the decrease in adsorption percentage from 90.30% for PU-PANI-ES to 81.50% for PU-PANI-EB is a consequence of the loss of positively charged amine groups in PU-PANI-ES when deprotonated to PU-PANI-EB, which in turn decreases the forms cation- π interaction with the aromatic benzene rings of EE2 [69]. PU is the most robust adsorbing polymer tested among other polymers in the previous study, owing to its polar nature [46]. PU consists of N-H and C=O functional groups that can form hydrogen bonding with the O-H terminal groups present in EE2 [70]. Herein, PU-PANI-ES fibers were chemically functionalised with an excess of amine groups present on the surface, as a result, enhanced the adsorption of EE2 on its surface as compared to the non-coated PU (as control). Furthermore, size-exclusion is another factor essential for membrane filtration, but it is unexpected here in the adsorption mechanism, which is primarily dependent on the molecule size of EE2, the pore size of fibers, and functional properties. The molecular size of hormones reported in the literature (0.79 nm) is far less than the mean porosity of the control PU fibers structure (0.47 μ m); hence this factor is excluded from consideration [46,71].

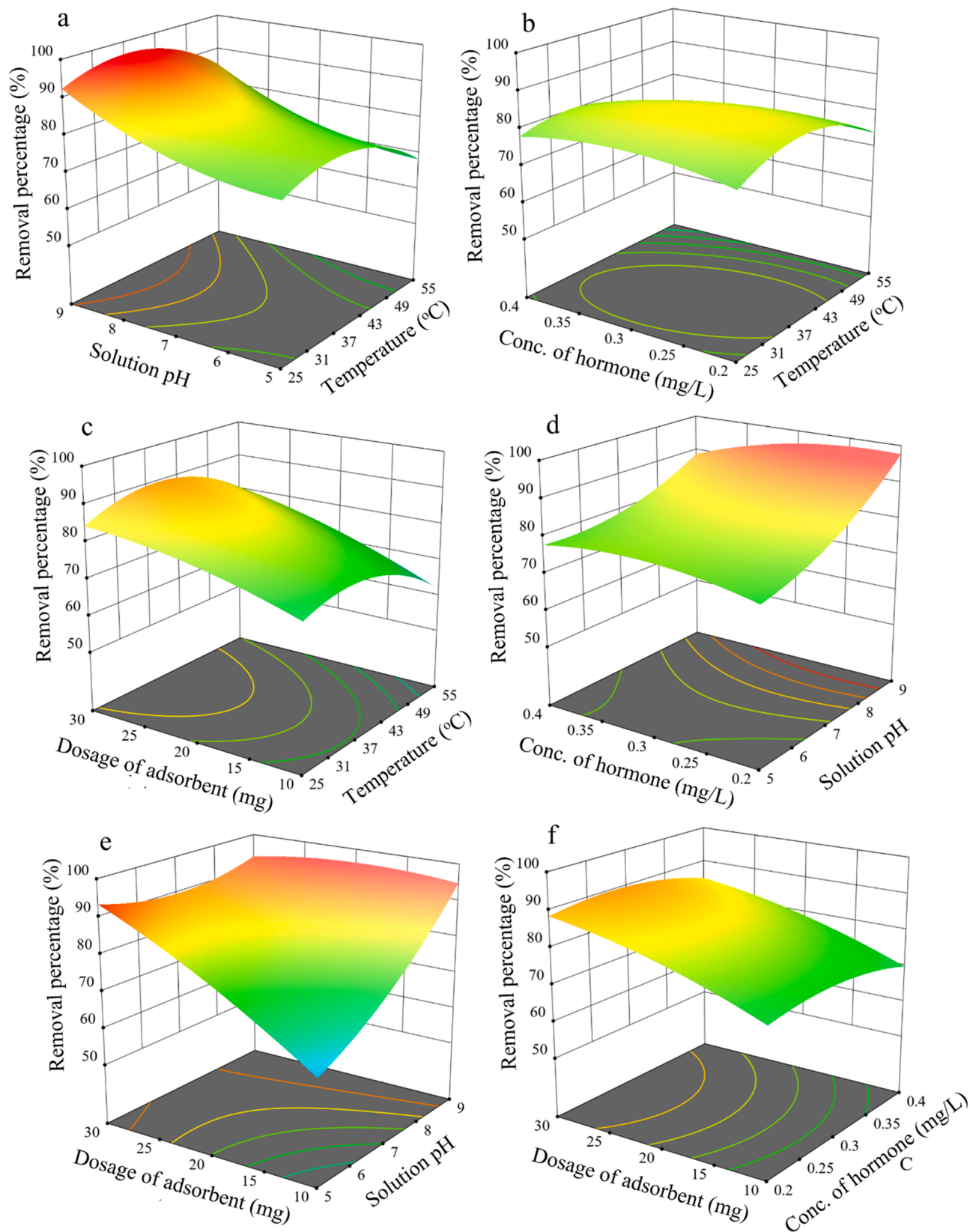


Fig. 6. 3D two parameter interaction response surface plot on the removal of EE2 hormone using PU-PANI-ES membrane.

3.9. Kinetic modelling

To better understand the effects posed on adsorption interactions and determination of the rate-limiting step, kinetic studies on the adsorption

process of the hormone was studied. In general, the evaluation of different kinetic models helps in the precise selection of best suited parameters for the optimum removal rates [72]. This is because several mechanisms occur together in a complex closed system which may cause

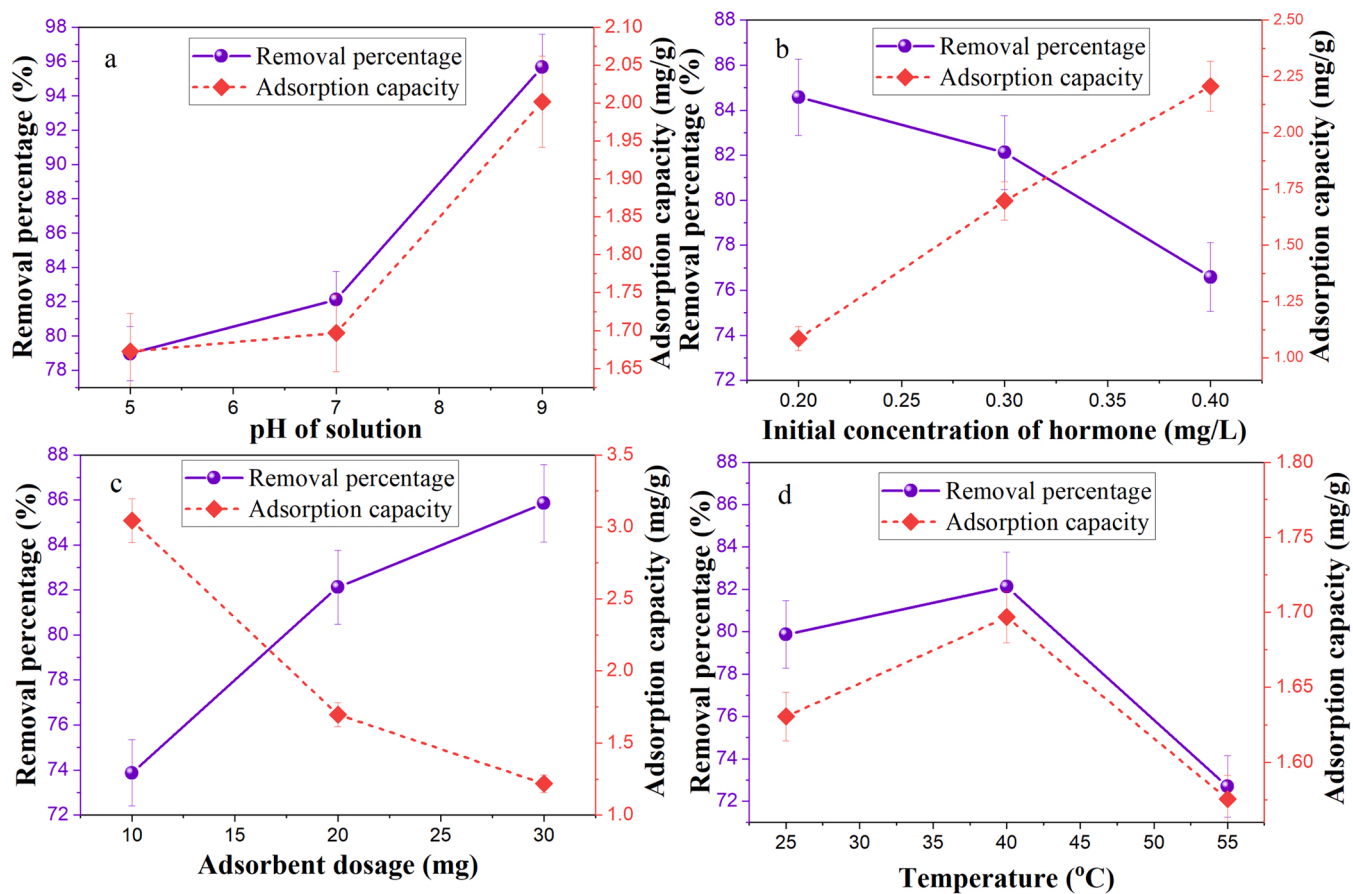
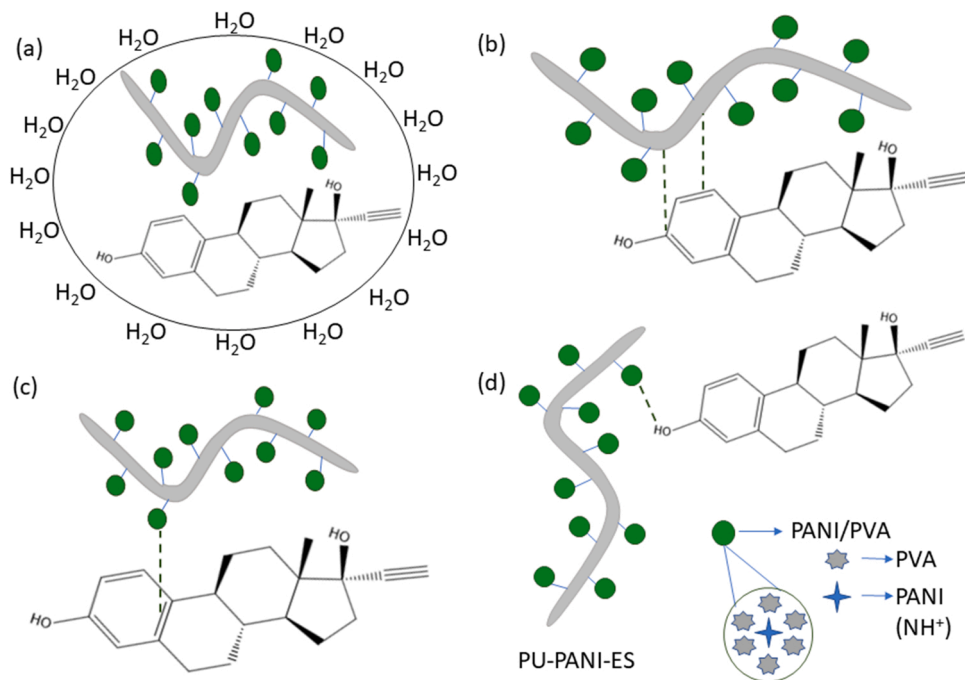


Fig. 7. Effects of different adsorption parameters on removal percentage and adsorption capacity: a) pH of the solution, b) initial concentration of EE2, c) adsorbent dosage, and d) temperature on the removal of EE2 hormone using PU-PANI-ES fibers.



Scheme 3. Possible interaction mechanisms between EE2 and PU-PANI-ES fibers; (a) hydrophobic interactions, (b) π - π stacking interaction, (c) Cation- π interaction, and (d) hydrogen bonding.

surface effects to overshadow the chemical effects during adsorption analysis. Thus, four of the most renowned kinetic models, pseudo-first-order, pseudo-second-order, Weber-Morris intraparticle diffusion, and Boyd's model, were employed for the data generated from the set of experimental values [53,64]. Pseudo-first order model is widely used for explaining the solid/liquids systems to evaluate the adsorption of an adsorbent in an aqueous medium. This model prescribes that the adsorption rate of EE2 hormone is directly proportional to the amount adsorbed from the given aqueous solution. The pseudo-second-order equation predicts the adsorption capacity of the adsorbent over the long-range experimental time. It assumes that the rate-determining step is caused by surface adsorption, which is guided by the physicochemical interactions owing to chemisorption between adsorbent-adsorbate phases. The Weber-Morris intraparticle model to obtain adsorption rates is related to the diffusion of adsorbate towards the adsorbent. This is proportionally dependent on its speed for diffusion. Boyd's model accounts for the free diffusion of a solid spherical adsorbent in a solution phase. The following equations of the stated models are given below, respectively.

$$\log(q_e - q_t) = \log q_e - \frac{K_1}{2.303} t \quad (5)$$

$$\frac{t}{q_t} = \frac{1}{K_2 q_e^2} + \frac{t}{q_e} \quad (6)$$

$$q_t = K_3 t^{0.5} + C \quad (7)$$

$$B_t = -0.4977 - \ln(1 - F) \quad (8)$$

where q_e and q_t (mg/g) represent the adsorption capacities at equilibrium and time, t , respectively. K_1 (min^{-1}) is the pseudo-1st order adsorption rate constant, K_2 (g/mg min) is the rate constant of the pseudo-2nd order adsorption process. Following the Pseudo-1st order equation, a plot of $\log(q_e - q_t)$ versus t (Fig. 8a) was deduced, and the values of K_1 and q_e were obtained from the slope and intercept, respectively. A graph of t/q_t versus t (Fig. 8b) was also plotted based on the pseudo-2nd order model to determine the values of K_2 and q_e from the slope and intercept, respectively. K_3 ($\text{mg/g min}^{0.5}$) is the intraparticle diffusion rate constant, C (mg/g) is the boundary layer effect that contributes to the rate-limiting adsorption step, Bt is the Boyd parameter related to the adsorption process, and F is the fraction of solute adsorbed at any time, t (min), estimated from $F = q_t/q_{max}$.

Comparing Fig. 8a and b, the difference between the dotted data set experimental points are far away scattered from the line of best fit (Fig. 8a), which indicates that the model was not completely suitable to describe the adsorption interaction between EE2 hormone and PU-PANI-ES adsorbent. Whereas Fig. 8b showed the best fitting with the experimental data indicating the pseudo-second-order model best describes the adsorption process. This is also evident by high regression coefficients and close agreement between the experimental adsorption capacities and the calculated values, represented in Table 5. Fig. 8c and d describe the kind of adsorption process occurring during the uptake of EE2 hormone by PU-PANI-ES. From Fig. 8c, two linear regions are visible (initial half and latter half), which relates to the initial and gradual adsorption

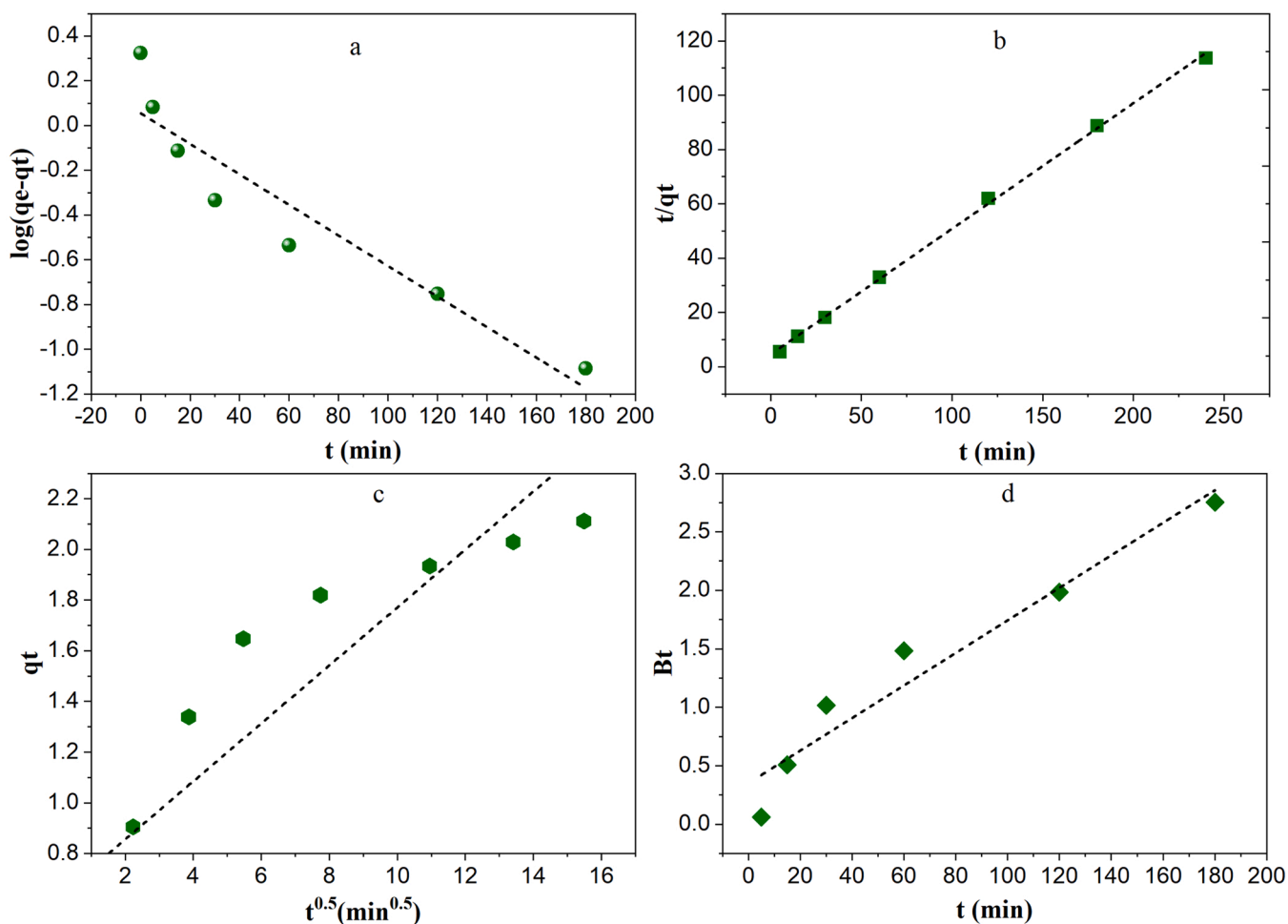


Fig. 8. Plots of the adsorption kinetics for the EE2 hormone on PU-PANI-ES fibers: (a) pseudo-first-order, (b) pseudo-second-order, (c) intraparticle diffusion model, and (d) Boyd model.

Table 5

Kinetic models and their determining parameters related to the removal of EE2 hormone using PU-PANI-ES fibers.

Pseudo-first-order		Pseudo-second order	
$q_e, \text{exp (mg/g)}$	2.11	$q_e, \text{exp (mg/g)}$	2.11
$q_e, \text{cal (mg/g)}$	1.13	$q_e, \text{cal (mg/g)}$	2.16
$K_1 \text{ (min}^{-1}\text{)}$	0.02	$K_2 \text{ (g/mg min)}$	0.04
R^2	0.892	R^2	0.998
χ^2	0.03	χ^2	0.12
SSE	0.16	SSE	0.57
Intraparticle diffusion		Boyd	
$K_3 \text{ (mg/g min}^{0.5}\text{)}$	0.11	R^2	0.939
$C \text{ (mg/g)}$	0.62	χ^2	0.07
R^2	0.872	SSE	0.29
χ^2	0.14		
SSE	0.84		

phase and then the equilibrium phase. In addition, the boundary-layer effect was depicted not to pass through the origin region, which indicates that the process was more intraparticle diffusion-controlled in the latter half of the experiment as a consequence of the surface control effect [64,65].

Among all the calculated models from the experimental data, it can be seen that EE2 adsorption on PU-PANI-ES fibers follows the pseudo-second-order model. The experimental data set points adhere completely to the line of best fit, also observed by the high regression coefficient (R^2) of 0.998 and the calculated adsorption capacity of 2.16 mg/g is extremely close to the experimental value of 2.11 mg/g. The plausible reason that indicates these findings could be the inhomogeneous surface of available active sites on the modified adsorbent PU membrane since the adsorption rate is dependent on the concentration of hormone in the solution and the number of available sites that can actively accommodate the hormone [73]. All the supporting values of the given models are presented in Table 5.

3.10. Thermodynamic study

In order to understand the thermodynamic behavior of the adsorption process for the removal of EE2 by PU-PANI-ES adsorbent, the Gibbs free energy change (ΔG), enthalpy change (ΔH), and entropy change (ΔS) were determined using Eqs. (9)–(11) [74,75]. The thermodynamic parameters were calculated based on the adsorption distribution coefficient (K_D) for the different studied temperatures.

$$K_D = \frac{C_s}{C_e} \quad (9)$$

$$\ln K_D = -\frac{\Delta H}{RT} + \frac{\Delta S}{R} \quad (10)$$

$$\Delta G = \Delta H - T\Delta S \quad (11)$$

where K_D is the distribution coefficient (a ratio of solid phase to solute concentrations), R (8.314 J/mol K) is the universal gas constant, C_s (mg/L) is the concentration of EE2 on the adsorbent, and T (K) is the absolute temperature. By plotting a Van't Hoff plot of $\ln K_D$ versus $1/T$, ΔS and ΔH were determined from the slope and intercept, respectively. Values of ΔG at different temperatures were then calculated and are given in Table 6.

Table 6

Thermodynamic parametric values for the adsorption of EE2 hormone.

Parameters	Temperature		
	298 K	313 K	328 K
ΔG (kJ/mol)	-37.52	-33.03	-28.53
ΔH (kJ/mol)	-12.67		
ΔS (J/mol K)	-29.94		

In accordance with calculated results, ΔG was determined to be negative, which is expected, indicating that the adsorption process was favourable and the reaction was spontaneous. ΔH value was negative, which confirmed the adsorption of EE2 onto the PU-PANI-ES membrane to be exothermic in nature. This explains the decrease in adsorption capacity at higher temperatures. In addition, the low ΔH value depicts the adsorption process favour more physical adsorption rather than chemical adsorption. The values deduced and phenomena observed in the present study are in close agreement with similar previous studies on the adsorption of estrogenic hormones [64,76]. The negative ΔS value indicates the adsorption process was more enthalpy driven.

3.11. Reusability study

It could be noticed from the results in Fig. 9 that the adsorption efficiency of PU-PANI-ES for EE2 hormone remains over 80% throughout the six adsorption cycles, while desorption gradually decreases and stay stagnant at around 60% in the last two cycles. A slight rise in adsorption with the increase in the number of cycles up to four cycles was observed, which could be due to improved swelling of the adsorbent when in contact with the ethanol (alkaline medium), resulting in high adsorption. However, the efficiency gets constant and near to that of the first cycle during the fifth and sixth cycles, which can be attributed to the decrease in the swelling reversibility of PU-PANI-ES. A similar increasing and then decreasing trend was reported in the literature for acid orange II and methylene blue removal [77].

3.12. Comparative study with other adsorbents

The following Table 7 demonstrates the adsorbent fibers and particles reported in the literature with their total adsorption capacities for capturing EE2 hormone compared to this study. As can be seen, the adsorption capacity of PU-PANI-ES reported in this study is 2.11 mg/g. This value is relatively high compared to similar reported previous studies. It is noteworthy to mention the significance of produced electrospun modified nanofibrous membrane in this study. However, considering Norit AC, Darco AC, and PA612 particles, the adsorption capacity value of these materials is still quite higher than the current study, which can be attributed to the nature of those materials and the relatively large surface area they possess (5.12–17.64 m²/g) in general as compared to fibrous materials.

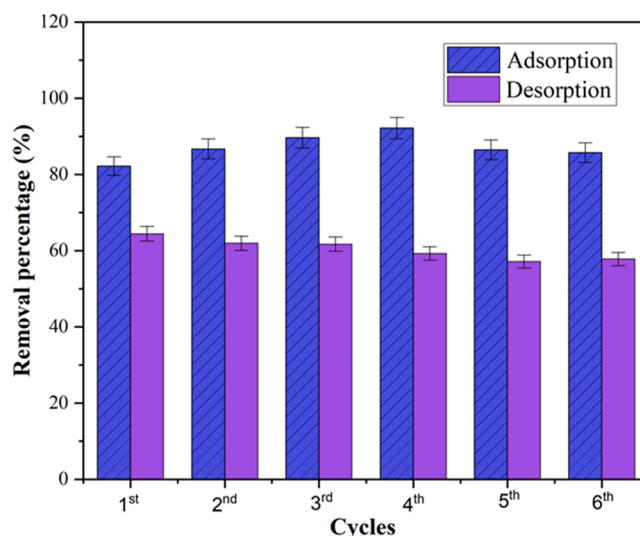


Fig. 9. Six adsorption-desorption cycles of EE2 by PU-PANI-ES fibers.

Table 7

Comparison of adsorbents for EE2 hormone removal.

Adsorbents	pH and temperature (°C)	Adsorption capacity (mg/g)	Reference
MWCNTs	6.30 and 25	0.47	[64]
PA612,	7.00 and 25	25.42	[78]
Darco AC,		27.61	
Norit AC		10.40	
Un-anthracite,	7.00 and 25	0.21	[79]
4 K		0.62	
anthracite			
PU Elastollan,	7.00 and 25	0.74	Our previous work
PU 918,		0.64	
PA		0.61	[46]
PU-PANI-ES	7.00 and 40	2.11	Present study

4. Conclusions

In this study, we successfully investigated the removal of a steroid hormone from water by lab synthesized spun polyurethane nanofiber membrane modified with PANI in PVA solution as the supporting polymer. The different spun and treated PU nanofiber membranes were chemically and morphologically characterized via FTIR, SEM, and optical microscopy. PU-PANI-ES as a modified material demonstrated to be the most efficient with 90.30% removal efficiency of the studied hormone as compared to its base form PU-PANI-EB (81.50%) and neat PU (55.40%) as control. PU-PANI-ES was further evaluated via an optimization study using the CCD model to determine its optimum removal conditions for EE2 hormone. According to the results obtained, the model proved to be significant for the optimization of the removal of the EE2 hormone with a high regression coefficient (R^2) of 0.983. The optimum parameters were found to be pH 7 (considering that wastewater or river water is in the range of pH 6–8), the temperature of 40 °C, 0.3 mg/L concentration of EE2, and 20 mg of PU-PANI-ES dosage. In addition, the adsorption was studied kinetically using different kinetic models, and the results depicted that the removal of EE2 hormone best fitted the pseudo-second-order model with maximum adsorption capacity determined as 2.11 mg/g. This obtained value proved to be significantly high compared to the other similar adsorbents in the literature. Furthermore, the adsorption efficiency was demonstrated to be temperature sensitive and decreased considerably at a higher temperature. This was supported by a thermodynamic study that showed the adsorption process is spontaneous and exothermic in nature. Finally, the recovery of EE2 hormone and reusability of PU-PANI-ES adsorbent depicted a good removal percentage which remained over 80% for tested six consecutive adsorption-desorption cycles. Overall, the reported results proved that the modification of the spun PU nanofiber with PANI significantly improved hormone removal from water and can be considered a promising adsorbent membrane for the remediation of different steroid hormones from water.

CrediT authorship contribution statement

Muhammad Yasir: Conceptualization, Methodology, Investigation, Formal analysis, Data curation, Writing – original draft, Writing – review & editing. **Fahanwi Asabuwa Ngwabebhoh:** Formal analysis, Data curation, Writing – review & editing. **Tomáš Šopík:** Methodology, Formal analysis, Data curation. **Hassan Ali:** Writing – review & editing. **Vladimír Sedlářik:** Conceptualization, Supervision, Project administration, Funding acquisition, Writing – review & editing.

Declaration of Competing Interest

The authors declare that they have no known competing financial interests or personal relationships that could have appeared to influence the work reported in this paper.

Acknowledgements

The authors gratefully acknowledge the financial support from the Ministry of Education, Youth and Sports of Czech Republic (DKRVO RP/CPS/2022/002 and RP/CPS/2022/005), the Internal Grant Agency of TBU in Zlin (grant no. IGA/CPS/2022/003). We would also like to acknowledge the Centre of Polymer Systems (CPS) situated at Tomas Bata University in Zlin, Czech Republic, to use the available research facilities to conduct this research work.

References

- [1] D.V. Henley, J. Lindzey, K.S. Korach, Steroid hormones, in: S. Melmed, P.M. Conn (Eds.), *Endocrinology*, Humana Press, Totowa, NJ, 2005, pp. 49–65, https://doi.org/10.1007/978-1-59259-829-8_4.
- [2] S.M. Choi, S.D. Yoo, B.M. Lee, Toxicological characteristics of endocrine-disrupting chemicals: developmental toxicity, carcinogenicity, and mutagenicity, *J. Toxicol. Environ. Health Part B* (2004), <https://doi.org/10.1080/716100635>.
- [3] M.E. Street, S. Angelini, S. Bernasconi, E. Burgio, A. Cassio, C. Catellani, F. Cirillo, A. Deodati, E. Fabbri, V. Fanos, G. Gargano, E. Grossi, L. Iughetti, P. Lazzeroni, A. Mantovani, L. Migliore, P. Palanza, G. Panzica, A.M. Papini, S. Parmigiani, B. Predieri, C. Sartori, G. Tridenti, S. Amarri, Current knowledge on endocrine disrupting chemicals (EDCs) from animal biology to humans, from pregnancy to adulthood: highlights from a national Italian meeting, *Int. J. Mol. Sci.* (2018), <https://doi.org/10.3390/ijms19061647>.
- [4] M.A. La Merrill, L.N. Vandenberg, M.T. Smith, W. Goodson, P. Browne, H. B. Patisaul, K.Z. Guyton, A. Kortenkamp, V.J. Cogliano, T.J. Woodruff, L. Rieswijk, H. Sone, K.S. Korach, A.C. Gore, L. Zeise, R.T. Zoeller, Consensus on the key characteristics of endocrine-disrupting chemicals as a basis for hazard identification, *Nat. Rev. Endocrinol.* 16 (2020) 45–57, <https://doi.org/10.1038/s41574-019-0273-8>.
- [5] R. Lauletta, A. Sansone, M. Sansone, F. Romanelli, M. Appetecchia, *Endocrine disrupting chemicals: effects on endocrine glands*, *Front. Endocrinol.* 10 (2019).
- [6] T.T. Schug, A.F. Johnson, L.S. Birnbaum, T. Colborn, L.J. Guillette, D.P. Crews, T. Collins, A.M. Soto, F.S. vom Saal, J.A. McLachlan, C. Sonnenschein, J.J. Heindel, Minireview: endocrine disruptors: past lessons and future directions, *Mol. Endocrinol.* 30 (2016) 833–847, <https://doi.org/10.1210/me.2016-1096>.
- [7] C.L.S. Vilela, J.P. Bassin, R.S. Peixoto, Water contamination by endocrine disruptors: impacts, microbiological aspects and trends for environmental protection, *Environ. Pollut.* (2018), <https://doi.org/10.1016/j.envpol.2017.12.098>.
- [8] Directive (EU) 2020/2184 on the quality of water intended for human consumption (recast), 2021.
- [9] M.R. Mills, K. Arias-Salazar, A. Baynes, L.Q. Shen, J. Churchley, N. Beresford, C. Gayathri, R.R. Gil, R. Kanda, S. Jobling, T.J. Collins, Removal of ecotoxicity of 17 α -ethinylestradiol using TAML/peroxide water treatment, *Sci. Rep.* (2015), <https://doi.org/10.1038/srep10511>.
- [10] C.L.S. Vilela, H.D.M. Villela, G.A.S. Duarte, E.P. Santoro, C.T.C.C. Rachid, R. S. Peixoto, Estrogen induces shift in abundances of specific groups of the coral microbiome, *Sci. Rep.* 11 (2021) 2767, <https://doi.org/10.1038/s41598-021-82387-x>.
- [11] X. Gao, S. Kang, R. Xiong, M. Chen, Environment-friendly removal methods for endocrine disrupting chemicals, *Sustainability* 12 (2020) 7615, <https://doi.org/10.3390/su12187615>.
- [12] Z. Křesinová, L. Linhartová, A. Filipová, M. Ezechiáš, P. Mašín, T. Cajthaml, Biodegradation of endocrine disruptors in urban wastewater using *Pleurotus ostreatus* bioreactor, *New Biotechnol.* 43 (2018) 53–61, <https://doi.org/10.1016/j.nbt.2017.05.004>.
- [13] R.M. Castellanos, J.P. Bassin, D.M. Bila, M. Dezotti, Biodegradation of natural and synthetic endocrine-disrupting chemicals by aerobic granular sludge reactor: Evaluating estrogenic activity and estrogens fate, *Environ. Pollut.* 274 (2021), 116551, <https://doi.org/10.1016/j.envpol.2021.116551>.
- [14] X. Wei, J. Li, Z. Liu, X. Yang, S. Naraginti, X. Xu, X. Wang, Visible light photocatalytic mineralization of 17 α -ethinyl estradiol (EE2) and hydrogen evolution over silver and strontium modified TiO₂ nanoparticles: mechanisms and phytotoxicity assessment, *RSC Adv.* 8 (2018) 4329–4339, <https://doi.org/10.1039/C7RA12638G>.
- [15] R.V. Carvalho, B.G. Isecke, E. Carvalho, F.J.C. Teran, Photocatalytic oxidation of 17-Ethinylestradiol by UV-activated TiO₂ in batch and continuous-flow reactor, *J. Chem. Eng. Mater. Sci.* (2017), <https://doi.org/10.5897/jcems2017.0293>.
- [16] A. Rafiq, M. Ikram, S. Ali, F. Niaz, M. Khan, Q. Khan, M. Maqbool, Photocatalytic degradation of dyes using semiconductor photocatalysts to clean industrial water pollution, *J. Ind. Eng. Chem.* 97 (2021) 111–128, <https://doi.org/10.1016/j.jiec.2021.02.017>.
- [17] M. Naz, A. Rafiq, M. Ikram, A. Haider, S.O.A. Ahmad, J. Haider, S. Naz, Elimination of dyes by catalytic reduction in the absence of light: a review, *J. Mater. Sci.* 56 (2021) 15572–15608, <https://doi.org/10.1007/s10853-021-06279-1>.
- [18] M. Yasir, M. Masar, T. Sopik, H. Ali, M. Urbanek, J. Antos, M. Machovsky, I. Kuritka, ZnO nanowires and nanorods based ZnO/WO₃/Pt heterojunction for efficient photocatalytic degradation of Estriol (E3) hormone, *Mater. Lett.* (2022), 132291, <https://doi.org/10.1016/j.matlet.2022.132291>.

- [19] T.A. Saleh, Carbon nanotube-incorporated alumina as a support for MoNi catalysts for the efficient hydrodesulfurization of thiophenes, *Chem. Eng. J.* 404 (2021), 126987, <https://doi.org/10.1016/j.cej.2020.126987>.
- [20] T.A. Saleh, Protocols for synthesis of nanomaterials, polymers, and green materials as adsorbents for water treatment technologies, *Environ. Technol. Innov.* 24 (2021), 101821, <https://doi.org/10.1016/j.eti.2021.101821>.
- [21] K.J. Choi, S.G. Kim, C.W. Kim, S.H. Kim, Effects of activated carbon types and service life on removal of endocrine disrupting chemicals: amitrol, nonylphenol, and bisphenol-A, *Chemosphere* (2005), <https://doi.org/10.1016/j.chemosphere.2004.11.080>.
- [22] E. Kim, C. Jung, J. Han, N. Her, C. Min Park, A. Son, Y. Yoon, Adsorption of selected micropollutants on powdered activated carbon and biochar in the presence of kaolinite, *Desalin. Water Treat.* (2016), <https://doi.org/10.1080/19443994.2016.1175972>.
- [23] A.O. Ifelebeuegu, Removal of steroid hormones by activated carbon adsorption—kinetic and thermodynamic studies, *J. Environ. Prot.* (2012), <https://doi.org/10.4236/jep.2012.36057>.
- [24] S.O. Badmus, T.A. Oyeohan, T.A. Saleh, Enhanced efficiency of polyamide membranes by incorporating cyclodextrin-graphene oxide for water purification, *J. Mol. Liq.* 340 (2021), 116991, <https://doi.org/10.1016/j.molliq.2021.116991>.
- [25] A.Q. Al-Gamal, T.A. Saleh, F.I. Alghunaimi, Nanofiltration membrane with high flux and oil rejection using graphene oxide/ β -cyclodextrin for produced water reuse, *Mater. Today Commun.* 31 (2022), 103438, <https://doi.org/10.1016/j.mtcomm.2022.103438>.
- [26] A.Q. Al-Gamal, W.S. Falath, T.A. Saleh, Enhanced efficiency of polyamide membranes by incorporating TiO₂-Graphene oxide for water purification, *J. Mol. Liq.* 323 (2021), <https://doi.org/10.1016/j.molliq.2020.114922>.
- [27] M.S. Islam, B.C. Ang, A. Andriyana, A.M. Affi, A review on fabrication of nanofibers via electrospinning and their applications, *SN Appl. Sci.* 1 (2019) 1248, <https://doi.org/10.1007/s42452-019-1288-4>.
- [28] I. Tlili, T.A. Alkanhal, Nanotechnology for water purification: electrospun nanofibrous membrane in water and wastewater treatment, *J. Water Reuse Desalin.* (2019), <https://doi.org/10.2166/wrd.2019.057>.
- [29] T.A. Saleh, Nanomaterials: classification, properties, and environmental toxicities, *Environ. Technol. Innov.* 20 (2020), 101067, <https://doi.org/10.1016/j.eti.2020.101067>.
- [30] F.A. AlAbduljabbar, S. Haider, F.A.A. Ali, A.A. Alghyamah, W.A. Almasry, R. Patel, I.M. Mujtaba, Efficient photocatalytic degradation of organic pollutant in wastewater by electrospun functionally modified polyacrylonitrile nanofibers membrane anchoring TiO₂ nanostructured, *Membranes* 11 (2021) 785, <https://doi.org/10.3390/membranes11100785>.
- [31] A.S.M. Ali, M.R. El-Aassar, F.S. Hashem, N.A. Moussa, Surface modified of cellulose acetate electrospun nanofibers by poly(aniline)/ β -cyclodextrin composite for removal of cationic dye from aqueous medium, *Fibers Polym.* 20 (2019) 2057–2069, <https://doi.org/10.1007/s12221-019-9162-y>.
- [32] S. Yan, Y. Yu, R. Ma, J. Fang, The formation of ultrafine polyamide 6 nanofiber membranes with needleless electrospinning for air filtration, *Polym. Adv. Technol.* 30 (2019) 1635–1643, <https://doi.org/10.1002/pat.4594>.
- [33] F.S. Victor, V. Kugarajah, M. Bangaru, S. Ranjan, S. Dharmalingam, Electrospun nanofibers of poly(vinylidene fluoride) incorporated with titanium nanotubes for purifying air with bacterial contamination, *Environ. Sci. Pollut. Res.* 28 (2021) 37520–37533, <https://doi.org/10.1007/s11356-021-13202-3>.
- [34] M.H. Mohraz, F. Golbabaee, L.J. Yu, M.A. Mansournia, A.S. Zadeh, S.F. Dehghan, Preparation and optimization of multifunctional electrospun polyurethane/chitosan nanofibers for air pollution control applications, *Int. J. Environ. Sci. Technol.* 16 (2019) 681–694, <https://doi.org/10.1007/s13762-018-1649-3>.
- [35] R. Sarika, D.R. Shankaran, Synthesis and characterization of curcumin nanoparticles loaded nanofibers for lead ion detection, *Sens. Lett.* (2016), <https://doi.org/10.1166/sl.2016.3707>.
- [36] S. Patel, M. Konar, H. Sahoo, G. Hota, Surface functionalization of electrospun PAN nanofibers with ZnO-Ag heterostructure nanoparticles: synthesis and antibacterial study, *Nanotechnology* (2019), <https://doi.org/10.1088/1361-6528/ab045d>.
- [37] M.M. Foomani, A. Khorshidi, A.F. Shojaei, Polyethyleneimine nanofibers functionalized with tetradentate Schiff base complexes of dioxomolybdenum(VI) as efficient catalysts for epoxidation of alkenes, *ChemistrySelect* (2019), <https://doi.org/10.1002/slct.201803047>.
- [38] B. Balusamy, A. Senthambizhan, T. Uyar, Functionalized electrospun nanofibers as a versatile platform for colorimetric detection of heavy metal ions in water: a review, *Materials* (2020), <https://doi.org/10.3390/ma13102421>.
- [39] R. Araga, C.S. Sharma, Amine functionalized electrospun cellulose nanofibers for fluoride adsorption from drinking water, *J. Polym. Environ.* (2019), <https://doi.org/10.1007/s10924-019-01394-2>.
- [40] L. Qian, X. Li, F. Qi, J. Li, L. Lu, Q. Xu, An amino-functionalized grooved nanofiber mat for solid-phase extraction of phenolic pollutants, *Microchim. Acta* (2017), <https://doi.org/10.1007/s00604-017-2313-1>.
- [41] J. Stejskal, P. Bober, M. Trchová, A. Kovalčík, J. Hodan, J. Hromádková, J. Prokeš, Poly(aniline) cryogels supported with poly(vinyl alcohol): soft and conducting, *Macromolecules* (2017), <https://doi.org/10.1021/acs.macromol.6b02526>.
- [42] Z. Zhang, Z. Wei, M. Wan, Nanostructures of polyaniline doped with inorganic acids, *Macromolecules* (2002), <https://doi.org/10.1021/ma020199v>.
- [43] J. Stejskal, Interaction of conducting polymers, polyaniline and polypyrrole, with organic dyes: polymer morphology control, dye adsorption and photocatalytic decomposition, *Chem. Pap.* (2020), <https://doi.org/10.1007/s11696-019-00982-9>.
- [44] M. Ayad, G. El-Hefnawy, S. Zaghlool, Facile synthesis of polyaniline nanoparticles; its adsorption behavior, *Chem. Eng. J.* (2013), <https://doi.org/10.1016/j.cej.2012.11.099>.
- [45] J. Stejskal, Conducting polymers are not just conducting: a perspective for emerging technology, *Polym. Int.* (2020), <https://doi.org/10.1002/pi.5947>.
- [46] M. Yasir, T. Šopík, L. Lovecká, D. Kimmmer, V. Sedlářik, The adsorption, kinetics, and interaction mechanisms of various types of estrogen on electrospun polymeric nanofiber membranes, *Nanotechnology* 33 (2021) 75702, <https://doi.org/10.1088/1361-6528/ac357b>.
- [47] S. Zaghlool, W.A. Amer, M.H. Shaaban, M.M. Ayad, P. Bober, J. Stejskal, Conducting macroporous polyaniline/poly(vinyl alcohol) aerogels for the removal of chromium(VI) from aqueous media, *Chem. Pap.* 74 (2020) 3183–3193, <https://doi.org/10.1007/s11696-020-01151-z>.
- [48] P. Humpolicek, V. Kasparkova, P. Saha, J. Stejskal, Biocompatibility of polyaniline, *Synth. Met.* (2012), <https://doi.org/10.1016/j.synthmet.2012.02.024>.
- [49] A.M. Khalil, A.I. Schäfer, Cross-linked β -cyclodextrin nanofiber composite membrane for steroid hormone micropollutant removal from water, *J. Memb. Sci.* 618 (2021), 118228, <https://doi.org/10.1016/j.memsci.2020.118228>.
- [50] T. Huang, S. wen Zhang, J. Xie, L. Zhou, L. fei Liu, Effective adsorption of quadrivalent cerium by synthesized laurylsulfonate green rust in a central composite design, *J. Environ. Sci.* (2021), <https://doi.org/10.1016/j.jes.2021.01.028>.
- [51] F.A. Ngwabebhoh, A. Erdem, U. Yildiz, Synergistic removal of Cu(II) and nitrazine yellow dye using an eco-friendly chitosan-montmorillonite hydrogel: Optimization by response surface methodology, *J. Appl. Polym. Sci.* 133 (2016) 1–14, <https://doi.org/10.1002/app.43664>.
- [52] J. Wang, H. Chi, A. Zhou, R. Zheng, H. Bai, T. Zhang, Facile synthesis of multifunctional elastic polyaniline/poly(vinyl) alcohol composite gels by a solution assembly method, *RSC Adv.* (2020), <https://doi.org/10.1039/d0ra02238a>.
- [53] A. Erdem, F.A. Ngwabebhoh, S. Çetintaş, D. Bingöl, U. Yildiz, Fabrication and characterization of novel macroporous Jeffamine/diamino hexane cryogels for enhanced Cu(II) metal uptake: optimization, isotherms, kinetics and thermodynamic studies, *Chem. Eng. Res. Des.* (2017), <https://doi.org/10.1016/j.cherd.2016.10.010>.
- [54] T.A. Saleh, Isotherm, kinetic, and thermodynamic studies on Hg(II) adsorption from aqueous solution by silica-multiwall carbon nanotubes, *Environ. Sci. Pollut. Res.* 22 (2015) 16721–16731, <https://doi.org/10.1007/s11356-015-4866-z>.
- [55] T.A. Saleh, The influence of treatment temperature on the acidity of MWCNT oxidized by HNO₃ or a mixture of HNO₃ / H₂SO₄, *Appl. Surf. Sci.* 257 (2011) 7746–7751, <https://doi.org/10.1016/j.apusc.2011.04.020>.
- [56] T.A. Saleh, Simultaneous adsorptive desulfurization of diesel fuel over bimetallic nanoparticles loaded on activated carbon, *J. Clean. Prod.* 172 (2018) 2123–2132, <https://doi.org/10.1016/j.jclepro.2017.11.208>.
- [57] A. Bahadur, M. Shoaib, A. Saeed, S. Iqbal, FT-IR spectroscopic and thermal study of waterborne polyurethane-acrylate leather coatings using tartaric acid as an ionomer, *E Polym.* (2016), <https://doi.org/10.1515/epoly-2016-0154>.
- [58] M. Shahi, A. Moghimi, B. Naderizadeh, B. Maddah, Electrospun PVA-PANI and PVA-PANI-AgNO₃ composite nanofibers, *Sci. Iran.* (2011), <https://doi.org/10.1016/j.scient.2011.08.013>.
- [59] H. Huang, J. Yao, L. Li, F. Zhu, Z. Liu, X. Zeng, X. Yu, Z. Huang, Reinforced polyaniline/poly(vinyl alcohol) conducting hydrogel from a freezing-thawing method as self-supported electrode for supercapacitors, *J. Mater. Sci.* (2016), <https://doi.org/10.1007/s10853-016-0137-8>.
- [60] O.F.S. Khasawneh, P. Palaniandy, P. Palaniandy, M. Ahmadipour, H. Mohammadi, M.R. Bin Hamdan, Removal of acetaminophen using Fe₂O₃-TiO₂nanocomposites by photocatalysis under simulated solar irradiation: optimization study, *J. Environ. Chem. Eng.* (2021), <https://doi.org/10.1016/j.jece.2020.104921>.
- [61] M. Galedari, M. Mehdipour Ghazi, S. Rashid Mirmasoomi, Photocatalytic process for the tetracycline removal under visible light: presenting a degradation model and optimization using response surface methodology (RSM), *Chem. Eng. Res. Des.* (2019), <https://doi.org/10.1016/j.cherd.2019.03.031>.
- [62] D. Lambropoulou, E. Evgenidou, V. Saliverou, C. Kosma, I. Konstantinou, Degradation of venlafaxine using TiO₂/UV process: Kinetic studies, RSM optimization, identification of transformation products and toxicity evaluation, *J. Hazard. Mater.* (2017), <https://doi.org/10.1016/j.jhazmat.2016.04.074>.
- [63] F. Esmaeeli, S.A. Gorbanian, N. Moazeei, Removal of estradiol valerate and progesterone using powdered and granular activated carbon from aqueous solutions, *Int. J. Environ. Res.* 11 (2017) 695–705, <https://doi.org/10.1007/s41742-017-0060-0>.
- [64] L.A. Al-Khateeb, A.Y. Obaid, N.A. Asiri, M. Abdel Salam, Adsorption behavior of estrogenic compounds on carbon nanotubes from aqueous solutions: Kinetic and thermodynamic studies, *J. Ind. Eng. Chem.* 20 (2014) 916–924, <https://doi.org/10.1016/j.jiec.2013.06.023>.
- [65] F.F. Qi, Y. Cao, M. Wang, F. Rong, Q. Xu, Nylon 6 electrospun nanofibers mat as effective sorbent for the removal of estrogens: kinetic and thermodynamic studies, *Nanoscale Res. Lett.* 9 (2014) 1–10, <https://doi.org/10.1186/1556-276X-9-353>.
- [66] L. Kovalova, D.R.U. Knappe, K. Lehnberg, C. Kazner, J. Hollender, Removal of highly polar micropollutants from wastewater by powdered activated carbon, *Environ. Sci. Pollut. Res.* (2013), <https://doi.org/10.1007/s11356-012-1432-9>.
- [67] S.A. Abdel-Gawad, H.M. Abdel-Aziz, Removal of ethinylestradiol by adsorption process from aqueous solutions using entrapped activated carbon in alginate biopolymer: isotherm and statistical studies, *Appl. Water Sci.* 9 (2019) 1–8, <https://doi.org/10.1007/s13201-019-0951-7>.
- [68] L.D. Nghiem, A.I. Schäfer, Adsorption and transport of trace contaminant estrone in NF/RO membranes, *Environ. Eng. Sci.* 19 (2002) 441–451, <https://doi.org/10.1089/109287502320963427>.

- [69] A.I. Schäfer, I. Akanyeti, A.J.C. Semião, Micropollutant sorption to membrane polymers: a review of mechanisms for estrogens, *Adv. Colloid Interface Sci.* 164 (2011) 100–117, <https://doi.org/10.1016/j.cis.2010.09.006>.
- [70] M. Yasir, T. Sopik, R. Patwa, D. Kimmer, V. Sedlarik, Adsorption of estrogenic hormones in aqueous solution using electrospun nanofibers from waste cigarette butts: Kinetics, mechanism, and reusability, *Express Polym. Lett.* 16 (2022) 624–648.
- [71] A.I. Schäfer, K. Stelzl, M. Faghih, S. Sen Gupta, K.R. Krishnadas, S. Heißler, T. Pradeep, Poly(ether sulfone) nanofibers impregnated with β -cyclodextrin for increased micropollutant removal from water, *ACS Sustain. Chem. Eng.* 6 (2018) 2942–2953, <https://doi.org/10.1021/acssuschemeng.7b02214>.
- [72] N. Sebeia, M. Jabli, A. Ghith, T.A. Saleh, Eco-friendly synthesis of Cynomorium coccineum extract for controlled production of copper nanoparticles for sorption of methylene blue dye, *Arab. J. Chem.* 13 (2020) 4263–4274, <https://doi.org/10.1016/j.arabjc.2019.07.007>.
- [73] E. Vazquez-Velez, L. Lopez-Zarate, H. Martinez-Valencia, Electrospinning of polyacrylonitrile nanofibers embedded with zerovalent iron and cerium oxide nanoparticles, as Cr(VI) adsorbents for water treatment, *J. Appl. Polym. Sci.* 137 (2020) 1–10, <https://doi.org/10.1002/app.48663>.
- [74] F.A. Ngwabebhoh, N. Mammadli, U. Yildiz, Bioinspired modified nanocellulose adsorbent for enhanced boron recovery from aqueous media: optimization, kinetics, thermodynamics and reusability study, *J. Environ. Chem. Eng.* 7 (2019), 103281, <https://doi.org/10.1016/j.jece.2019.103281>.
- [75] M. Carballa, G. Fink, F. Omil, J.M. Lema, T. Ternes, Determination of the solid-water distribution coefficient (K_d) for pharmaceuticals, estrogens and musk fragrances in digested sludge, *Water Res.* 42 (2008) 287–295, <https://doi.org/10.1016/j.watres.2007.07.012>.
- [76] Y.X. Ren, K. Nakano, M. Nomura, N. Chiba, O. Nishimura, A thermodynamic analysis on adsorption of estrogens in activated sludge process, *Water Res.* (2007), <https://doi.org/10.1016/j.watres.2007.01.058>.
- [77] W. Wang, J. Hu, R. Zhang, C. Yan, L. Cui, J. Zhu, A pH-responsive carboxymethyl cellulose/chitosan hydrogel for adsorption and desorption of anionic and cationic dyes, *Cellulose* 28 (2021) 897–909, <https://doi.org/10.1007/s10570-020-03561-4>.
- [78] J. Han, W. Qiu, Z. Cao, J. Hu, W. Gao, Adsorption of ethinylestradiol (EE2) on polyamide 612: Molecular modeling and effects of water chemistry, *Water Res.* 47 (2013) 2273–2284, <https://doi.org/10.1016/j.watres.2013.01.046>.
- [79] J. He, Q. Zhou, J. Guo, F. Fang, Characterization of potassium hydroxide modified anthracite particles and enhanced removal of 17 α -ethinylestradiol and bisphenol A, *Environ. Sci. Pollut. Res.* 25 (2018) 22224–22235, <https://doi.org/10.1007/s11356-018-2287-5>.

The adsorptive behaviour of electrospun hydrophobic polymers for optimized uptake of estrogenic sex hormones from aqueous media: kinetics, thermodynamics, and reusability study

Muhammad Yasir,^{*}  Fahanwi Asabuwa Ngwabebhoh,  Tomáš Šopík, 
Lenka Lovecká,  Dušan Kimmer  and Vladimír Sedlařík ^{*} 

Abstract

Background: Estrogenic hormones as micropollutants in water systems cause severe adverse effects on human health and marine life, leading to fatal diseases, such as breast, ovarian, and prostate cancer. Electrospun polymers have proven high stability and impressive performance in adsorption removal. In this study, electrospun polysulfone (PSU), polyvinylidene fluoride, and polylactic acid were prepared and characterized using scanning electron microscope (SEM), fourier-transform infrared spectroscopy (FTIR), thermogravimetric analysis (TGA), Brunauer Emmett Teller (BET), surface area measurement X-Ray diffraction (XRD), and pometry.

Results: Nanofibers possess a mean fiber diameter of 149–183 nm and a specific surface area of 1.6–6.3 m²/g. The adsorption efficiency of the simultaneous removal of estrone (E1), 17 β -estradiol (E2), estriol (E3), and 17 α -ethinylestradiol (EE2) in a mixed concentration was investigated using high performance liquid chromatography (HPLC). The results indicate that spun PSU fibers exhibited the highest removal of all four estrogens, with a maximum removal efficiency of 71.2%, 65.9%, 56.9%, and 36.1% and adsorption capacity of 0.508, 0.703, 0.550, and 0.354 mg/g for E1, EE2, E2, and E3, respectively. Additionally, the adsorption was optimised by varying parameters, such as concentration of adsorbate, pH, adsorbent dosage, and temperature, to statistically analyse one-way variance using ANOVA. The pseudo-second-order is best fitted for E1, EE2, and E2, while the pseudo-first-order is best for E3. The Langmuir–Freundlich isothermal model was most suitable for evaluation, and the thermodynamics depicted the adsorption to be exothermic and spontaneous.

Conclusion: The results indicate that spun PSU can be an efficient adsorbent in the simultaneous elimination of estrogens from wastewater and it exhibits a high regeneration performance of over 60% after six adsorption–desorption cycles.
© 2022 Society of Chemical Industry (SCI).

Keywords: electrospun nanofibers; kinetics; estrogenic hormones; adsorption mechanism; wastewater treatment

INTRODUCTION

Over the past few decades, rapid human population growth and industrialization have resulted in numerous environmental and energy issues. The persistent release of environmental contaminants has severely affected the bio-ecosystem due to their high toxicity and wide occurrence in aquatic environments.^{1–3} So far, various toxicants have been classified as having adverse effects on animals and humans alike.⁴ Several investigative reports have detected a high concentration of various types of pollutants, such as heavy metals, nitrates, per- and polyfluoroalkyl substances (PFAS), and endocrine-disrupting chemicals (EDCs). Estrogens classified under EDCs are by far the most toxic due to their high bio-toxicity and estrogenicity interfering with the normal functioning of the endocrine systems, even at ng L⁻¹ concentrations.^{5–8} These estrogenic chemicals exist mainly as estrone (E1), estradiol (E2), estriol (E3), and ethinylestradiol (EE2), and their

extensive synthetic use in the treatment of sexual disorders and as contraceptives have resulted in higher concentrations than recommended tolerance limit in aquatic resources.^{9,10} Globally, these steroids are potentially causing serious health issues by interfering with the naturally released hormones regulating various bodily functions. Several reports suggest that persistent exposure to these anthropogenic chemicals is correlated with serious health issues for humans and animals alike, including breast

^{*} Correspondence to: M Yasir or V Sedlařík, Centre of Polymer Systems, University Institute, Tomas Bata University in Zlín, Třída Tomáše Bati 5678, 76001 Zlín, Czech Republic. E-mail: yasir@utb.cz (Yasir); sedlarik@utb.cz (Sedlařík)

Centre of Polymer Systems, University Institute, Tomas Bata University in Zlín, Zlín, Czech Republic

cancer, skewed sex ratios, decreased fertility, feminization of males, *etc.*^{11,12}

Considering the above-mentioned highlights, proper remediation of these estrogenic hormones is of immediate scientific concern since less than 1% of the steroids present in rivers are expected to be removed by sediments.¹³ So far, various strategies have been employed to effectively remove and eliminate steroid hormones, as conventional methods are limited by their high energy cost and low removal efficiency.^{14,15} Some of the strategies that have been explored with promising results include UV photolysis, photocatalysis, advanced oxidation process, biodegradation, nanofiltration, reverse osmosis, and adsorption process.^{15–17} Out of these techniques, the adsorption process is considered an environmentally friendly technology with a high removal rate, ease of modification, and low operation cost.¹⁸ Various adsorbent materials with high adsorption capacity have been explored, including carbonaceous materials, biochar, activated carbon, charcoal, resin, *etc.*^{19–23} However, these highly adsorbent materials lack sufficient recyclability after a few cycles and are usually disposed after a limited life cycle. In this regard, electrospun polymer-based nanofibers have gained popularity for water treatment applications because of their unique properties, such as high surface area, porosity, controlled geometry, and low production cost.^{24,25} Out of several methods available for nanofiber production, electrospinning is the most common method since nanofibers in controlled dimensions, orientation, and morphology can be obtained.^{25,26} For the remediation of environmental pollutants, numerous types of polymeric membranes have been synthesized, including polyvinylchloride, cellulose acetate, polysulfone, polycarbonate, polypropylene, and polydimethylsiloxane.^{26–31} Additionally, the polymer-based nanofibers are functionalized with additive materials, such as zeolite, graphene oxide, ammine groups, *etc.*, to impart unique features that achieve high removal efficiency and selectivity based on the type of target molecule and application.^{32–34} However, little work has gone into investigating the optimized parameters for removing estrogenic hormones using electrospun fibers to eradicate them properly.

In the literature, some work has been conducted with commercial filters of polypropylene, nylon, cellulose acetate, polytetrafluoroethylene, regenerated cellulose, and glass microfibers for the removal of E1.³⁵ Another study reported the removal of EE2 by polyamide nanoparticles.³⁶ Next, polyethersulfone electrospun nanofibers were used for the adsorption of E2; also, a polyvinylidene fluoride membrane produced *via* the phase inversion method and doped with polyvinyl pyrrolidone and titanium dioxide was used for the removal of E1 and E2 hormones.^{37,38} However, these studies are limited to the removal of a single hormone, and these works require more in-depth studies related to optimization, kinetics, isotherms, and thermodynamics to understand the mechanisms involved in the adsorption of hormones by electrospun nanofibers and to discuss this matter in more detail. Thus, this gap highlights the necessity of developing electrospun nanofibers for a comprehensive study on the removal of estrogenic hormones.

This study aims to fabricate and test hydrophobic electrospun nanostructures of the thinnest fiber diameters and of ample surface area to volume ratios for more adsorption sites. To remove estrogenic hormones from wastewater, this research focused on using nanostructured membranes constructed from polymers with strong sorption activity. The goal is to simultaneously adsorb multiple estrogenic hormones from wastewater at a neutral pH in a one-step procedure and then quantify it by HPLC. To

understand the characteristics and interaction mechanisms involved, the feasibility of the results was further investigated using the experimental data to determine adsorption capacity with contact time and measure kinetics with appropriate models of pseudo-first-order, pseudo-second-order, intraparticle diffusion, Elovich, and fractional power models. Furthermore, one way variance in ANOVA was deployed for the optimized adsorption process by varying conditions, such as pH, temperature, concentration of adsorbate, and adsorbent dosage, to determine a suitable Isothermal model and thermodynamics. Finally, the research evaluates the reusability of prepared spun fibers over six adsorption–desorption cycles to determine their consistent effectiveness and recovery of estrogenic hormones.

MATERIALS AND METHODS

Materials and reagents

The estrogenic hormones used in this study were purchased from Sigma-Aldrich GmbH, Schnellendorf, Germany, and they include estrone (E1 ≥ 99%), 17β-estradiol (E2 ≥ 98%), estriol (E3 ≥ 97%), and 17α-ethinylestradiol (EE2 ≥ 98%). The Kynar Flex® 2801, a copolymer composed of poly(vinylidene fluoride)-co-hexafluoro propylene (PVDF) of molecular weight 455 kDa, was purchased from Arkema (Colombes, France). Ultrason Polysulfone (PSU) S6010 was purchased from BASF, Ludwigshafen, Germany. Polylactic acid (PLA), Ingeo™ 4060D, biopolymer, was purchased from NatureWorks LLC (Minnetonka, Minnesota, USA). *N*-Methyl-2-pyrrolidone (NMP) was purchased from Sigma-Aldrich, St. Louis, Missouri, USA. Acetone and *N,N*-dimethylformamide (DMF >99.5%) were bought from Lach-Ner, s.r.o., Neratovice, Czech Republic. Sodium tetra-borate decahydrate (borax) and citric acid were purchased from PENTA s.r.o., Prague, Czech Republic. As for the experimental solutions, acetonitrile (HPLC grade) was purchased from Honeywell, Prague, Czech Republic, and ethanol (HPLC grade >99%) from VWR, Stříbrná Skalice, Czech Republic. Deionized water (pH 7.3, 18.2 M Ω/cm) was sourced from a laboratory Milli-Q ultrapure (Type 1) water purification system, Biopak® Polisher; Merck, Burlington, Massachusetts, USA. All chemicals were used as received without any further purification throughout the study.

Preparation of spun nanofibers

First, the conductive components, citric acid and borax (CB), were used to prepare a solution in the ratio of 3:1, respectively. Then, 35 wt% of CB was dissolved in a DMF solution and agitated with a magnetic stirrer for 5 h at 400 rpm. The solution was used later dropwise for adjusting the electrical conductivity of polymeric solutions to optimum prior to electrospinning.

PSU of 20 wt. % was uniformly dissolved in NMP to reach a viscosity of 2 Pa/s and a conductivity of 116.3 μS/cm. PLA of 16 wt. % was dissolved in a solution of DMF/Acetone in a ratio of 4:1 to obtain a viscosity of 0.5 Pa/s and an electrical conductivity of 120.1 μS/cm. PVDF 20 wt. % was dissolved in DMF to a viscosity of 1.5 Pa/s and a conductivity of 118 μS/cm. Each solution was homogenized in a mixer (Heidolph, RZR 2041) by stirring at 500 rpm for 4 h and was treated with CB to achieve the reported conductivity values.

Electrospinning was performed on nano spider technology (NS Lab 200S spin line equipment, Elmarco, Liberec, Czech Republic) equipped with a patented (PCT/CZ2010/000042) rotating electrode comprising spinning elements containing a total of 32 nozzles (16 jets in each row). The process was conducted on

a 40 cm wide and 0.14 ± 0.01 mm thick, non-woven antistatic polypropylene (PP) continuous roller collector sheet in the laboratory of Tomas Bata University, Czech Republic, to produce fibers of a minimum diameter at optimum operating parameters; the thickness of the fibers together with the PP substrate sheet was measured to be 0.17 ± 0.01 mm for each material. The applied voltages were 55, 65, and 75 kV for PSU, PLA, and PVDF, respectively. The spacing between electrodes equaled 19 cm and the rotational speed of collecting PP spun bond was 0.1 m/min to prepare 5 m of each type of electrospun nanofiber in a total duration of 50 min. The pace of solution dosage was set at 0.17, 0.27, and 0.41 mL/min., and the average mass per unit area of the nanofibers reported were 0.59, 1.3, and 1.85 g/m², respectively. The operating room temperature was 26 ± 1 °C, with relative air humidity below 30%.

Characterization methods

Fourier-transform infrared spectroscopy (FTIR)

FTIR analysis was conducted using a Ge crystal in attenuated total reflectance (ATR) mode on a Nicolet 320 spectrometer (Thermo Scientific, Waltham, Massachusetts, USA). Adsorption of the estrogenic hormones on the surface of polymeric nanofibers was tested to determine the functional groups involved in the interaction. Spectra were recorded across 400–4000 cm⁻¹ under standard conditions with resolution and scan rate set at 4 cm⁻¹ and 16, respectively.

Scanning electron microscopy (SEM)

Nova 450 scanning electron microscope (SEM) (FEI; Thermo Fisher Scientific) was used to image electrospun fibers to observe the surface morphology and any defects, such as beads in the structures, that might be incorporated during electrospinning and to determine the desired diameter of fibers. The electron beam was operated at an accelerating voltage of 5–10 kV with a through-the-lens detector (TLD). The mean diameter of fibers was measured *via* ImageJ version 1.52a software (National Institutes of Health and the Laboratory for Optical and Computational Instrumentation (LOCI, University of Wisconsin), Madison, Wisconsin (USA)).

BET surface area and porosity analysis

Surface area and fiber surface pore diameter analysis were performed according to the Brunauer–Emmett–Teller (BET) method. To determine these quantities, a highly precise analyzer (BELSORP-mini II; BEL Japan Inc., Toyonaka, Japan) was used for specific surface area and pore size. Outgassing of the substrate was carried out for 12 h in a vacuum at 100 °C before starting measurements. Furthermore, according to ASTM F316-03 (2011), the pore size distribution of nanostructures and air permeability was tested and assessed by flow porometer NV, Belgium, using Galpor as a wetting liquid.

X-Ray diffraction

X-ray diffractograms (XRD) of electrospun fibers were recorded over the angle 2θ ranging from 5 to 90° *via* CoK_β ($\lambda = 1.79$ Å) as a source in a Miniflex™ 600 X-ray diffractometer (Rigaku, Tokyo, Japan). The operating parameters, such as voltage, current, step time, and step size, were 40 kV, 15 mA, 10°/s, and 0.02°, respectively.

Thermogravimetric analysis

To obtain the thermal stabilities of the produced nanofibers, a TGA Q500 thermogravimetric analyzer (TA Instruments, New Castle, Delaware, USA) was used with sample masses ranging from 12–20 ± 0.5 mg, depending on their densities. The samples were heated from 25 to 700 °C in an alumina crucible at a ramp of 15 °C/min under N₂ flow of 100 mL/min.

High-Performance liquid chromatography (HPLC) analysis

For the HPLC analysis of hormones (E1, E2, EE2, and E3), calibration standards and samples were carried out on an HPLC Dionex-UltiMate 3000 Series (Thermo Fisher Scientific, Karlsruhe, Germany). The separation was performed on a reversed-phase column Kinetex 2.6u C18 100 A (150 × 4.6 mm; Phenomenex, Torrance, California, USA) equipped with a security guard column (Phenomenex) at 30 °C. A combination of HPLC grade water and acetonitrile was used as the mobile phase (55:45, v/v) at a flow rate of 0.8 mL/min with an isocratic run time of 12 min. The sampler chamber was fixed at 5 °C and a 20 µL of volume was injected onto the column. Samples were performed in triplicate and elutes were analyzed using a wavelength of 200 nm to quantify the hormones' mean concentration by plotted calibration curve in Chromeleon software version 7.2 (Thermo Fisher Scientific).³⁹

For a preliminary test, a mixture of hormone solution was prepared containing 0.2 mg/L of each hormone with a total concentration of 0.8 mg/L and left for magnetic stirring overnight at 700 rpm, followed by 30 min of sonication before being stored in a dark place. Samples were collected *via* a micropipette (HTL Lab Solution, Poland) and passed through a glass microfiber (GMF) filter (Whatman, Prague, Czech Republic) with 25 mm of diameter and 0.45 µm of pore size before being dosed into 1.5 mL screw neck vials (VWR). Later, for optimization studies, a single high concentrated E1 (0.5 mg/L) solution was prepared as a stock solution that was diluted to prepare several different concentrations to test variation in adsorbate concentration (E1).

Adsorption study of spun polymeric nanofibers

Batch adsorption tests were conducted to determine the adsorption efficiency and capacity of each estrogenic hormone on spun nanofibers. Studies were performed similarly, as detailed in previous work.³⁹ 20 mg of each electrospun nanofiber was supplemented into 250 mL conical flasks filled with 100 mL solution from the prepared stock. The flasks were continuously agitated at 200 rpm on an orbital incubator shaker (Stuart® S1500; Barloworld Scientific Ltd., Stone, Staffordshire, UK). The influence of varying different parameters, such as initial concentration of hormone (mg/L), solution pH, adsorbent dosage (mg), and temperature of adsorbate solution (°C), was observed on the adsorption removal. Samples were withdrawn at predetermined time intervals using an optimized protocol to collect in vials *via* a GMF syringe filter and to measure the remaining concentration of estrogenic hormones present in the experimental flask. 4 mL of withdrawn sample was substituted with 4 mL of ultrapure water at each interval. To ensure precise results, the first 2 mL of the filtrate was passed through the GMF filter and discarded to avoid self-adsorption or residual permeate during the previous sampling. A set of triplicates of 'control' solution flasks were also included in the experimental run to obtain the initial reference mean concentration. The mean concentration values with standard deviation using Gaussian distribution were recorded and reported with reference to the control. The calculated percentage adsorption

removal and equilibrium adsorption capacity of each hormone at a given time (t) was determined by the expression in Eqns. (1) and (2), as follows:

$$\text{Removal (\%)} = \frac{C_i - C_t}{C_i} \times 100 \quad (1)$$

$$q_e = v \times \frac{C_i - C_e}{m} \quad (2)$$

Where C_i is the initial concentration (mg/L) and C_t is the concentration at time t (mg/L). The mass of adsorbent (m) is in grams, v is the volume of solution in liters, and q_e is equal to the equilibrium adsorption capacity in the adsorption process.

Adsorption kinetics study

The experimental results data were evaluated to study the factors involved in the adsorption process, including mass transfer and types of chemical interactions, to determine the rate-limiting step. Thus, kinetics models help select the optimized parameters and conditions required for full-scale elimination of the estrogenic hormone process. However, choosing the parameters and concluding the mechanisms involved in the complex heterogeneous systems is much more complicated because of superimposed surface effects on the chemical effects. Therefore, to deal with this concern, five models were deployed; Pseudo-first-order, Pseudo-second-order, Weber-Morris intra-particle/membrane diffusion, Elovich, and Fractional power model equations were best fitted with the experimental data to evaluate the simultaneous uptake of four estrogenic hormones by PSU fibers. The mentioned models are popular in describing the nature of aqueous/solid systems. Thus, these models can be expressed by the Eqns. (3), (4), (5), (6), and (7), respectively.

The pseudo-first-order introduced by Lagergren is the most common and widely used model for such a hormone adsorption study. It explains that the rate of estrogenic hormone adsorption on the surface of PSU fibers is directly dependent on the number of hormones adsorbed from the solution phase.⁴⁰

$$q_t = q_e (1 - e^{-k_1 t}) \quad (3)$$

Where q_t is the amount of hormone adsorbed per unit mass at time t (mg/g), q_e is the amount of hormone adsorbed per unit mass at equilibrium (mg/g), and k_1 is the first-order rate constant (L/min).

In contrast, the pseudo-second-order equation explains the hormone adsorption capacity and can exclusively predict the kinetic behavior over a long period. This model implies that surface adsorption is the rate-determining step due to the chemisorption that happens as a result of the physicochemical interactions between the PSU fibers and the hormone solution phase.⁴¹

$$\frac{t}{q_t} = \frac{1}{k_2 q_e^2} + \frac{t}{q_e} \quad (4)$$

Where k_2 is the second-order rate constant (g/(mg min)).

Next, the Weber-Morris intra-particle/membrane diffusion is a diffusion-controlled model; it suggests that the rate of adsorption is proportional to the speed of adsorbate with which it can diffuse towards the surface of the adsorbent. Primarily, the adsorption process occurs in a sequence of steps; first, the adsorbate moves

from the bulk of the solution to the surface of the adsorbent and then diffuses through the boundary layer to the outer surface of the adsorbent. Meanwhile, the adsorbate adsorbs on the active sites of the adsorbent and diffuses to penetrate through the pores. It is essential for validity that the linear convergence line of the best fit plotted for estrogenic hormone must intersect the coordinates of origin; then, this model is considered to be the rate-determining step.⁴²

$$q_t = k_3 t^{0.5} + C \quad (5)$$

Where k_3 is the intra-particle reaction rate constant (mg/g h^{1/2}) and C is the y-intercept constant (mg/g), which gives information about the boundary layer thickness.

Furthermore, in interactions where chemisorption is the only dominant mechanism for the adsorbate to be deposited on the surface of the adsorbent without desorption of products, the rate of adsorption gradually decreases with time due to the surface layer coverage. In such cases, the Elovich model is the most suitable for explaining the chemisorption process.⁴³

$$q_t = \beta \ln(\alpha\beta) + \beta \ln t \quad (6)$$

In Eqn. 6, α and β are the coefficients, such that α represents the initial adsorption rate (g/mg min) and β represents the desorption coefficient (mg/(g min)). These coefficients can be calculated from the slope and y-intercept of the plots, respectively.

Lastly, the fractional power model is the modified and advanced form of the Freundlich equation.⁴⁴

$$\ln q_t = \ln a + b \ln t \quad (7)$$

In Eqn. 7, a and b are the coefficients in the expression at the given condition that $b < 1$; the product of a and b is defined as the specific adsorption rate at a time of 1 min after the experiment is initiated.

Thermodynamic study

The impact that temperature has on the adsorption capacity of spun PSU was studied in a temperature-controlled system at 25, 35, and 45 °C. The thermodynamics of the adsorption process were estimated using the following equations.^{45,46}

$$K_D = \frac{C_s}{C_e} \quad (8)$$

$$\ln K_D = -\frac{\Delta H}{RT} + \frac{\Delta S}{R} \quad (9)$$

$$\Delta G = \Delta H - T\Delta S \quad (10)$$

Where ΔG is the Gibbs free energy change, ΔH is the enthalpy change, and ΔS entropy change. K_D is the distribution coefficient (a ratio of solid phase to solute concentrations), R (8.314 J/mol K) is the universal gas constant, C_s (mg/L) is the concentration of the hormone on the adsorbent, and T (K) is the absolute temperature.

Isotherm modeling

The adsorption isotherm study was performed at the initial pH of 7, temperature of 25 °C, and different initial concentrations of the E1 hormone mixture (0.1, 0.2, 0.3, 0.4, and 0.5 mg/L). Spun PSU was used as the adsorbent and samples were collected after 9 h of adsorption. The fitting of the adsorption equilibrium data was

evaluated using the Langmuir and Freundlich isotherms. The non-linear regression equations used for the models are shown in Eqns. (11) and (12), respectively:^{47–49}

$$q_e = \frac{Q_{\max} K_L C_e}{(1 + K_L C_e)} \quad (11)$$

$$q_e = K_F C_e^{1/n} \quad (12)$$

Where q_e is the amount of adsorbed hormone on PSU adsorbent at equilibrium (mg/g), C_e is the residual equilibrium hormone concentration (mg/L), Q_{\max} is the maximum adsorption capacity (mg/g), K_L is the Langmuir isotherm constant, K_F is the Freundlich constant, and n is the Freundlich heterogeneity factor.

Reusability study

For the desorption test, the nanofibers were extracted from the conical flasks containing the hormone solutions and washed thoroughly with distilled water, followed by gentle stirring at a constant 100 rpm for 10 min in a 100 mL mixture of 1:1 water and ethanol to entirely remove the hormones and elute in the mixture. Finally, the nanofibers were placed in 100 mL of water until the next adsorption cycle. The procedure was repeated for six consecutive adsorption–desorption cycles. The consecutive adsorption cycles were performed at the optimum conditions of pH 7, temperature 35 °C, 0.2 mg/L concentration of adsorbate (E1), and 40 mg dosage of adsorbent (PSU).

Statistical analysis

The data are displayed as mean \pm standard error. OriginLab software version 9.0 (OriginLab Corporation, Northampton, Massachusetts, USA) was used for statistical analysis. The difference between values was determined by a one-way analysis of variance (ANOVA). A value of $P < 0.05$ was determined as statistically significant.⁵⁰

RESULTS AND DISCUSSION

Characterization of materials

SEM analysis

Figure 1 reveals that the electrospun nanofibers were produced without beads or defects, as desired. The calculated average fiber diameters from SEM were in the range of 149–183 nm, which is firmly in compliance with the range of electrospun nanofibers (174–330 nm) reported in the literature.³⁹ These low achieved diameters are attributed to the optimized parameters used to prepare the electrospinning solutions, including low polymer concentration in the solution, intrinsic viscosity, and electrical conductivity. Further properties are mentioned in Table 1.

Table 1 shows that the mean pore size ranged from 0.39 to 1.10 μm and air permeability from 77 to 244 $\text{L}/\text{cm}^2 \text{ min bar}$, both of which are inversely dependent on the average mass of nanofiber per unit area (Table 2); the relative structural porosity is also visible in SEM micrographs at the same magnification. The measured BET surface area ranged from 0.3–6.3 m^2/g , which is directly dependent on the intrinsic viscosities of the solutions (PSU ~ 2.0 , PLA ~ 0.5 , and PVDF ~ 1.5 Pa.s) prior to electrospinning. The effect of the surface area is also evident in the preliminary test for the adsorption of hormones, where PSU was observed to adsorb and remove the highest percentage of hormones.

The physicochemical features of the electrospun nanofibers were investigated. The TGA graphs in Fig. 2(a)–(c) displayed that no

nanofiber degradation was observed up to 100 °C for any polymer. The slight initial dip in Fig. 2(a)–(c) is due to the evaporation of water, while the weight loss starting at around 200 °C was for PSU, at about 300 °C for PLA, and nearly at 400 °C for PVDF; these are far above the tested experimental range for adsorption in this study. Additionally, degradation with a rapid weight loss was observed at 517.73, 345.69, and 480.22 °C for PSU, PLA, and PVDF, respectively. The XRD (Fig. 2(d)) also revealed a broad peak region for each polymer at around $2\theta = 17\text{--}20^\circ$, indicating the semi-amorphous nature of the polymer electrospun nanofibers. For PVDF, two broad spikes are seen at around 18° and 22° that belong to the α and β phases, respectively.⁵¹

The IR spectra in Fig. 2(e) shows a characteristic peak at about 2974 cm^{-1} assigned to the CH_2 symmetric stretching present in all three polymeric nanofibers. Then, the spike at 1453 cm^{-1} for PVDF is the scissoring or in-plane bending of CH_2 in the α -phase. Furthermore, the rocking of CH_2 or CF_2 asymmetric stretching is observed at 840 cm^{-1} , and in-plane bending at 745 cm^{-1} is seen in the β -phase.⁵² PVDF appears in different crystal phases; the spike at 840 cm^{-1} is considerably large, representing the β -phase, and the peaks at 1431 and 1278 cm^{-1} define the crystalline phase. The peak at 1074 cm^{-1} is mainly due to the β -phase, but traces of other phases could also be found around this location in the literature.⁵¹ The absorption peak at 1187 cm^{-1} is due to the combination of β and γ phases, and the large peak at 880 cm^{-1} is a result of the combination of all existing phases, whereas peaks at 840 and 1278 cm^{-1} are the usual β -phase peaks.⁵³

In PLA, the characteristic peaks observed at 1754, 1267, and 754 cm^{-1} assigned to $\text{C}=\text{O}$ are due to the strength vibration, bending vibration, and torsion vibration, respectively. The peak located at 955 cm^{-1} corresponds to $\text{C}-\text{C}$ group. In addition, the spikes at 1132, 1045, and 867 cm^{-1} belong to $\text{C}-\text{O}$ groups for strength vibration. The deformation of $\text{C}-\text{H}$ appears at 1450 cm^{-1} and the symmetric and asymmetric strength vibrations of the -CH bond are indicated at 1362 and 1384 cm^{-1} . The peaks formed at 867 and 754 cm^{-1} are evidence of the amorphous and crystalline regions present in PLA, respectively.⁵⁴

The spectra peak intensity for PSU revealed at 1323 and 1293 cm^{-1} corresponds to the asymmetric absorption of the $\text{S}=\text{O}$ group, while the peak at 1169 cm^{-1} belongs to the symmetric absorption of the $\text{S}=\text{O}$ group. In addition, the characteristic absorption peaks at 1584 and 1487 cm^{-1} are attributed to the benzene rings.⁵⁵ The main characterized peaks are present at 1584, 1245, 1323, 1154, 1106, and 1013 cm^{-1} , corresponding to the stretching caused by aromatic $\text{C}=\text{C}$, $\text{C}-\text{O}-\text{C}$ (ether group), and $\text{O}=\text{S}=\text{O}$ bonds.⁵⁶

Batch adsorption studies

Preliminary adsorption for different prepared polymeric nanofibers

To evaluate and distinguish the efficiency of the prepared spun PSU, PLA, and PVDF nanofibers, short-term batch tests using the materials were performed to ascertain their adsorption efficiency against the four different hormones of E1, E2, EE2, and E3. According to deduced results (Fig. 3(a)), spun PSU showed more than 50% removal efficiency for almost all studied hormones. Removal efficiency for the different spun nanofibers was in the magnitude of $\text{PSU} > \text{PLA} > \text{PVDF}$. Based on this initial evaluation, spun PSU material was used for subsequent study due to its high adsorption capacity for different estrogenic hormones.

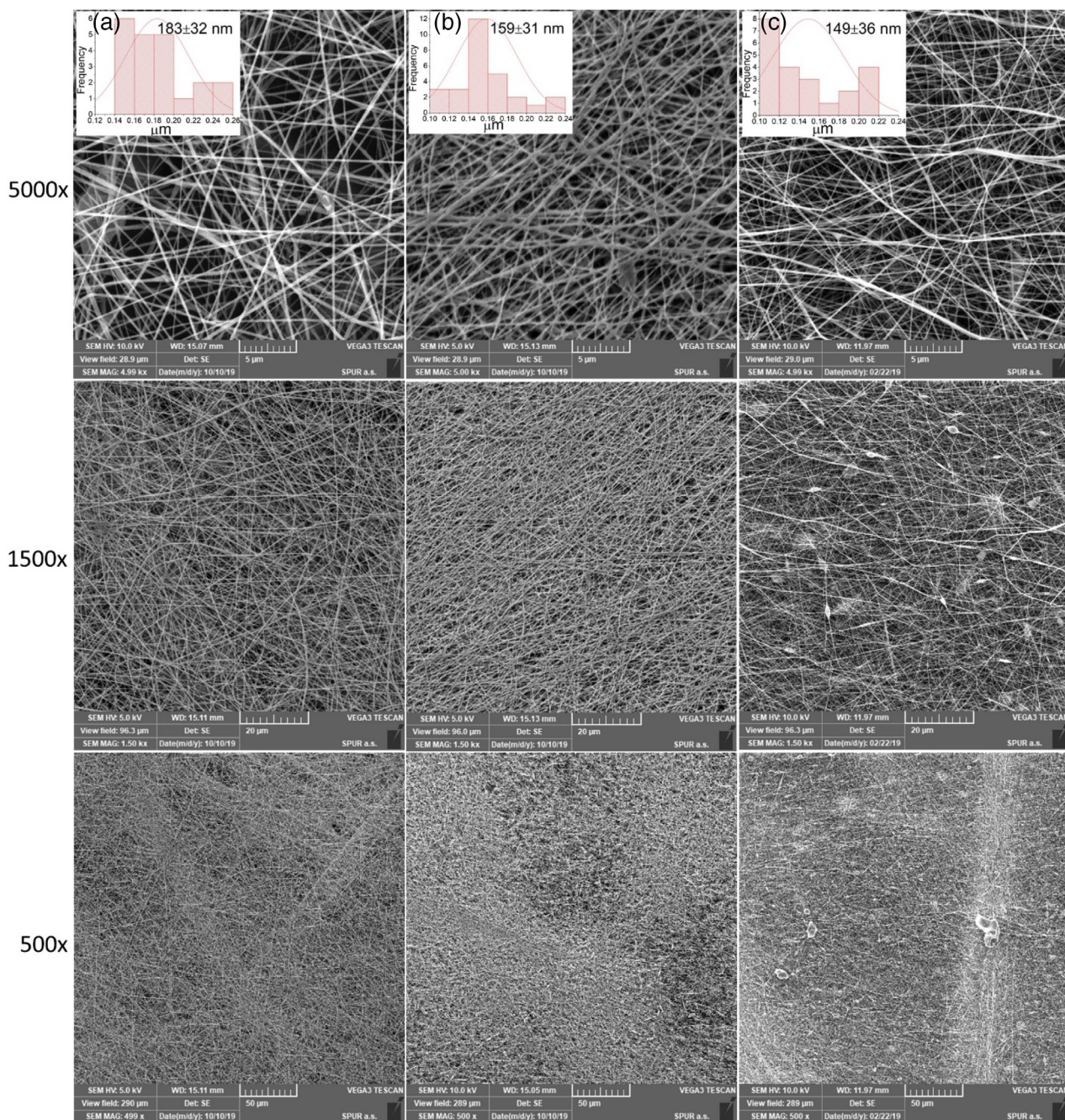


Figure 1. Electron micrographs with (inset) distribution of frequency size of the electrospun nanofibers PSU, PLA, and PVDF at different magnifications of 500x, 1500x, and 5000x.

Table 1. SEM, BET, and porometry data of electrospun polymeric fiber materials

Nanofiber	Average fiber diameter SEM (nm)	Porometry mean pore size (μm)	Air permeability ($\text{l}/\text{cm}^2 \cdot \text{min} \cdot \text{bar}$)	BET surface area (m^2/g)
PSU	183 ± 32	0.91	244	6.267
PLA	159 ± 31	1.10	197	0.302
PVDF	149 ± 36	0.39	077	1.612

Effect of contact time

The contact time plays a major role in the adsorption of the hormones onto the different spun nanofibers. The effect of contact time on the adsorption of the various hormones (E1, E2, EE2, and E3) by spun PSU, as the adsorbent with the highest adsorption capacity, was further investigated and is shown in Fig. 3(b). The initial uptake of the hormones occurred within the first 2 h, and after that, a gradual increase with time up to 9 h, which was depicted as the apparent equilibrium. This initial rapid uptake of the hormones could be due to the availability of the adsorption sites on the adsorbent materials. It was evident that the amount

Table 2. Properties of the polymeric solutions

Sample	Concentration (%)	Density (g/cm ³)	Intrinsic viscosity (Pa.s)	Electrical conductivity (μS/cm)	Av. mass per unit area (g/m ²)
PSU	20	1.25	2.0	116.3	0.59
PLA	16	1.25	0.5	120.1	1.30
PVDF	20	1.78	1.5	118.0	1.85

of hormones adsorbed onto the adsorbent increased by increasing the contact time. After 4 h, the removal of the hormones from the aqueous phase was more than 50%. The removal capacity of PSU for the different hormones was in the magnitude of E1 > EE2 > E2 > E3. This indicated that the E1 hormone had the highest binding affinity to PSU. This may be due to the stoichiometric structural arrangement of the E1 hormone molecule that favored more hydrogen bonds and π - π interactions with the adsorbent.³⁹

Adsorption kinetics

The adsorption of estrogenic hormones on PSU increased with time until equilibrium was achieved. The initial rate was fast for 60 min, and then it gradually decreased with an increased contact time, assuming saturation at 540 min. The adsorption kinetic plots for the adsorption of E1 on PSU nanofibers are shown in Fig. 4, and the obtained kinetic parameters from the models mentioned above are presented in Table 3.

Several kinetic models were used to investigate the experimental data that can best fit to understand the ability of concomitant adsorption of estrogenic hormones on the surface of PSU fibers. In Fig. 4(a), the plotting $\ln(q_e - q_t)$ vs. t shows a strong agreement of the E3 hormone with a linear best fit line covering the data set points, and the predicted adsorption capacity of 0.307 mg/g is close to the experimental equilibrium adsorption capacity of 0.354 mg/g with a high regression coefficient of 0.954. The theoretical adsorption capacities for E1, E2, and EE2 are 0.367, 0.423, and 0.451, all of which are unsatisfactory and reasonably less expected compared to the experimental values of 0.508, 0.550, and 0.703 mg/g, respectively. The rate constant, K_1 , is precise and similar for each estrogenic hormone, but the data set points do not match the generated lines of best fit for E1, E2, and EE2 for the pseudo-first-order equation.

For Fig. 4(b), the plots of t/q_t vs. t must be linear lines to accurately and precisely estimate the q_e and k_2 values from the slopes and y-intercepts of each data set, respectively. The results obtained clearly indicate that E1, E2, and EE2 estrogenic hormones follow pseudo-second order model kinetics. The data set points mostly match the lines of best fit with a high regression coefficient of 0.962, 0.970, and 0.975 for E1, E2, and EE2, respectively. Also, the calculated adsorption capacities of 0.528, 0.576, and 0.715 are strongly in compliance with the experimentally achieved values of 0.508, 0.550, and 0.703, respectively. The slightly lower values obtained during the experiment are referred to as the inhomogeneous active sites on the surface of PSU because the rate of adsorption is primarily dependent on the concentration of hormone solution and the number of available active sites present on the surface of the adsorbent material. Similar results have been observed and reported by Al-Khateeb *et al.* in the literature using MWCNTs as an adsorbent for these hormones. The adsorption

capacities reported were 0.423, 0.472, and 0.472 for E1, E2, and EE2, respectively.⁴³ Furthermore, E3 shows a clear mismatch using the pseudo-second-order model. The data points do not fit the linear best fit line, and in fact, two separate portions are observed: one for the first 120 min and the second from 180 min until the end of the experiment. The plots in Fig. 4(b) were used to determine the rate constants (k_2) and the calculated equilibrium adsorption capacities (q_e) expressed in Eqn. (4) to obtain the regression coefficient (R^2) shown in Table 3.

The plot of q_t vs. $t^{0.5}$ is shown in Fig. 4(c), representing the intraparticle diffusion model. The linear plots of all estrogenic hormones have a high regression coefficient of 0.992, 0.993, 0.995, and 0.975 for E1, E2, EE2, and E3, respectively, but the plots do not intercept through the origin. This indicates that intraparticle diffusion is involved in the adsorption process, but it is only a part of the mechanism and is not wholly the rate-determining step. A plausible reason could be that estrogenic hormones do not converge properly. This could be due to the surface boundary layer effects that might have dominated the interaction of the adsorption process in the latter half. Therefore, the diffusion rate decreases as the adsorption progresses, and a gentle slope is observed because of the low concentration of estrogenic hormones remaining in the solution.

The plot in Fig. 4(d) of q_t vs. $\ln t$ depicts high adsorption rates per minute, which indicates and elucidates that chemisorption is the most dominant adsorption mechanism in the interaction of estrogenic hormones with PSU nanofibers. EE2 had the highest adsorption capacity of 0.703 mg/g and an initial adsorption rate of 18.870 g/mg/min. The descending order of removal rates is in the magnitude of EE2 > E1 > E2 > E3, with E1 having the highest regression coefficient of 0.942 and the highest overall adsorption removal percentage (Fig. 3) due to its binding affinity to PSU. A plausible reason could be the stoichiometric structural arrangement of the E1 molecule that favored more hydrogen bonds and π - π interactions with the PSU fibers based on its structure.

In Fig. 4(e), the plots of $\ln q_t$ vs. $\ln t$ are represented. An entire mismatch is evident for most of the estrogenic hormones, except for E1, where a linear relationship is seen with a regression coefficient of 0.990, but the adsorption capacity is unsatisfactory. This indicates that the fractional power model is not appropriate for these estrogenic hormones. The calculated parameters using Eqns. (3), (4), (5), (6), and (7) are shown in Table 3.

Adsorption based on the variation of single parameters

Following the preliminary adsorption, contact time, and kinetics studies, the E1 hormone was selected as the most suitable hormone for further investigation of adsorption due to its high interaction with the adsorbents leading to the highest removal efficiency. As one of three major endogenous estrogens found in humans, this hormone serves as a suitable candidate. Different

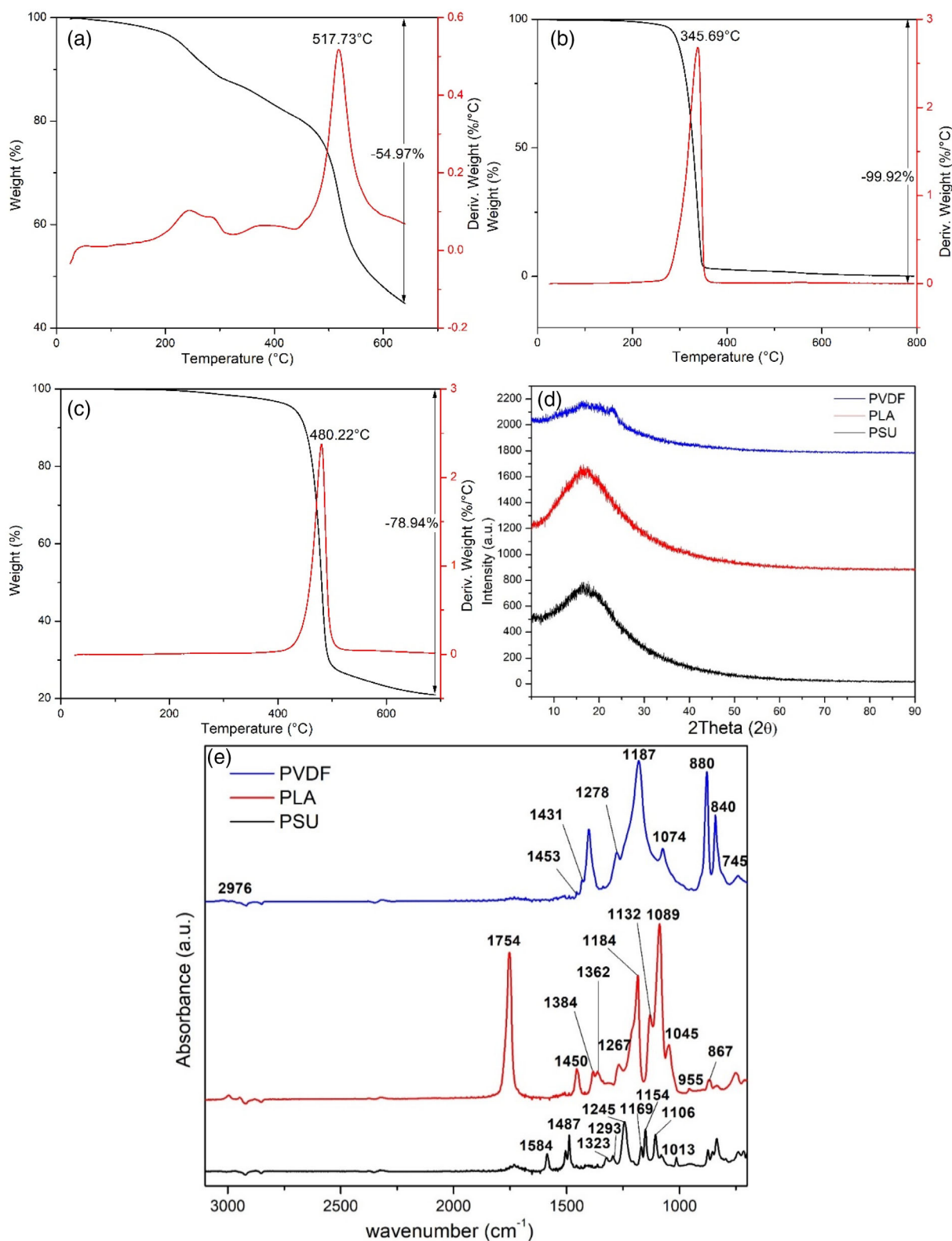


Figure 2. Thermogravimetric analyses of (a) PSU, (b) PLA, and (c) PVDF; (d) X-ray diffractograms and (e) FTIR spectra of the different electrospun nanofibers.

adsorption parameters of solution pH, hormone concentration, adsorbent dosage, and temperature effect were investigated by varying one factor and keeping the others constant.

Effect of solution pH

Solution pH is a vital index controlling parameter for the adsorption performance of an adsorbent. The solution pH was varied from 3 to

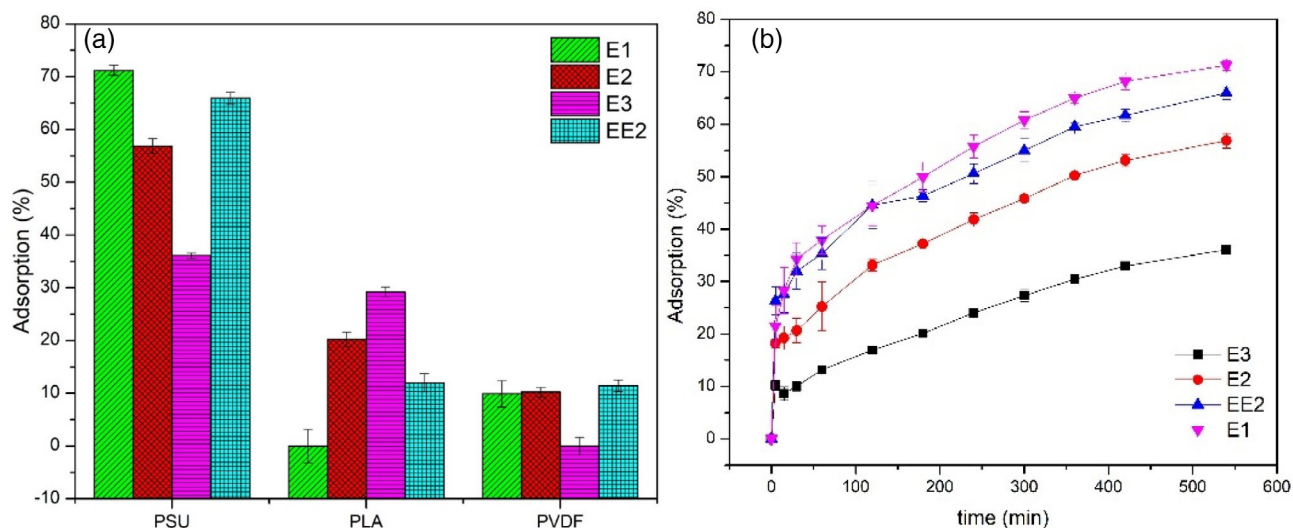


Figure 3. (a) Comparative adsorption efficiency of hormones (E1, E2, E3, and EE2) on PSU, PLA, and PVDF electrospun nanofibers (left panel), and (b) adsorption efficiency trends of E1, E2, E3, and EE2 hormones on PSU nanofibers as a function of time (right panel). Conditions: pH: 7, concentration of each hormone: 0.2 mg/L, and testing duration: 9 h.

9 at a constant dosage of 20 mg, 0.2 mg/L hormone concentration, and temperature 25 °C under shaking at 150 rpm. Figure 5(a) reveals that the hormone uptake by PSU is slightly affected by the initial solution pH ranging from 3.0 to 7.0, while the adsorption efficiency significantly increased from pH 7 to 9. The lowest removal efficiency of 44.32% was observed at pH 3, compared to the 79.92% determined at pH 9.0. This observation can be traced to the ionization state of the estrone (E1) hormone molecule. Generally, estrogen hormones are considered weak Lewis acids, and their ionization state is strongly dependent on solution pH. The reported value in literature for pKa of E1 is approximately 10.34.⁵⁷ pKa represents the acid dissociation constant of E1; above this value, the hormone deprotonates and becomes negatively charged, thereby losing its hydrogen atom affinity. As such, the adsorption study was investigated below pH 9 to favor interactions between the hormone molecules and the adsorbent materials.⁵⁸ Though maximum adsorption was achieved at pH 9, for environmental health and better safety handling of the system, a pH of 7, which shows more than 50% removal efficiency, was selected as the most suitable solution pH.

Effect of hormone concentration

The effect of the initial concentration of the hormone on spun PSU adsorption properties was investigated and presented in Fig. 5(b). According to the plot, the amount of hormone adsorbed on spun PSU was evaluated by varying initial concentrations from 0.1 to 0.5 mg/L at a dosage of 20 mg, pH 7, and temperature of 25 °C under shaking at 150 rpm. It was observed that the amount of hormone adsorption increased with an increase in initial concentration. However, the removal efficiency decreases with an increase in initial hormone concentration. As depicted in Fig. 5(b), the removal efficiency decreased from 52.95% to 48.62%. This phenomenon was attributed to the gradual saturation of the adsorbent adsorption sites with an increase in initial hormone concentration.⁵⁹

Effect of adsorbent dosage

The dosage of adsorbent plays a crucial role in the whole adsorption process. Investigations were performed by varying the amount of spun PSU (10, 20, 30, and 40 mg) while keeping the

other factors constant at 0.2 mg/L, pH 7, and temperature 25 °C under shaking at 150 rpm. Figure 5(c) shows that increasing the amount of adsorbent led to increased adsorption capacity. This is ascribed to more adsorption sites being available as the amount of the adsorbent increases, thus allowing for an increase in the number of hormone pollutants attached to the adsorbent.⁶⁰ It is evident that increasing the amount of the adsorbent directly increases the adsorption surface, giving rise to an increased removal percentage of the hormone from an aqueous phase. The removal efficiency rises from 37.42% to 79.82% by increasing the adsorbent amount from 10 mg to 40 mg. In addition, it was observed that the removal percentage was >50% when using adsorbent amounts ≥ 20 mg.

Effect of temperature

The effect on removal efficiency of the hormone by spun PSU was investigated by varying the medium's temperature (25, 35, and 45 °C) at constant 20 mg, 0.2 mg/L, and pH 7 under shaking at 150 rpm. Based on the obtained results (Fig. 5(d)), low temperatures (25 and 35 °C) favoured a higher adsorption capacity as compared to a decrease in adsorption at elevated temperatures (45 °C). This observation was mainly attributed to the exothermic nature of the adsorption process.⁶¹ In addition, low adsorption at elevated temperatures may be related to the denaturing of the molecular hormone structure, thus affecting the binding affinity to the adsorbent adsorption sites. The adsorption efficiency of the hormone was most significant at 35 °C, with a removal capacity of 65.33% compared to 40.26% for higher temperatures. This suggested that adsorption at mild room temperature best suited the removal of the hormone and that continued heating would decrease the adsorption efficiency. Thus, for economic and environmental considerations, the best conditions for removing the estrogenic hormone were determined to include temperatures between 25 and 35 °C.

Adsorption mechanism

The types of mechanism depend on several factors, such as the hydrophobic nature of the hormone, the surface area of the polymeric nanofiber available for active sites interaction, the

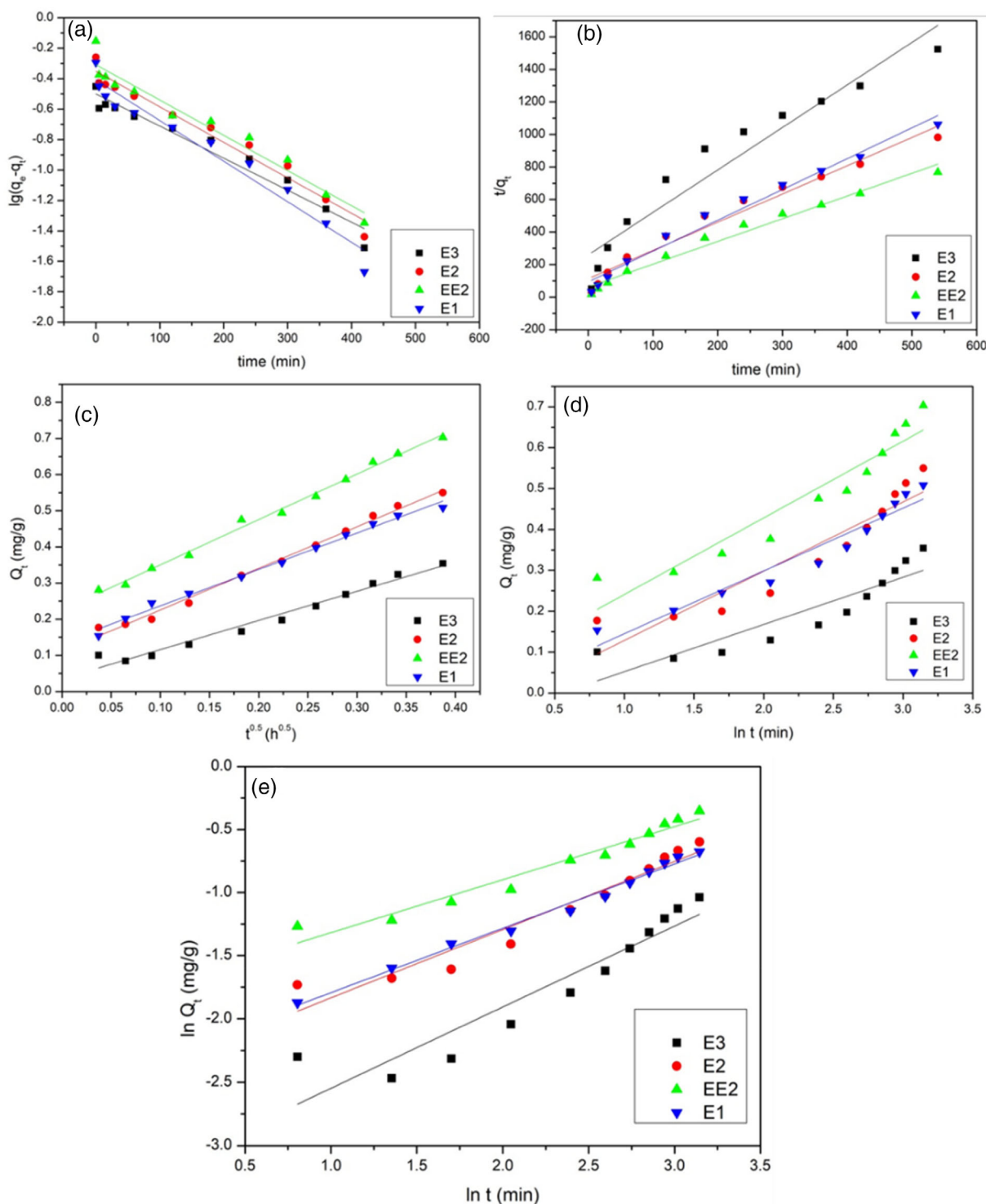


Figure 4. Adsorption kinetics plots of the four estrogenic hormones (E1, E2, EE2, E3) on PSU nanofibers: (a) Pseudo-first-order, (b) Pseudo-second-order, (c) Weber-Morris intraparticle diffusion, (d) Elovich, and (e) Fractional power model.

functional groups present on the hormone and nanofiber, and the pH of the solution. There can be more adsorption mechanisms present together that can lead to the adsorption of E1 on PSU nanofibers, as shown in Fig. 6. Size exclusion can contribute to a negligible amount of adsorption on the surface of PSU nanofibers (BET mean pore diameter on the fiber surface was 10.288 nm and SEM mean fiber diameter equaled 183 ± 32 nm). This is expected

because the reported diameter size of the E1 molecule in literature is approximately 0.8 nm (calculated using the Stokes-Einstein equation).⁶² Thus, a minuscule amount of E1 molecules can be entrapped in the pores on the fiber surface. However, most of the E1 molecules can readily pass through the porous non-woven structure of nanofibers due to its mean porosity of 0.91 μm and similarly for PLA (1.10 μm) and PVDF (0.39 μm). Additionally, the

Table 3. The kinetic models' parameters with each hormone using PSU electrospun nanofibers

Model parameters	Hormones			
	E1	E2	EE2	E3
$q_{e, \text{ expt}}$ (mg/g)	0.508	0.550	0.703	0.354
Pseudo-first order model				
k_1 (min^{-1})	0.003	0.002	0.002	0.002
$q_{e, \text{ cal}}$ (mg/g)	0.367	0.423	0.451	0.307
R^2	0.962	0.970	0.975	0.954
Pseudo-second order model				
k_2 (g/mg min)	0.038	0.027	0.031	0.026
$q_{e, \text{ cal}}$ (mg/g)	0.528	0.576	0.715	0.383
R^2	0.980	0.968	0.981	0.929
Intraparticle diffusion model				
k ($\text{mg/g h}^{0.5}$)	1.009	1.152	1.256	0.807
l (mg/g)	0.136	0.110	0.225	0.035
R^2	0.992	0.993	0.995	0.975
Elovich model				
α (g/mg min)	11.641	7.302	18.870	5.796
β (mg/g min)	0.077	0.085	0.094	0.058
R^2	0.942	0.881	0.909	0.819
Fractional power model				
a	0.100	0.093	0.176	0.041
b	0.255	0.270	0.210	0.320
$a + b$	0.025	0.025	0.037	0.013
R^2	0.990	0.939	0.957	0.885

dissociation of hydroxyl groups of E1 attached to its aromatic rings is dependent on the acid dissociation constant (pK_a); this value of E1 is 10.34, which is higher than that of phenol ($pK_a = 10$). This indicates that E1 would not deprotonate and stay predominantly neutral at $\text{pH} < 10.5$; therefore, the influence of electrostatic charge is absent in this system. The other possibility of E1 adsorption on the PSU internal and external surfaces could be due to hydrophobic interactions; the $\log K_{ow}$ (octanol–water partitioning coefficient) is 3.43, which is a greater value than 2.5. Therefore, this suggests that E1 could readily be adsorbed on the hydrophobic surfaces of PSU, PLA and PVDF nanofibers. Next, the electron-rich and deficient benzene aromatic rings possessed by both the adsorbate (E1) and the adsorbent (PSU) will lead to π - π interactions by the overlapping double-bonded C=C atoms present in the two molecules. Furthermore, the phenolic hydroxyl and carbonyl functional groups present on E1 can facilitate the formation of hydrogen bonding by acting as either a proton donor or acceptor. However, in this case, the -OH terminal group present in E1 molecules will serve as a proton donor and bind with the groups containing highly electronegative oxygen atoms in the structure of PSU nanofibers.⁶² Similarly, the C=O bond present at 1754 cm^{-1} in PLA (Fig. 2(e)) is responsible for its hydrogen bonding with hormones; however, this interaction is absent in the case of PVDF. This is the strongest of all the interactions and provides a boost in the rapid adsorption of the E1 hormone. Similar hydrogen bonding interactions of nylon 6,6 membrane and electrospun polyurethane fibers with E1 are reported in the literature.^{35,39} Hence, a similar interaction behavior is expected to occur in the remaining hormones (E2, EE2, E3) of the same estrogenic family.⁵⁷

Therefore, comparing the types of adsorption interaction mechanisms between estrogenic hormones and PSU nanofibers with PLA and PVDF, the overall descending trend of hormone

adsorption on nanofibers is as $\text{PSU} > \text{PLA} > \text{PVDF}$, which is also evident from Fig. 3(a).

Thermodynamic study

The thermodynamic parameters were estimated by plotting a Van't Hoff plot of $\ln K_D$ versus $1/T$, while values of ΔS and ΔH were determined from the slope and intercept, respectively. Values of ΔG at different temperatures were then calculated and are given in Table 4.

In general, the adsorption capacities of the PSU sample decreased at higher temperatures (Fig. 5(d)). The highest increase in adsorption capacity occurred by increasing the temperature from 25 to 35 °C. This increase in temperature may have facilitated the diffusion of the hormone molecules through the spun PSU material's matrix, thereby favoring adsorption. The calculated thermodynamic parameters from Eqns. (8), (9), and (10) summarized in Table 4 depicted ΔH and ΔG values to be negative. This indicated that the adsorption process of the estrogenic hormone onto PSU was exothermic and spontaneous, demonstrating favourability at lower temperatures. The values of ΔG ranging from -0.536 to -0.59 kJ/mol imply that evaluated estrogenic hormones were adsorbed onto PSU through the mechanism of physical adsorption. The ΔH value (≤ 20 kJ/mol) determined for the hormone adsorption on PSU also suggested that adsorption occurred through the mechanism of physical adsorption.⁵⁸ The negative ΔS entropy value suggested a decrease in randomness at the solute/solid interface.

Isotherm modeling

By plotting q_e vs. C_e , the equilibrium adsorption data were fitted with isotherm models as presented in Fig. 7, while the calculated isotherm parameters are given in Table 5.

The Langmuir model is based on the assumption of monolayer coverage on a homogenous surface with identical adsorption sites, given there is no interaction between the adsorbate molecules, while the Freundlich model describes multilayer adsorption with the interactions between adsorbate molecules and the heterogeneous adsorbent surface for various adsorption sites.^{63,64} The adsorption capacities of spun PSU increased with initial hormone concentrations, although the characteristic plateau was not achieved in the investigated concentration range. According to R^2 values (> 0.990), both models fit well with the experimental. This was supported by the low values obtained for the other error analysis parameters (sum of squared errors and chi-squared). However, the experimental data best fit with the Freundlich isotherm model. This indicates that the adsorption of the hormones on the surface of PSU was mainly heterogeneous. Freundlich parameter K_F is an indication of the PSU capacity, while n is a measure of the surface heterogeneity. For the investigated hormone, the n value was below one, indicating the heterogeneous surface of the adsorbent. The maximum adsorption capacity calculated from the Langmuir isotherm was 10.65 mg/g for the hormone; this was in close agreement with that calculated from the combined Langmuir–Freundlich isotherms (12.88 mg/g), indicating the suitability of these isotherms in describing the adsorption process of the hormone on the adsorbent. Similar results for the same hormone have been reported by Patel *et al.*⁶⁰ and Prokić *et al.*,⁴⁷ with maximum adsorption capacities determined as 10.12 and 12.66 mg/g, respectively.

A comparative study with other adsorbents

Table 6 compares the reported electrospun nanofibers to other adsorbent particles reported in the literature for the effective removal of E1 hormone.

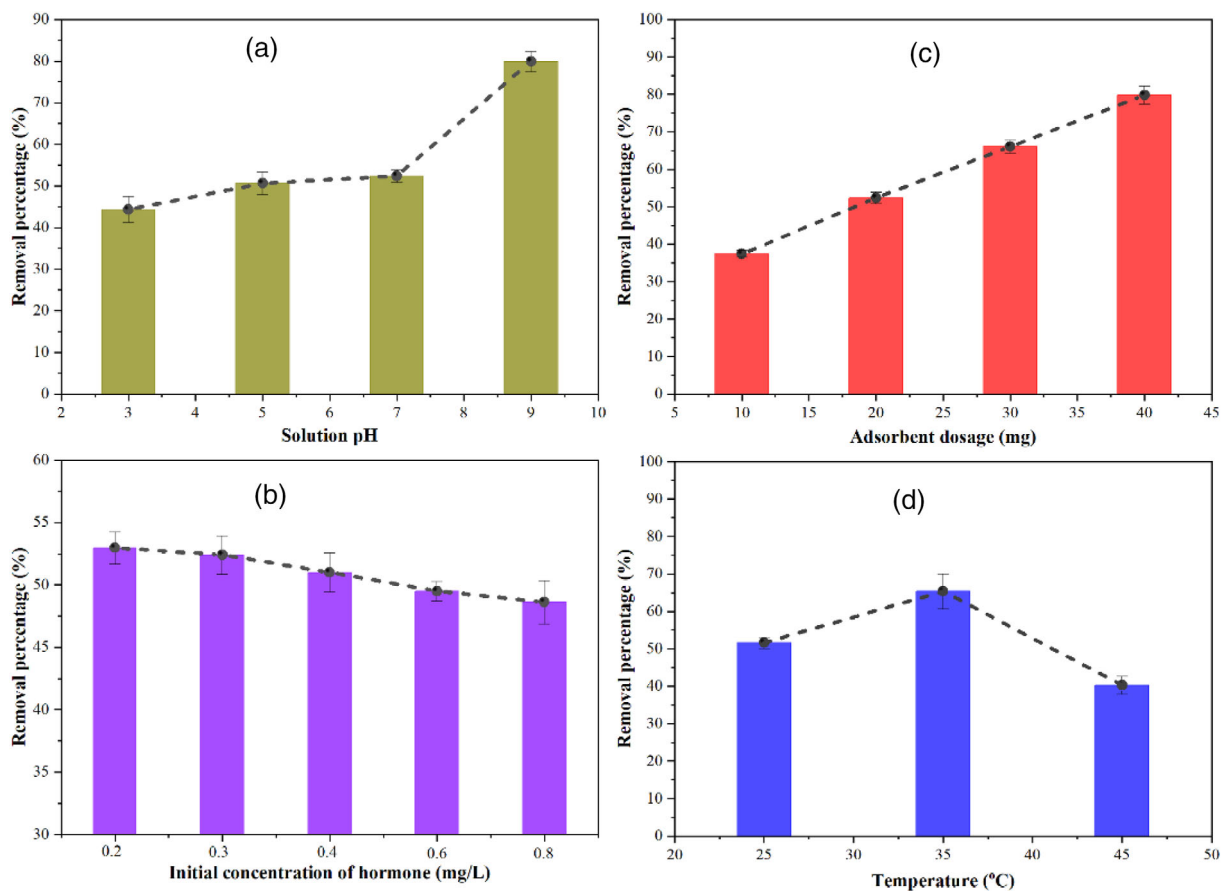


Figure 5. Effects of different adsorption parameters: (a) solution pH, (b) initial adsorbate concentration, (c) adsorbent dosage, and (d) temperature on the removal of E1 hormone using spun PSU nanofibers.

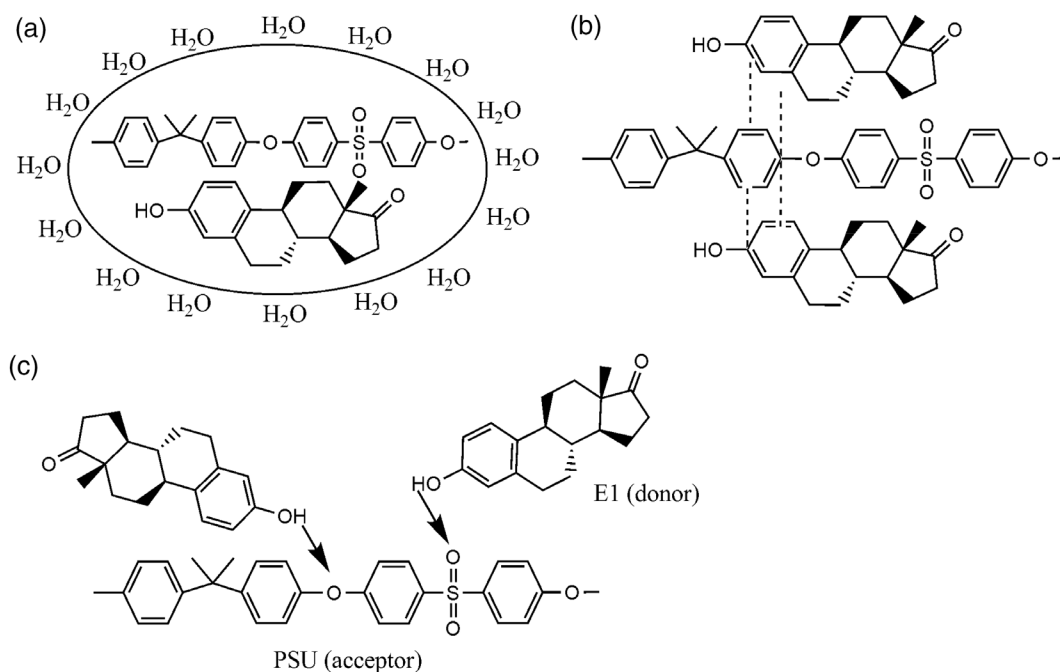
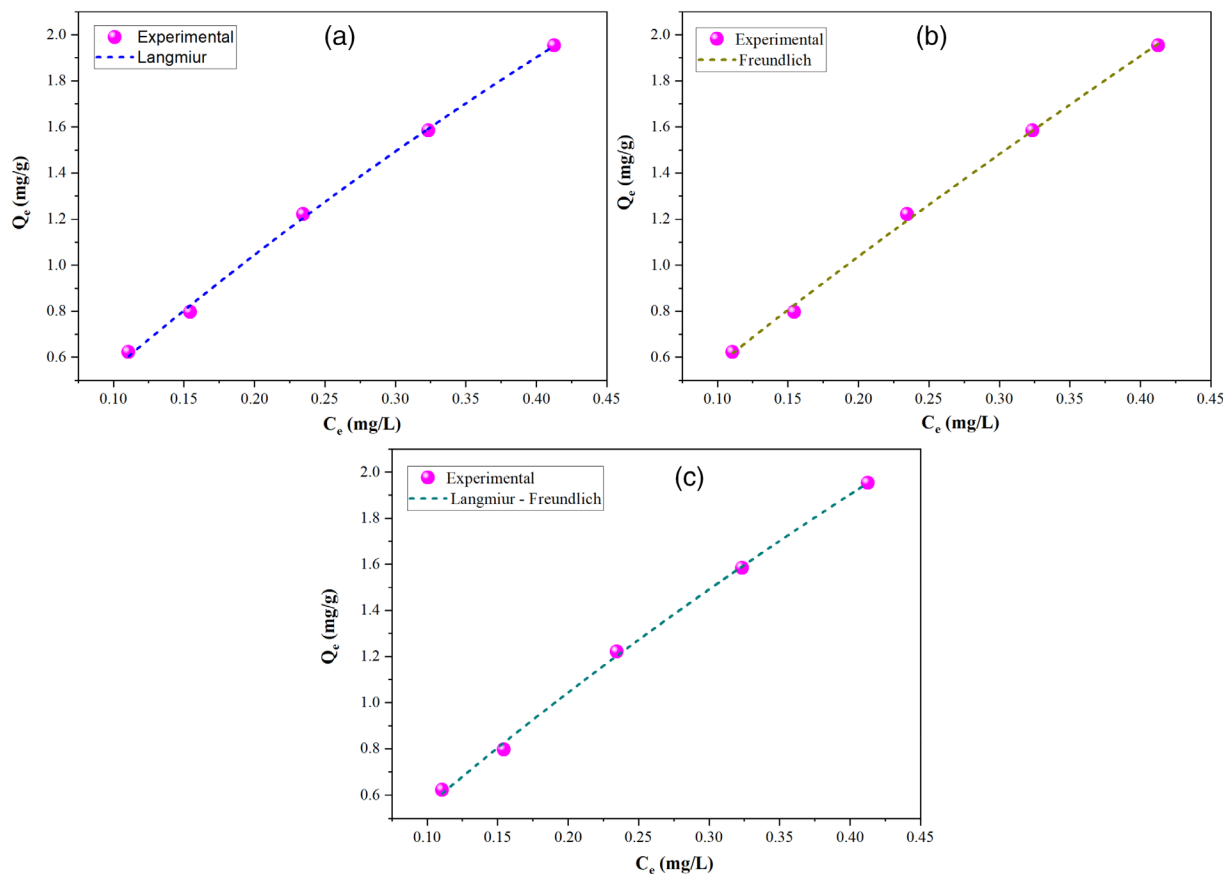


Figure 6. Schematic representation of the possible different interaction mechanisms between PSU nanofibers and E1 hormone: (a) hydrophobic interactions, (b) π - π stacking interaction, and (c) hydrogen bonding. Strong bonding interactions are represented with bold arrows, while weak interactions are represented with dotted lines.

Table 4. Thermodynamic parametric values for the adsorption of E1 hormone

Parameters	Temperature		
	298 K	308 K	318 K
ΔG° (kJ/mol)	-0.596	-0.566	-0.536
ΔH° (kJ/mol)	-1.478		
ΔS° (J/mol K)	-2.958		

PSU possesses a high adsorption capacity due to its surface area of 6.3 m²/g, which is relatively low for the other compared materials reported in the literature. The results revealed that PSU nanofibers at pH 7 and room temperature (25 °C) possessed a cumulative adsorption capacity of 2.115 mg/g with an individual adsorption capacity for E1 of 0.508 mg/g. This value is higher than the adsorption capacity of the compared electrospun nanofibers, MWCNTs, activated sludge, and hollow fiber membrane shown in Table 6. However, the value is slightly low compared to that of carbonized hydrothermal carbon because of carbon's high surface

**Figure 7.** Adsorption isotherms for E1 hormone using PSU electrospun nanofibers: (a) Langmuir, (b) Freundlich, and (c) Langmuir–Freundlich model.**Table 5.** Calculated adsorption isotherm parameters for the adsorption of the E1 hormone

Langmuir model						
Q_{\max} (mg/g)	K_L (L/mg)	R_L	R^2	SSE	χ^2	
10.651	0.543	0.696–0.887	0.998	0.00144	0.00048	
Freundlich model						
K_F (mg/g)(L/mg)	n		R^2	SSE	χ^2	
4.267	0.878		0.999	0.00172	0.00057	
Langmuir – Freundlich model						
Q_{\max} (mg/g)	K_{LF}	n	R^2	SSE	χ^2	
12.888	0.424	0.975	0.996	0.00142	0.00071	

SSE, sum of squared errors; χ^2 , Chi-square.

Table 6. Comparison of adsorption capacity of E1 hormone using PSU to various adsorbents

Material	Hormone	pH and temperature (°C)	Adsorption capacity (mg/g)	Reference
PES nanofibers	E1	7 and 25	0.442	39
PAN nanofibers	E1	7 and 25	0.396	39
PA nanofibers	E1	7 and 25	0.331	39
MWCNTs	E1	7 and 25	0.423	43
Activated sludge	E1	7 and 25	0.002533	43
Hydrophobic hollow fiber membrane	E1	7 and 25	0.000062	43
Carbonized hydrothermal carbon	E1	7 and 25	0.95	48
PSU nanofibers	E1	7 and 25	0.508	Present study

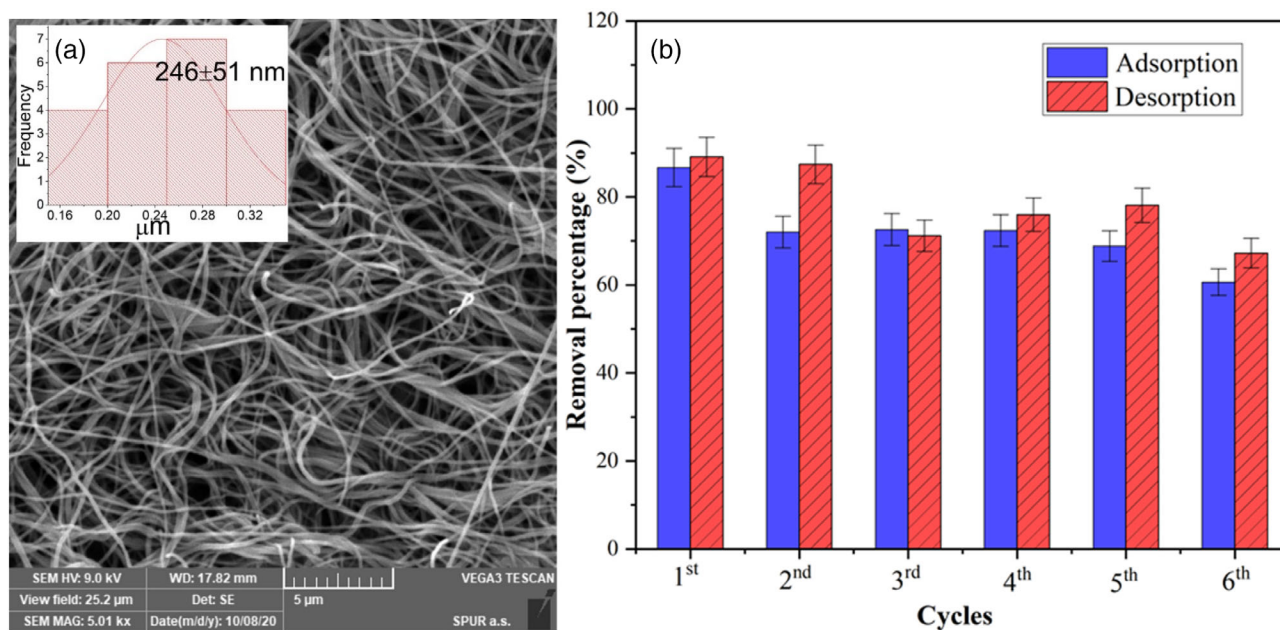


Figure 8. SEM micrograph after study with (inset) distribution of the fiber diameter (left panel) and cycles of adsorption–desorption for E1 by PSU nanofibers (right panel).

area compared to the electrospun nanofibers. When comparing PSU with the other electrospun nanofibers reported in the literature, the value for PSU nanofibers is high due to its high surface area and small average fiber diameter of 183 ± 32 nm (PES: 199 ± 51 nm, PAN: 330 ± 73 , PA: 220 ± 51 nm), its structure that allows hydrophobic and π - π interactions, and the functional groups present on the surface that facilitate hydrogen bonding with E1 hormone, as discussed in the Adsorption mechanism section.

Adsorption–desorption study

Fig. 8 shows that the highest adsorption was achieved at around 82.2%, which was gradually reduced, reaching the efficiency of about 60% after six adsorption cycles; this is evidence of the high performance of PSU nanofibers. Desorption cycles followed the same trend, but the efficiency remained slightly higher in most of the cycles using the desorption of E1 from PSU nanofibers; this clearly indicates the effectiveness of the process for the recovery of E1 hormones from the nanofibers. Additionally, the SEM image shows the surface morphology of the nanofibers after six cycles. A slight increase in the diameter of the nanofiber is observed,

increasing from 183 to 246 nm. A plausible reason for this swelling could be the interaction between the nanofiber and the ethanol while they were in contact during the desorption cycles.³⁹

CONCLUSIONS

Polymeric nanofibers that include PSU, PLA, and PVDF were successfully produced *via* the facile electrospinning method and they could adsorb all types of estrogenic hormones. These fibers possessed a mean fiber diameter of 149–183 nm and a specific surface area of 1.6–6.3 m²/g. The preliminary study showed that PSU was the best among these polymers, with the highest percentage of removal (71.2%) of E1. The adsorption of hormones on PSU is significantly high compared to those of other polymers due to the hydrogen bonding interactions. Therefore, five models (pseudo-first-order, pseudo-second-order, intraparticle diffusion, Elovich, and fractional power model) were deployed on the experimental data to obtain the adsorption kinetics and to understand the characteristics of PSU fibers with contact time. The obtained results showed that E3 followed pseudo-first-order kinetics, while E1, E2, and EE2 best fit pseudo-second-order kinetics. PSU fibers had maximum removal efficiencies of 71.2, 65.9, 56.9, and 36.1%

for E1, EE2, E2, and E3, respectively. Adsorption obeyed Langmuir–Freundlich isothermal adsorption models; thermodynamics and mechanisms were evaluated, revealing that the adsorption process of E1 was exothermic and spontaneous in nature. The adsorption–desorption cycles were conducted over six cycles to determine the reusability and effectiveness of PSU, both of which remained above 60%. Overall, the results indicate that PSU can be a potential and efficient adsorbent for the effective simultaneous removal of estrogenic hormones from water streams.

ACKNOWLEDGEMENTS

The authors gratefully acknowledge the financial support from the Ministry of Education, Youth, and Sports of the Czech Republic (RP/CPS/2022/002 and RP/CPS/2022/005) and the Internal Grant Agency of TBU in Zlin (grant no. IGA/CPS/2022/003). We would also like to acknowledge the Centre of Polymer Systems (CPS) situated at Tomas Bata University in Zlin, Czech Republic, for the use of their available research facilities to conduct this research work.

CONFLICT OF INTEREST

The authors declare that there exists no form of competing interests.

AUTHOR CONTRIBUTIONS

Muhammad Yasir: Conceptualization, Methodology, Investigation, Formal analysis, Data curation, Writing- original draft, Writing- Review & editing. Fahanwi Asabuwa Ngwabebhoh: Formal analysis, Data curation, Writing- Review & editing. Tomáš Šopík: Methodology, Formal analysis, Data curation. Lenka Lovčáková: Formal analysis, Data curation. Dušan Kimmer: Conceptualization, Supervision, Review & editing. Vladimír Sedlářik: Conceptualization, Supervision, Project administration, Funding acquisition, Review & editing.

REFERENCES

- AlAbduljabbar FA, Haider S, Ali FAA, Alghyamah AA, Almasry WA, Patel R *et al.*, Efficient photocatalytic degradation of organic pollutant in wastewater by electrospun functionally modified Polyacrylonitrile nanofibers membrane anchoring TiO₂ nanostructured. *Membranes* **11**:785 (2021).
- Wu X, Cobbina SJ, Mao G, Xu H, Zhang Z and Yang L, A review of toxicity and mechanisms of individual and mixtures of heavy metals in the environment. *Environ Sci Pollut Res* **23**:8244–8259 (2016).
- Hamid N, Junaid M and Pei D-S, Combined toxicity of endocrine-disrupting chemicals: A review. *Ecotoxicol Environ Saf* **215**:112136 (2021).
- Haddaoui I and Mateo-Sagasta J, A review on occurrence of emerging pollutants in waters of the MENA region. *Environ Sci Pollut Res* **28**: 68090–68110 (2021).
- Balali-Mood M, Naseri K, Tahergorabi Z, Khazdair MR and Sadeghi M, Toxic mechanisms of five heavy metals: mercury, Lead, chromium, cadmium, and arsenic. *Front Pharmacol* **12**:643972 (2021).
- Kocour Kroupová H, Valentová O, Svobodová Z, Šauer P and Máchová J, Toxic effects of nitrite on freshwater organisms: a review. *Rev Aquac* **10**:525–542 (2018).
- Chambers WS, Hopkins JG and Richards SM, A review of per- and Polyfluorinated alkyl substance impairment of reproduction. *Frontiers in Toxicology* **3**:732436 (2021).
- La Merrill MA, Vandenberg LN, Smith MT, Goodson W, Browne P, Patisaul HB *et al.*, Consensus on the key characteristics of endocrine-disrupting chemicals as a basis for hazard identification. *Nat Rev Endocrinol* **16**:45–57 (2020).
- Hilakivi-Clarke L, de Assis S and Warri A, Exposures to synthetic estrogens at different times during the life, and their effect on breast cancer risk. *J Mammary Gland Biol Neoplasia* **18**:25–42 (2013).
- Czarny K, Szczukocki D, Krawczyk B, Gadzała-Kopciuch R and Skrzypek S, Toxicity of single steroid hormones and their mixtures toward the cyanobacterium *Microcystis aeruginosa*. *J Appl Phycol* **31**:3537–3544 (2019).
- Street ME, Angelini S, Bernasconi S, Burgio E, Cassio A, Cattellani C *et al.*, Current knowledge on endocrine disrupting chemicals (EDCs) from animal biology to humans, from pregnancy to adulthood: highlights from a national Italian meeting. *Int J Mol Sci* **19**:1647 (2018).
- Kumar M, Sarma DK, Shubham S, Kumawat M, Verma V, Prakash A *et al.*, Environmental endocrine-disrupting chemical exposure: role in non-communicable diseases. *Frontiers in Public Health* **8**:553850 (2020).
- Henley DV, Lindzey J and Korach KS, Steroid hormones, in *Endocrinology*, ed. by Melmed S and Conn PM. Humana Press, Totowa, NJ, pp. 49–65 (2005).
- Koh YKK, Chiu TY, Boobis A, Cartmell E, Scrimshaw MD and Lester JN, Treatment and removal strategies for estrogens from wastewater. *Environ Technol* **29**:245–267 (2008).
- Gao X, Kang S, Xiong R and Chen M, Environment-friendly removal methods for endocrine disrupting chemicals. *Sustainability* **12**:7615 (2020).
- Muhammad Y, Milan M, Tomas S, Hassan A, Michal U, Jan A *et al.*, ZnO nanowires and nanorods based ZnO/WO₃/Pt heterojunction for efficient photocatalytic degradation of Estriol (E3) hormone. *Mater Lett* **319**:132291 (2022).
- Yasir M, Sopik T, Patwa R, Kimmer D and Sedlarik V, Adsorption of estrogenic hormones in aqueous solution using electrospun nanofibers from waste cigarette butts: kinetics, mechanism, and reusability. *Express Polym Lett* **16**:624–648 (2022).
- Hartmann J, Beyer R and Harm S, Effective removal of estrogens from drinking water and wastewater by adsorption technology. *Environ Process* **1**:87–94 (2014).
- Peiris C, Nawalage S, Wewelwela JJ, Gunatilake SR and Vithanage M, Biochar based sorptive remediation of steroidal estrogen contaminated aqueous systems: A critical review. *Environ Res* **191**:110183 (2020).
- Ogata F, Tominaga H, Yabutani H and Kawasaki N, Removal of estrogens from water using activated carbon and ozone. *J Oleo Sci* **60**: 609–611 (2011).
- Wang X, Liu N, Liu Y, Jiang L, Zeng G, Tan X *et al.*, Adsorption removal of 17 β -estradiol from water by Rice straw-derived biochar with special attention to pyrolysis temperature and background chemistry. *Int J Environ Res Public Health* **14**:1213 (2017).
- O. Ifealebuegu A, Removal of Steroid hormones by activated carbon adsorption—kinetic and thermodynamic studies. *J Environ Prot* **03**: 469–475 (2012).
- Jiang L, Liu Y, Liu S, Zeng G, Hu X, Hu X *et al.*, Adsorption of estrogen contaminants by graphene nanomaterials under natural organic matter preloading: comparison to carbon nanotube, biochar, and activated carbon. *Environ Sci Technol* **51**:6352–6359 (2017).
- Cheng C, Li X, Yu X, Wang M and Wang X, Chapter 14 – electrospun nanofibers for water treatment, in *Micro and Nano Technologies*, ed. by Ding B, Wang X, JBT-EN Y. William Andrew Publishing, pp. 419–453 (2019). <https://doi.org/10.1016/B978-0-323-51270-1.00014-5>
- Agrawal S, Ranjan R, Lal B, Rahman A, Singh SP, Selvaratnam T *et al.*, Synthesis and Water Treatment Applications of Nanofibers by Electrospinning. *Processes* **9**:1779 (2021).
- Matei E, Covaliu-Mierla CI, Ţurcanu AA, Răpă M, Predescu AM and Predescu C, Multifunctional membranes—A versatile approach for emerging pollutants removal. *Membranes* **12**:67 (2022).
- Mat Nawi NI, Chean HM, Shamsuddin N, Bilad MR, Narkkun T, Faungnawakij K *et al.*, Development of hydrophilic PVDF membrane using vapour induced phase separation method for produced water treatment. *Membranes* **10**:121 (2020).
- Goetz LA, Naseri N, Nair SS, Karim Z and Mathew AP, All cellulose electrospun water purification membranes nanotextured using cellulose nanocrystals. *Cellulose* **25**:3011–3023 (2018).

- 29 Liu L, Lin Z, Niu J, Tian D and He J, Electrospun polysulfone/poly(lactic acid) nanoporous fibrous mats for oil removal from water. *Adsorpt Sci Technol* **37**:438–450 (2019).
- 30 Rosalam S, Chiam CK, Widyaparamitha S, Chang YW and Lee CA, Water desalination by air-gap membrane distillation using meltblown polypropylene nanofiber membrane. *IOP Conf Ser Earth Environ Sci* **36**:12032 (2016).
- 31 Li X, García-Payo MC, Khayet M, Wang M and Wang X, Superhydrophobic polysulfone/polydimethylsiloxane electrospun nanofibrous membranes for water desalination by direct contact membrane distillation. *J Memb Sci* **542**:308–319 (2017).
- 32 Rahman ROA, El-Kamash AM and Hung Y-T, Applications of Nano-zeolite in wastewater treatment: an overview. *Water* **14**:137 (2022).
- 33 Ivanoska-Dacikj A, Makreski P and Bogoeva-Gaceva G, Fabrication of biodegradable polyurethane electrospun webs of fibers modified with biocompatible graphene oxide nanofiller. *J Ind Text* **0**(0):1–25 (2021). <https://doi.org/10.1177/15280837211003165>
- 34 Almasian A, Chizari Fard G, Parvinzadeh Gashti M, Mirjalili M and Mokhtari SZ, Surface modification of electrospun PAN nanofibers by amine compounds for adsorption of anionic dyes. *Desalin Water Treat* **57**:10333–10348 (2016).
- 35 Han J, Qiu W and Gao W, Adsorption of estrone in microfiltration membrane filters. *Chem Eng J [Internet]* **165**:819–826 (2010). <https://doi.org/10.1016/j.cej.2010.10.024>.
- 36 Han J, Qiu W, Cao Z, Hu J and Gao W, Adsorption of ethinylestradiol (EE2) on polyamide 612: molecular modeling and effects of water chemistry. *Water Res* **47**:2273–2284 (2013).
- 37 Schäfer AI, Stelzl K, Faghih M, Sen Gupta S, Krishnadas KR, Heißler S *et al.*, Poly(ether sulfone) nanofibers impregnated with β -Cyclodextrin for increased micropollutant removal from water. *ACS Sustain Chem Eng* **6**:2942–2953 (2018).
- 38 Wang M, Qu F, Jia R, Sun S, Li G and Liang H, Preliminary study on the removal of steroidal estrogens using TiO₂-doped PVDF ultrafiltration membranes. *Water* **8**:1–12 (2016).
- 39 Yasir M, Šopík T, Lovecká L, Kimmer D and Sedlařík V, The adsorption, kinetics, and interaction mechanisms of various types of estrogen on electrospun polymeric nanofiber membranes. *Nanotechnology* **33**:75702 (2021).
- 40 Qi FF, Cao Y, Wang M, Rong F and Xu Q, Nylon 6 electrospun nanofibers mat as effective sorbent for the removal of estrogens: kinetic and thermodynamic studies. *Nanoscale Res Lett* **9**:1–10 (2014).
- 41 Ersali S, Hadadi V, Moradi O and Fakhri A, Pseudo-second-order kinetic equations for modeling adsorption systems for removal of ammonium ions using multi-walled carbon nanotube. *Fuller Nanotub Carbon Nanostructures* **3**:150527104639002 (2013).
- 42 Tian Y, Wu M, Liu R, Li Y, Wang D, Tan J *et al.*, Electrospun membrane of cellulose acetate for heavy metal ion adsorption in water treatment. *Carbohydr Polym [Internet]* **83**:743–748 (2011).
- 43 Al-Khateeb LA, Obaid AY, Asiri NA and Abdel SM, Adsorption behavior of estrogenic compounds on carbon nanotubes from aqueous solutions: kinetic and thermodynamic studies. *J Ind Eng Chem* **20**:916–924 (2014).
- 44 Ho YS and McKay G, Application of kinetic models to the sorption of copper (II) on to peat. *Adsorpt Sci Technol* **20**:797–815 (2002).
- 45 Ngwabebhoh FA, Mammadli N and Yildiz U, Bioinspired modified nanocellulose adsorbent for enhanced boron recovery from aqueous media: optimization, kinetics, thermodynamics and reusability study. *J Environ Chem Eng* **7**:103281 (2019).
- 46 Carballa M, Fink G, Omil F, Lema JM and Ternes T, Determination of the solid-water distribution coefficient (K_d) for pharmaceuticals, estrogens and musk fragrances in digested sludge. *Water Res* **42**:287–295 (2008).
- 47 Prokić D, Vukčević M, Kalijadis A, Maletić M, Babić B and Đurkić T, Removal of Estrone, 17 β -estradiol, and 17 α -Ethinylestradiol from water by adsorption onto chemically modified activated carbon cloths. *Fibers Polym* **21**:2263–2274 (2020).
- 48 Prokić D, Vuk M, Mitrović A, Maletić M, Kalijadis A, Janković I *et al.*, Adsorption of estrone, 17 β -estradiol, and 17 α -ethinylestradiol from water onto modified multi-walled carbon nanotubes, carbon cryogel, and carbonized hydrothermal carbon. *Environ Sci Pollut Res* **29**:4431–4445 (2021).
- 49 Ngwabebhoh FA, Erdem A and Yildiz U, Synergistic removal of Cu(II) and nitrazine yellow dye using an eco-friendly chitosan-montmorillonite hydrogel: optimization by response surface methodology. *J Appl Polym Sci* **133**:1–14 (2016).
- 50 Yasir M, Ngwabebhoh FA, Sopik T, Ali H and Sedlařík V, Electrospun polyurethane nanofibers coated with polyaniline / polyvinyl alcohol as ultrafiltration membranes for the removal of ethinylestradiol hormone micropollutant from aqueous phase. *J Environ Chem Eng* **10**:107811 (2022).
- 51 Kaspar P, Sobola D, Částková K, Knápek A, Burda D, Orudzhev F *et al.*, Characterization of polyvinylidene fluoride (Pvdf) electrospun fibers doped by carbon flakes. *Polymers* **12**:1–15 (2020).
- 52 Lanceros-Méndez S, Mano JF, Costa AM and Schmidt VH, FTIR and DSC studies of mechanically deformed β -PVDF films. *J Macromol Sci Phys* **40B**:517–527 (2001).
- 53 Sengupta D, Kottapalli AGP, Chen SH, Miao JM, Kwok CY, Triantafyllou MS *et al.*, Characterization of single polyvinylidene fluoride (PVDF) nanofiber for flow sensing applications. *AIP Adv* **7**:105205 (2017).
- 54 Sepahi S, Kalaei M, Mazinani S, Abdouss M and Hosseini SM, Introducing electrospun polylactic acid incorporating etched halloysite nanotubes as a new nanofibrous web for controlled release of amoxicillin. *J Nanostructure Chem* **11**:245–258 (2021).
- 55 Rosid SM, Ajji A, Hasbullah H, Rosid SJM, Ismail AF and Goh PS, Physicochemical characteristics of polysulfone nanofiber membranes with iron oxide nanoparticles via electrospinning. *J Appl Polym Sci* **139**:1–10 (2022).
- 56 Mazoochi T, Hamadani M, Ahmadi M and Jabbari V, Investigation on the morphological characteristics of nanofibrous membrane as electrospun in the different processing parameters. *Int J Ind Chem* **3**:1–8 (2012).
- 57 Schäfer AI, Akanyeti I and Semião AJC, Micropollutant sorption to membrane polymers: A review of mechanisms for estrogens. *Adv Colloid Interface Sci* **164**:100–117 (2011).
- 58 Duan Q, Li X, Wu Z, Alsaedi A, Hayat T, Chen C *et al.*, Adsorption of 17 β -estradiol from aqueous solutions by a novel hierarchically nitrogen-doped porous carbon. *J Colloid Interface Sci* **533**:700–708 (2019).
- 59 Zhang J, Nguyen MN, Li Y, Yang C and Schäfer AI, Steroid hormone micropollutant removal from water with activated carbon fiber-ultrafiltration composite membranes. *J Hazard Mater* **391**:122020 (2020).
- 60 Patel S, Han J and Gao W, Sorption of 17 β -estradiol from aqueous solutions on to bone char derived from waste cattle bones: kinetics and isotherms. *J Environ Chem Eng* **3**:1562–1569 (2015).
- 61 Gong K, Lin Y, Wu P, Jin X, Owens G and Chen Z, Removal mechanism of 17 β -estradiol by carbonized green synthesis of Fe/Ni nanoparticles. *Chemosphere* **291**:132777 (2022).
- 62 Jin X and Hu J, Role of water chemistry on estrone removal by nanofiltration with the presence of hydrophobic acids. *Front Environ Sci Eng* **9**:164–170 (2015).
- 63 Tagliavini M, Engel F, Weidler PG, Scherer T and Schäfer AI, Adsorption of steroid micropollutants on polymer-based spherical activated carbon (PBSAC). *J Hazard Mater* **337**:126–137 (2017).
- 64 Ngwabebhoh FA, Gazi M and Oladipo AA, Adsorptive removal of multi-azo dye from aqueous phase using a semi-IPN superabsorbent chitosan-starch hydrogel. *Chem Eng Res Des* **112**:274–288 (2016).